

Lecture Notes in Mechanical Engineering

Vitalii Ivanov · Justyna Trojanowska ·
Ivan Pavlenko · Jozef Zajac ·
Dragan Peraković *Editors*

Advances in Design, Simulation and Manufacturing IV

Proceedings of the 4th International
Conference on Design, Simulation,
Manufacturing: The Innovation
Exchange, DSMIE-2021,
June 8–11, 2021, Lviv, Ukraine –
Volume 1: Manufacturing
and Materials Engineering

 Springer

Lecture Notes in Mechanical Engineering

Series Editors

Francisco Cavas-Martínez, Departamento de Estructuras, Universidad Politécnica de Cartagena, Cartagena, Murcia, Spain

Fakher Chaari, National School of Engineers, University of Sfax, Sfax, Tunisia

Francesco Gherardini, Dipartimento di Ingegneria, Università di Modena e Reggio Emilia, Modena, Italy

Mohamed Haddar, National School of Engineers of Sfax (ENIS), Sfax, Tunisia

Vitalii Ivanov, Department of Manufacturing Engineering Machine and Tools, Sumy State University, Sumy, Ukraine

Young W. Kwon, Department of Manufacturing Engineering and Aerospace Engineering, Graduate School of Engineering and Applied Science, Monterey CA, USA

Justyna Trojanowska, Poznan University of Technology, Poznan, Poland

Francesca di Mare, Institute of Energy Technology, Ruhr-Universität Bochum, Bochum, Nordrhein-Westfalen, Germany

Lecture Notes in Mechanical Engineering (LNME) publishes the latest developments in Mechanical Engineering—quickly, informally and with high quality. Original research reported in proceedings and post-proceedings represents the core of LNME. Volumes published in LNME embrace all aspects, subfields and new challenges of mechanical engineering. Topics in the series include:

- Engineering Design
- Machinery and Machine Elements
- Mechanical Structures and Stress Analysis
- Automotive Engineering
- Engine Technology
- Aerospace Technology and Astronautics
- Nanotechnology and Microengineering
- Control, Robotics, Mechatronics
- MEMS
- Theoretical and Applied Mechanics
- Dynamical Systems, Control
- Fluid Mechanics
- Engineering Thermodynamics, Heat and Mass Transfer
- Manufacturing
- Precision Engineering, Instrumentation, Measurement
- Materials Engineering
- Tribology and Surface Technology

To submit a proposal or request further information, please contact the Springer Editor of your location:

China: Ms. Ella Zhang at ella.zhang@springer.com

India: Priya Vyas at priya.vyas@springer.com

Rest of Asia, Australia, New Zealand: Swati Meherishi at swati.meherishi@springer.com

All other countries: Dr. Leontina Di Cecco at Leontina.dicecco@springer.com

To submit a proposal for a monograph, please check our Springer Tracts in Mechanical Engineering at <http://www.springer.com/series/11693> or contact Leontina.dicecco@springer.com

Indexed by SCOPUS. All books published in the series are submitted for consideration in Web of Science.

More information about this series at <http://www.springer.com/series/11236>

Vitalii Ivanov · Justyna Trojanowska ·
Ivan Pavlenko · Jozef Zajac ·
Dragan Peraković
Editors

Advances in Design, Simulation and Manufacturing IV

Proceedings of the 4th International
Conference on Design, Simulation,
Manufacturing: The Innovation Exchange,
DSMIE-2021, June 8–11, 2021,
Lviv, Ukraine – Volume 1: Manufacturing
and Materials Engineering

 Springer

Editors

Vitalii Ivanov
Sumy State University
Sumy, Ukraine

Justyna Trojanowska
Poznan University of Technology
Poznan, Poland

Ivan Pavlenko
Sumy State University
Sumy, Ukraine

Jozef Zajac
Technical University of Kosice
Presov, Slovakia

Dragan Peraković
University of Zagreb
Zagreb, Croatia

ISSN 2195-4356

ISSN 2195-4364 (electronic)

Lecture Notes in Mechanical Engineering

ISBN 978-3-030-77718-0

ISBN 978-3-030-77719-7 (eBook)

<https://doi.org/10.1007/978-3-030-77719-7>

© The Editor(s) (if applicable) and The Author(s), under exclusive license
to Springer Nature Switzerland AG 2021

This work is subject to copyright. All rights are solely and exclusively licensed by the Publisher, whether the whole or part of the material is concerned, specifically the rights of translation, reprinting, reuse of illustrations, recitation, broadcasting, reproduction on microfilms or in any other physical way, and transmission or information storage and retrieval, electronic adaptation, computer software, or by similar or dissimilar methodology now known or hereafter developed.

The use of general descriptive names, registered names, trademarks, service marks, etc. in this publication does not imply, even in the absence of a specific statement, that such names are exempt from the relevant protective laws and regulations and therefore free for general use.

The publisher, the authors and the editors are safe to assume that the advice and information in this book are believed to be true and accurate at the date of publication. Neither the publisher nor the authors or the editors give a warranty, expressed or implied, with respect to the material contained herein or for any errors or omissions that may have been made. The publisher remains neutral with regard to jurisdictional claims in published maps and institutional affiliations.

This Springer imprint is published by the registered company Springer Nature Switzerland AG
The registered company address is: Gewerbestrasse 11, 6330 Cham, Switzerland

Preface

This volume of Lecture Notes in Mechanical Engineering contains selected papers presented at the 4th International Conference on Design, Simulation, Manufacturing: The Innovation Exchange (DSMIE-2021), held in Lviv, Ukraine, on June 8–11, 2021. The conference was organized by the Sumy State University, Lviv Polytechnic National University, and International Association for Technological Development and Innovations, in partnership with Technical University of Kosice (Slovak Republic), Kielce University of Technology (Poland), University of West Bohemia (Czech Republic), Poznan University of Technology (Poland), Association for Promoting Innovative Technologies—Innovative FET (Croatia), and Society for Robotics of Bosnia and Herzegovina (Bosnia and Herzegovina).

DSMIE-2021 is the international forum for fundamental and applied research and industrial applications in engineering. The conference focuses on a broad range of research challenges in the fields of manufacturing, materials, mechanical, and chemical engineering, addressing current and future trends in design approaches, simulation techniques, computer-aided systems, innovative production approaches, Industry 4.0 strategy implementation for engineering tasks solving, and engineering education. DSMIE-2021 brings together researchers from academic institutions, leading industrial companies, and government laboratories worldwide to promote and popularize the scientific fundamentals of manufacturing.

DSMIE-2021 received 175 contributions from 27 countries around the world. After a thorough peer-review process, the program committee accepted 100 papers written by authors from 20 countries. Thank you very much to the authors for their contribution. These papers are published in the present book, achieving an acceptance rate of about 57%. Extended versions of selected best papers will be published in scientific journals: Management and Production Engineering Review (Poland), Archives of Mechanical Technology and Materials (Poland), Journal of Engineering Sciences (Ukraine), Advances in Thermal Process and Energy Transformation (Slovak Republic), and Assembly Techniques and Technologies (Poland).

We would like to thank members of the program committee and invited external reviewers for their efforts and expertise in contributing to reviewing, without which it would be impossible to maintain the high standards of peer-reviewed papers. Program committee members and invited external reviewers devoted their time and energy to peer-reviewing manuscripts. Our reviewers come from all over the world and represent 18 countries and are affiliated with more than 70 institutions.

Thank you very much to keynote speakers: Vitalii Pasichnyk (Ukraine), Katarzyna Antosz (Poland), and Alper Uysal (Turkey) for sharing their knowledge and experience.

The book “Advances in Design, Simulation and Manufacturing IV” was organized into two volumes according to the main conference topics: Volume 1—Manufacturing and Materials Engineering and Volume 2—Mechanical and Chemical Engineering. Each volume is devoted to research in design, simulation, and manufacturing in the main conference areas.

The first volume consists of five parts. The first part includes recent developments in product design and manufacturing processes. Notably, it presents ways for ensuring the technological parameters of automobile engines, studying the contact pressure in parts, the development of approaches for recognition cutting parts of cutters during machining, and fractal analysis of metal structures. This part also includes the research of spindle units for multi-operational lathes, technological inheritability and damageability of materials, studies of wear characteristics for hardened steels using laser–ultrasonic surface treatment, and rational design modeling of an interference fit. Recent developments in designing implants via additive technologies, dynamic modeling of automatic clamping mechanisms, optimal designing of automobile pipe adapters, and grinding hard alloys using solid lubricants are also presented in this part. Finally, the first part includes studies in ensuring technological parameters of surface shaping, design calculation of electrohydraulic drives and technological equipment, optimizing the interelectrode gap during electrical discharge grinding, and designing thread joints for thin-walled shells.

The second part includes studies in the implementation of intelligent solutions within the Industry 4.0 strategy. Notably, ways to implement blockchain information management systems and agile project management for IMS and IT projects are analyzed. This part also consists of optimization work with a digital human model, the implementation of Industry 4.0 supported by service robots in production processes, intelligent numerical control of profile grinding, and carrier behavior strategy. Autonomous data-driven integration systems, 3D technology radar models to evaluate emerging technologies, and ensuring the reliability of transport systems are also included. Finally, the second part presents an intelligent scheduling system architecture for manufacturing systems and a new approach for providing internal logistics according to Industry 4.0 concept and corresponding requirements.

The third part is devoted to contributing to ICT in engineering education. Mainly, it presents studies aimed at developing a mobile application for test control, integrated quality assurance at HEI, and Android application for explaining form deviations based on 3D models. This part also includes recent developments in

in-campus transfer technology and information and communication technologies for enhancing engineering creativity.

The fourth part is based on numerical simulation and experimental studies of milling, honing, burnishing, turning, abrasive finishing, hobbing, fine boring, gear shaping, and abrasive processing. Ways for modeling crack formation during thermomechanical processing of materials and the study of the impact of heat flows on the machine tool's wheelhead are also presented in this part. Finally, the fourth part includes numerical, experimental, and statistical results for surface layer operational characteristics and machining parts under dry, MQL, and nanofluid MQL conditions.

The fifth part aims at presenting recent developments in advanced materials and their applications. Remarkably, ways for strengthening centrifugal pumps' shafts by chemical–thermocycling treatment are proposed. The influence of synthesis modes on ceramic coatings' properties is analyzed. Optimal composite shelled sandwich structures with a honeycomb filler are designed. Ways for preparation and characterization of biocomposites, advanced manufacturing technologies for obtaining high-quality castings, the ion bombardment modeling of nano-periodic composite structures, and the rational choice of material for orthopedic purposes are proposed. Finally, the fifth part presents investigations in surface bandage

We appreciate the partnership with Springer, StrikePlagiarism, EasyChair, and our sponsors for their essential support during the preparation of DSMIE-2021.

Thank you very much for DSMIE Team. Their involvement and hard work were crucial to the success of the conference.

DSMIE's motto is "*Together we can do more for science, technology, engineering, and education*".

June 2021

Vitalii Ivanov
Justyna Trojanowska
Ivan Pavlenko
Jozef Zajac
Dragan Perakovic

Organization

Steering Committee

General Chair

Vitalii Ivanov Sumy State University, Ukraine

Co-chair

Ihor Hrytsai Lviv Polytechnic National University, Ukraine

Members

Oleksandr Gusak Sumy State University, Ukraine
Yaroslav Kusyi Lviv Polytechnic National University, Ukraine
Oleksandr Liaposhchenko Sumy State University, Ukraine
Ivan Pavlenko Sumy State University, Ukraine
Vadym Stupnytsky Lviv Polytechnic National University, Ukraine

Program Committee

Gabriel Abba University of Lorraine, France
Jean-Francois Antoine University of Lorraine, France
Katarzyna Antosz Rzeszow University of Technology, Poland
Jose Manoel Balthazar Institute of Aeronautics and Space, Brazil
Kristina Berladir Sumy State University, Ukraine
Jozef Bocko Technical University of Kosice, Slovak Republic
Ricardo Branco University of Coimbra, Portugal
Dagmar Caganova Slovak University of Technology,
Slovak Republic
Emilia Campean Technical University of Cluj-Napoca, Romania
Robert Cep VSB-Technical University of Ostrava,
Czech Republic

Yelizaveta Chernysh	Sumy State University, Ukraine
Olivian Chiver	Technical University of Cluj-Napoca, Romania
Vasile George Cioata	Polytechnic University of Timisoara, Romania
Olaf Ciszak	Poznan University of Technology, Poland
Oguz Colak	Eskisehir Technical University, Turkey
Radu Cotetiu	Technical University of Cluj-Napoca, Romania
Nadezda Cubonova	University of Zilina, Slovak Republic
Ivan Cvitic	University of Zagreb, Croatia
Predrag Dasic	University Union "Nikola Tesla," Serbia
Yuliia Denysenko	Sumy State University, Ukraine
Oleksandr Derevianchenko	Odessa National Polytechnic University, Ukraine
Sergey Dobrotvorskiy	National Technical University "Kharkiv Polytechnic Institute," Ukraine
Mihai Dragomir	Technical University of Cluj-Napoca, Romania
Kostiantyn Dyadyura	Sumy State University, Ukraine
Milan Edl	University of West Bohemia, Czech Republic
Sulaymon Eshkabilov	North Dakota State University, USA
Mathieu Gautier	University Lyon, France
Renata Gnatowska	Czestochowa University of Technology, Poland
Mihaly Gorbe	John von Neumann University, Germany
Marta Grabowska	Poznan University of Technology, Poland
Domenico Guida	University of Salerno, Italy
Oleksandr Gusak	Sumy State University, Ukraine
Michal Hatala	Technical University of Kosice, Slovak Republic
Ihor Hurey	Lviv Polytechnic National University, Ukraine
Vitalii Ivanov	Sumy State University, Ukraine
Maryna Ivanova	National Technical University "Kharkiv Polytechnic Institute," Ukraine
Lydmila Kalafatova	Donetsk National Technical University, Ukraine
Isak Karabegovic	University of Bihac, Bosnia, and Herzegovina
Gennadii Khavin	National Technical University "Kharkiv Polytechnic Institute," Ukraine
Lucia Knapcikova	Technical University of Kosice, Slovak Republic
Kateryna Kostyk	National Technical University "Kharkiv Polytechnic Institute," Ukraine
Jan Krmela	Alexander Dubcek University of Trencin, Slovak Republic
Ivan Kuric	University of Zilina, Slovak Republic
Yaroslav Kusyi	Lviv Polytechnic National University, Ukraine
Vladimir Lebedev	Odessa National Polytechnic University, Ukraine
Oleksandr Liaposhchenko	Sumy State University, Ukraine
Slawomir Luscinski	Kielce University of Technology, Poland
Jose Mendes Machado	University of Minho, Portugal
Angelos Markopoulos	National Technical University of Athens, Greece
Mykola Melnychuk	Lutsk National Technical University, Ukraine

Ronald L. Mersky	Widener University, USA
Viktor Molnar	University of Miskolc, Hungary
Ronald Iosif Moraru	University of Petrosani, Romania
Dmitriy Muzylyov	Kharkiv Petro Vasylenko National Technical University of Agriculture, Ukraine
Marek Ochowiak	Poznan University of Technology, Poland
Daniela Onofrejova	Technical University of Kosice, Slovak Republic
Oleh Onysko	Ivano-Frankivsk National Technical University of Oil and Gas, Ukraine
Vitalii Pasichnyk	National Technical University of Ukraine “Kyiv Polytechnic Institute named after I. Sikorskyi,” Ukraine
Ivan Pavlenko	Sumy State University, Ukraine
Dragan Perakovic	University of Zagreb, Croatia
Marco Perisa	University of Zagreb, Croatia
Oleksandr Permiakov	National Technical University “Kharkiv Polytechnic Institute,” Ukraine
Jan Pitel	Technical University of Kosice, Slovak Republic
Grigore Marian Pop	Technical University of Cluj-Napoca, Romania
Oleksandr Povstyanoy	Lutsk National Technical University, Ukraine
Erwin Rauch	Free University of Bolzano, Italy
Michal Rogalewicz	Poznan University of Technology, Poland
Andrii Rogovyi	Kharkiv National Automobile and Highway University, Ukraine
Yiming Rong	Southern University of Science and Technology, China
Alessandro Ruggiero	University of Salerno, Italy
Vira Shendryk	Sumy State University, Ukraine
Robert Sika	Poznan University of Technology, Poland
Lesya Shkitsa	Ivano-Frankivsk National Technical University of Oil and Gas, Ukraine
Vsevolod Sklabinskyi	Sumy State University, Ukraine
Volodymyr Sokolov	V. Dahl East Ukrainian National University, Ukraine
Marcin Sosnowski	Jan Dlugosz University of Czestochowa, Poland
Vadym Stupnytskyk	Lviv Polytechnic National University, Ukraine
Antoni Swic	Lublin University of Technology, Poland
Yuliia Tarasevych	AGH University of Science and Technology, Poland
Volodymyr Tonkonogyi	Odessa National Polytechnic University, Ukraine
Justyna Trojanowska	Poznan University of Technology, Poland
Michael Tseitlin	National Technical University “Kharkiv Polytechnic Institute,” Ukraine
Nicolae Ungureanu	Technical University of Cluj-Napoca, Romania
Alper Uysal	Yildiz Technical University, Turkey
Leonilde Rocha Varela	University of Minho, Portugal

George-Christopher Vosniakos	National Technical University of Athens, Greece
Jerzy Winczek	Czestochowa University of Technology, Poland
Szymon Wojcechowski	Poznan University of Technology, Poland
Oleg Zabolotnyi	Lutsk National Technical University, Ukraine
Jozef Zajac	Technical University of Kosice, Slovak Republic
Volodymyr Zavalov	National University of Food Technologies, Ukraine
Przemyslaw Zawadzki	Poznan University of Technology, Poland
Jan Zdebor	University of West Bohemia, Czech Republic
Lianyu Zheng	Beihang University, China
Predrag Zivkovic	University of Nis, Serbia

Invited External Reviewers

Frantisek Botko	Technical University of Kosice, Slovak Republic
Vladimir Bulej	University of Zilina, Slovak Republic
Alina Crisan	University of Agricultural Sciences and Veterinary Medicine, Romania
Liviu Adrian Crisan	Technical University of Cluj-Napoca, Romania
Maryna Demianenko	Sumy State University, Ukraine
Jan Gorecki	Poznan University of Technology, Poland
Damian Grajewski	Poznan University of Technology, Poland
Jakub Hajkowski	Poznan University of Technology, Poland
Nadiia Kharchenko	Sumy State University, Ukraine
Serhii Khovanskyi	Sumy State University, Ukraine
Vladyslav Kondus	Sumy State University, Ukraine
Dmytro Konovalov	Admiral Makarov National University of Shipbuilding, Ukraine
Ivan Kozii	Sumy State University, Ukraine
Dmytro Kryvoruchko	Sumy State University, Ukraine
Agnieszka Kujawska	Poznan University of Technology, Poland
Stanislaw Legutko	Poznan University of Technology, Poland
Dmytro Levchenko	Innovative Solutions LLC, Ukraine
Svitlana Lugova	JSC Nasosenergomash Sumy, Ukraine
Janosch Luttmmer	University of Duisburg-Essen, Germany
Oleh Lychak	Karpenko Physico-Mechanical Institute of the National Academy of Sciences of Ukraine, Ukraine
Dariusz Mazurkiewicz	Lublin University of Technology, Poland
Jakub Michalski	Poznan University of Technology, Poland
Iurii Merzliakov	Sumy State University, Ukraine
Panagiotis Karmiris	National Technical University of Athens, Greece
Obratanski	
Emmanouil Papazoglou	National Technical University of Athens, Greece

Robin Pluhnau	University of Duisburg-Essen, Germany
Mykola Radchenko	Admiral Makarov National University of Shipbuilding, Ukraine
Michal Sajgalik	University of Zilina, Slovak Republic
Serhii Sharapov	Sumy State University, Ukraine
Dimitrios Skondras-Giousios	National Technical University of Athens, Greece
Maksym Skydanenko	Sumy State University, Ukraine
Viktoriia Vakal	Sumy State University, Ukraine
Radoslaw Wichniarek	Poznan University of Technology, Poland
Dmytro Zhyhlyii	Sumy State University, Ukraine

DSMIE Team

Kristina Berladir	Sumy State University, Ukraine
Oleksandr Gusak	Sumy State University, Ukraine
Ihor Hrytsai	Lviv Polytechnic National University, Ukraine
Vitalii Ivanov	Sumy State University, Ukraine
Yaroslav Kusyi	Lviv Polytechnic National University, Ukraine
Oleksandr Liaposhchenko	Sumy State University, Ukraine
Ivan Pavlenko	Sumy State University, Ukraine
Andrii Slipchuk	Lviv Polytechnic National University, Ukraine
Vadym Stupnytskyi	Lviv Polytechnic National University, Ukraine

Contents

Product Design and Manufacturing Processes

Ensuring the Technological Parameters of Cast Block Crankcase of Automobile's Diesel Engine	3
Oleg Akimov, Kateryna Kostyk, Stepan Klymenko, Pavel Penzev, and Leonid Saltykov	
The Contact Pressure in Drawing Parts Without Clamping the Workpiece Flange	12
Roman Arhat, Ruslan Puzyr, Viktor Shchetynin, Viacheslav Puzyr, and Tetiana Haikova	
Complex Recognition Approach for Cutting Part of Cutters in Finishing Turning	21
Oleksandr Derevianchenko and Oleksandr Fomin	
Fractal Analysis of Structural and Phase Changes in the Metal of Welded Steam Pipe Joints	31
Yaroslav Garashchenko, Alyona Glushko, Olena Kobets, and Olena Harashchenko	
Research of the Spindle Units for Multioperational Lathes in the APM WinMachine Environment	41
Oleg Krol and Volodymyr Sokolov	
Technological Inheritability of Product Material Using the Criterion of Technological Damageability	52
Yaroslav Kusyi	
Wear Characteristics of Carbon and Tool Steels Hardened by Combined Laser-Ultrasonic Surface Treatment	62
Dmytro Lesyk, Silvia Martinez, Bohdan Mordyuk, Vitaliy Dzhemelinskyi, and Aitzol Lamikiz	

Rational Design Solution Based on Mathematical Modeling of an Interference Fit	73
Vladimir Nechiporenko, Valentin Salo, Petro Litovchenko, Valeriya Rakivnenko, and Andriy Horbunov	
Design and Engineering Assurance for the Customized Implants Production Using Additive Technologies	81
Vitalii Pasichnyk, Maksym Kryvenko, Svitlana Burburska, and Oleksandr Haluzynskyi	
The Dynamic Model of the Automatic Clamping Mechanism with a Rotating Input Link	95
Borys Prydalnyi	
The Optimal Conditions for Adding Strain to the Deformation Zone During the Expansion of Automobile Pipe Adapters	104
Ruslan Puzyr, Eduard Klimov, Andrii Chernish, Serhii Chernenko, and Yuliia Sira	
Diamond Spark Grinding of Hard Alloys Using Solid Lubricants	114
Aleksandr Rudnev, Yuriy Gutsalenko, Elena Sevidova, Larisa Pupan, and Oksana Titarenko	
Technological Parameters of Hole Shaping in the Cones Rolling-Cutter Row of Roller Cone Bits	123
Andrii Slipchuk and Roman Jakym	
Design Calculation of Automatic Rotary Motion Electrohydraulic Drive for Technological Equipment	133
Volodymyr Sokolov, Olga Porkuian, Oleg Krol, and Oksana Stepanova	
Optimization of the Interelectrode Gap in Electrical Discharge Grinding with Changing Electrode Polarity	143
Roman Strelchuk and Oleksandr Shelkovyi	
Determination of Radial Displacement Coefficient for Designing of Thread Joint of Thin-Walled Shells	153
Tetiana Tutko, Olha Dubei, Liubomyr Ropyak, and Vasyl Vytvytskyi	
Solutions for Industry 4.0	
Investments in Blockchain Information Management Systems Based on Business Angels' Criteria	165
Andrei Davydovitch, Tatjana Vasiljeva, Julija Novinkina, and Bohdan Haidabrus	
Agile Project Management Based on Data Analysis for Information Management Systems	174
Bohdan Haidabrus, Janis Grabis, and Serhiy Protsenko	

Optimization Work with a Digital Human Model	183
Pavel Kábele and Milan Edl	
The Implementation of Industry 4.0 Supported by Service Robots in Production Processes	193
Isak Karabegović, Edina Karabegović, Mehmed Mahmić, Ermin Husak, and Predrag Dašić	
Intelligent Numerical Control of Profile Grinding	203
Vasily Larshin, Natalia Lishchenko, Oleksandr Lysyi, and Sergey Uminsky	
Choice of Carrier Behavior Strategy According to Industry 4.0	213
Dmitriy Muzylyov, Natalya Shramenko, and Mykola Karnaukh	
Autonomous Data-Driven Integration into ERP Systems	223
Janis Peksa	
Three Dimensional Technology Radar Model to Evaluate Emerging Industry 4.0 Technologies	233
Erwin Rauch and Eugenio Vinante	
Applicability of Traditional Project Closeout Approaches in Agile Developed IT Projects	243
Philipp Rosenberger and Jozsef Tick	
Reliability of Road Transport Means as a Factor Affecting the Risk of Failure – The Transport Problem Case Study	253
Piotr Trojanowski and Justyna Trojanowska	
An Intelligent Scheduling System Architecture for Manufacturing Systems Based on I4.0 Requirements	262
Leonilde Varela, Vaibhav Shah, Aurélio Lucamba, Adriana Araújo, and José Machado	
A New Approach for the Evaluation of Internal Logistics Processes and Their Readiness for the Industry 4.0 Concept	275
Michal Zoubek, Michaela Koubovská, and Michal Šimon	
ICT for Engineering Education	
Mobile Application for Test Control of Knowledge Among Mechanical Engineering Students	289
Alexander Alexeyev, Tetiana Malandii, and Alina Moshna	
Institutional Aspects of Integrated Quality Assurance of Engineering Study Programs at HEI Using ICT	301
Vitaliy Kobets, Vira Liubchenko, Ihor Popovych, and Svitlana Koval	

An Android Application for Explaining Form Deviations Using 3D Models	311
Grigore Marian Pop, Radu Comes, and Liviu Adrian Crisan	
In-campus Way of the Insight Transfer Technology	322
Lesya Shkitsa, Volodymyr Kornuta, Olena Kornuta, Vasyl Bui, and Iryna Bekish	
Information and Communication Technology Tools for Enhancing Engineering Students' Creativity	332
Olena Titova, Petro Luzan, Natalia Sosnytska, Serhii Kulieshov, and Olena Suprun	
Numerical Simulation and Experimental Studies	
Development of Optimum Thin-Walled Parts Milling Parameters Calculation Technique	343
Sergey Dobrotvorskiy, Serhii Kononenko, Yevheniia Basova, Ludmila Dobrovolska, and Milan Edl	
Measurement of Contact Pressure for Conical Honing	353
Eshreb Dzhemilov and Ruslan Dzhemalyadinov	
Simulation Methodology of Diamond Burnishing	363
Vladimir Fedorovich, Ivan Pyzhov, Janos Kundra, Larisa Pupan, and Irina Voloshkina	
Optimal Milling Conditions for Complex Shaped Thin-Walled Components	373
Anton Germashev, Yuri Vnukov, Mark Kuchuhurov, Viktor Logominov, and Bert Lauwers	
Study of Dynamic and Power Parameters of the Screw Workpieces with a Curved Profile Turning	385
Ivan Hevko, Andrii Diachun, Oleg Lyashuk, Yuriy Vovk, and Andriy Hupka	
Effect of Abrasive Finishing on the Electrical Parameters of S-B and Rectangular Waveguides	395
Natalia Honchar, Pavlo Tryshyn, Dmytro Stepanov, and Olena Khavkina	
Prediction the Durability of Hobs Based on Contact and Friction Analysis on the Faces for Cutting Teeth and Edges During Hobbing	405
Ihor Hrytsay and Vadym Stupnytsky	
Modelling of the Effect of Slide Burnishing on the Surface Roughness of 42CrMo4 Steel Shafts	415
Rafał Kluz, Tomasz Trzepieciniski, Magdalena Bucior, and Katarzyna Antosz	

Analytical Modelling of Crack Formation Potential in Thermomechanical Processing of Materials 425
 Maksym Kunitsyn, Anatoly Usov, and Yulia Sikirash

The Influence of Grinding Modes on the Quality of the Surface Layer 434
 Maksym Kurin, Serhii Nyshnyk, and Anatolii Dolmatov

Improvement of the Gear Shaping Effectiveness for Bimetal Gears of Internal Gearing with a Friction Coating 444
 Mykola Korotun, Yuliia Denysenko, Olaf Ciszak, and Oleksandr Ivchenko

Penetration Depth of the Critical Temperature into the Workpiece Material During Grinding 453
 Vladimir Lebedev, Tatiana Chumachenko, Nataliya Klymenko, Olga Frolenkova, and Serhii Yevtifieiev

Justification of Technological Possibilities for Reducing Surface Roughness During Abrasive Processing 463
 Fedir Novikov, Dmytro Novikov, Andrii Hutorov, Yevhen Ponomarenko, and Oleksii Yermolenko

Geometric Modeling of Lathe Cutters for Turning High-Precision Stainless Steel Tapered Threads 472
 Oleh Onysko, Iulia Medvid, Vitalii Panchuk, Vesna Rodic, and Cristian Barz

Interaction of Flexural and Torsional Shapes Vibrations in Fine Boring with Cantilever Boring Bars 481
 Alexandr Orgiyan, Gennadiy Oborskyi, Vitalii Ivanov, Anna Balaniuk, and Ruslan Matzey

Heat Flows Affected on the Wheelhead of a Cylindrical Grinding Machine 490
 Mykhaylo Stepanov, Petro Litovchenko, Larysa Ivanova, Maryna Ivanova, and Magomediemmin Gasanov

Simulation Research of Machining-Induced Surface Layer Operational Characteristics 501
 Vadym Stupnytskyy, Ihor Hrytsay, and She Xianning

An Experimental and Statistical Investigation on Cutting Forces in Turning of AISI 304 Stainless Steel Under Dry, MQL and Nanofluid MQL Conditions 513
 Youssef Touggui, Alper Uysal, Uğur Emiroglu, and Eshreb Dzhemilov

Advanced Materials

Strengthening of the NKV Type Centrifugal Pump's Shaft by Chemical-Thermocycling Treatment	525
Kristina Berladir, Tetiana Hovorun, and Oleksandr Gusak	
The Influence of Synthesis Modes on Operational Properties of Oxide Ceramic Coatings on Aluminum Alloys	536
Nataliya Imbirovych, Oleksandr Povstyanoy, Olha Zaleta, Sergey Shymchuk, and Olga Priadko	
Optimal Design of Composite Shelled Sandwich Structures with a Honeycomb Filler	546
Andrii Kondratiev, Olexander Potapov, Anton Tsaritsynskyi, and Tetyana Nabokina	
Preparation and Characterization of a Biocomposite Based on Casein and Cellulose	556
Mykola Melnychuk, Victoria Malets, Marcin Sosnowski, Ivanna Mykhaylyuk, and Inna Boyarska	
Advanced Technologies of Manufacturing Readily Removable Cores for Obtaining High-Quality Castings	565
Olga Ponomarenko, Igor Grimzin, Nataliia Yevtushenko, Tatiana Lysenko, and Dmytro Marynenko	
The Use of Ion Bombardment Modeling as a Component of the Structural Engineering of Nanoperiodic Composite Structures	575
Oleg Sobol, Nataliia Pinchuk, Andriy Meilekhov, and Mariia Zhadko	
Powder Technology and Software Tools for Microstructure Control of AlCu₂ Samples	585
Oleg Zabolotnyi, Viktoriya Pasternak, Nataliia Ilchuk, Nataliia Huliieva, and Dagmar Cagánová	
Rational Choice of a Material for Orthopedic Insoles Based on the Mechanical Characteristics and Practical Application Purposes	594
Ruslan Zaloha, Kostiantyn Dyadyura, Viliam Zaloga, and Michal Hatala	
Structure and Properties of Surface Bandage Shelves for the Gas Turbine Engine's Blades	602
Natalia Zaichuk, Sergii Shymchuk, Anatolii Tkachuk, Yurii Feshchuk, and Jacek Szczot	
Author Index	613

Product Design and Manufacturing Processes



Ensuring the Technological Parameters of Cast Block Crankcase of Automobile's Diesel Engine

Oleg Akimov¹ , Kateryna Kostyk¹  ^(✉), Stepan Klymenko² , Pavel Penzev¹ ,
and Leonid Saltykov¹ 

¹ National Technical University “Kharkiv Polytechnic Institute”, 2,
Kyrpychova Street, Kharkiv 61002, Ukraine

² Physico-Technological Institute of Metals and Alloys of the National
Academy of Sciences of Ukraine, 34/1, Vernadskogo Blvd., Kyiv 03142, Ukraine

Abstract. The relevance of computer-integrated technologies for manufacturing parts is significant in the world. The purpose of this work is to analyze the quality of cast block crankcase using a universal technology of complex computer-integrated design of cast parts of internal combustion engines using engineering modeling of thermal and hydrodynamic parameters of casting. The results of computer-engineering modeling of thermal and hydrodynamic processes of block crankcase casting have shown that gas-shrinkage defects can be stress concentrators in the part's structural elements. Therefore, they can affect the strength characteristics during operation. The developed 3D model of block crankcase casting with a technological gating-feeding system allowed creating a finite-difference model of casting and tooling and performing engineering modeling of casting processes in the ICS NovaFlow. The analysis of physical features of the processes of filling and cooling the castings in the mold was performed for the cast block crankcase of 4DTNA1 automobile diesel, the locations and sizes of gas-shrinkable defects were determined according to the Niyama criterion. The research results allowed us to form boundary and initial conditions for modeling the stress-strain state of the block crankcase in the places of gas-shrink porosity formation. Further development of the above studies will be carried out for castings of new types, configurations, other casting technologies, newly synthesized alloys.

Keywords: Solidworks · Novaflo · Block crankcase · Engines · 3D model · Casting defects

1 Introduction

Modern computer-aided design of cast engine parts is a powerful tool for developing new parts and upgrading existing ones. Current systems for computer-engineering modeling of production processes and analysis of the thermal and stress-strain state of cast parts of internal combustion engines are the most effective in design and technological design.

Processes computer-aided design, technological preparation, and production of cast engine parts are an integral part of a systematic approach inherent in the CALS-technologies, i.e., a set of the corresponding time sequence of state changes of the part.

In current conditions, the main requirements for manufactured products are high quality, low cost, and minimum development time for new products, which can be achieved using computer modeling [1] and parameter identification [2] in technological design.

Most of the cast parts for transport and particular purpose types of diesel are made by casting method, which should be based on manufacturing's technological aspects, namely various casting defects [3]. These defects occur due to the lack of methods and tools to influence the technological modes of production. The design documentation and technical specifications usually specify the size and number of various casting defects that are not allowed in part, which means that such defects affect its quality and reliability.

The diesel's central part under consideration is a block-case, the quality of which will depend on the required characteristics laid down at the design stage. According to the technical conditions, requirements for the quality and reliability of cast parts of internal combustion engines are laid and fulfilled at the production stage using methods for determining technological defects [4].

Obtaining a high-quality block crankcase at the casting stage consists of two main processes: pouring molten metal into the mold and forming the cast part during the phase transition during cooling and crystallization.

2 Literature Review

The relevance of computer-integrated technologies for manufacturing parts occupies an essential place in the world. For many years, computer systems (CAE, CAD, and CAM) have been used to increase production productivity [5].

The most crucial advantage of computer-integrated technologies is that they emphasize the advanced capabilities of engineering analysis. For example, based on the finite element method [6]. The most striking feature of CAD/CAM systems is the so-called solid-state creation (modeling) of the product exclusively on the computer screen, viewing on the screen (visualization) of the process of processing parts and transmitting the generated data over computer networks to the CNC equipment [7].

Computer modeling becomes an integral part of designing new parts and designing technological processes for their manufacture. It acquires the status of an essential and often decisive competitive advantage. Increasingly, customers for foundry products in the list of requirements for the manufacturer of these products put forward a need for the mandatory use of computer modeling.

In a market economy, improving product quality and reducing metal and energy consumption is an urgent task. Consequently, the latest technologies are introduced in the production using computer modeling programs, which improves the quality of products without special costs for energy, metal, etc.

The advantages of automated modeling systems for foundry processes are described in many works [8, 9]. The main advantage is the ability to work out the nuances of casting technology on a virtual prototype of the cast, which reduces or eliminates the need for the production of test castings, reduces the process of designing the technology, and reduces the cost of casting [10]. The research work [11] shows that the visualization of physical processes foundry technology, such as the filling melt the mold cavity, cooling and solidification of metal warping under the action of thermal stress allows a better

understanding of these processes, and therefore better manage them for reducing scrap in molding and increase yield.

Full-scale CAD/CAM/CAE systems are complex multifunctional systems that include a large set of modules (from 40 to 50) for various functional purposes [12].

In practice, various specialized and universal CAD/CAE/CAM systems of various versions and configurations are in operation in most enterprises. Very often, different strategies are used in divisions of the same organization. Sometimes this is even the case at the level of individual developers.

In the application of design of cast parts of modern systems (CAD/CAM/CAE/PDM and CIM), it is possible to provide [13]:

- Reduce production time and increase competitive products and output. Due to programs that provide speed for creating 3D models, regardless of the time spent on producing drawings on paper [14, 15];
- They can also provide significant cost savings. By using a software package that reduces the number of ongoing changes that accompany any design process, as well as errors [16];
- Improving the vibration reliability [17] and quality of manufacture. With the help of effective analysis of the created products, it can be tracked related defects in some software packages [18];
- It will allow you to design and produce better models [19] continuously;
- Maximum error elimination. Due to the visualization of the designed product, which allow us to eliminate typical errors in production promptly [20];
- Introduction of newer and more modern methods that allow us to develop productive strategies of 3D model design, as well as their visualization, consideration of fill processes, as well as possible defects [21];
- Avoiding large-scale layout products will reduce the time to create a specific part [22].

Modern design in foundry production includes developing a 3D model of a part, casting system, and equipment. The processes that occur must be consistent with practical methods that allow getting high-quality parts with higher performance characteristics [23].

The purpose of this work is to analyze the quality of cast block crankcase using a universal technology of complex computer- integrated design of cast parts of internal combustion engines using engineering modeling of thermal and hydrodynamic parameters of casting. Computer modeling of casting processes occurring in the manufacture of a cast part of the block crankcase is performed to identify the places of formation of defects, determine their location and estimated size, as well as for subsequent analysis of the phase transition process when cooling the casting of the block crankcase in the form.

3 Research Methodology

For achieving this objective, the following sequence of stages was proposed, according to the method of computer modeling of thermal and hydrodynamic casting processes:

- determination of the initial conditions;
- development of a 3D casting model based on a 4DTNA1 diesel block crankcase with a technological gating-feeding system;
- computer-integrated modeling of foundry processes for the production of cast block crankcase;
- analysis of the results of computer simulation;
- study of the nature of filling the mold with metal and the location of casting defects.

A cast 4DTNA1 diesel crankcase was selected as the studied part for computer-integrated modeling (Fig. 1).

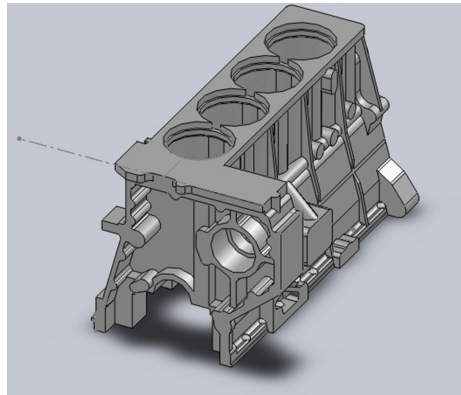


Fig. 1. Cast block crankcase of 4DTNA1 diesel.

A 3D model of block crankcase casting with a technological gating-feeding system was created in the ICS SolidWorks (Fig. 2). The gating-feeding system created is a “tapering type” system that ensures by its design the correct and gradual filling of the form with metal to avoid the ingress of slag inclusions into its cavity.

The boundary conditions and initial data for modeling according to the following sequence were set:

- 3D import (converting a file to *.stl format) and creating a finite-difference model;
- the purpose of the material for casting and tooling, as well as the separation coating, applied to the surface of the tooling;
- setting the initial temperature of the melt and process equipment, and cooling with various heat carriers;
- setting the total production cycle time for a single casting.

Using the 3D import module built into the ICS NovaFlow, the block crankcase model with a gating-feeding system and the equal model were converted into a finite-volume model.

The optimal cell parameters are set based on the calculation time-adequacy of the results (Fig. 2). The cell size is 3.7 mm.



Fig. 2. Final-volume model of the casting in the chill with the displayed cells.

The assignment of boundary conditions for the material of casting elements and technological equipment is made by dividing into separate parts, each of which is given its color:

- block crankcase casting material is AlSi5Cu1Mg;
- materials of technological equipment are Steel 20, Grey Cast Iron 20;
- The chill forms are coated with chill paint with a thickness of 0.2 mm, which has a thermal conductivity of $\lambda = 0.3 \text{ W/m}^*\text{K}$.

To prevention moisture from entering the forming surface and a high-temperature difference when pouring, the process equipment was preheated to $T = 523 \div 553 \text{ K}$.

The melt temperature before pouring into the mold was 983 K.

4 Results

The obtained results of computer-engineering modeling are presented graphically in filling the mold with a melt, the direction of crystallization during cooling (transition from the liquid to the solid phase), and displaying the location of gas-shrinkable defects.

The filling in the form plays an essential role in creating favorable conditions for directed crystallization. The velocity of the melt movement when filling the mold in separate parts did not exceed the critical values of $V_{kr} > 0.8 \text{ m/s}$, with a smooth filling of the mold, without splashes, and with small vortices according to the requirements [17] (Fig. 3).

The results of computer simulation analysis showed that the movement of the melt in the mold could be considered as satisfying the following requirements:

- passing through the elements of the gating system, the melt does not acquire a turbulent character of movement;

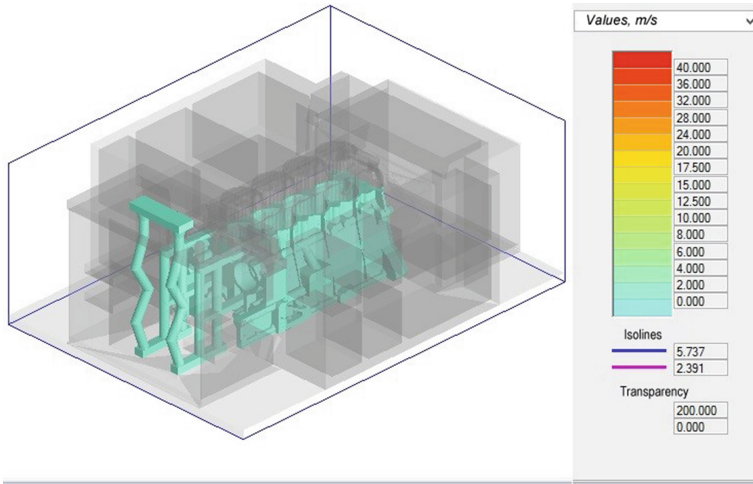


Fig. 3. General view of filling the form with melt.

- the mold is filled in without exceeding critical speeds.

The analysis of the results of computer-integrated simulation of the cooling process of the part in the technological mold (chill) was carried out under the parameters:

- the transition from the liquid to the solid phase during cooling of the part in the form (Fig. 4);
- gas-shrinkage defects expressed by the Niyama criterion [24] (Fig. 5).

Analysis of the dynamics of cooling of the casting, the phase transition, the connectivity of the zones that crystallize last allowed to determine the places of the possible occurrence of gas-shrinkable defects.

The conclusion is based on the analysis of the location of defects expressed in the ICS NovaFlow by the Niyama criterion.

The criterion for determining the location of gas-shrinkable defects and their magnitude is Niyama, which we use to predict microporosity and gas-shrink porosity large enough to be detected by radiographic testing. This criterion is a reliable predictor of porosity for simple castings. Still, in the case of castings with complex geometries, its use requires a more thorough analysis of the simulation results since many factors affect the formation of gas-shrink porosity.

Analysis of the locations of defects showed that the most prone to shrinkage places are:

- edge cavities of the cylinders;
- the upper plane in the front part of the block, in the places of attachment under the head;
- arrays of bosses on the sides of the block.
- Modeled defects allow us to forecast that the cast product may be defective by 5–6%.

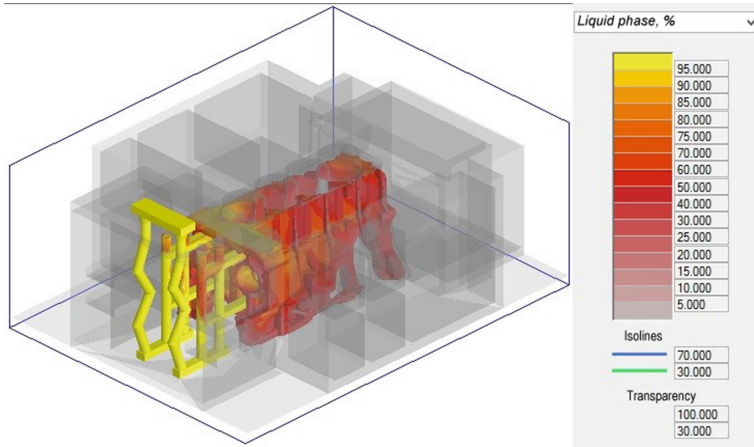


Fig. 4. The transition from the liquid to the solid phase during the cooling of the part in the chill.

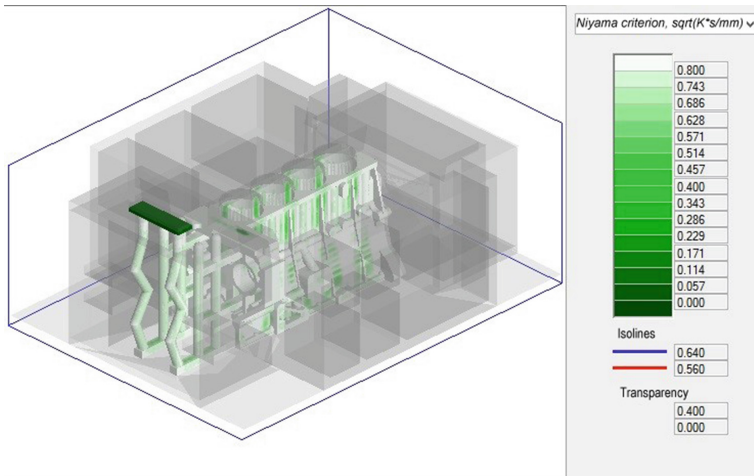


Fig. 5. Locations of gas shrinkage defects according to the Niyama criterion.

From the results of computer-engineering modeling of thermal and hydrodynamic processes of block crankcase casting, it follows that gas-shrinkage defects can be stress concentrators in the part's structural elements. Therefore, it can affect the strength characteristics during operation.

5 Conclusions

The developed 3D model of block crankcase casting with a technological gating-feeding system allowed creating a finite-difference model of casting and tooling and performing engineering modeling of casting processes in the ICS NovaFlow. The analysis of physical

features of the processes of filling and cooling the castings in the form was performed for the cast block crankcase of 4DTNA1 automobile diesel, the locations and sizes of gas-shrinkable defects were determined according to the Niyama criterion.

The research results allowed us to form boundary and initial conditions for modeling the stress-strain state of the block crankcase in the places where gas-shrink porosity is formed.

Further development of the above studies will be carried out for castings of new types, configurations, other casting technologies, newly synthesized alloys.

References

1. Mehrabi, M.G., Ulsoy, A.G., Koren, Y.: Reconfigurable manufacturing systems: key to future manufacturing. *J. Intell. Manuf.* **11**, 403–419 (2000). <https://doi.org/10.1023/A:1008930403506>
2. Pavlenko, I., Trojanowska, J., Ivanov, V., Liaposhchenko, O.: Parameter identification of hydro-mechanical processes using artificial intelligence systems. *Int. J. Mechatron. Appl. Mech.* **2019**(5), 19–26 (2019)
3. Prasad, R.: Progress in investment castings. In: *Science and Technology of Casting Processes*. IntechOpen (2012)
4. Thomas, D.S., Gilbert, S.W.: Costs and cost effectiveness of additive manufacturing. *NIST Spec. Publ.* **1176**, 12 (2012). <https://doi.org/10.6028/NIST.SP.1176>
5. Milchev, G., Miltchev, R.: Development of information technologies, planned obsolescence and modification of the life-cycle of the CAD/CAM/CAE systems. *Eur. J. Sustain. Dev.* **7**(3), 217 (2018). <https://doi.org/10.14207/ejsd.2018.v7n3p217>
6. Rao, S.S.: *The Finite Element Method in Engineering*. Butterworth-Heinemann (2017)
7. Sang, Z., Xu, X.: The framework of a cloud-based CNC system. *Procedia CIRP* **63**, 82–88 (2017). <https://doi.org/10.1016/j.procir.2017.03.152>
8. Kumar, V., Madan, J.: A system for computer-aided gating design for multi-cavity die-casting dies. *Proc. Inst. Mech. Eng. Part B: J. Eng. Manuf.* **231**(11), 1983–1999 (2017). <https://doi.org/10.1177/0954405415614727>
9. Khan, M.A.A., Sheikh, A.K.: A comparative study of simulation software for modelling metal casting processes. *Int. J. Simul. Model.* **17**(2), 197–209 (2018). [https://doi.org/10.2507/IJSIMM17\(2\)402](https://doi.org/10.2507/IJSIMM17(2)402)
10. Kozłowski, J., Sika, R., Górski, F., Ciszak, O.: Modeling of foundry processes in the era of Industry 4.0. In: Ivanov, V., et al. (eds.) *DSMIE. LNME*, pp. 62–71. Springer, Cham (2019). https://doi.org/10.1007/978-3-319-93587-4_7
11. Bianchi, M.F., Gameros, A.A., Axinte, D.A., Lowth, S., Cendrowicz, A.M., Welch, S.T.: On the effect of mould temperature on the orientation and packing of particles in ceramic injection moulding. *J. Eur. Ceram. Soc.* **39**(10), 3194–3207 (2019). <https://doi.org/10.1016/j.jeurceramsoc.2019.03.049>
12. Ng, C.B.R.: *A concurrent design facility architecture for education and research in multi-disciplinary design of complex systems* (2019)
13. Wang, X., Bi, Z.: New CAD/CAM course framework in digital manufacturing. *Comput. Appl. Eng. Educ.* **27**(1), 128–144 (2019). <https://doi.org/10.1002/cae.22063>
14. Akimov, O., Soloshenko, V., Kostyk, K.: Computer-integrated design of cast parts on the criterion of performance on the example of the turbine wheel turbocharger. In: *CEUR Workshop Proceedings*, vol. 2353, pp. 324–338 (2019)

15. Akimov, O.V., et al.: Computer engineering and design of cast parts for internal combustion engine crankcase. *J. Eng. Sci.* **6**(2), E24–E30 (2019). [https://doi.org/10.21272/jes.2019.6\(2\).e4](https://doi.org/10.21272/jes.2019.6(2).e4)
16. Dhahad, H.A., Alawee, W.H., Marchenko, A., Klets, D., Akimov, O.: Evaluation of power indicators of the automobile engine. *Int. J. Eng. Technol.* **7**(4.3), 130–134 (2018)
17. Pavlenko, I., Ivanov, V., Kuric, I., Gusak, O., Liaposhchenko, O.: Ensuring vibration reliability of turbopump units using artificial neural networks. In: Trojanowska, J., Ciszak, O., Machado, J.M., Pavlenko, I. (eds.) *MANUFACTURING 2019. LNME*, pp. 165–175. Springer, Cham (2019). https://doi.org/10.1007/978-3-030-18715-6_14
18. Boboulos, M.A.: *CAD-CAM & Rapid Prototyping Application Evaluation*. Bookboon (2010)
19. Kumar, S.L.X.: State of the art-intense review on artificial intelligence systems application in process planning and manufacturing. *Eng. Appl. Artif. Intell.* **65**, 294–329 (2017). <https://doi.org/10.1016/j.engappai.2017.08.005>
20. Laurel, B.: *Design Research: Methods and Perspectives*. MIT Press (2003)
21. Otto, K.N.: *Product design: techniques in reverse engineering and new product development* (2003)
22. Khan, M., Khan, S.S.: Data and information visualization methods, and interactive mechanisms: a survey. *Int. J. Comput. Appl.* **34**(1), 1–14 (2011)
23. Parsons, J.L., Campbell, J.R.: Digital apparel design process: placing a new technology into a framework for the creative design process. *Cloth. Text. Res. J.* **22**(1–2), 88–98 (2004). <https://doi.org/10.1177/0887302X0402200111>
24. Ignaszak, Z.: Discussion on usability of the niyama criterion for porosity predicting in cast iron castings. *Arch. Foundry Eng.* **17**(3), 196–204 (2017). <https://doi.org/10.1515/afe-2017-0115>



The Contact Pressure in Drawing Parts Without Clamping the Workpiece Flange

Roman Arhat¹(✉) , Ruslan Puzyr² , Viktor Shchetynin¹ , Viacheslav Puzyr¹ ,
and Tetiana Haikova¹

¹ Kremenchuk Mykhailo Ostrohradskiy National University, 20, Pershotravneva Street,
Kremenchuk 39600, Ukraine

² Kremenchuk Mykhailo Ostrohradskiy National University College, 7, Chumatskyi Shliakh
Street, Kremenchuk 39621, Ukraine

Abstract. In the paper, dependence has been obtained to calculate the contact pressures when drawing down the axisymmetric workpiece without a blank flange collet. The solution is based on the assumptions of the momentless theory of shells. The adequacy of the mathematical model is confirmed by experimental data for a narrow interval of forging blanks. The experiments have been carried out on a specially designed tooling to measure load cell deformation using a strain gauge. All the equipment used has passed metrological control. To calculate the meridional and tangential stresses on the torus-shaped portion of the matrix, dependencies were obtained that contain a term connecting the thickness of the workpiece with the value of the stresses arising during drawing, which more accurately describes their distribution on the drawing edge of the matrix. The expression for calculating the surface contact pressure during the drawing of a cylindrical part makes it possible to consider the friction stresses at the radius of the matrix rounding and calculate the drawing force. The obtained dependence differs from the conventional ones in its simplicity and clarity and can be used at the preliminary stage of choosing equipment for stamping. It is shown that the friction stresses between the contacting surfaces can be controlled over a wide range while achieving a significant change in the stress state and the distribution of deformations in the volume of the workpiece.

Keywords: Metal drawing · Plastic deformation · Die body radius · Drawing punch · Contact pressure

1 Introduction

Drawing of axisymmetric parts is characterized not only by the loss of flange part stability but also by the deformation localization in the zone of the transition of the wall to the bottom and the destruction of the workpiece given location [1, 2]. The destruction and localization of deformations can be eliminated by reducing the tensile stress value. When drawing down with a collet, this problem is solved by reducing the collet force, using highly effective lubricants, and also polishing the die body contact surfaces and the blank holder [3–5].

2 Literature Review

The drawing down without workpiece flange pressing is limited by the formation of workpiece uncompressed part. The bottom separation can occur if the process of workpiece retraction into the die body hole continues, ignoring the folds on the flange. As shown in the papers [6, 7], it is possible to extend the interval of non-collet forging by increasing the resistance of the flange, loss of stability, or increasing tensile stresses in the initial stage of deformation. The blank flange practically does not contact the surface of the die body, since when the punch is lowered, the flange portion rises above the die body and forms a conical surface with an angle α at the apex [8–11]. Therefore, the contact of the workpiece with the die body occurs along its toroidal surface with a certain rounded radius. The stresses in the drawn metal, the force, the drawing coefficient, and the corrugation and destruction of the blank depending on the radius of curvature of the drawing edge of the matrix [6, 12]. Therefore, it is chosen very carefully in each specifically selected technological process [3, 13]. The existing analytical dependences for calculating stresses at the radius of curvature do not fully consider all the minute details and technological factors of the drawing process, and their accuracy is not satisfactory [14, 15]. The presence of refined formal dependencies describing the distribution of stresses on the drawing edge of the matrix, taking into account friction, bending moments, contact pressure, blank thickness, and others, will make it possible to expand the range of drawn products without pressing the flange and reduce rejects to a minimum. Therefore, it is of great scientific interest to theoretically determine the contact stresses on the torus-shaped section of the matrix and the factors that make it possible to control the value of these stresses to find conditions for expanding the possibilities of drawing without a folding holder. This will enable finding more accurate theoretical dependences for calculating and analyzing the stress field when drawing cylindrical parts.

3 Research Methodology

To determine the contact stresses, we start from the equilibrium equations for the torus [6, 16], but taking into account the surface load

$$\left. \begin{aligned} \frac{\partial R_2 N_1}{\partial \phi} + \frac{\partial((R_1 \sin \theta)T)}{\partial \theta} - N_2 \frac{\partial R_2}{\partial \phi} + T \frac{\partial R_1 \sin \theta}{\partial \theta} &= 0, \\ \frac{\partial((R_1 \sin \theta)N_2)}{\partial \theta} + R_2 \frac{\partial T}{\partial \phi} - N_1 \frac{\partial(R_1 \sin \theta)}{\partial \theta} + T \frac{\partial R_2}{\partial \phi} &= 0, \\ \frac{N_1}{R_1} + \frac{N_2}{R_2} &= q. \end{aligned} \right\} \quad (1)$$

where N_1, N_2, T – are internal meridional, tangential, and shear stresses;
 q – is the contact pressure.

We take into account the fact that the deformation is axisymmetric, and therefore the terms of the system (1) containing $\partial \phi$, as well as the shearing force T , and that $R_1 = \frac{R}{\sin \theta} = \frac{a(1+k \sin \theta)}{k \sin \theta}$, $R_2 = a$, $k = \frac{a}{R}$, then we will have [5, 17]:

$$\left. \begin{aligned} N_2 a \cos \theta + \frac{\partial N_2}{\partial \theta} \frac{a}{k} (1 + k \sin \theta) - N_1 a \cos \theta &= 0, \\ \frac{N_1 \sin \theta}{R} + \frac{N_2}{a} &= q. \end{aligned} \right\} \quad (2)$$

Next, we calculate according to the procedure [8, 18, 19] with the only difference that the pressure on the workpiece when it slides along the edge of the die body is applied from within half a torus.

where R_d – is the radius of the drawing part;

r_m The radius of the die body input edge; $R = R_d + a \sin \theta$; $a = r_m$.

When the torus is affected by a surface load with loss of stability in the form of bulge formation, the expression for q has been obtained by the authors of [8, 20, 21] as $k \rightarrow 0$:

$$q = \frac{E}{12(1 - \mu^2)} \left(\frac{s}{a}\right)^3 (n^2 - 1), \quad (3)$$

where μ – is Poisson's ratio;

E – is Young's modulus;

n – is the number of emerging half-waves with loss of stability.

Regarding our drawing conditions, it should be slightly modified. For further calculation, we use the cylindrical rigidity of the shell corresponding to the secant modulus $D \approx D' = \frac{E_c s^3}{9}$, we sort out the value of n for which $(n^2 - 1) = 1$. Further, since $E_c = \frac{\sigma_i}{\varepsilon_i}$, we accept $\sigma_i = \sigma_{cp}$, and $\varepsilon_i = \frac{1}{2} \varepsilon_\theta$ [22, 23]. The draw ratio is $m = \frac{D}{D_0}$, hence $\varepsilon_\theta = 1 - m = 1 - \frac{D}{D_0}$, where D and D_0 are the diameter of the workpiece and the diameter of the blank, respectively. Then expression (6) will have the form:

$$q = \frac{2\sigma_s}{9\left(1 - \frac{D}{D_0}\right)} \left(\frac{s}{r_m}\right)^3. \quad (4)$$

We substitute this relation into the formulas for the internal forces and, passing to the stresses, we get:

$$\sigma_\rho = \frac{\sigma_s}{9\left(1 - \frac{D}{D_0}\right)} \left(\frac{s}{r_m}\right)^2, \quad (5)$$

$$\sigma_\theta = -\frac{1 + \frac{k}{2} \sin \theta}{1 + k \sin \theta} \frac{2\sigma_s}{9\left(1 - \frac{D}{D_0}\right)} \left(\frac{s}{r_m}\right)^2. \quad (6)$$

Formerly [6, 24], formulas were derived from calculating the magnitude of the stress tensor components on the torus-like part of the die body without considering the surface load. Using the principle of superposition [16, 25] and carrying out simple transformations, the final dependencies for calculation of meridional and tangential stresses on the rounded radius of the die body at $\theta = 90^\circ$ will look like:

$$\sigma_\rho = \sigma_s \left(\ln \frac{R_0}{R_d + r_m} - \frac{r_m}{R_d + r_m} + 0, 1 \frac{R_0}{R_0 - R_d} \left(\frac{s}{r_m}\right)^2 \right), \quad (7)$$

$$\sigma_\theta = -\sigma_s \left(1 - \ln \frac{R_0}{R_d + r_m} + \frac{r_m}{R_d + r_m} + 0, 22 \frac{1 + \frac{k}{2}}{1 + k} \frac{R_0}{R_0 - R_d} \left(\frac{s}{r_m}\right)^2 \right). \quad (8)$$

In contrast to correlations [6, 26], to calculate the meridional and tangential stresses on the torus-like part of the die body, the dependences (7) and (8) contain a term that relates the thickness of the blank to the value of the stresses arising while drawing, which describes their distribution on the drawing edge of the die body more accurately.

Below there are stress graphic dependences (Fig. 1) – the blank thickness for $R_0 = 50$ mm, $R_d = 25$ mm and matrix rounding radius $r_m = 10$ mm, created according to formulas (7), (8).

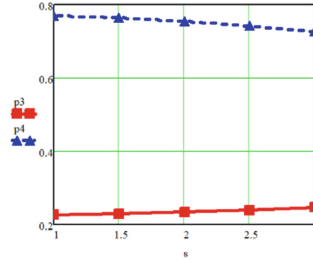


Fig. 1. Stress graphs (σ/σ_s) – the blank thickness (s), created according to dependences (7), (8).

Using the second system Eq. (2), as well as (10) and (8) and carrying out simple transformations, we find the surface pressure, which causes the plastic deformation of the blank during drawing without workpiece collet:

$$\frac{q}{s} = \sigma_s \left(\begin{aligned} & \left(\ln \frac{R_0}{R_d+r_m} - \frac{r_m}{R_d+r_m} \right) \frac{R_d}{(R_d+r_m)^2} \\ & + \frac{R_0}{R_0-R_d} \left(\frac{s}{r_m} \right)^2 \left(\frac{1}{9(R_d+r_m)} - \frac{2}{9r_m} \frac{1+\frac{k}{2}}{1+k} \right) - \frac{1}{r_m} \end{aligned} \right). \tag{9}$$

We analyze the terms of the expression for given deformation parameters – $R_0 = 50$ mm, $s = 2$ mm, $R_d = 25$ mm and $r_m = 10$ mm. The first and second terms are of the same order of smallness and can be neglected with an error up to the third decimal place. Then the surface load is the following:

$$q = -\frac{s}{r_m} \sigma_s. \tag{10}$$

To verify the obtained dependence by determining contact pressures, experiments have been carried out to measure the load cell deformations caused by frictional forces. Experimental and theoretical studies demonstrate [13, 18, 27, 28] that the frictional stresses between the surfaces to be contacted can be controlled within wide limits while achieving a significant change in the stress state and the distribution of deformations in the volume of blank, which is of great importance for the production of high-quality workpieces using drawing down.

Since the flange of the workpiece practically does not contact with the mirror of the die body while drawing down without the blank holder, and friction occurs mainly along the rounded radius of the latter, it is of great interest to determine the frictional stresses and to study their effect on the occurrence of the loss of flange stability.

The experiments were carried out on a tensile machine of UME-10TM type with a force of 10 tf [14, 24, 29].

The experimental equipment appeared to be a special die body with an inlet of 50 mm and a set of punches with diameters of 49.3 mm; 46.4 mm; 49 mm, providing the drawing of blanks without thinning the stiffening plate of 08kp steel with a thickness of 0.15 mm, of aluminum A2 with a thickness of 1.4 mm and copper M4 of 0.25 mm correspondently. The dying body was installed on the lower traverse of the tensile machine. The exchangeable punches were on the upper traverse. Both traverses were equipped with clamping elements.

Special equipment appeared to be a dying body, with an insert for the drawing radius, which can be displaced in the direction of movement of the punch during drawing and the punch of a conventional design (Fig. 2) [15, 30, 31].

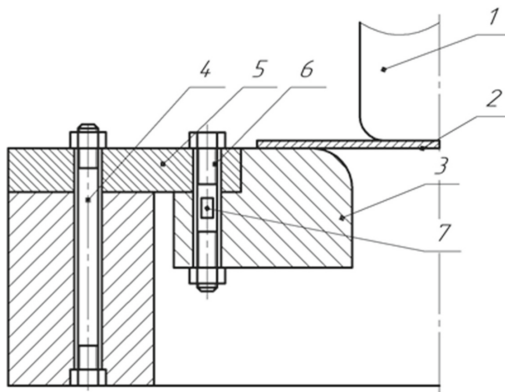


Fig. 2. Equipment for measuring frictional stresses at the rounded radius of the exhaust die body: 1 – punch; 2 – blank; 3 – movable insert; 4 – a fixing bolt; 5 – a connecting ring; 6 – load cell; 7 – strain gage.

The equipment for measuring the load cell deformations is a strain gauge operational amplifier MCP606-I/P, ADC E14–440, power supply unit AX-1803D and personal computer Pentium 4 CPU 2.40 GHz 1.0 GB RAM. Load cell deformations caused by frictional forces during drawing determined strain gages deformation, which is included in a quarter-bridge scheme without compensation of temperature stresses [32]. This, in turn, caused the change in the resistance of the resistor and the current in the circuit. The current oscillations were amplified by an operational amplifier and transmitted to the ADC. On the computer monitor, these current readings were recorded for a predetermined time. It was KF 5P1–5-200-A-12 strain gage, with an operating resistance of $R = 199.7 \pm 0.2 \Omega$ and a base of 5 mm. The label of the resistors was produced with the “cyacrine” glue according to the technology described in the paper [33, 34].

4 Results

Thus, the contact pressure between the hemispherical surface of the die body and the workpiece was measured. Measurements were subjected to a minimum of 16 blanks for

each metal and alloy with different coefficients of drawing. The load cell rounded radius $r_m = 4$ mm and $r_m = 1.5$ mm, without lubrication of the surfaces of the workpiece and the tool. Simultaneously, the depth of the punch's progress was recorded, such as force increase; a sharp force increase meant the occurrence of corrugations that made it difficult to draw a flat workpiece into the hole in the die. Based on the measurement results, typical ADC voltage-time charts are shown (Fig. 3). Also, the experimental data are used to verify the adequacy of the mathematical model of the distribution of contact pressures on the die body rounded radius when drawing without collet.

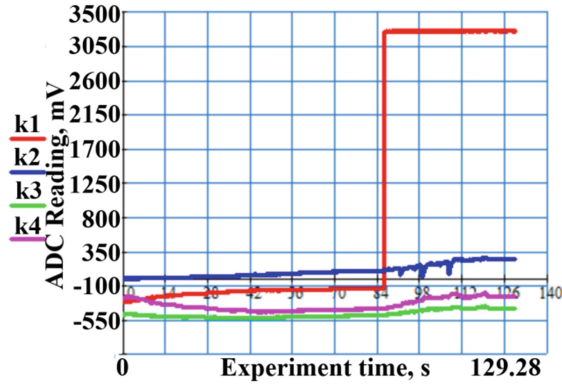


Fig. 3. A typical schedule of measurement of load cell deformations: k1 – the first load cell (breakage); k2 – the second load cell; k3 – the third load cell; k4 – the fourth load cell.

For greater accuracy of contact pressure measurements, the first lot of blanks was chosen in such a size that their diameter was equal $D_0 = D + 2r_m$, where D is the diameter of the drawing workpiece. This was to minimize the effect of blank flange deformation and reduce the impact of the bending moment on the torus-like section. The remaining two lots of blanks were selected with dimensions $D_0 = D + 4r_m$ and $D_0 = D + 6r_m$ correspondently. The results of the experimental data have been subjected to statistical processing [12, 35, 36], then averaged and summarized in Table 1. Processing experimental data on the measurement of contact pressures showed that their distribution is subjected to normal law at a significance level $q = 0.05$. The confidence error in the results of the experiment was assumed to be symmetric and amounted to $\Delta = \pm 0.26$ MPa.

In Table 1, in the numerator of the values of the diameter, the draw ratio, the stroke of the punch, the value of the contact pressure, which relate to the drawing option with the rounding radius of the die body $r_m = 4.0$ mm; in the denominator it is the same for $r_m = 1.5$ mm; $\Delta, \%$ is deviations of the experimental data from the theoretical ones, calculated from the dependence (3).

Table 1. Results of experimental studies on the contact pressures measurement.

Material	Deformation parameters					Contact pressure	Estimated contact pressure	Δ , %
	s, [mm]	D ₀ , [mm]	k	r _m , [mm]	h, [mm]	q, [MPa]	q, [MPa]	
Steel 08kp	0.15	58/52	1.16/1.04	4/1.5	8.0/6.0	58/38	17.25/46.0	71.3/17.2
		66/54	1.32/1.08	4/1.5	8.0/6.0	94/55		81.7/16.9
		74/56	1.48/1.12	4/1.5	8.1/6.0	133/57		87.1/19.4
Aluminum A2	1.4	58/52	1.16/1.04	4/1.5	8.2/6.1	27/46	42/56	35.1/17.4
		66/54	1.32/1.08	4/1.5	8.3/6.0	37/48		10.6/12.6
		74/56	1.48/1.12	4/1.5	8.0/6.0	46/51		8.7/7.5
Copper M4	0.25	58/52	1.16/1.04	4/1.5	8.0/6.0	21/17	10/26.6	52.3/34.3
		66/54	1.32/1.08	4/1.5	7.9/6.0	34/21		70.5/20.3
		74/56	1.48/1.12	4/1.5	7.9/6.0	43/24		76.7/6.7

5 Conclusions

The results of experimental studies showed that the greatest coincidence with theory is 6.7% for drawing with $k = 1.12$ and $r_m = 1.5$ mm for copper and the greatest discrepancy in calculations is up to 87% for steel with $r_m = 4.0$ mm a rounded radius of the die body. The discrepancy between the results of experimental studies and calculated data in general can be explained by the imperfection of the mathematical model, where all factors of constructive and technological nature are not taken into account, as well as hardening of the metal during plastic deformation [37, 38]. The best coincidence between the results of theoretical and experimental studies, which does not exceed 20% (except copper drawing, $k = 1.04$, $r_m = 1.5$ mm), showed data for all metals with $r_m = 1.5$ mm. However, as can be seen from Table 1, an increase in the flange width results in an increase in the contact pressure, and the best coincidence of the results is observed precisely with the drawing of blanks with an enlarged flange. Therefore, the completion of the dependence is obvious. A further direction of research on this issue will concern its refinement in terms of considering the bending moments acting on the radius of the matrix rounding, which should result in greater adequacy of solutions.

References

1. Golovlev, V.: The initial stage of drawing sheet metal. Forging and stamping production. Mater. Work. Press. 7, 4–10 (1995)
2. Kalyuzhnyi, O.: Intensification of forming processes of cold sheet stamping. Sik Group Ukraine LLC, Kyiv (2015)
3. Yan, G., Wang, X., Deng, L.: A study of hole flanging-upsetting process. Adv. Mater. Res. 939, 291–298 (2014). <https://www.scientific.net/AMR.939.291>
4. Luo, J.: Study on stamping-forging process and experiment of sheet metal parts with non-uniform thickness. Huazhong Univ. Sci. Technol. 51, 45–54 (2011).

5. Gavas, M., Izciler, M.: Effect of blank holder gap on deep drawing of square cups. *Mater. Des.* **28**, 1641–1646 (2007)
6. Puzyr, R., Savelov, D., Argat, R., Chernish, A.: Distribution analysis of stresses across the stretching edge of die body and bending radius of deforming roll during profiling and drawing of cylindrical workpiece. *Metall. Min. Ind.* **1**, 27–32 (2015)
7. Popov, E.: *Fundamentals of the theory of sheet punching*. Engineering, Moscow (1977)
8. Volmir, A.: *Stability of Deformable Systems*. The Science, Moscow (1967)
9. Ogorodnikov, V.A., Dereven'ko, I.A., Sivak, R.I.: On the influence of curvature of the trajectories of deformation of a volume of the material by pressing on its plasticity under the conditions of complex loading. *Mater. Sci.* **54**(3), 326–332 (2018). <https://doi.org/10.1007/s11003-018-0188-x>
10. Salenko, Y., Puzyr, R., Shevchenko, O., Kulynych, V., Pedun, O.: Numerical simulation of local plastic deformations of a cylindrical workpiece of a steel wheel rim. In: Ivanov, V., et al. (eds.) *DSMIE 2019. LNME*, pp. 442–451. Springer, Cham (2020). https://doi.org/10.1007/978-3-030-50794-7_43
11. Yang, C., Li, P., Fan, L.: Blank shape design for sheet metal forming based on geometrical resemblance. *Procedia Eng.* **81**, 1487–1492 (2014)
12. Anishchenko, O., Kukhar, V., Grushko, A., Vishtak, I., Prysiaznyi, A., Balalayeva, E.: Analysis of the sheet shell's curvature with lame's superellipse method during superplastic forming. *Mater. Sci. Forum* 945, 531–537 (2019). <https://www.scientific.net/MSF.945.531>
13. Borisevich, V., Zahirnyak, M., Drabobetsky, V.: Choosing the optimal parameters for extracting sheet blanks. *Forging and stamping production. Mater. Work. Press.* **2**, 38–41 (2009)
14. Sosenushkin, E., Yanovskaya, E., Sosenushkin, A., Emel'yanov, V.: Mechanics of nonmonotonic plastic deformation. *Russ. Eng. Res.* **35**(12), 902–906 (2015). <https://doi.org/10.3103/S1068798X15120199>
15. Guo, Y., Batoz, J., Naceur, H., Bouabdallah, S., Mercier, F., Barlet, O.: Recent developments on the analysis and optimum design of sheet metal forming parts using a simplified inverse approach. *Comput. Struct.* **78**, 133–148 (2000). [https://doi.org/10.1016/S0045-7949\(00\)00095-X](https://doi.org/10.1016/S0045-7949(00)00095-X)
16. Sivak, R.: Evaluation of metal plasticity and research of the mechanics of pressure treatment processes under complex loading. *East.-Eur. J. Enterp. Technol.* **6/7**(90), 34–41 (2017). <https://doi.org/10.15587/1729-4061.2017.115040>
17. Anishchenko, A., Kukhar, V., Artiukh, V., Arkhipova, O.: Application of G. Lamé's and J. Gielis' formulas for description of shells superplastic forming. *MATEC Web of Conf.* **239**, 06007 (2018). <https://doi.org/10.1051/mateconf/201823906007>
18. Ogorodnikov, V., Savchinskij, I., Nakhajchuk, O.: Stressed-strained state during forming the internal slot section by mandrel reduction. *Russ. J. Heavy Mach.* **12**, 31–33 (2004)
19. Leyu, W., Daxin, E.: Numerical simulation analysis of variable BHF drawing of rectangular cup on curve blank-holder. *Mod. Manuf. Eng.* **2**, 73–74 (2006)
20. Wang, X., Ouyang, K., Xia, J.: FEM analysis of drawing-thickening technology in stamping-forging hybrid process. *Forg. Stamp. Technol.* **34**(4), 73–78 (2009). <https://doi.org/10.3969/j.issn.1000-3940.2009.04.017>
21. Akbari-Mousavi, S., Barrett, L., Al-Hassani, S.: Explosive welding of metal plates. *J. Mater. Process. Technol.* **202**(1–3), 224–239 (2008)
22. Del', G., Tomilov, F., Ogorodnikov, V.: Stressed state during the hot extrusion of steel. *Steel USSR* **5**(4), 223–224 (1975)
23. Comsa, D., Banabic, D.: Numerical simulation of sheet metal forming processes using a new yield criterion. *Key Eng. Mater.* **344**, 833–840 (2007)

24. Puzyr, R., Haikova, T., Trotsko, O., Argat, R.: Determining experimentally the stress-strained state in the radial rotary method of obtaining wheels rims. *East-Eur. J. Enterp. Technol.* **4**(1(82)), 52–60 (2016). <https://doi.org/10.15587/1729-4061.2016.76225>
25. Puzyr, R., Savelov, D., Shchetynin, V., Levchenko, R., Haikova, T., Kravchenko, S., Yasko, S., Argat, R., Sira, Y., Shchipkovakyi, Y.: Development of a method to determine deformations in the manufacture of a vehicle wheel rim. *East-Eur. J. Enterp. Technol.* **4**(1(94)), 55–60 (2018). <https://doi.org/10.15587/1729-4061.2018.139534>
26. Renne, I., Ogorodnikov, V., Nakhaichuk, V.: Plotting plasticity diagrams by testing cylindrical samples in combined tension and torsion. *Strength Mater.* **8**(6), 733–737 (1976)
27. Mori, K., Nakano, T.: State-of-the-art of plate forging in Japan. *Prod. Eng. Res. Dev.* **10**(1), 81–91 (2015). <https://doi.org/10.1007/s11740-015-0648-1>
28. Zagirnyak, M., Drahobetskiy, V.: New methods of obtaining materials and structures for light armor protection. In: *International Conference 2015, ICMT*, vol. 1, pp. 705–710 (2015)
29. Ogorodnikov, V.A., Grechanyuk, N.S., Gubanov, A.V.: Energy criterion of the reliability of structural elements in vehicles. *Mater. Sci.* **53**(5), 645–650 (2018). <https://doi.org/10.1007/s11003-018-0119-x>
30. Harpell, E., Worswick, M., Finn, M., Jain, M., Martin, P.: Numerical prediction of the limiting draw ratio for aluminum alloy sheet. *J. Mater. Process. Technol.* **100**, 131–141 (2000). [https://doi.org/10.1016/S0924-0136\(99\)00468-9](https://doi.org/10.1016/S0924-0136(99)00468-9)
31. Del, G., Ogorodnikov, V., Nakhaichuk, V.: Criterion of deformability of pressure shaped metals. *Notification High. Educ. Inst. Mech. Eng.* **4**, 135–140 (1975)
32. Zagirnyak, M., Kalinov, A., Ogar, V., Lotous, V.: Experimental assessment of the accuracy of the method for determination the power on an induction motor shaft. In: *18th International Conference 2017, CPEE* (2017). <https://doi.org/10.1109/CPEE.2017.8093054>
33. Markov, O., Zlygoriev, V., Gerasimenko, O., Hrudkina, N., Shevtsov, S.: Improving the quality of forgings based on upsetting the workpieces with concave facets. *East-Eur. J. Enterp. Technol.* **5**(1(95)), 16–24 (2018). <https://doi.org/10.15587/1729-4061.2018.142674>
34. Kukhar, V., Yelistratova, N., Burko, V., Nizhelska, Y., Aksionova, O.: Estimation of occupational safety risks at energetic sector of Iron and Steel Works. *Int. J. Eng. Technol. (UAE)* **7**(2), 216–220 (2018). <https://doi.org/10.14419/ijet.v7i2.23.11922>
35. Markov, O.E., Perig, A.V., Zlygoriev, V.N., Markova, M.A., Kosilov, M.S.: Development of forging processes using intermediate workpiece profiling before drawing: research into strained state. *J. Braz. Soc. Mech. Sci. Eng.* **39**(11), 4649–4665 (2017). <https://doi.org/10.1007/s40430-017-0812-y>
36. Anishchenko, A., Kukhar, V., Artiukh, V., Arkhipova, O.: Superplastic forming of shells from sheet blanks with thermally unstable coatings. In: *MATEC Web of Conference*, vol. 239, p. 06006 (2018). <https://doi.org/10.1051/mateconf/201823906006>
37. Sotiria, H., Spyros, A.: Stability of long transversely-isotropic elastic cylindrical shells under bending. *Int. J. Solids Struct.* **47**, 10–24 (2010). <https://doi.org/10.1016/j.ijsolstr.2009.09.004>
38. Logesh, K., Raja, V., Krishnan, D., Azeemudeen, M., Andrew, A., Hariprasath, K.: Experimental investigation and analysis of tensile and forming behaviour of cold rolled sheet metal. *Int. J. Mech. Eng. Technol. (IJMET)* **8**(11), 252–264 (2017)



Complex Recognition Approach for Cutting Part of Cutters in Finishing Turning

Oleksandr Derevianchenko^(✉)  and Oleksandr Fomin 

Odessa National Polytechnic University, 1, Shevchenko Avenue, Odessa 65044, Ukraine
algdrv@opu.ua

Abstract. In the conditions of finishing and precision turning, the traditional approach to laboratory assessment of the condition of cutters by periodically recording the parameters of the wear zone along the flank surface and subsequent recognition is, in the authors' opinion, insufficiently effective. It does not consider significant changes (due to wear) in the geometry of the cutting edges and, in particular, in the forming of their sections, the state of which directly affects the quality of the processed surface. Therefore, there is a need for complex control and complex recognition of cutting part states. The article aims to develop an approach to complex recognition of cutters cutting part in finishing turning. The scientific novelty consists of creating classifiers for complex recognizing the states of cutters for finishing turning, using the most informative features of the shape of all wear zones, and analyzing their effectiveness. The research was carried out under conditions of processing hardened steel 115CrV3 on a lathe model TPC - 125 BH1P. On a special laboratory stand, equipped with a vision system, comprehensive periodical monitoring of the condition of the cutting part of the cutters for finishing was carried out. Practical usefulness consists of developing a method for predicting the residual life of cutters for finishing turning, using a set of features characterizing the shape and size of defects and microdefects of all wear surfaces of the cutting part. Timely replacement of a failed tool with a new one provides a significant economic effect.

Keywords: Tools failures · States of cutters · Complex of classifiers

1 Introduction

In the conditions of finishing and precision turning, the traditional approach to laboratory assessment of the condition of cutters by periodically recording the parameters of the wear zone along the flank face and subsequent recognition is, in the authors' opinion, insufficiently effective.

Nowadays, in cutting tools (CT) technical diagnostics, a trend is being developed based on smart diagnostic systems. These systems can create, compare, and transform CT models of a given subject area to make decisions based on accumulated knowledge and without the operator's participation in this process. The cutting part (CP) of any CT is characterized by a certain structure and geometry determined by the tasks required

by the processing results. We can say that the working part of the cutting edge (CE) is a variable structure system. It does not take into account significant changes (due to wear) in the geometry of the cutting edges and, in particular, in the forming section of the CE, the state of which directly affects the quality of the processed surface. Therefore, there is a need for complex control and complex recognition of CP states.

The connection of the wear zones of the flank and rake face leads to significant gradual changes in the shape and geometry of the working sections of the CP.

The development carried out was focused on recognizing the states of the worn flank face of tools. However, in finishing and precision machining conditions, it is also necessary to recognize the rake surface and CE conditions.

2 Literature Review

The 5G technology in the next future will have a major impact on the industry [1]. This will enable manufacturers to complete end-to-end automation with the virtual deployment of new product lines or the entire factory. 5G will enable growth and transformation in Industry 4.0. In production conditions of Industry 4.0 became an actual new technological process. For example, in [2] is proposed progressive manufacturing process, based on the concept of intensification of machining and application of multi-axis equipment. It made the possibility to reduce the complexity of the manufacturing process (in drilling, milling, and boring operations).

One major challenge is designing the strategy for communication between the factory modules and the identification of adequate communication technologies [3].

Now the tasks of intelligent forecasting of the operability of modern technical systems are becoming relevant. For example, deep learning model creation is used for predicting the remaining useful life of the machining tools [4].

An artificial neural network model is developed to predict the main cutting force, and its ability to predict cutting force was analyzed in [5]. An effort is made to optimize the cutting parameters to accomplish minimum cutting force using a genetic algorithm. In work [6] features, obtained by processing the cutting force, vibration signal, and surface texture of the machined surface in turn, which are found by tool condition monitoring, are used to estimate cutting tools states.

Cutting tool failure in the manufacturing industry causes damage to the cutting tools; leads to serious accidents [7]. So, a wear monitoring system is required to mitigate these negative effects in the metal cutting manufacturing process. More and more diverse mathematical models are beginning to be used in the metalworking industry when creating mathematical and software for monitoring systems of machine tools and tools. In particular, the application of discrete and continuous Markov chains is promising [8].

It is especially noteworthy is the development of new promising strategies in CAD / CAM systems [9] and their use in diagnostic and monitoring systems for modern automated manufacturing [10].

An important role in data collections and modern computing technology are playing cloud computing and cloud manufacturing (CM) [11–13]. CM as a new technological paradigm has been attracted a large amount of research interest. When solving various diagnostic problems, such intelligent technologies as pattern recognition [14–16], the

formation of statistical classifiers [15], digital image processing [14, 17], and others are increasingly used. They will begin to find application for building classifiers and recognizing the states of cutting tools (CT) [11, 14]. In the publication [11], we show the prospects for using cloud technologies and creating a central laboratory for the development of classifiers of instrument states based on the use of direct and indirect control methods. Therefore, the need to develop an approach to complex recognition of the states of the cutting part (CP) of worn-out tools is obvious.

The article aims to develop an approach to complex recognition of cutting parts of cutters in finishing turning.

3 Research Methodology

The experimental research was carried out under conditions of processing hardened steel 115CrV3 on a lathe model TPC - 125 BH1P. On a special laboratory stand, equipped with a vision system (Fig. 1), comprehensive periodical monitoring of the condition of the cutting part of the cutters for finishing was carried out. Digital images of CP wear zones were recorded. The formation of signs and recognition of the states of the flank faces is discussed in detail in our work [11]. Therefore, the main attention is paid to determining the signs of the states of the CP rake face and cutting edges. For cutting part states recognizing and of the CT residual life predicting – is shown on Fig. 1.

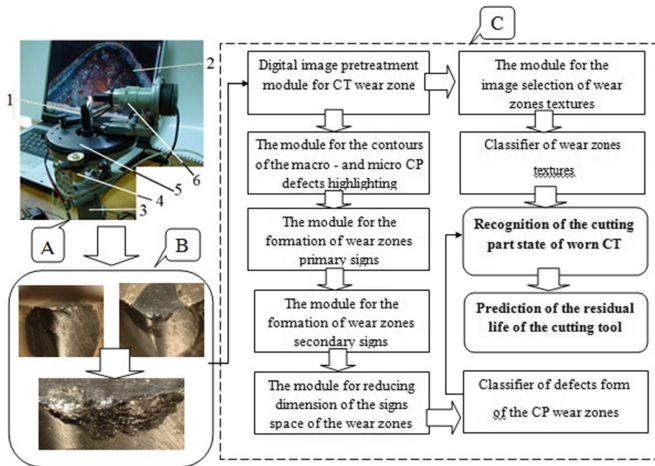


Fig. 1. Fragment of a smart system for cutting part (CP) states recognizing and of the CT residual life predicting.

The scheme contains 3 functional zones (A, B, C). In zone A, a fragment of the stand is shown for sequential monitoring of the wearing tool. The stands main elements: 1–CT; 2–a digital image of the wear zone of the rake face on the monitor screen; 3–control system fundament; 4–table rotation mechanism; 5–turntable on which the controlled tool is mounted; 6–digital camera. If necessary, it provides registration of many digital panoramic CP images, which can form a 3D - CP model.

In zone B, some of the samples of CT images in different projections are shown. They are the source data for obtaining the primary signs of the shapes and textures of the CP wear zones. Zone C represents a fragment of the of smart system intellectual component. Zone C shows the sequential operations of complex processing and analysis of images for each worn surface. Due to the limitations of the volume of the article, we will consider only some of them.

4 Results

Consider fragments of the image processing of the front surface of a worn CNB cutter after wearing CT monitoring. (Fig. 2). In the resulting image 1, a fragment of the wear zone 2 (crater wear) is selected with subsequent scaling (3). After its conversion to binary (4), wear zone contour (5) is selected, and feature sets are formed (6, 7).

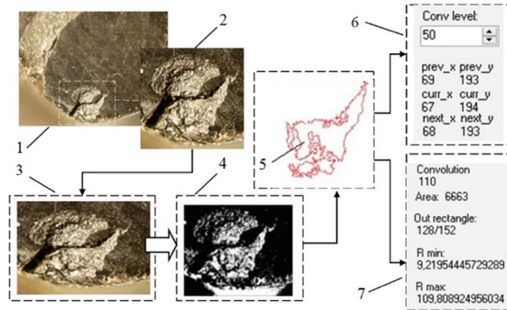


Fig. 2. Fragments of the image processing of the rake face with the crater wear of a worn CNB cutter.

In the structure of the process of complex recognition of the states of worn CT of cutters for finishing, an important place belongs to recognizing the states of the cutting edges. The representation of the classes of form changes of the CT in the process of wear of the cutting part is shown in Fig. 3.

When registering digital images of the rake face of the CT in the initial state ($\hat{R}_{CE}^{\tau_0}$) and the state of wear ($\hat{R}_{CE}^{\tau_1}$) - zone 1 - as a result of the processing $\mu_{CE}^{\tau_0}$ of the binary image (2), there is a selection (3) of the CE contours of the new ($\bar{R}_{CE}^{\tau_0}$) and worn (not shown in Fig. 3) cutter. The combination of these contours gives the contours of the displacement of the CE as a result of wear.

Several classes of these contour shapes are highlighted (in position 1 is shown the class Ω_1). At the bottom of Fig. 3 schematically shows the combined projections of the CE on the main plane ($R_{CE}^{\tau_0}, R_{CE}^{\tau_1}, R_{CE}^{\tau_2}, R_{CE}^{\tau_3}$) for the moments of processing τ_1, τ_2, τ_3 (the shaded outline corresponds to the class Ω_1).

In the structure of Fig. 3 indicates the coordinate system $\hat{Y}\hat{X}$, in which the projections are combined, and the coordinate system $X(D_S), Y$, where is the vector D_S of movement of the cutter feed. Complex contour shapes are caused by the formation of grooves on the CT rear surface. Attention should be paid to the sequential change in the positions

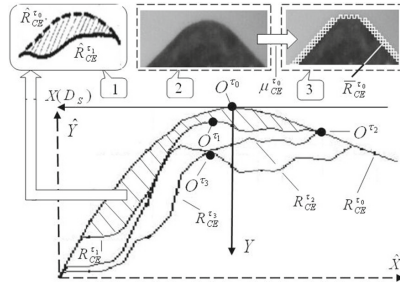


Fig. 3. Representation of the classes of form changes of the CE in the process of wear of the cutting part (fragment).

of the points of the tops ($O^{T0}-O^{T1}-O^{T2}-O^{T3}$), which is due to the radial wear of the CT. Recognition of classes of contours ($\Omega_1-\Omega_5$) is a component of the complex recognition of the state of the CT source. Let's move on to some of the CP defects and microdefects. In Fig. 4 shows images of zones of concentrated wear of the flank face (1), the groove-notch wear (2), and the lowering section of the cutting edge (3).

The following parameters are determined from such images: h_{CE} the amount of lowering (CE displacement) due to the closure of wear zones, the groove's height. Grooving and concentrated wear zones are common when machining hardened steels. The grooves weaken the cutting part of the CT and can cause its local destruction. Therefore, the growth of the parameter h_{GRV} is taken into account in the complex forecasting of the residual resource of the CT. With the formation of traces of concentrated wear on the forming section of the CE, the machined surface quality deteriorates sharply. Due to the closure of the wear zones on the front and rear surfaces, the effect of lowering the cutting edge section to a height h_{CE} and the formation of a small threshold on the front surface is formed.

When this parameter reaches the limit value, the chips stop coming off the rake face because they rest against the threshold and moves vertically upward. This prevents the chip breaking process; chips fill the treatment area, leading to an accident.

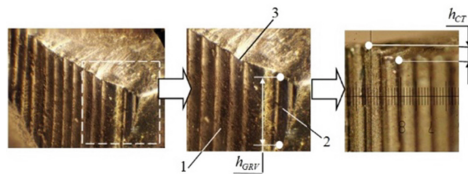


Fig. 4. Images of wear zones of the flank wear of the cutter with traces of defects.

This is especially true on flexible production modules. Therefore, the growth of the parameter h_{CE} is taken into account in the complex forecasting of the residual resource of the CT. The main results of the formation of classifiers are shown in Figs. 5, 6, 7, 8 and 9. Let's move on to a comparative analysis of the quality of classifiers for complex recognition of CP states.

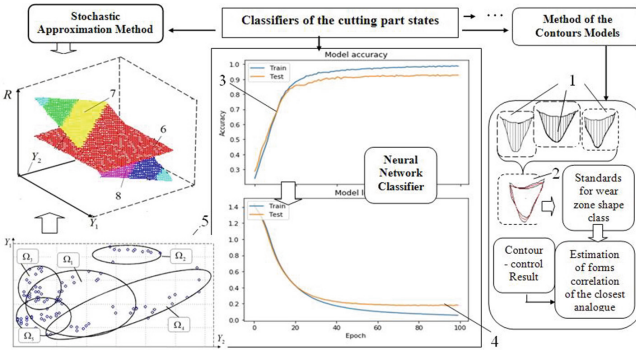


Fig. 5. Some results of a comparative analysis of the quality of classifiers for complex recognition of CP states.

Here 1 is a set of contours of the flank wear zones recorded under the same processing conditions; 2 - reference contour (shape class), formed as a result of processing set 1; 3, 4 - respectively, graphs of changes in the accuracy of the neural network on the training and examination samples; 5 - an example of the intersection of regions of 5 classes of states of the flank wear cp; positions 6–8 show an example of the work of the classifier generated by the stochastic approximation method (6 - classifier; 7 – class 1; 8 - class 2). Figure 5 demonstrated the scheme of classifiers set, which can be used in the experiments. Classifiers were built using the method of contours models of wear zones (1, 2), stochastic approximation method, and neural networks. In cases where the probability density functions of the diagnostic features in the training set are known, the stochastic approximation method (SAM) is effectively used. However, in practice, and especially in the production environment, such estimates are not accurate or completely absent. In this case, a device of neural networks can give a good result. The results of computational experiments show that even simple neural networks created using Python (a programming language) and Keras (libraries for constructing and training neural networks) demonstrate a high recognition quality of CT states. An example of using the Python programming language and the Keras library to build a neural network-based cutting tool state classifier is presented below (Fig. 6). The algorithm includes the following steps: 1. Import of required modules and libraries; 2. Loading the training data set; 3, dividing the training sample into training and examination; 4. Neural network training with Keras; 5. Train the neural network with executing code; 6. I am checking the accuracy of the training data; 7. They are obtaining the conclusion.

The process of neural network training (for recognizing classes of states of the worn back face of the cutters CP) is presented in Fig. 7. After 100 training epochs (it will take around a minute), the training accuracy is reached 94.5% (Fig. 7) - so the model is trained.

In a wide range of external conditions, the use of genetic algorithms becomes justified. The results of computational experiments using the Python programming language and the Deap library of genetic algorithms - demonstrate the fast and effective construction of diagnostic features space of minimum dimension (Fig. 8). So, from a set of 8 primary signs, the algorithm selected 4 of the most informative ones. This base CT

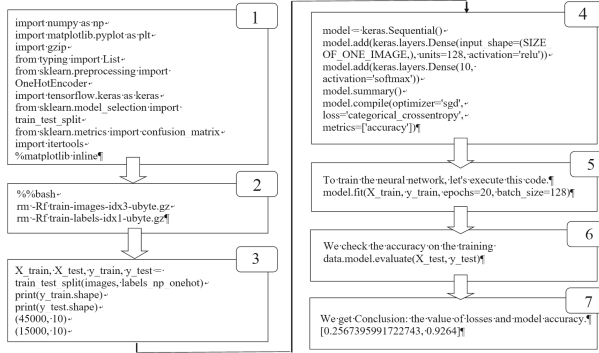


Fig. 6. An example of using the Python programming language and the Keras library to build a neural network-based cutting tool state classifier.

model is constructed in the form of a neural network, which provides the recognition quality of CT states of 98.5%, so the preference is given to the neuron set method. Let's move on to the analysis space of signs and predict CT residual life (Fig. 9).

After receiving the secondary signs of wear zones, internal and external micro defects (traces of concentrated wear, groves at the cut layer borders, the appearance of lowering sections of the CE, etc.), process formation of the Y attribute space occurs.

In this conditionally multidimensional CP state space, the areas of the tool state classes are displayed ($\Omega_1, \Omega_2, \Omega_3$). Class Ω_1 - incisors are worn flank wear surfaces without visible micro-defects. In this class, at the control moments τ_1, τ_2 , two states (c_{τ_1}, c_{τ_2}) are identified, which correspond to feature vectors (y^{τ_1}, y^{τ_2}).

Epoch							
1600 1600	[=====]	- 1s	600us/step	- loss:	1.3835	- acc:	0.3019
Epoch							
1600 1600	[=====]	- 0s	60us/step	- loss:	1.3401	- acc:	0.3369
Epoch							
1600 1600	[=====]	- 0s	72us/step	- loss:	1.2986	- acc:	0.3756
Epoch							
1600 1600	[=====]	- 0s	63us/step	- loss:	1.2525	- acc:	0.4100
Epoch							
1600 1600	[=====]	- 0s	62us/step	- loss:	1.1982	- acc:	0.4675
.							
.							
Epoch							
1600 1600	[=====]	- 0s	55us/step	- loss:	0.0400	- acc:	0.9937
Epoch							
1600 1600	[=====]	- 0s	62us/step	- loss:	0.0390	- acc:	0.9950
Epoch							
1600 1600	[=====]	- 0s	57us/step	- loss:	0.0390	- acc:	0.9937
Epoch							
1600 1600	[=====]	- 0s	60us/step	- loss:	0.0380	- acc:	0.9950

Fig. 7. The neural network training (for recognizing classes of states of the worn back face of the cutters CP).

The indicated states of the cutter differ in the size of the flank wear zone. The wear process is conventionally depicted by $W^{(\tau_1 - \tau_2)}$. Further CT wear ($W^{(\tau_2 - \tau_3)}, W^{(\tau_3 - \tau_4)}$) leads to the appearance of new wear zones traces of concentrated wear; section of lowering the cutting edge (due to the closure of the wear zones). They are significant in finishing (class Ω_2) - state c_{τ_3}, c_{τ_4} (a digital image corresponding to the state c_{τ_4} is given conditionally here).

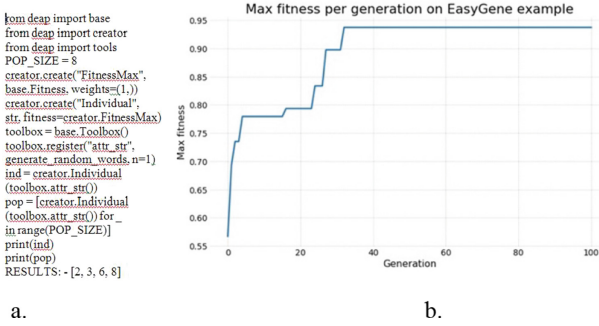


Fig. 8. Features space selection using genetic algorithm.

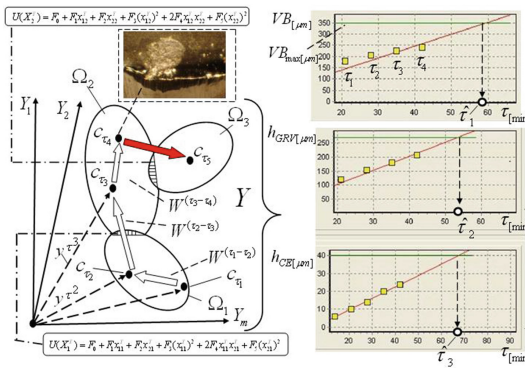


Fig. 9. Schema of the cutter states changing (as it wears out) in the space of signs and complex prediction of its residual life.

Pay attention to the fact that there is an intersection of class areas $\Omega_1, \Omega_2, \Omega_3$ (shaded areas). In this case, the use of the SAM becomes an alternative. The corresponding classifiers (sets of decision rules - separating hypersurfaces $((U(X1), U(X2)))$ are polynomials of the 2nd degree.

The right part of Fig. 9 shows the prediction schemes for the residual life of the cutter (with the conditional use of a linear model) according to four parameters ($VB_{[\mu m]}$; $h_{GRV}[\mu m]$; $h_{CE}[\mu m]$). Here: $h_{GRV}[\mu m]$ - groove height; $h_{CE}[\mu m]$ - CE lowering value. Green lines indicate the limit values of each parameter. From the obtained values of the time period for the loss of CT workable state ($\hat{\tau}_1; \hat{\tau}_2; \hat{\tau}_3$), the smallest is selected. The prediction result is transmitted to the CNC system.

5 Conclusions

The smart system has been developed for complex recognizing states and predicting the residual life of a cutting tool. A special laboratory stand was tested for direct monitoring of CT states using vision systems; image processing of wear zones ensured the formation of sets of CT states signs. A number of wear zones ststateigns were obtained, which

were used to form the corresponding classifiers. We tested 3 types of CT state classifiers constructed using SAM, method of contours models of wear zones, and neural networks. The related software packages have been developed using the programming languages Python and Keras library. The best results were shown by the neural network classifier, which will be used in further studies.

The dimensionality of the CP states space reduced using genetic algorithms. From a set of 8 primary signs, the algorithm selected 4 of the most informative ones. The cutting state's models were constructed in the form of a neural network, which provides the probability of correctly recognizing CT states of 98.5%.

In future investigations, authors planning to create fuzzy – neuron classifier for CT states complex recognition (to provide 100% quality of state recognition).

References

1. Peraković, D., Periša, M., Zorić, P., Cvitić, I.: Development and implementation possibilities of 5G in Industry 4.0. In: Ivanov, V., Trojanowska, J., Pavlenko, I., Zajac, J., Peraković, D. (eds.) DSMIE 2020. LNME, pp. 166–175. Springer, Cham (2020). https://doi.org/10.1007/978-3-030-50794-7_17
2. Ivanov, V., Dehtiarov, I., Zaloga, V., Kosov, I., Savchuk, V.: Increasing productivity of connecting rods machining. In: Ivanov, V., Trojanowska, J., Pavlenko, I., Zajac, J., Peraković, D. (eds.) DSMIE 2020. LNME, pp. 264–275. Springer, Cham (2020). https://doi.org/10.1007/978-3-030-50794-7_26
3. Mukku, V.D., Lang, S., Reggelin, T.: Integration of LiFi technology in an Industry 4.0 learning factory. *Procedia Manuf.* **31**, 232–238 (2019). 9th Conference on Learning Factories, Braunschweig, Germany
4. Liu, C., Zhang, L., Niu, J., Yao, R., Wu, C.: Intelligent prognostics of machining tools based on adaptive variational mode decomposition and deep learning method with attention mechanism. *Neurocomputing* **417**, 239–254 (2020)
5. Leo Dev Wins, K., Anuja Beatrice, B., Ebenezer Jacob Dhas, D.S., Anita Sofia, V.S.: Artificial neural network and genetic algorithm-based models for predicting cutting force in turning of hardened H13 steel. In: Vijayan, S., Subramanian, N., Sankaranarayananasamy, K. (eds.) Trends in Manufacturing and Engineering Management. LNME, pp. 627–635. Springer, Singapore (2021). https://doi.org/10.1007/978-981-15-4745-4_56
6. Cheng, M., Jiao, L., Shi, X., Wang, X., Yan, P., Li, Y.: An intelligent prediction model of the tool wear based on machine learning in turning high strength steel. *J. Eng. Manuf.* **234**(13), 1580–1597 (2020)
7. Marani, M., Zeinali, M., Kouam, J., Songmene, V., Mechefske, C.K.: Prediction of cutting tool wear during a turning process using artificial intelligence techniques. *Int. J. Adv. Manuf. Technol.* **111**(1–2), 505–515 (2020). <https://doi.org/10.1007/s00170-020-06144-6>
8. Olekh, T., Gogunskii, V.: Use of discrete and continuous markov chains for system absorbing states. In: 2019 IEEE International Conference on Advanced Trends in Information Theory, ATIT 2019 - Proceedings, pp. 518–521 (2019)
9. Dodok, T., Cubonova, N., Cisar, M., et al.: Utilization of strategies to generate and optimize machining sequences in CAD/CAM. In: 12th International Scientific Conference of Young Scientists on Sustainable, Modern and Safe Transport Location: High Tatras. *Procedia Engineering*, vol. 192, pp. 113–118 (2017).
10. Kuric, I., Cisar, M., Tlach, V., Zajačko, I., Gál, T., Więcek, D.: Technical diagnostics at the department of automation and production systems. In: Burduk, A., Chlebus, E., Nowakowski,

- T., Tubis, A. (eds.) ISPEM 2018. AISC, vol. 835, pp. 474–484. Springer, Cham (2019). https://doi.org/10.1007/978-3-319-97490-3_46
11. Fomin, O., Derevianchenko, O.: Improvement of the quality of cutting tools states recognition using cloud technologies. In: Ivanov, V., Trojanowska, J., Pavlenko, I., Zajac, J., Peraković, D. (eds.) DSMIE 2020. LNME, pp. 243–252. Springer, Cham (2020). https://doi.org/10.1007/978-3-030-50794-7_24
 12. Liu, Y., Wang, L., Vincent Wang, X.: Cloud manufacturing: latest advancements and future trends. In: 8th Swedish Production Symposium, pp. 62–73. Waterfront Convention Centre Stockholm, Sweden (2018). *Procedia Manuf.*
 13. Newman, S.T., Nassehi, A., Xu, X.W., Rosso, R.S.U., Wang, L., Yusof, Y., et al.: Strategic advantages of interoperability for global manufacturing using CNC technology. *Robot. Comput.-Integr. Manuf.* **24**(6), 699–708 (2008)
 14. Antoshchuk, S., Derevianchenko, O., Tkachenko, E.: The hierarchical objects analysis on images of cutting tool wear zones. In: International Conference TCSET 2006 Conference Proceedings. pp. 253–255 (2007)
 15. Vapnik, V.: *The Nature of Statistical Learning Theory*. Springer, Heidelberg (2013)
 16. Aivazjan, S., Buxshtaber, V., Enjukov, I., Mechalkin, L.: *Applied statistics. Classification and dimension reducing*. Finance and Statistics, Moscow (1989). (in Russian)
 17. Jahne, B.: *Digital Image Processing*. Springer, Heidelberg (2005)



Fractal Analysis of Structural and Phase Changes in the Metal of Welded Steam Pipe Joints

Yaroslav Garashchenko^(✉) , Alyona Glushko , Olena Kobets ,
and Olena Harashchenko 

National Technical University “Kharkiv Polytechnic Institute”,
2, Kyrpychova St, Kharkiv 61002, Ukraine

Abstract. The research results of the ability to assess the boundaries of structural components’ geometric complexity, which are visible in a metallographic analysis of the metal samples of Welded Steam Pipe Joints, considering the operating time, are presented. The estimation of the complexity of grain boundaries was made based on a statistical analysis of fractal dimensions obtained by the cellular method for measuring the grain boundary length. The fractal analysis of micro-section images is carried out using a developed program. The computer system was tested for several samples cut from sections of steam pipelines with different operating times, operated under conditions of creep and low-cycle fatigue. A comparative analysis of fractal dimensions of structural components’ boundaries in the microsections images of various metal sections with different operating times is carried out. The research and comparative analysis are carried out for the heat-affected zone, base metal, weld, and substrate areas. As a result, the possibility of assessing the complexity of the boundaries of structural components in the steam pipelines metal and their welded joints was confirmed based on the analysis of statistical characteristics of the distribution of their fractal dimension.

Keywords: Metallographic analysis · Boundaries of structural components · Geometrical complexity · Fractal dimension

1 Introduction

Structural changes in the steam pipelines metal made of heat-resistant pearlitic steel 12Cr1MoV (analog of steel 14MoV6-3, 1.7715 EN 10216-2:2020), which are operated under conditions of creep and low-cycle fatigue, lead to a deterioration in their properties. Identifying premature degradation processes in metal by forming defects based on metallographic analysis of structural changes is essential to ensure a trouble-free operation of steam pipelines [1].

The use of fractal analysis is one of the approaches for quantifying metallographic images. It is known that the fractal dimension of metallographic image components can be used as a characteristic of the fatigue of metal polycrystals [2]. The fractal dimension of a metal’s structural components is an effective quantitative characteristic

of the process of self-organization of the material structure during fatigue. It depends on the initial structure of the material and the duration of cyclic loads [2].

2 Literature Review

The development of methods for assessing the materials structure and modern computer technologies has brought to a new level the ability to carry out their quantitative assessment [3]. The metal structure is represented by space-filling irregular elements [4]. The correlation between parameters of the metal structure and their physical and mechanical properties has been studied by many authors [5, 6]. The presence of an element of subjectivity in assessing the metal structure lies in the fact that many of its elements, due to their complex configuration, are difficult to quantitatively describe [7]. This fact leads to the loss of important information about the “structure-property” tandem. The structure’s geometric description is usually presented at the following three levels [4]: qualitative, quantitative, and topographic. The quantitative assessment of grain structures usually calculates the average grain size, grain boundary density, statistical grain size distribution, and porosity [7].

There is an approach that integrates 3D-modeling and visual analysis of metal structure [8]. Modeling produces valid polygonal 3D-representations of the structure by adopting a physics-based particle packing procedure.

Known studies [9] have shown that the self-organization model of metal structure can be used for cyclic actions. The specific features of the formation of microstructure and substructure [10] of metal under long-term cyclic influences in the form of dissipative structures make it possible to use the theory of fractals to describe them [11]. Fractal image analysis is used in many scientific fields [12, 13]. In materials science, fractal analysis is used to study the metal’s microstructure since its structure can be interpreted as a fractal image [13, 14]. Fractal dimension and lacunarity are determined by the results of fractal analysis [11]. There are many methods for determining the fractal dimension for an image proposed in [15, 16]. Using these methods produces differing results. Comparative assessment of several methods is presented in [17].

The value of fractal dimension characterizes the quantitative parameters of structural elements and the physical properties of these elements’ boundaries [10]. Determining the correlation between specified properties and fractal dimension of grain boundaries is a rather complicated but solvable problem [13].

This research shows a hypothesis about the statistical analysis of the fractal dimension distribution of the boundaries of selected structural components using the cellular measurement method, which will make it possible to scientifically determine their geometric complexity and consider this complexity when assessing the material structure effect on the properties and the residual resource.

The purpose of the research is to substantiate the assessment of boundaries complexity of the structural components of steam pipeline metal and its welded joints based on cellular method, considering the operating life.

3 Research Methodology

Analysis of metallographic images of metal samples of steam pipelines was carried out using statistical fractal analysis of images developed at NTU “Kharkiv Polytechnic Institute” (Ukraine). This system quantifies the metal structure based on the pixel array analysis using *RGB* and *HSV* color models. A subsystem has been developed to solve the problem and is shown in Fig. 1.

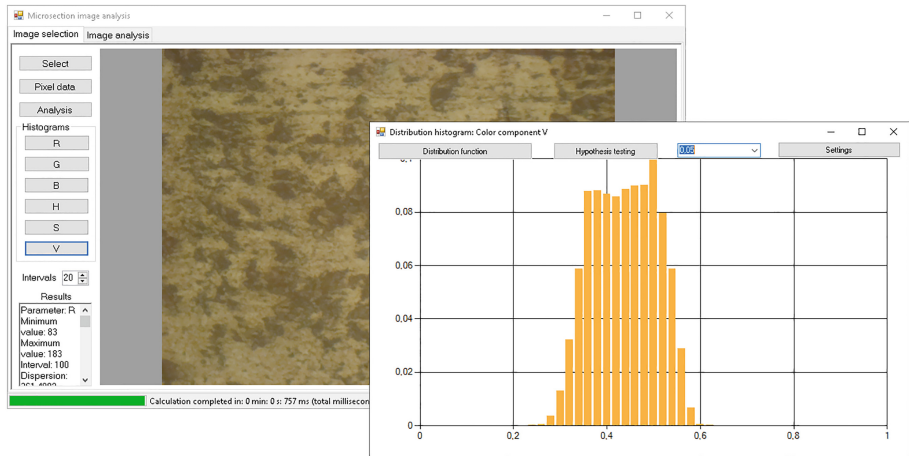


Fig. 1. Screen form of the fractal image analysis system.

This system (Fig. 1) gives a user the following basic capabilities:

- forming of pixels array with the definition of color components using *RGB* and *HSV* models;
- image visualization;
- determination of main statistical characteristics of color components distribution;
- determination of fractal dimension for a given range of scales (scaling area) to measure the length of the contour of selected pixels;
- statistical distribution analysis of the selected pixels over the width and length of the image;
- visualization of analysis results in the form of density or cumulative probability function.

The definition of *RGB* and *HSV* color model components for pixel array is performed by defining their properties: Red, Green, Blue, Hue, Saturation, Brightness (Value).

The research of possibilities of assessing the fractal dimension of boundary pixels was carried out using metallographic images of four samples of welded joints microsections cut from operating steam pipelines. One sample is taken as a baseline version, which has no operating time. For the rest of the samples, the operating time was 120 and 150

Table 1. Chemical composition of steel 12Cr1MoV (GOST 5520-79).

C, %	Si, %	Mn, %	Ni, %	P, S, %	Cr, %	Mo, %	V, %	Cu, %
0.08 ÷ 0.15	0.17 ÷ 0.37	0.4 ÷ 0.7	<0.3	<0.025	0.9 ÷ 1.2	0.25 ÷ 0.35	0.15 ÷ 0.30	<0.2

thousand hours. All samples' base material is heat-resistant pearlitic steel 12Cr1MoV (the chemical composition is presented in Table 1).

The scheme for determining the fractal dimension of selected image pixels in the developed system (Fig. 1) is shown in Fig. 2.

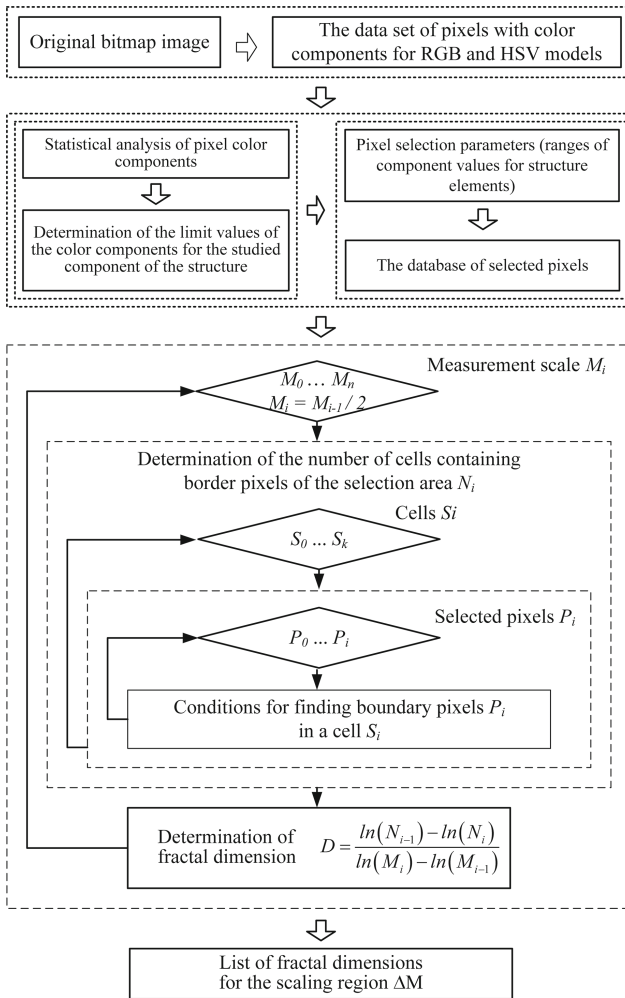


Fig. 2. Scheme for calculating the fractal dimension of selected image pixels.

The selection areas of metal structure elements in the microsection image (Fig. 1) are formed by setting the value range of selected RGB or HSV color components. Consequently, closed selection areas are formed consisting of an array of pixels related to the studied structural element. Such areas are obtained due to the values of pixel color components falling within a specific range. In most cases, selection regions are created based on a need to consider the structure's main component. For the contours of selection areas, we take the boundary selected pixels, defining the condition for the location of unselected pixels next to them (one or more that do not fall outside the specified cell). At the same time, the typical problem of fractal geometry to determine the length of a curved line using an array of cells with specified dimensions (which is called the "measurement scale" [7]) is quite applicable to the contours. Solving this problem is the coefficient of fractal dimension D of contour for a particular scaling area ΔM (range of cell sizes).

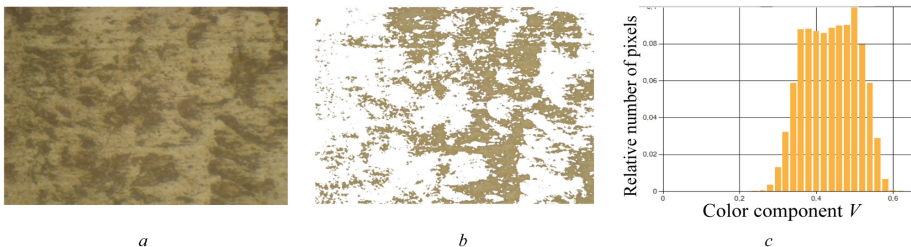
Given the theoretical background [18], fractal dimension D quantifies a contour's complexity (it contains border pixels) as a factor of change in detail with a change in scale. Fractal dimension is determined by the following formula [7]:

$$D = \frac{\ln(N_{i-1}) - \ln(N_i)}{\ln(M_i) - \ln(M_{i-1})}, \quad (1)$$

where M_i - measure (cell size) for the i -th measurement of the length of structural element boundaries under study; N_i is the number of scales (cells with size M_i) covering the contour (boundary pixels).

Coefficient D obtained by formula (1) can take a non-integer value, characterizing the degree of filling the image with the studied boundary pixels [19].

According to this scheme (Fig. 2), with a sequential change in the scale, the process of measuring the length of boundaries of selected areas of metal structure elements is repeated by several scales of N_i (cell size M_i) that cover entirely the boundary pixels [7] (Fig. 3 shows an example of microsection image with selected pixels). The pearlite zones' selection in the microsection image was carried out by replacing the original color (Fig. 3a) with white (Fig. 3b). As a threshold value of color brightness, $V_{max} = 0.46$ was visually selected to highlight pearlite in the image of a metal microsection. This value is also seen in density function (brightness) component values V for the HSV color model.



a - original image; b - image with selected pixels;
 c - histogram of the V component (brightness) for the HSV color model

Fig. 3. Visual analysis of the microsection image of the weld metal without operating time.

As applied to the cellular method, a scale is called a cell (square) of size M . The scale should be significantly less than the measured contour length or a total number of boundary pixels ($M \ll L$). In formula (1) number N will increase with decreasing value M (a more significant number of more minor scales are required to cover the boundary pixels fully).

Concerning a contour consisting of boundary pixels, its complexity and, accordingly, the fractal dimension will depend on the scaling area $\Delta M = M_{i-1} - M_i$. When measuring a real contour using a measure $M \rightarrow 0$, the length $L = const$. In this case, according to formula (1), the fractal dimension will correspond to the Euclidean dimension of the contour $D = 1$. If we consider increasing the image resolution (decreasing the pixel size $p_{image} \rightarrow 0$) applied to a perfectly etched sample, the contour length increases $L \rightarrow L_{ideal}$. Therefore, the fractal dimension of the contour obtained by the sequential arrangement of boundary pixels will always be $D \in (1, 2]$ (on condition that the cell size M does not exceed the contour size).

There are always restrictions on the minimum and maximum value of measurement scale M [20] in practice. In this study, the measurement scale's limitations will be the image size and the condition for determining the boundary pixel. Therefore, a cell with dimensions of 2×2 pixels will be the minimum acceptable. Accordingly, the initial measures M_i were chosen from the list $M_i = \{2, 4, 8, 16, 32, 64\}$ pixels (at image resolution - 1536×1152). The values of measures were set in a geometric progression with a common ratio $r = 2$. The number of contour length measurements was performed up to 5 times to obtain a wider scaling area of ΔM .

The studied images of microsections have the exact resolution. Accordingly, the use of specified M values for all images made it possible to obtain the fractal dimension's relative values, which can be compared. This circumstance makes it possible to carry out a comparative analysis of the studied grains' contours (boundary pixels) for all samples.

A separate study was carried out to substantiate the visually determined value of the brightness threshold V_{max} for the selected area of the microsections structural element. For this purpose, the fractal dimension of boundary pixels (the contour of the selected area) was determined depending not only on the measurement scale but also on the specified threshold V_{max} . 3D plot for $D = f(M, V_{max})$ is shown in Fig. 4 using the example of a steam pipeline weld with an operating time of 150 thousand hours.

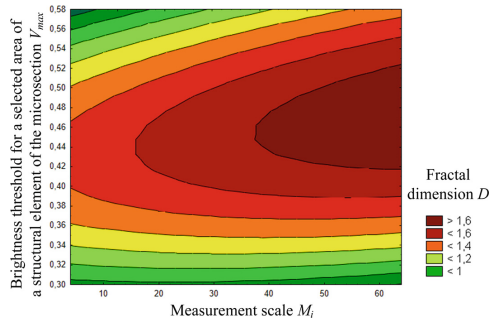


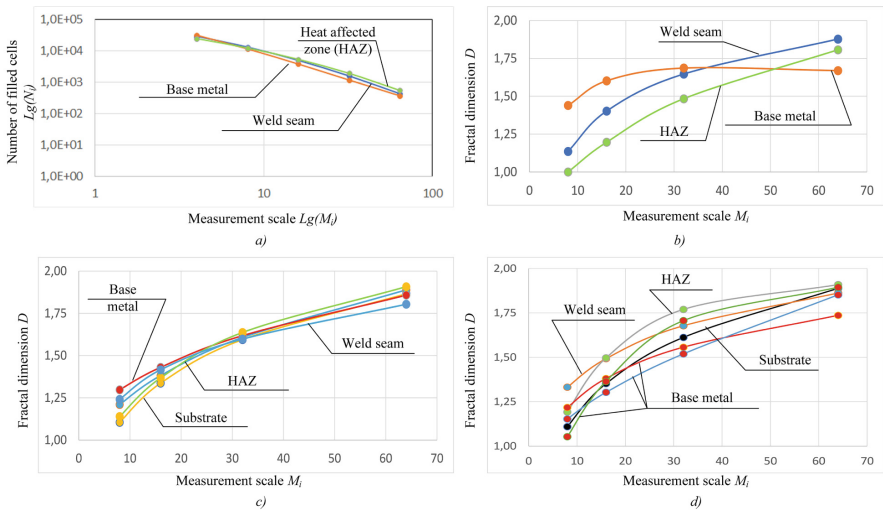
Fig. 4. Brightness threshold correlation for the selected area of the microsection structural element and the measurement scale with a fractal dimension of boundary pixels.

In the microsection image shown in Fig. 3, the main structural element is pearlite, which has the highest relative content in the metal. The main structural element's real boundary will be highlighted in the area of maximum fractal dimension and the largest measurement scale on graph $D = f(M, V_{max})$ (Fig. 4).

The largest fractal dimension is observed in the domain of the most significant values of measurement scale $M_i = 64$ pixels and $V_{max} = 0.46 \pm 0.04$ (Fig. 4). In this way, we confirm the correctness of value's (V_{max}) choice for the studied microsections component's contour (Fig. 3). This V_{max} value is correct for samples obtained under similar laboratory conditions.

4 Results

Results of calculations to determine the fractal dimension of selected components contours for microsections of test samples are shown in Fig. 5. The graph of the typical influence of measurement scale on the number of filled cells with boundary pixels is shown in Fig. 5a. This graph confirms the fractal analysis application's validity since it has a nearly linear relation of log-transformed characteristics $lg(N) = lg(M)$. This relation is typical for fractal contours.



a - influence of the measurement scale on the number of filled cells with boundary pixels for a sample without operating time; *b*, *c*, *d* - the relationship between the measurement scale and the fractal dimension for samples with an operating time of 0, 120, and 150 thousand hours respectively.

Fig. 5. Results of fractal analysis of microsection images.

Figure 5 b-d shows the different options for the relation between the measurement scale and the microsection fractal dimension for steam pipeline samples. All dependencies are characterized by an increase in the fractal dimension with growth in the measurement scale. This case was separately studied by grouping the fractal analysis results by measurement scale (statistical analysis using the “Box Whiskers” swing chart is shown in Fig. 6.) Such a diagram shows general trends and significant differences in the ranges of fractal dimension values depending on the measurement scale. The greatest overlap of the fractal dimension domain was noted for the measurement scales $M_i = \{16, 8\}$ pixels. The smallest is for $M_i = \{32, 16\}$ pixels. In general, the results obtained do not contradict the well-known studies of the fractal dimension of contours or components of the metal structure [6, 12]. The most informative for assessing the steam pipeline residual resource can be considered the measurement scale $M_i = 8$, since the largest range of values of the fractal dimension D_i is observed.

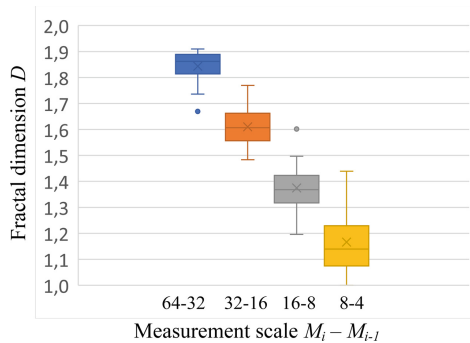


Fig. 6. Statistical analysis of the fractal dimensions of boundary pixels, grouped by measurement scale, regardless of operating time.

The statistical analysis of fractal dimensions grouped by metal sections (weld, base metal, heat-affected zone, and substrate) and the operating time is shown in Fig. 7. Heat-affected zone has the most extensive range of values according to experimental microsections D_i . For the initial sample (without operating time), the base metal has the smallest range of D_i values, which is entirely explainable due to the lack of influence of external factors on a metal structure.

There are identified trends. If for the initial sample arithmetic mean value \overline{D}_i for the base metal is more significant compared with a weld and heat-affected zone, then with an increase in operating time, the opposite situation is observed, that is, a significant relative decrease in \overline{D}_i . There is also a growing trend of D_i for all areas under the study with an operating time. Therefore, with the operating time, the contours’ complexity for the tested element of metal structure increases. This feature is the most pronounced for the heat-affected zone. This feature’s study makes it possible to determine the residual resource of a steam pipeline.

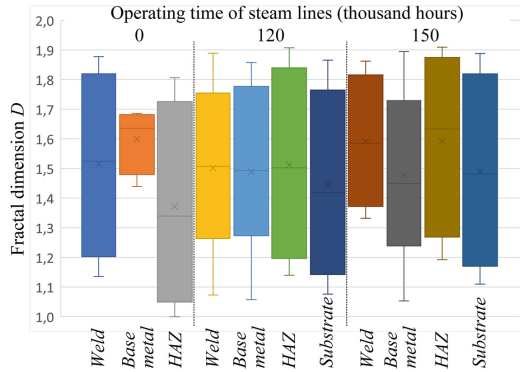


Fig. 7. Statistical analysis of the fractal dimensions of boundary pixels, grouped by metal sections and the operating time.

5 Conclusions

Statistical analysis of the distribution of fractal dimension of microsections of steam pipelines metal, obtained by the cellular method, makes it possible to scientifically determine grain boundaries' geometric complexity (areas of structural elements).

The original study of the effect of V_{max} and measurement scale M_i on the fractal dimension D_i carried out for the first time and made it possible to obtain a universal idea of the complexity of the contours of all structural components of the microsection image under study. The dependence $D_i = (V_{max}, M_i)$ made it possible to substantiate the threshold value of color brightness for studying the boundaries of pearlite, which is the structure's main component.

The influence of steam pipeline time on structural changes, expressed by an increase in fractal dimension and, accordingly, by the complexity of structural components contours, has been confirmed.

Further research is an analysis of the correlation between obtained data and the mechanical properties of the metal. This analysis will expand the possibilities for identifying structure parameters based on metallographic and fractal analyses and predicting a steam pipeline's residual resource.

References

1. Glushko, A.: Research into defectiveness of welded joints of steam pipes operated over a long time. *East. Eur. J. Enterp. Technol.* **6**(1 (84)), 14–20 (2016). <https://doi.org/10.15587/1729-4061.2016.85852>
2. Kuznetsov, P., Petrakova, K., Schreiber, Y.: Fractal dimension as a characteristic of fatigue of metal polycrystals. *Phys. Mesomech.* **7**(S1-1), 389–392 (2004)
3. Suryanarayana, C.: Microstructure: An Introduction. In: Prasad, E., Wanhill, R.J.H. (eds.) *Aerospace Materials and Material Technologies*. IIMS, pp. 105–123. Springer, Singapore (2017). https://doi.org/10.1007/978-981-10-2143-5_6
4. DeHoff, R.T.: Microstructology: the realistic and quantitative description of microstructural evolution. *Metall. Microstruct. Anal.* **1**, 244–258 (2012). <https://doi.org/10.1007/s13632-012-0042-8>

5. Dmytryk, V., Glushko, A., Tsaryk, A.: Recrystallization in the metal of welding joints of steam trucks. *Prob. Atomic Sci. Technol.* **5**, 49–52 (2019)
6. Miletić, I., Ilić, A., Nikolić, R.R., Ulewicz, R., Ivanović, L., Sczygiol, N.: Analysis of selected properties of welded joints of the HSLA steels. *Materials* **13**(6), 1301 (2020)
7. Bolshakov, V., Volchuk, V., Dubrov, Y.: *Fractals in Materials Science*, 1st edn. PGACA (2006)
8. Rodrigues, A.M., Bardella, F., Zuffo, M.K., Leal Neto, R.M.: Integrated approach for geometric modeling and interactive visual analysis of grain structures. *Comput. Aided Des.* **97**, 1–14 (2018)
9. Anisovich, A., Tovpenets, R.: Synergetic approach to describing structural changes during cyclic thermal effects. *Eng. Phys. J.* **75**(1), 15–20 (2002)
10. Tovpenets, P., Anisovich, A.: Possibility of using the fractal analysis to describe alloys' structures after pulse processing. *Cast. Metall.* **1**(37), 143–145 (2006)
11. Stoffel, A., Rabkin, M.: Use multifractal analysis to estimate the properties of structural steel. *Metall. Mater. Sci.* **10**(31), 24–27 (2016). [in Russian]
12. Moskvina, P., Balytska, N., Melnychuk, P., Rudnitskyi, V., Kyrylovykh, V.: Special features in the application of fractal analysis for examining the surface microrelief formed at face milling. *East. Euro. J. Enterp. Technol.* **2**(1(86)), 1–7 (2017). <https://doi.org/10.15587/1729-4061.2017.96403>
13. Krivonosova, E.A., Krivonosova, E.K., Trushnikov, D.: Fractal geometry in metallurgy of welding and coatings. *Mater. Sci. Forum* **893**, 252–256 (2017)
14. Fernández, R., González-Doncel, G., Garcés, G.: Fractal analysis of strain-induced microstructures in metals. In: *Fractal Analysis - Selected Examples* (2020)
15. Li, J., Du, Q., Sun, C.: An improved box-counting method for image fractal dimension estimation. *Pattern Recogn.* **42**, 2460–2469 (2009)
16. Liu, J., Jiang, X., Huang, X., Shaohua, W.: Morphological characterization of super fine pulverized coal particle. Part 2. AFM investigation of single coal particle. *Fuel* **89**(12), 3884–3891 (2010). <https://doi.org/10.1016/j.fuel.2010.07.001>
17. Risović, D., Pavlović, Ž.: Performance assessment of methods for estimation of fractal dimension from scanning electron microscope images. *Scanning* **35**(6), 402–411 (2013)
18. Albers, A., Gerald, A., Mandelbrot, B.: *In His Own Words. Mathematical People: Profiles and Interviews*. AK Peters, Wellesley (2008)
19. Falconer, K.: *Fractal Geometry: Mathematical Foundations and Applications*. Wiley, New York (2014)
20. Perrier, E., Tarquis, A., Dathe, A.: A program for fractal and multifractal analysis of two-dimensional binary images: computer algorithms versus mathematical theory. *Geoderma* **134**(3–4), 284–294 (2006)



Research of the Spindle Units for Multioperational Lathes in the APM WinMachine Environment

Oleg Kroi^(✉)  and Volodymyr Sokolov 

Volodymyr Dahl East Ukrainian National University, 59-a,
Central Ave., Severodonetsk 93400, Ukraine

Abstract. The problem of modeling the spindle unit's design for multi-operational lathes equipped with a set of modular tooling according to the rigidity criterion is considered. Structural and calculation schemes of a two-support structure in the form of a constant cross-section beam on duplexed angular contact ball bearings considering linear and angular stiffness are proposed. The procedure for constructing an analytical static formula of a spindle as an analytical dependence of its general compliance on the cantilever's dimensions is used, which adequately reflects the conditionally constant (spindle on two supports) and replaceable (modular tooling) parts of the object under consideration. With the help of this formula, it is possible to express procedure probing the machine's working space according to the compliance indicator. Analytical dependencies for finding a rational ratio of the spindle main design parameters from the standpoint of maximum rigidity are proposed. This approach is most effective for typical double-support spindles equipped with a variety of tooling. The efficiency of the APM Structure3D module in solving problems of assessing the stress-strain state, considering the complex mechanism of deformations in supports, is shown. The stress fields, which predetermine the picture of the researched object's deformation state, are presented. For a comprehensive study of the spindle unit, the capabilities of APM Structure3D to determine the set of natural frequencies and the corresponding vibration modes are used.

Keywords: Machine tools · Spindle-cantilever stiffness · Optimal size ratio · Static formular · Stress field

1 Introduction

In connection with the increase in machining processes' productivity and efficiency, the issue of modeling the forming units of metal-cutting machines in modern CAD systems is becoming increasingly important. The analysis of the balance of flexibility and vibration modes of the primary units of lathes showed that the central forming units: spindle – workpiece and support group – tool block, predetermine the quality of the machine as a whole. The spindle's rigidity and vibration resistance characteristics on elastic supports depend on the size of the cantilever part of both the spindle itself and the length of the

workpiece. Fixing a processing scheme with a particular overhang and building on these basic design schemes and 3D models of the main units of the machine [1, 2] do not make it possible to effectively control the rigidity and vibration resistance within the working space of the machine. In [2], a library of models of generalized multi-axis machine tool configurations is presented.

The widespread introduction of the 3D modeling apparatus in designing machine tools is also presented in [3]. Comprehensive research of the operability of machine tools and technological equipment is carried out using CAD SOLIDWORKS and CAE ANSYS software. Within three-dimensional libraries, 3D models of the spindle and its research by the finite element method are presented. As the author notes, choosing the best modeling method is key to creating an accurate model. The main apparatus of the 3D modeling software is CAD SOLIDWORKS to create the spindle model. To effectively use the finite element method, the CAE ANSYS interface is used for import from SOLIDWORKS, followed by an analysis of the spindle's stress-strain state using ANSYS. Often, spindle researchers use multi-node bar models with three degrees of freedom at each node. For these models, the dynamic characteristics at natural frequencies and modes of vibration of the spindle are carried out, taking into account the changing load. Authors often follow the path of simplifying the original 3D model (removing chamfers and small holes, and other structural elements) when converting 3D file formats between SOLIDWORKS and ANSYS.

An integrated approach to assessing the indicators of rigidity and vibration resistance is presented in [4]. The idea of a modular modeling system based on information about the forming units: spindle-tool and table-workpiece are proposed. The universality of such a structure for presenting information is provided by analytical models and arrays of experimental data, concentrated in the databases' corresponding sections. This article [4] identifies critical parameters and associated constraints based on the data embedded in the database on the characteristics of machine elements' dimensions and rigidity, coordinate matrices, and node vectors. Simultaneously, the issues of the optimal ratio of the spindle size and the tooling component to maximize rigidity and the relationship with the finite element analysis procedure are not addressed in this work.

A promising approach is an approach to constructing the static formula for s_f of the spindle, presented in [5]. This approach is effective when using unified spindle units equipped with a wide range of modular tooling. Simultaneously, the authors considered one variant of loading with a single cantilever force without considering various loading schemes, particularly the forces in the gearing "gearbox output shaft – spindle".

2 Literature Review

The research of the spindle units' structures of metal-cutting machines according to the criterion of rigidity and the influence of technological tooling on design decision-making is widely presented in the machine-tool literature.

In [6], determining the accuracy of the technological operation of boring holes when changing the dimensional parameters of the spindle unit (SpU) and its rigidity is considered. When obtaining an analytical expression for the SpU compliance, considering the spindle's deflection and its supports, the value of the restraint force in the front support

was taken into account. The advantage of this work is to consider the variety of boring machine tool designs. Simultaneously, as is known, the parameters of their matching (joint) also affect the level of deformations of the “boring bar – boring cutter” assembly, which in turn affects the rigidity of the forming spindle unit. It is an aspect of the influence of tooling that is not considered in this work. Information about the features of the influence of duplexed angular contact ball bearings and, in particular, the consideration of their angular compliance on the stiffness of the SpU as a whole is also not given.

The work [7] considers the nature of the relationship between the stiffness characteristics of the forming units of multi-operational machines of the drilling-milling-boring type for processing accuracy. Of interest is a new approach associated with the study of the space of change in static stiffness by introducing the concept of “generalized stiffness”, covering the machine tool’s entire working area. The authors implement the procedure for forming 3D and parametric models on the scale of multi-axis processing space. This achieves an effective procedure for assessing and predicting possible processing errors. Nevertheless, at the same time, the procedure for changing the technological tool is not presented in work. The task of finding the ratio of the dimensions for the inter-support part of the spindle and the cantilever part, reflecting the dimensions of the technological tooling, providing minimal deformations of the forming unit, is not posed either. The same approach to assessing stiffness is used in [8] but without advanced 3D modeling and parameterization tools.

The great opportunities in terms of automation of the main procedures for evaluating structures by the stiffness criterion are provided by the integrated CAD APM WinMachine [9, 10], which includes the APM Structure3D module – a module for calculating the stress-strain state, stability, natural and forced vibrations of parts and structures by the finite element method [11]. In this system, a more efficient procedure is proposed for determining the stiffness of structural supports considering linear and angular compliance.

Based on the analysis carried out, the task of this study can be formulated as follows: To develop an analytical toolkit for assessing the stiffness of a double-bearing spindle assembly and the choice of the optimal ratio of the sizes of its elements using various types of technological equipment in the environment of the APM Structure-3D module.

3 Research Methodology

3.1 Determination of the Spindle-Tooling Structure Stiffness

Consider a variant of combined loading of a unified two-bearing spindle unit (Fig. 1) for a multi-purpose lathe mounted on duplexed angular contact ball bearings 4-46209 and 4-46112, mounted according to the “tandem-O” scheme with a spring-type preload (rear support) and a preload using two spacers for duplexed front support [12, 13].

Let us consider the problem of calculating the rigidity of the spindle unit’s structure (spindle-modular tooling) of the main motion drive for a multi-operational lathe (for example, model MS03), the structural diagram of which is shown in Fig. 1b.

This spindle unit design can be presented in the form of a constant cross-section beam on two hinged supports, the design diagram of which is shown in Fig. 1c.

At the same time, the rolling bearings on the rear (r) and front (f) bearings have finite stiffness, and their action in the design scheme can be conditionally replaced by springs with stiffness j_r and j_f (the springs can perceive both compressive and tensile stresses). This assumption is in good agreement with practice if the bearings are preloaded. The rigidity of bearings 4-46112 GOST 831-75 (front support) and 4-46209L GOST 831-75 (rear support) can be determined analytically or graphically. Using the graph [1], we determine the rigidity of the above duplexed angular contact bearings: $j_r = 8.8 \cdot 10^4$ N/mm – for bearings 4-46209L; $j_f = 9.2 \cdot 10^4$ N/mm – for bearings 4-46112.

The radial compliance A of the rear and front supports will be $A_r = 0.113 \cdot 10^{-4}$ mm/N and $A_f = 0.109 \cdot 10^{-4}$ mm/N, respectively. The radial compliance of support consisting of several angular contact ball bearings is determined by the formula [1] and is $0.652 \cdot 10^{-5}$ mm/N. The presence of a preload $P_{pl} = 930$ N in the front support, following the recommendations [1], increases the rigidity by 15–20%; in this case, the front support A_f 's compliance $0.522 \cdot 10^{-5}$ mm/N.

To determine the analytical model for assessing the spindle unit's compliance with the MS03 machine tool, we will use the method of initial parameters in the matrix formulation [5, 14]. According to the proposed design scheme, the SpU is represented as a statically indeterminate elastic system “spindle-cantilever” (S-C) on two supports that have linear $\{A_r; A_f\}$ and angular $\{a_r; a_f\}$ by compliances with 4 unknowns: reactions in the rear and front support $\{R_r; R_f\}$ and corresponding reaction moments $\{m_r; m_f\}$ in these supports.

To assess the characteristics of the spindle unit's compliance considering the size of the machine working area, the program was developed in the mathematical environment “Maple”. Using the kernel of symbolic mathematics, a static form was obtained $s_f = f(l_k)$ for various cantilever lengths l_k of the spindle unit (e.g., multi-operational machine MS03).

We represent the mathematical model of the S-C system in the form of a matrix Eq. (1):

$$\begin{bmatrix} 1 & 1 & 0 & 0 \\ l + l_1 & l_1 & -1 & -1 \\ A_r - \frac{l^3}{6EI} & -A_f & a_r l + \frac{l^2}{2EI} & 0 \\ \frac{-l^2}{2EI} & 0 & a_r + \frac{l}{EI} & -a_f \end{bmatrix} \times \begin{bmatrix} R_r \\ R_f \\ m_r \\ m_f \end{bmatrix} = \begin{bmatrix} R' \\ -R' l_k \\ 0 \\ 0 \end{bmatrix}, \quad (1)$$

where l – inter-support distance, mm; l_1 – length of the cantilever part of the spindle, mm; l_k – length of the cantilever (modular equipment and workpiece), mm; E – elastic modulus of structural steel – Steel 20X, $E = 2.1 \cdot 10^5$, MPa; I – a moment of inertia of the spindle cross-section, mm^4 ; R' – the unit force applied at the cutting point, N.

With the help of the above-developed program in the Maple environment, a static formula for s_f of the SpU machine model MS03 was obtained, presented in the form of an analytical dependence of the spindle compliance (taking into account the support compliance) on the length of the cantilever:

$$s_f = 0.29 \cdot 10^{-4} + 0.332 \cdot 10^{-6} l_k + 0.507 \cdot 10^{-8} l_k^2. \quad (2)$$

The resulting analytical formula is an effective toolkit for determining and modeling the characteristics of rigidity within the machine's working space. A similar approach for

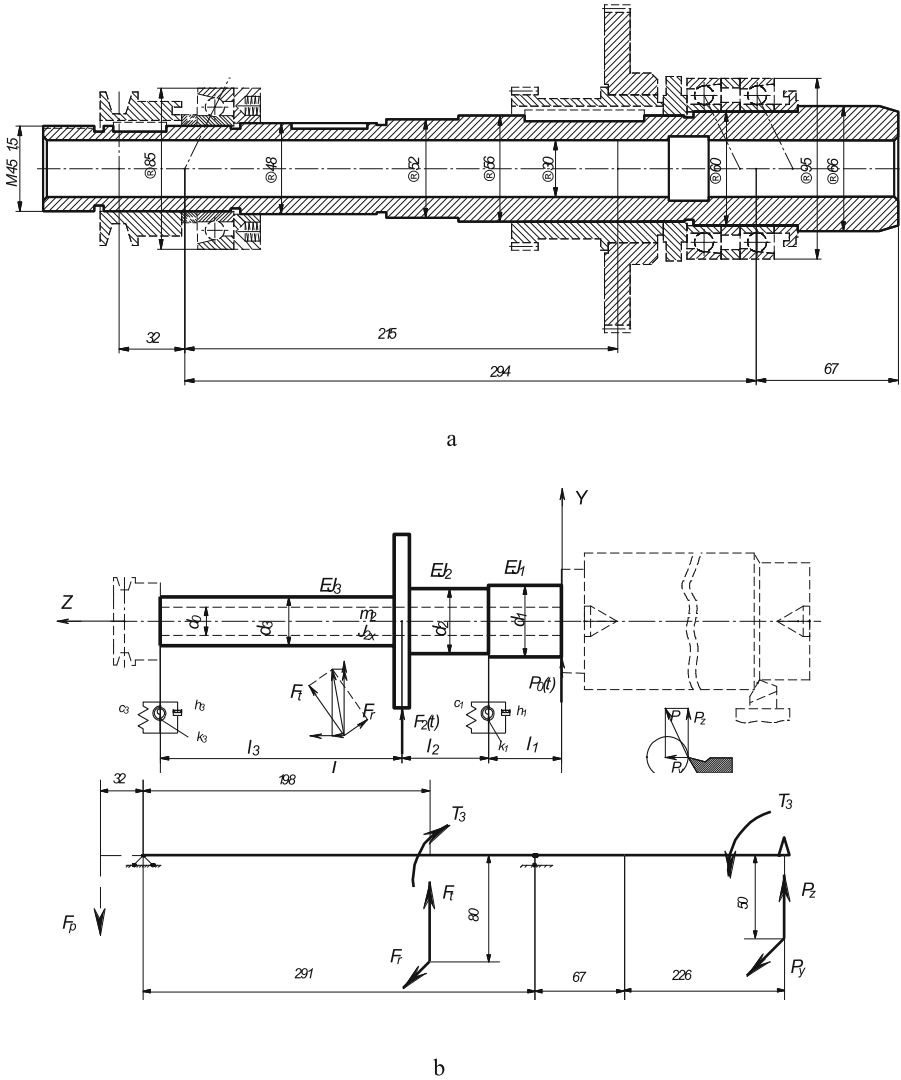


Fig. 1. Spindle unit: a – spindle design; b – structural diagram of the spindle with tooling.

the problem of optimizing the design of a fixture for multi-axis processing of lever-type parts with statistical and modal analysis is presented [15]. The resulting static formula for s_f becomes promising in the problem-oriented analysis of complex details [16, 17].

3.2 Finding the Optimal Ratio of Spindle and Cantilever Sizes

A specific reserve of the spindle structure’s rigidity can be formed depending on the ratio of its main parameters: the inter-support (spindle span) distance l and the span diameter d_0 [18, 19].

Let us consider the option of loading the spindle's cantilever on two supports by the force P . The displacement of the spindle end caused by the deformation of its supports can be represented as [1, 20]:

$$y_1 = \delta_f \left(1 + \frac{l}{l_1}\right) + \delta_r \left(\frac{l}{l_1}\right), \quad (3)$$

where δ_f, δ_r – deformations, respectively, of the front and rear spindle bearings.

Having introduced designations $\lambda = \frac{l}{l_1}$, characterizing the relative span length, the deformations of the supports can be written as:

$$\delta_f = \frac{P(\lambda + 1)}{\lambda \cdot j_f}; \quad \delta_r = \frac{P}{\lambda \cdot j_r}, \quad (4)$$

where j_f, j_r – stiffness's of the front and rear supports, respectively.

Then expression (3) takes the form: $y_1 = \frac{P}{j_f} \cdot \frac{(\lambda+1)^2}{\lambda^2} + \frac{P}{j_r} \cdot \frac{1}{\lambda^2}$.

The deflection of the spindle end as an elastic beam can be represented as:

$$y_2 = \frac{Pl_1^2 l}{3E \cdot j_r} + \frac{Pl_1^3 l}{3E \cdot j_f} = \frac{P}{j_0} \left(1 + \lambda \frac{j_f}{j_r}\right), \quad (5)$$

where $j_0 = \frac{3Ej_f}{l_1^3}$ – conditional stiffness of the spindle cantilever.

Summing up the elastic displacements of the spindle end, we obtain the overall compliance of the spindle unit:

$$\delta = \frac{1}{j} = \frac{(\lambda + 1)^2}{j_f \lambda^2} + \frac{1}{j_r} \cdot \frac{1}{\lambda^2} + \frac{1}{j_0} \left(1 + \lambda \frac{j_f}{j_r}\right). \quad (6)$$

For spindles on rolling bearings, additional constraints are introduced on the smallest distance between the supports ($\lambda_{min} \geq 2.5$) since the runout of the bearings with a further decrease in the inter-support distance increases the runout of the spindle end [1, 21]. This stiffness limitation allows the use of an approximate ratio between the diameter (average) of the spindle span d_0 and its inter-support distance l .

Let us consider the procedure for determining the optimal ratio of the cantilever's lengths and inter-support parts. This machine's spindle is a hollow shaft with an average outer diameter $d_0 = 60$ mm and an inner diameter d_i loaded with a cantilever force $P = 400$ N.

The optimization problem involves considering the spindle as beams on two supports with a preload, which are conditionally replaced by springs. The optimization problem in this formulation is limitation two processing methods: for turning and boring operations.

Using the core of symbolic mathematics in the MAPLE environment, we define the displacement of the spindle's end due to the deformation of its supports, which can be represented as follows: $y_1 = \frac{0.001668(\lambda+1)^2}{\lambda^2}$.

The deflection of the spindle's end as an elastic beam can be represented as: $y_2 = 0.0008533 + 0.000547 \cdot \lambda$. The total compliance of the spindle assembly, reduced to the cantilever part, will be:

$$\delta = \frac{0.001668(\lambda + 1)^2}{\lambda^2} + \frac{0.001668}{\lambda^2} + 0.000853 + 0.000547 \cdot \lambda. \quad (7)$$

The components of compliance and the general compliance of the designed spindle unit are shown in Fig. 2.

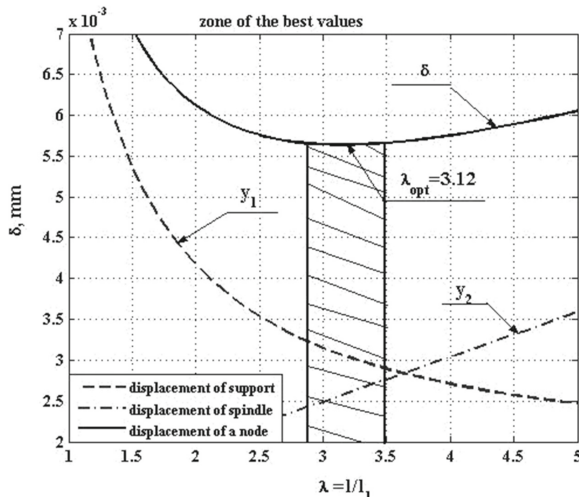


Fig. 2. The optimal ratio of the spindle sizes.

Analysis of the results obtained shows the presence of a significant reserve of rigidity (the maximum deflection on the spindle's cantilever (Fig. 1) is $y_{max} = 0.027$ mm, and the angle of rotation of the cantilever section is 0.0289 rad). In this case, the deflection arrow on the inter-support part at $[y] = 0.0003 \cdot l$ should not exceed $[y_{max}] = 0.0873$ mm. The permissible rotation angle of the spindle's end must not exceed $[\theta] = 0.0572^\circ$.

Similar numerical values of compliance are also obtained due to calculations using the APM Shaft module [10].

The practical implementation of the results obtained was carried out for a multifunctional lathe in analytical models for determining the rigidity of the elastic spindle-workpiece system with a variable length of the overhang of modular equipment workpiece. These results are most typical for turning parts such as bodies of rotation and boring holes when using special boring bars.

4 Result

Simultaneously, the APM Shaft module cannot take into account the angular compliance of the spindle unit, which affects the deformation parameters of the designed structure [22, 23].

For effective modeling, calculation of the stress-strain state, taking into account the supports' angular compliance, we use the module for complex analysis of three-dimensional structures APM Structure3D [8]. In the process of modeling, a "skeleton" model of the spindle structure is created (Fig. 3). In this model, the boundaries of the bar elements are determined by the nodes at those points where the load or the bending

stiffness of the section changes are applied. Each bar has specific dimensions and is connected with nodes to the rest of the structure bars.

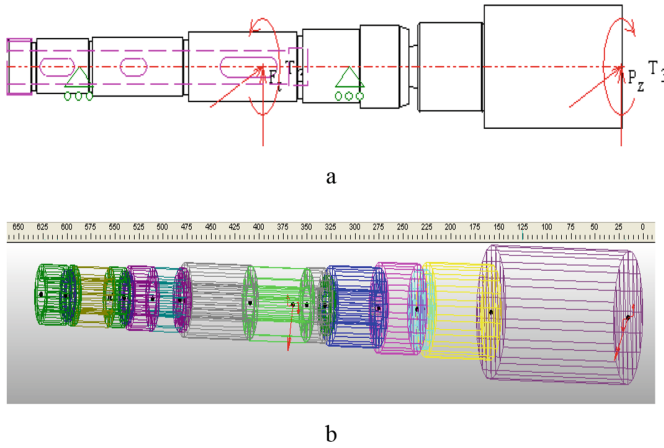


Fig. 3. Skeleton model of the spindle structure.

The spindle assembly is divided into various types of sections associated with various functional elements, including spline and keyway connections, different shapes of grooves and chamfers, fillets. The APM Structure-3D module used operates with various shapes of arbitrary cross-sections, including multiply connected. This is an expandable section library into which custom cross-sections can be added. For the spindle skeleton model being created, a parametric model of a spline straight-sided section of the middle series was built, which was entered into the library.

The picture of the spindle's general loading is formed from several types of force factors that differ in magnitude and mode of action. For these purposes, a special auxiliary toolkit – “Loading” has been introduced in the APM Structure-3D module. With the help of this toolkit, an abstract part of the load space is allocated in the spindle into which a part of the force factors acting on the elements of the model is placed.

A feature of specifying supports is the ability to combine the rigid and elastic fastening, each of which is an entirely different object. They will work together when they act in different directions of the coordinate system at the node. In the rigid restraint mode, by turning on the checkboxes in the fields of displacement in the direction of the axis, restrictions on displacement in the direction of the X and Y and rotations around the same axes should assign.

Calculation in the APM Structure3D environment (Fig. 4) allows one to show the stress field specific for a typical turning operation performed on a multipurpose machine MS03 and stress distribution in the i -th section of the spindle.

Following the color scale (Fig. 4, a), the maximum values of the equivalent stress SVM (according to the energy theory of strength) do not exceed the permissible yield stresses ($[\tau] = 635$ MPa for the spindle's material of the steel DIN 20Cr4), even with a yield factor $k_\tau = 2$.

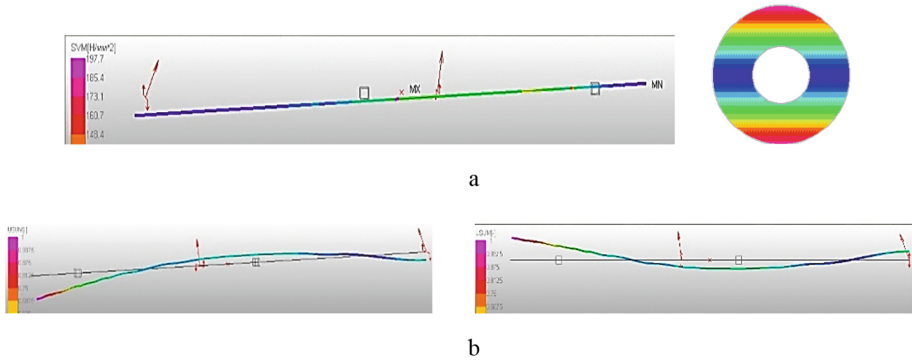


Fig. 4. The stress field of the machine spindle MS03.

In the APM Structure 3D module, estimates of the dynamic quality of functioning are effectively calculated [24]. These estimates are associated with the determination of natural frequencies and the corresponding natural vibration modes. The APM Structure 3D module performed by default the calculation for 16 natural frequencies and forms with an accuracy of 0.01%. In Fig. 4b shows the 3rd and 4th natural forms, describing the spindle model's configuration, oscillating with the corresponding frequencies.

5 Conclusion

A procedure for determining the stress-strain state of structures of double-bearing spindles of multi-operation lathes equipped with a set of modular equipment has been developed. Constructive and design schemes of the spindle assembly have been formed.

An analytical procedure for constructing static formulas of spindle nodes in the Maple environment, reflecting the flexibility of the spindle and cantilever parts (modular equipment) has been implemented. A numerical solution was obtained using the example of a machine model MC03: $s_f = 0.29 \cdot 10^{-4} + 0.332 \cdot 10^{-6}l_k + 0.507 \cdot 10^{-8}l_k^2$. On this basis, the level of deformations of the node under consideration was determined in express mode at various lengths of the cantilever part.

The optimal ratio of the parameters: the lengths of the inter-support and cantilever parts of the spindle, which minimizes the overall flexibility of the assembly, is found. The analysis of the results obtained showed that there is a significant reserve of rigidity for the optimal ratio of these two parameters (the maximum deflection on the spindle console is $y_{max} = 0.027$ mm, and the angle of rotation of the cantilever section is 0.0289 rad).

The modeling and calculation of the stress-strain state were performed considering the linear and angular compliance of the supports in the module's environment for complex analysis of three-dimensional structures APM Structure-3D. An essential feature of modeling in APM Structure-3D has been noted, combining rigid and elastic fastening in one support.

References

1. Avramova, T.M., Bushuev, V.V., Gilova, L.Y.: Handbook on Metal-Cutting Machine Tools. Mechanical Engineering, Moscow (2012)
2. Li, J., Song, Y., Liu, Y.: Development of post-processing system for three types of five-axis machine tools based on solid model. In: ASME 2017 12th International Manufacturing Science and Engineering, vol. 3, pp. 118–132 (2017)
3. Kong, J., Cheng, X.: Modal analysis of CNC lathe's spindle based on finite element. *Adv. Eng. Res.* **148**, 318–321 (2017)
4. Brecher, C., Fey, M., Daniels, M.: Modeling of position-, tool- and workpiece-dependent milling machine dynamics. *High Speed Mach.* **2**, 15–25 (2016)
5. Popov, V.A., Loktev, V.A.: Dynamics of Machines. Technique, Kyiv (1975)
6. Saninskij, V.A., Rjabova, K.L., Platonov, Y., Osadchenko, E.N.: Effect of rigidity and geometric parameters of the spindle pinol assembly on the accuracy of boring of coaxial holes. *Mod. Prob. Sci. Educ.* **4**, 15–21 (2013)
7. Gao, X., Li, B., Hong, J., Guo, J.: Stiffness modeling of machine tools based on machining space analysis. *Int. J. Adv. Manuf. Technol.* **86**(5–8), 2093–2106 (2016). <https://doi.org/10.1007/s00170-015-8336-z>
8. Ugrinov, P.: Rigidity of machining centers of medium size. *Autom. Control Mech. Eng.* **5**, 43–47 (2001)
9. Krol, O., Sokolov, V.: 3D modelling of angular spindle's head for machining centre. *J. Phys. Conf. Ser.* **1278**, 012002 (2018)
10. Zamriy, A.A.: Design and Calculation by the Finite Element Method in the APM Structure 3D Environment. APM, Moscow (2010)
11. Neduzha, L., Shvets, A.: Application of APM winmachine software for design and calculations in mechanical engineering. *Sci. Prog. Transp.* **2**(62), 129–147 (2016)
12. Krol, O., Sokolov, V.: Parametric modeling of transverse layout for machine tool gearboxes. In: Gapiński, B., Szostak, M., Ivanov, V. (eds.) MANUFACTURING 2019. LNME, pp. 122–130. Springer, Cham (2019). https://doi.org/10.1007/978-3-030-16943-5_11
13. Yakovenko, I., Permyakov, A., Prihodko, O., Basova, Y., Ivanova, M.: Structural optimization of technological layout of modular machine tools. In: Tonkonogyi, V., et al. (eds.) InterPartner 2019. LNME, pp. 352–363. Springer, Cham (2020). https://doi.org/10.1007/978-3-030-40724-7_36
14. Brecher, C., Bäumlner, S., Daniels, M.: Prediction of dynamics of modified machine tool by experimental substructuring. In: Allen, M., Mayes, R., Rixen, D. (eds.) Dynamics of Coupled Structures, Volume 1. CPSEMS, pp. 297–305. Springer, Cham (2014). https://doi.org/10.1007/978-3-319-04501-6_28
15. Ivanov, V., Dehtiarov, I., Pavlenko, I., Liaposhchenko, O., Zaloga, V.: Parametric optimization of fixtures for multiaxis machining of parts. In: Hamrol, A., Kujawińska, A., Barraza, M.F.S. (eds.) MANUFACTURING 2019. LNME, pp. 335–347. Springer, Cham (2019). https://doi.org/10.1007/978-3-030-18789-7_28
16. Ivanov, V., Dehtiarov, I., Pavlenko, I., Kosov, M., Hatala, M.: Technological assurance and features of fork-type parts machining. In: Ivanov, V., et al. (eds.) Advances in Design, Simulation and Manufacturing II. DSMIE-2019. LNME, pp. 114–125. Springer, Cham (2020). https://doi.org/10.1007/978-3-030-22365-6_12
17. Ivanov, V., Pavlenko, I., Zaloga, V., Liaposhchenko, O., Pirogov, D.: Technological features of locating charts in fixture design. In: Karabegović, I. (ed.) NT 2020. LNNS, vol. 128, pp. 66–74. Springer, Cham (2020). https://doi.org/10.1007/978-3-030-46817-0_7
18. Vasilkov, D.V., Weitz, V.L., Shirladze A.G.: Electromechanical drives of metalworking machines. In: Calculation and Design: Textbook. Polytechnic, SpB (2011)

19. Khomyakov, S., Kochinev, N., Sabirov, F.: Simulation and experimental study of the dynamics for spindle nodes characteristics. *Izvestiya TSU* **3**, 251–258 (2011)
20. Chermensky, O., Fedotov, N.: Rolling bearings. Mechanical Engineering, Moscow (2003)
21. Gasanov, M., Kotliar, A., Basova, Y., Ivanova, M., Panamariova, O.: Increasing of lathe equipment efficiency by application of gang-tool holder. In: Gapiński, B., Szostak, M., Ivanov, V. (eds.) *MANUFACTURING 2019. LNME*, pp. 133–144. Springer, Cham (2019). https://doi.org/10.1007/978-3-030-16943-5_12
22. Kurov, A.V.: Modeling and engineering analysis of overhead crane structures using APM WinMachine. *Polytech. Youth J. MSTU N.E. Bauman* **72**(17), 1–9 (2017)
23. Urbikain, G., Campa, F., Zulaika, J.: Preventing chatter vibration in heavy-duty turning operations in large horizontal lathes. *Sound Vib.* **340**, 317–321 (2015)
24. Türkeş, E.: Chatter stability analysis approach for stability analysis of rotating machinery vibrations. *J. Eng. Sci.* **3**, 1–17 (2017)



Technological Inheritability of Product Material Using the Criterion of Technological Damageability

Yaroslav Kusyi^(✉) 

Lviv Polytechnic National University, 12, Bandera St, Lviv 79013, Ukraine
jarkym@ukr.net

Abstract. Product Life Cycle Support (PLS) becomes a priority direction in mechanical manufacturing. That realize by providing the rational operational parameters and reliability indicators for manufactured machines and their products. The PLS - concepts are an effective tool for the development of functionally-oriented technological processes. The prediction of the product behavior during exploitation using technological inheritability of its properties is an important problem for modern mechanical manufacturing. The technological damageability is proposed to estimate the technological inheritability of material properties during manufacturing products from castings. Analyzing of material degradation of manufactured products using the LM-hardness method is suggested. LM-hardness method, used for control of the dissipation of the material's mechanical properties, received by means of special devices in fixed conditions. In general, the degree of the material degradation of manufactured products is described using the Weibull coefficient (m). For the first time, it was proposed technological damageability D for analyzing of degradation of the products material structure for castings in sand molds. The influence of the design parameters of the "Sandvik" tool during end milling on the technological inheritability of material properties using the distribution of Weibull coefficient (m) is analyzed.

Keywords: Technological inheritability · Homogeneity · Technological damageability · Weibull coefficient

1 Introduction

Technological providing operational characteristics and prediction of reliability indicators of products when designing the functionally-oriented technological processes is an important and priority task of mechanical engineering manufacturing [1, 2]. The Product Life Cycle Support is closely related to the functionally-oriented technologies for the technological process design [3, 4].

Functionally-oriented technological process (FOTP) or functionally-oriented technology is a rational technological process that aims at providing the most important and necessary operational characteristics of the mechanical engineering product in compliance with the scheduled parameters of accuracy and the characteristics of surface

engineering of product assigned by the designer. Solution of this important problem is possible using the automated control of the technological process and careful analysis of the whole technological chain from a blank to a final product from technological heredity and inheritability, by the system-integrated CAD/SAE/CAPP/CAM software products [3]. When designing the FOTP, the substages of the Life Cycle of a Product: design and technological preparation of production are intensified. This is necessary to obtain the desired positive result from the standpoint of cost/reliability during the design of FOTP in the customer-manufacturer chain [4].

The technological process as an operational unit of the production process has an important and decisive influence on the set of the quality parameters of mechanical engineering products starting from the initial blank production to the final product with regulated technical characteristics [5]. However, the relations between technological parameters, modes of surface engineering, operational parameters, and reliability indicators are complex and difficult to predict (Fig. 1) [6]. In many cases, the process of formation and transformation of the necessary operational characteristics and reliable indicators of the mechanical engineering product at the stage of its development and production can lead to the most adverse conditions to the product fracture at the stage of its operation [7, 8].

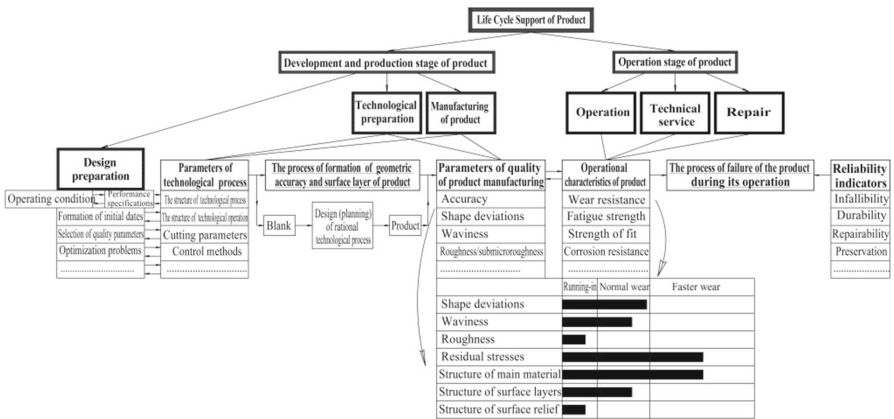


Fig. 1. Relations between technological parameters, modes of surface engineering, operational parameters, and reliability indicators.

An initial blank produced by casting, forging, press forming, etc., is a reference link of the technological process [9]. However, the importance of blanking production in the manufacturing process structure is not sufficiently considered when the influence of technological inheritability on the final product’s quality parameters and operational characteristics is analyzed [10]. The performed investigations [11] showed that the material structure and initial properties of blanks were closely related to the inheritability of liquid metal alloy. Previous studies explained that about 75% of workpiece quality properties are achieved during pouring and crystallization of the liquid alloy during cooling in the mold. Only 25% of numbers of properties of initial raw materials are transferred to the workpiece during machining or finishing treatment [10, 11].

On the other hand, the rational modes of surfaces machining in the technological process contribute to forming the necessary operational parameters and reliability characteristics of the product [11, 12]. They also minimize the initiation and transformation of technological defects at the stage of its development and production, transforming into technological damages at the stage of its operation [13].

Technological providing of the necessary operational characteristics and predicted reliability indicators of mechanical engineering products requires a complex systematic approach, which consists not only in the investigations of real physical processes in the product material at submicroscopic, microscopic, and macroscopic levels but also in their step-by-step tracking at all substages and stages of the Life Cycle of a Product from the position of the technological inheritability [9, 14].

Technological inheritability is a complex process of transferring the properties of product material from previous technological operations to subsequent ones. Preservation of these properties of the product material is called technological heredity. The system principle of the Product Life Cycle Support from the position of the technological inheritability requires a direct and rational connection of technological preparation of production with the stage of operation with not step-by-step, but parallel and coordinated work of technologist and designer. Therefore, the operations of technological processes of manufacturing machine parts must be considered with the help of structural units of the technological chain, from the production of initial blanks to finished products in the formation of their final operating parameters [8, 10].

2 Literature Review

The irrational technological process causes inadmissible failures of the mechanical engineering product. They are classified into three main groups (Fig. 2) [7].

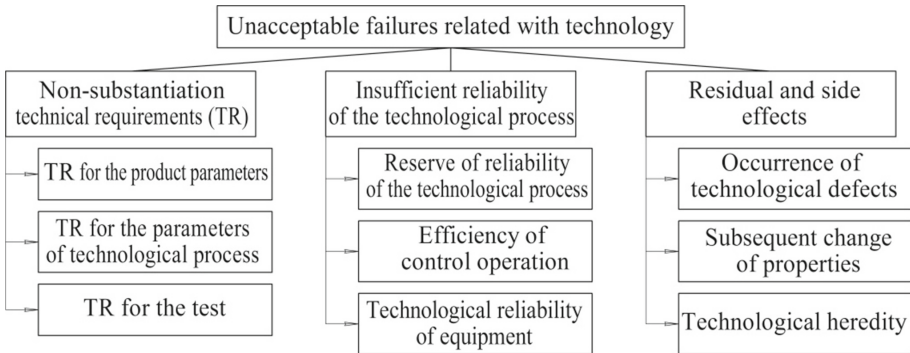


Fig. 2. Classification of impermissible failures that were formed during product manufacturing.

The first group of unacceptable failures is closely connected, first of all, with shortcomings of the designer’s work. Such shortcomings are embedded in the mechanical engineering products at the substage of technological preparation of production. They

are implemented during their manufacturing at product development and production (Fig. 2) [7].

The second group of unacceptable failures is closely related to the insufficient reliability of the structural elements of the technological environment. The technological environment is a set of necessary technological objects that interact with the studied technological object at a certain stage of manufacturing of mechanical engineering parts and/or assembly of the machine (Fig. 2) [7].

The third group of impermissible failures needs the most investigations. This group [7] is closely related to technological process imperfections using the indicator of technological inheritability (Fig. 2). It is worth noting that all subgroups of group III are interconnected. The processes of initiation and formation of defects at the stage of product development and production due to the phenomenon of technological inheritability of material properties can have two development options. According to the first option, the initiation and formation of defects can progress and transform into damage during operation. According to the second option, their impact can be minimized or even completely eliminated due to the technological process's optimal blank and rational structure.

Inheritability of product properties during its manufacturing is most often described using the graph theory.

The quality parameter on the p -th technological operation is determined by introducing the coefficients of technological inheritability [5]:

$$R_1 = a_1 \cdot R_0^{b_1}, \dots, R_{p-1} = a_{p-1} \cdot R_{p-2}^{b_{p-1}}; R_p = a_p \cdot R_{p-1}^{b_p}, \tag{1}$$

where $R_0 \dots R_p$ is a set of quality parameters of mechanical engineering product; $a_1, b_1, \dots, a_{p-1}, b_{p-1}, a_p, b_p$ are coefficients of technological inheritability according to the sequence of operations of the certain technological process.

According to (1), the current state of a certain link in the technological chain is described by the coefficients of technological inheritance, which relate to the functional relationships between technological modes and quality parameters of products. These coefficients are obtained by transforming the regression dependencies found by the methods of experiments planning [5]:

$$R_p = a_p \cdot a_{p-1}^{b_p} \cdot a_{p-2}^{(b_p \cdot b_{p-1})} \cdot \dots \cdot a_1^{(b_p \cdot b_{p-1} \cdot \dots \cdot b_1)} \cdot R_0^{(b_p \cdot b_{p-1} \cdot \dots \cdot b_1)}. \tag{2}$$

From formula (2), it follows that a set of final parameters of product quality are closely related to the parameters of initial blank quality through a set of coefficients of technological inheritability.

But the determination of all coefficients of technological inheritance greatly complicates the work of the technologist.

Consider the complex relationships between the technological process parameters, the parameters of processing quality, operational characteristics, and reliability indicators from the position of technological inheritability of material properties (Fig. 3).

The Life Cycle of a Product (LCP) consists of two stages: the product's development and production stage and operation stage. The substages of design preparation, technological preparation of production, and the substages of product manufacturing are part of the stage of development and production. The stage of operation provides the using, technical service, and repair of the product (Fig. 3) [10].

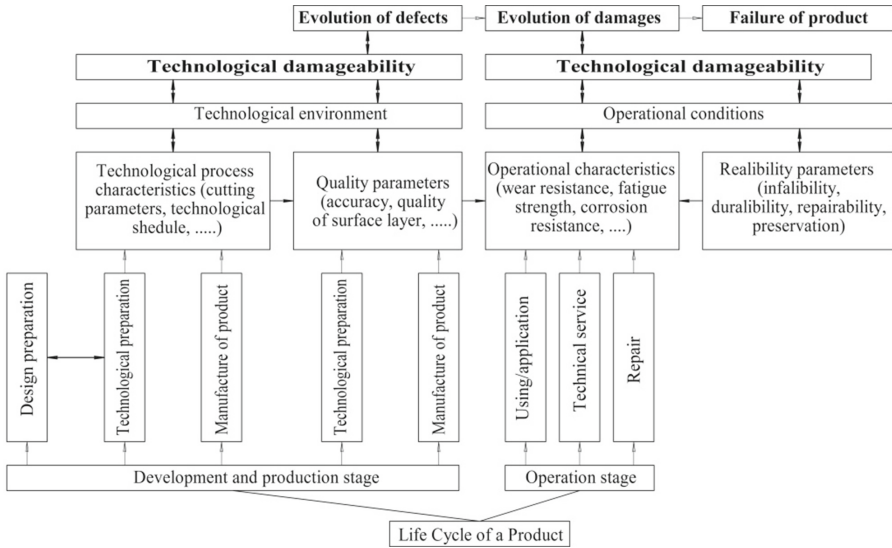


Fig. 3. Analysis of LCP using damageability of material properties.

At present, there isn't any parameter that could characterize in detail the whole technological chain of product manufacturing. In my opinion, the technological inheritability of the properties of products at all substages and stages of their Life Cycle should be analyzed using their technological damageability.

In the general case, single damage is a process of a pronounced and uneven change in the geometric state of the friction surfaces of the product, the structure, and properties of the surface layers of the material. Damage is the main result of damage, manifested in negative changes in structure, macrogeometric characteristics, properties, and stress-strain state of the product surface layers. On the other hand, the analysis of Product Life Cycle Support shows that single damage results from its operation due to the "revival" of defects formed at the stage of development and production [13].

The properties of the blanks and the forming technological environment determine the product's properties (machine). The technological environment is the carrier of the mechanism of inheritability and transformation of the properties of products in the process of their manufacture, which is shown in Fig. 3.

Technological damageability combines the technological providing of the technological process from one side and the evolution of defects/damage on the other [11].

In product manufacturing, defects occur depending on the type of blank, processing modes, control methods, the degree of automation, etc. There are typical types of defects for each technological process, as a rule, associated with a violation of the technological process or an unfavorable combination of factors. The initiation, formation, and development of defects result from the technological process of manufacturing the product, and damage is a consequence of its operation (Fig. 3) [13].

According to traditional machine-building production, machining by cutting has a significant impact on the performance of products.

However, the technological providing the product performance is a priority task to prevent damage of the product during its Life Cycle [15, 16].

Analyzing the technological damageability of the mechanical engineering product throughout the technological chain, it is possible to predict the probability of its failure at a specific time and for specific operating conditions [13].

The processes of defects development and their transformation into damages from the stage of development and production to the stage of operation of the Life Cycle of a Product are multi-scale and multi-stage. They develop simultaneously at all levels: submicroscopic, microscopic, and macroscopic. This means a combination of different types of models. Multi-stage processes require new approaches and techniques to provide operational characteristics and reliability indicators depending on the operating conditions of the product [11].

Also, the use of rational criteria for the analysis of real physical processes during the manufacture of the product can make technical problems more efficient [10].

We can investigate the change in technological damageability for the entire technological chain and obtain a step-by-step analysis of the technological inheritance of the product material properties. But in some cases, we can investigate the change of technological damageability for some operations of the technological route to obtain a partial analysis of the technological inheritance of the material properties of a certain part of the technological chain.

3 Research Methodology

3.1 Methods of Research

Determination of technological damageability has its characteristics for different types of blanks. The formation of the structure of castings is a complex process. Therefore the method of calculating the technological damageability for castings is suggested.

In modern mechanical manufacturing, in solving applied problems, LM-hardness, developed under the guidance of Academician A.O. Lebedev, provides high efficiency, is used. A critical feature of the LM-hardness method is scattering the parameters of the product's material instead of its raw parameters. The proposed method is easiest for implementing in mechanical manufacturing, using hardness for control of material degradation, the defined value used to assess product material properties [17] indirectly.

Time dependence of the "homogeneity" parameter integrally characterizes the material structure during statistical processing of the obtained experimental results of hardness measurements [18]. It is estimated through calculation of the Weibull coefficient called m [17]:

$$m = \frac{d(n)}{2,30259 \cdot S(\lg(H))}, \quad (3)$$

where $d(n)$ is a dependent parameter, the number of measurements n increases $d(n)$ value.

$$S(\lg(H)) = \sqrt{\frac{1}{n-1} \cdot \sum_{i=1}^n (\lg(H_i) - \overline{\lg(H)})^2}, \quad \overline{\lg(H)} = \frac{1}{n} \cdot \sum_{i=1}^n \lg(H_i). \quad (4)$$

Technological damageability D , defined here, allows assessing the degradation of the structure of the material of the product [11]:

$$D = 1 - m_i/m_{matr.}, \quad (5)$$

where m_i is the Weibull coefficient value for the i -th cross-section of the measurements; $m_{matr.}$ is the Weibull coefficient value for the main material.

Suppose we have a distribution of the homogeneity coefficient (m) along the entire cross-section of the sample. In that case, we can analyze the technological inheritability of material properties by the change of its technological damageability D using Eq. (5) (direct method). But suppose the Weibull coefficient (m) distribution along the entire cross-section of the sample is unknown. In that case, we must analyze the technological inheritability of material properties by the change of Weibull coefficient (m), which is indirectly related to technological damageability D (indirect method). In this case, we use Eqs. (3), (4). The large value of the Weibull coefficient (m) corresponds to a low level of scattering of hardness characteristics and a low degree of damageability; for the lower value of the homogeneity coefficient (m), vice versa, the degree of damage ability is higher.

3.2 Experimental Researches Planning

Experimental Samples

The blank size $165 \times 155 \times 20$ mm was cast in a traditional sand mold and used for experimental studies. The initial material was AK21M2.5H2.5 (GOST 1853-93).

Machine-Cutting Tools and Cutting Machine

End milling was used for machining the casting. End milling cutters were used with a diameter of $\emptyset 6$ mm, $\emptyset 8$ mm, $\emptyset 10$ mm, $\emptyset 12$ mm for rough and semi-rough milling. The experimental sample was machined on HAAS MINIMILL [10].

Technological Route and Cutting Conditions

It was planned 2 series of investigations for different machining of experimental samples. At first, the surface of the experimental sample was milled by all four end milling cutters for semi-rough milling. All four end milling cutters machined the sample surface for rough milling during the next stage. Hardness was controlled after each stage. The cutting parameters are selected according to the tool manufacturer's recommendations [3]. The cutting parameters consisted of cutting depth (t), feed per teeth (S_z), rotary speed (n), cutting speed (V). The cutting parameters were for $\emptyset 6$ mm: $t = 3.0$ mm, $S_z = 0.1$ mm/teeth, $n = 3100 \text{ min}^{-1}$, $V = 58.43$ m/min; for $\emptyset 8$ mm: $t = 3.0$ mm, $S_z = 0.1$ mm/teeth, $n = 4000 \text{ min}^{-1}$, $V = 100.53$ m/min; for $\emptyset 10$ mm: $t = 3.0$ mm, $S_z =$

0.1 mm/teeth, $n = 5800 \text{ min}^{-1}$, $V = 182.21 \text{ m/min}$; for $\varnothing 12 \text{ mm}$: $t = 3.0 \text{ mm}$, $S_z = 0.1 \text{ mm/teeth}$, $n = 5800 \text{ min}^{-1}$, $V = 218.65 \text{ m/min}$ [10].

The Device for Hardness Control

The device TP-5006 was used for hardness control. Loading value 588.4 N was applied with a ball $\varnothing 3.175 \text{ mm}$. 30 measurement samples were obtained in each experiment [10, 11].

The hardness of the surface layers was measured after each machining.

4 Results

We did not have a Weibull coefficient (m) distribution over the entire cross-section of the sample. Therefore, we analyzed the technological inheritability of material properties by changing the Weibull coefficient (m), which is indirectly related to the technological damageability D .

Mathcad 15 was used to calculate the Weibull coefficient (m) through Eq. (3) for obtained results of experimental research. The diagram $m = f(d_c)$ is presented in Fig. 4, where d_c is the diameter of the end milling cutter.

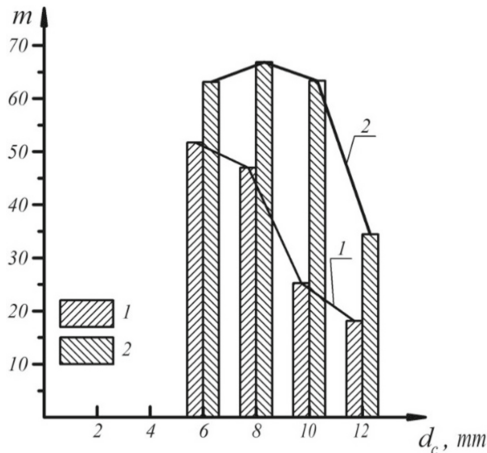


Fig. 4. Dependence of the homogeneity parameter (m) on the diameter of the end milling cutter: after rough (1) and semi-rough (2) machining.

Figure 4 shows the change in the technological inheritability of the properties of the product material by analyzing the technological damageability, starting with the first processing for the technological route.

After rough machining, an increase in the diameter of the end milling cutter (with increasing rotary speed n and cutting speed V) at the same feed on the tooth and the depth of cut leads to a decrease in the Weibull homogeneity coefficient (m). This is due to the increase in load characteristics and the intensification of the cutting process. This

indirectly indicates an increase in technological damageability after rough machining of the casting (Fig. 4).

After semi-rough machining, the Weibull homogeneity coefficient (m) increases for each end milling cutter. The removal explains the increase in the Weibull homogeneity coefficient (m) by cutting the defective layer (about 3 mm) after the first treatment – rough end milling. After semi-rough machining, the Weibull homogeneity coefficient (m) is stabilized for the end milling cutters of a diameter \varnothing 6 mm, \varnothing 8 mm, \varnothing 10 mm. But the Weibull homogeneity coefficient (m) increases about twice for the end milling cutter of a diameter of \varnothing 12 mm (Fig. 4).

5 Conclusions

For the first time, it was introduced technological damageability D parameter to assess the technological inheritability of material properties during the product manufacture from castings. The actual technological damageability D can be calculated by the known distribution of homogeneity coefficient (m) along the entire cross-section of the sample. Changes in the technological inheritability by the Weibull coefficient value (m) should be analyzed in other variants because the parameter of the damageability D is inversely proportional to the m .

The tool's design parameters influence the formation of technological damageability D of the product material for the first treatment – rough machining for the technological route of cutting. An increase in the diameter of the end milling cutters from \varnothing 6 mm to \varnothing 12 mm leads to a decrease in the Weibull homogeneity coefficient (m) from 51.70 to 18.15 for aluminum alloy AK21M2.5H2.5. This determines the increase in the technological damageability D . After the second treatment – semi-rough machining for the technological route, the Weibull homogeneity coefficient (m) increases for each end milling cutter. In this case, the technological damageability D decreases.

The obtained research results for mechanical engineering products showed a good correlation with the investigations of Academician A.O. Lebedev [10] for turbine manufacturing, aircraft and space industries, etc.

Further research should be performed for another material usable for mechanical engineering products and technological treatments, for example, milling and subsequent grinding, to implement the developed research method into mechanical manufacturing.

References

1. Denkena, B., Mörke, T., Krüger, M., Schmidt, J., Boujnah, H., Meyer, J., Gottwald, P., Spitschan, B., Winkens, M.: Development and first applications of gentelligent components over their life-cycle. *CIRP J. Manuf. Sci. Technol.* **7**(2), 139–150 (2014)
2. Gubaydulina, R.H., Gruby, S.V., Davlatov, G.D.: Analysis of the lifecycle of mechanical engineering products. *IOP Conf. Ser.: Mater. Sci. Eng.* **142**(1), (2016)
3. Stupnytskyy, V.: Features of functionally-oriented engineering technologies in concurrent environment. *Int. J. Eng. Res. Technol.* **2**(9), 1181–1186 (2013)
4. Stupnytskyy, V., Hrytsay, I.: Comprehensive analysis of the product's operational properties formation considering machining technology. *Arch. Mech. Eng.* **67**(2), 1–19 (2020)

5. Kheifetz, M.L., Gretskey, N.L., Prement, G.B.: Technological control of the heredity of operational quality parameters in the engine camshaft recovery. *Adv. Mater. Technol.* **1**, 12–20 (2019)
6. Kheifetz, M.L., Vasilyev, A.S., Klimenko, S.A.: Technological control of the heredity of operational quality parameters for machine parts. *Adv. Mater. Technol.* **2**(14), 8–18 (2019)
7. Aftanaziv, I.S., Shevchuk, L.I., Strohan, O.I., Kuk, A.M., Samsin, I.L.: Improving reliability of drill pipe by strengthening of thread connections of its elements. *Naukovi Visnyk Natsionalnoho Hirnychoho Universytetu* **4**, 22–29 (2019)
8. Lachmayera, R., Mozgovaa, I., Reimcheb, W., Colditzc, F., Mrozb, G., Gottwalda, P.: Technical inheritance: a concept to adapt the evolution of nature to product engineering. *Procedia Technol.* **15**, 178–187 (2014)
9. Jiang, Z., Tang, X.: Optimization of fixture flexibility for irregular geometries of workpiece based on metamorphic mechanisms. *Int. J. Adv. Manuf. Technol.* **103**, 325–342 (2019)
10. Kusyi, Y.M., Kuk, A.M.: Investigation of the technological damageability of castings at the stage of design and technological preparation of the machine Life Cycle. *J. Phys.: Conf. Ser.* **1426**, 012034 (2020). <https://doi.org/10.1088/1742-6596/1426/1/012034>
11. Kusyi, Ya., Stupnytskyi, V.: Optimization of the technological process based on analysis of technological damageability of casting. In: Ivanov, V., Trojanowska, J., Pavlenko, I., Zajac, J., Peraković, D. (eds.) *Advances in Design, Simulation and Manufacturing III. DSMIE-2020. Lecture Notes in Mechanical Engineering*, pp. 276–284. Springer, Cham (2020). https://doi.org/10.1007/978-3-030-50794-7_27
12. Fyodorov, V.P., Averchenkov, V.I., Nagorkin, M.N.: Controlling the parameters of the component quality using program means while performing mechanical machining. *Procedia Eng.* **150**, 899–905 (2016)
13. Lian, J., Sharaf, M., Archie, F., Münstermann, S.: A hybrid approach for modelling of plasticity and failure behavior of advanced high-strength steel sheets. *Int. J. Damage Mech.* **22**(2), 188–218 (2013)
14. Baurova, N.I., Zorin, V.A., Prikhod'ko, V.M.: Taking into account the factors of technological heredity by technological mechanics. *Polym. Sci. Ser. D* **9**(4), 402–406 (2016)
15. Fesenko, A., Basova, Y., Ivanov, V., et al.: Increasing of equipment efficiency by intensification of technological processes. *Periodica Polytech. Mech. Eng.* **63**(1), 67–73 (2019)
16. Franciosa, P., Gerbino, S., Ceglarek, D.: Fixture capability optimization for early-stage design of assembly system with compliant parts using nested polynomial chaos expansion. *Procedia CIRP* **41**, 87–92 (2016)
17. Lebedev, A., Golubovskii, E., Lokoshchenko, A., Muzyka, N., Lamashevskii, V., Shvets, V., Efimenkova, E.: Assessment of the limiting levels of dispersed damage in materials under steady-state conditions of static and cyclic loading. *Strength Mater.* **44**, 579–584 (2012)
18. Muzyka, N.R., Shvets, V.P.: Studies on the material damageability by the scratching method. *Strength Mater.* **48**(3), 394–400 (2016)



Wear Characteristics of Carbon and Tool Steels Hardened by Combined Laser-Ultrasonic Surface Treatment

Dmytro Lesyk¹ (✉) , Silvia Martinez² , Bohdan Mordyuk³ ,
Vitaliy Dzhemelinskiy¹ , and Aitzol Lamikiz⁴

¹ National Technical University of Ukraine “Igor Sikorsky Kyiv Polytechnic Institute”,
37, Peremohy Ave., Kyiv 03056, Ukraine

lesyk_d@ukr.net

² University of the Basque Country, 202, Bizkaia Science and Technology Park,
Zamudio 48170, Spain

³ G.V. Kurdyumov Institute for Metal Physics of the NAS of Ukraine, 36,
Academician Vernadsky blvd., Kyiv 03142, Ukraine

⁴ University of the Basque Country, Alameda Urquijo s/n, Bilbao 48013, Spain

Abstract. To increase the wear resistance of the subsurface layers, AISI 1045 carbon steel and AISI D2 tool steel samples were hardened by a laser heat treatment (LHT) followed by ultrasonic impact treatment (UIT). This paper focuses on studying the effects of the separately applied LHT, UIT, and combined LHT + UIT processes on the wear behavior of the hardened surface of carbon and tool steel. The comparison of the surface roughness and hardness after surface treatments are also addressed. The hardened samples were examined after the short-term (15 min), and long-term (45 min) wear tests under oil-lubricated conditions in the quasi-static and dynamic loading conditions. An optical 3D profilometer evaluated the wear tracks. The results demonstrated that the formed fine-grained martensitic structure coupled with high surface hardness and low surface roughness after combined treatment lead to a significant reduction of the wear loss regardless of the steel type.

Keywords: Laser hardening · Ultrasonic peening · AISI 1045 steel · AISI D2 steel · Roughness · Hardness · Wear

1 Introduction

One of the most promising directions for extending the life of metal components (e.g., shafts, gears, molds, dies, blades of gas turbine engines) is the improvement of technological processes for the surface modification by highly concentrated energy sources (electron beam, plasma arc, and laser beam). The application of the surface heat treatments combined with the mechanical surface treatments may significantly increase the wear and corrosion resistance of the structural/tool steel parts. Therefore, the development and implementation of new combined surface hardening technologies is an essential and urgent task in the mechanical engineering industry.

2 Literature Review

The metal components' wear resistance is enhanced through the purposeful control of the microstructure, phase/stress state, surface roughness, and hardness.

Currently, a plasma surface hardening technique is widely used to process large-sized parts due to the low cost of the technological process [1]. In contrast to the plasma surface hardening, the electron beam surface hardening method is usually applied for the surface treatment of small-sized metal parts [2]. Compared to the plasma and electron beam surface treatment, the laser heat treatment (LHT) is a more promising technique for processing complex shapes' metal components [3, 4]. At the same time, recently developed laser systems using fiber [5, 6], diode [7], and disk [8] lasers combined with modern scanning optics can significantly improve the efficiency and productivity of the LHT process. Additionally, the laser spot size can be significantly increased by the advanced 2D/3D scanning optics [9, 10]. In most cases, it allows avoiding the overlapping of the laser beam, which caused the heterogeneous microhardness in the near-surface layer of the carbon [11, 12] and alloy [13] steels via the tempered martensitic structure.

It is well-known that LHT induces the fine-grained martensitic structures through phase transformations, increasing the dislocation density [14, 15]. The martensitic-austenitic structure depends on the LHT parameters and alloy carbon concentration [16, 17]. Increasing the concentration of carbon in the hypoeutectoid steels is accompanied by an increase in the hardening depth through increment the calcination. On the contrary, reducing the hardening depth and increasing the hardening width in the hypereutectoid steels occurs with increasing the carbon content due to the reduction of thermal conductivity [6, 14, 18]. Additionally, increasing the steel's carbon content causes a significant amount of residual austenite in the subsurface layer at the LHT with a melting, which leads to a reduction of the mechanical properties [19].

For decreasing the surface roughness and residual austenite, mechanical surface treatments can be applied after LHT. Simultaneously, the grain refinement and a deeper compressive residual stress are provided by a severe plastic deformation [10, 20]. Consequently, an improvement in both the surface quality and structural parameters in the near-surface layer led to enhance the wear/corrosion resistance and fatigue life of a material. The study of the effects of surface plastic deformation by the ultrasonic impact treatment (UIT) on the wear behavior of structural/tool steel hardened by LHT using advanced laser systems becomes especially relevant.

This work aims to compare the surface roughness and hardness of the AISI 1045 and AISI D2 steel hardened by laser heat treatment, ultrasonic impact treatment, and combined laser-ultrasonic treatments. Particular attention is paid to the study of wear behavior under oil-lubricated conditions in the quasi-static and dynamic loads.

3 Research Methodology

The AISI 1045 carbon steel samples of ~20 mm thick and AISI D2 tool steel samples of ~10 mm thick were studied. The sample thickness was chosen differently to provide appropriate overcooling rates to obtain similar hardness. Unlike the samples of AISI D2 steel, the AISI 1045 steel samples were polished before the post-treatments of their

surfaces. For evaluating both the running-in stage and steady stage of the wear process, the surface roughness should be minimized.

The samples were hardened by a 1 kW power Rofin Sinar FL010 fiber laser combined with 2D scanning optics, which was mounted in a milling center [10, 15]. A proportional-integral controller was used that adjusts the laser power value to keep the nominal surface temperature during LHT. The LHT process was carried out at a sample feed rate of 90 mm/min and a scanning velocity of 1000 mm/s, changing a heating temperature (1200 °C for AISI 1045 steel and 1270 °C for AISI D2 steel).

The samples' surface plastic deformation was carried out using an ultrasonic seven-pin impact head, which was mounted at the horn tip (vibration amplitude of ultrasonic horn was 18 μm , vibration frequency of ultrasonic horn was 21.6 kHz). The ultrasonic tool was pressed to the sample surface at a static load of 50 N while the impact head was forcedly rotated at a speed of 76 rpm [10]. The UIT process lasted for 60 s (AISI 1045 steel) and 120 s (AISI D2 steel).

The surface roughness was determined using a Leica DCM3D optical profilometer. The surface hardness was measured using a Computest SC hardness tester at a load on an indenter of 5 kg. The hardened samples were tested in both the quasi-static and dynamic loading conditions using a computer-assisted tribological complex (Fig. 1). The wear test system was described in more detail elsewhere [21]. Each wear track was evaluated by an optical 3D profilometer (Infinite Focus G5 Alicona).

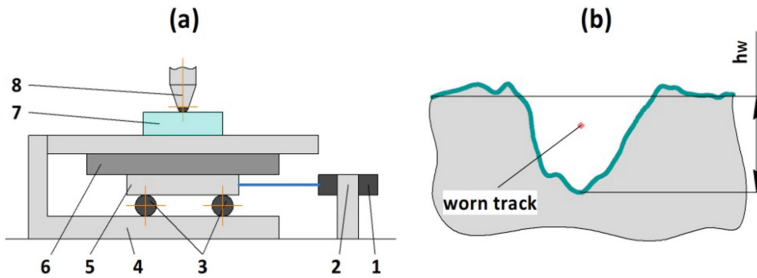


Fig. 1. Scheme of the tribological complex (a) consisting of a friction force sensor (1), clip (2), two pairs of balls (3), stand with a slide (4), support (5), ring spring (6), test sample (7), and counterbody (8); 2D view of the worn track (b): h_w – the height of the worm tracks.

4 Results

4.1 Surface Roughness

The behavior of the surface roughness parameter R_a (arithmetical mean deviation of the assessed profile within 0.8 mm) is presented in Fig. 2. The AISI D2 tool steel samples ($R_a = 2.60 \mu\text{m}$) were notably rougher compared to the AISI 1045 carbon steel samples ($R_a = 0.61 \mu\text{m}$). The surface roughness almost does not change after laser surface hardening regardless of the initial state. This is because the melting of microasperities' peaks did

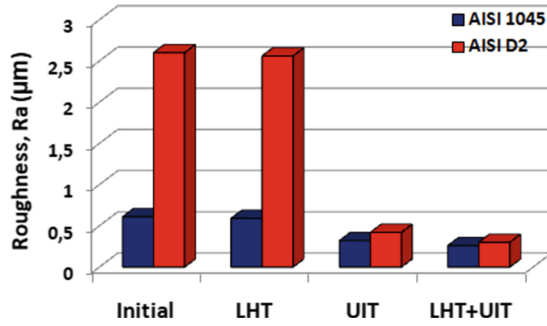


Fig. 2. Surface roughness of the initial sample and the LHT, UIT, and combined LHT + UIT processed AISI 1045 and AISI D2 steel samples.

not occur. At the same time, an oxide film is formed due to the sample surface's reaction heated by a laser beam with the atmosphere.

In contrast to the LHT, the UIT technique's use allows a significant reducing the Ra parameter (Fig. 2) irrespective of the initial state of steel. The Ra parameter was reduced by UIT from $0.61 \mu\text{m}$ to $0.32 \mu\text{m}$ for AISI 1045 steel, and from $2.60 \mu\text{m}$ to $0.42 \mu\text{m}$ for AISI D2 steel. Moreover, the combined LHT + UIT hardened samples show a slightly better surface roughness than the single UIT-processed samples. In particular, the Ra parameter of untreated/polished samples (AISI 1045 steel) was decreased twice. The Ra parameter of the unpolished tool steel samples was reduced by combined LHT + UIT technique from $2.60 \mu\text{m}$ to $0.30 \mu\text{m}$.

4.2 Surface Hardness

Along with the surface roughness, the surface hardness is also of particular importance for the surface layer's wear resistance. The results showed that the combined LHT + UIT and single LHT processes lead to an almost triple and double increase in the surface hardness (Fig. 3), respectively, due to the fine-grained martensitic structure formed [10, 21].

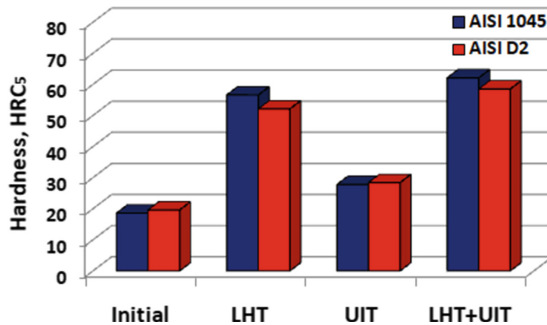


Fig. 3. Surface hardness of the initial sample and the LHT, UIT, and combined LHT + UIT processed AISI 1045 and AISI D2 steel samples.

In contrast to the AISI 1045 steel samples, the surface hardness of AISI D2 steel samples is lower due to the presence of more residual austenite. In comparison with the untreated state, the UIT induced surface hardening by ~50% due to the increased dislocation density and grain refinement. The hardness's highest values were obtained after the combined treatment (62.1 HRC₅ for AISI 1045 steel and 58.5 HRC₅ for AISI D2 steel).

4.3 Wear

The wear loss magnitudes were determined according to Fig. 1b using the 2D/3D micrographs and the worn tracks' profiles on the surfaces (Figs. 4, 5 and 6) made by laser microscopy.

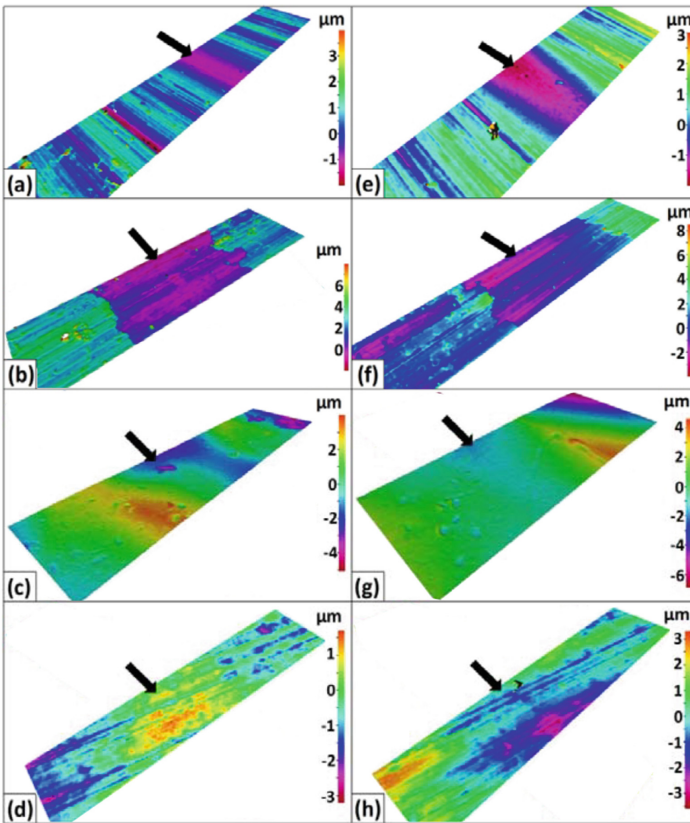


Fig. 4. 3D micrographs of the worn tracks on the surfaces after the short-term (a–d) and long-term (e–h) tests in the quasi-static condition for the initial sample (a, e) and the LHT (b, f), UIT (c, g), and combined LHT + UIT (d, h) processed samples of AISI 1045 steel.

It can be seen that the width/depth of the worn tracks (indicated by arrows) is larger after dynamic tests (Figs. 4 and 5). It is of interest that as compared to the single LHT

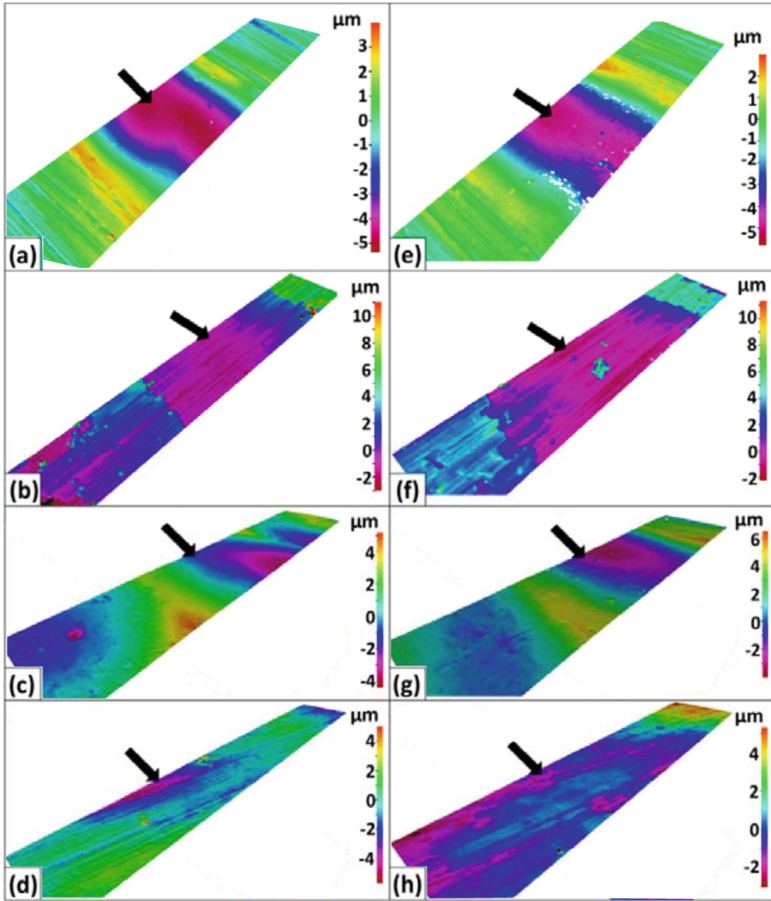


Fig. 5. 3D micrographs of the worn tracks on the surfaces after the short-term (a–d) and long-term (e–h) tests in the dynamic condition for the initial sample (a, e) and the LHT (b, f), UIT (c, g), and combined LHT + UIT (d, h) processed samples of AISI 1045 steel.

process (Figs. 4b, f, 5b, f, and 6b), the UIT process after LHT results in the fragmentation and removal of the oxide film from the surface (Figs. 4 d, h, 5 d, h, and 6 d). As seen in Fig. 6 b the oxide film has a thickness of 2–3 μm . The spherical counterbody formed the semi-circular worn track patterns with the pile-ups area in the initial sample and UIT-processed sample after the long-term tests (Fig. 6a, c). Unlike the UIT-treated sample, the semi-circular worn track patterns were not observed in the LHT, and combined LHT + UIT treated samples (Fig. 6b, d) due to a high surface hardness (Fig. 3).

The wear loss magnitudes of AISI 1045 and AISI D2 steels registered after quasi-static and dynamic tests lasted for 15 min (short-term tests) and 45 min (long-term tests) are given in Figs. 7 and 8, respectively. During the running-in stage of the wear process (quasi-static tests), the LHT formed oxide layers being fragmented during the tests exert a deteriorative influence on the wear resistance provoking adhesive and abrasive wear

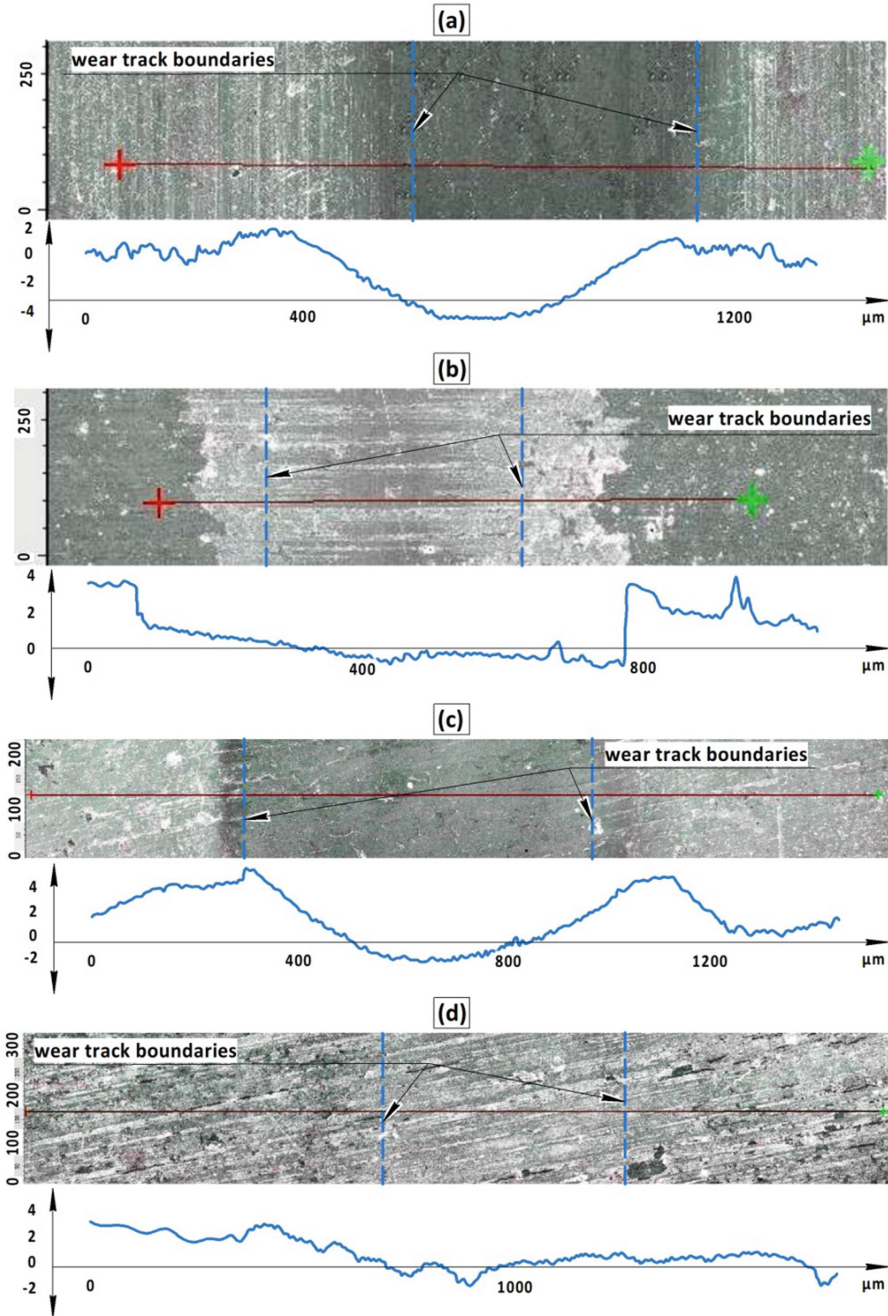


Fig. 6. 2D micrographs and profiles of the worn tracks on the surfaces after the long-term tests in the dynamic condition for the initial sample (a) and the LHT (b), UIT (c), and combined LHT + UIT (d) processed samples of AISI 1045 steel.

(Fig. 7). It should also be noted that as compared to the initial state, the single UIT process unexpectedly deteriorates the wear resistance of the AISI 1045 steel samples due to the formation of wavy microrelief with high peaks. The formed fine-grained martensitic structure coupled with high surface hardness and low surface roughness after the combined LHT + UIT process resulted in a significant reduction of the wear loss values regardless of the studied material type.

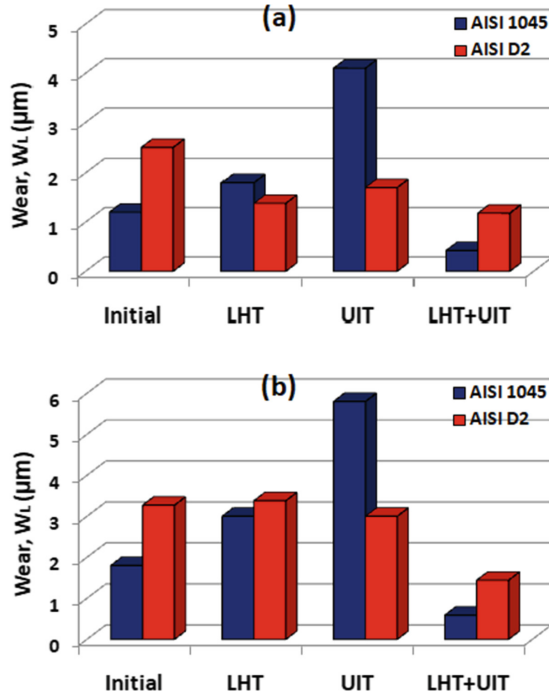


Fig. 7. Wear loss after the short-term (a) and long-term (b) tests in the quasi-static condition for the initial sample and the LHT, UIT, and combined LHT + UIT processed samples AISI 1045 and AISI D2 steel.

As compared to the initial sample (Fig. 8), the hardened samples of AISI 1045 steel/AISI D2 steel demonstrate the wear losses after long-term tests (45 min) in the dynamic condition decreased by 34.95/41.33% after the LHT process, by 4.85/68.32% after the UIT process, and by 83.88/75.18% after the LHT + UIT process.

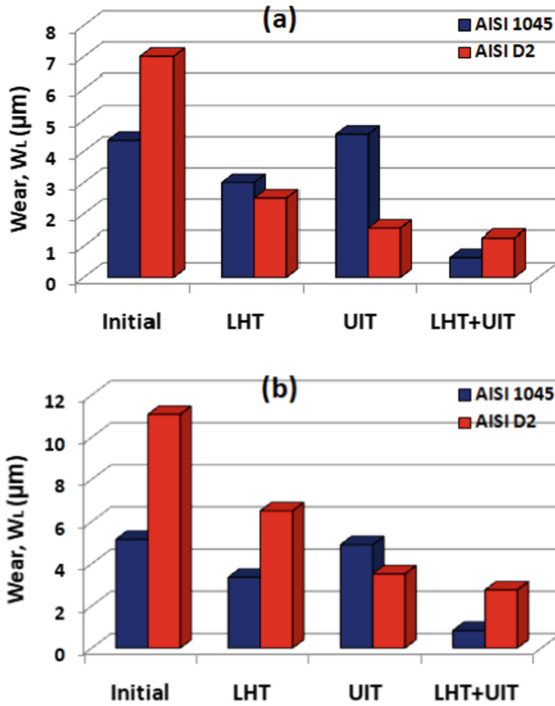


Fig. 8. Wear loss after the short-term (a) and long-term (b) tests in the dynamic condition for the initial sample and the LHT, UIT, and combined LHT + UIT processed samples of AISI 1045 and AISI D2 steel.

5 Conclusions

The results of this study can be summarized as follows:

1. The combined treatment provides the lowest surface roughness (Ra parameter $\sim 0.25 \mu\text{m}$) and the highest surface hardness ($\sim 62 \text{ HRC}_5$) for AISI 1045 steel.
2. Compared to the untreated sample, the hardened samples demonstrate the wear losses of AISI 1045 and AISI D2 steel after long-term tests in the dynamic condition decreased by ~ 84 and $\sim 75\%$ after the combined treatment. The combined LHT + UIT method can be used to increase the wear resistance of structural and tool steel.
3. The application of a diode laser for LHT is planned for further research. Simultaneously, the surface plastic deformation of LHT-treated samples will be performed by a shot peening, cavitation peening, ultrasonic peening, and laser peening.

Acknowledgments. This study is supported financially by the Erasmus Mundus program and partially supported by the National Academy of Sciences of Ukraine (Project #0119U001167). The authors would also like to acknowledge Dr. G.I. Prokopenko to discuss the obtained results and Dr. K.E. Grinkevych for his help with the wear tests.

References

1. Ismail, M.I.S., et al.: Surface hardening of tool steel by plasma arc with multiple passes. *Int. J. Technol.* **5**, 79–87 (2014)
2. Petrov, P.: Optimization of carbon steel electron-beam hardening. *J. Phys: Conf. Ser.* **223**, (2010)
3. Montealegr, M.A., et al.: Surface treatments by laser technology. *Contemp. Mater.* **19**, 19–30 (2010)
4. Grum, J., et al.: The influence of different conditions of laser-beam interaction in laser surface hardening of steels. *Thin Solid Films* **453–454**, 94–99 (2004)
5. Sancho, P., et al.: Dynamic control of laser beam shape for heat treatment. *J. Laser Appl.* **30**, 032507 (2018)
6. Qiu, F., et al.: Surface hardening of AISI 4340 steel by laser linear oscillation scanning. *J. Surf. Eng.* **28**, 569–575 (2012)
7. Skvarenina, S., et al.: Predictive modeling and experimental results for laser hardening of AISI 1536 steel with complex geometric features by a high power diode laser. *Surf. Coat. Technol.* **201**, 2256–2269 (2006)
8. Hruska, M., et al.: 3D Scanning laser hardening, *Proceedings of the Materials 23rd International Conference on Metallurgy and Materials, Metal*, pp. 921–926 (2014)
9. Klocke, F., et al.: Optimization of the laser hardening process by adapting the intensity distribution to generate a top-hat temperature distribution using freeform optics. *Coatings* **7**, 1357–1366 (2017)
10. Lesyk, D., Martinez, S., Mordiyuk, B., Dzhemelinskyi, V., Danyleiko, O.: Combined laser-ultrasonic surface hardening process for improving the properties of metallic products. In: Ivanov, V., et al. (eds.) *Advances in Design, Simulation and Manufacturing. DSMIE 2018. Lecture Notes in Mechanical Engineering*, pp. 97–107. Springer, Cham (2019). https://doi.org/10.1007/978-3-319-93587-4_11
11. Giorleo, L., et al.: Modelling of back tempering in laser hardening. *J. Adv. Manuf. Technol.* **54**, 969–977 (2011)
12. Kim, J.D., et al.: Laser transformation hardening on rod-shaped carbon steel by Gaussian beam. *Met. Soc. China* **19**, 941–945 (2009)
13. Yao, C., et al.: Study on the softening in overlapping zone by laser-overlapping scanning surface hardening for carbon and alloyed steel. *Opt. Lasers Eng.* **48**, 20–26 (2010)
14. Orazi, L., et al.: An efficient model for laser surface hardening of hypo-eutectoid steels. *Appl. Surf. Sci.* **256**, 1913–1919 (2010)
15. Lesyk, D., Martinez, S., Mordiyuk, B., Dzhemelinskyi, V., Danyleiko, O.: Effects of the combined laser-ultrasonic surface hardening induced microstructure and phase state on mechanical properties of AISI D2 tool steel. In: Ivanov, V., et al. (eds) *Advances in Design, Simulation and Manufacturing II. DSMIE-2019. Lecture Notes in Mechanical Engineering*, pp. 188–198. Springer, Cham (2020). https://doi.org/10.1007/978-3-030-22365-6_19
16. Zhang, P., et al.: Effect of laser surface hardening on the microstructure, hardness, wear resistance and softening of a low carbon steel. *Laser Eng.* **28**, 135–149 (2014)
17. Slatter, T., et al.: The influence of laser hardening on wear in the valve and valve seat contact. *Laser Eng.* **267**, 797–806 (2009)
18. Hung, T.P., et al.: Temperature modeling of AISI 1045 steel during surface hardening processes. *Metar.* **11**, 1815 (2018)
19. Li, C., et al.: Microstructure, hardness and stress in melted zone of 42CrMo steel by wide-band laser surface melting. *Opt. Lasers Eng.* **49**, 530–535 (2011)

20. Fan, Z., et al.: Surface nanocrystallization of 35# type carbon steel induced by ultrasonic impact treatment (UIT). *Int. J. Fatigue* **27**, 1718–1722 (2012)
21. Milman, YuV, et al.: New opportunities to determine the rate of wear of materials at friction by the indentation data. *Prog. Phys. Met.* **21**, 554–579 (2020)



Rational Design Solution Based on Mathematical Modeling of an Interference Fit

Vladimir Nechiporenko^(✉) , Valentin Salo , Petro Litovchenko ,
Valeriya Rakivnenko , and Andriy Horbunov 

National Academy of the National Guard of Ukraine, 3, Zakhysnykiv Ukrayiny Square,
Kharkiv 61001, Ukraine

Abstract. The paper proposes a significant improvement in the integrated methodology for automated calculation and selection of interference fits. The study's main task was to find a rational combination of the values of the variable parameters of the complex mathematical model of the area of existence of the fit. The specified search was carried out in the range of a finite set of permissible parameter values that correspond to the conditions for calculating the fit. As an effective tool for performing a large volume of numerical and analytical calculations, the author's computer program for the automated design of interference fit was used. The research object was the geometric image of the model of the area of existence of the fit parameters in the form of a three-dimensional body as part of the complex of a multiparametric mathematical model. For solving this problem, one of the projections of the model of the area of existence of fit parameters is described analytically based on the theory of R -functions. In the research process, the influence of the fit diameter's value (the main geometric characteristic of the fit) on the quality and reliability of the shroud joint during its thermal assembly and during the operation was determined. The research results are recommended for improving the mathematical and software tools for computer-aided design of interference fits when choosing the most rational design solution for the given operating conditions and assembly of the joint.

Keywords: Multiparametric model · Area of existence · Fit parameters · Fit diameter · Working fit length · Computer-aided design · Theory of R -functions

1 Introduction

One of the main directions of improving modern machines' operational characteristics and mechanisms is the quality and reduction of the terms of technological preparation of production. This is possible by increasing the automation level of the design of their units and assemblies and modern methods for finding rational options for design solutions.

The introduction of computer-aided design of interference fits makes it possible to increase the design process's productivity by considering the maximum number of factors affecting the fit's strength and reliability and choosing a rational design solution from a finite set of acceptable ones.

Therefore, this work aims to study the effect of the fit diameter on the qualitative choice of interference fit using a multiparametric mathematical model of the area of existence of the shroud joint parameters during its thermal assembly.

Considering this, the research results aimed at developing methods and means of computer-aided design of effective joints with an interference fit are relevant.

2 Literature Review

Interference fits on a smooth surface are among the most common types of conditionally detachable joints and are widely used in various branches of modern technology. Thus, in [1], a study of the influence of interference fit on the distribution of stresses and the mode of destruction of the riveted joint is presented as the most reliable way of joining the aircraft fuselage skin. A 3D model is used to analyze the mechanical characteristics of flat head riveted joints. The three-parameter probabilistic model of the strength of cylindrical joints with interference, proposed in the article [2], made it possible to calculate the permissible value of the load and obtain curves of strength and failure of joints, which are consistent with experimental data. In work [3], a joint's strength analysis with an interference fit of an oval-shaped underwater pipeline with a mechanical connector was performed to repair. The necessity of an interference fit in case of pipeline damage was indicated. The ANSYS software and the theory of a thick-walled cylinder were used to analyze the pipeline's contact characteristics. According to the results obtained, the pipeline's contact stress practically depends on the equivalent interference and not on ovality, which only significantly affects the uniformity of the distribution of the contact stress on the joining interference surfaces. Electromagnetic riveting has ample opportunities for engineering applications in production and assembly as an advanced technology for joining with an interference fit, which is the subject of theoretical and experimental studies in [4]. Here, an analytical interference fit model is derived from stress wave theory and shell theory. The presented analytical solutions are in good agreement with the experimental values. Using the proposed model, which considers many process parameters, it is possible to predict the distribution of residual stresses as an important factor in fatigue life.

One of the promising directions in improving existing and creating new structures is the widespread use of composite materials. The intensive growth in the use of composites is due to a significant decrease in the weight of critical products and an increase in their performance and reliability. Therefore, the development of effective and reliable methods for calculating composite joints, which, in particular, is widely used in the assembly of thin-walled sheets in the aviation industry, is of great scientific and practical importance. So, article [5] is devoted to analyzing the mechanism of microscopic damage in the composite during the installation of the pin with an interference fit, which is of great importance for the optimal design of joints with interference. In this regard, the work proposes a new approach to multiscale modeling of microscopic damage using 2D finite element models on the ABAQUS platform. In [6], an analytical method was developed for calculating the stress around the holes for interference fit on composite plates under tensile loading. For checking the accuracy of this method, the experiment results were used, which give sufficient agreement.

In [7], using the probability density function and convolution, a methodology for analyzing the statistical distribution of contact pressure and rigidity of the mating surface between the shaft and the bearing, depending on the degree of interference, was developed. For illustrating the methodology, a roller bearing with a nominal diameter of 50 mm is taken as an example, for which, as shown by the results, there is a high probability of obtaining a clearance of up to 0.5 μm , which implies a loss of contact stiffness. For solving this problem, two approaches are investigated in this work: using a tighter tolerance of the bearing inner ring or a larger deviation of the shaft diameter. An analytical formulation for evaluating the evolution of contact pressure in interference joints operating in a high-temperature regime at the creeping stage was proposed in [8]. The proposed analytical solution correlates contact pressure with creep properties of the material and can be used to improve the design or evaluate joints' serviceability that transfer a load through an interference fit.

In [9], the results of the fit process of a double hinge of a full-scale model of a vacuum vessel ITER (VV) mounted on nine VV gravity supports (VVGs) are presented. For such a joint, a heat-shrink fit method was chosen for the sleeve's mutual mating into the hole of the hinge block. In [10], the strength of joints with an interference fit is considered, and a device for sliding bearing units is proposed in cases where the coefficient of linear expansion of the hole is greater than the same parameter for the shaft. This option provides a significant increase in the joint's strength due to the intense heat removal from the sleeve. As follows from the literature review analysis [1–10], a considerable amount of research has been devoted to an interference fit. Most of them consider joint strength problems under static loads, and for the construction of mathematical models, as a rule, the finite element method is used. At the same time, topical issues of rational and optimal choice of fit have practically not been studied, and the regularities and parameters of frictional contact, which determine the strength, reliability and durability of fit fits, have not been sufficiently studied.

3 Research Methodology

In this work, studies are continued, which are based on the use of the article's developments [11] when calculating the fit with an interference fit of the ring gear rim of a cylindrical wheel on the smooth base of the hub during thermal assembly. The authors' research methods are numerical and analytical, based on the analysis of the initial data and the results of the automated calculation of interference fits. As a research tool, the author's computer program Interference Fit [11] was used, which allows, based on this calculation's results, to select a rational design solution from a finite set of admissible ones.

The methodology for choosing a rational joint is based on the construction of a three-dimensional mathematical model of the existence of interference fits in the lpN coordinate system (l is the working length of the joint, p is the specific contact pressure, N is the interference). The proposed model is part of a comprehensive multiparametric mathematical model and considers all the strength, operational and technological parameters of the projected fit, which are necessary for its reasonable choice.

Based on the theory of R -functions, a two-parameter model pN of the area of existence of interference fits, as well as the shapes of a finite set and a localized reliable zone of

suitable interference fits, are described analytically. The considered area is one of the precise criteria for choosing the final design solution at a particular value of the fit diameter as the interference function's main argument. When its value changes in a specific range, the localization zone can change significantly, and the choice of fit will depend on a subjective factor.

To improve the methodology and software for automated calculation, the authors have constructed a graphical interpretation of the mathematical model of the existence of rational fit with interference in the coordinate system dIN (d is the fit diameter). This model is built based on new research results and is an essential part of a multiparametric model's considered complexity, which will allow the designer with greater confidence to reasonably choose a design solution from a finite set of alternative ones.

4 Results

4.1 Conditions for Ensuring Strength and Existence of Fits Depending on Geometric Parameters in Integrated Modeling

The initial data for the study of mathematical models of the fit parameters' area of existence in the form of graphical spatial images were taken the same as in the study [11]. In this case, the fit diameter's varied values were set in the form of a matrix of a discrete series of d_j values, which is determined from a normalized series of standard values within the range of the fit diameters $d_{\min} - d_{\max}$. For reasons of ensuring sufficient rigidity of the joint parts, a general recommendation was adopted, corresponding to the condition:

$$d_{\min} \leq d_j \leq d_{\max} = (d_1 + 15) \leq d_j \leq (d_2 - 15), \quad (1)$$

where $d_{\min} = (d_1 + 15)$ and $d_{\max} = (d_2 - 15)$ are, respectively, the minimum and maximum recommended limiting values of the joint rim diameter, within which it is possible to ensure the specified joint strength. For the considered example, $d_{\min} = d_1 + 15 = 50 + 15 = 65$ mm; $d_{\max} = d_2 - 15 = 130 - 15 = 115$ mm. For an interference fit, the actual value of the fit length l_k is recommended when the condition is met:

$$l_{cr} \leq l_k \leq l_{r\max}, \quad (2)$$

where l_{cr} – the minimum critical value of the working length at which the condition for the strength of the joint is met; $l_{r\max}$ – recommended maximum working length for fit parts (made of steel $l_{r\max} \leq 4d^{0.7}$; made of cast iron $l_{r\max} \leq 1,25d$; made of light alloys – $l_{r\max} \leq 1,5d$; at high bending loads and accurate centering $l_{r\max} \leq (1.5-2.0)d$). This condition's boundaries determine the recommended area of existence of suitable interference parameters along with the coordinate axis $0 l$. In this case, the l_{cr} value will ensure the fit's immobility, and the value $l_{r\max}$ will be limited only structurally, for example, by the length of the gear hub. Let us note that the fulfillment of the following conditions $l_k > l_{r\max}$ is also possible, but its effectiveness and expediency are doubtful. Therefore it is not recommended. The following condition can determine the minimum critical value of the working length:

$$l_{cr} = [p_{\min}]_k \cdot l_k / [p_{\min}], \quad (3)$$

where $[p_{\min}]_k$ – the permissible minimum specific pressure in the joint, at a certain actual value of the fit working length l_k .

In the range $0 < l_k < l_{cr}$, an interference fit is unacceptable, because in this case, the weakest fit part may be destroyed. In this case, the permissible minimum specific pressure and the corresponding permissible minimum design interference under the strength conditions will exceed the maximum permissible values ($[p_{\min}] > [p_{\max}]$ and $[N_{\min}] > [N_{\max}]$).

4.2 Mathematical Modeling of the Area of Existence of Fits Depending on Geometric Parameters Integrated Modeling

The form elements of the basic mathematical model lpN , considered in [11], connect some parameters with the investigated model dlN (Figs. 1 and 2). Both of these models are constituent parts of the multiparametric model complex. For them are the standard coordinate plane lN (with its corresponding coordinate axes $0l$ and $0N$).

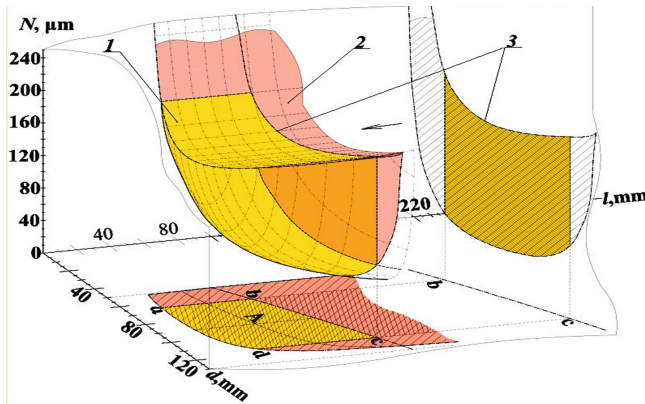


Fig. 1. The spatial area of the existence of interference fit and the location of the secant surface.

In Fig. 1 are marked: 1 – recommended area of existence of interference fit; 2 – an area of the possible existence of interference fit; 3 – secant surface, delimiting the values of the recommended parameters from all possible.

On the coordinate plane lN (see Fig. 2), the lines of admissible interference values of the area of existence of the fit parameters are projected, formed by the extreme points of the segments of the range $[N_{\min}] - [N_{\max}]$ as the value of the working fit length l_k increases. At $l_k \rightarrow \infty$ the value of the minimum limiting interference decreases $[N_{\min}] \rightarrow 0$, and the maximum $[N_{\max}]$ remains constant. Between the lines of the boundaries of this growing area, the number of suitable standard fits is sequentially increasing, the parameters of which fit into the specified area (with the method of complete interchangeability).

On the coordinate plane dN (see Fig. 2), the projection of the area of existence of the fit parameters (for the ranges of values $[N_{\min}] - [N_{\max}]$ and $d_{\min} - d_{\max}$ at $l_{cr} - l_{r \max}$) and

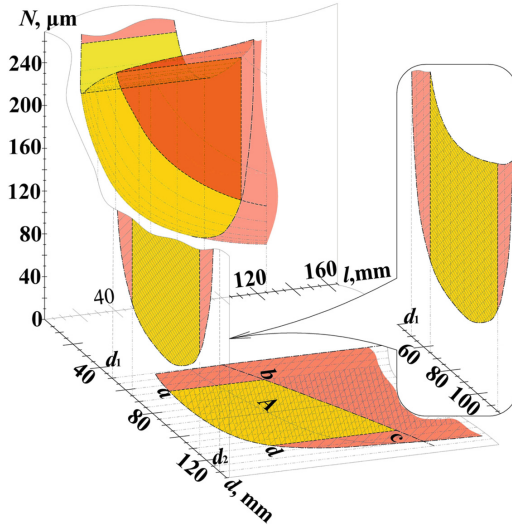


Fig. 2. The projections of the volumetric model of the area of existence of interference fit onto the coordinate planes.

the projection of the secant surface 3 (see Fig. 1) are shown. Line *bc* of the allowable effective interferences is plotted on this projection depending on the fit diameter and recommended maximum joint working length for steel materials. As an example (Fig. 3), several stepped ranges of probabilistic interferences values are projected onto the *dN* plane, depending on the range of nominal diameters recommended for the standard-fit H7/v7. On the coordinate plane *dl* (Fig. 2 and 3), the projection of the area of existence of the geometric parameters of the fits (for the ranges of values $d_1 - d_2$ and $l_{cr} - l_{r\max}$) and the center of symmetry (point *A*) of the flat image *abcd* of the model in the coordinate axes *dl* is shown.

The area of existence of the geometric parameters of fits, represented in the form of a flat figure in the coordinate axes *dl*, is described in an analytical form using the mathematical apparatus of the theory of *R*-functions [12, 13]:

$$\left. \begin{aligned} \Omega_{ld} = \Omega_{l_1} \wedge_0 \Omega_d \wedge_0 \Omega_{l_2}, \quad \Omega_d = \left[\left(\frac{(d_2 - 15) - (d_1 + 15)}{2} \right)^2 - (d - d_A)^2 \right], \\ \Omega_{l_1} = \left[\left(l_{cr} - \frac{l_{r\max} + l_{cr}}{2} \right)^2 - (l - l_A)^2 \right], \quad \Omega_{l_2} = \left[\left(l_{r\max} - \frac{l_{r\max} + l_{cr}}{2} \right)^2 - (l - l_A)^2 \right], \end{aligned} \right\} \quad (4)$$

where \wedge_0 – *R*-conjunction symbol [14, 15]; (*d*, *l*) – coordinates of the values of the fit diameter *d* (mm) and fit working length *l* (mm); (d_A , l_A) – coordinates of the center of symmetry *A* of a flat figure *abcd* of admissible values of the ranges of the fit diameter d_A (mm) and the fit working length l_A (mm); d_1 – the diameter of the inner surface of the covered part (mm); d_2 – conventional outer diameter of the covering part (mm); Ω_d – set of permissible recommended values of the fit diameter of the joint in the form of a vertical strip (for $(d_1 + 15)$ and $(d_2 - 15)$); Ω_{l_1} and Ω_{l_2} are the sets of permissible values of the fit working length of the joint in the form of curved strips.

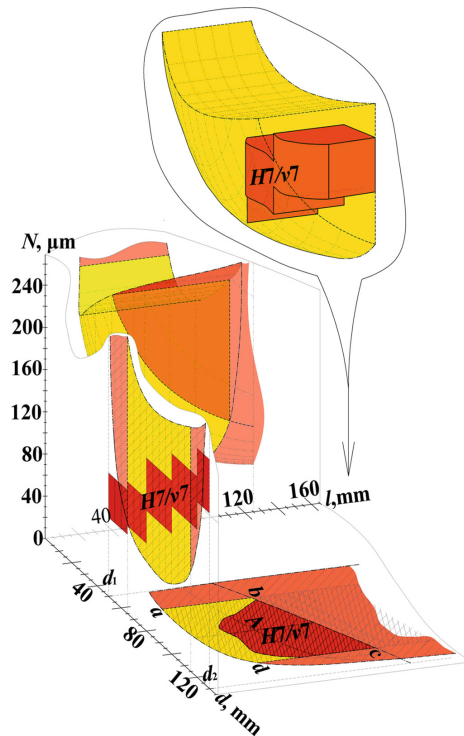


Fig. 3. Recommended area of existence of fit parameters and localization of the model of interference fit $H7/v7$.

For the considered example (see Fig. 3), the $H7/v7$ fit model has the largest volume (among other alternative ones), occupying a large part within the recommended area of existence of its parameters. Therefore, such a joint can be considered the most rational and taken as a criterion as a final design solution. The study results make it possible to reasonably choose rational parameters (first of all, the fit diameter) and one design solution – a suitable standard interference fit with computer-aided design and significantly reduce the influence of the subjective factor.

5 Conclusions

When using the effective software Interference Fit in the calculations for the automated calculation of interference fits, an essential criterion for choosing the final design solution is developed considering the influence of the fit diameter as the main argument of the interference function.

As a result, a visual representation of numerical calculations in the form of a graphic illustration of the material is created. The proposed approach is reasoned and qualified for the choice of the rational fit. The analysis of the obtained research results shows that this direction's complex mathematical modeling is a relatively effective tool.

The model of the existence of interference fit parameters, which is a part of the general multiparametric model in complex mathematical modeling, is analytically described using the effective mathematical apparatus of the theory of R -functions. This circumstance makes it possible to modernize the software for computer-aided design of fits significantly.

In the future, we plan to modernize the author's computer program "Interference Fit" by adding a graphical application.

References

1. Jin, K., Wang, H., Tao, J., Tian, J.: Effect of the interference fit on the stress distribution and failure mode of a flat-head riveted GLARE joint. *Comp. Struc.* **235**, (2020)
2. Gallio, G., Lombardia, M., Rovarinob, D., Finoa, P., Montanaro, L.: Influence of the mechanical behaviour of different adhesives on an interference-fit cylindrical joint. *Int. J. Adhes. Adhes.* **47**, 63–68 (2013)
3. Cao, Y., Zhang, L., Sun, Y., Shi, Y., He, Y., Zhen, Y.: Strength analysis of the interference joint of the oval submarine pipeline to the mechanical connector. *Appl. Oc. Res.* **101**, (2020)
4. Zhang, X., Jiang, H., Luo, T., Hu, L., Cui, J.: Theoretical and experimental investigation on interference fit in electromagnetic riveting. *Int. J. Mech. Sci.* **156**, 261–271 (2019)
5. Song, D., Li, Y., Zhang, K., Cheng, H., Liu, P., Hu, J.: Micromechanical analysis for microscopic damage initiation in fiber/epoxy composite during interference-fit pin installation. *Mat. Des.* **89**, 36–49 (2016)
6. Wu, T., Zhang, K., Cheng, H., Liu, P., Li, Y.: Analytical modeling for stress distribution around interference fit holes on pinned composite plates under tensile load. *Comp. Part B: Eng.* **100**, 176–185 (2016)
7. Tsai, J.-Ch., Chou, T.-T., Chang, Ch.-K.: Statistical analysis of contact stiffness for shaft-bearing assembly with tolerancing and fit. *Proc. CIRP* **92**, 45–50 (2020)
8. Esposito, L., Bruno, M., Bertocco, A.: Analytical formulation of the contact pressure evolution for interference joints under creep regime. *Int. J. Pres. Ves. and Pip.* **185**, (2020)
9. Cheon, J., Park, Ch., Moon, H., Chung, W.-H., Kim, Yu.-G.: Interference fit process development for the ITER Vacuum Vessel Gravity Support mock-up fabrication. *Fus. Eng. Des.* **146** Part B, 1907–1911 (2019)
10. Svyatukha, A.A., Plakhotnikova, I.B.: Features of thermal assembly of parts of fixed joints of sliding bearing units. *Bull. NTU "KhPI". Ser. New Solu. Mod. Technol.* **26**(999), 160 (2013)
11. Nechiporenko, V., Salo, V., Litovchenko, P., Yemanov, V., Horielyshev, S.: Method of design of interference fit based on complex mathematical modeling. In: Ivanov, V., Trojanowska, J., Pavlenko, I., Zajac, J., Peraković, D. (eds.): *Advances in Design, Simulation and Manufacturing III. DSMIE 2020. Lecture Notes in Mechanical Engineering*, pp. 45–54. Springer, Cham (2020), https://doi.org/10.1007/978-3-030-50794-7_5
12. Awrejcewicz, J., Kurpa, L., Shmatko, T.: Investigating geometrically nonlinear vibrations of laminated shallow shells with layers of variable thickness via the R -functions theory. *Compos. Struct.* **125**, 575–585 (2015)
13. Balestrino, A., Caiti, A., Crisostomi, E., Grammatico, S.: Stabilizability of linear differential inclusions via R -functions. *IFAC Proc.* **43**(14), 1092–1097 (2010)
14. Varvak, M.: Ellipsoidal/radial basis functions neural networks enhanced with the Rvachev function method in application problems. *Eng. Appl. Artif. Intell.* **38**, 111–121 (2014)
15. Pokras, V., Rvachev, M.: Application of the R -functions method to viscoplastic analysis in metal forming. *J. Mater. Process. Technol.* **60**(1–4), 493–500 (1996)



Design and Engineering Assurance for the Customized Implants Production Using Additive Technologies

Vitalii Pasichnyk¹ (✉) , Maksym Kryvenko¹ , Svitlana Burburska^{1,2} ,
and Oleksandr Haluzynskyi² 

¹ National Technical University of Ukraine “Igor Sikorsky Kyiv Polytechnic Institute”, 37,
Peremohy Ave, Kyiv 03056, Ukraine

v.pasichnyk@kpi.ua

² SI, the Institute of Traumatology and Orthopedics” by NAMS of Ukraine, 27,
Bulvarno-Kudriavska St, Kyiv 01601, Ukraine

Abstract. The development and dissemination of practical additive technologies applications have become a significant trend in technology development in various activity fields. Medical engineering is one of the industries where such technologies already have a tangible effect and will become even greater in the future, especially in the manufacture of customized implants. In many cases, customized implants provide the patient with a quality of life that other solutions cannot offer. Simultaneously, the correct application of medical engineering solutions in this area requires enhanced engineering support. The point here is not about the optimal modes of implant formation but the engineering support system for decisions at every step from the initial condition analysis to surgery. So far, considerable practical experience has been gained, and many publications have appeared describing individual case implementation. Simultaneously, there is a lack of publications that would give an idea of the wide range of possibilities for using additive technologies in creating customized implants and their entire system of engineering support. This paper’s results are based on the authors’ own practical experience, implemented based on the Laboratory of Biomedical Engineering at the Institute of Orthopedics and Traumatology of the National Academy of Medical Sciences of Ukraine.

Keywords: Additive technologies · 3D printing · Endoprosthesis · Customized implants

1 Introduction

From the first steps of surgery development, the engineering solutions are always nearby. New materials, new designs, new technologies that could provide the surgeon with a solution to the patient’s problems were actively tested and applied. We are currently witnessing the rapid development of *additive technologies* (AT), and orthopedics, especially customized (patient-specific), has become a field of many advanced innovations that radically change the perception of patient’s capabilities [1].

2 Literature Review

Customized implants (CI) became one of the first successful additive technologies in the medical field [2]. Over time, many other applications have emerged, such as limb repair procedures, where the complexity is associated with defects that are not easy to repair with ready-made sizes or implant shapes [3]. AT, due to the ability to accurately reproduce complex shapes and the ability to print contralateral anatomy for use as a reference for anatomical reconstruction, is ideal for creating CI [4].

Cases are severe in patients, especially young people, adolescents, where the only possible option is to block the joints or even amputation. AT development allowed the emergence of a fairly large number of engineering solutions when a CI is created to replace a certain area of a bone or joint [5].

AT economics became an important success factor of such applications. Conventional subtractive technologies for the manufacture of parts are an exponential dependence of cost on complexity. The more complex the part is by the number of elements, their shape, and accuracy, the more expensive the manufacturing process challenging the technologist with an increasing number of technological limitations (trimming elements, lack of access to cutting tools, catastrophic drop in stiffness of parts and tools preventing cutting, etc. A significant difference of AT, almost a paradox, is that the more complex the shape of the part is (due to shape optimization), the cheaper it is to make such a part on an additive machine (AM) [6]. Today, engineers who traditionally make implants based on subtractive processing need to change and expand their design thinking.

Projects for CI creation and installation in orthopedics are complex and require a high level of knowledge in engineering and medicine. A clear understanding of the work sequence on such projects, as incorrectly defined source data can nullify all work performed. Significant practical experience has already been gained in using CIs made using AT, but systemic aspects of engineering support are underrepresented in the literature. This paper concerns the engineering aspects of supporting CI additive manufacturing.

3 Research Methodology

The structural-logical scheme reflects the authors' own practical experience, implemented based on the Laboratory of Biomedical Engineering at the Institute of Orthopedics and Traumatology of the National Academy of Medical Sciences of Ukraine [7].

It is known that the processes of additive production can be divided into three successive technological stages: Preprocessing, Processing, and Post-processing [8]. It is also possible to consider a more general manufacturing CI process and accompanying equipment with AT integrated.

Preprocessing. Reverse engineering – CT/MRI data processing. Creating a three-dimensional model of the target area, taking into account the main vessels and nerves' spatial location. Surgical planning to determine the type of surgical access, the size of resection. Zone definition – assessment of bone condition. Analysis of existing standard designs of endoprostheses. Decision-making on CI manufacture.

Equipment. Computer tomography, MRI machine, PC, specialized software.

Processing. Navigation systems modeling for resections, future CI prototype modeling, strength calculations. FDM/SLA printing of the target organ model, printing of navigation systems, implant prototype printing. “Operation to operation” analysis. Testing main stages of implantation. Correction. SLM/EBM manufacturing of CI.

Equipment. PC with specialized software, additive machines based on FDM, SLA, SLM/EBM technologies with related equipment, surgical instruments for resection and installation.

Post-processing. CI processing – cleaning, heat treatment, machining (threading, grinding, etc.). Accuracy control. Checking the quality and accuracy of the implant. Coating. Titanium shielding, coating for osteointegration. Preparation for implantation sterilization, packaging.

Equipment. PC with specialized software, heat treatment equipment, CNC machines for machining, coating plants, sterilization, and packaging equipment.

4 Results

Substance and technological features of implementing engineering support stages. Let us consider the detailed substance and engineering features of implementing engineering support stages for AT-based CI manufacture, presented in Sect. 2.

4.1 Engineering Support for Collecting Initial Information

Computed tomography (CT) and magnetic resonance imaging (MRI) scans can provide a basic set of patient characteristics.

In determining the choice and features of CT and MRI, one should consider the different nature of the physical phenomena used in these devices. CT uses X-ray radiation, which gives an idea of the physical state of a matter. MRI uses constant and pulsating magnetic fields and radiofrequency radiation, which provides information about the distribution of protons (hydrogen atoms), i.e., tissues’ chemical structure. Therefore, CT allows a physician to see not only the tissues but also their X-ray density, which changes with the course of the disease; in the case of MRI, the physician visually evaluates the image only. In general, MRI better distinguishes soft tissues. The bones may not be visible – there is no resonance of calcium, and bone tissue on MR scans is visible only indirectly [9].

CT allows the physician to see the most detailed picture of the body condition in situations of studying damage to bones and teeth; studying joint lesions; diagnosing injuries (fresh bleeding is clearly visible); detecting spine diseases, including hernias, osteoporosis, scoliosis, and others; studying brain damage; examining the thoracic cavity (detection of tuberculosis, pneumonia, and other diseases); examining thyroid and parathyroid glands; examining hollow organs (stomach, intestines); studying the vascular condition, diagnosing aneurysms, atherosclerosis; examining genitourinary system (visible tumors, stones, cysts) [10].

MRI is usually prescribed for examination of tissues, joints, and blood vessels; examination on suspicion of a tumor in soft tissues; examination of intracranial nerves; structures of the brain and spinal cord; study of spinal cord and brain membranes; examination of patients with multiple sclerosis and other neurological diseases, as well as stroke patients; study of ligaments and muscles; study of the condition of joint surfaces [11].

As can be seen, a single study method is not enough to assess the condition, decide on the scope and features of surgery, and hence on the engineering support of CI manufacture and technological means of surgery. That is why a comprehensive study using CT/MRI should be used as initial data for planning and creating CI and ancillary structures. When obtaining the results, many prerequisites should be provided to ensure initial data completeness and quality. CT studies require [12] the minimum possible cross-sections; metal artifacts suppression if structures have already been implanted in the scanning area; noise minimization on images. MRI studies require [13] isotropic voxel, minimum inter-slice gap, noise minimization.

Since bone surfaces are the basic surfaces for CI construction in orthopedics-traumatology, CT is the main radiological diagnosis type. If there is a need for additional visualization of soft tissues, nerves, and blood vessels, a combination of images from two study methods is used in specialized programs to process already combined images. Due to the fact that CT and MRI are performed on different devices, given that it is very difficult to ensure the same position of patient when scanning, the processing of combined CT/MRI images is a complex semi-automatic process (Fig. 1).

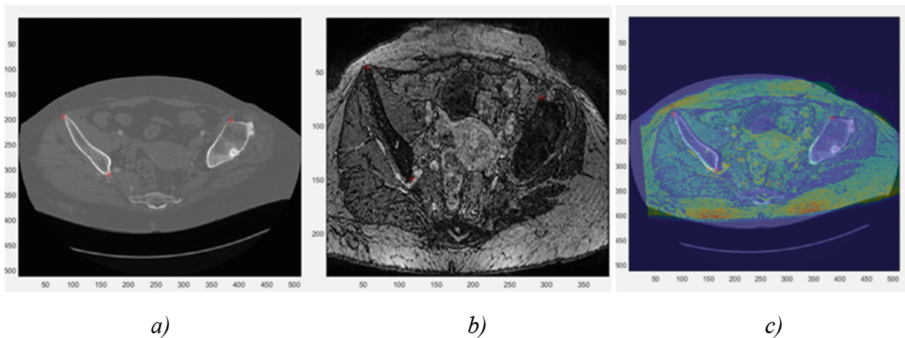


Fig. 1. CT/MRI integration: a – slice on CT scan, b – similar slice on MRI scan, c – CT and MRI combined scan.

4.2 Formation of Virtual and Full-Scale Model of an Anatomical Object

After receiving CT/MRI scans, one should create a virtual and full-scale model of the anatomical object. Various programs facilitate 3D models based on tomography data: RadiAnt, 3D Doctor, Simplant, ScanIp, Simpleware. To a large extent, the 3D model accuracy will depend on the specialist's engineering skills [14].

The first step in creating an individual prototype is to process multiple images that have been obtained using CT/MRI scanning. Processing includes analysis, noise removal, and image segmentation. This work is performed per each section in three study planes [15].

Specialized software is used to perform image processing. DICOM is the most common source data format. The software makes it possible to automate the segmentation process, as it can distinguish more than a hundred degrees of tissue density [9].

Initial data processing generates STL, VRML, PLY, or DXF files. STL format is preferably used to manufacture parts on an additive machine [16]. STL-file requires analysis and adjustment to correctly display and prevent errors in the polygonal grid, for example, in Autodesk NetFabb [17]. When the finished bone model is obtained, it is necessary to prepare data for AM implementation. AM perceives information in the G-code, determining conditions for the working body trajectory move, the preparatory and final actions. To form a trajectory in one plane, one should proceed to a set of sections based on a 3D model in STL format. To do this, special slicer programs are being used that allow setting printing parameters: location of the part in AM working area, temperature and speed according to the material, the configuration of supports, density of filling the part, and more. This stage is illustrated in Fig. 2.

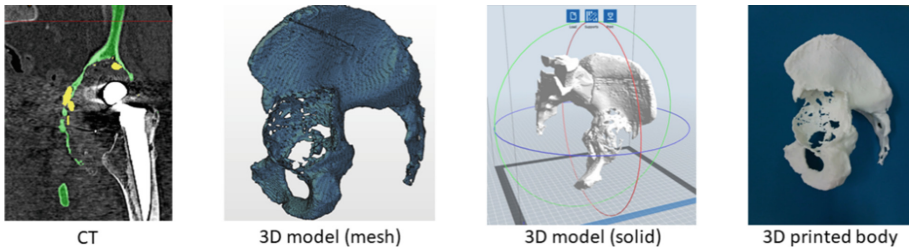


Fig. 2. Figure showing the process of converting CT/MRI into a 3D model and printed details.

4.3 Surgical Planning Using Full-Scale Models of Anatomical Objects Made Using AT

The presence of a full-scale model of an anatomical object, which on a scale of 1:1 with color separation reflects the features of clinical presentation of the patient's bone and soft tissues, is extremely clear and useful when planning a surgery. The resulting model can be divided to view and understand the anomalies before the actual surgery. The whole process can be modeled before the actual surgery, allowing surgeons to choose the best method and reduce time.

The main tasks of surgical planning include [18]:

- Identifying surgical target, its location, and relevant surrounding structures. The main vessels and nerves are determined by 3D model visual analysis, as damage to these structures can lead to bleeding and limb sensitivity loss. Considering the location of

vessels and nerves near the implant site is an important factor influencing future CI design.

- Planning surgical access – access point/location and path to a specific target structure to minimize damage to surrounding structures. During surgery, access should be provided to a body or operation site. Access should be physiological, anatomical, and sufficient to achieve the goal. Sufficient means a minimal incision that provides a comfortable area for surgery.
- Determining the position of surgical instruments and probes for treatment delivery and/or implants placement.
- Prognosticating and evaluating the expected treatment outcome, including radiation therapy, cryoablation, brachytherapy, stent placement, brain stimulation electrode or orthopedic implant, etc.

4.4 Design of a Customized Implant

CI design should take into account:

- Position of the target organ relative to access (it is not desirable to move and rotate the implant in the surgical wound, as this will injure the surrounding structures), minimally invasive access (minimal incision provides less blood loss and rapid recovery but prevents implantation of large structures).
- Assessment of bone quality. Specialized software allows estimating the bone density, which will affect the choice of type (spongy or cortical, with or without locking), direction, and length of screws.

CI design includes several zones (Fig. 3): working zone, zone of primary fixation, zone of secondary fixation-osteointegration, auxiliary zones. The engineer's task is to make a functional, safe implant, the design of which will allow preserving biological tissues (bone) as much as possible and providing a possibility of design revision in the future.

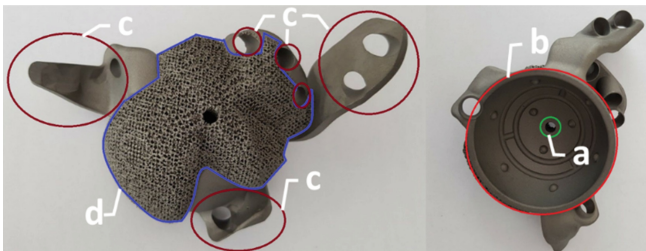


Fig. 3. Zones of customized implants (on the example of an individual acetabular component): a - auxiliary zone (hole for fixing the impactor tool); b - working zone (base surface for installing the cement component of the endoprosthesis); c - zone of primary fixation (flanges with holes for screws); d - zone of secondary fixation-osteointegration (trabecular surface).

Working Zone. This is the main CI zone, which performs the main functions of the organ. For example, for joint implants, the working zone is a friction pair that allows

joint moving. The working zone is performed as anatomically as possible (repeats the organ's shape, has the correct biomechanical spatial arrangement).

Primary Fixation Zone. For orthopedic CI, the primary fixation is made with screws. Flanges are built to place the screws, which are resting on the support zones of the bone. The contact surface of the flange with the bone reflects the surface of the bone in this zone.

Zone of Secondary Fixation-Osteointegration. This is the CI-bone contact zone, which involves further ingrowth of bone into the implant structure. It is exactly osteointegration, which ensures reliable, long-term fixation. For this purpose, the surface of CI-bone contact is made mesh-like (trabecular), duplicating the bone surface. The secondary fixation zone can be saturated with bone grafting to improve osteointegration.

Auxiliary Zone. This is the attachment zone for the impactor (implant placement tool).

Zones that come into contact with biological tissues and do not provide osteointegration should be safe for surrounding tissues, namely, do not cause tissue irritation due to a smooth surface, rounding of corners, etc. The right material is one of the important aspects of making CI. The material must meet the objectives, with due regard given to its strength and elasticity. The requirements for an implant and its material will depend on the placement site and potential load.

4.5 Regular and Stochastic Structures in Customized Implants

AT becomes effective and significantly expands the possibilities of engineering support through various regular and stochastic structures. Regular structures are divided into two- and three-dimensional. Stochastic structures can be open and closed. These solutions are integrated into implant design to improve bone tissue proliferation, approximation of CI mass, and mechanical characteristics to biological ones.

Face-centered cubic (BCC) and *body-centered cubic* (FCC) are the most common, or variations thereof, such as the inclusion of z-struts (BCCZ and FCCZ) named after similar crystal structures. Other topologies are based on struts, such as cubic, octet-truss, diamond, dodecahedron, truncated cup-tahedron, and gyroid [19]. Some designs have a high stiffness to mass ratio, others better dampen energy, and some are aimed at the aesthetic component. Such structures can withstand heavy loads, so it is possible to create a continuous-trabecular CI, to reduce the cost and weight. However, when analyzing such implant operation, one can conclude that design elements damage the soft tissues, and therefore it is advisable to use only in areas of contact with the bones.

4.6 Engineering Verification of the Customized Implant Design

Identifying Mechanical Characteristics. *Computer-aided engineering* (CAE) is the main tool for identifying CI mechanical characteristics based on computer simulation for different boundary conditions that determine the load on individual CI sections and zones. In complex cases, field experiments may be required to determine mechanical CI characteristics.

The computing power of the available computer can be one of the limitations at this stage. A modern home PC may be sufficient for continuous CI computer-aided engineering. However, if the CI design provides for solutions to reduce weight and improve performance (integrated trusses, topological optimization, generative design, and lattice structures), then, in most cases, it is necessary to use powerful workstations.

Design Optimization. When working with the project, one needs to conduct a detailed analysis and optimization of the working area. The main criteria for optimization are the approximation of the implant weight to the weight of bone under replacement and the minimization of load takeoff in the placement area.

It is necessary to study the contact areas to avoid underloading and overloading certain areas to distribute the load as evenly. Uneven loading can reduce CI service life. CI weight criterion is important to ensure patient comfort, as significant deviations in CI weight from the bone being replaced will create discomfort for the patient.

Determining the Location for Primary Fixation Elements. When designing, it is important to ensure the correct and constant location of CI in the patient's body. This problem is addressed by determining the position and stroke of the screws. There are auxiliary structures or navigators (Fig. 4) aimed to simplify the surgery and increase placement accuracy. In most cases, navigators are made using AT method from polymers. These designs, as well as CI, are developed patient-specific and disposable.

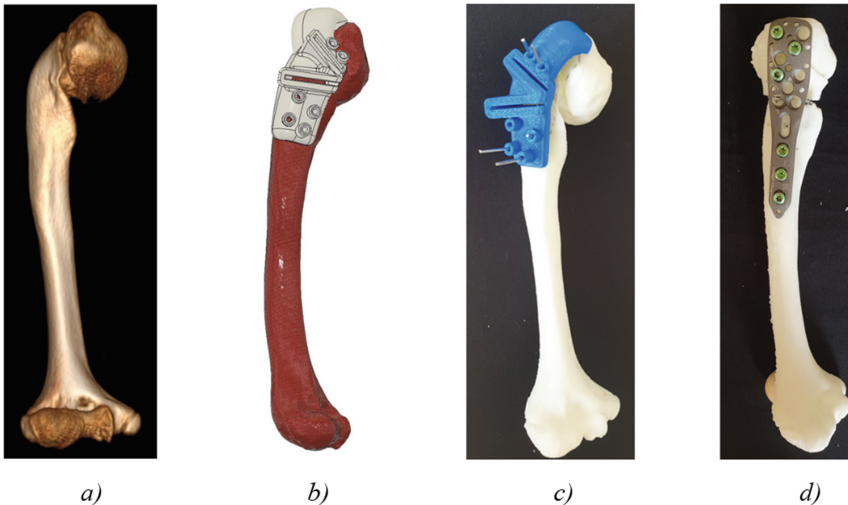


Fig. 4. Surgical navigators for correcting bone geometry, made using AT: a – baseline condition of patient's bone; b – a computer model of a bone with an overlaid navigator; c – navigator superimposed on a bone model made on a 3D printer using FDM technology; d – verifying geometry of the bone on its model.

Usually, these elements design can provide for the direction of screws, rods, placement of cutting areas. Using navigators, the surgeons can correctly guide the drill and

saw and constructively predict the depth of drilling or the range of possible cuts. Fastening of the navigator occurs with spokes through apertures in a design. Spokes do not allow design sliding on a bone during manipulations.

4.7 Choice Specifics and Application of Technologies

In CI manufacture, AT serves as the basis, but in addressing issues of achieving high surface cleanliness or thread formation, conventional machining technologies are used. When printing a thread, there is a problem with overhanging surfaces, and these areas pose a high probability of defect formation [20]. At this stage of development, it is advisable to use a set of technologies.

Post-processing of individual products should be applied in such a way as to take into account the previously defined requirements for the product. The choice of post-processes depends on the design, material, and manufacturing process. Metallic materials typically require heat treatment to reduce residual stresses and meet technical requirements. For friction surfaces, implants for joint replacement are necessary to grind and polish because these areas require high surface cleanliness to reduce resistance to motion in the future.

Individual products for implantation must be sterile at the end of production. Lattice endoprostheses especially need to be thoroughly cleaned to remove any powder particles or residues, such as dirt from abrasive paste or coolant from computer digital control processes. Typical methods include ultrasonic cleaning and the use of sterilization processes.

4.8 Quality Control of Customized Implants

Before completing the manufacturing process, product quality requires verification, even though both software and specialists constantly monitor the product during the manufacture. Currently, AMs have sufficient control over process parameters [21]. However, minor defects, uneven cooling, internal stress, and sub-optimal printing parameters can lead to defects that are sometimes so difficult to detect that a defective part can be put into operation.

ATs allow creating parts with very complex geometry, which complicates further the verification of their quality [22]. For example, lattice structures or topological optimization allow generating a part with a maximum specific strength. The geometric accuracy of products is assessed only by measuring the critical parameters of the product. However, conventional non-destructive testing methods do not apply to such parts, as the outer layer of the part may block access to its internal structure – for example, lattice filling. The only way to determine the internal component's size is to destroy the sample area and use the usual coordinate method of measurement using a coordinate measuring machine (CMM). Internal designs are completely inaccessible and require the use of non-destructive testing methods to assess product quality [23].

To optimize the quality of parts obtained using AT, it is necessary to adjust an accurate, reliable, and stable inspection and control process. One such verification method was developed by ANSYS, Synopsys, and North Star Imaging (NSI). This method uses

CT data to build a three-dimensional model. Then, Synopsys Simpleware software converts these into a final element model, the calculation of which can be performed with ANSYS. The resulting layered images should be processed using specialized software, which allows, for example, selecting fragments of the model area, in which there are differences between the design and actual geometry of the part. The obtained three-dimensional finite element model can be imported into ANSYS Mechanical to perform a calculation for strength, comparing how much the mechanical characteristics will change compared to the design.

X-ray computed tomography provides a unique method of non-destructive assessment of internal areas and structures of parts that are manufactured additively, and is increasingly used by the additive manufacturing industry to evaluate the relevant products [24].

Since additive production is based on the concept of constructing an object through the sequential application of material layers, the main parameter that characterizes the accuracy of object construction is the layer thickness of material used to build the object, i.e., the application layer. Thus, the accuracy of 3D printing is the minimum allowable layer height printed by a 3D printer. Modern FDM 3D printers can provide a thickness of up to 20 μ . Modeling of object deposition with melting allows measuring the roughness parameters Ra , Rz , and $Rmax$ not worse than 50 μ m. Also, an important element of the final stage is to reduce the surface roughness of the constructed object. Reducing the object's roughness is carried out using appropriate solvents or laser polishing, which reduces the roughness up to 1.4 μ m, which cannot be achieved by machine processing [25, 26].

Also, the necessary product documentation is generated during verification, which indicates the functional characteristics of specific parts of the implant, recommendations for placement, and auxiliary systems and tools to simplify and improve placement accuracy.

One of the verification stages can include the study of duplicate parts, which are an exact copy of the developed implant and made in one AM working chamber. This approach is possible in cases where it is not possible to calculate the created structure, and it is necessary to check the performance of the structure before placement. The copy part is exposed to a potential load or can be destroyed to obtain data on the maximum possible load.

In addition to machine processing, the parts need a special coating to improve bone tissue proliferation and reduce the body's response to a foreign body. Titanium and titanium alloys are coated with hydroxyapatite using several methods. CI coating with calcium phosphate leads to a strong early porous fixation of the implant and early bone ingrowth.

As it is shown in Sect. 4.7, the processes implemented by engineers and surgeons cannot be interrupted. In preparation for surgery, a team of surgeons is involved in the implant's planning and development. The action is worked out using plastic models and prototypes (so-called "operation to operation"). At this stage, the composition of the surgical team is being determined and the tools for intervention. A sterile model of the target area is taken to the operation theatre. This guides the surgeon during the surgery because they can access the implantation site through a small incision. Also, a map plan

or surgical equipment is provided to the operation theatre. This document describes the stages of surgery, the sequence of using navigation systems, and the defined maximum lengths of screws in different zones.

4.9 Implementation of Engineering Support System in the Manufacture of Customized Implants of the Acetabular Component Based on Additive Technologies

Anamnesis. Patient N., 54 y.o., condition after total arthroplasty of the right hip joint (fracture of the right femur neck in 2007). Aseptic instability of endoprosthesis components. Pain syndrome.

According to the methodology described in the article, Fig. 5 illustrates all stages of engineering support of the acetabular department's surgical operation.

Stage 1. Obtaining primary objective information about the patient's condition. X-ray densitometry allows assessing the structural condition of bone tissue in the individual implant fixation zone. This allows identifying bone support zones to construct primary fixation flanges and aids in deciding on which screws to choose (locked, unlocked).

Stage 2. FDM full-scale printed model. A plastic model printed at a scale of 1:1 (Fig. 5c) is currently the best method of visualizing bone defects in the acetabulum area. Using this model, the surgeon makes final decision on the appropriateness of using an individual implant.

Stage 3. FDM-printed model after first analysis by the surgical team (blue indicates the iliac support plane, red – flanges location, black – reference planes of cup reverse side contact with the strongest “bone” of the cavity bone bed).

Stage 4. CAD-based determining the correct biomechanical position of the future customized implant.

Stage 5. Final CAD model of the customized implant with the designation of screws maximum lengths.

Stage 6. Fitting of the navigation system for screws on a plastic model.

Stage 7. The customized implant of the acetabular component, made by additive technology SLM (Selective Laser Melting).

Stage 8. Fitting of the customized implant to the FDM-printed model.

Stage 9. Surgical operation (not shown in Fig. 5).

Stage 10. Post-surgery X-ray.

Clinic of Orthopedics and Traumatology in Adults ITO NAMS performed revision endoprosthesis of the right hip joint: removal of endoprosthesis components, placement of the customized acetabular system, revision leg. Bone alloplasty of acetabular defects.

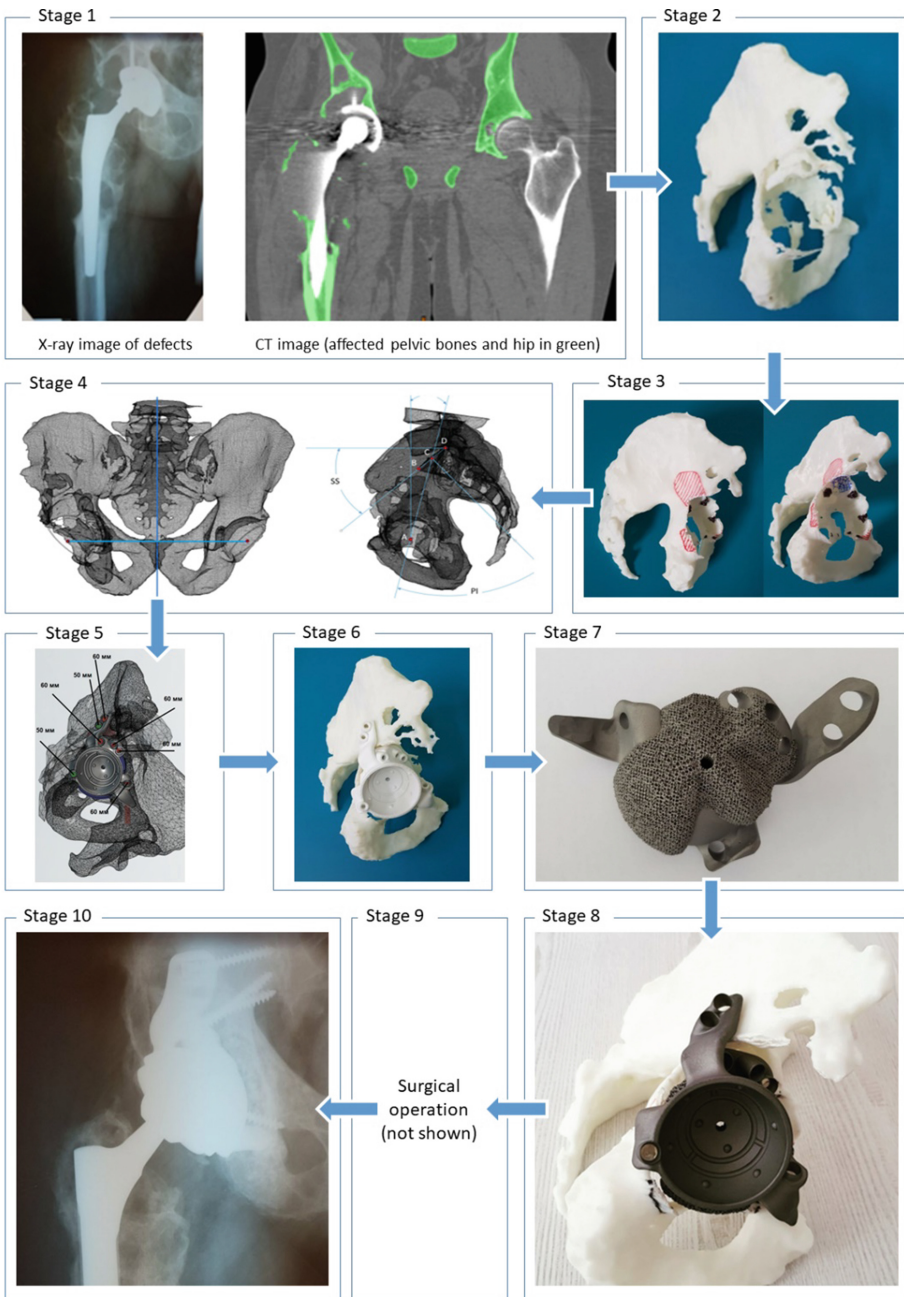


Fig. 5. Stages on the engineering support of surgery of the acetabular component.

5 Conclusions

This paper summarizes the authors' experience in terms of engineering support for the manufacture of customized implants based on the Laboratory of Biomedical Engineering at the Institute of Orthopedics and Traumatology of the National Academy of Medical Sciences of Ukraine. The general structural and logical sequence of processes described are built around the basic process of making customized implant – additive technology. According to the established division of additive technologies into Preprocessing, Processing, Post-processing, these are integrated into three stages. The necessary set of technological equipment and software has been identified, comprehensively providing a sufficient level of engineering support for complex surgeries. It is shown how and for what purposes the additive technologies of work with plastic and metals can be used. All these examples are implemented in surgeries on patients.

References

1. Jakus, A.E.: An Introduction to 3D Printing - Past, Present, and Future Promise, 3D Printing in Orthopaedic Surgery, pp. 1–15. Elsevier Inc, Amsterdam, Netherlands (2019)
2. Gaiko, G., Galuzinsky, O., Burburskaya, S.: Application of additive technologies in orthopedics and traumatology. In: *New Technologies in Orthopedics and Traumatology*, pp. 17–18. Kyiv (2018)
3. Liang, H., Zhang, Y., Yifei, W., Tao, J.: Reconstruction with 3D-printed pelvic endoprostheses after resection of a pelvic tumour. *Bone Joint J.* **99B**(2), 267–275 (2017). <https://doi.org/10.1302/0301-620X.99B2.BJJ-2016-0654.R1>
4. Christensen, A.M., Rybicki, F.J., Grant, G.T.: 3D Printing and Patient-Matched Implants, 3D Printing in Medicine: A Practical Guide for Medical Professionals, pp. 85–95. Springer International Publishing AG (2017)
5. Sourabh, M.S., Chi, Z.: Basic of 3D printing: Engineering Aspect, 3D Printing in Orthopaedic Surgery, pp. 1–15. Elsevier Inc, Amsterdam, Netherlands (2019)
6. Pasichnyk, V., Yentyn, O., Kudin, S.: Additive production: current state and prospects. In: *XIX International Science and Technology Conference on Progressive Technology, Technology and Engineering Education*, vol. 2, pp. 28–31. KPI, Kyiv (2018)
7. Laboratory of Biomedical Engineering SI “The Institute of Traumatology and Orthopedics” by NAMS of Ukraine Homepage. <https://3dlab.in.ua/>. Accessed 20 Oct 2020
8. Ahsan, N., Khoda, B.: AM optimization framework for part and process attributes through geometric analysis. *Addit. Manuf.* **11**, 85–96 (2016). <https://doi.org/10.1016/j.addma.2016.05.013>
9. Marusina, M.Ya., Kaznacheeva, A.O.: Modern types of tomography. SPbGU ITMO, SPb (2006). [in Russian]
10. O’Rourke, R., Brundage, B., Froelicher, V., et al.: Consensus document on electron-beam computed tomography for the diagnosis and prognosis of coronary artery disease. *Am. Heart Assoc. Exp. Am. Coll. Cardiol.* **102**, 126–140 (2000). <https://doi.org/10.1161/01.CIR.102.1.126>
11. Fayad, Z., Worthley, S., Helft, G., et al.: Magnetic resonance imaging of the vasculature system. In: Fuster, V., Alexander, R.W., O’Rourke, R.A. (eds.) *Hurst’s The Heart*, pp. 609–627. McGraw-Hill, New York, NY (2001)
12. Hofer, M.: *Computed Tomography. Basic Guide*. 3rd edn. Med. Lit., Moscow (2011). [in Russian]

13. Currie, S., Hoggard, N., Craven, I., et al.: Understanding MRI: basic MR physics for physicians. *Postgrad. Med. J.* **89**(1050), 209–223 (2013). <https://doi.org/10.1136/postgradmedj-2012-131342>
14. Lantada, A.D., Morgado, P.L.: Enhancing product development through CT images, computer-aided design and rapid manufacturing: present capabilities, main applications and challenges. In: Homma, N. (ed.) *Theor. Appl. CT Imaging Anal.*, pp. 269–290. Rijeka, Croatia (2011)
15. Wang, C.-S., Wang, W.-H.A., Lin, M.-C.: STL rapid prototyping bio-CAD model for CT medical image segmentation. *Comput. Ind.* **61**(3), 187–197 (2010). <https://doi.org/10.1016/j.compind.2009.09.005>
16. Kurenov, S., et al.: Three-dimensional printing to facilitate anatomic study, device development, simulation, and planning in thoracic surgery. *J. Thorac. Cardiovasc. Surg.* **149**(4), 973–979 (2015). <https://doi.org/10.1016/j.jtcvs.2014.12.059>
17. Khoda, B.: *Computer-Aided Design of Additive Manufacturing Components, Laser-Based Additive Manufacturing of Metal Parts*. Taylor & Francis Group (2018)
18. Essert, C., Joskowicz, L.: Chapter 32 - Image-based surgery planning. In: Zhou, S.K., Rueckert, D., Fichtinger, G. (eds.) *The Elsevier and MICCAI Society Book Series, Handbook of Medical Image Computing and Computer Assisted Intervention*, pp. 795–815. Academic Press (2020). <https://doi.org/10.1016/b978-0-12-816176-0.00037-5>
19. Tao, W., Leu, M.C.: Design of lattice structure for additive manufacturing. In: *2016 International Symposium on Flexible Automation (ISFA)*, pp. 325–332. Cleveland, OH (2016). <https://doi.org/10.1109/isfa.2016.7790182>
20. Munsch, M.: Laser additive manufacturing of customized prosthetics and implants for biomedical applications (2017). <https://doi.org/10.1016/B978-0-08-100433-3.00015-4>
21. Neyezhnikov, P.L., Skliarov, V.V., Prokopov, A.V.: Analysis of the capability of the national measurement standards of Ukraine for assurance of traceability in the field of additive manufacturing. *Ukrainian Metrol. J.* **1**, 22–29 (2018). <https://doi.org/10.24027/2306-7039.1.2018.134056>
22. Pasichnyk, V., Burburska, S., Kutuza, V.: Nutrition of parameters in the accuracy of endoprostheses, in the preparation of additive technologies. In: *XX International Science and Technology Conference on Progressive Technology, Technology and Engineering Education*, vol. 2, pp. 223–226. KPI, Kyiv (2019)
23. Waller, J., Parker, B.H., Hodges, K.L., Burke, E.R., Walker, J.L.: *Non-destructive Evaluation of Additive Manufacturing. State-of-the-Discipline Report*, NASA/TM-2014–218560 (2014)
24. Angel, J., De Chiffre, L.: *Inter-laboratory Comparison of Industrial Computed Tomography. CIA, CT Comparison* (2013)
25. Sikder, S., Barari, A., Kaji, F., Kishawy, H.: Using acetone vapour treatment to improve secondary finishing operations in additive manufacturing. *Proc. ASPE* 3898 (2014)
26. Alfieri, V., Argenio, P., Caiazzo, F., Sergi, V.: Reduction of surface roughness by means of laser processing over additive manufacturing metal parts. *Materials* **10**(1), 30, 1–12 (2017). <https://doi.org/10.3390/ma10010030>



The Dynamic Model of the Automatic Clamping Mechanism with a Rotating Input Link

Borys Prydalnyi^(✉) 

Lutsk National Technical University, 75, Lvivska St., Lutsk 43018, Ukraine
b.prydalnyi@lutsk-ntu.com.ua

Abstract. Some features of a new design of clamping mechanism drive for automatic fixing of cylindrical objects in metalworking machines are considered. One of the proposed design features is a rotating input link, which receives input energy in the form of rotational motion. The presented drive's operation is considered a part of the clamping mechanism with a collet chuck. Furthermore, the clamping mechanism's interaction with a drive of the main movement of a lathe is described. The dynamic model is presented as a system with lumped parameters, consisting of rigid bodies connected by inertialess elastic-dissipative links. The stages of the backlash elimination and conversion of the mechanism elements' kinetic energy into the system's stressed state's potential energy are considered separately. The obtained results can contribute to the development of methods for calculating this type's structures' parameters. They can be helpful in the determination of more optimal geometric-mass parameters of the elements of these structures.

Keywords: Clamp drive · Spindle assembly · Lathe

1 Introduction

It is known that the productivity of processing on metalworking machines can be improved by increasing the cutting modes. That is, it is necessary to increase the rate of chip removal or chip load. Increasing the spindle assembly's rotation speed (SA) requires improving the dynamic characteristics of its design and the ability to balance accurately and more [1, 2]. Increasing the feed during machining increases the cutting forces acting on the object fixed (tool or workpiece) and requires an increase in the clamping forces for effective fixation. Providing the required parameters for clamping workpiece or cylindrical tool in metalworking machines depends on the clamping mechanism (CM) operation, which is part of the SA. One of the main and largest subsystems of the CM is its drive (actuator) ACM. For eliminating these shortcomings and improving the conditions of workpiece processing, a new ACM design [3] was developed.

2 Literature Review

Several scientific papers present mathematical models and studies of spindle assemblies' characteristics as a single system without singling out clamping mechanisms.

The operation principles of new clamping mechanisms of the CNC lathe are described in [4]. Mathematical models of trajectories spindle with lumped parameters have been developed [5]. In [6], ultra-precision spindle's dynamic properties at different speeds are investigated using experimental impact tests. Machine tool dynamics is modeled using the finite element approach [7]. Using the design matrix, a flow-chart for the dynamics design method coupled with multisource information was obtained in [8]. In [9], carbon fiber reinforced plastic is described as a promising material for enhancing machine tools' spindle performance. The paper [10] covers diagnostics and monitoring CNC machine tools, industrial robots, and production lines. The paper [11] proposes an alternative method of balancing motorized spindles based on the real-time position data of CNC machine tools to reduce the costs associated with external balancing instruments and improve the dynamic balancing process's efficiency. The method of estimation the cutting forces and vibrations at the milling tool from accelerometers mounted on the spindle housing is presented in [12]. A specific electromagnetic excitation device is used to measure the Frequency Response Function of the spindle at high speeds, and the evolution with the speed of the eigenfrequencies and the radial stiffness is analyzed in [13]. In the paper [14] an experimental approach based on accurate characterizations of the dynamic behavior for different spindle conditions (repaired or damaged) is proposed. For improving the spindle system during the design and predict the tool dynamics, the paper [15] proposes modeling of spindle-holder assembly and presents an investigation on the contact characteristic under clamping and centrifugal forces. The paper [16] examines the influence of different clamping chucks on energy consumption parameters, tool wear, and surface qualities, thereby focusing on important sustainability indicators in machining operations. In [17], clamping force-deformation characteristics are plotted for implementing a corrective clamping mechanism to control workpiece deformations. In the study [18], experimental studying has been carried out for discussing dynamic characteristics of spindle imbalance, which induces forced oscillations and the impact on surface generation during diamond turning. For minimizing the duration of the clamping and unclamping processes, it is necessary to ensure the high speed of the CM and, as a result, significant acceleration of its elements. This shows the feasibility of analyzing the dynamic characteristics of the CM structures.

3 Research Methodology

The developed model (Fig. 1), which describes the CM's work with the new ACM, is a system with lumped parameters, comprising perfectly rigid bodies interconnected by inertial elastic-dissipative elements. The pliability and dissipative forces of internal friction in the material of only the most strained elements and the losses due to sliding friction in their conjugations were taken into account to simplify the dynamic model. For example, it does not take the spindle and rotor's torsional stiffness into account because they are much larger than other elements to neglect their torsional pliability.

The creation of the clamping force in CM with the presented ACM occurs with the torque's participation from the main motion drive (spindle rotation). The SA receives a rotational motion with torque M_{sh} and angular velocity ω_{sh} from the main electric motor through a set of gears that form a kinematic connection of the main drive with

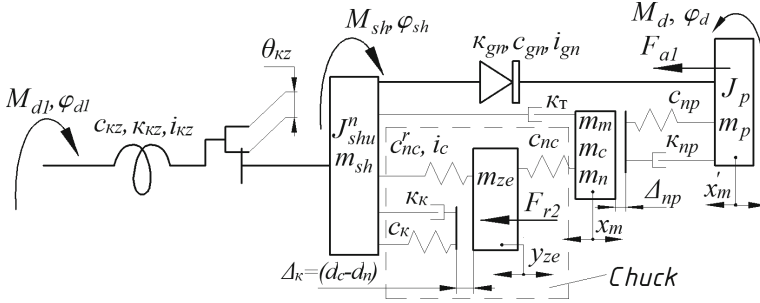


Fig. 1. The dynamic model of the new ACM [3] as a part of CM of the lathe.

a total gear ratio i_{kz} and damping characteristics (dissipation) and stiffness k_{kz} and c_{kz} respectively. The main electric motor drive's stator interacts with the rotor with a mass m_{p1} through an electromagnetic field with a damping factor k_{ed1} and stiffness c_{ed1} , which ensures its rotation with torque M_{d1} and angular velocity ω_{d1} . Thus, the rotor's rotation angle of the main motor drive ϕ_{d1} and the spindle ϕ_{sh} are related by the dependence $\phi_{sh} = \phi_{d1}, i_{kz} \pm \theta_{kz}$ and $\phi_d = \phi_{sh} + \phi$.

At the rear end of the spindle with mass m_{sh} (Fig. 1) there is a threaded surface with a diameter d_1 and pitch h on which the rotor of the motor ACM with the outer diameter d_2 , mass m_p and moment of inertia J_p is screwed. The threaded surfaces of the spindle and rotor form a self-braking screw-type gear with a transmission ratio i_{gn} . The ACM rotor interacts with the stator through an electromagnetic field with damping k_{ed} and stiffness c_{ed} characteristics, which allows the ACM rotor to rotate to the machine body with torque M_d and angular velocity ω_d that differs from ω_{sh} . The forces of friction in the screw self-braking gear determine its damping characteristics k_{gn} and create the braking torque M_g^T . The resultant of torques M_{sh} and M_d cause the rotor's rotation relative to the spindle with force F_{a1} speed $\omega_{\Delta} = \omega_d - \omega_{sh}$, and axial movement of the rotor ACM approximately equal to the movement value x'_T of the output link-rod to transmit force to the clamping chuck (Fig. 1). The moments of inertia of rotation of the elements rotating together with the spindle relative to its axis are reduced to the flywheel with the moment of inertia J_{shu}^n .

The transmission of axial force F_{a1} to the clamping chuck occurs after backlash elimination $\Delta_{\Pi p}$ appears in the CM as a specific feature of the installation, adjustment, and wear. This reduces the magnitude of the axial movement of the input link of the clamping chuck by the value $x_m = x'_m - \Delta_{np}$. The axial force F_{a1} is transmitted through a set of transmission links with total stiffness $c_{\Pi p}$ and damping k_{np} to the output link-rod, collet chuck and workpiece with masses m_T, m_c and m_π respectively. The movement of these masses in the axial direction is counteracted by friction forces S_T^T , which occur mainly in the contacts of the surfaces of the spindle and the link-rod. This interaction is characterized by the damping coefficient K_T .

The processes that take place in the clamping chuck (in Fig. 1. the area is indicated by a dashed line) are presented in a simplified form. Axial movement x_T is transmitted with force F_{a1} from the link-rod to the clamping elements of the collet chuck through the petals with the coefficient of tensile deformation $c_{\Pi c}$ (Fig. 1). This causes the force

interaction in the wedge mechanism of the collet with the gear ratio i_u . The clamping elements of the collet with the mass m_{ze} is also moving in the radial direction by the value, which is counteracted by the force of elastic deformation of the collet petals with a coefficient $c_{\Pi c}^{\gamma}$. When the clamping elements are moving in the radial direction, it causes the backlash elimination (mainly between the surfaces of the workpiece and the clamping elements) with the total value Δ_k , and the workpiece is clamping with effort $F_{\gamma 2}$. The contact characteristics of the clamping elements with the spindle and the workpiece and the size of the gaps are described by the coefficient of elasticity c_k , damping K_k , and the size of the gap $\Delta_K = (d_c - d_{\Pi})$, where d_c , d_{Π} are the diameters of the collet hole and the workpiece, respectively.

The rotation of the ACM rotor in the opposite direction to the spindle rotation can be obtained when the ACM engine is running in the mode of electric machine brake. One of the recommended modes is regenerative braking, which provides certainty of the rotor speed ω_d , which it seeks to achieve due to braking – synchronous motor frequency. This improves the conditions for regulation the work of ACM – obtaining the required value ω_{Δ} . The maximum torque M_d on the rotor ACM in this mode is slightly higher than in the driving mode due to resistance losses in the stator, which in the driving mode leads to a decrease in torque, and in the generator – to additional use (consumption) of the external driving torque, ie. braking.

Two variants of the initial operating conditions of the ACM can be distinguished at $\omega_d = \omega_{sh}$, ($\omega_{\Delta} = 0$): SA is stopped $\omega_{sh} = 0$; the SA rotates $\omega_{sh} \neq 0$. When at the initial stage SA rotates ($\omega_{\Delta} = 0$, $\omega_{sh} \neq 0$), there are two ways to ensure the difference ω_{Δ} in angular velocities of the rotor and spindle ($\omega_d \neq \omega_{sh}$) for the ACM operation:

1. The ACM motor is only switched on during clamping or unclamping processes. Outside these processes, the magnetic field's influence on the rotor ACM is absent, so it rotates with the spindle under the action of the moment M_{sh} from the drive of the main motion. The process of switching on the ACM motor can be accompanied by negative effects in the CM which is associated with transients.
2. The ACM motor idles during spindle rotation and provides rotation of the rotor under the influence of torque M_{π} with a frequency identical to the spindle speed $\omega_d = \omega_{sh}$ ($\omega_{\Delta} = 0$). This requires constant monitoring of the actual speeds of the spindle and rotor ACM and their coordination. For performing clamping (unclamping), the current characteristics U, I, v are changed by the controller device to ensure rotation of the rotor with an angular velocity ω_d that differs in modulus or direction from the angular velocity of the spindle ω_{sh} by a given value $\omega_{\Delta} = \omega_d - \omega_{sh}$.

Depending on the parameters of the CM's elements with ACM, control system, and method of obtaining ω_{Δ} , the number of stages of its work may be different. In the most general case, we can distinguish two stages of the CM:

1. Transients in ACM during its uncontrolled acceleration from the state of rest and the absence of resistance forces on the output link to the output axial force's appearance. This stage is characterized by the beginning of the movement and active acceleration of moving masses during backlash elimination $\Delta_{\Pi p}$ and Δ_K without the emergence of

deformations of links and tension in the system. Energy is also spent on overcoming friction forces. There is an increase in the kinetic energy of the CM

2. The value of the axial force on the output link increases from zero to the maximum steady-state, which is accompanied by the appearance of elastic deformations of the links of the CM (the appearance of the stress state of the system). The kinetic energy of the motion of the CM links is transformed into the potential energy of the stress state of the system. The engine ACM rotor rotation speed rapidly approaches the spindle rotation speed, which ends with self-braking in the screw-type gear.

The nature of the transients during the operation of the CM depends on the features of its design. Backlashes θ_{KZ} , $\Delta_{\Pi p}$ and Δ_K which exist in the kinematic pairs of the CM, are expressed in the form of a conditional resulting angular gap which is reduced to the input link and can determine the features of operating the CM at the initial stage. If this angular backlash's magnitude is significant, then the transient electromagnetic process associated with the ACM motor's start can be considered completed during the backlash elimination. It means that before the ACM motor starts work under the load from the resistance torque, there is the process of some free run with non-zero initial speed and torque. In the mathematical model, this can be expressed by other initial conditions and the appearance of an additional equation of motion. In the case of small gaps in the kinematic pairs, we can assume that the torque of resistance applies to the rotor ACM at the initial moment of start-up and remains invariant for some time. Self-braking transmission with a gear ratio $i_{g\pi}$ conditionally divides the elastic-deformable torsional system of the MR into two sections. In the absence of action M_d (the ACM motor is switched off), the torque of elastic deformation $M_c = f(\phi, c_{\Pi p}, c_{\Pi c}, c_{\Pi c}^\gamma, c_K)$ forces can unscrew the elements of the transmission of the ACM in the opposite direction to what it was during the clamping. The self-braking screw gear transmission remains locked if elastic forces' moment does not exceed the moment of friction forces M_g^T in the transmission created during the clamp. Under these conditions, after the ACM engine shutdown, its rotor performs decaying oscillations due to the action of the CM links' elastic forces (c_{zm}) and dissipative factors with damping coefficient K_{zm} (Fig. 1). If the maximum value of the torque from elastic forces exceeds the self-braking torque M_g^T , there is braking-off (release) of the system, which reduces workpiece clamping forces and reduces ACM work reliability. To unclamp the workpiece, the condition braking-off the ACM $M_d > M_g^T$ must be met. The ACM motor creates peak torque at the initial stage due to statical friction forces. Dynamic displacements caused by the elastic characteristics of the CM links (c_{zm}) (Fig. 2) can be considered as forced oscillations (torsional) of the multi-mass system near the "equilibrium" motion of the system elements with rigid links. Oscillations are caused by the action of active forces and forces of inertia.

When the rotor's rotation speed with the moment of inertia J_p is changing by the value ω_Δ , there is a dynamic torque $M_{Jp} = J_p \frac{d\omega_\Delta}{dt} = J_p \ddot{\phi}(t)$. The rotation of the rotor relative to the spindle is also associated with the movement in the axial direction of lumped masses m_p, m_T, m_c, m_π , so the action of inertia of these links must be reduced to the rotor in the form of a moment of inertia $J_p^P = f(m_p, m_T, m_c, m_\pi, m_{ze}, i_{g\Pi}, i_c)$, which corresponds to the torque $M_p^P = J_p^P \frac{d\omega_\Delta}{dt} = J_p^P \ddot{\phi}(t)$. As a result of the force interaction of the rotor with the spindle through the links of the CM (Fig. 2) with elastic-dissipative

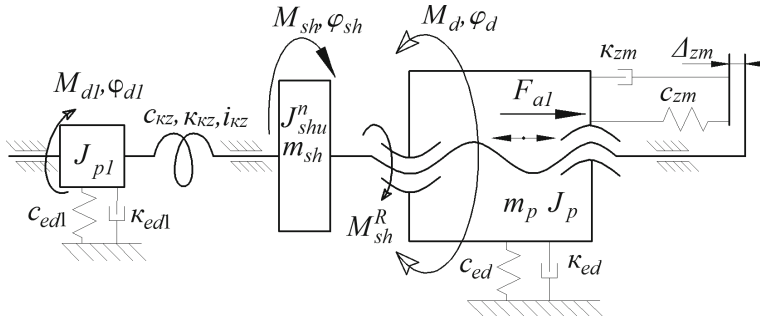


Fig. 2. Interaction of CM with other subsystems of the machine.

characteristics c_{zm} and K_{zm} there are torques from the action of elastic forces $M_C = f(\phi, c_{\Pi p}, c_{\Pi c}, c_{\Pi c}^y, c_k)$ and dissipative forces $M_k = f(t, \phi, K_{\pi p}, K_T, K_K)$ that counteract the rotation of the rotor relative to the spindle during clamping of a workpiece. Thus, the torques M_d and M_{Jp} arising on the rotor of the ACM motor during the clamp are counterbalanced by the torque of resistance $M_R = M_K + M_C + M_{Jp}^P$ applied to the rotor from the CM.

$$M_d - M_{Jp} = M_K + M_C + M_{Jp}^P \quad (1)$$

The electromagnetic torque M_π in the mode of high deceleration $\omega_d \rightarrow \omega_{sh}$ under the action M_R can be represented as a function of speed and supply voltage $M_d = f(\dot{\phi}_d, U)$, and the condition of providing the required value of the clamping forces $F_{\gamma 2}$ is presented as M_d^{maxR} . If $M_d = 0$, the expression implies the condition of the clamp due to the action of inertia.

At the final stage of the clamp, the kinetic energy of motion of the CM elements is converted into the stress state's potential energy, so when the rotor slows down under the action of active forces (M_K and M_C) the value $\frac{d\omega_\Delta}{dt}$ became negative and torques M_{Jp} and M_{Jp}^P change direction. Overcoming the torque M_R of resistance of the rotor rotation relative to the spindle due to the action on the rotor of the torques M_π and M_{Jp} causes the appearance of equal in modulus and opposite in direction reactive torque $M_w^R = M_\theta - M_{Jp}$ on the spindle.

The torque M_{d1} from the main drive motor is transmitted to the SA through the gears with the common gear ratio i_{kz} and characteristics of damping K_{Kz} and stiffness c_{kz} . In the steady-state mode of rotation of the spindle at a constant speed, $\omega_{sh} = \omega_{d1} \cdot i_{kz}$ it is counteracted by the torque M_{sh} that arises as a result of the action of dissipative factors, so it fulfilled equality $M_{d1} \cdot i_{kz} = M_{sh}$. The influence of the torque M_{sh}^R that occurs during the ACM operation causes a change in the speed of rotation of the SA and causes the appearance of a dynamic torque $M_{Jsh}^P = J_{shu}^\pi \frac{d\omega_{sh}}{dt}$, which also counteracts M_{d1} . Thus the mathematical equality is fulfilled.

$$M_{d1} \cdot i_{kz} = M_{sh} + M_{sh}^R + M_{Jsh}^P \quad (2)$$

The dynamic qualities of this system, which contains the drive of the main motion and the CM with the new ACM, can be approximately estimated by the transients' duration. During the transition process, the torques M_{sh} and M_{sh}^R are constant values, the time dt corresponding to the change of the angular velocity $d\omega_{sh}$ can be determined from the equation of motion by the formula.

$$dt = J_{shu}^n \frac{d\omega_{sh}}{M_{d1} \cdot i_{kz} - M_{sh} - M_{sh}^R} \tag{3}$$

The transient processes that appear in the spindle drive resulting from operation ACM cause the change of spindle rotation speed from ω_{sh} to $\omega_{sh} + \omega_{sh}^R$. They can be found by integrating the previous expression.

$$t = \int_{\omega_{sh}}^{\omega_{sh} + \omega_{sh}^R} \frac{J_{shu}^\pi \cdot d\omega_{sh}}{M_{d1} \cdot i_{kz} - M_{sh} - M_{sh}^R} = \frac{J_{shu}^\pi \cdot \omega_{sh}^R}{M_{d1} \cdot i_{kz} - M_{sh} - M_{sh}^R} \tag{4}$$

This system's tendency to oscillations, and, as a consequence, the margin of stability can be characterized by the maximum value of the torque on the spindle ($M_{sh} + M_{sh}^R$) relative to the steady-state value M_{sh} after the transition process.

$$G = \frac{(M_{sh} + M_{sh}^R) - M_{sh}}{M_{sh}} = \frac{M_{sh}^R}{M_{sh}} \tag{5}$$

4 Results

The mathematical description of the processes occurring during the work the CM with the new ACM and their influence on the main motion drive of the machine can be reduced to a system of equations with a description of the motion of two sections of the system – the main electromotor with transmission and the SA which are connected by elastic-deformable connection with the characteristics K_{kz} , c_{kz} and i_{kz} (Fig. 1, 2). The torque of the engine of the drive of the main movement $M_{\pi 1}$ is counteracted by the moments of active forces M_C^{KZ} , M_K^{KZ} and $M_{Jp1} = J_{p1} \frac{d\omega_{d1}}{dt} = J_{p1} \ddot{\phi}_{dt}(t)$ forces of inertia. Thus, the torque M_C^{KZ} is counteracted by the torques M_{sh} and M_{sh}^R the dynamic torque $M_{jsh}^P = J_{shu}^n \frac{d\omega_{sh}}{dt} = J_{shu}^n \ddot{\phi}_{sh}(t)$.

Therefore, the change in the rotation speeds ω_{d1} of the main drive and ACM elements depends on the magnitude of the driving moments M_{d1} and M_d . The control of the CM's characteristics with the new ACM can be performed by adjusting the values M_d and ω_d , which also affects ω_{d1} due to changes in the load on the motor of the main motion drive. The magnitude of the change ω_{d1} depends on the stiffness of the mechanical characteristics of the motor of the main motion drive, which reflects the nature of the

change in the angular velocity of the engine $\Delta\omega_{d1}$ with a change in torque ΔM_{d1} , $\beta = \frac{\Delta M_{d1}}{\Delta\omega_{d1}}$. Therefore $\omega_{d1} = f(M_d, \beta)$.

$$\left\{ \begin{array}{l} M_{d1} - M_C^{kz} - M_K^{kz} = J_{p1} \frac{d\omega_{d1}}{dt} = J_{p1} \ddot{\phi}_{d1}(t); \\ M_C^{kz} - M_{sh} - M_{sh}^R = J_{shu}^n \frac{d\omega_{sh}}{dt} = J_{shu}^n \ddot{\phi}_{sh}(t); \\ M_C^{kz} = c_{kz}(\phi_{sh} - \phi_{d1} \cdot i_{kz} \pm \theta_{kz}); M_K^{kz} = K_{kz} \frac{d\phi_{dt}}{dt}; \\ \omega_{d1} = \frac{\omega_{sh}}{i_{kz}}; \phi_{sh} = \phi_{d1} \cdot i_{kz}; \omega_{\Delta} = \omega_d - \omega_{sh}; \\ M_{sh} = \frac{M_{d1}}{i_{kz}}; M_{sh}^R = M_d - M_{Jp} = M_K + M_C + M_{Jp}^P; \\ M_C = f(\phi, c_{np}, c_{nc}, c_{nc}^r, c_k); M_{Kf}(t, \dot{\phi}, k_{np}, K_T, K_k); \\ M_d = f(\phi_d, U); \phi_d = \phi_{sh} + \phi; \\ M_{Jp} = J_p \frac{d\omega_{\Delta}}{dt} = J_p \ddot{\phi}(t); M_{Jp}^P = J_p^P \frac{d\omega_{\Delta}}{dt} = J_p^P \ddot{\phi}(t). \end{array} \right. \quad (6)$$

After substituting the second equation of the system for the first one we obtain

$$M_{d1} - \left(J_{shu}^n \frac{d\omega_{sh}}{dt} + \frac{M_{d1}}{i_{kz}} + M_d - M_{Jp} \right) - M_K^{kz} = J_{p1} \frac{d\omega_{dt}}{dt}$$

$$M_{d1} \left(1 - \frac{1}{i_{kz}} \right) - K_{kz} \omega_{d1} - \dot{\omega}_{d1} (J_{p1} + J_{shu}^n, i_{kz} + J_p \cdot i_{kz}) = M_d - J_p \dot{\omega}_d \quad (7)$$

5 Conclusions

The identified dependencies show the patterns of influence of the characteristics of the machine's main driver on the CM's operation with the new ACM. A dynamic model is compiled, and mathematical dependences are presented, which describe the geometric-mass, kinematic, and force characteristics of the CM operation. The peculiarities of the stages of the CM with the new ACM depending on the size and presence of gaps, characteristics of the elasticity of kinematic connections, the mass of elements, and specifics of control are revealed. The use of the obtained dependences promotes the development of the parametric synthesis of this type's structures.

References

1. Cisar, M., Kuric, I., Cubonova, N., Kandra, M.: Design of the clamping system for the CNC machine tool. In: 13th International Conference on Modern Technologies in Manufacturing, pp. 14–20. EDP Sciences, Cluj-Napoca (2017)
2. Mori, K., Bergmann, B., Kono, D., Denkena, B., Matsubara, A.: Energy efficiency improvement of machine tool spindle cooling system with on-off control. CIRP J. Manuf. Sci. Technol. **25**, 14–21 (2019)
3. Kuznetsov, Y., Prydalnyi, B., Redko, R.: Device for clamping rod-shaped material. Patent of Ukraine 95323 (2011)
4. Alquraan, T., Kuznetsov, Y., Tsyvd, T.: High-speed clamping mechanism of the CNC lathe with compensation of centrifugal forces. Procedia Eng. **150**, 689–695 (2016)

5. Fedorynenko, D., Sapon, S., Boyko, S.: Accuracy of spindle units with hydrostatic bearings. *Acta Mech. Automatica* **10**(2), 117–124 (2016)
6. Foremny, E., Schenck, C., Kuhfuß, B.: Dynamic behavior of an ultra precision spindle used in machining of optical components. *Procedia CIRP* **46**, 452–455 (2016)
7. Grossi, N., Scippa, A., Montevecchi, F., Campatelli, G.: A novel experimental-numerical approach to modeling machine tool dynamics for chatter stability prediction. *J. Adv. Mech. Des. Syst. Manuf.* **10**(2), 1–10 (2016)
8. Jia, Q., Li, B., Wei, Y., Chen, Y., Yuan, X.: Axiomatic design method for the hydrostatic spindle with multisource coupled information. *Procedia CIRP* **53**, 252–260 (2016)
9. Kono, D., Mizuno, S., Muraki, T., Nakaminam, M.: A machine tool motorized spindle with hybrid structure of steel and carbon fiber composite. *CIRP Ann.* **68**(1), 389–392 (2019)
10. Kuric, I., Cisar, M., Tlach, V., Zajacko, I., Gal, T., Wiecek, D.: Technical diagnostics at the department of automation and production systems. In: Burduk, A., Chlebus, E. (eds.) *ISPEM 2018, Advances in Intelligent Systems and Computing*, vol. 835, pp. 474–484. Springer, Cham (2019)
11. Zhang, L., Zha, J., Zou, C., Chen, X., Chen, Y.: A new method for field dynamic balancing of rigid motorized spindles based on real-time position data of CNC machine tools. *Int. J. Adv. Manuf. Technol.* **102**(5–8), 1181–1191 (2018). <https://doi.org/10.1007/s00170-018-2953-2>
12. Postel, M., Aslan, D., Wegener, K., Altintas, Y.: Monitoring of vibrations and cutting forces with spindle mounted vibration sensors. *CIRP Ann.* **68**(1), 413–416 (2019)
13. Rabréau, C., Ritou, M., Le Loch, S., Furet, B.: Investigation of the evolution of modal behavior of HSM Spindle at high speed. *Procedia CIRP* **58**, 405–410 (2017)
14. Ritou, M., Rabréau, C., Le Loch, S., Furet, B., Dumur, D.: Influence of spindle condition on the dynamic behavior. *CIRP Ann.* **67**(1), 419–422 (2018)
15. Wan, S., Hong, J., Du, F., Fang, B., Li, X.: Modelling and characteristic investigation of spindle-holder assembly under clamping and centrifugal forces. *J. Mech. Sci. Technol.* **33**(5), 2397–2405 (2019). <https://doi.org/10.1007/s12206-019-0438-3>
16. Thorenz, B., Westermann, H.-H., Kafara, M., Nützel, M., Steinhilper, R.: Evaluation of the influence of different clamping chuck types on energy consumption, tool wear and surface qualities in milling operations. *Procedia Manuf.* **21**, 575–582 (2018)
17. Yadav, M.H., Mohite, S.S.: Controlling deformations of thin-walled Al 6061–T6 components by adaptive clamping. *Procedia Manuf.* **20**, 509–516 (2018)
18. Zhang, S., Yu, J., To, S., Xiong, Z.: A theoretical and experimental study of spindle imbalance induced forced vibration and its effect on surface generation in diamond turning. *Int. J. Mach. Tools Manuf.* **133**, 61–71 (2018)



The Optimal Conditions for Adding Strain to the Deformation Zone During the Expansion of Automobile Pipe Adapters

Ruslan Puzyr¹(✉) , Eduard Klimov² , Andrii Chernish² , Serhii Chernenko² ,
and Yuliia Sira¹

¹ Kremenchuk Mykhailo Ostrohradskyy National University College,
7, Chumatskyi Shliakh Street, Kremenchuk 39621, Ukraine

² Kremenchuk Mykhailo Ostrohradskyy National University, 20, Pershotravneva Street,
Kremenchuk 39600, Ukraine

Abstract. It is shown that pipe parts with an increased diameter of the edge portion are widely used in the automobile industry as connecting adapters for fuel and exhaust systems. Moreover, one of the requirements for the manufacture and further operation of adapters consists of the same wall thickness of the part in each of its sections. This requirement is almost impossible to meet if the diameter of the end of the tubular billet is increased using a traditional expansion process. To increase the thickness of the part at the end after the expansion, various methods of adding strain to the deformation zone in the form of retaining rings, bandages, and spring elements are used. This increases the cost of technology. The paper presents the results of a numerical experiment to determine the optimal conditions for additional loading of the deformation zone using conical protrusions on the punch generatrix. It is shown that this method of increasing the thickness of the finished part wall is efficient and does not require special costs. The thickness of the finished product at the end of the billet will depend on the location of the conical protrusion on the punch, its length, and the geometric characteristics of the tubular billet. A punch with a protrusion at the end of the conical surface's generatrix has better results compared to a tool with a straight generatrix.

Keywords: Tubular billet · Plastic deformation · Increase of the billet thickness

1 Introduction

Tubular billets with an enlarged neck diameter on one or both sides have found their application as connecting elements for automobiles' fuel and exhaust systems [1, 2]. It is well known that the automobile's power is increased up to 10% of the designed one due to the use of direct-flow resonators and improved exhaust manifolds [2–4]. Moreover, high operational requirements are imposed on the design and material of these parts. They must be resistant to corrosion, which is especially prone to the walls of the exhaust manifold. Here, the temperature of gases during operation can exceed 1000 °C; when the engine is stopped, sharp cooling occurs, which entails the formation of condensate and

increased corrosive wear. The resonator and exhaust manifold operate under conditions of increased vibrations. Therefore, they are susceptible to mechanical damage in cracks in the base metal and welds [5, 6]. An increase in diameter at the end of a tubular billet is required for welded joints with larger diameter pipes or seats, flanges, and adapters.

The equality of the thicknesses of the joined parts is one of the conditions ensuring the tightness and strength of such a connection. The main method of making sockets on pipes is their expansion in a cold state. However, an increase in the pipe end diameter entails a decrease in the wall thickness from the end of the billet to the non-deformable part according to the linear law [7, 8]. The expansion process is characterized by the simplicity of tooling, a press table in the form of a thrust element, and a punch as a deforming tool. Equipment in the form of a single-action press is used [9, 10]. An increase in the billet diameter is limited by the loss of stability of the non-deformable part of the pipe and the localization of deformations at the end, and destruction in the form of longitudinal cracks [11, 12]. Therefore, the efforts of researchers and practitioners are aimed at studying the stress-strain state in the deformation zone to predict the final dimensions of parts depending on the initial conditions, tool design, technological factors and determine the optimal conditions for shaping.

2 Literature Review

The influence of the anisotropy of the billet metal and various expansion factors is given in [13–15], where the relationship between the punch half-cone angle and the expansion ratio with an increase in relative stresses is shown experimentally. Moreover, the expansion ratio had a greater influence on the increase in relative stresses. Papers [16, 17] contain analytical dependences for calculating the stress field during the expansion of a tubular billet and comparing the calculation results with finite element modeling. This comparison showed good agreement between the results of the two calculation methods. The authors of [18, 19] studied the effect of various types of loading on buckling during the expansion of tubular billets theoretically. Prediction of the stress-strain state during pipe expansion is described by analytical models [20, 21], which consider the process's various design and technological parameters. In papers [22–24], an elastoplastic model of the expansion process for thick-walled cylinders was developed. Also, the author [25] states that between the rigid punch and the molded part during deformation in certain intervals of the taper angle of the tool, constant pressure is observed during plastic deformation of the billet. All the studies described above are of great interest, but the achievements [12, 26] should be specially noted. Here the authors provide analytical and experimental solutions for predicting the length and thickness of the pipe wall after deformation, which will be discussed in this paper. In papers [27, 28], it is said that the thickness of the end part of the pipe during expansion can be increased by adding stress to the edge of the billet with retaining elements.

This paper aims to research the influence of the geometric parameters of the deforming tool on the change in the wall thickness of the socket of the finished detail.

3 Research Methodology

To increase the wall thickness of the part during the expansion of the billet, the end support in the form of a sleeve tube made of a softer metal has a positive effect. Deforming together with the billet has an additional impact in pressure on its end part [29, 30]. Preparatory operations for removing the sleeve tube and its further molding for the subsequent operation of expansion lengthen the production cycle and increase the technological cost of production as a whole. Previously, the positive effect of the structural step of the punch on the increase in the wall thickness of the edge part of the finished product was demonstrated [30, 31]. Moreover, the zone with an increased diameter of the tool was located in the center of the generatrix of the punching cone and at the beginning and the end. In all cases, an increase in the diameter of the generatrix of the conical surface led to a decrease in the logarithmic deformations in the direction of the coordinate axes X and Y, which indicated an increased thickness of the end face of the part in comparison with similar parts made by a punch with a straight generatrix.

This research continues to study the effect of a sharp change in the punch diameter at a certain section of the generatrix, which simulates the support of the billet end and aims to determine the optimal position of the support along the generatrix of the punch and its dimensions from the point of view of the smallest radial logarithmic deformations.

In the numerical experiment, deforming tools with protrusions along the generatrix of a conical surface were used. The protrusions were located at the beginning, in the middle, and at the end of the generatrix of the conical punch. However, for the first variant, the length of the protrusions was 2.8 mm, for the second –4.2 mm (Fig. 1). The height of the punches and the expansion ratio for all deformation variants were the same and amounted to 15 mm and $k = 1.38$, respectively. The smaller punch diameter was $d = 21$ mm, the larger one was $D = 29$ mm. Geometric dimensions of the pipe: inner diameter $d_0 = 21$ mm, wall thickness $t = 2$ mm, and length $l = 50$ mm.

The task was modeled in a 3D setting in the finite element analysis software package Simulia Abaqus – student edition. The billet was represented as a deformable solid, while the punch was modeled as a completely rigid discrete three-dimensional body. “Revolution” is the construction method for both models. The pipe was assigned the following mechanical material characteristics (deformable aluminum type AD (A199.0)): $\rho = 2700$ kg/m³; $E = 70 \cdot 10^9$ Pa; $\mu = 0.33$, $\sigma_{0.2} = 50 \cdot 10^6$ Pa, $\sigma_v = 110 \cdot 10^6$ Pa [32]. It was believed that the material is initially isotropic, possessing isotropic strengthening in the form of $\sigma_{0.2} = 50 + 0.64e^{0.62}$ [33, 34]. At the initial step of the calculation, the billet was fixed with the lower end along all degrees of freedom. At the next step (Dynamic Explicit), surface interactions between the punch and the pipe billet were formed in the form of a kinematic contact with the final formulation of friction and the coefficient of friction equal to 0.15 [35, 36]. The boundary conditions imposed restrictions on the movement and rotation of the billet during the lowering of the punch [37, 38]. The billet was loaded with a given speed of movement of the punch along the axis of symmetry of the pipe, which was 0.25 mm/s [39].

The finite element mesh for the billet was created by a structural method of construction with a hexahedral shape of an element from a standard library of 3D stress components of the C3D8R type (eight-corner rectangular with linear order and a small-time integration step). The punch was also covered with a mesh, mainly consisted of cubic

elements using the free construction technique. The type of elements was selected from the standard library of rigid discrete bodies of the R3D4 type (four-corner volumetric bilinear rigid quadrangles).

4 Results

The results of the model experiment are presented in the figures in the form of color diagrams showing the change in stresses according to von Mises at the end of the punch stroke and graphs of the force and logarithmic deformation. For a more accurate analysis of the process, the wall thickness of the billet is divided into two layers in all experiments.

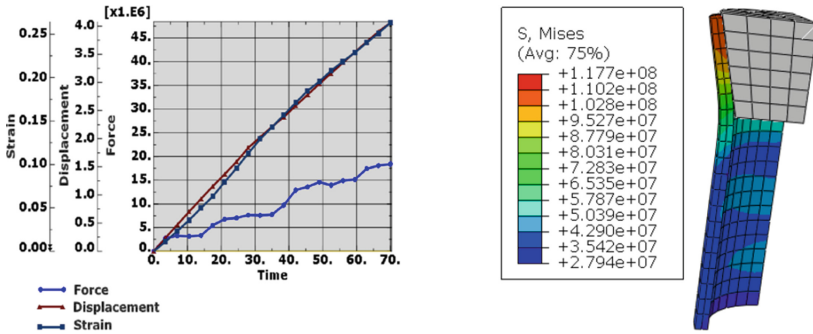


Fig. 1. Expansion of a tubular billet by a punch without a protrusion: on the left – a graph of the force, logarithmic deformation along with the billet thickness and movement of the billet end, depending on the deformation time; on the right – contour graph of stress distribution according to von Mises.

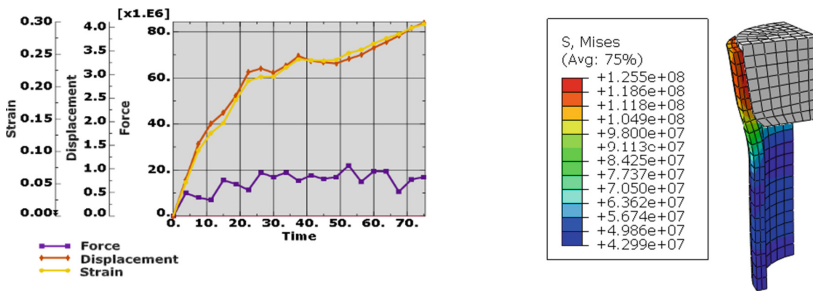


Fig. 2. Expansion of a tubular billet by a punch with a protrusion at the bottom of the generatrix (length $2/\sin 45^\circ$): on the left – a graph of the force, logarithmic deformation along with the billet thickness and displacement of the billet end depending on the deformation time; on the right – contour graph of stress distribution according to von Mises.

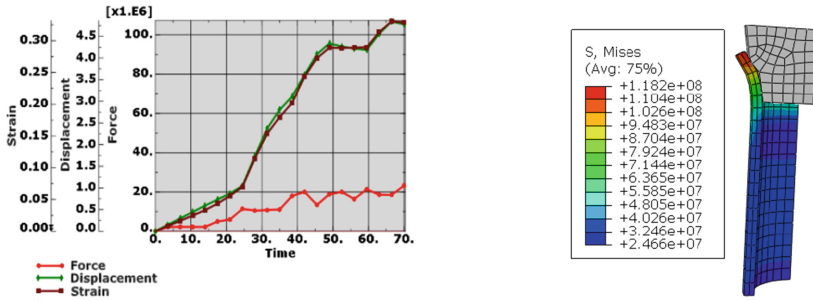


Fig. 3. Expansion of a tubular billet by a punch with a protrusion in the middle of the generatrix (length $2/\sin 45^\circ$): on the left – a graph of the force, logarithmic deformation along with the billet thickness and displacement of the billet end face depending on the deformation time; on the right – contour graph of stress distribution according to von Mises.

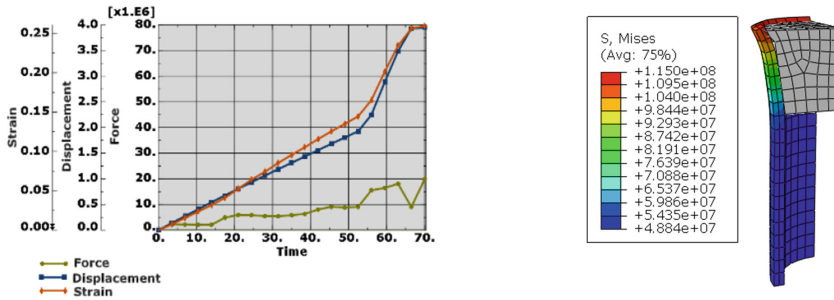


Fig. 4. Expansion of a tubular billet by a punch with a protrusion at the end of the generatrix (length $2/\sin 45^\circ$): on the left – a graph of the force, logarithmic deformation along with the billet thickness and movement of the billet end face depending on the deformation time; on the right – contour graph of stress distribution according to von Mises.

The presented contour graphs demonstrate that the zone of the billet with the largest diameter is exposed to the highest stress intensity. Moreover, for the billet, which is expanded by a punch with a protrusion at the beginning of the generatrix, it has the greatest value $\sigma_1 = 125 \text{ MPa}$. For a billet deformed by a punch with a protrusion at the end of the generatrix, the value is the smallest $\sigma_1 = 115 \text{ MPa}$. The expansion force and the actual logarithmic deformations are also of interest for analysis. They can be used to judge the degree of reduction in the wall thickness of the tubular billet. The figures show the graphs of the distribution of these values at the time of the forming process, as can be seen that in the course of deformation the force increases for all researched tool shapes. In the presence of a sharp increase in the diameter of the punch, there is a sharp increase in the force on the graph, which indicates the supporting action of the protrusions of the punches (Figs. 3, 4). Also, on the force-time charts, peak fluctuations in the values of the deformation force are characteristic of punches with protrusions (Figs. 2, 3 and 4). This may indicate fluctuations in the friction forces between the billet with a punch when the billet moves away and again contacts the tool’s surface. The billet end is subject to the greatest logarithmic deformations in thickness. So, upon reaching the given expansion

ratio $k = 1.38$, i.e., when the displacement of the edge of the billet is 4 mm, the largest logarithmic deformations are characteristic for the variant a straight generatrix of the conical surface of the tool and are equal to $\epsilon_s = 0.126$. The smallest deformations are typical of the variant with thickening at the end of the generatrix, equal to $\epsilon_s = 0.093$. An intermediate position is occupied by the results of logarithmic deformation for a punch with a protrusion in the middle of the generatrix $\epsilon_s = 0.098$ and with the deformation at the beginning of the generatrix $\epsilon_s = 0.112$.

Below are the graphs of the distribution of the expansion forces, logarithmic deformations, and displacement of the end surface of the billet for punches with a protrusion length of $3/\sin 45^\circ$ (the second variant).

As expected, the deformation force increases abruptly when the billet begins to deform by the protrusion. This creates the effect of additional loading of the deformation zone. The effectiveness of this technique can be judged by the distribution of the logarithmic deformation over the thickness at the end of the billet. So, when moving the end of the billet by 4 mm, the largest logarithmic deformations were: for a punch with a protrusion at the end of the generatrix $\epsilon_s = 0.074$ (Fig. 5); for a punch with a protrusion in the middle $\epsilon_s = 0.077$ (Fig. 6); for a punch with a protrusion at the beginning of the generatrix $\epsilon_s = 0.086$ (Fig. 7). However, it should be noted that shaping by punches with protrusions at the beginning and in the center of the generatrix of the conical surface of the tool is limited by the loss of stability of the non-deformable part of the billet. This occurs with further lowering of the punch when the billet edge moves away from the tool's surface and its movement exceeds 4 mm.

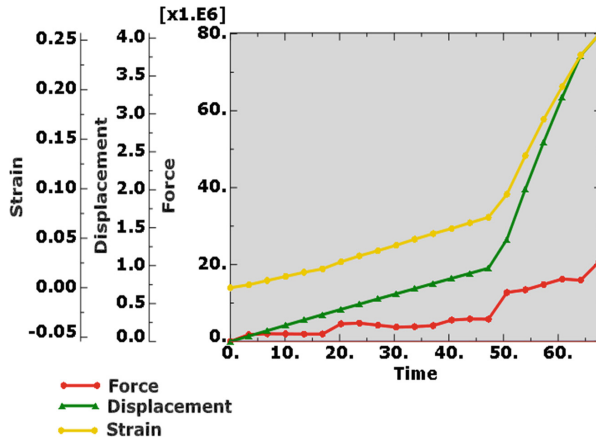


Fig. 5. Expansion of a tubular billet by a punch with a protrusion at the end of the generatrix (length 4.2 mm).

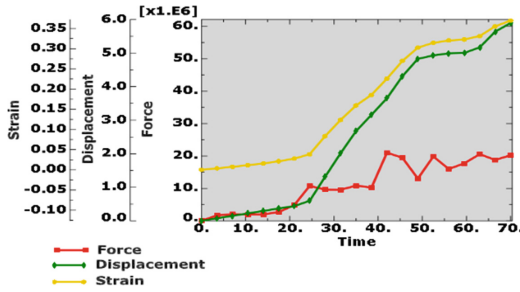


Fig. 6. The punch with a protrusion in the middle of the generatrix (length 4.2 mm).

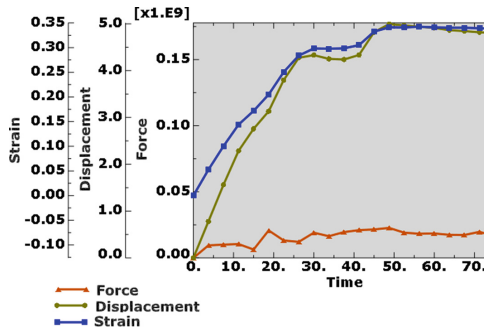


Fig. 7. The punch with a protrusion at the beginning of the generatrix (length 4.2 mm)

5 Conclusions

The performed numerical experiments make it possible to state that the presence of a step on the punch during the expansion of the tubular billet increases the wall thickness of the finished product. However, the placement of the step of the difference in diameters relative to the generatrix of the conical surface and its diameter affects the degree of thinning of the billet at the end. The best results in each group of experiments were obtained for a punch with an increased diameter at the end of the generatrix of the conical surface of the tool. For a punch with a protrusion length equal to $2/\sin 45^\circ$, the logarithmic deformation along the thickness of the billet at the end was $\epsilon_s = 0.093$, and for a punch with a protrusion length equal to $3/\sin 45^\circ - \epsilon_s = 0.074$. This is in the first case by 26%, and in the second by 41% less compared to the logarithmic deformation during expansion by a punch with a straight line generatrix, where it is equal to $\epsilon_s = 0.126$. Intermediate results were obtained by placing the protrusion in the middle of the generatrix. So with the length of the protrusion $2/\sin 45^\circ \epsilon_s = 0.098$ (22%), with the length $3/\sin 45^\circ - \epsilon_s = 0.077$ (39%). An increase in the diameter of the punch at the beginning of the generatrix led to a decrease in the thickness of the billet at the end by 11% (length $2/\sin 45^\circ$) and by 32% (length $3/\sin 45^\circ$).

Therefore, it can be assumed with confidence that if it is necessary to obtain a socket at the end of a tubular billet of a certain length with an increased wall thickness, then for this it is required to design a protrusion on the punch at the end of the generatrix

of the conical surface of the tool. With the same inclination of the generatrix of the protrusion to the punch axis, its length should be taken as long as possible, providing expansion without loss of stability of the non-deformable part of the billet. Further, it can be assumed that for certain expansion ratios, the height of the sockets, and the geometric dimensions of the billets, there are quite certain dimensions of the protrusions on the punch, with which one can maximally increase the thickness of the edge of the finished product. This task will be the subject of further development on this topic.

References

1. Karjalainen, P., Pirjola, L., Heikkilä, J., Lähde, T., Tzamkiozis, T., Ntziachristos, L., Keskinen, J., Rönkkö, T.: Exhaust particles of modern gasoline vehicles: a laboratory and an on-road study. *Atmos. Environ.* **97**, 262–270 (2014). <https://doi.org/10.1016/j.atmosenv.2014.08.025>
2. Sassykova, L., Aubakirov, Y., Sendilvelan, S., Tashmukhambetova, Z., Faizullaeva, M., Bhaskar, K., Batyrbayeva, A., Ryskaliyeva, R., Tyussyupova, B., Zhakupova, A., Sarybayev, M.: The main components of vehicle exhaust gases and their effective catalytic neutralization. *Orient. J. Chem.* **35**(1), 110–127 (2019). <https://doi.org/10.13005/ojc/350112>
3. Moroz, M., Korol, S., Boiko, Y.: Social traffic monitoring in the city of Kremenchuk. *Actual Probl. of Econ.* **1**(175), 385–398 (2016)
4. Ikpe, A., Orhororo, E., Gobir, A.: Engineering material selection for automotive exhaust systems using CES software. *Int. J. Eng. Technol.* **3**(2), 50–60 (2017)
5. Yang, M., Zhao, T., Liu, Y., Liu, X., Hou, H.: A case study of interior booming noise control in an HEV. In: *International Conference on Innovative Material Science and Technology*, pp. 232–238 (2016)
6. Martins, L., Guimarães, G., Fragassa, C.: Acoustical performance of helmholtz resonators used as vehicular silencers. *FME Trans.* **46**, 497–502 (2018). <https://doi.org/10.5937/fmet1804497R>
7. Salenko, Y., Puzyr, R., Shevchenko, O., Kulynych, V., Pedun, O.: Numerical simulation of local plastic deformations of a cylindrical workpiece of a steel wheel rim. In: Ivanov, V., Trojanowska, J., Pavlenko, I., Zajac, J., Peraković, D. (eds.) *Advances in Design, Simulation and Manufacturing III. DSMIE-2020. Lecture Notes in Mechanical Engineering*, pp. 442–451. Springer, Cham (2020). https://doi.org/10.1007/978-3-030-22365-6_9
8. Yang, C., Li, P., Fan, L.: Blank Shape design for sheet metal forming based on geometrical resemblance. *Procedia Eng.* **81**, 1487–1492 (2014). <https://doi.org/10.1016/j.proeng.2014.10.178>
9. Haikova, T., Puzyr, R., Levchenko, R.: Experimental studies on the stress-strain state under drawing aluminum-copper bimetal parts rectangular in plan. *Russ. J. Non-Ferrous Metals* **61**(4), 404–412 (2020)
10. Fung-Huei, Y.: Study of tube flaring forming limit in the tube flaring process. *J. Strain Anal. Eng. Des.* **42**(5), 315–324 (2007). <https://doi.org/10.1243/03093247JSA272>
11. Maslov, A., Batsaikhan, J., Puzyr, R., Salenko, Y.: The determination of the parameters of a vibration machine of the internal compaction of concrete mixtures. *Int. J. Eng. Technol.* **7**(4.3), 12–19 (2018). <https://doi.org/10.14419/ijet.v7i4.3.19545>
12. Razooqi, A.: Experimental and numerical analysis of expanded pipe using rigid conical shape. *J. Eng.* **8**(24), 106–119 (2018). <https://doi.org/10.31026/j.eng.2018.08.09>
13. Othman, T., Khalaf, H., Alyan, J.: Experimental study of steady-state tube expansion by using conical mandrel. *J. Eng. Technol.* **33** (2015)

14. Dasappa, P., Inal, K., Mishra, R.: The effects of anisotropic yield functions and their material parameters on prediction of forming limit diagrams. *Int. J. Solids Struct.* **49**, 3528–3550 (2012). <https://doi.org/10.1016/j.ijsolstr.2012.04.021>
15. Cardoso, R., Adetorob, O.: A Generalisation of the Hill's quadratic yield function for planar plastic anisotropy to consider loading direction. *Int. J. Mech. Sci.* **128–129**, 253–268 (2012). <https://doi.org/10.1016/j.ijmecsci.2017.04.024>
16. Fischer, F., Rammerstorfer, F., Daxner, T.: Flaring-an Analytical Approach. *Int. J. Mech. Sci.* **48**, 1246–1255 (2006)
17. Moroz, M., Korol, S., Yelistratov, V., Moroz, O.: Development of a moderator of the pump controlled drive for the engine. In: Conference 2019, MEES, vol. 9(23), pp. 30–33. IEEE, Kremenchuk, Ukraine (2019)
18. Shakeri, M., Salehghaffari, S., Mirzaeifar, R.: Expansion of circular tubes by rigid tubes as impact energy absorbers. *Exp. Theoret. Inv.* **12**(5), 493–501 (2007)
19. Pilipenko, O., Feofanova, A., Zharkov, A.: Creasing during the distribution of a tube billet from anisotropic material. *Izvestia TulSU. Series. Mech. Deformable Solid Metal Process.* **2**, 140–145 (2006)
20. Renne, I., Kayushin, V.: Distribution of the pipe with a conical punch, limited by the loss of stability of the cylindrical shape of the workpiece. *Forging Stamping* **3**, 20–21 (1988)
21. Karrech, A., Seibi, A.: analytical model for the expansion of tubes under tension. *J. Mater. Process. Technol.* **210**, 356–362 (2010)
22. Popov, E.: *Fundamentals of the theory of sheet stamping*. Mechanical Engineering, Moscow (1977)
23. Perry, J. Aboudi J.: elasto-plastic stresses in thick walled cylinders. *J. Press. Vessel Technol.* **125**, 248–252 (2003)
24. Yang, J., Lou, M., Hua, Y., Lu, G.: Energy absorption of expansion tubes using a conical cylindrical die: experiments and numerical simulation. *Int. J. Mech. Sci.* **52**, 716–725 (2010)
25. Sosenushkin, E., Yanovskaya, A., Sosenushkin, A., Emel'yanov, V.: Mechanics of nonmonotonic plastic deformation. *Russ. Eng. Res.* **35**(12), 902–906 (2015). <https://doi.org/10.3103/S1068798x15120199>
26. AL-Abri, O.S.: *Analytical and Numerical Solution for Large Plastic Deformation of Solid Expandable Tubular (USA)*, 152370 (2011)
27. Al-Abri, O.S., Pervez, T.: Structural behavior of solid expandable tubular undergoes radial expansion process- analytical. numerical and experimental approaches. *Int. J. Solids Struct.* **50**, 2980–2994 (2013)
28. Venugopal, L., Prasad, N., Geeta, K., Praveen, L.: Simulation studies on tube end expansion of AA2014 alloy tubes. In: Conference 2017, IOP Conference Series: Materials Science and Engineering, vol. 30. Hyderabad, India (2017)
29. Neto, D., Oliveira, M., Alves, J., Menezes, L.: Influence of the plastic anisotropy modelling in the reverse deep drawing process simulation. *Mater. Des.* **60**, 368–379 (2014). <https://doi.org/10.1016/j.matdes.2014.04.008>
30. Luo, J.: Study on stamping-forging process and experiment of sheet metal parts with non-uniform thickness. *Huazhong Univ. Sci. Technol.* **51**, 49–54 (2011)
31. Markov, O., Zlygoriev, V., Gerasimenko, O., Hrudkina, N., Shevtsov, S.: Improving the quality of forgings based on upsetting the workpieces with concave facets. *Eastern-European J. Enterp. Technol.* **5/1**(95), 16–24 (2018). <https://doi.org/10.15587/1729-4061.2018.142674>
32. Zagirnyak, M., Drahobetskyi, V.: New methods of obtaining materials and structures for light armor protection. In: Chenchevoy, V. et al. (eds.) Conference 2015, ICMT, pp. 1–6. IEEE, Brno, Czech Republic (2015)
33. Burda, M., Sova, Z., Drzal, K., Masiolek, A.: Method and apparatus for shaping various cross-sections on metal pipes. Patent of Polska WO 135266 (2006)

34. Haikova, T., Puzyr, R., Savelov, D., Dragobetsky, V., Argat, R., Sivak, R.: The research of the morphology and mechanical characteristics of electric bimetallic contacts. In: Chenchevoy, V. et al. (eds.) Conference 2020, PAEP, pp. 579–582. IEEE, Kremenchuk, Ukraine (2020). <https://doi.org/10.1109/paep49887.2020.9240847>
35. Geselbracht, Margaret J., Ellis, Arthur B., Penn, Rona L., Lisensky, George C., Stone, Donald S.: Mechanical properties of metals: experiments with steel, copper, tin, zinc, and soap bubbles. *J. Chem. Educ.* **71**(3), 254 (1994)
36. Matsuda, K., Hashimoto, D., Nakamura, K.: Real contact area and friction property of rubber with two-dimensional regular wavy surface. *Tribol. Int.* **93**(part B), 523–529 (2016)
37. Anishchenko, O., Kukhar, V., Grushko, A., Vishtak, I., Prysiashnyi, A., Balalayeva, E.: Analysis of the sheet shell's curvature with lame's superellipse method during superplastic forming. *Mater. Sci. Forum* **945**, 531–537 (2019). <https://doi.org/10.4028/www.scientific.net/MSF.945.531>
38. Sawant, P., Warstler, M., Saiful, B.: Exhaust tuning of an internal combustion engine by the combined effects of variable exhaust pipe diameter and an exhaust valve timing system. *Energies* **11**(6), 1545 (2018). <https://doi.org/10.3390/en11061545>
39. Hrudkina, N., Aliieva, L., Abhari, P., Markov, O., Sukhovirska, L.: Investigating the process of shrinkage depression formation at the combined radialbackward extrusion of parts with a flange. *Eastern-Eur. J. Enterp. Technol.* **5**(1–101), 49–57 (2019). <https://doi.org/10.15587/1729-4061.2019.179232>



Diamond Spark Grinding of Hard Alloys Using Solid Lubricants

Aleksandr Rudnev¹ , Yuriy Gutsalenko¹ , Elena Sevidova¹ , Larisa Pupan¹ ,
and Oksana Titarenko²  

¹ National Technical University «Kharkiv Polytechnic Institute», 2,
Kyrypchova Street, Kharkiv 61002, Ukraine

² National Academy of the National Guard of Ukraine, 3, Zakhysnykiv Ukrainy Square,
Kharkiv 61001, Ukraine

Abstract. The article focuses on the results and comparative analysis of diamond spark grinding of titanium-tungsten hard alloy T15K6 using various lubricating media - cooling technological mean with irrigation (3% soda solution of water) and solid lubricants (technical stearin, sebacic acid, mixture (1:1) of stearin with sebacic acid. Specific energy intensity B_M estimated the efficiency of the process, detailed work A_s , productivity Q , relative consumption of diamonds in wheel q , and prime cost C_g . The best combination of the indicated characteristics ensures using a solid lubricant based on a mixture (1:1) of stearin with sebacic acid: the increase in productivity Q is 13.8%, the decrease in the indices q is 33.3%, and C_g is 14.5%. The grinding speed exerts the biggest influence on B_M and A_s . The intensity of these growths during grinding with the introduction of a solid lubricant mixture (1:1) of stearin with sebacic acid into the cutting zone is much less (by 12%) compared to the technological cooling mean with irrigation, which makes it possible to increase the range of grinding speeds, the processing efficiency and makes the diamond spark grinding of hard alloys less wasteful and more environmentally friendly.

Keywords: Cooling technological means · Hart-to-machine materials · Irrigation · Stearin · Sebacic acid · Specific energy intensity · Specific grinding work · Productivity · Consumption of diamonds · Surface roughness · Diamond wheel

1 Introduction

The ability to effectively distribute the heat during cutting guarantees increasing the durability of the cutting tool, which improves the quality of the surface layer of the resulting products, reducing the time and costs of the technological process. One variant of the traditional approach to the intensification of heat removal from the cutting zone is associated with an increase in the consumption of lubricating and cooling technological means (CTM), especially when cutting difficult materials. Thus, in 2016, consumption of mineral-based CTM amounted to 13.726 million tons with a projected annual increase of 1% [1]. Such excessive CTM use gives rise to many problems associated with significant

manufacturing costs, transportation, utilization of CTM, human life safety, depletion of natural resources, and the forced replacement of individual components with expensive synthetic analogs [2].

Particularly relevant is the issue of abandoning CTM use with irrigation for diamond spark grinding (DSG), implemented using diamond wheels on conductive metal bonds with the supply of electrical energy to the processing zone. The method for intensifying the grinding process with an additional energy source has proven its effectiveness in processing heat-resistant steels, hard alloys, and super-hard materials. However, the CTM consumption with irrigation in these cases can reach 50–600 l/min.

Among the modern methods of minimizing or replacing liquid CTM, the most promising for the DSG process are those that are capable of exerting a complex (anti-adhesive, antifriction) effect on the workpiece surface and the diamond wheel, do not require large energy costs to remove the materials, are economical in the consumption of diamonds, and provide comparable or better process performance. After a careful review of the open literature, it was found that no study offers clear and comprehensive research of the effects as well as the mechanisms associated with minimizing or replacing CTM in the DSG process.

2 Literature Review

Over the last 15 years, new research into creating reduced consumption and more environmentally friendly lubrication and cooling methods have been developed in minimum quantity lubrication (MQL), cryogenic techniques, dry cutting, and cutting technologies using solid lubricants (cutting with solid lubricants). The introduction of each of the methods into the manufacturing requires significant changes in the system and method of supplying CTM, the choice of composition and preparation of components (for example, the addition of non-metallic and metallic nanoparticles) according to the type of machining material and the cutting process itself [3].

The most widespread technologies are MQL, which involves the pressure spraying of CTM microdoses mixed with compressed air into the cutting zone. Positive results have been shown for significant reductions in CTM consumption and surface roughness, a decrease in required cutting forces, and an increase in tool wear resistance during the processes of turning [4], milling [5], drilling [6], and grinding [7, 8]. The biggest difficulties in the introduction of MQL technology, including high investment costs, are typical for hard-to-machine materials – hardened and corrosion-resistant steels [9, 10], titanium alloys [11, 12], hard alloys [1], etc. In [13], it is shown that the MQL method has more lubricating than cooling ability. Therefore, its application is limited by machining titanium alloys and nickel-based alloys.

In certain cases, cryogenic cooling provides improvements in tool life and productivity due to increased cutting speeds. However, machining can be accompanied by a reconfiguration of the cutting tool and the workpiece parameters due to the increased hardness, deformability, and cracking resistance of materials under the influence of low temperatures. In titanium alloys machining, cryogenic cooling often requires the addition of extra lubricating components. The widespread implementation of the method is hindered by the problems of ensuring the safety of work and the problem of the suitability of the technology for various types of equipment [14].

The main disadvantage of using air as CTM is poor lubricity. One of the more promising air cooling methods of the cutting zone is the application of activated air media, for example, cooled ionized air [15].

An alternative and less costly substitute for the CTM components during abrasive machining can be solid lubricants – SL [16, 17]. When they are introduced into the cutting zone, it is possible to reduce the cutting forces significantly, the temperature on the contact surfaces, and greatly increase the durability of the abrasive tool [18] due to the lubricating, damping, and dispersing action of the SL components [17]. The choice of the SL composition (graphite, wax, Teflon, silicone, paraffin, MoS₂, hBN, etc.) and the method of its introduction into the cutting zone (impregnation of the grinding wheel with powder paste, continuous/intermittent SL supply by clamping devices) [13] is selected for each specific case in terms of process efficiency and surface finish. Thus, in [19], it was shown that the usage of SL during grinding, compared with the traditional method of cooling with irrigation, can reduce the surface roughness of titanium-tungsten hard alloy T15K6 (15% TiC, 6% Co, 79% WC). The SL composition can favorably affect the quality of the surface layer due to the activation of the removal work in the surfactants environment. Thus, in grinding hardened high-speed steels with cubic boron nitride wheels, the SL introduction into the cutting zone made it possible to reduce the intensity of undesirable phase transformations in the machined surface layer [20].

In general, the DSG process of hard alloys using the SL instead of liquid CTM has been little studied; therefore, it is of interest to assess the effectiveness of such a replacement and further develop practical recommendations for choosing the SL composition and features of its application.

This work aims to study the characteristics of diamond-spark grinding of titanium-tungsten hard alloy T15K6 using various cooling technological means.

3 Research Methodology

DSG process with various SL was investigated concerning the processing of T15K6 carbide inserts.

Experimental studies were carried out on a universal grinding machine model 3D642E, modernized for implementing the DSG process by installing a power supply 6 and additional conductive devices (Fig. 1). A special HO6506 pulse generator was used as a power source, which converts an alternating current with a voltage of 380 V into a unipolar pulse with an adjustable frequency and amperage.

The impulse current was supplied to the grinding zone through the graphite brush 5. Simultaneously, it was possible to connect one pole of the generator to the brush and diamond wheel 3. The other pole to processed carbide insert 7 was affixed to the device on the machine table.

Diamond spark grinding was carried out with reverse polarity (diamond wheel – anode, processed carbide plate – cathode), as the introduction of additional energy into the processing zone in this way provides better self-sharpening of the diamond wheel and less electric discharges energy acts upon the processed carbide alloy, which reduces the likelihood cracking.

The experiments were carried out with an average value of the current $I = 4 \dots 6$ A, open circuit voltage $U = 60 \dots 80$ V, duty cycle $S = 2$ at a pulse frequency $f = 66$ kHz.

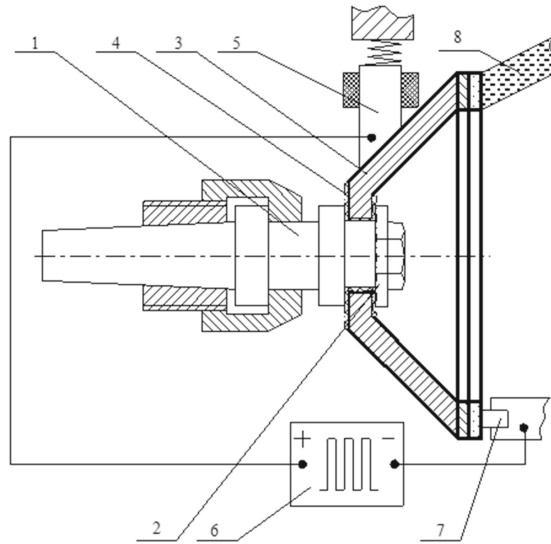


Fig. 1. Upgraded system machine - device - tool - part (MDTP). for researching the DSG process: 1 – machine spindle; 2 – parts for fastening the circle; 3 – diamond wheel body; 4 – dielectric coating; 5 – current lead brush; 6 – pulse generator; 7 – processed carbide insert; 8 – solid lubricant.

Grinding speed V was varied in the range from 15 to 35 m/s. Grinding was carried out according to an elastic scheme, where the transverse feed is not carried out rigidly by the feed mechanism but is set with the help of weights on a special device under a predetermined force. Normal-pressure P_n varied in the range from 0.8 to 1.6 MPa.

The tangential cutting force P_z was measured with a dynamometer.

During our research, cup-shaped diamond wheels 12A2-45°AC6-100/80 M1-01-4 were used. For their electrical isolation, a coating 4 with a thickness of 30...45 μm was applied to the borehole by the method of plasma electrolytic oxidation according to the previously developed technological recommendations [21].

SL was fed by the contact method. A cast cylinder made of SL with a diameter of $D = 10...12$ mm was installed in the device. With a small force, $P = 5$ g was pressed against the wheel at an angle $\alpha = 60^\circ$, which ensured continuous contact of the lubricant with the working surface of the diamond wheel during grinding.

The SL composition was guided by the recommendations [17]. The base components should provide a high lubricating effect – to reduce micro-seizure, scuffing, frictional heating, and frictional forces in the “part-tool” contact zone. Compared with the traditional watering method with a 3% soda solution of water, three SL compositions were used: 1 – technical stearin; 2 – sebacic acid; 3 – a mixture of stearin with sebacic acid (1:1).

A comparative analysis of diamond spark grinding using various lubricating media was carried out based on studying the energy and economic characteristics of the process. Specific energy intensity B_M [22], particular work of grinding A_s [23], the productivity of the process Q , relative consumption of diamonds q , and prime cost for grinding C_g were estimated as the main criteria.

Specific energy consumption of grinding B_M , J/kg, was determined by the energy (work) spent on removing mass from the hard alloy ΔM :

$$B_M = \frac{A}{\Delta M}, \quad (1)$$

where A – the work of grinding, J; ΔM – the mass of removed material, kg.

The specific work of grinding A_s , J/mm³, spent on removing the volume of material, was determined from the ratio:

$$A_s = \frac{P_z V}{Q}, \quad (2)$$

where P_z – the tangential component of the cutting force, N; V – cutting speed, m/s; Q – process productivity, mm³/min.

The productivity of the grinding process Q was determined from the ratio:

$$Q = \frac{F \Delta h}{T}, \quad (3)$$

where F – the cross-sectional area of the grinded hard alloy insert, mm²; Δh – linear material removal, mm; T – grinding time, min.

The relative consumption of diamonds q , mg/g, was determined by the ratio of worn diamonds to the mass of the ground material [24]:

$$q = \frac{M_d}{M_m} = \frac{878 \cdot 10^3 \cdot \pi (D_1^2 - D_2^2) \cdot c \cdot \Delta S}{4F \cdot \Delta h \cdot \rho}, \quad (4)$$

The equation calculated the number of consumed diamonds for a cup-shaped circle of any concentration M_d , mg, for 1 h of work:

$$M_d = \frac{878(D_1^2 - D_2^2)\pi \cdot c \cdot \Delta S}{4 \cdot 10^5}, \quad (5)$$

where D_1 – outer diameter of the diamond ring, mm; D_2 – inner diameter of the diamond ring, mm; c – concentration of grains in a circle, %; ΔS – linear wear of the diamond wheel in thickness, mm.

The amount of removed hard alloy M_m during the same operation time was determined from the expression:

$$M_m = \frac{F \Delta h \rho}{10^6}, \quad (6)$$

where ρ – density of the processed hard alloy, kg/m³.

The prime cost for grinding C_g was determined from the relationship:

$$C_g = \frac{30 + A_d + P_m + E + W}{v}, \quad (7)$$

where 30 – the hourly wages of the grinder worker, currency unit (c.u)/h; A_d – depreciation c.u/h; P_m – costs for the current repair of the machine, reduced to 1 h of work, c.u/h; E – costs of electricity, c.u/h; W – costs associated with depreciation for the wear of the diamond wheel, taking into account its cost, reduced to 1 h of work, c.u/h; v – the volume of polished material per 1 h of work, cm³/h.

4 Results

The results of the values of the performance indicators of diamond wheels in the process of diamond spark grinding using the investigated SL and CTM with irrigation show (Fig. 2) that the best productivity indicators Q , the specific consumption of diamonds q , as well as the prime cost C_g are provided by the use of SL based on a mixture of stearin – sebacic acid (1:1). As a result, compared with the traditional DSG process of using CTM by jet irrigation, the recorded increase in productivity Q is 13.8%, and the decrease in q and C_g is 33.3% and 14.5%, respectively.

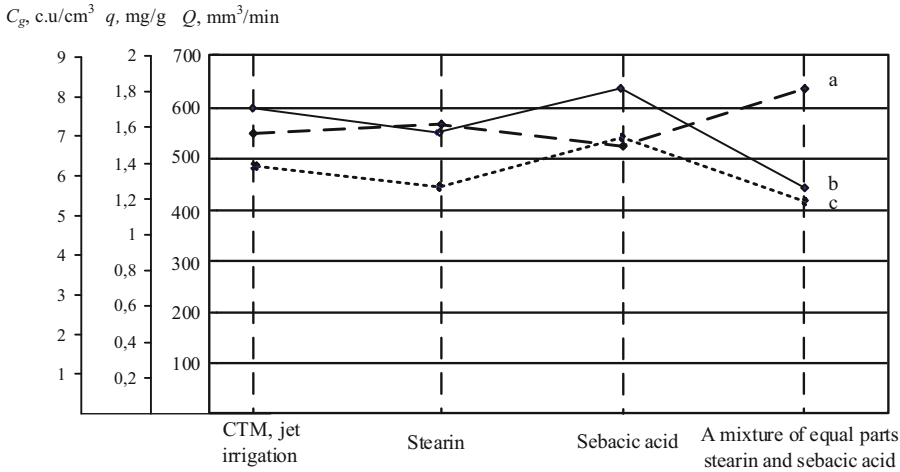


Fig. 2. Dependence of the DSG process energy and economic criteria of the T15K6 hard alloy on the CTM composition: a – productivity of the grinding process Q , b – relative consumption of diamonds q , c – prime cost C_g .

The results obtained for a mixture of stearic-sebacic acid (1:1) indicate a reduction in friction on the contact surfaces between the diamond grain and the bond of the wheel and the processed hard alloy. Consequently, the stearin-sebacic acid mixture (1:1) has the optimum lubricating properties among the considered SL and CTM, and, accordingly, its use reduces the specific energy consumption. Sebacic acid, in this context, shows the worst performance. Subsequently, all studies of the DSG process were carried out using a mixture of stearin – sebacic acid (1:1).

From the research results on the effect of normal pressure on the energy consumption of the DSG process (Fig. 3), it can be seen that in the entire range of changes in normal pressures and the values of the specific energy consumption of the process B_M are lower for SL compared to CTM irrigation (by 11–18% with a change in P_n from 0.8 up to 2.0 MPa, respectively). A proportional increase in grinding performance can explain the general tendency for a slight change in the energy consumption index with an increase in normal pressure.

In comparison with the value of normal pressure, the cutting speed has a much larger effect on the energy consumption of the process B_M (Fig. 4). With an increase in the

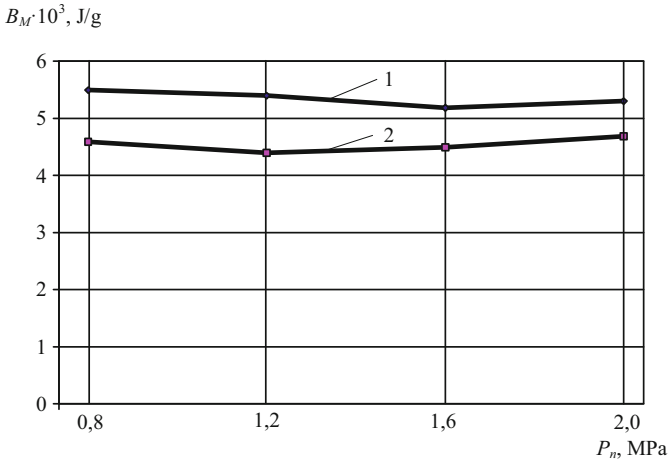


Fig. 3. Dependence of specific energy capacity on normal pressure during diamond spark grinding of hard alloy T15K6 with speed $V = 25$ m/s: 1 – CTM with irrigation, 2 – SL.

grinding speed V from 15 to 35 m/s, the specific energy consumption increases both by CM grinding with irrigation and SL. This can be explained by an increase in the thermal grinding power released in the contact zone. At the same time, the intensity of the increase in the specific energy consumption during grinding with the introduction of a solid lubricant into the cutting zone is much less (the change in B_M is 42% in the studied range of change in grinding speeds) than in the case of traditional CTM (the change in B_M is 54% in the same range of V). The observed effect can be explained by the more active self-sharpening of the cutting surface of the diamond wheel and, accordingly, a large removal of material.

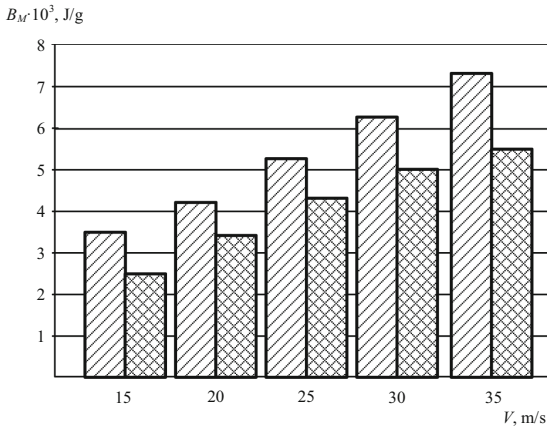


Fig. 4. Dependence of the DSG specific energy consumption of hard alloy T15K6 on the cutting speed at normal pressure $P_n = 1.2$ MPa: ▨ – CTM with irrigation; ▩ – SL.

5 Conclusions

A present experimental study has attempted to explore the machining performance of the DSG process of T15K6 hard alloy using various lubricating media. A comparative analysis of the energy and economic characteristics of the process using CTM with irrigation, SL of different compositions made it possible to establish that the best combination of processing productivity Q , specific consumption of diamonds q , and prime cost C_g ensures the application of an SL based on mixtures of equal parts of stearin and sebacic acid. SL of this composition provides a stable and significant advantage of the indicated characteristics compared to liquid CTM: the increase in productivity Q is 13.8%, and the decrease in the indices q and C_g is 33.3% and 14.5%, respectively.

Among technological indicators of the process, the grinding speed exerts the biggest influence on the specific energy consumption B_M and specific work A_s . Simultaneously, the intensity of the growth of the B_M during grinding with the introduction of an SL into the cutting zone is much less (by 12%) than the liquid CTM, which makes it possible to increase the range of grinding speeds and the processing efficiency.

The results indicate numerous practical benefits of the DSG process using SL: tool wear is lower, chips formed are easier to recycle, the setup cost is very slight, the dry working area is more appropriate for machines for sharpening and finishing of hard alloys inserts.

Based on the research performed, it can be considered that the usage of a solid lubricant is a better alternative to liquid CTM for particularly difficult-to-cut materials under DSG conditions. It is a very promising direction that meets modern trends in the development of minimal lubrication technology.

Further studies are related to understanding the mechanisms (tribological and heat transfer) of a solid lubricant approach and how physically these mechanisms affect the DSG process performance for hard-to-machine materials.

References

1. Said, Z., Gupta, M., Hegab, H., Arora, N., Khan, A.M., Jamil, M., Bellos, E.: A comprehensive review on minimum quantity lubrication (MQL) in machining processes using nano-cutting fluids. *Int. J. Adv. Manuf. Technol.* **105**(17), 2057–2086 (2019)
2. Ezugwu, E.O., Bonney, J., Da Silva, R.B., Cakir, O.: Surface integrity of finished turned Ti–6Al–4 V alloy with PCD tools using conventional and high-pressure coolant supplies. *Int. J. Mach. Tool Manuf.* **47**(6), 884–891 (2007)
3. Ghadimi, A., Saidur, R., Metselaar, H.: A review of nanofluid stability properties and characterization in stationary conditions. *Int. J. Heat Mass Transf.* **54**(17), 4051–4068 (2011)
4. Sampaio, M.A., Machado, A.R., Laurindo, C.A.H., Torres, R.D., Amorim, F.L.: Influence of minimum quantity of lubrication (MQL) when turning hardened SAE 1045 steel: a comparison with dry machining. *Int. J. Adv. Manuf. Technol.* **98**(1–4), 959–968 (2018)
5. Tosun, N., Huseyinoglu, M.: Effect of MQL on surface roughness in milling of AA7075-T6. *Mater. Manuf. Process.* **25**(8), 793–798 (2010)
6. Tasdelen, B., Wikblom, T., Ekered, S.: Studies on minimum quantity lubrication (MQL) and air cooling at drilling. *J. Mater. Process. Technol.* **200**(1–3), 339–346 (2008)

7. Tawakoli, T., Haddad, M., Sadeghi, M.H., Daneshi, A., Sadeghi, B.: Minimum quantity lubrication in grinding: effects of abrasive and coolant–lubricant types. *J. Clean. Prod.* **19**(17–18), 2088–2099 (2011)
8. Khan, A.M., Jamil, M., Mia, M., Pimenov, D., Gasiyarov, V., Gupta, M., He, N.: Multi-objective optimization for grinding of AISI D2 steel with Al₂O₃ wheel under MQL. *Materials* **11**(11), 2269 (2018)
9. Tawakoli, T., Haddad, M.J., Sadeghi, M.H., Daneshi, A., Stöckert, S., Rasifard, A.: An experimental investigation of the effects of workpiece and grinding parameters on minimum quantity lubrication – MQL grinding. *Int. J. Mach. Tool Manuf.* **49**(12–13), 924–932 (2009)
10. Sadeghi, M.H., Haddad, M.J., Tawakoli, T., Vesali, A., Emami, M.: An investigation on surface grinding of AISI 4140 hardened steel using minimum quantity lubrication – MQL technique. *Int. J. Mater. Form.* **3**(4), 241–251 (2010)
11. Sadeghi, M.H., Haddad, M.J., Tawakoli, T., Emami, M.: Minimal quantity lubrication – MQL in grinding of Ti–6Al–4 V titanium alloy. *Int. J. Adv. Manuf. Technol.* **44**(5–6), 487–500 (2009)
12. Pervaiz, S., Anwar, S., Qureshi, I., Ahmed, N.: Recent advances in the machining of titanium alloys using minimum quantity lubrication (MQL) based techniques. *Int. J. Precis. Eng. Manuf.-Green Tech.* **6**(1), 133–145 (2019)
13. Nadolny, K., Kieraś, S., Sutowski, P.: Modern approach to delivery coolants, lubricants and antiadhesives in the environmentally friendly grinding processes. *Int. J. Precis. Eng. Manuf.-Green Tech.* (2020). <https://doi.org/10.1007/s40684-020-00270-y>
14. Kireinov, A.V., Esov, V.B.: Modern trends in the use of lubricating and cooling technological aids in blade processing of difficult-to-machine materials. *Eng. J.: Sci. Innov.* **2**(62), 1–15 (2017). [in Russian]
15. Boswell, B., Islam, M.N., Davies, I.J., Pramanik, A.: Effect of machining parameters on the surface finish of a metal matrix composite under dry cutting conditions. *Proc. Inst. Mech. Eng. B J. Eng. Manuf.* **231**(6), 913–923 (2017)
16. Uzunyan, M.D., Pyzhov, I.M., Agu, A.C.: Solid lubricant for the combined processing of materials with conductive abrasive tools. Patent No. 58078, Ukraine (2011) [in Ukrainian]
17. Khudobin, L.V. (ed.): Lubricating and cooling technological aids and their use in cutting: a handbook. Mechanical Engineering, Moscow (2006) [in Russian]
18. Panaioti, V.A.: Applying solid lubricant to the grinding-wheel surface. *Russ. Eng. Res.* **37**(4), 359–362 (2017)
19. Agu, A.C., Uzunyan, M.D.: Investigation of surface roughness during diamond-spark grinding of hard alloys using minimal lubrication technology. *Cut. Tool. Technol. Syst.* **91**, 12–17 (2017). [in Russian]
20. Panaioti, V.A.: Effect of solid lubricants on the phase composition of the ground surface of high-speed steels. In: Proceedings of the IV International Scientific Conference “Fundamental Research and Innovative Technologies in Mechanical Engineering 2015”, FRITME-2015, pp. 189–191. IMASH RAS, Moscow (2015) [in Russian]
21. Sevidova, E., Pupan, L., Gutsalenko, Yu., Rudnev, A., Titarenko, O.: Effect of morphological features on dielectric properties of plasma electrolytic oxidation coatings on D16T aluminum alloy. In: Ivanov, V., et al. (eds.) *Advances in Design, Simulation and Manufacturing III*. DSMIE-2020, LNME, pp. 542–551. Springer, Cham (2020)
22. Maslov, E.N.: Grinding materials theory. Mechanical Engineering, Moscow (1974) [in Russian]
23. Popov, S.A., Malevsky, N.P., Tereshchenko, A.M.: Diamond-abrasive treatment of metals and hard alloys. Mechanical Engineering, Moscow (1977) [in Russian]
24. Loladze, T.N., Bokuchava, G.V.: Wear of diamonds and diamond wheels. Mechanical Engineering, Moscow (1967) [in Russian]



Technological Parameters of Hole Shaping in the Cones Rolling-Cutter Row of Roller Cone Bits

Andrii Slipchuk¹ (✉)  and Roman Jakym² 

¹ Lviv Polytechnic National University, 12, Bandera Street, Lviv 79013, Ukraine
ands1@ukr.net

² Drohobych Ivan Franko State Pedagogical University, 24,
Ivan Franko Street, Drohobych 82100, Ukraine

Abstract. In this paper, the examination will be focused only on roller cone bits with three cones. The results show that most problems with deviation from the profile are fixed on the holes. The purpose of this is to increase the accuracy of the holes in the rolling-cutter row of the cone for the tungsten carbide insert cutters. For this purpose, from the batch of tungsten carbide insert cutters a statistically controlled group of tungsten carbide insert cutters was selected. The geometric parameters of the shank for the detection of deviations in the surface profile were studied. The obtained data make it possible to state that the cutting speed within the studied limits does not significantly affect the magnitude of the holes breakdown when fine reaming the holes in the rolling-cutter row of the cone body for the tungsten carbide insert cutters fit. Such results indicate significant reserves in improving the accuracy of molding by monolithic carbide reamers. The effect of technological parameters on the statistical relationship between the magnitude of the hole deployment and the roughness of the processing surfaces was also studied. For the sake of clarity of the advantages of solid carbide reamers and reamers compared with those with soldered hard-alloyed plates, the comparative data for two types of reamers are presented.

Keywords: Tungsten carbide insert cutter · Accuracy · Drilling · Breakdown · Hardness · Reaming · Fretting fracture · Roughness

1 Introduction

Roller cone bits are working in extremely difficult drilling conditions; therefore, there are strict requirements for their durability and efficiency. Analysis of used bits and damaged rock-destroying equipment often revealed cases when the tungsten carbide insert cutter was scrolling [1, 2]. Sometimes there were cases of destruction or loss of insert cutter [3, 4]. A wide range of requirements is necessary for a high grade of materials, design, and construction, the technology of manufacturing cone drill bits. Special attention is required to study the processes shaping the accuracy of conjugate elements, the connection of the shank's tungsten carbide insert cutter with the cone. It

is also essential to study the features and nature of stress distribution connected with “tungsten carbide insert cutter – cone” [5, 6]. It is essential to know features of physical and mechanical indicators rolling-cutter row of the cone in which holes for a fit of insert cutter are carried out for this purpose. The geometry of the connection surface “insert cutter – cone” is also valuable [7]. Therefore, the research is devoted to studying technological parameters of the shaping holes in the rolling-cutter row of the cone and geometric, physical, and mechanical features in the connection surface “tungsten carbide insert cutter – cone”. The research objective is to study engineering and design parameters that determine the reliability of the connection “insert cutter – cone”.

2 Literature Review

It is known that in operation, the tungsten carbide insert cutter undergoes bending loads [8, 9]. Therefore, considerable stresses occur in the conjugated sections of the cutter’s exit from the body of the cone rolling-cutter row and in the bottom area [10, 11]. When overloaded or with insufficient steel strength of the cone, plastic deformation, fretting fracture, and microcracks occur. Insufficient quality coupling in the connection contributes to the fact that the tungsten carbide inserts cutters are displaced, then loosens, and in some cases, falls out or “turns out” from the hole (see Fig. 1).

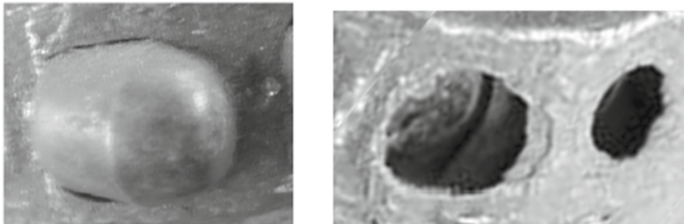


Fig. 1. Plastic deformations in the tungsten carbide insert cutters in the exit area.

Changing the orientation of workloads, which is carried out during each cycle of rotation of the cone and thus rolling over the face (the tungsten carbide insert cutter enters the rock, destroys it, turns it out of the hole, leaves the hole, undergoes sliding) there is a cyclic stress redistribution in the conjugated section not only in separately conjugated “tungsten carbide insert cutters - the body of the cone”, but also in adjacent tungsten carbide insert cutters systems that are close to each other. Practice shows that in these areas, the concentration of stresses can dramatically increase by almost 1.5 or even 2 times [4]. This is due to the change in the resultant load angle from 20° to 60° . In a number of cases, when significant deviations in the form of holes were registered (significant deformations and destruction of the holes walls were detected when cutting the used cones in the area of the holes) [12, 13].

The presence of variables according to the cyclic law (according to the design and size of the cone) of stresses in the area of conjugation “tungsten carbide insert cutters - body of the cone” causes fatigue wear not only of the tungsten carbide insert cutters, but also the

bodies of the rolling-cutter row. This causes the origin and growth of fatigue cracks [14, 15]. Such processes' peculiarity and nature depend on the stress concentration magnitude in the cutter entrance area into the cone and at the contact "facet of the cutter's shank - bottom of the hole" [5, 16]. The rates that characterize the destroying viscosity of the bit's steel determine the strength of the cone rolling-cutter row. The simplest criteria used in production are of great practical importance, and the standard indicators of strength and plasticity are the indicator DI [4]. Simultaneously, more detailed information is provided by a thorough study of the structural sensitivity to cracking appearance, as shown in [2].

3 Research Methodology

First of all, we studied features of design and physic-mechanical properties in the connection "insert cutter-cone". When we identified the features of the requirements for the quality of the shape's hole, after that, we studied the nature of the influence of cutting parameters on the quality of the formation's holes for fit inserts. In research, we used standard equipment for bit production. Shaping of the hole was carried out on the CNC machine - MCV500. Planning of experimental researches and statistical data processing was carried out according to the mathematical theory of experiments and mathematical statistics and the principles generally accepted in engineering technology. The analysis of the waste cones revealed the effect of tungsten carbide insert cutters slipping around their axes. Therefore, the task was to study the causes of this phenomenon. For this purpose, from the batch of tungsten carbide insert cutters a statistically controlled group of insert cutters was selected. The shank's geometric parameters were investigated to detect deviations in the surface profile (see Fig. 2). The results show that most problems with deviation from the profile are fixed on the holes. For tungsten carbide insert cutters, a calibration operation can be applied. Concerning the holes, the detected nature of the deviations makes it possible to set specific tasks for the rational designation of the manufacturing operation parameters to shape cone's holes. The purpose of this is to increase the accuracy of the holes in the rolling-cutter row of the cone for the tungsten carbide insert cutters. The zero point (origin of coordinates) is on the destructive part to the base for measuring the insert cutter (Fig. 2), and the other zero point is on the surface to the bottom for holes (Fig. 3). We took 6 insert cutters from a batch for studying and obtaining substantiated statistically subordinate data for analysis. Also, the cone holes were measured, which were obtained on one cone when we have one setup and one instrument.

To estimate the steel strength parameters in the section hole, the hardness was measured, followed by establishing the hardness distribution gradient in the section hole (see Fig. 4). Hardness was measured using a hardness tester PMT-3.

It was defined by the analysis that along the neutral lines of stretches - the compression in the areas of the operational wedging surface of an insert cutter - there appear sliding planes. Under unfavorable conditions, the stress distribution in the cutter-to-hole coupling occurs sudden appearance of the propagation of trunk cracks, leading to the sudden destruction of the tungsten carbide insert cutters [9]. Therefore, the accuracy of the connection is crucial.

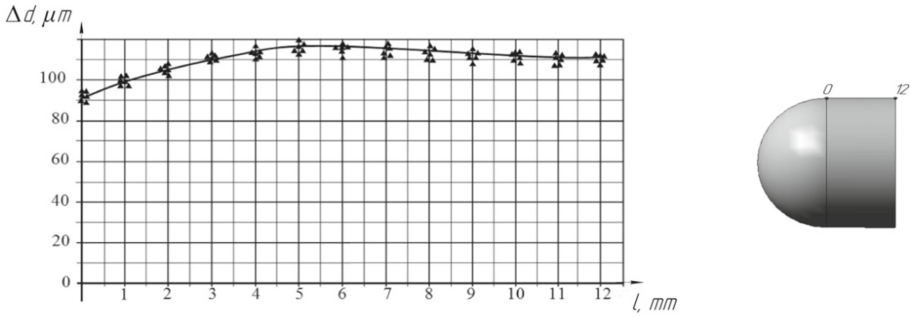


Fig. 2. The character of the profiles deflection of the generatrix shanks of tungsten carbide insert cutters (hardmetal HG20 (Germany)).

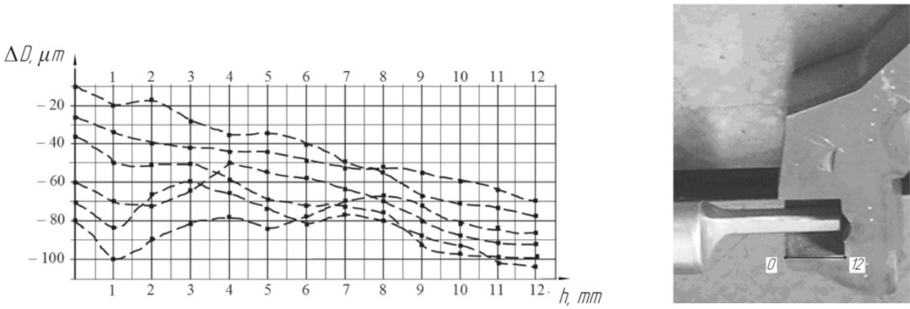


Fig. 3. The character of the profiles deflection of the wall of holes in the cone's rolling-cutter row (AISI 9315H).

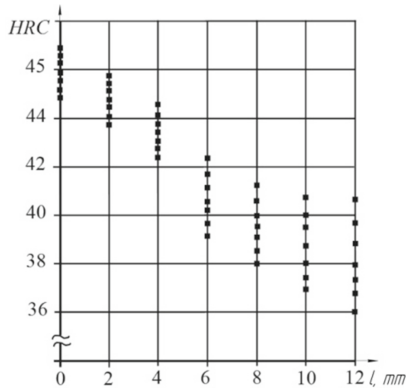


Fig. 4. Hardness distribution on the depth of the rolling-cutter row parallels to the depth of the hole.

4 Results

Measuring the geometric parameters of the holes in the cones revealed that in most cases, and it is 68%, and in some batches up to 85%, a reverse cone is formed (the diameter of the hole in the upper section is smaller than the diameter in the lower section). The size difference can fluctuate significantly. For example, for 18 mm holes, it is in the range of 24–31 μ , and sometimes more. At the holes of smaller diameters, the following figures are slightly smaller: 18–23 μ . In some cases, and it can be up to 45% in the batch, the hole breaking in its top is fixed. The value of the difference in diameters against the middle part of the hole can range from 18 to 32 μ . The formation of the holes' shapes can be explained by the appearance of elastic deformations during the processing of the rolling-cutter row on the body with areas of different hardness (Fig. 4). The dimensional instrument's nature with the reduced incoming part and problems with the instrument positioning cause these deviations. Therefore, the additional dimensional processing of the tungsten carbide insert cutters does not exclude errors in holes. Extra semi-final fine reaming is only insignificantly capable of improving the accuracy of the hole shaping.

According to the manufacturing process, the holes' size distribution measured after the first processing was equal to 25–141 μ , then after the final machining – to 49–106 μ . Fine reaming is performed by a tool with a much more reduced part than the conventional incoming part, which is typical for the processing of the small depth blind holes.

The tool's beating against the hole's axis, especially when there are significant discrepancies because the machining is carried out with different tools, increases the diameter's value in the upper section. Besides, it was found [16, 17] that the deformation and distortion of the cones significantly increase the scattering of the rates of deviations from the documentary regulated. This can be dramatically changed by machining the holes with a setup with monolithic hard-alloyed reamers, which allows single processing of the hole and the machined bottom. For ensuring the wear resistance of such tools from 26 min to the guaranteed 45 min, the first machining can be performed with one tool and the final one with another. Such technology can be effectively implemented on the processing MCV tools of the “Kovosvit” company, which have proven themselves well in the bit industry.

Studies to determine the influence of technological parameters of forming the cones rolling-cutter row holes on the accuracy of their design parameters have been carried out (Table 1). For core drilling and reaming, the diameter tolerance was 0.6 mm. The diameter tolerance was 0.1 mm for the first reaming, and the side tolerance was 0.05 mm. The diameter's tolerance is 0.05 mm for the final reaming and 0.025 mm for the side reaming. The deviation from the cross-section of the axes of the holes with the cone axis was no more than 0.13 mm, and at the top for all other holes up to 0.25 mm.

It is known [18] that fluctuations in the values of the radial component of the cutting force P_V cause an increase in the value of the holes breaking when they are formed. The heterogeneity of the steel, different hardness, significant cylindricity deviation of the holes is the reasons which cause both the general wear of the cutting part of the tool and the chipping of the cutting edges (Fig. 5).

Table 1. The results of the study of the cutting speed influence V on the value of the holes breakdown in the rolling-cutter row of the cone in the roller cone bits 311,1, which was performed with monolithic carbide reamer Ø 18.5 mm ($t_{0,05} = 0.445$).

№	Cutting speed V, (meter per minute)	The obtained values x_i (µm)						$\bar{x}_i(\mu\text{m})$	$s_i^2(-)$	$c^2(-)$	τ (-)
		1	2	3	4	5	6				
1	42	24	28	26	22	25	22	24.5	5.5	5.4	0.982
2	46	26	30	23	24	26	24	25.5	6.3	7.4	1.175
3	48	30	28	23	27	26	25	26.5	5.9	4.7	0.97
4	50	31	27	29	26	28	24	27.5	5.9	4.9	0.831
5	52	28	33	30	28	25	27	28.5	7.5	5.1	0.680
6	56	30	31	26	34	29	33	30.5	8.3	13.1	1.578
7	58	34	29	36	28	32	30	31.5	9.5	15.8	2.821
8	60	28	32	37	34	35	29	32.5	12.3	8.7	0.707

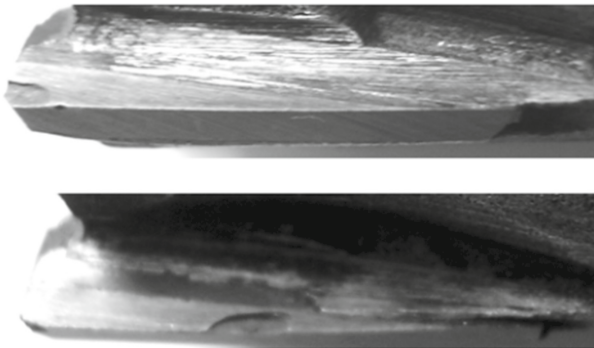


Fig. 5. Characteristic chipping of hard-alloyed plates in the sections of working edges.

Using a well-tried method, namely the method of sequential subtraction [19, 20], the estimate for σ_0^2 the sample data was determined:

$$c^2 = \frac{\sum a_i^2}{2(n - 1)}, \tag{1}$$

and the evaluation criterion

$$\tau = \frac{c^2}{s^2} \tag{2}$$

The results of the calculations c^2, s_i^2, τ are summarized in Table 1.

\bar{x}_i – measurement average; s_i^2 – dispersion; c^2 – assessment criterion; τ – assessment criterion.

Considering that the minimal permissible boundary τ for a significance level of 5% [20], then the randomness hypothesis is true and statistically subordinated to the normal distribution law.

According to the criterion

$$T_l = \frac{s_{max}^2}{s_{min}^2} \tag{3}$$

the variance of the sample variances s_i^2 is $T_l = 2, 236$. Since, $k_1 = m - 1 = 6 - 1 = 5$, $k_2 = n = 8$ for the confidence probability $P = 0,05$ [20] the tabular value of the criterion $T = 3,69$ then $T_l < T$. This is sufficient proof of the selected hypothesis of the sample variances random divergence.

The sample averages were then checked for homogeneity. For this purpose, the nature and magnitude of the difference in the sample averages' adjacent values were evaluated. For this purpose, the Student's criterion was applied:

$$t_i = \frac{(\bar{x}_i - \bar{x}_{i+1})}{\sqrt{n(s_i^2 + s_{i+1}^2)}} \sqrt{\frac{n^2(2n - 2)}{2n}}. \tag{4}$$

According to the probability $P(|t| \geq t_1)$, the Student's distribution of at $k_1 = n_1 + n_2 - 2 = 10$ [20] to each calculated value t_i corresponds probability P_i .

The results of calculations and statistics data are presented in Table 2. The obtained probabilities are not small. They are greater than the confidence level $P = 0.05$. This gives grounds to claim that the experiments' obtained values are randomly different from the tabular ones, and the hypothesis of random difference of sample averages (or their homogeneity) is accepted correctly. Therefore, the compared samples belong to the same general totality.

Table 2. Computational results of probability P_i for each value t_i

$t_i(-)$	0.651	0.640	0.611	1.125	0.530	0.479
$P_i(-)$	0.535	0.540	0.562	0.297	0.590	0.655

A standard characterizes the dispersion of the values of the holes deployment

$$\sigma_o = \frac{\bar{s}}{H_n} \tag{5}$$

where H_n is the coefficient that depends on the sample volume $n = 8$, and according to [11] $H_n = 0, 92$. So, $\bar{s} = 2, 766$, then $\sigma_o = 3, 007$.

Therefore, the actual value of the holes deployment for the test reamer will be within

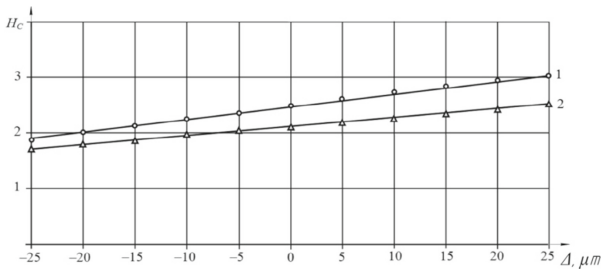
$$\pm 3\sigma_o = \pm 9, 021. \quad x_o - 3\sigma_o < \Delta < x_o + 3\sigma_o, \quad 19, 354 < \Delta_1 < 37, 396.$$

The effect of technological parameters on the statistical relationship between the magnitude of the hole deployment and the roughness of the processing surfaces was also studied. The results of studies on a statistically subordinate number of the holes (150) in a cones batch are presented in Table 3.

Table 3. The range of values distribution of the deployment of holes by the indication of their processing purity.

		Deployment of the hole Δ , (μm)										
		-16	-12	-8	-4	0	4	8	12	16	20	24
The magnitude of the change in the purity of the processing R_a (μm)	0,2	1	–	3	1	–	–	–	–	–	–	–
	0,6	–	4	10	10	2	–	–	–	–	–	–
	1,0	–	–	18	19	4	–	–	–	–	–	–
	1,4	–	–	2	1	–	–	–	–	–	–	–
	1,8	–	–	–	6	2	3	1	–	–	–	–
	2,2	–	–	–	2	1	20	2	–	–	–	–
	2,6	–	–	–	–	4	4	6	3	–	–	–
	3,0	–	–	–	–	–	–	–	2	5	2	–
	3,4	–	–	–	–	–	–	–	–	–	3	4
	3,8	–	–	–	–	–	–	–	–	–	3	2
		Frequency distribution of the magnitude of the deployment (number of deployed holes with appropriate frequency)										

For the sake of clarity of the advantages of solid carbide reamers and reamers compared with those with soldered hard-alloyed plates in Fig. 6, the comparative data for two types of reamers are presented.



1 – reamer with plates HG20 (Germany), 2 - monolithic carbide reamer HG012 (Germany)

Fig. 6. Comparison of the nature of the size effect of the holes deployment on their processing purity. 1 – reamer with plates HG20 (Germany), 2 - monolithic carbide reamer HG012 (Germany)

5 Conclusions

The holes' ovality should be reduced to 0.02 mm because with the increase of tolerance around the hole there is an unfavorable stress distribution, which leads to the destruction of the conjugated elements of a tungsten carbide insert cutter and a hole of the cone on the rolling-cutter row. A stable profile can be achieved by introducing an additional final reaming operation, which would serve as the hole's final calibration. For this purpose, it is effective to use monolithic carbide reamers, which provide higher stability and quality of the machined holes in contradistinction to the reamers with soldered hard-alloyed plates.

The obtained data make it possible to state some results. The cutting speed does not significantly affect the holes' breakdown magnitude when fine reaming the holes. We can say about cutting speed when it is within the studied limits. Therefore, the average value of the holes' deployment when using the reamer is equal to 28 μm . Such results indicate significant reserves in improving the accuracy of molding by monolithic carbide reamers.

Further improvement of the selective assembling technology should be used.

References

1. Prakash, S., Mukhopadhyay, A.: Reliability analysis of tricone roller bits with tungsten carbide insert in blasthole drilling. *J. Int. J. Min. Reclam. Environ.* **34**(2), 101–118 (2020). <https://doi.org/10.1080/17480930.2018.1530055>
2. Yong, D., Chen, M., Jin, Y., Yakun, Z., Daiwu, Z., Lu, Y.: Theoretical and experimental study on the penetration rate for roller cone bits based on the rock dynamic strength and drilling parameters. *J. Nat. Gas Sci. Engin.* **36**, 117–123 (2016)
3. Pandey, P., Mukhopadhyay, K., Chattopadhyaya, S.: Reliability analysis and failure rate evaluation for critical subsystems of the dragline. *J. Braz. Soc. Mech. Sci. Engin.* **40**(2), 1–11 (2018). <https://doi.org/10.1007/s40430-018-1016-9>
4. Yakim, R., Petrina, Yu.D.: Theory and Practice of Quality Assurance and Operational Indicators of Cemented Parts of Cone Drill Bits. Monograph. IFNTUNG Publ., Ivano-Frankovsk (2011)
5. Slipchuk, A., Yakim, R.: The influence of technological factors during pressing tungsten carbide insert cutter in the cone of the roller cone bits for the reliability connection. *New Solut. Mod. Technol.* **3**(5), 1–10 (2020). <https://doi.org/10.20998/2413-4295.2020.01.01>
6. Hu, Q., Zhu, H., Ren, H.: Research on shape parameters of circular arc disc teeth for three-cone bit. *Petroleum* **4**(1), 108–114 (2018)
7. Gustafson, A., Schunnesson, H., Kumar, U.: Reliability analysis and comparison between automatic and manual load haul dump machines. *Q. Reliab. Eng. Int.* **31**(3), 523–531 (2015). <https://doi.org/10.1002/qre.1610>
8. Ratnam, M.: Factors affecting surface roughness in finish turning. *Ref. Module Mat. Sci. Mat. Eng.* **1**(1), 1–25 (2016)
9. Pyalchenkov, V., Kulyabin, G., Dolgushin, V.: Analytical and experimental study of the deformation of roller cone bit parts. *Int. J. Mech. Eng. Technol.* **10**(3), 204–213 (2019)
10. Gupta, A., Chattopadhyaya, S., Hloch, S.: Critical investigation of wear behaviour of WC drill bit buttons. *Rock Mech. Rock Eng.* **46**(1), 169–177 (2013). <https://doi.org/10.1007/s00603-012-0255-9>

11. Nickel, J., Shuaib, A.N., Allam, I.M.: Wear studies of tungsten carbide cutting tools using micro-beam techniques. *J. Tribol.* **121**(1), 177–184 (1999). <https://doi.org/10.1115/1.2833800>
12. Rezvanizani, S., Barabady, J., Valibeigloo, M., Asghari, M., Kumar, U.: Reliability analysis of the rolling stock industry. *Int. J. Perform. Eng.* **5**(2), 167–175 (2009)
13. Huang, Z., Li, Q., Zhou, Y., Jing, S., Ma, Y., Hu, W., Fan, Y.: Experimental research on the surface strengthening technology of roller cone bit bearing based on the failure analysis. *Eng. Fail. Anal.* **29**, 12–26 (2013)
14. Chen, S., Dahlem, J., Rayburn, C.: A study of drilling performance of energy balanced roller cone bit. *SPE Asia Pac. Oil Gas Conf. Exhib. Jakarta* (2003). <https://doi.org/10.2118/80493-ms>
15. Shigemi, N.: Feasibility study on roller-cone bit wear detection from axial bit vibration. *J. Petrol. Sci. Eng.* **82**, 140–150 (2012)
16. Bybee, K.: Drilling performance of an energy-balanced roller-cone bit. *J. Petrol. Technol.* **12**, 49–50 (2003)
17. Schroder, J.: Cone retention and tapered bearing preload system for roller cone bit (2011). Patent of US № 20130105229A1
18. Jon, S., Maurizio, D.P., Alun, R., Jesse, Y.: Bearing innovations extend roller-cone bit life. *Oil Gas J.* **114**(6), 50–55 (2016)
19. Meeker, W., Escobar, L.: *Statistical Methods for Reliability Data*. Wiley, New York (2014)
20. Solonin, I.: *Mathematical statistics in engineering technology*. Mechanical engineering Publ., 176 (1960)



Design Calculation of Automatic Rotary Motion Electrohydraulic Drive for Technological Equipment

Volodymyr Sokolov^(✉) , Olga Porkuian , Oleg Krol , and Oksana Stepanova 

Volodymyr Dahl East Ukrainian National University, 59-a, Pr. Central,
Severodonetsk 93400, Ukraine

Abstract. The article is devoted to the development of electrohydraulic drives for technological equipment. The engineering method for the design calculation of automatic electrohydraulic rotary motion drive with volume regulation was presented. This method allows evaluating the main parameters and choice drive elements and devices using the maximum load moment and hydraulic motor rotation velocity, predicting its static and dynamic characteristics. The electrohydraulic drive's automatic control system was proposed considering the control object's observation noise and stochastic perturbation. The example of design calculation for the automatic electrohydraulic drive parameters for technological equipment for the following input data was performed: maximum load moment $M_{max} = 120$ N.m; maximum rotation frequency $n_{max} = 2100$ rpm; reduced inertia moment of the rotating parts $J = 0,8$ kg.m². The possibility of using a serially produced axial piston-regulated pump with an inclined disk and an unregulated hydraulic motor with an inclined washer was shown. The drive's mathematical model parameters as an object of automatic control were determined based on hydraulic machines' passport data. The research of the system's dynamic characteristics was carried out.

Keywords: Engineering method · Volume regulation · Automatic control system · Dynamic characteristics

1 Introduction

The use of hydraulic drive in mechanical engineering allows us to simplify kinematics, reduce metal consumption, increase accuracy, reliability, and automation of technological equipment [1, 2]. The achievement of arbitrary kinematics of the working body and the possibility of implementing the optimal laws of its movement [3, 4] are ensured by using automatic electrohydraulic drives with volume regulation in equipment with a capacity of more than 5 kW [5, 6].

The advantages of the volume regulation method over the throttle [7, 8] are significantly less energy loss and more stringent load characteristics. The disadvantages are the structural complexity and increased cost of adjustable hydraulic machines [9, 10]. These factors have led to the predominant use of hydraulic drives with volume regulation

at medium equipment powers (10–25 kW) and mandatory use at high power (more than 50 kW).

In this regard, the urgent task is to develop methods for the design calculation of automatic electrohydraulic drives for technological equipment with volume regulation.

2 Literature Review

In the general case, there are various hydraulic drives with volume regulation, which differ in the circulation of the working fluid, volume regulation, and branching of energy flows [11, 12].

Known hydraulic drives with the closed and open circulation of the working fluid [13, 14]. The hydraulic drive velocity can be regulated through the adjustable pump, adjustable hydraulic motor, or two adjustable hydraulic machines. Notably, there is smooth and stepwise regulations of the working volume of the hydraulic machine. Along with single-flow hydraulic transmissions, dual-flow ones are used to simultaneously operate hydraulic and mechanical transmissions [15, 16].

Volumetric hydraulic drives with the working fluid's closed circulation have comparatively smaller overall dimensions and weight, all other things being equal. Closed circulation of the working fluid is used when using hydraulic motors with the same effective areas of the working chambers [17, 18]. The essential properties of volumetric hydraulic drives with the closed circulation of the working fluid are the possibility of breaking the operating mechanism and resistance to the associated load using driving motor instead of throttling the fluid flow, which significantly reduces the heating of fluid and ensures the recovery of electric energy in the indicated operating modes [19, 20].

According to the method of implementing the volume method of speed regulation, three structural schemes of hydraulic drives are distinguished: with adjustable pump and uncontrolled hydraulic motor, unregulated pump and adjustable hydraulic motor, and both adjustable hydraulic machines. Volumetric hydraulic drive with adjustable pump and the unregulated hydraulic motor is the most common. Hydraulic drives with such a structure are used in many types of technological equipment and various mechanisms [21, 22]. Under consideration, the hydraulic drive provides a smooth start-up and stepless velocity regulation of the equipment working body through a single control unit [23, 24].

This work aims to develop an engineering method for the design calculation of automatic rotary motion electrohydraulic drive for technological equipment with volume regulation, allowing the values of the maximum load moment and rotation frequency of the hydraulic motor to evaluate the main parameters and to choose elements and devices of the drive, to predict its static and dynamic characteristics.

3 Research Methodology

Based on the analysis of the issue's status, we can propose the following engineering method to calculate the automatic rotary motion electrohydraulic drive for technological equipment with volume regulation.

To calculate the hydraulic drive with the rotational movement of the output link, the next parameters should be taken as input data: M_{max} – maximum load moment (N.m); n_{max} – maximum rotation frequency (rpm); J – reduced inertia moment of the rotating parts (kg.m^2).

3.1 Construction of the Settlement and Principal Scheme for Hydraulic Drive

In the settlement scheme, the drive's principal elements and devices are reflected, the relationships between them are formed, and the main drive parameters are presented. When developing the principal scheme, analogues of the designed equipment and the developers' experience are considered.

3.2 Choice of the Working Fluid and the Nominal Working Pressure

In addition to the main function of transferring energy from pump to hydraulic motor, the working fluid performs a number of essential functions: lubricating the surfaces of the rubbing parts; removal of wear products of rubbing pairs; protecting them from corrosion; cooling of the hydraulic system. Therefore, the correct choice of the working fluid determines the performance and durability of hydraulic equipment. As a rule, the working fluid is selected based on the technical requirements for equipment or the recommendations in the main hydraulic equipment's technical data (i.e., the pump and the hydraulic motor) and considering the operating mode of hydraulic drive, climatic and temperature conditions.

The hydraulic system's pressure depends on the pump type and the hydraulic drive's purpose on the equipment under consideration. The pump pressure should be greater, the greater the load or power of the driven working mechanism. Small pressures lead to an increase in size and weight but contribute to smooth and stable operation; high pressures lead to a reduction in dimensions and weight, complicate the design and operation of hydraulic systems, and reduce hydraulic durability equipment [25, 26]. The working pressure's nominal value in the hydraulic system p_{nom} is a set from the standard series, MPa: 6.3; 10; 12.5; 16; 20; 25; 32; 40.

3.3 Determination of the Working Volume and Choice of the Hydraulic Motor

The working volume of the hydraulic motor q_m considering hydraulic losses in the system, is estimated by the expression

$$q_m \geq (1, 2 \dots 1, 5) \frac{2\pi M_{max}}{p_{nom}}. \quad (1)$$

According to the parameters q_m and p_{nom} , taking into account n_{max} , the hydraulic motor is selected from the range of series-produced hydraulic equipment. In hydraulic drives of medium and high power (more than 10 kW), rotary-piston hydraulic machines are used mainly, which have a fairly high efficiency coefficient (0,85 ... 0,92) and acceptable weight and size indicators (0.5–10 kg/kW) [8, 25].

In the absence of a suitable series-produced engine, the technical assignment is drawn up to develop the original hydraulic motor. In further calculations, the technical data for the value of the working volume for the hydraulic motor q_m is considered.

3.4 Choice the Pump

When assessing the maximum working volume $q_{p,max}$ of the adjustable pump, the volumetric losses in the hydraulic system (leakage) should be considered, and the nominal rotary velocity of the pump shaft, which can be taken from the technical data pumps used for this type of equipment.

Therefore, it is recommended to evaluate the maximum working volume of the pump according to the expression

$$q_{p,max} \geq (1,1 \dots 1,2) q_m \frac{n_{max}}{n_{p,nom}}, \tag{2}$$

where $n_{p,nom}$ – nominal rotary frequency of the pump shaft.

According to the parameters $q_{p,max}$ and p_{nom} , the pump is selected from the range of series-produced hydraulic equipment. It should be noted that when choosing pumps, they are also mainly oriented to rotary-piston hydraulic machines. In further calculations, the technical data for the value of the maximum pump working volume $q_{p,max}$ is considered.

3.5 Determination of the Parameters for Mathematical Model of Hydraulic Drive Power Unit

Assuming a rigid load characteristic, the structural diagram of the mathematical model can be represented in the form shown in Fig. 1, where the following parameters are indicated: T_{rp} – time constant of the regulation process for pump working volume; T_{pd} – time constant of the drive power part; $k_{\gamma U}$ – transfer coefficient for the inclination angle γ of the titling washer (cylinder block) by the control voltage U ; $k_{\Omega \gamma}$ – transfer coefficient of the drive power unit (transfer coefficient for the rotary velocity Ω by the inclination angle of the titling washer); α – rotation angle of the motor shaft; s – Laplace variable [27, 28].

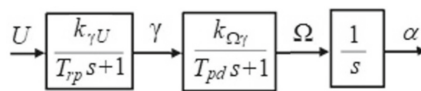


Fig. 1. The structural scheme of the mathematical model.

The transfer coefficient for the inclination angle of the pump washer by the control voltage

$$k_{\gamma U} = \frac{\gamma_{nom}}{U_{nom}} \approx \frac{\gamma_{max}}{U_{max}}, \tag{3}$$

where γ_{nom} , U_{nom} , γ_{max} , U_{max} – nominal and maximum values for the inclination angle of the washer (cylinder block) and the control voltage.

The transfer coefficient of the drive power unit

$$k_{\Omega \gamma} \approx \frac{\Omega_p}{\gamma_{max} \frac{q_{p,max}}{q_p}}, \tag{4}$$

where Ω_p – nominal rotation velocity of the pump shaft (rad/s), which is related to its rotation frequency (rpm) by the dependence

$$\Omega_p = \frac{\pi n_{p,nom}}{30}. \quad (5)$$

If the mathematical model of the power unit is considered for dimensionless variables

$$\bar{\gamma} = \frac{\gamma}{\gamma_{max}} \bar{\Omega} = \frac{\Omega}{\Omega_{max}} \quad (6)$$

where $\Omega \frac{\Omega_p q_{p,max}}{q_{m,max}}$ – maximum rotation speed of the hydraulic motor shaft;

It is easy to see that the transfer coefficients (3), (4) in this case are equal to unity

$$k_{\gamma U} = 1; k_{\Omega \gamma} = 1. \quad (7)$$

The time constant of the process control of the pump's working volume T_{rp} can be directly set in the passport data of the pump, or indirectly determined from the passport data of dynamic characteristics [25, 29] such as response time with a sharp change in oil flow, time of reversal of oil flow and other.

The time constant of the drive power part T_{pd} can be estimated from the values of the relative damping coefficient ζ_m for the hydraulic motor and its time constant T_m

$$T_{pd} \approx 2\zeta_m T_m. \quad (8)$$

According to the calculated dependence [25, 30], the hydraulic motor's relative damping coefficient is difficult. Therefore, at the preliminary calculation stage, it is recommended to set

$$\zeta_m \approx 0.4 - 1.2. \quad (9)$$

The expression can estimate the time constant of the hydraulic motor

$$T_m \approx (6 - 14) \sqrt{\frac{J}{q_m E_f}}. \quad (10)$$

where E_c – elastic modulus of the working fluid.

Thus, the rotary motion electrohydraulic drive's mathematical model parameters with volume regulation as automatic control objects are determined.

3.6 Assessment of the Static Characteristics for Hydraulic Drive

Usually of practical interest is the velocity static characteristic - the dependence of the rotation velocity on control voltage $\Omega(U)$ for the unloaded drive, the load characteristic – the dependence of the rotation velocity on the load moment $\Omega(M)$ at the nominal working volume of the adjustable pump, and the dependence of power consumption on rotation velocity $N(\Omega)$ and the efficiency coefficient on regulation depth $\eta(\Omega)$. The methods for calculating the static characteristics of hydraulic drives with volume regulation are quite fully described in the technical literature [11, 25] and differ in the degree of accepted assumptions.

3.7 Synthesis of the Automatic Control System

Methods for developing the automatic control system (ACS) by hydraulic drives for technological equipment are presented in papers [28, 29]. For rotary motion electrohydraulic drive, the ACS can be recommended, which considers the observation noise and stochastic disturbance of the control object. The structural scheme of this ACS is shown in Fig. 2.

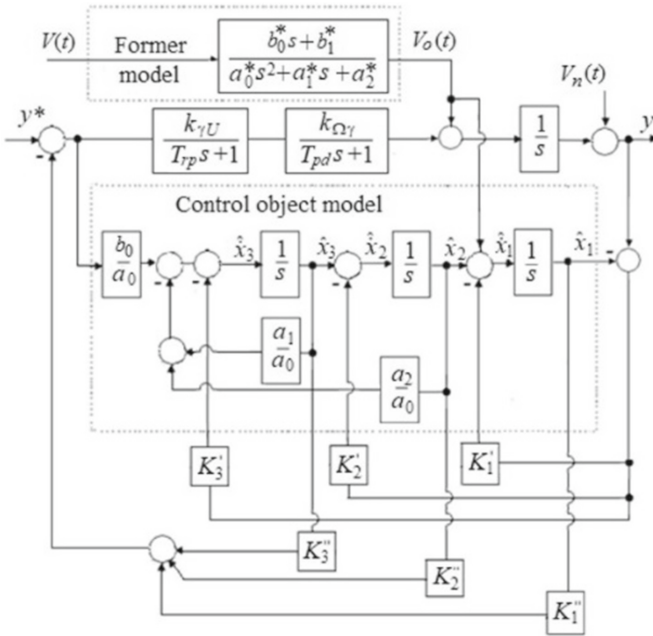


Fig. 2. The structural scheme of the ACS.

On the diagram are indicated: α^* – given control law for the rotation angle of the hydraulic motor shaft; x_1, x_2, x_3 – phase variables; K_1', K_2', K_3' – gain coefficients of the Kalman-Bucy filter; K_1'', K_2'', K_3'' – feedback gain coefficients of the controller; $V_o(t)$ – color noise of the control object; $V_n(t)$ – white observation noise; $b_0^*, b_1^*, a_0^*, a_1^*, a_2^*$ – coefficients for the transfer function of the color noise former for the control object;

$$a_0 = T_{rp}T_{pd}; a_1 = T_{rp} + T_{pd}; a_2 = 1; a_3 = 0; \tag{12}$$

$$b_0 = k_{\gamma U}k_{\Omega \gamma}. \tag{13}$$

4 Results

We show an example of calculating the parameters of an automatic hydraulic drive of the rotational movement of equipment for machining materials for the following input

data: maximum load moment $M_{max} = 120 \text{ N.m}$; maximum rotation frequency $n_{max} = 2100 \text{ rpm}$; reduced inertia moment of the rotating parts $J = 0.8 \text{ kg.m}^2$.

Below are the main results of the calculation.

We accept the scheme for a volumetric hydraulic drive with the working fluid's closed circulation with an adjustable pump and unregulated hydraulic motor. The hydraulic drive's settlement and principal scheme are shown in Fig. 3 (P1 – main pump; P2 – auxiliary pump; HM – hydraulic motor; CV1, CV2 – check valves; SV1 – SV4 – safety valves; F – filter; T – tank).

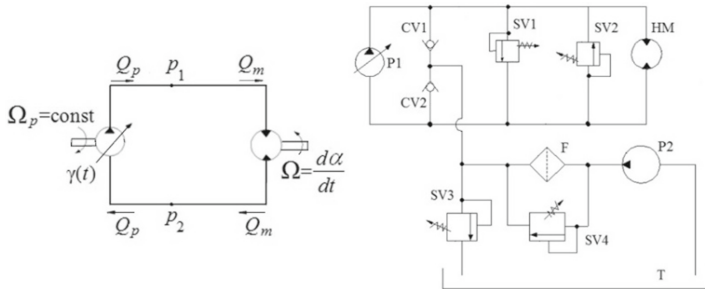


Fig. 3. The structural scheme of the ACS.

We choose the industrial oil IGP-30. We accept the nominal working pressure in hydraulic system $p_{nom} = 20 \text{ MPa}$.

The working volume of the hydraulic motor

$$q_m \geq (1, 2 \dots 1, 5) \frac{2\pi M_{max}}{p_{nom}} = 1, 3 \cdot \frac{2 \cdot 3, 14 \cdot 120}{20 \cdot 10^6} = 49 \cdot 10^{-6} \text{ m}^3 = 49 \text{ sm}^3. \quad (14)$$

We select the unregulated axial-piston hydraulic motor with titling washer MFS 52 (PJSC “Hydrosila APM”, Ukraine), which has the following main technical data parameters: working volume 51.6 cm^3 ; nominal pressure 22.5 MPa ; maximum rotary frequency 3100 rpm ; nominal rotary frequency 1500 rpm ; the nominal power 29 kW . Further, we consider the working volume's technical data value for the hydraulic motor $q_m = 51.6 \cdot 10^{-6} \text{ m}^3$.

The maximum working volume of the pump

$$q_{p, max} \geq (1, 1 \dots 1, 2) q_m \frac{n_{max}}{n_{p.HOM}} = 1, 15 \cdot 51, 6 \cdot 10^{-6} \cdot \frac{2100}{1500} = 83, 08 \cdot 10^{-6} \text{ m}^3 \approx 83 \text{ sm}^3. \quad (15)$$

We select the axial-piston adjustable pump PVS 90 EP with electric proportional control (PJSC “Hydrosila APM”, Ukraine), which has the following main technical data parameters: maximum working volume 89 cm^3 ; nominal pressure 22.5 MPa ; nominal rotary frequency 1500 rpm ; maximum inclination angle of the washer $\pm 18^\circ$; the maximum control voltage $\pm 24 \text{ V}$; the nominal power 63.3 kW . Further, we consider the maximum working volume's technical data value for the pump $q_{p, max} = 89 \cdot 10^{-6} \text{ m}^3$.

We consider the automatic drive's mathematical model for dimensionless variables (6), (7). Therefore, we have

$$k_{\gamma U} = 1; k_{\Omega\gamma} = 1. \quad (16)$$

Further,

$$\zeta_m = 1,0; T_m = 10 \sqrt{\frac{0,8}{51,6 \cdot 10^{-6} \cdot 1,0 \cdot 10^9}} \approx 0,04 \text{ s}; T_{rp} = 2 \cdot 1,0 \cdot 0,04 = 0,08 \text{ s}. \quad (17)$$

To control the drive, we use the ACS with the structural scheme according to Fig. 2. Transient processes in the ACS using the Kalman-Bucy filter and without it are shown in Fig. 4. The perturbing effect on the control object was considered in the form of white noise with spectral density $S_y(\omega) = 1$ and transfer function $W_f(s) = 0,02$ for the former model (Fig. 2). Researches have shown that the Kalman-Bucy filter performs optimal filtration and provides the ability to achieve the required quality of control by drive. In particular, it significantly reduces the duration of the transient process.

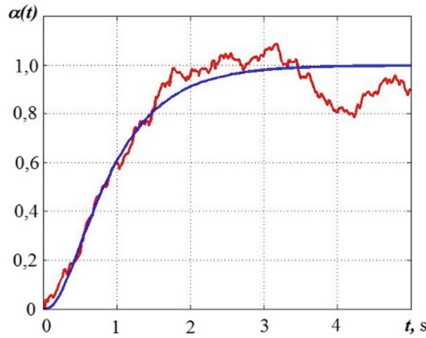


Fig. 4. The transient processes in the ACS.

5 Conclusions

Thus, the engineering method for the design calculation of an automatic electrohydraulic rotary motion drive with volume regulation is presented. The method evaluates parameters and choices that drive elements and devices using the maximum load moment and predicts hydraulic motor rotation velocity. The distinctive feature of the proposed engineering method is determining the transfer coefficients and time constants of the mathematical model and constructing a structural scheme of the ACS by drive. The recommended ACS by the electrohydraulic drive of the technological equipment considers the observation noise and stochastic disturbance of the control object.

The example of design calculation for the automatic electrohydraulic drive parameters for technological equipment for the following input data has been performed: maximum load moment $M_{max} = 120$ N.m; maximum rotation velocity $n_{max} = 2100$ rpm; reduced moment inertia of the rotating parts $J = 0.8$ kg.m². The possibility of using a serially produced axial piston regulated pump with an inclined disk and an unregulated hydraulic motor with an inclined washer is shown. Based on hydraulic machines' passport data, the mathematical model parameters for the drive as object of automatic control are determined. To control the drive, ACS is used, taking into account the observation noise and stochastic perturbation of the control object. The research of the system's dynamic characteristics is carried out. It was shown that the Kalman-Bucy filter performs optimal filtering and provides the ability to achieve the required quality of drive control.

References

1. Petrakov, Yu.: Automatic control of material machining by cutting. UkrNSIAT, Kyiv (2003)
2. Fedorovich, V., Mitsyk, A.: Mathematical simulation of kinematics of vibrating boiling granular medium at treatment in the oscillating reservoir. *Key Eng. Mat.* **581**, 456–461 (2014)
3. Abrahamova, T., Bushuyev, V., Gilova, L.: *Metal-cutting Machine Tools. Machinery Engineering*, Moscow (2012)
4. Ivanov, V., Dehtiarov, I., Pavlenko, I., Liaposhchenko, O., Zaloga, V.: Parametric optimization of fixtures for multiaxis machining of parts. In: Hamrol, A., et al. (eds.) *Advances in Manufacturing II. LNME*, vol. 3, pp. 335–347. Springer, Cham (2019)
5. Sveshnikov, V.: Hydrodrives in modern mechanical engineering. *Hydraul. Pneum.* **28**, 10–16 (2007)
6. Krutikov, G., Stryzhak, M.: *Hydraulic drive systems*. NTU 'KhPI', Kharkiv (2014)
7. Rydberg, K.-E.: *Hydraulic Servo Systems: Dynamic Properties and Control*. Linköping University Electronic Press, Linköping (2016)
8. Guan, C., Pan, S.: Adaptive sliding mode control of electro-hydraulic system with nonlinear unknown parameters. *Control Eng. Pract.* **16**(11), 1275–1284 (2008)
9. Burennikov, Y., Kozlov, L., et al.: Mechatronic hydraulic drive with regulator, based on artificial neural network. *IOP Conf. Ser. Mater. Sci. Eng.* **209**, 012071 (2017)
10. Rogovyi, A., Korohodskiy, V., Medvediev, Y.: Influence of Bingham fluid viscosity on energy performances of a vortex chamber pump. *Energy* **218**, (2021)
11. Popov, D.: *Mechanics of Hydro- and Pneumodrives*. MSTU, Moscow (2001)
12. Andrenko, P., Rogovyi, A., Hrechka, I., et al.: Characteristics improvement of labyrinth screw pump using design modification in screw. *J. Phys. Conf. Ser.* **1741**, 012024 (2021)
13. Rogovyi, A., Khovanskyi, S., Hrechka, I., Gaydamaka, A.: Studies of the swirling submerged flow through a confuser. In: Ivanov, V., et al. (eds.) *Advances in Design, Simulation and Manufacturing III. DSMIE 2020. LNME*, vol. 2, pp. 85–94. Springer, Cham (2020)
14. Rogovyi, A., Khovanskyi, S., et al.: The wall erosion in a vortex chamber supercharger due to pumping abrasive mediums. In: Ivanov, V., et al. (eds.) *Advances in Design, Simulation and Manufacturing II. DSMIE 2019. LNME*, pp. 682–691. Springer, Cham (2020)
15. Krol, O., Sokolov, V.: Modeling carrier system dynamics for metal-cutting machines. In: *2018 International Russian Automation Conference (RusAutoCon)*. IEEE (2018)
16. Kundrák, J., Mitsyk, A., Fedorovich, V., Morgan, M., Markopoulos, A.: The use of the kinetic theory of gases to simulate the physical situations on the surface of autonomously moving parts during multi-energy vibration processing. *Materials* **12**(19), 3054 (2019)

17. Popov, D., Panaiotti, S., Ryabinin, M.: *Hydromechanics*. MGТУ, Moscow (2014)
18. Sokolov, V., Krol, O., Baturin, Y.: Dynamics research and automatic control of technological equipment with electrohydraulic drive. In: 2019 International Russian Automation Conference (RusAutoCon). IEEE (2019)
19. Stepanov, M., Ivanova, L., Litovchenko, P., Ivanova, M., Basova, Y.: Model of thermal state of the system of application of coolant in grinding machine. In: Ivanov, V., et al. (eds.) *Advances in Design, Simulation and Manufacturing*. DSMIE 2018. LNME, pp. 156–165. Springer, Cham (2019)
20. Sokolov, V.: Transfer functions for shearing stress in nonstationary fluid friction. In: *Proceedings of the 5th International Conference on Industrial Engineering (ICIE 2019)*. ICIE 2019. LNME, vol. 1, pp. 707–715. Springer, Cham (2020)
21. Gasanov, M., Kotliar, A., Basova, Y., Ivanova, M., Panamariova, O.: Increasing of lathe equipment efficiency by application of gang-tool holder. In: *Advances in Manufacturing II*. LNME, vol. 4, pp. 114–125. Springer, Cham (2019)
22. Kotliar, A., Basova, Y., Ivanov, V., et al.: Ensuring the economic efficiency of enterprises by multi-criteria selection of the optimal manufacturing process. *Manage. Prod. Eng. Rev.* **11**(1), 52–61 (2020)
23. Pavlenko, I., Trojanowska, J., Ivanov, V., Liaposhchenko, O.: Parameter identification of hydro-mechanical processes using artificial intelligence systems. *Int. J. Mechatron. Appl. Mech.* **5**, 19–26 (2019)
24. Kovalevskyy, S., Kovalevska, O., et al.: Using wave signatures for identifying mechanical objects. *IOP Conf. Ser. Mater. Sci. Eng.* **568**, 012117 (2019)
25. Sveshnikov, V.: *Hydrodrives of tools*. Machinery Engineering, Moscow (2008)
26. Wang, L., Book, W., Huggins, J.: A hydraulic circuit for single rod cylinders. *J. Dyn. Syst. Meas. Control* **134**, (2012)
27. Kim, D.: *Theory of Automatic Control*, vol. 1. Linear systems. Fizmathlit, Moscow (2003)
28. Lurie, B., Enright, P.: *Classical Automation Control Methods*. BHV-Petersburg, Saint-Petersburg (2004)
29. Tsankov, P.: Modeling of vertical spindle head for machining center. *J. Phys. Conf. Ser.* **1553**, 012012 (2020)
30. Pupkov, K., Egupov, N.: *Methods of classical and modern theory for automation control*, vol. 3. *Synthesis of Controllers for Automation Control Systems*. MSTU, Moscow (2004)



Optimization of the Interelectrode Gap in Electrical Discharge Grinding with Changing Electrode Polarity

Roman Strelchuk^(✉)  and Oleksandr Shelkovyi 

National Technical University “Kharkiv Polytechnic Institute”,
2, Kyrpychova Street, Kharkiv 61002, Ukraine

Abstract. The paper investigates the process of electrical discharge diamond grinding with changing the polarity of electrodes in time in the cutting zone for processing various materials, and the value of the interelectrode gap is determined. The study aims to determine the optimal value of the interelectrode gap during electrical discharge grinding using the mathematical method of planning experiments. The mathematical method of planning experiments was used, which allows solving the optimization problem under conditions of incomplete knowledge of physical processes' mechanism. The experiment's planning gave the result with small errors and made it possible to minimize the number of experiments. As a result of experimental studies, a mathematical model of the limiting interelectrode gap from the electrical modes of electrical discharge diamond grinding was built. The functional dependence of the interelectrode gap was obtained, with the help of which it is possible to determine the value of the optimal interelectrode gap for various electrical parameters of electrical discharge grinding. It was established that the most significant factors that affect the interelectrode gap are the voltage of the ignition pulse and the amplitude of the discharge current.

Keywords: Diamond grinding · Interelectrode gap · Voltage · Current amplitude · Frequency · Duty cycle · Electrode polarity

1 Introduction

The change of the polarity on the electrodes in time and the corresponding pulse repetition rate provides stable conditions for electro-discharge diamond grinding. By changing the electrical parameters with a corresponding change in the polarity of the electrodes, it is possible to directly regulate the process itself up to an equilibrium state, providing an equivalent manifestation of electrophysical and electrochemical (even if they are insignificant) processes relative to both electrodes with an optimal interelectrode gap [1–3].

The processing zone for electro-discharge diamond grinding is where the cutting grains of the wheelwork in the interelectrode gap, where the discharges act. Electric discharges in the grinding zone act on the cut-off chips, on the surface of the workpiece

material, and on the grinding wheel – on the bond in the intergranular space and, indirectly, on the dielectric grains. The effect of discharges on metal has been thoroughly studied [4]. However, in the grinding zone, it has its peculiarities.

The state of the processing zone and the nature of the action of the discharges depends on the technological conditions of processing and the structure of the cutting relief of the tool, on the value of the interelectrode gap (the distance between the bond of the wheel and the surface of the part) and various electrical parameters. In the technology of electrical discharge machining, discharges with an energy of 5 . . . 0.05 J (or less) with a frequency of 0.4–8.0 kHz, with a pulse duration of 10^5 –20 μ s (or less) are used. The discharges with a duration of less than 10^{-7} s are considered short (spark).

The intensity of the discharges' action and the restoration of the cutting ability of the tool depend primarily on the electrical parameters, which are selected, considering the non-damage of the grains in the wheel and the repetition rate of the discharges. The intensity of electrical erosion is significantly affected by the composition of the liquid medium [5].

In the presence of an interelectrode gap in the processing zone, electric discharges arising from the interelectrode medium's breakdown are dominant. In the absence of a gap and the presence of elements bridging the interelectrode gap, the discharge is initiated by explosive electrical erosion, which melts the chips.

2 Literature Review

Analysis of works on electrical discharge diamond grinding [6, 7] showed that the process of interaction of the tool with the metal being processed under the conditions of the action of discharges had been little studied, and the zone of combined processing under conditions of changing the polarity of the electrodes in time has not been studied at all. In this regard, an attempt was made to describe the processes and phenomena occurring in the zone of electrical discharge diamond grinding and to establish the optimal value of the interelectrode gap under various electrical conditions. The processing zone for electrical discharge diamond grinding is a complex electrophysical system. It is simultaneously the place of micro-cutting and the action of discharges in the interelectrode gap. When a voltage is applied in this zone, an electric current arises, which passes through the current-conducting bridges that bridge the interelectrode gap, a working fluid with a specific electrical conductivity, and through the channel of the resulting discharge during its action. The value of the processing zone is determined by the width of the tool front and the value of the interelectrode gap, i.e., the distance between the wheel's bond and the surface of the part.

In the processing zone, along with chip formation and the action of discharges, complex mechanical and electrophysical processes occur: contact-frictional, thermal, electrical, electrohydraulic, and plasma-chemical; high-frequency oscillations and cavitation of the liquid medium take place, hydrogen absorption and embrittlement of the surface layers of the cathode material of the electrode can occur.

The main dominant effect of electrical energy in the processing zone is manifested in electro-erosion processes and phenomena of a combined nature of various duration and intensities. They take place in the areas of contact and non-contact interaction of

the wheel with the cut-off chips and the processed material, where the surfaces of these electrodes come close to each other and where contact is possible, the formation of intermittent or tight contacts and their rupture. Thus, the zone of electrical discharge diamond grinding is characterized by contact and non-contact electro-erosion [8].

In the grinding zone, electric discharges occur during the breakdown of the inter-electrode medium between the chips or the surface of the metal and the bond, when the chips slide along the bond – discharges initiated by the explosive electric erosion of the bridging elements, as well as discharges associated with the rupture of the electric circuit in the places where the chips are separated from the material being processed during the end of micro-cutting.

All these electro-erosion processes are associated with electrical discharges, which can have different initiation and formation conditions and differ in their nature, parameters, and intensity of action on the electrodes [9].

When studying the influence of electrical parameters on the combined grinding process, it was established [10, 11] that for specific conditions, there is an optimal value of the interelectrode gap, at which the action of the discharge is most effective, the material removal from the electrodes is the highest. As the gap increases or decreases, the volume of the wells decreases. Therefore, when working with the interelectrode gap, it is necessary to take into account the effect of the discharge on the bond – the necessary removal must be provided, and the effect of electro-erosion processes on the surface processed must be reduced, where the requirements for the quality of processing can be a limiting factor.

3 Research Methodology

The experimental studies were carried out based on a 3D642E machine tool. When choosing the 3D642E grinding machine tool, first of all, the possibility of manufacturing workpieces with the required dimensions, shape, and quality of the processed surfaces has been determined. The 3D642E grinding machine corresponds to the above possibilities. Additional energy was introduced into the cutting zone from a NO 6506 pulse generator, which converts 380 V alternating current into a unipolar pulse current. Voltage, discharge current amplitude, frequency, and duty cycle were controlled using a pulse generator.

An end-face grinding scheme was used, which was carried out with conical cup wheels 12A2-45° 150 × 10 × 3 × 32 on a bond M1-01 with diamond grains AC6 with a grain size of 160/125 and a concentration of 4. Before conducting the experiments, diamond wheels were preliminarily straightened and run in for 5–10 min. The workpiece material was VK6 carbide plates with dimensions of 14 × 14 × 5 mm. VK6 carbide has been chosen as the processed material due to the fact that it belongs to superhard and difficult-to-machine materials. The ED grinding process is especially effective for superhard and difficult-to-machine materials.

The size of the interelectrode gap was determined as follows. With the impulse generator turned off, the workpiece was brought down to mutual contact with the grinding wheel using the machine table's longitudinal feed limb. After that, the part was moved apart at a distance of 0.5 mm, counted along the machine table's longitudinal feed limb. Then the pulse generator was turned on, and the part was brought together with the

grinding wheel. With the help of an electronic oscilloscope, the beginning of a stable electrical discharge flow was recorded. The value of the interelectrode gap, according to this method, was determined by the readings of the longitudinal feed limb of the machine table.

The study of the regularities of electrical discharge diamond grinding highlights the study of the interelectrode gap formed by the workpiece material's interacting surfaces and the metal bond of the diamond grinding wheel. In this case, it is necessary to take into account the specific features of the process. Since electrical discharges are randomly distributed along the periphery of the rotating diamond wheel and the rectilinear moving surface of the part, the interelectrode gap is determined as the average value of the instantaneous electrical gaps S_i :

$$S = \frac{\sum_{i=1}^n S_i}{n} \quad (1)$$

where n – the number of discharges passed along the periphery of the diamond wheel and the part's surface.

The instantaneous electric gap S_i is the distance between two points of the electrode surfaces, which at a given time corresponds to the small dielectric strength of the gap [12]. The rotation of the diamond wheel during electrical discharge grinding contributes to the working fluid's intensive pumping, which excludes the deposition of erosion products on the electrodes. In this regard, the instantaneous electric gap is equal to the instantaneous geometric gap and is defined as the distance between the most noticeable irregularities on the metal bond's surfaces and the part's surface (Fig. 1).

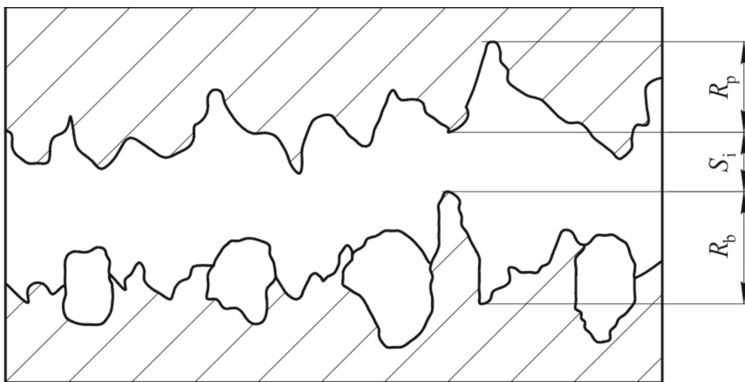


Fig. 1. Scheme for determining the instantaneous interelectrode gap.

Building a mathematical model of the limiting interelectrode gap is of the most significant theoretical and practical interest. In this case, the limiting gap will be understood as the maximum value of the geometric gap, at which a stable flow of electric discharges begins. The mathematical model of the limiting interelectrode gap is a function of several variables that makes it possible to determine the gap's value with the required accuracy at all points of a predetermined region for determining the electrical modes and process conditions.

A theoretical solution to the problem of building such a model is currently not possible. In this regard, the most expedient is the use of mathematical methods for planning experiments, making it possible to solve such problems in conditions of incomplete knowledge of the mechanism of phenomena [13, 14]. The experiment’s design gives the result with a minor error and allows minimizing the number of experiments.

Based on qualitative analysis, it was established that the most significant effect on the value of the limiting interelectrode gap is exerted by the energy characteristics of electrical discharge grinding, determined by the electrical modes of the process. As factors in building a mathematical model of the limiting interelectrode gap were chosen: U – ignition pulse voltage; I – discharge current pulse amplitude; f – pulse frequency; q – pulse duty cycle. The intervals and levels of variation of factors are shown in Table 1.

Table 1. Levels and intervals of a variety of factors.

Natural designation of a factor	U, V	I, A	f, KHz	q
Factor code designation	X_1	X_2	X_3	X_4
Top level	45	22	66	1.5
Lower level	5	2	22	0.5
Main level	25	12	44	1.0
Variation interval	20	10	22	0.5

The sought a power function of the type represented functional dependence:

$$S = CU^xI^yf^zq^v, \tag{2}$$

where – C, x, y, z, v constants determined after implementing the planned experiments.

In order to obtain a power dependence, the optimization parameter was transformed by considering the logarithm. To set up the experiment, a complete factorial design of type 2^4 was implemented in four randomized series, which made it possible to assess each factor’s influence independently. The planning matrix and the results of the experiments are presented in Table 2.

The formulas determined the regression coefficient values:

$$b_i = \frac{\sum_{i=1}^N x_{iu}\bar{y}}{N}; \tag{3}$$

$$b_u = \frac{\sum_{i=1}^N \bar{y}}{N}; \tag{4}$$

$$b_{ij} = \frac{\sum_{i=1}^N x_{iu}x_{ju}\bar{y}}{N}; \tag{5}$$

where $x_{iu} - x_i$ factor value in u -th experiment; $x_{ju} - x_{ju}$ factor value in u -th experiment; \bar{y} – optimization parameter value in the same experiment; N – number of experiments.

Table 2. Levels and intervals of factor variation.

Experiment no.	X_1	X_2	X_3	X_4	$\bar{S}, \mu\text{m}$
1	5	2	22	0,5	14
2	45	2	22	0,5	43
3	5	22	22	0,5	37
4	45	22	22	0,5	111
5	5	2	66	0,5	10
6	45	2	66	0,5	31
7	5	22	66	0,5	26
8	45	22	66	0,5	79
9	5	2	22	1,5	11
10	45	2	22	1,5	32
11	5	22	22	1,5	27
12	45	22	22	1,5	82
13	5	2	66	1,5	7
14	45	2	66	1,5	23
15	5	22	66	1,5	20
16	45	22	66	1,5	59

The coefficients' significance was assessed by comparing the coefficient's absolute value with the value of the confidence interval.

The analysis showed that the coefficients b_0 , b_1 , b_2 , b_3 , and b_4 could be considered significant with a 95% confidence level. The regression coefficients for pairwise interactions and also for higher-order interactions are statistically insignificant. Thus, the regression equation is as follows:

$$y = 7.10 + 1.06X_1 + 1.69X_2 - 0.06X_3 - 2.06X_4 \quad (6)$$

The adequacy of the model, that is, its ability to predict the actual response values with the required accuracy, was tested by Fisher's criterion:

$$F = \frac{S_{ad}^2}{S_{\{y\}}^2} \quad (7)$$

where $S_{\{y\}}^2$ – experiment reproducibility variance; S_{ad}^2 – residual variance or variance of adequacy.

The Fisher criterion's calculated value turned out to be less than the tabular value at a 5% significance level. Therefore the resulting model is adequate. After decoding and potentiating, the mathematical model of the limiting interelectrode gap can be represented as:

$$S = 7.10 \frac{U^{1.06} I^{1.69}}{f^{0.06} q^{2.06}}. \quad (8)$$

4 Results

Figures 2, 3 and 4 show a graphical interpretation of the obtained mathematical model after experimental studies.

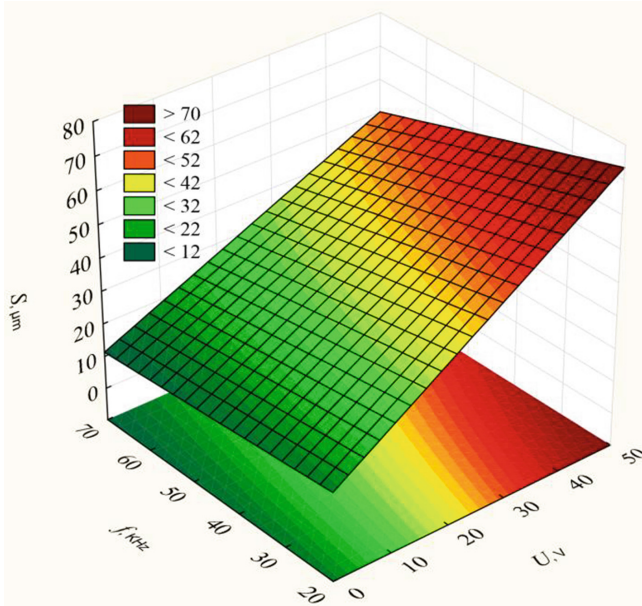


Fig. 2. Response surface $S - (U, f)$. Parameters of calculation $I = 12 \text{ A}$, $q = 1.0$.

Graphical dependency analysis: Fig. 2 shows that with an increasing voltage of the ignition pulse, the limiting gap increases. This can be explained by increasing the voltage with all other equal parameters, the electric field strength increases and facilitates the breakdown of the gap between the electrodes.

An increase in the discharge current amplitude (Fig. 3) leads to an increase in a gap. In this case, the volume of the vapor-gas mixture in the gap increases, facilitating breakdown and leading to an increase in the limiting gap.

The pulse frequency and duty cycle (Fig. 4) have less influence on the value of the limiting interelectrode gap. With all other equal parameters, an increase in frequency

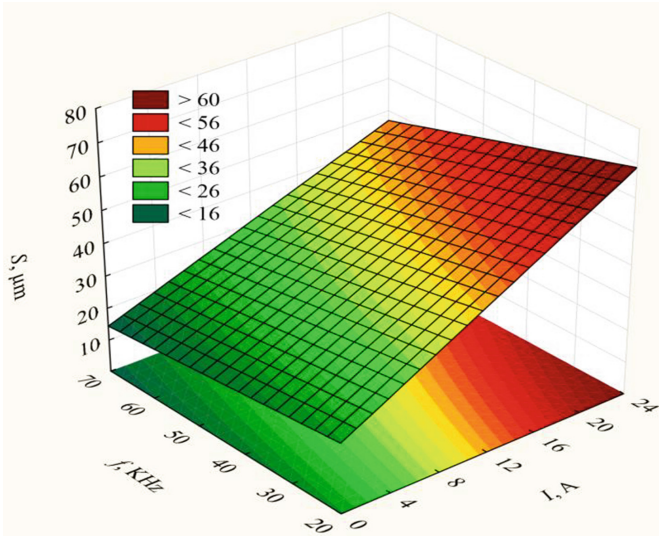


Fig. 3. Response surface $S - (I, f)$. Parameters of calculation $U = 25 \text{ V}, q = 1.0$.

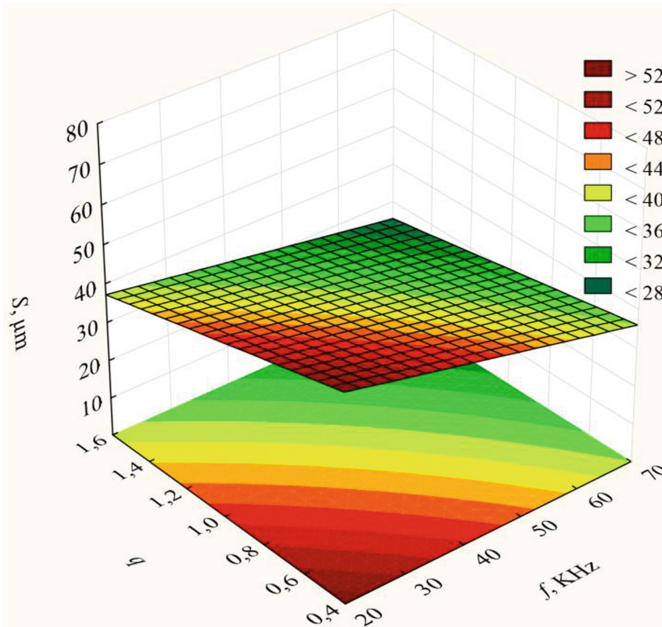


Fig. 4. Response surface $S - (f, q)$. Parameters of calculation $U = 25 \text{ V}, I = 12 \text{ A}$

and duty cycle leads to a decrease in the interelectrode gap. This fact can be explained as follows. One of the prerequisites for breakdown is conducting conductive bridges due to the redistribution of solid particles suspended in a liquid [15, 16].

With long pulses, chains and bridges are formed faster and reach longer distances than with short ones. An increase in the pulse frequency and duty cycle leads to a decrease in the pulse duration, while the gradient of the breakdown potential of the liquid dielectric increases and the interelectrode gap at which a stable flow of electric discharges begins decreases.

It was experimentally established that the most significant factors that affect the interelectrode gap are the voltage of the ignition pulse and the amplitude of the discharge current. When working with an optimal interelectrode gap, the role of pre-fracture of cut thin layers of the workpiece material on the cutting surface increases significantly since this surface is not shielded by chips, which can receive the primary energy of the electric discharge. Thus, under the conditions of electro-discharge grinding, electric discharge erosion acts in the interelectrode gap. Its action on the cutting surface in the place of the most significant cut thickness contributes to the chip formation process's facilitation due to the cut layer's pre-destruction.

5 Conclusions

It was found that the processing zone is characterized by an interelectrode gap with the dominance of breakdown discharges, with the bridging bridges-chips with the initiation of discharges excited by explosive electric erosion.

The size of the interelectrode gap has a significant effect on the processes of the ED gap development. As a result of the study, it was found that the most significant effect on the value of the interelectrode gap is exerted by the energy characteristics of ED grinding, determined by the electrical modes of the process.

The functional dependence of ED gap value has been obtained with which it is possible to determine the value of the optimal interelectrode gap for various electrical parameters of ED grinding. It was found that the most significant factors that affect the interelectrode gap are the voltage of the ignition pulse and the amplitude of the discharge current. The frequency and duty cycle of pulses have a minor effect on the ED gap limit's value. All other things being equal, an increase in frequency and duty cycle leads to a decrease in the interelectrode gap.

In the future, experimental studies will be directed to determine the value of the ED gap from the mechanical modes of grinding and the characteristics of the tool: the speed of the grinding wheel V , the depth of cut t , the tool grit z , the concentration of diamonds in the wheel k . Undoubtedly, these parameters will affect the size of the EDM gap. Due to the high complexity of the complete factorial experiment's implementation, only electrical modes of the grinding process have been used in work: the voltage of the ignition pulse U , the amplitude of the discharge current pulse I , the pulse frequency f , and the duty cycle q .

References

1. Arun, I., Yuvaraj, C., Jyothibabu, P., Sekhar Reddy, G.C.: Influence of silica on microstructural modification of electrical discharge composite coating and its wear performance. *Silicon* **12**, 2375–2386 (2020)

2. Ermilina, O.V., Chemodanov, V.B.: Extreme approach to optimizing the process of electrical discharge profiling of diamond tool. *TEM J.* **9**, 527–540 (2020)
3. Ruszaj, A., Cygnar, M., Grabowski, M.: The state of the art in electrochemical machining process modeling and applications. In: *AIP Conference Proceedings*. American Institute of Physics Inc. (2018)
4. Montes, J.M., et al.: Modelling and simulation of the electrical resistance sintering process of iron powders. *Met. Mater. Int.* **26**, 1045–1059 (2020)
5. Rao, X., Zhang, F., Lu, Y., Luo, X., Chen, F.: Surface and subsurface damage of reaction-bonded silicon carbide induced by electrical discharge diamond grinding. *Int. J. Mach. Tools Manuf.* **154**, 103564 (2020)
6. Giridharan, A., Samuel, G.L.: Investigation into erosion rate of AISI 4340 steel during wire electrical discharge turning process. *Mach. Sci. Technol.* **22**, 287–298 (2018)
7. Rajeswari, R., Shunmugam, M.S.: Finishing performance of die-sinking EDM with ultrasonic vibration and powder addition through pulse train studies. *Mach. Sci. Technol.* **24**, 245–273 (2020)
8. Lu, Y., et al.: Efficient and precise grinding of sapphire glass based on dry electrical discharge dressed coarse diamond grinding wheel. *Micromachines* **10**, 625 (2019)
9. Sharma, R., Gupta, A., Vates, U.K., Singh, G.K.: Electrical discharge diamond grinding (EDDG): a review. In: *Lecture Notes in Mechanical Engineering*, pp. 523–533. Pleiades Publishing (2019)
10. Gutsalenko, Y., Bratan, S., Roshchupkin, S., Dyadichev, V., Menyuk, S.: Investigation of the structure and properties of copper-tin bonding M2-01 in diamond grinding wheel introducing additional energy in the form of electric discharges into the processing zone. In: *Materials Today: Proceedings*, pp. 586–590. Elsevier Ltd. (2019)
11. Choudhary, S., Doon, R., Jha, S.K.: Prediction of the material removal rate and surface roughness in electrical discharge diamond grinding using best-suited artificial neural network training technique. In: *Advances in Intelligent Systems and Computing*, pp. 487–495. Springer (2019)
12. Strelchuk, R., Trokhymchuk, S., Sofronova, M., Osipova, T.: Revealing patterns in the wear of profile diamond wheels. *East.-Eur. J. Enterp. Technol.* **3**, 30–37 (2020)
13. Zhang, C., Ordóñez, R.: *Extremum-Seeking Control and Applications*. Springer, London (2012)
14. Straus, J., Krishnamoorthy, D., Skogestad, S.: On combining self-optimizing control and extremum-seeking control – applied to an ammonia reactor case study. *J. Process Control* **78**, 78–87 (2019)
15. Wang, T., Liu, H., Wu, C., Cheng, J., Chen, M.: Three-dimensional modeling and theoretical investigation of grinding marks on the surface in small ball-end diamond wheel grinding. *Int. J. Mech. Sci.* **173**, 105467 (2020)
16. Kahraman, M.F., Öztürk, S.: Experimental study of newly structural design grinding wheel considering response surface optimization and Monte Carlo simulation. *Meas. J. Int. Meas. Confed.* **147**, 106825 (2019)



Determination of Radial Displacement Coefficient for Designing of Thread Joint of Thin-Walled Shells

Tetiana Tutko , Olha Dubei , Liubomyr Ropyak  , and Vasyl Vytvytskyi 

Ivano-Frankivsk National Technical University of Oil and Gas, 15, Karpatska Street,
Ivano-Frankivsk 76019, Ukraine
L_ropjak@ukr.net

Abstract. The oil and gas industry uses drilling, casing, and compressor pipes connected by threaded couplings. Variable tensile forces load a drill string during its operation in a well. Experience shows that pipes are destructed on the body of the pipe or in the thread's roots. It indicates the importance of studying the contact stresses in the elements of threaded joints. To theoretically determine the distribution of contact stresses in a "pipe - coupling - pipe" thread joint, an integral equation is drawn up with the thread joint's contact pressure as an unknown variable. To develop this equation, it is necessary to determine the radial displacements and angles of rotation of the normal in the coupling and pipes caused by a single annular force or a single annular moment applied in any normal cross-section. Based on the theory of thin shells of finite length, a method for determining the radial displacements of shell middle surface points (coupling), due to the annular force applied in its arbitrary cross-section, as well as the angles of rotation of the normal to its middle surface caused by these force factors. The fact that the annular moments in the right and left parts of the coupling are opposite has been considered.

Keywords: Pipe · Coupling · Thread joint · Shell · Force loads · Contact pressure

1 Introduction

Pipes are widely used in the oil and gas industry for drilling and operation of wells and transportation of production products. Pipes are connected by welding or by thread joints. A key advantage of thread joints over other connection methods is that they can be disassembled and reused. In particular, thread joints are widely used to maintain the structural integrity and tightness of drill pipes, casings, and tubes in wells. Distribution of load and contact stresses among thread elements of compressor pipes and casings significantly impact the optimization of joint structures, control of the pre-tightening force, and prevent threads' failure [1]. In addition to the aforementioned joints, designs of many machine and mechanism designs envisage thread joints of thin-walled parts (for example, head-cylinder block connection in internal combustion engines). In this

case, shells can schematize the thread joints' parts when calculating the strength and load distribution between turns of a thread.

The distribution of load and contact stresses in thread joints have been studied in many works, and general approaches to such problems can be divided into three main areas [1, 2]. The first direction is based on analytical methods, the work of the second direction is based on the finite element method, and the third direction – uses field experiments. Our work develops the first analytical direction of research.

2 Literature Review

Experience in drilling shows that drilling tools operate in difficult conditions under high loads and high temperatures [3]. When designing contact pairs, it is important to use modern methods to ensure the desired properties of contact surfaces and wear resistance of parts. Therefore, the study of diffusion processes [4], modeling of plastic deformation [5, 6], and the study of structural changes [7] are relevant for the development of materials for pipes.

Imperfections in pipe design and cyclic loads cause most destruction of thread joints of pipes [8]. Pipes are made of different materials, and protectors, dampers, and hubs improve pipes' operating conditions and threads [9, 10]. Frictional hardening [11], laser hardening [12], and coating [13–15] are used to strengthen pipes and their threads. The use of polymers is also promising [16, 17].

Also, the workability of thread joints is significantly affected by technological methods of their manufacture [18, 19], equipment [20], and errors in the manufacture of thread profile [21]. Therefore, the main trends in improving the reliability of thread joints are improving engineering methods of calculation, increasing structural strength, the technology of manufacture, assembly, and operation [22–24].

Analysis of modern research indicates some basic directions concerning estimation of contact stresses in thread joints in engineering practice.

The first direction is to schematize a real object of calculation and develop simplified mechanical and mathematical models to describe its behavior analytically by classical means of mechanics of a deformable solid body [25, 26]. Analytical approaches to calculating layered structures' strength and rigidity under local and temperature loads [27, 28] remain relevant and continue developing. A method for determining the contact stresses on the surfaces of conjugate parts and finding the relationships between the load and the slip zone's size in contact with friction is proposed [29]. Clarification of contact interaction models of rod surface with an elastic or inelastic medium is required for the safe operation of long objects [26, 30]. The work [31] has proposed a method to refine pressure calculation and temperature distribution along the good pipes; the study [32] has investigated stress distribution in pipes and [33] – influence of the drill string geometry in the well on its cleaning quality.

The second direction of research is the use of numerical methods to determine contact stresses in thread joints. Researchers often use the finite element method and universal software for automated engineering calculations [30, 31, 33]. Modern numerical methods for stating and solving contact problems on the interaction of elastic bodies are presented in [34–36] and pipes [37].

The third direction of research is based on the results of laboratory or industrial experiments [38]. It aims to consider all the essential contact interaction parameters in thread joints and identify features of threads' behavior under operating loads.

When analyzing the load distribution problem on turns of thread joints, authors usually use the theory of thin-walled shells and eventually come to the key integral equation to determine the contact pressure on the side surfaces of thread turns [1, 2, 39]. To develop an equation in each case, it is necessary to find the so-called coefficients of influence for the thread joint elements. For engineering practice, it is essential to develop a simple method of determining such coefficients for the finite shell. This need has become the main motivation of our study.

3 Research Methodology

A coupling of pump-compressor pipes is under tensile forces during operation. The contact forces between the turns of the pipe-coupling thread cause three distributed force factors q_z , q_n , m on the cylindrical surfaces of thread roots, which is schematically shown in Fig. 1 [39]. Axial forces q_{z1} , q_{z2} react axial load Q and cause stretching of pipes and couplings. Normal annular forces q_{z1} , q_{z2} and annular moments m_1 im_2 lead to radial displacements of the middle surface points of the coupling and the pipe.

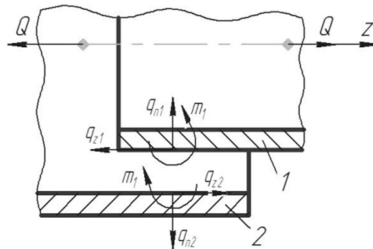


Fig. 1. The model of contact interaction in the pipe - coupling thread joint: 1 – pipe, 2 – coupling.

The work [39] has studied the problem of load distribution in thread joints of shells. The authors obtained an integral equation where pressure on the surface of the thread turns of two shells is unknown. Similarly, the integral equation is obtained for the coupling of two pipes when all the elements of such a connection are shells. To solve this equation, it is necessary to pre-determine many variables for the coupling and the pipes.

It should be determined the following: radial displacement of shell middle surface points in the cross-section z refer to single annular force in the cross-section ξ (variable $K_{n2}(z, \xi)$); and the angles of rotation of the normal to the middle surface of the shell caused by both single annular force and annular moment in cross-section z refer to specified annular force factors applied in the ξ cross section (variable $K'_{n2}(z, \xi)$).

In this paper, a restriction is made on the definition of the mentioned above variables. They can be specified only for the coupling that joins the two pipes. Given this, we formulate the purpose of this work.

The aim is to specify radial displacement of shell middle surface points and angles of rotation of the normal to the middle surface of the shell for coupling to solve the integral equation for determining the pressure on the turns' working surfaces.

To achieve this goal, it is necessary to solve the following tasks:

- solve the boundary problem to determine the radial displacement of shell middle surface points (coupling) due to the annular force applied in its arbitrary cross-section;
- specify the angles of rotation of the normal to the middle surface of the shell caused by annular moments of the left and right halves, directed in opposite directions.

In this research, we neglect the details of the thread material's deformation and consider the contact bodies as thin shells. A finite shell of length L is considered. An arbitrary annular force $P(\xi)$ is applied in its arbitrary normal cross-section ξ . The edges of the shell are free of load. It is necessary to find the radial displacements w of its middle surface points (Fig. 2).

For a circular cylindrical shell under an axisymmetric load, the differential equation of equilibrium has the form [39, 40]:

$$\frac{d^4w}{dz^4} + 4\beta^4w = \frac{q}{D}, \tag{1}$$

where w is the radial displacement (deflection) of the shell; $\beta^4 = \frac{3(1-\nu^2)}{r^2h^2}$; r, h – radius of the middle surface and thickness of the shell; D – is the cylindrical stiffness of the shell $D = \frac{Eh^3}{12(1-\nu^2)}$; E, ν – modulus of elasticity and Poisson's ratio of the shell material; q – component of radial load.

For the shell under consideration:

$$q = P(\xi)\delta_+(z - \xi), \tag{2}$$

where $P(\xi)$ – annular force, $\delta_+(z - \xi)$ – asymmetric impulse function [38], $\delta_+(z - \xi) = \frac{d}{dz}S_+(z - \xi)$, and $S_+(z - \xi)$ – asymmetric unit function $\left(S_+(z - \xi) = \begin{cases} 0 & \text{npuz} - \xi \leq 0, \\ 1 & \text{npuz} - \xi > 0 \end{cases} \right)$.

Given (2) and the conditions at the edges of the shell, there have been obtained the boundary value problem:

$$\frac{d^4w}{dz^4} + 4\beta^4w = \frac{P(\xi)}{D}\delta_+(z - \xi), \tag{3}$$

$$\left. \frac{d^2w}{dz^2} \right|_{z=0} = 0, \quad \left. \frac{d^3w}{dz^3} \right|_{z=0} = 0, \quad \left. \frac{d^2w}{dz^2} \right|_{z=L} = 0, \quad \left. \frac{d^3w}{dz^3} \right|_{z=L} = 0 \tag{4}$$

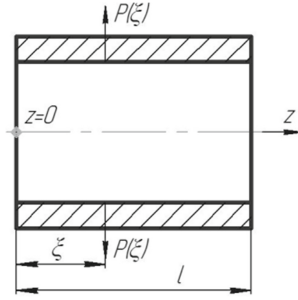


Fig. 2. The finite shell loaded with annular force $P(\xi)$.

We have found an analytical solution to the problem (3) and (4)

$$\begin{aligned}
 w = & \frac{P(\xi)}{4\beta^3 D} \frac{V_3(\beta L)V_2(\beta(L-\xi)) - V_4(\beta L)V_1(\beta(L-\xi))}{V_3^2(\beta L) - V_4(\beta L)V_2(\beta L)} V_1(\beta z) \\
 & + \frac{P(\xi)}{4\beta^3 D} \frac{V_3(\beta L)V_1(\beta(L-\xi)) - V_2(\beta L)V_2(\beta(L-\xi))}{V_3^2(\beta L) - V_4(\beta L)V_2(\beta L)} V_2(\beta z) \\
 & + \frac{P(\xi)}{\beta^3 D} V_4(\beta(z-\xi))S_+(z-\xi).
 \end{aligned} \quad (5)$$

which is expressed through Krylov functions

$$\left. \begin{aligned}
 V_1(\beta z) &= \text{ch}\beta z \cos \beta z, \quad V_2(\beta z) = \frac{1}{2}(\text{ch}\beta z \sin \beta z + \text{sh}\beta z \cos \beta z), \\
 V_3(\beta z) &= \frac{1}{2}\text{sh}\beta z \sin \beta z, \quad V_4(\beta z) = \frac{1}{4}(\text{ch}\beta z \sin \beta z - \text{sh}\beta z \cos \beta z);
 \end{aligned} \right\}$$

If we substitute $P(\xi) = 1N$ in (5), we obtain the desired valuable $K_{n2}(z, \xi)$ I.e., the displacement of the shell middle surface points (coupling) in section z from the single annular force placed in section ξ (the notation [39] is preserved here).

Taking the derivative of z from the analytical expression (5) for $P(\xi) = 1N$, we obtain the formula for angles of rotation of the normal to the middle surface of the shell, which occur when it is loaded by the annular force in the arbitrary cross-section

$$\begin{aligned}
 K'_{n2}(z, \xi) = & -\frac{1}{4\beta^2 D} \frac{V_3(\beta L)V_2(\beta(L-\xi)) - V_4(\beta L)V_1(\beta(L-\xi))}{V_3^2(\beta L) - V_4(\beta L)V_2(\beta L)} V_4(\beta z) \\
 & + \frac{1}{4\beta^2 D} \frac{V_3(\beta L)V_1(\beta(L-\xi)) - V_2(\beta L)V_2(\beta(L-\xi))}{V_3^2(\beta L) - V_4(\beta L)V_2(\beta L)} V_1(\beta z) \\
 & + \frac{1}{\beta^2 D} V_3(\beta(z-\xi))S_+(z-\xi).
 \end{aligned} \quad (6)$$

We proceed to consider the boundary value problems for determining the radial displacements of the shell middle surface points, which arise when the annular moments are applied on its inner side (Fig. 3). The annular moments for the left and right halves have opposite directions.

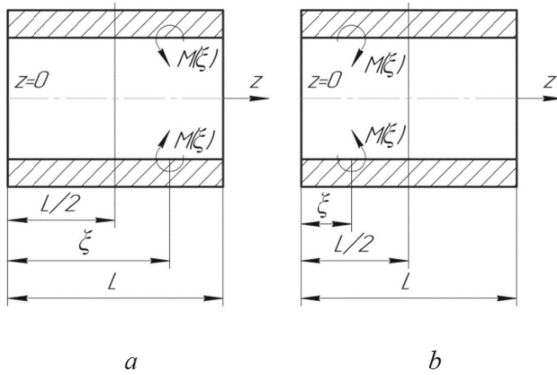


Fig. 3. The finite shell loaded with annular moments: *a* – for the left half of the shell; *b* – for the right half of the shell.

Given the shell with the length of L . The annular moments $M(\xi)$ are applied on its inner side, the directions of which differ for the left and right halves of the shell. The end sections of the shell are free from bending moments and transverse forces. It is necessary to find the radial displacement of shell middle surface points (coupling).

The surface load is specified as

$$q = -\frac{M(\xi)}{D} \delta'_+(z - \xi) \operatorname{sgn}\left(\xi - \frac{L}{2}\right).$$

As a result, we obtain a boundary value problem:

$$\frac{d^4 w}{dz^4} + 4\beta^4 w = -\frac{M(\xi)}{D} \delta'_+(z - \xi) \operatorname{sgn}\left(\xi - \frac{L}{2}\right) \tag{7}$$

$$\left. \frac{d^2 w}{dz^2} \right|_{z=0} = 0, \quad \left. \frac{d^3 w}{dz^3} \right|_{z=0} = 0, \quad \left. \frac{d^2 w}{dz^2} \right|_{z=L} = 0, \quad \left. \frac{d^3 w}{dz^3} \right|_{z=L} = 0 \tag{8}$$

$$w = \left\{ \frac{M(\xi)}{4\beta^2 D} \frac{V_1(\beta(L-\xi))}{V_3^2(\beta L) - V_4(\beta L)V_2(\beta L)} [V_2(\beta L)V_2(\beta z) - V_3(\beta L)V_1(\beta z)] \right. \\ \left. + \frac{M(\xi)}{\beta^2 D} \frac{V_4(\beta(L-\xi))}{V_3^2(\beta L) - V_4(\beta L)V_2(\beta L)} [V_3(\beta L)V_2(\beta z) - V_4(\beta L)V_1(\beta z)] \right. \\ \left. - \frac{M(\xi)}{\beta^2 D} V_3(\beta(z - \xi)) S_+(z - \xi) \right\} \operatorname{sgn}\left(\xi - \frac{L}{2}\right). \tag{9}$$

The function $K'_{m2}(z, \xi)$ of the angle of rotation of the normal to the middle surface in the section z refer to a single annular moment in the section is found by differentiating of formula (9) for $M(\xi) = 1Nm$.

As a result, we have obtained

$$\begin{aligned}
 K'_{m2}(z, \xi) = & \left\{ \frac{V_1(\beta z)}{4\beta D} \frac{V_1(\beta(L - \xi))V_2(\beta L) + 4V_4(\beta(L - \xi))V_3(\beta L)}{V_3^2(\beta L) - V_4(\beta L)V_2(\beta L)} \right. \\
 & + \frac{V_4(\beta z)}{\beta D} \frac{V_1(\beta(L - \xi))V_3(\beta L) + 4V_4(\beta(L - \xi))V_4(\beta L)}{V_3^2(\beta L) - V_4(\beta L)V_2(\beta L)} \\
 & \left. - \frac{1}{\beta D} V_2(\beta(z - \xi))S_+(z - \xi) \right\} \operatorname{sgn}\left(\xi - \frac{L}{2}\right). \tag{10}
 \end{aligned}$$

4 Results

There have been developed graphs according to relations (5), (10).

Figure 4 shows the graphical dependences of $K_{n2}(z, \xi)$ for different values of $\xi = 0, 03; 0,05; 0,07$ m obtained by formula (5) for the coupling HKM-89-E State Standard GOST 633-80.

Parameters of this coupling: nominal diameter 89 mm, length $L = 146$ mm.

Analyzing the graphical dependences (Fig. 4), we see that the cross-section of the shell with maximum $K_{n2}(z, \xi)$ coincides with the coordinate of the annular force application.

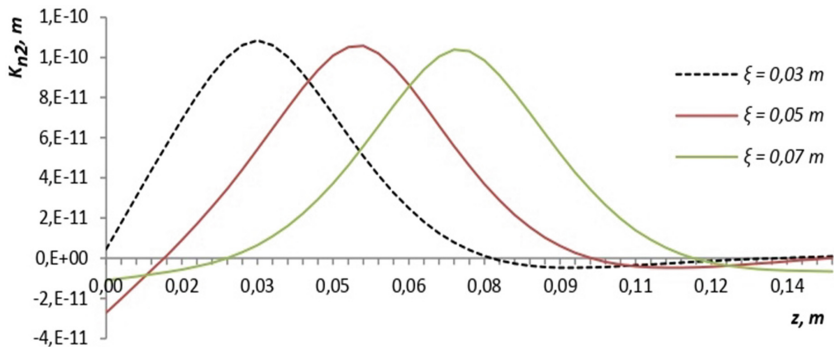


Fig. 4. Radial displacement of the shell middle surface points (coupling) caused by the annular force.

Figure 5 shows the graphical dependences of $K'_{m2}(z, \xi)$, i.e., radial displacement of shell middle surface points from the single annular moment for different values of $\xi = 0, 03; 0,05; 0,07$ m obtained by formula (9) for the coupling HKM-89-E State Standard GOST 633-80.

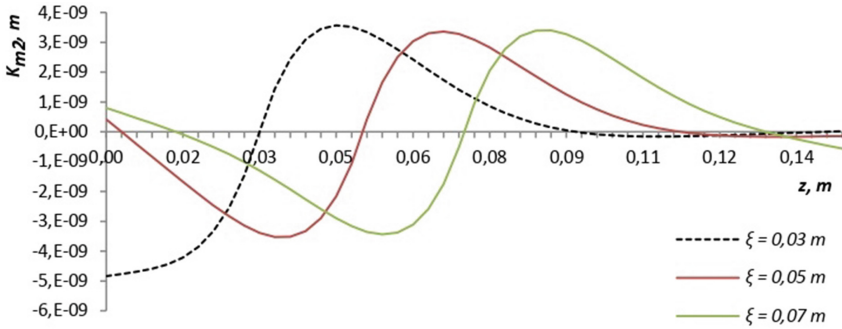


Fig. 5. Radial displacement of shell middle surface points refer to the single annular moment $M(\xi) = 1Nm$.

5 Conclusions

As a result of the new analytical studies, there have been specified the radial displacement and the angles of rotation of the normal of the finite shell (coupling) caused by the single annular force $P(\xi)$ or the single annular moment applied in the arbitrary section of this shell. It is established that the shell's cross-section with maximum coincides with the coordinate of the annular force application.

Thus, analytical relations of influence functions have been obtained to develop integral equations of contact problems for cylindrical shells' thread joints. Further research is planned to improve the method of solving integral equations for contact pressure on the coupling-pipe thread joints' working surfaces.

References

1. Xu, H., Shi, T., Zhang, Z., Shi, B.: Loading and contact stress analysis on the thread teeth in tubing and casing premium threaded connection. *Math. Probl. Eng.* **2014**, (2014)
2. Zhang, D., Gao, S., Niu, S., Liu, H.: A prediction method for load distribution in threaded connections. *J. Theor. Appl. Mech.* **56**(1), 157–168 (2018)
3. Ropyak, L.Ya., Pryhorovska, T.O., Levchuk, K.H.: Analysis of materials and modern technologies for PDC drill bit manufacturing. *Prog. Phys. Met.* **21**(2), 274–301 (2020)
4. Radchenko, T.M., Tatarenko, V.A.: Atomic-ordering kinetics and diffusivities in Ni-Fe permalloy. *Defect Diffus. Forum* **273–276**, 525–530 (2008)
5. Kozak, L.Y.: Discrete models of plastic deformation of solids under the action of high hydrostatic pressure. *Mat. Sci.* **52**(1), 108–112 (2016)
6. Ostapovets, A., Molnár, P., Jäger, A.: Visco-plastic self-consistent modelling of a grain boundary misorientation distribution after equal-channel angular pressing in an AZ31 magnesium alloy. *J. Mat. Sci.* **48**(5), 2123–2134 (2013)
7. Striletskyi, Y.Y., Melnychuk, S.I., Gryga, V.M., Pashkevych, O.P.: Using broadband signals for structural change detection in metal details. *Naukovyi Visnyk Natsionalnoho Hirnychoho Universytetu* **2020**(3), 19–26 (2020)
8. Belkacem, L., Abdelbaki, N., Gaceb, M., Bouali, E., Bettayeb, M.: Drill string fatigue failure and lockup risks assessment in tortuous trajectory well in Algeria. *Chem. Eng. Trans.* **61**, 1099–1104 (2017)

9. Velichkovich, A.S.: Design features of shell springs for drilling dampers. *Chem. Petrol. Eng.* **43**(7–8), 458–461 (2007)
10. Shatskyi, I., Velychkovych, A., Vytvytskyi, I., Seniushkovych, M.: Analytical models of contact interaction of casing centralizers with well wall. *Eng. Solid Mech.* **7**(4), 355–366 (2019)
11. Gurey, V., Hurey, I.: Influence of surface hardened nanocrystalline layers on the resistance of contact fatigue destruction. In: Ivanov, V., Trojanowska, J., Pavlenko, I., Zajac, J., Peraković, D. (eds.) *Advances in Design, Simulation and Manufacturing III. DSMIE-2020. Lecture Notes in Mechanical Engineering*, pp. 483–491. Springer, Cham (2020). https://doi.org/10.1007/978-3-030-50794-7_47
12. Kostyuk, G., Nechyporuk, M., Kostyk, K.: Determination of technological parameters for obtaining nanostructures under pulse laser radiation on steel of drone engine parts. In: *Conference Proceedings of 2019 10th International Conference on Dependable Systems, Services and Technologies, DESSERT 2019*, pp. 208–212 (2019)
13. Tarel'nyk, V.B., Paustovskii, A.V., Tkachenko, Y.G., Konoplianchenko, E.V., Martsynkovskiy, V.S., Antoszewski, B.: Electrode materials for composite and multilayer electrospark-deposited coatings from Ni–Cr and WC–Co alloys and metals. *Powder Metall. Metal Ceram.* **55**(9–10), 585–595 (2017)
14. Tarel'nik, V.B., Konoplyanchenko, E.V., Kosenko, P.V., Martsinkovskii, V.S.: Problems and solutions in renovation of the rotors of screw compressors by combined technologies. *Chem. Petrol. Eng.* **53**(7–8), 540–546 (2017)
15. Perepl'otchikov, E.F., Vasylyv, K.B., Vynar, V.A., Ryabtsev, I.O., Zakiev, V.I.: Elevation of the wear resistance of low-alloy structural steel by plasma-powder surfacing with alloys based on iron, chromium, and nickel. *Mat. Sci.* **54**(3), 378–386 (2018)
16. Berladir, K.V., Hovorun, T.P., Bilous, O.A., Baranova, S.V.: The modeling of the composition and properties of functional materials based on polytetrafluoroethylene. *Funct. Mat.* **25**(2), 342–347 (2018)
17. Berladir, K., Gusak, O., Demianenko, M., Zajac, J., Ruban, A.: Functional properties of PTFE-composites produced by mechanical activation. In: Ivanov, V. et al. (eds.) *Advances in Design, Simulation and Manufacturing II. DSMIE-2019. Lecture Notes in Mechanical Engineering*, pp. 391–401. Springer, Cham (2020)
18. Onysko, O.R., Kopey, V.B., Panchuk, V.G.: Theoretical investigation of the tapered thread joint surface contact pressure in the dependence on the profile and the geometric parameters of the threading turning tool. *IOP Conf. Ser. Mat. Sci. Eng.* **749**(1), (2020)
19. Onysko, O., Kopei, V., Medvid, I., Pituley, L., Lukan, T.: Influence of the thread profile accuracy on contact pressure in oil and gas pipes connectors. In: *Lecture Notes in Mechanical Engineering*, pp. 432–441 (2020)
20. Yakovenko, I., Permyakov, A., Prihodko, O., Basova, Y., Ivanova, M.: Structural optimization of technological layout of modular machine tools. In: *Lecture Notes in Mechanical Engineering*, pp. 352–363 (2020)
21. Pryhorovska, T., Ropyak, L.: Machining error influence on stress state of conical thread joint details. In: *Proceedings of the International Conference on Advanced Optoelectronics and Lasers, CAOL, 9019544*, pp. 493–497 (2019)
22. Shats'kyi, I.P., Lyskanych, O.M., Kornuta, V.A.: Combined deformation conditions for fatigue damage indicator and well-drilling tool joint. *Strength Mat.* **48**(3), 469–472 (2016)
23. Shatskyi, I., Ropyak, L., Velychkovych, A.: Model of contact interaction in threaded joint equipped with spring-loaded collet. *Eng. Solid Mech.* **8**(4), 301–312 (2020)
24. Onysko, O., Borushchak, L., Kopei, V., Lukan, T., Medvid, I., Vryukalo, V.: Computer studies of the tightness of the drill string connector depending on the profile of its tapered thread. In: *Lecture Notes in Networks and Systems. LNNS*, vol. 128., pp. 720–729 (2020)

25. Dutkiewicz, M., Gołębiowska, I., Shatskyi, I., Shopa, V., Velychkovych, A.: Some aspects of design and application of inertial dampers. *MATEC Web Conf.* **178**, 06010 (2018)
26. Grydzhuk, J., Chudyk, I., Velychkovych, A., Andrusyak, A.: Analytical estimation of inertial properties of the curved rotating section in a drill string. *East. Eur. J. Enterp. Technol.* **1**(7–97), 6–14 (2019)
27. Tatsii, R.M., Pazen, O.Y.: Direct (classical) method of calculation of the temperature field in a hollow multilayer cylinder. *J. Eng. Phys. Thermophys.* **91**(6), 1373–1384 (2018)
28. Volchenko, N., Volchenko, A., Volchenko, D., Poliakov, P., Malyk, V., Zhuravliov, D., Vytvytskyi, V., Krasin, P.: Features of the estimation of the intensity of heat exchange in selfventilated disk-shoe brakes of vehicles. *East. Eur. J. Enterp. Technol.* **1**(5–97), 47–53 (2019)
29. Shatskyi, I., Popadyuk, I., Velychkovych, A.: Hysteretic properties of shell dampers, In: Awrejcewicz, J. (ed.) *Dynamical Systems in Applications. DSTA 2017. Springer Proceedings in Mathematics & Statistics*, vol. 249, pp. 343–350. Springer, Cham (2018)
30. Levchuk, K.G.: Diagnosis of catches of metal drill pipes by their stress-strain state in a sloping well. *Metallofiz. Noveishie Tekhnol.* **40**(5), 701–712 (2018)
31. Panevnyk, O.V., Dubei, O.Ya.: Determination of the pressure and temperature distribution along the oil well bore. *Naukovyi Visnyk Natsionalnoho Hirnychoho Universytetu* (4), 98–103 (2015)
32. Mandryk, O., Artym, V., Shtohry, M., Zaytsev, V.: Scientific rationale for the movable pipeline technology for transporting CNG by sea. *Manage. Syst. Prod. Eng.* **28**(3), 168–177 (2020)
33. Vytyaz, O., Chudyk, I., Mykhailiuk, V.: Study of the effects of drilling string eccentricity in the borehole on the quality of its cleaning. In: *New Developments in Mining Engineering 2015: Theoretical and Practical Solutions of Mineral Resources Mining*, pp. 591–595 (2015)
34. Pryhorovska, T.: Rock heterogeneity numerical simulation as a factor of drill bit instability. *Eng. Solid Mech.* **6**(4), 315–330 (2018)
35. Pryhorovska, T.O., Chaplinskiy, S.S., Kudriavtsev, I.O.: Finite element modelling of rock mass cutting by cutters for PDC drill bits. *Shiyu Kantan Yu Kaifa/Petroleum Exploration and Development* **42**(6), 812–816 (2015)
36. Pryhorovska, T.A., Chaplinskiy, S.S.: Finite element modeling of rock mass cutting by cutters for PDC drill bits. *OIJ* **1**, 38–41 (2018). <https://doi.org/10.24887/0028-2448-2017-1-38-41>
37. Dzhus, A., Rachkevych, R., Andrusyak, A., Rachkevych, I., Hryhoruk, O., Kasatkin, S.: Evaluation the stress-strain state of pumping equipment in the curvilinear sections of the wells. *Manage. Syst. Prod. Eng.* **28**(3), 189–195 (2020)
38. Martsynkowsky, V., Kundera, C., Gudkov, S.: Selected dynamic problems of the face packing seal. *Procedia Eng.* **136**, 150–156 (2016)
39. Birger, I.A., Iosilevich, G.B.: Threaded and flanged connections. *Mechanical engineering, Moscow* (1990). (in Russian)
40. Beer, F., Johnston, E., DeWolf, J., Mazurek, D.: *Mechanics of Materials*. McGraw-Hill Education, New York (2015)

Solutions for Industry 4.0



Investments in Blockchain Information Management Systems Based on Business Angels' Criteria

Andrei Davydovitch¹  , Tatjana Vasiljeva¹ , Julija Novinkina¹ ,
and Bohdan Haidabrus^{1,2} 

¹ Riseba University of Applied Science, 3 Meza Street, Riga 1046, Latvia

² Riga Technical University, 1 Kalku Street, Riga 1658, Latvia

Abstract. Blockchain technology bears an enormous potential to revolutionize markets and economies. Previous research studies on investments in blockchain technology were carried out as part of the paradigm of investing in speculative assets without focusing on the launch of the blockchain at the company level. Currently, there is no scientific basis for properly evaluating the investments in blockchain information management systems that help managers and investors in the decision-making process. Authors assume that the evaluation/scoring model for investment in blockchain information systems, based on business angels' investment criteria, is the solution for this market. The study's research problem is that the vast majority of the stakeholders do not look at blockchain investments through the paradigm of investing in blockchain information management systems from the company perspective. The research aims to identify the main groups of investment criteria for blockchain investments and create a theoretical framework based on the literature overview for further analysis.

Keywords: Blockchain technology · Initial coin offering · Distributed ledger · Theoretical framework

1 Introduction

The growing number of start-ups using blockchain as an information management system active in industries ranging from education to insurance services to telecom and supply chain shows the quick adoption of this technology across many major domains of our everyday life [1–4]. To be more precise, Gartner predicts that by 2025 the blockchain will have added slightly over \$176 billion to the overall capitalization of businesses worldwide, which will then surge by 2030 to exceed \$3.1 trillion [5].

From the authors' point of view, scam is the main reason why the amount of funds raised with the help of Initial Coin Offering ICOs is dramatically decreasing since Q2 2018 [6]. Authors think that ICO received a bad reputation as a fundraising method, and blockchain start-ups need to find alternative fundraising sources. It is very important to notice that ICO scams also became possible due to the lack of analysis and due diligence from the investors' side.

The study's research problem is that the vast majority of the stakeholders do not look at blockchain investments through the paradigm of investing in blockchain information management systems from the company perspective.

The research aims to identify the main groups of investment criteria for blockchain investments and create a theoretical framework based on the literature overview for further analysis.

2 Literature Review

At the phase of problem identification, the authors have analyzed the literature sources describing the investments in the blockchain area and business angels' investment criteria.

To understand the main trends in the academic studies related to blockchain technology, authors created a database consisting of 6,494 articles published from 2015 to 2019, selected for the keyword "blockchain" in the following scientific databases:

- SSRN, 844 articles
- Scopus, 2,312 articles
- Springer, 2,054 articles
- EmeraldInsight, 37 articles
- EBSCO, 985 articles
- ScienceDirect, 246 articles
- Web of science 16 articles

After reviewing the theses, the authors received a general opinion on blockchain technology research and revealed a lack of publications on blockchain start-ups' investments.

To determine the main research topics and the position of the scientific community concerning investments in areas related to the blockchain, authors structured the collected database, focusing on three keywords: "Initial Coin Offering", "ICO", "Security Coin Offering", "Security Token Offering", "STO" and "invest".

As a result of this structuring, 169 references were selected for detailed analysis. Focusing on the relevance of the topic of investment in the blockchain, 128 literary sources were selected.

Previous researchers reviewed investments in areas related to blockchain from different points of view.

The paper "Initial Coin Offerings" claims that the management team's quality is a first-order predictor for virtual currency projects' success. Highly visionary projects trade at a discount due to an increased probability of failure. Also, the ICO market is very sensitive to adverse industry events [7]. This article also focuses on the factors not related to investments in blockchain technology or projects utilizing it.

The study ICOs to Finance New Ventures For investors indicates that high investment risk can be reduced by a careful evaluation of several characteristics, such as the venture's source code and the technical information provided in a white paper. This also implies that it may be worthwhile for investors to familiarize themselves with DLT to understand the

technical information the venture provides more accurately. This study further indicates that traditional venture quality indicators may not be as useful in the ICO context as they are in other domains of entrepreneurial finance [8].

The authors agree that the venture's source code and the technical information presented in the white paper are important, but this approach is not too complicated. Many projects are not ready to publish source code. The technical data provided in a white paper is can only provide a vision of technological perspective.

Traditional venture quality indicators provide a more complex overview of the project.

The article Initial Coin Offerings and Entrepreneurial Finance: the Role of Founders' Characteristics provides tests on the effects of disclosure of founders' background information and the founding team's collective human capital on ICO outcomes. Authors of this article find both the disclosure of founders' information and the founding team's human capital are associated with better ICO outcomes measured either by the total amount raised or the fundraising speed. The results highlight the importance of information disclosure and human capital in entrepreneurial finance. The list of factors reviewed in this article is below [9].

In the articles about blockchain investments, the top three groups of topics are ICO regulation and Legal aspects; General information about the ICO as a fundraising method; General information about the cryptocurrency investments. Authors assume that researchers look at blockchain technology as a fundraising method but not as technology like the internet, virtual reality, or even electricity.

Some researchers are trying to understand the reasons to invest in the Initial Coin Offerings that is why authors reviewed articles related to the following topics: ICO selection/scoring [8, 10–12] and ICO success determinants [7, 9, 13].

3 Research Methodology

Table 1 summarized previous researchers' vision regarding the reasons to invest in the ICOs and formed a basis of our research methodology. Due to the specific ICO investments, the focus of the observed research was on the ICO characteristics, social and informational aspects, and online ratings. The majority of the authors highlight the importance of the ICO project team.

These articles are also focused on the investments in speculative assets powered by blockchain technology but not in blockchain technology.

Nowadays, the scientific community is focusing on the use of blockchain technology for fundraising needs. The researchers are not focused on the investments in blockchain technology from a company perspective.

Based on the literature overview, the authors assume that this approach leads to one of the possible research gaps – a scoring model for investments in blockchain start-ups.

Since the investment process is associated with an informational asymmetry between the investor and the project, the authors will adhere to contract theory.

As far as an investment process for blockchain investors is associated with profit expectation, authors will also adhere to rationalism theory.

Table 1. Summary of the factors for investments in ICO/STO

Author	Year	Factors/Investment criteria/Groups of criteria	Country
Yadav [12]	2017	Legal aspects, Company age, Token characteristics, Token distribution, sentiments of the crypto community around the projects; Promotion bounties and paid promotion; Information quality in the project White paper	Germany
Hargrave, Sahdev and Feldmeier [10]	2018	Market of the Token, Competitive advantage, Management team, User adoption (publicity), Token Mechanics,	USA and EU
Rhue [11]	2018	Social/information, Ratings	USA
Fisch et al. [8]	2018	Ideological motives, Technological motives, Financial motives (not factors or criteria)	Netherlands
Momtaz [7]	2018	Management team	USA
Fisch [8]	2018	Source code, Technical information	Netherlands
An et al. [9]	2018	ICO characteristics, Founder characteristics, Team characteristics, Market characteristics	Scotland
de Jong, Roosenboom and van der Kolk [13]	2018	Informational transparency, Quality rating by cryptocurrency experts, ICO stages and timing, Pre- ICO GitHub repository, Project team	Netherlands
Martino, Bellavitis and DaSilva [14]	2019	Democratized participation in global capital markets, subsequent appreciation in the value of investments	Italy New Zealand Switzerland
Ante and Fiedler [15]	2019	Project team, advisors, and social media network	Germany
Albrecht, Lutz and Neumann [16]	2019	Social media network	Germany
Momtaz [17]	2020	Chief Executive Officer (management team)	USA

(continued)

Table 1. (continued)

Author	Year	Factors/Investment criteria/Groups of criteria	Country
Meyer and Ante [18]	2020	Jurisdiction of ICO, blockchain infrastructure, token allocation, length of an ICO campaign, whitepaper	Germany

Table 2. Major groups of business angels' investment criteria

Author	Year	Groups of criteria	Country
Haar et al. [19]	1988	Managing team, market, track record	USA
Mason and Harrison [20]	1996	Entrepreneur/managers; market; financial criteria	UK
Landstrom [21]	1998	Entrepreneur, product/market, financial criteria	Sweden
Yasuhisa [22]	1999	Competitiveness of goods/services; entrepreneurial skills and "chemistry" in relations with an entrepreneur	Japan
Feeney et al [23]	1999	Entrepreneur; growth potential; profit	UK (Scotland)
Van Osnabrugge [24]	2000	Entrepreneur; market/product; financial criteria	UK
Stedler and Peters [25]	2002	Entrepreneur/management; product; market; financial criteria; growth potential	Germany
Mason and Harrison [26]	2002	Development stage; industry/technology; location	UK
Mason and Harrison [27]	2003	Presentation; market; product	UK
Mason and Stark [28]	2004	Entrepreneur/managers; investor involvement; financial criteria	UK
Sudek [29]	2006	Entrepreneur; trust; management team; exit	USA
Clark [30]	2008	Entrepreneur/management; market, product	UK
Maxwell et al. [31]	2011	Product; market, entrepreneur/management; financial criteria	Canada
HBAN and EBAN [32]	2013	Management team; exit potential, income potential	Iceland

The theoretical framework of the research is based on the results of a brief literature review. Independent variables – groups of investment criteria connected with the dependent variable "Investment decision" through the mediating variable investor's personality.

Authors assume that business angels as a type of investor are the most important and applicable source for determining investment criteria for blockchain start-ups.

Based on the research described in Table 2, the authors have created the conceptual model that assumes that there are six main groups of investment criteria for business angels: criteria related to the characteristics of the entrepreneur (founder) and the management team; criteria related to the market and growth potential; criteria related to the characteristics of the product/service; financial criteria; criteria related to exit from the investment (exit); criteria related to the involvement of a business angel in the project. The authors intend to adopt these groups of investment criteria for projects utilizing blockchain technology.

The authors propose that, despite the blockchain technology’s novelty, the adopted traditional groups of investment criteria are applicable for the blockchain start-ups and investors. These groups of investment criteria are marked as independent variables in Fig. 1.

The authors have identified a potential prospective solution for investments in blockchain information management systems based on business angels’ investment criteria as a scoring model.

4 Results

The authors developed the theoretical framework based on the traditional groups of investment criteria for business angels. These groups of investment criteria are marked as independent variables in Fig. 1. They impact the dependent variable (investment decisions) through mediating variables (investors’ personality).

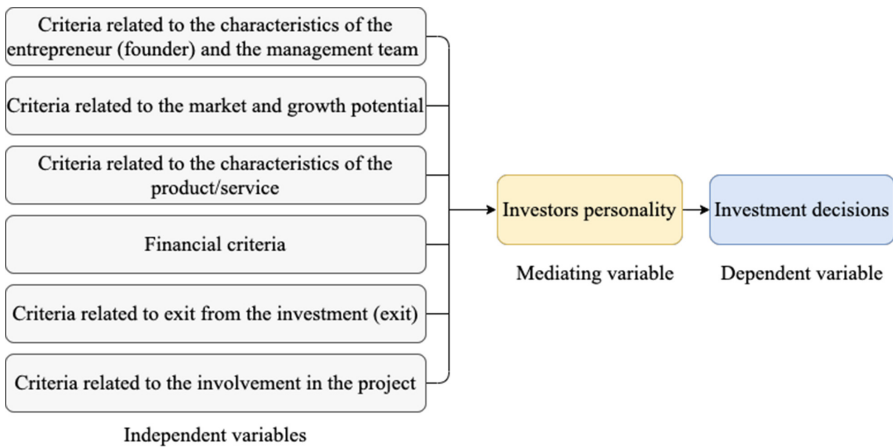


Fig. 1. The theoretical framework of further research

The authors have defined methods and research steps that formed the basis for the convergent approach to forming the presented theoretical framework (Table 3).

The data collection and validation of results will also be divided into two steps:

1. The first step is interviewing experts and developing surveys using the Delphi method.

Table 3. Methods and research steps

Phase	Proposed process step	Method and approach
Problem identification	State of research	Literature review
Data collection and validation of results	Interviews with experts	Delphi, Interview
	Survey for investors and managers/founders	Survey
Development and implementation	Scoring model development/differences identification	Statistical methods, Methods of mathematical analysis
Evaluation of results	Interviews with experts	Interview

2. The second is two polls: a survey of blockchain investors and a survey of managers/founders of blockchain start-ups.

The development and implementation phase will have two results:

1. Scoring model for investments in blockchain start-ups.
2. The list of differences in vision regarding investment criteria between investors and blockchain start-ups.

These results will be achieved, and further research will be conducted based on data collected with a survey using statistical methods and mathematical analysis methods. The authors are going to evaluate the results of the study with the help of expert interviews.

5 Conclusions

As a result of the research, the authors identified the six main groups of business angels' investment criteria applicable to blockchain investments. The scientific community is trying to understand the general aspects of investing in ICO/cryptocurrency at this stage, paying special attention to the legal aspects. Researchers view investments in blockchain technology through the ICO/STO paradigm. ICO/STO projects are very speculative investments and often utilize blockchain technology only to issue a token – a speculative asset. Despite the high level of interest from the scientific community to the blockchain field, investment criteria or scoring model for investment in blockchain start-ups has not yet been developed.

References

1. Cbinsights Homepage, Banking Is Only the Beginning: 50 Big Industries Blockchain Could Transform. <https://www.cbinsights.com/research/industries-disrupted-blockchain/>. Accessed 06 Apr 2019

2. Chen, G., Xu, B., Lu, M., Chen, N.-S.: Exploring blockchain technology and its potential applications for education. *Smart Learn. Environ.* **5**(1), 1 (2018). <https://doi.org/10.1186/s40561-017-0050-x>
3. IBM Homepage, The building block of an insurance revolution education. <https://www.ibm.com/downloads/cas/N3XRQABZ>. Accessed 06 Apr 2019
4. Karabegovic, I., Karabegovic, E., Mahmic, M., Husak, E.: The role of smart sensors in production processes and the implementation of Industry 4.0. *J. Eng. Sci.* **6**(2), B8–B13 (2019). [https://doi.org/10.21272/jes.2019.6\(2\).b2](https://doi.org/10.21272/jes.2019.6(2).b2)
5. Gartner Homepage, Practical Blockchain: A Gartner Trend Insight Report, <https://www.gartner.com/en/documents/3628617>. Accessed 04 Oct 2019
6. ICORATING Homepage, Market Statistics. <https://icorating.com/statistics/market/>. Accessed 04 June 2019
7. Momtaz, P.: Initial Coin Offerings (2018). https://papers.ssrn.com/sol3/papers.cfm?abstract_id=3166709. Accessed 05 Jan 2019
8. Fisch, C., et al.: Motives to Invest in Initial Coin Offerings (ICOs) (2018). <https://doi.org/10.2139/ssrn.3287046>. Accessed 25 Jan 2019
9. An, J., et al.: Initial coin offerings and entrepreneurial finance: the role of founders' characteristics. *J. Altern. Invest.* (2018)
10. Hargrave, J., Sahdev N.K., Feldmeier, O.: How Value is Created in Tokenized Assets (2018). https://papers.ssrn.com/sol3/papers.cfm?abstract_id=3146191. Accessed 05 Jan 2019
11. Rhue, L.: Trust is All You Need: An Empirical Exploration of Initial Coin Offerings (ICOs) and ICO Reputation Scores (2018). <https://doi.org/10.2139/ssrn.3179723>. Accessed 23 Jan 2019
12. Yadav, M.: Exploring Signals for Investing in an Initial Coin Offering (ICO) (2017). https://papers.ssrn.com/sol3/papers.cfm?abstract_id=3037106. Accessed 05 Jan 2019
13. de Jong, A., Roosenboom, P., van der Kolk, T.: What Determines Success in Initial Coin Offerings? (2018)
14. Martino, P., Bellavitis, C., DaSilva, C.M.: Blockchain and Initial Coin Offerings (ICOs): A New Way of Crowdfunding (2019)
15. Ante, L., Fiedler, I.: Cheap signals in security token offerings (STOs). *Quant. Finan. Econ.* **4**(4), 608–639 (2020). <https://doi.org/10.3934/QFE.2020028>
16. Albrecht, S., Lutz, B., Neumann, D.: The behavior of blockchain ventures on Twitter as a determinant for funding success. *Electron. Mark.* **30**(2), 241–257 (2019). <https://doi.org/10.1007/s12525-019-00371-w>
17. Momtaz, P.: CEO emotions and firm valuation in initial coin offerings: an artificial emotional intelligence approach. *Strat. Manage. J.* (2020)
18. Meyer, A., Ante, L.: Effects of initial coin offering characteristics on cross-listing returns. *Digit Finance* (2020)
19. Haar, N., Starr, J., MacMillan, I.: Informal risk capital investors: investment patterns on the east coast of the USA. *J. Bus. Ventur.* **3**(1), 11–29 (1988)
20. Mason, C., Harrison, R.: Why 'Business Angels' say no: a case study of opportunities rejected by an informal investor syndicate. *Int. Small Bus. J.* **14**(2), 35–51 (1996)
21. Landstrom, H.: Informal investors as entrepreneurs. *Technovation* **18**(5), 321–333 (1998)
22. Yasuhisa, T.: Business angels in Japan. *Ventur. Capital Int. J. Entrep. Fin.* (1999).
23. Feeney, L., Haines, G., Riding, A.: Private investors' investment criteria: insights from qualitative data. *Ventur. Capital Int. J. Entrep. Fin.* **1999**(2), 121–145 (1999)
24. Van Osnabrugge, M.: A comparison of business angel and venture capitalist investment procedures: an agency theory-based analysis. *Ventur. Cap.* **2**(2), 91–109 (2000)
25. Stedler, H., Peters, H.: Business angels in Germany: an empirical study. *Ventur. Cap.* **5**(3), 269–276 (2002)

26. Mason, C., Harrison, R.: Barriers to investment in the informal venture capital sector. *Entrep. Reg. Dev.* **14**(3), 271–287 (2002)
27. Mason, C., Harrison, R.: Auditioning for money: what do technology investors look for at the initial screening stage? *J. Priv. Equity* **6**(2), 29–42 (2003)
28. Mason, C., Stark, M.: What do investors look for in a business plan? A comparison of the investment criteria of bankers, venture capitalists and business angels. *Int. Small Bus. J.* **22**(3), 227–248 (2004)
29. Sudek, R.: Angel investment criteria. *J. Small Bus. Strat.* Fall 2006/Winter 2007, 89–103 (2006)
30. Clark, C.: The impact of entrepreneurs' oral 'pitch' presentation skills on business angels' initial screening investment decisions. *Ventur. Cap.* **10**, 257–279 (2008)
31. Maxwell, A., Jeffrey, S., Levesque, M.: Business angel early stage decision making. *J. Bus. Ventur.* **26**(2), 212–225 (2011)
32. Halo Business Angel Network, and European Business Angel Network, Raising Business Angel Investment European Booklet for Entrepreneurs. <http://www.eban.org/wp-content/uploads/2014/09/17.-European-Booklet-for-Entrepreneurs.pdf>. Accessed 04 Jan 2017



Agile Project Management Based on Data Analysis for Information Management Systems

Bohdan Haidabrus^{1,2} , Janis Grabis¹, and Serhiy Protsenko³

¹ Riga Technical University, 1, Kalku Street, Riga 1658, Latvia

² Riseba University of Applied Science, 3, Meza Street, Riga 1056, Latvia

³ Sumy State University, 2, Rymyskogo-Korsakova Street, Sumy 40007, Ukraine

Abstract. Nowadays, many projects and product managers, industry, and portfolio leads understand that data from the project or portfolio can be valuable for increasing their activities. There are many different types of project and portfolio lifecycle processes of managers daily duties: pre-sales and sales, mobilization, delivery, and closure phases. Definitely, in research, we focus on the processes, staffing, governance, and reporting activities. The day-by-day tasks are quite regulated and clearly described using templates and techniques as a company standard. Our literature review shows that Data Science methods can increase the level of project management and project success in several business problems. This study gives new opportunities to improve project management evaluation and results for managers, industry, and delivery leads. The proposed approach allows doing a project, portfolio management, and agile development more accurately, considering best practices and project performance data. Moreover, our results can provide more efficient benefits for different internal and external stakeholders.

Keywords: Agile development · Lean · Scrum · Safe · Project management · Data science · Data analysis · Machine learning

1 Introduction

In the last years, more and more companies are coming to understand that the data will be very useful for analyzing their success. Of course, this is more related to project-oriented companies implementing project management methodology in their activities. Different types of IT projects such as custom web applications, software-as-a-service products, mobile business apps, application programming interface (API), and integration require improvement of project management and software development business processes.

This study developed an approach based on Data Science for searching internal historical data from different projects. In particular, it includes specific project and portfolio management methods and guides (PMBOK PMI, Prince 2, IPMA ICB 4.0, SAFe, etc.) and software development techniques and approaches (Waterfall, Agile framework: Scrum, Kanban, Lean, XP, etc.) [1]. We identified the data from many PM's templates and Agile Development reports, from Mobilization Overview, Staffing process, Delivery, and others. Key performance indicators based on data analysis help organizations be successful in a long-term perspective.

2 Literature Review

Nowadays, the ability to analyze and use data is one of the key factors affecting the IT companies' ability to work effectively in the long perspective [2, 3]. There are many methodologies that follow the Agile framework. The most well-known among them are Scrum, Kanban, Extreme Programming, Lean Software Development, Test-Driven Development, Scaled Agile Framework, Large Scale Scrum, etc. [4–6]. Each methodology is unique and follows its own rules and techniques. Nevertheless, all of them incorporate elements of iterative development and continuous feedback during mobile apps development. An Agile framework makes it focused on methods and methodologies aimed at making the project and portfolio team think, work and make decisions more efficiently and successfully [7], including the use of recent AR/VR [8, 9] and smart technologies [10].

The main factor affecting the projects' successful implementation can be described with the so-called overall Agile framework. Three horizons from Agile project lifecycle consist of the following components which answering for such questions: how we sell, how we set up, how we manage, how we share? There are several ways to investigate planning indicators related to the deadlines [11]:

- *Pre-Sales and Sales* is focused on answering the questions of how we sell. Pre-Sales usually takes place at target right clients, accounting planning, and deal organization. A good Sales plan is updated during the project and consists of: quality opportunities, develop and submit a proposal, finalize and sign a contract.
- *Mobilization* takes place at the start of each process iteration, staffing processes, tools, and facilities. The main question at this step is: how we set up?
- *Delivery* processes are designed to coordinate work and how to manage: governance and reporting, compliance controls, business continuity, quality reviews, continuous improvement, client satisfaction.
- *Closure* is focused on answering the questions of how we share and cover innovation success stories, credentials and lessons learned, and project closure processes.

First, it emphasizes that plans are created for different reasons. The daily schedule is very precise, the iteration plan is less accurate and lists user stories for each iteration, while the release planning is the least accurate of all and only contains a prioritized list of desired features for the project. Secondly, such three-level planning helps view the project from different perspectives. As we know from our projects, the development process is not amorphous. It is filtered with planning throughout each phase and each level instead of a long and all-or-nothing plan from the start. Although long-term planning is more open-ended, you still can set main goals and push for them - keep those objectives in mind throughout each release and each iteration [12].

Project planning success depends on a large number of factors. Therefore, it is necessary to build and analyze the system of key performance indicators at all steps on the lifecycle, from the idea to the final product. A product owner, business stakeholders, and development team (scrum master, business analyst, UI/UX designer, developers (front-end/back-end), quality assurance engineers) need to have information on the project's current status. It is necessary to provide the key information about project management

and realization: the process kick-off, product backlog, release plan, sprints, minimum viable product (MVP), etc.

3 Research Methodology

Using Data Analysis for Managing IT Projects can be divided into two parts:

- *The Best Practices Approach*: historically integrated analysis of the best practices and failures of the projects;
- *The Historical Data Science Approach*: analysis of historical data for project planning depends on the requirements specification artefacts and user stories by using data.

According to *Project Lifecycle Support*, we have analyzed agile software product delivery processes of such IT projects from *Latvia Accenture Technology Center (LATC)* (accenture.com) [11]. The documentation is developed as a support document for LATC to secure a common agile framework to indemnify a successful run using Agile focused on six key pillars: happy growth, services marketing, change management, consulting, technology center amplified, client whitespace.

The delivery process consists of seven steps on the way from governance to the controls: governance and reporting, compliance controls, the business community, quality reviews, continuous improvement, client satisfaction, financial controls (Table 1).

Table 1. Delivery process

Stage	Description
Governance & reporting	It is critical to have the right framework to monitor delivery performance and support the teams executing projects. Governance models outline the connections for various leadership groups to connect and discuss the work in a portfolio. The Early Warning (EW) system is designed to find the risky opportunities and contracts and determine where further action is needed. Need to ensure that proper risk assessment is conducted already during the opportunity stage
Compliance management	Compliance management is the process of assessing and monitoring compliance against Accenture and engagement policies such as client data protection, records management, identify and track corrective actions to avoid or mitigate engagement risks
Business continuity	Business Continuity Plan (BCP) is a plan of action taken to ensure the continuation of essential project business processes and services in response to an interruption caused by any internal or external factor. It is a set of documents that defines the strategy of recovery in case of crisis. It considers the following aspects: - <i>People</i> - safety and security of our people - <i>Infrastructure</i> - the ability of the office to support service delivery in case of a power failure and ensure security - <i>Technology</i> - the impact of technology assets on service delivery

(continued)

Table 1. (continued)

Stage	Description
Quality reviews	Quality is a critical way how we protect our reputation internally as well as our external Brand. This involves informal coaching as well as structured reviews. We expect quality assurance to be applied to all areas of work/services we deliver and across all stages of the project lifecycle - starting with proper risk assessments from the opportunity stages through quality assurance and continuous risk monitoring and mitigation by adopting best practices
Continuous improvement	Productivity improvements are part of the value proposition to our clients. To deliver more value to our clients and Accenture, we should strive for more efficient delivery over time. <i>A continuous improvement process</i> is an ongoing effort to improve products, services, or processes. <i>Lean</i> is a principle-based approach that focuses on reducing the lead time, accelerate the velocity and reduce the cost of operation by continuously identifying wastes (non-value-adding activities) in the process (value stream) and eliminating them: <i>Map the AS-IS process, Identify Value and Waste, Eradicate Waste, Identify Automation opportunities, Identify Automation opportunities</i>
Client satisfaction	Client Team Satisfaction Survey (CTSS) allows us to understand our client team's (company on-site team's) assessment of the services and value we delivered, how well we delivered to the client's overall expectations, and the overall strength of the relationship
Financial controls	Cost to serve helps us ensure that money we spend to deliver service meets our contractual obligations to our clients. Whenever you ask yourself, " <i>Does my project meet financial targets?</i> " you need to clarify your project Cost to Serve and then compare it with what was agreed with On-site or Client (Target Cost to Serve). " <i>How can I do this?</i> " – you may ask? Well, let's break it down together!

Based on *The Agile Software Delivery*, the massive data with target as an integral evaluation of the project success allows for the complex correlations between separate different features. This approach, which is presented in "Fig. 1", allows describing all complex correlations between various project features, consider the importance of the feature, and zero the importance of those features that have a weak effect on the target. It means that the IT Project Manager should consider such features as a low-priority.

In the research, we are working with not so big dataset. In our case, there are not enough data, but there are too many features. The features do not cover all multidimensional data space, and it is necessary to use the special approaches for very small data sets processing, where the main challenge is to avoid overfitting.

The machine learning approach's main goal is to create such models that summarize the data from the training dataset in a way when the model trained on the new data could predict the target in the right way. On the one hand, we should try to develop such models which appreciate the basic interaction with data and models adjust excessively to the training data, and as a result, to do non-correct predict on the new unknown data. On the other hand, using very simple models (Under Fit) leads to losing the possibility of predicting complex patterns in the data (Fig. 2).

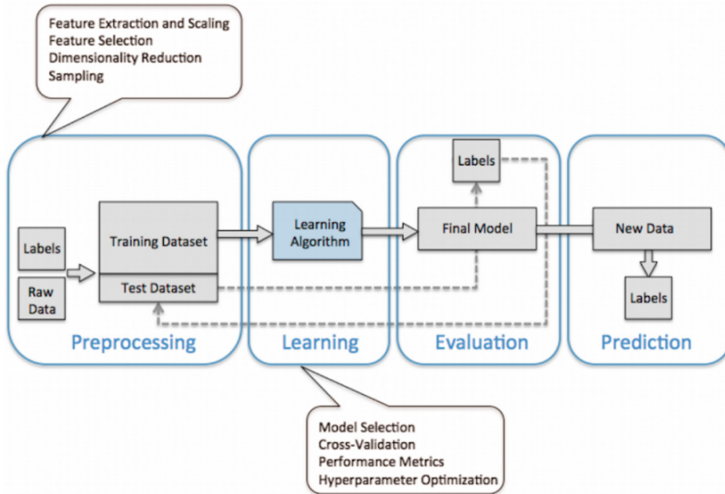


Fig. 1. ML system roadmap for agile software development and delivery

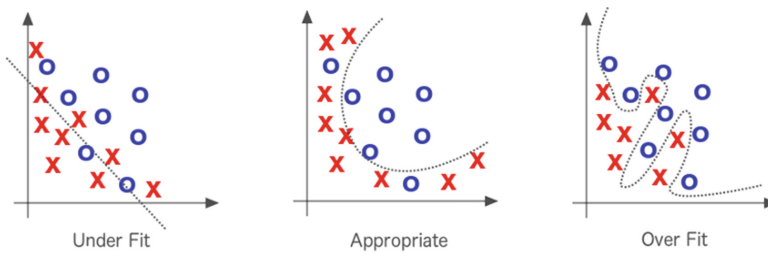


Fig. 2. Model for assessing the data analysis approach

It is common knowledge to have smaller samples for training, and more features lead to more accurate and consistent models. The disadvantage of this approach may result in the complexity of presenting different projects in one vector space. Because there are no identical projects, and there is another problem associated with a small number of observations in multidimensional space. Considering the information mentioned above, classical ML models such as linear models, random forest, or boosting will not always give good results, but certainly, they will be more adequate than using deep learning based on such types of datasets.

4 Results

We have a dataset with only data 37 samples. The complex models will realize very complicated and less related real predictions, which are almost perfectly explained in the train datasets, but probably poorly predicted the test dataset.

In our case, we use an approach where we try not to use complicated models with many parameters (such as artificial neural networks). The approaches of using different

forms of regularization are generally accepted. For linear regression, it is possible to use L1 and L2 regularization. [13, 14] (Fig. 3).

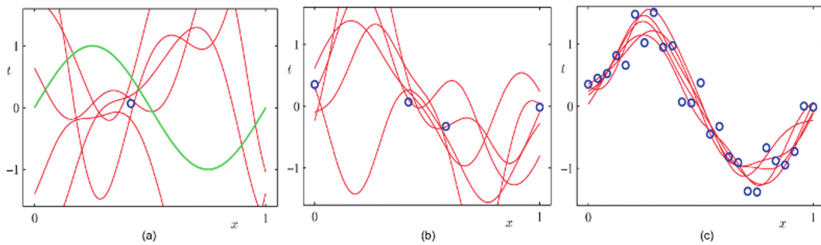


Fig. 3. Models for L1 and L2 regulations

In our research, the very important step of multidimensional project vectors is the initial preprocessing and features selections for this stage, and we have used a statistical approach based on Bayesian statistics Automatic Relevance Determination (ARD) [15, 16]. As a result, we received smaller dimensional vectors with features that were of greater statistical weight, and in this case, the use of classical ML models gave an adequate result.

$$Y = W \bullet X + e, \quad (8)$$

where, e - is a random normal error and the coefficients W are equal [1, 2, 3, 4, 5, 0, 0, ..., 0], that is, only the first five coefficients are nonzero, and the signs from the 6th to the 30th generally do not affect the real value of Y . We only have data - X and Y -, and we need to calculate the coefficients W :

```
# prepare the data, separate target and form Xtrain ta Ytrain.
Xtrain = data.iloc[:,1:-1].
Ytrain = data.iloc[:,-1].
#Check the size of our massive.
Xtrain.shape, Ytrain.shape.
```

Using the *ARDRegression()*, we will see which features are important and affect the target:

```
ard = ARDRegression().
ard.fit(Xtrain, ytrain).
ard.fit(Xtrain, ytrain).
# The higher of coefficient value, so it is more important for
the target.
print (ard.coef_).
```

And the results are:

```
[ 1.92557895e-03 -9.51988416e-04
-2.13868725e-04 -7.21210062e-04
```

1.51514818e-02 4.13840050e-01
 5.14818026e-01 8.82658008e-04
 9.09728493e-04]

Based on the ARD process model’s created model [17, 18], we can analyze the results, which show that in our case study, the coefficient of determination R^2 has a set of points r^2_score equal 0.9 (Fig. 4). In our research, we can see the efficiency of the Lasso regression analysis method [19, 20], t-distributed stochastic embedding algorithm, and random decision forest method (max_depth show the depth of separate tree in the forest) [12] not so high as using ARD.

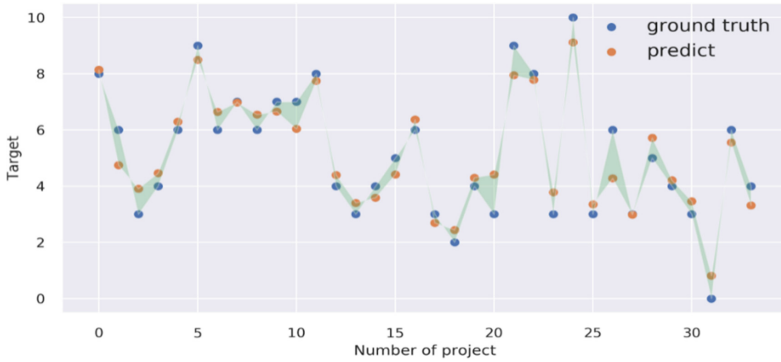


Fig. 4. ARD regression algorithm for correlation of targets and number of projects

Based on our research, we can see that application Synthetic Minority Over-sampling Technique and other synthetic addition data generation methods will increase the level of our results. Variance reduction and increase the opportunity of prediction can be possible by using different models with hyperparameters.

According to *The Historical Data Science Approach*, it is necessary to analyze the previous project data from the company’s analytical systems: Jira, Confluence, MS Teams, code repository (GitHub, GitLab, etc.), the Project Process Maturity Assessment, Project Subject Matter Expert Reviews, automation assessments, Delivery Quality Assurance Reviews, and another useful source of information. The project processes are proposed as an acyclic graph-theoretical model, specifically Probabilistic Graphical Models (PGM). Such a network may represent probabilistic relationships between estimates and inputs; it can be used to calculate the probabilities of evaluation of successful realization with the different inputs that will be considered with their weights.

As for small-scale datasets, statistic algorithms based on the Bayesian interpretation of probability, such as Bayesian Paradigm and Ridge Regression and Automatic Relevance Determination (ARD), deliver a posterior estimation and distribution of the variance components as coefficients of weights with a low level of dispersion.

5 Conclusions

In this research, we concluded that while operating with a small-scale dataset and comparatively sizeable quantity of modifications of increasing IT-readiness criteria, it is necessary to implement methods and algorithms based on the Machine Learning approach to avoid overfitting and predicting false data. An important step in the transition from simple regression problems to multiclass classification (for example, 3 classes) using traditional regularization linear models will allow obtaining a satisfactory result. To increase the efficiency of implementing IT projects, it is also advisable to use automatic determination of relevance using Bayesian statistic algorithms. Combining such synthetic algorithms as forecasts from multiple models and implementing the SMOTE-Simple Genetic Algorithm would be a perspective direction for the future increasing the level of quality our algorithms.

References

1. Akintoye, A.S., MacLeod, M.J.: Risk analysis and management in construction. *Int. J. Project Manage.* **15**(1), 31–38 (1997)
2. Labuschagne, C., Brent, A.C.: Sustainable project life cycle management: the need to integrate life cycles in the manufacturing sector. *Int. J. Project Manage.* **23**(2), 159–168 (2005)
3. Rivera, R., Burnaev, E.: Forecasting of commercial sales with large scale Gaussian Processes. arXiv preprint: [arXiv:1709.05548](https://arxiv.org/abs/1709.05548), [adsabs.harvard.edu](https://arxiv.org/abs/1709.05548). Accessed 17 Sep 2017
4. Bushuyev, S., Friedrich Wagner, R.: IPMA delta and IPMA organizational competence baseline (OCB): new approaches in the field of project management maturity. *Int. J. Manage. Proj. Bus.* **7**(2), 302–310 (2014)
5. Kritsky, D.N., Druzhinin, E.A., Pogudina, O.K., Kritskaya, O.S.: Decision making by the analysis of project risks based on the FMEA method. In: *Proceedings of IEEE 13th International Scientific and Technical Conference on Computer Sciences and Information Technologies, CSIT 2018*, pp. 187–190, Lviv (2018)
6. Siddique, L., Hussein, B.A.: Practical insight about risk management process in agile software projects in Norway. In: *IEEE International Technology Management Conference, ITMC*, pp. 1–4, Chicago (2014)
7. Rosenberger, P., Tick, J.: Suitability of PMBOK 6th edition for agile-developed IT Projects. In: *Proceedings of 18th IEEE International Symposium on Computational Intelligence and Informatics, CINTI 2018*, pp. 241–245, Budapest (2018)
8. Ivanov, V., Pavlenko, I., Trojanowska, J., Zuban, Y., Samokhvalov, D., Bun, P.: Using the augmented reality for training engineering students. In: *4th International Conference of the Virtual and Augmented Reality in Education, VARE 2018*, pp. 57–64 (2018)
9. Buñ, P., Trojanowska, J., Ivanov, V., Pavlenko, I. The use of virtual reality training application to increase the effectiveness of workshops in the field of lean manufacturing. In: *4th International Conference of the Virtual and Augmented Reality in Education, VARE 2018*, pp. 65–71 (2018)
10. Karabegovic, I., Karabegovic, E., Mahmic, M., Husak, E.: The role of smart sensors in production processes and the implementation of Industry 4.0. *J. Eng. Sci.* **6**(2), B8–B13 (2019). [https://doi.org/10.21272/jes.2019.6\(2\).b2](https://doi.org/10.21272/jes.2019.6(2).b2)
11. Accenture, October 2020. <https://www.accenture.com/lv-en>. Accessed 01 Oct 2020
12. Chenarani, A., Druzhinin, E.A., Kritskiy, D.N.: Simulating the impact of activity uncertainties and risk combinations in R & D projects. *J. Eng. Sci. Technol. Rev.* **10**(4), 1–9 (2017)

13. Jan Drugowitsch: Variational Bayesian inference for linear and logistic regression. arXiv preprint [arXiv:1310.5438](https://arxiv.org/abs/1310.5438), arxiv.org, last accessed 2013/10/13.
14. Piironen, J., Vehtari, A.: Projection predictive model selection for Gaussian processes. In: IEEE 26th International Workshop on Machine Learning for Signal Processing (MLSP), pp. 18–22, Salerno (2016).
15. Kampars, J., Grabis, J.: Near real-time big-data processing for data driven applications. In: Proceedings of 2017 International Conference on Big Data Innovations and Applications, Innovate-Data 2017, pp. 35–42, Prague (2018)s
16. Wu, A., Koyejo, O., Pillow, J.: Dependent relevance determination for smooth and structured sparse regression. *J. Mach. Learn. Res.* **20**, 1–49 (2019)
17. Karpus, V.E., Ivanov, V.A.: Choice of the optimal configuration of modular reusable fixtures. *Russian Engineering Research*, 213–219 (2012).
18. Xu, T., Sun, J., Bi, J.: Longitudinal LASSO: jointly learning features and temporal contingency for outcome prediction. In: Proceedings of the 21th ACM SIGKDD International Conference on Knowledge Discovery and Data Mining. ACM (2015)
19. Kiyko, S.G., Druzhinin, E.A., Koba, S.A., Haidabrus, B.V.: A mathematical background for information technology of project's processes integration taking into account risk factors. *J. Metall. Mining Ind.* **6**(3), 66–77 (2014)
20. Vasiljeva, T., Berezkina, E.: Determining project management practices for enterprise resource planning system projects. In: Proceedings of the 30th International Business Information Management Association Conference on Proceedings, IBIMA 2017 - Vision 2020: Sustainable Economic development, Innovation Management, and Global Growth, pp. 573–584 (2015SS7)



Optimization Work with a Digital Human Model

Pavel Kábele[✉]  and Milan Edl 

University of West Bohemia, 22, Univerzitní St., Pilsen 326 00, Czech Republic
pkabele@kpv.zcu.cz

Abstract. Ergonomics is a scientific discipline that today brings together several major scientific disciplines that deal with the rationalization of workspace design. It tries to unite these fields into one comprehensive one: to adapt the environment, especially the working environment, to humans so that it consumes as few biological reserves as possible when using it. This environment should therefore be pleasant for people, not negatively affect their physical and mental strength. In the past, the ergonomics of workplaces were not much addressed. First, a machine, tool, or workplace was created, and only then has an operator sought them. One had to adapt to the machine in order to use its help. The relationship between a person and his workplace began to be resolved only with the emergence of the first ergonomic companies. This work describes the Rula analysis and the relationship between ergonomic analysis and REFA time analysis. The application of individual methods is followed by evaluating results and determining individual problems at workplaces. Based on the identified shortcomings, proposals are made that partially or entirely eliminate these shortcomings. The effectiveness of the designs is retrospectively tested by ergonomic methods and subsequently evaluated.

Keywords: Ergonomics · Tecnomatix jack · Rula · Analysis · REFA · Time analysis · Workplace introduce

1 Introduction

In recent years, health and safety at work have become an increasingly relevant topic. The case study describes the procedure for optimizing the workplace using a simulation model. There is a very close relationship between health and work, as the amount and method of work performed by him is further developed based on the employee's health. In the work environment, operators are often exposed to the negative influences that cause occupational diseases. Therefore, the employer is obliged to classify individual job positions and observe the necessary measures to ensure greater safety and health at work.

The constant expansion of science and technology brings new technologies, machines, or methods of work. There is a certain imbalance between a person's abilities, skills, and abilities and the requirements for the activities and demands that the new technology requires. It is essential not to overlook this imbalance, as all new technologies or work methods must be performed and operated. Ignoring it can cause an overload of a

person, which leads to either his fatigue, failure, or even a crash of the entire system with possible health damage. Moreover, ergonomics is the task of not overlooking a person's limits but to respect all his abilities and limitations when designing a workplace [1, 2].

2 Literature Review

The concept of ergonomics was created by combining two Greek words “ergon” - work, “nomos” law. We can therefore say that ergonomics is the doctrine of the laws of human labor [3].

There are many definitions of ergonomics, one that was adopted by the International Ergonomic Association (IEA) in 2001:

“Ergonomics is a scientific discipline that optimizes the interaction between humans and other elements of the system and uses theory, knowledge, principles, data, and methods to optimize human well-being and system performance” [3, 4].

According to ČSN EN 614–1: 2006, the definition of ergonomics is as follows:

“Ergonomics is a scientific discipline that optimizes the interaction between humans and other elements of the system and uses theory, knowledge, principles, data, and methods to optimize human well-being and system performance” [5].

According to Jacobs, the main tasks of ergonomics include [6]:

- Creating organizational and technical conditions for effective human work,
- Increasing work well-being and reducing unpleasant workloads,
- Limiting the conditions for human error and failure,
- Achieve efficient production without the risk of health damage to operators,
- To adapt work equipment, procedures, and the environment to human abilities to perform his work tasks as efficiently and without harm to his health [6].

A workspace is a place in the workplace or a part thereof that is defined by an employee or multiple employees, which is used to perform a work task [7]. Each workspace designed to perform work is equipped with elements that affect the operation of the entire work activity. The individual elements and their use are governed by the relevant normative regulation [7, 8].

2.1 Ergonomic Analysis

The RULA analysis, full name Rapid Upper Limb Assessment, helps to assess the degree of risk of upper limb disease for a given procedure. The risk of damage to the upper limbs is determined by the position, muscle use, weight of the load, the duration of the operation, and the operation's frequency. Indicates the degree to which the risk of damage to the upper limbs must be reduced. The load on the operator's upper limbs, neck and torso is expressed by scoring according to a scale. It also determines whether the position is acceptable or changes will need to be made. Another possibility is to pay more attention to the task, such as performing an analysis that calculates the risk factor from the joint's angle, the rotation of arms, wrists, neck, and legs [9]. In most cases, the RULA methodology is used to assess the position, force, and movement associated with sedentary tasks. The four main applications of RULA analysis include:

- Measure musculoskeletal risk, usually as part of ergonomic analysis
- Compare musculoskeletal loads of current and modified workplaces
- Evaluate results such as productivity or equipment suitability
- Educate employees about the risks caused by various bad work attitudes [8].

In the first part of the RULA methodology, it is first necessary to assign individual points to the right or left-hand positions. In the upper arm, the arm’s angle in the work process plays the most significant role. An example is an angle that makes more than 90°, so this position is rated 4 points, as it is non-physiological. If the arm is supported, 1 point is deducted from the score. For the forearms and wrists, the principle is similar, but in addition, it distinguishes whether the movement does not take place through the center of the body or to the side. Subsequently, it is necessary to specify the type of load and the intensity of the work. The given principle is also followed in evaluating the position of the neck, torso, and legs [8–10].

In the second part, an evaluation is performed, where a gradual matrix search in the tables leads to a specific result. The evaluation for the upper limbs’ position is performed in the table marked with the letter “A”, when the score is determined by searching. The muscle, strength, and load scores must be added to this score. The result for the upper limbs’ position is a score of C [10, 11].

The ratings for neck, torso, and legs are given in the table marked “B”. This evaluation is searched for similarly as in the previous step, i.e., matrix. After adding the muscle, strength, and load scores, the resulting value for the neck, torso, and legs is marked with a score of D. The total score is determined by a matrix search in the table for scores C and D. As a rule, C and D scores higher than 9 are automatic to the 4th category. These categories are explained below [10, 12].

In total will be included in one of 4 categories (Table 1):

Table 1. Color categories in RULA methodology [13].

Categories	Risk and urgency of the measure
1–2	The work is acceptable; no changes are needed
3–4	The work is slightly risky; it is possible to make slight changes
5–6	Marked in orange - risky work; changes made are desirable
7	Hazardous work; urgent requests for changes

2.2 Software for Ergonomic Simulation

Tecnomatix Jack is an ergonomic tool for simulating and optimizing the work environment. This software works in a 3D environment and enables comprehensive control, simulation, and evaluation of the impact of work on humans. It is used in medicine, ergonomics, and also by health and safety operators. They use it to assess the working environment to protect operators’ health, fatigue, and safety. It can also be used to optimize work performance [13–15].

The software helps designers, ergonomists, experts through various assemblies to see the operator's reach, what the operator in a given position sees, whether it fits into a certain space. Jack is capable of detailed ergonomic analysis and simulation of future workplaces and workplaces operations. If the human factor is included in the analyses, the workplace can be freely optimized before its creation, thus saving many costs and the operator's health [12, 13].

2.3 Time Analysis

The REFA work system applies as a general model of work. Defined system terms can describe the working system. Work analyzes, resp. Work studies are ways of describing and evaluating work systems. The work system is in its function operating units of power and, at the same time, the building blocks of processes [1, 2]. The REFA toolkit is particularly successful when it contains change projects initiated by the company's management concerning a closed and agreed target system, using up-to-date information and communication media tailored to the relevant use case, and in particular the following factors [2, 12, 14]:

- Adjustment of work
- Process modification
- Data and time management (process data management)
- Quality management
- Cost management
- Management of remuneration and working hours
- Employee participation

3 Research Methodology

The study included the task of optimizing the production workplace depending on ergonomics. The procedure was the mapping of problematic workplaces – an execution of time surveys before optimization. Subsequently, the creation of a simulation program. Evaluation and subsequent verification of new time values.

The analyzes mentioned above were performed on the male 95th percentile and the female 5th percentile. According to NV 361/2007 Coll, range zones were assessed within the workplace, RULA analysis, and evaluation. Everything for predetermined working positions - reach into KLT boxes (into the blue box on the left, into the gray KLT box on the work table, reach into the blue KLT box on the right) - everything was assessed for the upper positions of KLT boxes, then the basic working position at the working table and placing parts in the trash for operators.

3.1 Description of Analyzed Workplace

The workplace consists of two worktables (Fig. 1), including the upper space intended for placing KLT boxes of various sizes. A technological jig is also mounted on one worktable, intended for easier execution of assembly operations on the final product,

which is the BMS stabilizer. There are then two smaller tables on both sides of the workplace on which the KLT boxes are located.

First, the basic working positions for the position of the operator were performed. An operator stands at a desk and holds a product, see the picture below.

In the following section, three workplace operator positions are selected for the workplace, which is the most demanding to perform. All human models are taken from the GERMAN anthropometric database and are always the 95th percentile for men and the 5th percentile for women.



Fig. 1. Model of the selected workplace.

3.2 Measurement of Current Workplace

The analysis was performed by taking a snapshot of the work operation. From the analysis, it is possible to read the required time per unit produced $t_e = 43s$. Calculations obtained this time from the measured times during the 45-min measurement. During this time, the production of 8 pieces was measured. There were 2 minor fluctuations in production speed. The second measured piece was made faster, which was probably because the storage space was freed, and the operator did not have to wait for it to be released.

The available zones analysis showed that all KLT boxes are out of their reach zone for men in the 95th percentile, and it is not possible to get into the boxes without a tread or a large incline. Subsequently, the RULA analysis was performed, which is a suitable tool for the initial ergonomic screening of the workplace. After performing the RULA analysis, the working position was rated 7 (Fig. 2) points, so it falls into the worst category, where there is a very high risk of health problems, and immediate changes in the workplace are needed.

Task Entry	Reports	Analysis Summary						
Job Title:	<input type="text" value="Daikin"/>	Job Number: <input type="text"/>						
Location:	<input type="text"/>	Analyst: <input type="text"/>						
Comments:	<input type="text"/>	Date: <input type="text"/>						
Body Group A Posture Rating								
Upper arm:	5							
Lower arm:	3							
Wrist:	2							
Wrist Twist:	2							
Total:	7							
Body Group B Posture Rating								
Neck:	5							
Trunk:	3							
Total:	7							
<table border="1"> <tr> <td>Muscle Use:</td> <td>Normal, no extreme use</td> </tr> <tr> <td>Force/Load:</td> <td>< 2 kg intermittent load</td> </tr> <tr> <td>Arms:</td> <td>Not supported</td> </tr> </table>			Muscle Use:	Normal, no extreme use	Force/Load:	< 2 kg intermittent load	Arms:	Not supported
Muscle Use:	Normal, no extreme use							
Force/Load:	< 2 kg intermittent load							
Arms:	Not supported							
<table border="1"> <tr> <td>Muscle Use:</td> <td>Normal, no extreme use</td> </tr> <tr> <td>Force/Load:</td> <td>< 2 kg intermittent load</td> </tr> </table>			Muscle Use:	Normal, no extreme use	Force/Load:	< 2 kg intermittent load		
Muscle Use:	Normal, no extreme use							
Force/Load:	< 2 kg intermittent load							
Legs and Feet Rating								
Standing, weight even. Room for weight changes.								
<table border="1"> <tr> <td>Grand Score: 7</td> </tr> <tr> <td>Action: Investigation and changes are required immediately.</td> </tr> </table>			Grand Score: 7	Action: Investigation and changes are required immediately.				
Grand Score: 7								
Action: Investigation and changes are required immediately.								
<input type="button" value="Update Analysis"/>								

Fig. 2. The result of the current state.

Subsequently, according to NV 361/2007 Coll., the working position was evaluated, thanks to which the biggest transgressions against ergonomics were revealed. The most problematic area is the left shoulder, which is in an unacceptable working position (flexion and abduction). The KLT box should be moved lower.

3.3 Outputs of Analyzes

According to the RULA analysis results, it is clear that the most stressed parts of the musculoskeletal system are mainly the back muscles, especially their lower half, and again the area of the cervical spine and upper limbs. In general, this position is very unsuitable for long-term and repeated stresses, and immediate changes must be made without the operator having to make similar movements.

In unsuitable positions, the operator is forced to keep stretching, which keeps him from working. REFA analysis revealed that the operator is forced to spend 7% of his working time stretching.

The results of repeated analyses also show increased activation of the lower back muscles, and a large load is placed on them in this position. However, it should be noted that the lifted object (part) has a very low weight. For this reason, the overall load on the lower back is still the norm and should not lead to more serious injuries, even with frequent work (Fig. 3).

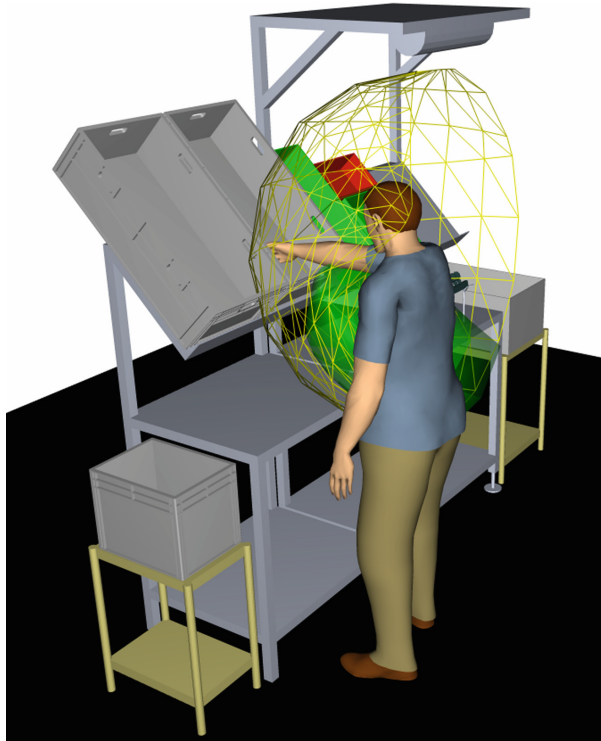


Fig. 3. Stressed positions.

4 Results

The whole study is based on the topic of the dissertation. Specifically, the methodology of ergonomic improvement and time plans was used. First, the original workplace was mapped. The layout of the workplace was drawn into a simulation program, and the current state was modeled.

An example of the results is the SF4 workplace, where 3 operations are performed. After evaluation for the 95th percentile (Table 2), it is necessary to adjust the workplace ergonomics. In particular, 2 operations is very critical. For the analysis to be as meaningful as possible, it was necessary to subject the workplaces to an analysis for percentile 5. This is an operator of very small stature.

Table 2. Evaluation of current workplace.

Percentile 95	Operation 1	Operation 2	Operation 3
RULA	4	7	4
Back	Unsatisfactory	Unsatisfactory	Unsatisfactory
Hands		Unsatisfactory	Unsatisfactory
Percentile 5	Operation 1	Operation 2	Operation 3
RULA	5	6	7
Back	Unsatisfactory	Unsatisfactory	Unsatisfactory
Hands		Unsatisfactory	Unsatisfactory

A new workplace model has been created in the Tecnomatix program that meets the company’s investment costs and at the same time improves in the form of Table 3. The proposed condition was created for the 50th percentile. The proposed condition was created for the 50th percentile.

Table 3. Evaluation of new workplace.

Percentile 50	Operation 1	Operation 2	Operation 3
RULA	2	3	2
Back	Satisfactory	Unsatisfactory	Satisfactory
Hands		Unsatisfactory	Satisfactory

The most problematic movements of the hands and back were evaluated. From the proposed solution, it is necessary to deal with operation 2. However, this value is no longer critical. In the next procedure, the preparation will be adjusted so that it is more suitable for handling.

Verification of the production cycle can be seen in Fig. 4. By improving the ergonomics of the workplace and rationalizing work processes, the production cycle was shortened by 10 s.

The main benefit for the practice is the use of ergonomic methods in conjunction with the Tecnomatix Jack software. So far, ergonomics in workplaces has not been much addressed, so the work can also guide what direction to take when creating a new workplace or what methodology to use when innovating an existing workplace.

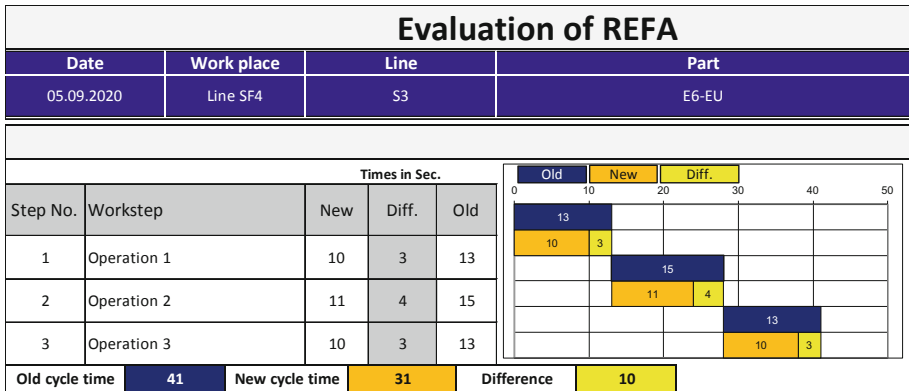


Fig. 4. Evaluation of REFA analysis.

5 Conclusion

As part of the study, a snapshot of the work process was prepared using the REFA methodology, which was used to understand the operation of the workplace, the assembly process, and the time required for the operations performed. The RULA method was chosen to assess the workload, work intensity, and assess the body’s working positions, which was subsequently confirmed by the Tecnomatix Jack program.

Simultaneously with the time analysis, a RULA analysis was performed, which identified problematic workplace places.

From the above ergonomic analyzes, it is clear that long-term work in the workplace shown could cause health problems that would lead to back, neck, and upper limb pain. It is, therefore, appropriate to consider adjusting working conditions using the solutions outlined above. Adjustments should take into account both short and large operators; it is essential to reach a compromise.

Another possible solution to improve working conditions at the workplace and thus increase the ergonomics of the entire workplace is the acquisition of rubber pads to soften the concrete surfaces on which operators would stand in their activities’ performance.

Problems that have arisen during observation and analysis must be rectified as soon as possible. REFA time analysis results revealed that after adjusting the workplace ergonomics, the operator is not limited by stretching during the work task. This eliminates unnecessary movements and simplifies the work process.

The dependence of productivity on workplace ergonomics will be verified for another study. A methodology for how to increase productivity depending on the ergonomics of the workplace will be determined.

The performed analyzes were a significant contribution to the detection of ergonomic shortcomings and based on them a new work procedure was developed with a number of rationalization solutions in the workplace.

Acknowledgment. This paper was supported by the Internal Grant Agency of the University of West Bohemia, project No. SGS-2012–063 - “Integrated design of manufacturing system as metaproduct with a multidisciplinary approach and with using elements of virtual reality.” This paper was created with the subsidy of the project CZ.1.05/2.1.00/03.0093 “RTI - Regional Technological Institute” carried out with the support of the Ministry of Education, Youth and Sports.

References

1. Mašín, I., Vytlačil, M.: *New Ways to Higher Productivity - Industrial Engineering Methods*. 1st ed. Institute of Industrial Engineering, Liberec (2000).
2. Malý, S., Král, M., Hanáková, E.: *ABC Ergonomics*, 1st edn. Professional Publishing, Prague (2010)
3. Porter, M.E.: *Competitive Strategies - Methods for Industry and Competitor Analysis*. Victoria Publishing, Prague (1994)
4. Gilbertová, S., Matoušek, O.: *Ergonomics: Optimization of Human Activity*, 1st edn. Grada, Prague (2002)
5. Bridger, R.: *Introduction to Ergonomics*, 3rd edn. CRC Press, Boca Raton (2009)
6. Jacobs, K.: *Ergonomics for Therapists*, 3rd edn. Mosby, St. Louis, Mo (2008)
7. Bercaw, R.: *Lean Leadership For Healthcare: Approaches To Lean Transformation*. CRC Press, Boca Raton, FL (2013)
8. Hanáková, E., Matoušek, O.: *Hygiene of work*, 1st edn. Oeconomica, Praha (2006)
9. Chundela, L.: *Ergonomics*, 2nd edn. CTU Publishing House, Prague (2005)
10. Salvendy, G.: *Handbook of Human Factors and Ergonomics*, 4th edn. Wiley, Hoboken (2012)
11. Ferenčíková, D.: Ergonomic aspects of product development and innovation. In: *Proceedings of the 2nd International Conference on Innovation and Entrepreneurship*. Academic Conferences Ltd, Bangkok (2014)
12. Berlin, C., Adams, C.: *Production Ergonomics: Designing Work Systems to Support Optimal Human Performance*. Ubility Press, London (2017)
13. Guastello, S.J.: *Human Factors Engineering and Ergonomics: A Systems Approach*. Lawrence Erlbaum Associates, Mahwah, N. J. (2006)
14. Singh, L.P.: *Work Study and Ergonomics*, 1st edn. Cambridge University Press, Cambridge (2018)
15. Hatiar, K., Bršiak, V.: Industrial revolution and prevention of work-related problems of the musculoskeletal system. In: *Living conditions and health: collection of scientific works*. Comenius University in Bratislava (2018)



The Implementation of Industry 4.0 Supported by Service Robots in Production Processes

Isak Karabegović¹ , Edina Karabegović² , Mehmed Mahmić²,
Ermin Husak² , and Predrag Dašić³ 

¹ Academy of Sciences and Arts of Bosnia and Herzegovina, 7, Bistrik Street, 71000 Sarajevo, Bosnia and Herzegovina

² University of Bihać, 2/2, PapeIvanaPavla II Street, 77000 Bihać, Bosnia and Herzegovina

³ High Technical Mechanical School of Professional Studies, 19, RadojaKrstića Street, 37240 Trstenik, Serbia

Abstract. The ongoing implementation of Industry 4.0 in all segments of society will improve many aspects of human life and initiate many changes in business, production processes, and supply chains from raw materials to finished products. The implementation of new business methods leads to the transformation of production models and production processes, consumption, transport, and supply. Industry 4.0 enables the adaptation of production processes in the industry to full intelligent automation. In other words, it enables the introduction of self-automation, self-configuration, self-diagnosis and solution, knowledge, and intelligent decision-making, owing to the innovations and their implementation in robotics, smart sensors, 3D printers, Internet of Things (IoT), and Big Data technology. The essential quality shift in the implementation of Industry 4.0 in production processes is the implementation of AGV service robots (automatically guided vehicles) in the automation of transport operations in the production process itself (such as transport of raw materials, semi-products, and finished products), on assembly lines, storage of finished products and supply of finished products. The implementation of service robots in the production process is amortized very quickly if they are in operation for 24 h, while the investments can pay off in 2–3 years, and the system operates for about 15 years. The availability of work itself is about 98.5%. The implementation of service robots optimizes production time and costs, thus providing high productivity. The paper presents the annual application of service robots in logistics and the application of AGV service robots with different structures in production processes.

Keywords: Industry 4.0 · Smart factory · Service robots · Automatic guided vehicles · Transportation · Logistic · Production process

1 Introduction

Industry 4.0 represents a vision of advanced industrial production, which is already partially implemented by applying new technologies to automate production processes, data exchange, and processing. A new value chain is formed with the implementation of

Industry 4.0 that primarily relies on CPS – Cyber-Physical-Systems, which is another name for the Internet of Things, and its associated services, most often realized through Cloud Computing [1]. The analysis and discussion of Industry 4.0 have the task of raising awareness of participants about its implementation, comprehensiveness, and speed of technological change and its multiple impacts [2]. It is well known that a large number of both industrial and service robots have been installed in the production processes in all branches of industry, especially in the metalworking and automotive industries. We have to mention that the first-generation industrial robots were installed in the production processes, which were separated with fences to not harm the workers in the production process [3, 4]. The development of new technologies, primarily robotic, sensor and information-communication technology, and their implementation, leads to the development of collaborative robots and AGV service robots (automatic guided vehicle) [5, 6]. Their implementation in production processes represents the most significant qualitative change in the automation of transport operations, production, assembly lines, and warehouses [7, 8]. The implementation of service and collaborative robots in production processes has achieved many advantages such as: improving product quality, increasing homogeneity, reducing demand for the workforce in performing routine and reproduction processes, reducing production costs, reducing maintenance costs, satisfying the requirements of the global market such as stricter quality standards [9]. Robotic technology and its implementation in production processes and all segments of society present one of the Industry 4.0 foundations.

2 Literature Review

As it is well known, the following revolutions have been recorded in the world [10]:

- the first industrial revolution that occurred with the invention of the steam engine in 1784,
- the second industrial revolution with the discovery of electricity in 1870,
- the third industrial revolution with the application of IT systems and the Internet in 1969,
- today we are in the fourth industrial revolution, i.e., Industry 4.0.

The evaluation of the industrial revolutions is shown in Fig. 1.

The difference between the third industrial revolution and the fourth industrial revolution, i.e., Industry 4.0, is as follows: physical labor and automated production are characteristics of the third industrial revolution production process, whereas Industry 4.0 engage intellectual labor and automatic design [3]. Development and implementation of these technologies at the very beginning have increased the application of innovations in computer hardware, software, operating technologies, and information technologies that are becoming more sophisticated and integrated, enabling the transformation of society as a whole, thus leading us into a global economy. The implementation of Industry 4.0 in production processes is leading towards the smart-intelligent production process that has its characteristics, as shown in Fig. 2.

The production process of Industry 4.0 has its characteristics such as intelligence, awareness, connectivity, and manageability. The production process is equipped with

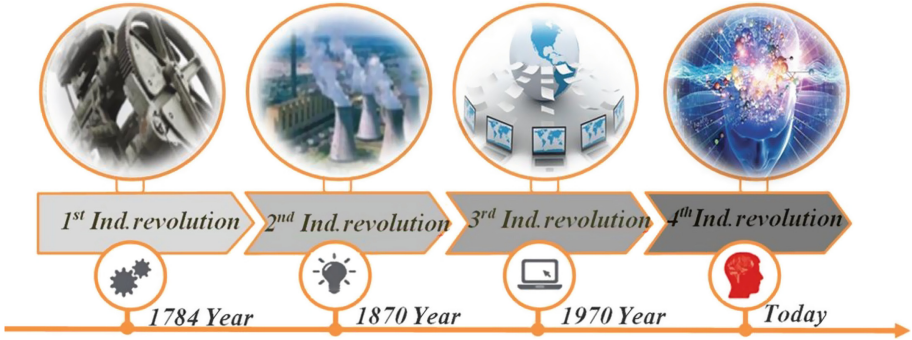


Fig. 1. Industrial revolutions and their evaluation in the world.

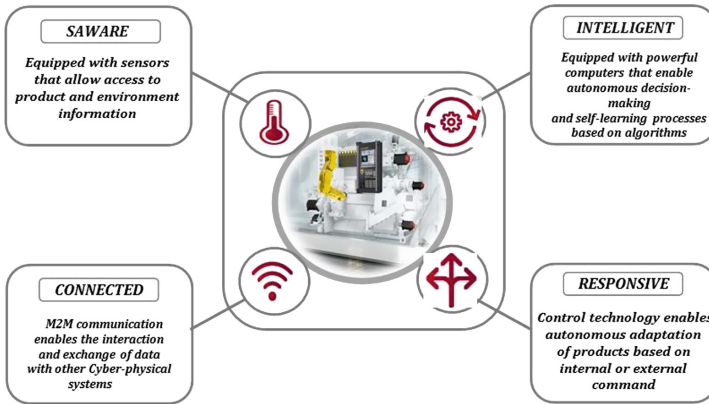


Fig. 2. The smart production process of Industry 4.0 and its characteristics.

advanced sensors that allow access to information about the state of production and the environment, and it is also equipped with powerful computers that allow autonomous decision-making and the process of self-organization based on an algorithm [13].

3 Research Methodology

Based on [18], it is known that the continuous robot market is expanding. The trend of industrial robotics has been increasing further in recent years. The need for robot applications is certainly increasing based on the labor shortage aspect and the reduction of the working population since the low birth rate and aging population, including developed countries: the need for quality service without errors and exemption from aspects such as hard work, a simple repetitive work, and poor working conditions. [19]. For security reasons, much space is needed to install conventional robots. However, by developing collaborative robots, implementation becomes possible next to the workers without any safety fences, and the installation hurdles regarding space are reduced. So we can state that the possibility for robotization is still increasing. We analyzed the trend of service

robot implementation based on statistics on the application of service robots from the UN Economic Commission for Europe (UNECE), the Organization for Economic Co-operation and Development (OECD), and the International Federation of Robotics (IFR) [20].

4 Results

The reference [3] concludes that the trend of application of innovations from the mentioned technologies of Industry 4.0 is continuously increasing in the world. The automotive industry holds first place in the implementation and application of innovations from Industry 4.0. Such order is a great global competition in the world because all companies invest heavily in research, development, and implementation of Industry 4.0 core technologies to remain competitive in the global market [11]. All production processes require flexible automation in all industries and the reduction of production and sales time of permanently high-quality products. It is expected that the introduction of innovative technologies in the industry will lead to greater flexibility, increased productivity, increased product quality, and customer cooperation in order to increase sales of finished products [12]. There has also been an exponential evolution in robotic technology, as shown in Fig. 3.

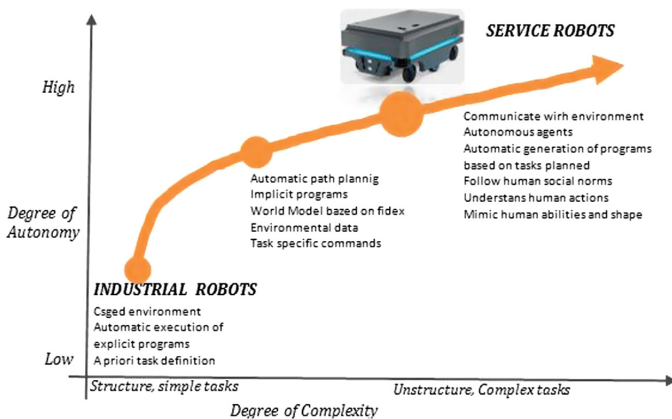


Fig. 3. The trend of evolution of robotics.

Based on Fig. 3, we can conclude that industrial robots (first-generation robots) have a very low degree of autonomy, they are locked in a cage for worker safety, they employ automatic execution of tasks and explicit programs, and need to have defined tasks for execution [13, 14]. The first evolution occurred in terms of automatic path planning, implicit programs, with task-specific commands and environment data. Due to new technologies, the implementation of patents in robotics is coming to a new evolution. Robots can communicate with the environment, have automatic program generation and autonomous agents, understand human procedures, and imitate human abilities [15]. Owing to the implementation of patents in robotics, there has been an evolution of both

industrial and collaborative robots and service robots. As they are most commonly called, service robots are classified into two groups according to their role in the community, i.e., service robots for personal/home use and service robots for professional purposes [16, 17]. Logistics robots implemented in production processes are classified in the group of service robots for professional use, which also include: military service robots, field robots (agriculture, livestock, and forestry), service robots for medicine, service robots for professional cleaning, service robots for inspection and maintenance, service robots for rescue and surveillance, underwater systems, mobile platforms for general use, public relations service robots, and other service robots [12].

The application of service robots in the world is shown in Fig. 4, which demonstrates the trend of applying service robots in the world from 2005 to 2013. The statistics shown in the diagrams were obtained from the International Federation of Robotics (IFR), the United Nations Economic Commission for Europe (UNECE), Organization for Economic Co-operation and Development (OECD) and references [19, 20].

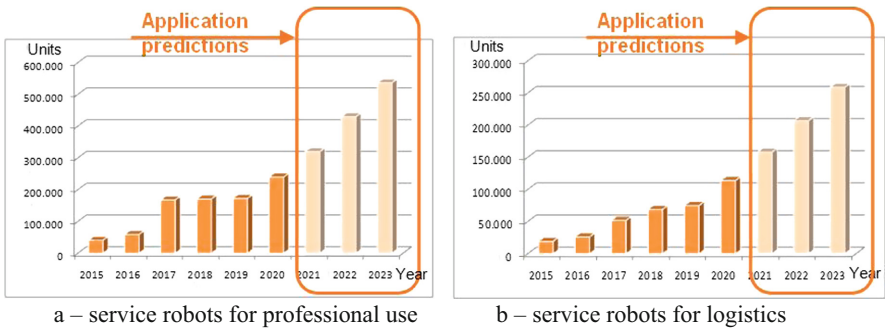


Fig. 4. The trend of implementation of professional service robots and service robots for logistics for the period 2015–2020 and estimate of application to 2023.

The trend of application of professional service robots (Fig. 4.a) has grown six times in just five years so that in 2019 the application amounted to 173,000 robot units. An exponential increase is expected in the coming period as well, so that in 2023 (according to the reports of the International Federation of Robotics – IFR) the application of about 537,000 robot units is expected. Of all professional service robots, the application of service robots for logistics holds the first place, as shown in Fig. 4.b. The trend of application of service robots for logistics is exponential so that with 19,400 robot units applied in 2015, the application increased to 75,000 robot units in 2019. It is estimated that the application will increase in the future, and the application of about 259,000 robot units in production processes of logistics is expected by 2023. To create a factual representation of the application of service robots for professional use, Fig. 5 shows the percentage ratio of applications for 2019 [19].

As can be seen, of the total amount of service robots used for professional purposes, service robots for logistics hold first place with 43%. The second place is held by service robots for the public environment with 12%, followed by service robots for defense with 11%, service robots for inspection with 9%. We must note that the medical application

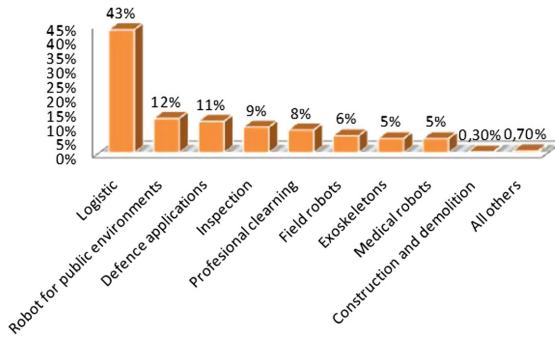


Fig. 5. The representation of professional service robots in 2019.

of robots is only 5%, which should raise concern because the number of applications in medicine should be far more significant. If we compare the percentages of robot applications for logistics for 2019 (43%) to 2013 when only 10% of robots were applied for logistics [18], we conclude that the application has increased 4.3 times in seven years. The answer to this trend is the implementation of Industry 4.0 in the industry's production processes where service robots are mainly used, i.e., the automotive industry with the highest implementation of Industry 4.0. Service robots of the latest generation must be aware, or in other words, it must be equipped with smart sensors that allow access to information about the state of the product they are manipulating or working with and the environment in which they perform operations. It needs to be connected by M2M communication that enables interaction and data exchange with other machines in the environment and with other cyber-physical systems. Control technology must allow robots autonomous adaptation based on an internal or external command. The robot must be intelligent and equipped with a powerful computer that allows autonomous decision-making and self-learning processes based on algorithms. The industrial robots conceived in this way will accelerate the implementation of Industry 4.0 in production processes. Many automotive companies are driven by the implementation of Industry 4.0 in production processes. Companies engaged in the development and production of service robots for logistics have developed various designs of service robots. Due to paper limitations, we can present only two solutions to implement service robots for logistics. Company MiR – Mobile Industrial Robots has developed a service robot for logistics MiR500 and MiR1000 to optimize internal transport in companies for heavy loads on pallets up to 1000 kg. Before implementing service robots for logistics, transport in production processes was performed manually, as shown in Fig. 6 a) [3, 21].

MiR service robots are collaborative and autonomous. They maneuver safely around all kinds of obstacles. If a person comes out in front of them, they will stop. Advanced technology and sophisticated software allow the robot to navigate independently and choose the most efficient route to its destination.

When an obstacle occurs on the path of the service robot, the robot automatically moves around it and redirects its path to avoid stopping or delaying the delivery of materials. The service robots are equipped with the latest laser scanner technology and provide a 360-degree visual image for optimal safety. The 3D cameras on the front have

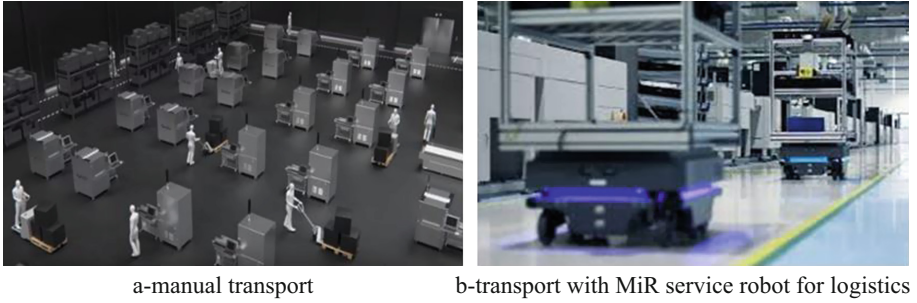


Fig. 6. Transport in the production process with service robots for logistics of company MiR.

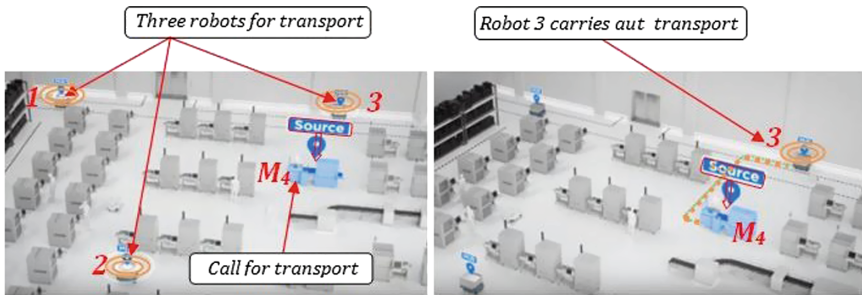


Fig. 7. Optimization of the path of a service robot for logistics in the production process of the company MiR [3, 21]

a range of 30 to 2000 mm above the floor level, while two sensors at each corner ensure that the robot can see pallets and other obstacles, which robots usually have a hard time seeing. The method of order processing for robot transport is shown in Fig. 7.

The working machine communicates with service robots for logistics. For example, when a machine M_4 gives an order for the transport of the finished product, we can see that three robots can perform the given order. Software optimization is performed, and a decision is made that the robot which is the closest to the given machine M_4 and whose path is the shortest should perform the task. This example is robot 3, which takes the processing order and performs transport, as shown in Fig. 7. During operation, service robots consume energy from the battery. After the battery is discharged, it is necessary to recharge it. Battery charging connectors are installed in the workspace, so the service robot can reach the connector and turn it on to charge the battery (the robot can perform 1000 cycles with one charging). When the battery is charged, the robot is ready to process the following order.

Another example is the company “KUKA”, which developed a service robot for logistics “KMR iiwa”, shown in Fig. 8.

When an order for transport is given in the production process, optimization is performed through ERP (Enterprise Resource Planning) to verify which service robot is free and the closest to execute the production order. After path optimization, ERP gives the robot the command to execute the task, and the service robot starts execution.

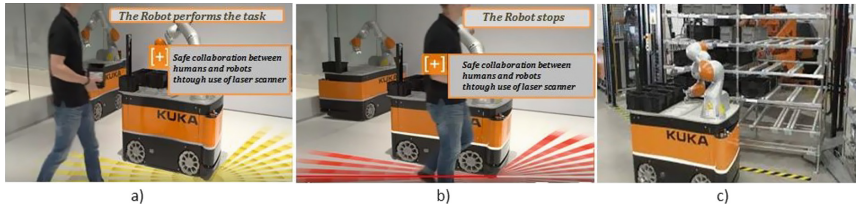


Fig. 8. Service robot “KMR iiwa” – safety cooperation between people and barriers with a laser scanner [22, 23].

However, suppose it encounters obstacles along the way that may be different, such as workers in the production process, other service robots performing other tasks or some other obstacle. In that case, the robot stops or bypasses the obstacle because the safety of the service robot is provided with a laser scanner, as shown in Fig. 8. We must note that many companies in the world are developing both industrial and service robots, but due to limitations, we cannot present their designs and implementation methods. We can easily conclude that service robots for logistics, using all the above technologies that form the basis of Industry 4.0, are entirely prepared for implementation in the production processes of Industry 4.0. This is the path that will lead to smart production processes in industries. Service robots for logistics perform tasks exclusively in industrial automation to make it more flexible.

5 Conclusions

The implementation of the technologies that form the foundation of the fourth industrial revolution, Industry 4.0, such as robotics and automation, cloud computing, intelligent sensors, 3D printers, and radio frequency identification – RFID, changed the production processes and supply chains. Industry 4.0 relies on advances in the use and exchange of information, thus giving companies the ability to connect almost all devices and drastically improve their efficiency. Using a large number of smart sensors in the production process, we always have information about production devices and machines based on which we make decisions when to replace devices and machines, thus conducting permanent maintenance. It seems to many that Industry 4.0 serves only large companies that perform large and complex operations in production processes, but this is not the case. Small and medium-sized companies can also benefit from what Industry 4.0 offers because by using these technologies, they can process and store data more efficiently and improve the way they design, manufacture, and deliver the products.

The development of new technologies is guiding us towards the automation and modernization of production processes and the implementation of Industry 4.0, thus creating the conditions for the application of service robots that are becoming more demanding and complex. The trend of applying service robots is continually growing, as shown in the paper, which will continue in the years to come. Besides, the trend of implementing service robots for logistics in production processes is growing exponentially, as shown in Fig. 4b. Service robots for logistics are the most commonly used service robots, and in 2019 the ratio was 43% of the total amount of installed robots.

AGV logistics service robots have advantages over other robots, such as increased reliability, increased productivity, reduced labor costs, controlled movement with ± 10 mm accuracy, reduced damage to the elements they transport, increased flexibility and safety, and the reprogrammed trajectory of robots. The implementation of Industry 4.0 in production processes depends on the implementation of robotic technology in production processes because robotic technology is one of the pillars of Industry 4.0. Both industrial and service robots are installed in production processes. The paper has shown that the highest application of service robots for logistics is in the production processes, thus leading us to smart production processes and smart factories, which is the ultimate goal of Industry 4.0. It is expected that in the coming period, the implementation of robots and Industry 4.0 will have a growing trend worldwide.

References

1. Schwab, K.: The Fourth Industrial Revolution. World Economic Forum. Geneva, Switzerland (2016)
2. Pelster, B., Schwartz, J. (eds.): Rewriting the rules for the digital age. Deloitte Global Human Capital Trends, Deloitte University Press (2017)
3. Karabegović, I., Kovačević, A., Banjanović-Mehmedović, L., Dašić, P.: Handbook of Research on Integration Industry 4.0 in Business and Manufacturing. IGI Global, Hershey, Pennsylvania, USA (2020)
4. Mathieu, d'A.: Data analytics beyond data processing and how it affects Industry 4.0. Insight Centre for Data Analytic, Dublin, Irska (2017)
5. Kusmin, K.-L.: Industry 4.0 Analytical Article, IFI8101 - Information Society Approaches and ICT Processes. School of Digital Technologies, Tallinn University, Estonia (2016)
6. Bechtold, J., Lauenstein, C., Kern, A., Bernhofer, L.: Executive Summary: The Capgemini Consulting Industry 4.0 Framework. Capgemini Consulting, Pariz, France (2017)
7. Davies, R.: Industry 4.0: Digitalisation for productivity and growth (2015)
8. Bunse, B., Kagermann, H., Wahlster, W.: Smart Manufacturing for the Future. Germany Trade & Invest, Berlin, Germany (2017)
9. Freund, E., Stern, O.: Robotertechnologie I. Institut für Roboterforschung, Dortmund (1999)
10. Löhner, M., Kerpen, D., Lemm, J., Saggiomo, M., Gloy, Y.S.: Intelligent assistance systems for a competence-enhancing in industrial textile work environments. In: 8th International Conference on Education and New Learning Technologies, pp. 1054–1056. Barcelona, Spain (2016)
11. Dev Anand, M., Selvaraj, T., Kumanan, S., Raj, A.B.T.: Robotics in online inspection and quality control using moment algorithm. *Adv. Prod. Eng. Manage.* 7(1), 27–38 (2012)
12. Dev Anand, M., Selvaraj, T., Kumanan, S.: Fault detection and fault tolerance methods for industrial robot manipulators based on hybrid intelligent approach. *Adv. Prod. Eng. Manage.* 7(4), 225–236 (2012)
13. Kadri-Liis, K.: Industry 4.0 Analytical Article, IFI8101 - Information Society Approaches and ICT Processes. School of Digital Technologies, Tallinn University, Estonia (2016)
14. Sihm, W., Jäger, A., Hummel, V., Ranz, F.: Implications for Learning Factories from Industry 4.0. ESB Business School, Reutlingen University, Reutlingen (2016)
15. Ulrich, E., Maximilian, H.: Industrial IoT Risk Assessment of Smart Factories. PLUS-2016, Munchen, Deutschland (2016)
16. Buchmeister, B., Friscic, D., Palcic, I.: Impact of demand changes and supply chain's level constraints on bullwhip effect. *Adv. Prod. Eng. Manage.* 8(4), 199–208 (2013)

17. Dev Anand, M., Selvaraj, T., Kumanan, S., AjithBosco Raj, T.: Robotics in online inspection and quality control using moment algorithm. *Adv. Prod. Eng. Manage.* **7**(1), 27–38 (2012)
18. Karabegović, I., Karabegović, E., Mahmić, M., Husak, E.: The application of service robots for logistics in manufacturing processes. *Adv. Prod. Eng. Manage.* **10**(4), 185–194 (2015)
19. World Robotics 2019: The International Federation of Robotics, Statistical Department. Frankfurt am Main, Germany(2019)
20. Karabegović, E.: Implementation of industry 4.0 and robots in production processes of the metal industry. *Int. J. Adv. Eng. Res. Sci. (IJAERS)* **7**(12), 169–176 (2020)
21. Optimized Internal Transportation of Heavy Loads and Pallets with MiR1000 and MiR500. <https://www.mobile-industrial-robots.com>. Accessed 22 Dec 2020
22. Autonomous transportation with mobile robot KMR iiwa,KUKA - Robots & Automation. <https://www.kuka.com/en-de>. Accessed 22 Dec 2020
23. Autonomous Mobile Robots (AMRs) - Latest News. <https://www.cobottrends.com/category/amrs/>. Accessed 24 Dec 2020



Intelligent Numerical Control of Profile Grinding

Vasily Larshin¹ , Natalia Lishchenko² , Oleksandr Lysyi³ ,
and Sergey Uminsky⁴ 

- ¹ Odessa National Polytechnic University, 1, Shevchenko Ave., Odessa 65044, Ukraine
² Odessa National Academy of Food Technologies, Kanatna St., Odessa 11265039, Ukraine
³ Odessa Military Academy, 10, Fontanskaya doroga St., Odessa 65009, Ukraine
⁴ Odessa State Agrarian University, 13, Panteleymonovskaya St., Odessa 65012, Ukraine

Abstract. The use of a single computer-aided control to automate production and its preparation creates a common technical base when the adjustable online model of the profile gear grinding operation allows compensating for the lack of online sensors built into the gear grinding system. In this case, the automation of design and production within a single integrated CAD/CAM/CAE system appears to be a single technological process in which not only general but also phased results are defined. This becomes possible by optimizing the entire (and not only partial) sequence of work performed. The introduction of negative feedback from the built-in online sensors of technological information (when such sensors are available) allows, based on monitoring the grinding system state and output parameters, to correct the setting of the CAE-system which is used not only offline but also in the online mode of CNC machine work. When the adjustment of the CAE system is regulated by deviation, this approach to control makes it possible to increase the efficiency of automated grinding systems. The paper provides a fundamental solution to the problem of making adjustments to the control program of a CNC machine based on the results of measuring the state and output parameters of the grinding system. Given as an example, a step-by-step sequence of actions to determine the parameters of grinding of complex-shaped machine parts (for example, gear wheels) makes it possible to understand the algorithm of operation of an intelligent self-training grinding system.

Keywords: CAD/CAM/CAE · Product life cycle · Product design · Process design · Self-training grinding system

1 Introduction

The world economy is going through the fourth industrial revolution of its development. A distinctive feature of this “Industry 4.0” revolution is the widespread use of automation and computerization of technological processes and technological systems to ensure the efficiency of various industries (not only mechanical engineering) and the so-called sustainable economic development. The role and significance of complex production automation can hardly be overestimated when the risk of human-made disasters,

climatic changes in the environment (global warming), pandemic (COVID-19), etc. In these conditions, computer automation of production in mechanical engineering technology and other economic branches plays a paramount role for the world and domestic economy.

There are two definitions of the term “automation” for manufacturing processes and manufacturing systems. According to the first automation definition, manual labor and manual control are replaced by machine labor and machine control, respectively. According to the second automation definition, it is developing new manufacturing processes and manufacturing systems that cannot be implemented manually.

Mechanical engineering technology is a complex engineering and scientific discipline about the manufacture of machines of the required quality, in a given quantity, and at a given time, with the lowest labor intensity and cost of their manufacture. The production process of making machines includes all actions at the stages of production and its technical preparation. Production planning of modern production is a process that consists of a product design (computer-aided design or CAD) and a process design (computer-aided manufacturing or CAM) as well as a production schedule. The CAD and CAM allow significantly reducing production costs and are currently carried out within the integrated CAD/CAM/CAE system, the structure of which corresponds to the product design (CAD) and process design (CAM) stages in the product life cycle.

At the first stage (CAD), the product computer-aided design is performed based on the product geometric 3D model. The result of this stage is a geometric information model (plan) of the product, which can be represented by a set of design documentation, to wit: working drawings of parts, assembly drawings of a product structure, hydraulic, electrical, and other schemes.

At the second stage (CAM), computer-aided process design (planning) for product manufacturing (machining and assembling) is performed. The initial information for automated process (e.g., grinding operation) design is the product information geometric model developed at the previous CAD stage. The process design stage (CAM stage) is the automated preparation of control programs based on the computer-aided programming system’s post-processor. Thus, the created CNC control program results from sequential actions along the CAD/CAM/CNC chain and indicates the end of the pre-production stage. This is the so-called open-loop control scheme, i.e., without feedback and provided by CAD/CAM/CNC means and experienced technologists.

Obviously, with the technological systems’ actual operation developed at the CAM stage (implementation stage), the process’s basic parameters (state parameters and output parameters) will not equal the corresponding designed values. In this regard, an urgent task is to develop a methodology for correcting decisions made at the pre-production stage. One of the possible ways to solve this problem is developing self-training technological (grinding) systems, which becomes possible when using such areas of automation as adaptive and intelligent control systems.

2 Literature Review

The appearance of onboard measuring systems on CNC machines [1] makes it possible to use measuring information to correct technological operations’ progress on the

machines tools. When analyzing the state of the issue, several intelligent numerical control directions for metal cutting were established, including adaptive and intelligent automation systems.

There are researches connected with CAD/CAM/CAE integrated system advantages [2], new operation features (e.g., tool deflection) [3], and application examples [4]. There is a study in which analysis features can be automatically converted to a script code for finite element analysis through feature mapping [5]. Therefore, an attempt was made to consider these three systems (CAD, CAM, and CAE) as components of a single integrated system for the production preparation stage. However, the information flow direction in the CAD/CAM/CAE integrated system is not accompanied by its return via feedback to have a possibility of correcting previously made decisions. In other words, it is not possible to make adjustments to the previous stages of the multistage path CAD/CAM/CAE based on the actual data obtained during onboard measurements on a CNC machine.

There are examples [6, 7] when the CAE system, as part of the CAD/CAM/CAE, is used to correct the machine tool control program based on the CAE system's cutting process simulation. However, there is no channel to consider the actual cutting conditions measurement data to correct the CAE model.

A new approach for the design of intelligent systems is proposed, including the statement that the control intelligence is hierarchically distributed according to the principle of increasing precision with decreasing intelligence (IPDI), evident in all hierarchical management systems [8]. This principle allows considering production management as a single process covering the stages of production preparation (the upper level of the hierarchy) and production itself (the lower level of the hierarchy). However, in [8], nothing is said about the flow of information from the lower level to the upper one for correcting decisions made at the upper level.

Finishing operations, such as grinding ones, are the most difficult to automate than metal cutting operations, especially in freeform surface grinding of the dental crown [9] and profile grinding [10]. First of all, this is caused by the high temperature, e.g., in the grinding wheel's contact zone and the workpiece to be ground, e.g., in surface [11, 12] and gear [13, 14] grinding. Temperature models, both analytical [15] and computer [16, 17] ones, are based on the differential heat conduction equation [18]. On- and offline measurements in these works are done, but only for experimental verification of models, i.e., not for the correction of these models.

There are studies on the material removal rate in a special virtual media [19], on the grinding wheel dressing condition control based on AE signal with a fuzzy model [20], and on the quantitative grinding wheel loading evaluation from the AE signals [21]. A knowledge-based analytical tool is established through the correlation between grinding power and grinding conditions [22], and a model to evaluate specific energy consumption in grinding is proposed [23]. However, the established information links or embedded models do not have a constantly working feedback between the calculated (according to the information link or model) and measured parameters in all these cases.

Thus, the analysis of literary sources showed that the lack of effective online sensors of information about the performing grinding system state is compensated by modeling and simulating the grinding system state. Besides, the grinding system state simulation

is carried out in the CAE system at the pre-production stage. However, it is known that any modeling (including using finite element analysis) is relative, and its quantitative results must be corrected, for example, by applying feedback from online information sensors embedded on the operating equipment. There is no information in the literature on implementing such an approach to self-training of a grinding system when a working model is adjusted (self-trained or self-learned) based on a comparison of the simulation results (parameters found by the model) with the measurement results of the same quantities.

The study aims to find a generalized solution to this problem for any technological systems, i.e., not only grinding ones. A specific example of the development of computer subsystems for designing an operation, monitoring, and technological diagnosis is given on the example of the profile gear grinding.

3 Research Methodology

The emergence of the flexible manufacturing system (FMS) is the current state-of-the-art automation level in the sphere of manufacturing technology. An FMS deals with high-level information processing (information flow) and material flow and consists of CNC machines, cells, industrial robots, inspection machines, computer-aided handling, and storage systems. Conventional manufacturing consists of several stages, which are consistent with the product life cycle, namely, (1) the product design, (2) process planning, (3) implementation, and (4) production management. With the development and improvement of control computers, all these stages were gradually integrated into a single integrated manufacturing system based on the so-called CAD/CAM kernel (Fig. 1).

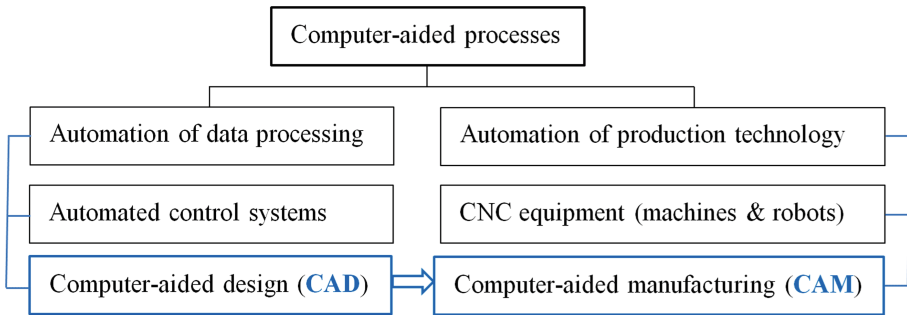


Fig. 1. Computer-aided manufacturing processes containing CAD/CAM kernel.

For a long time, CAD/CAM kernel idea remained a general trend in developing automated production in mechanical engineering. Simultaneously, two more manufacturing automation trends developed simultaneously: computer-aided engineering (CAE) and model reference adaptive control.

Finally, the moment came when these two trends merged due to the lack of reliable sensors of primary technological information, on the one hand, and due to the complexity of the physical processes occurring during machining and assembly, on the other hand (Fig. 2).

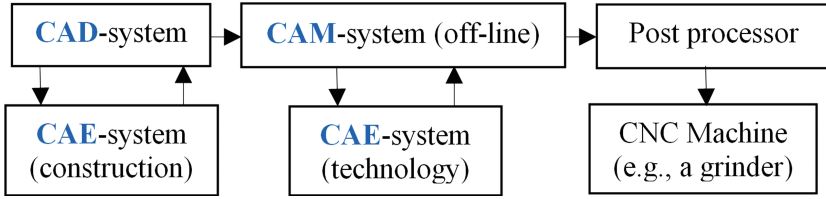


Fig. 2. Integrated CAD/CAM/CAE system shows CAE-system position in CAD- and CAM-systems (offline).

New CAD/CAM/CAE kernel mainly corresponds to the product life cycle stages [7]. Besides, the CAE system may contain the product testing and the process assessing means. However, as it was shown in the literature review, new technologies of automated production should be flexible and take into account the individual characteristics of the parts to be machined, especially complex-shaped parts made from difficult-to-machine materials. Figure 2 shows that the CAM system output is a control program for a CNC machine, which is generated by a post-processor and fed to this machine, for example, the gear grinding CNC machine Höfler Rapid 1250. Obviously, the technological parameters assumed (predicted) at the pre-preparation stage (grinding system state and output parameters) will not coincide with the operating grinding system’s actual online parameters. As follows from Fig. 2, it is impossible to bring these parameters to equality by making adjustments to the CAE system in automatic mode without human intervention. However, it is possible to introduce an unusual (i.e., novel, previously absent) negative feedback, as well as new blocks and connections between them, as shown in Fig. 3. In this case, the actual online values of the grinding system state and output parameters can be compared automatically with their calculated values that are available in the CAE system and obtained either by analytical calculations or by online modeling in the appropriate FEM or FDM system (e.g., in the FEM-system COMSOL Multiphysics).

Technological parameters Q'_w and V'_w in Fig. 3 characterize the intensity of the stock removal (Q'_w) during grinding, for example, gear grinding, and the current resource consumption (V'_w) of the grinding wheel. The value of these parameters is formed considering the actual parameters of grinding (hereinafter gear grinding).

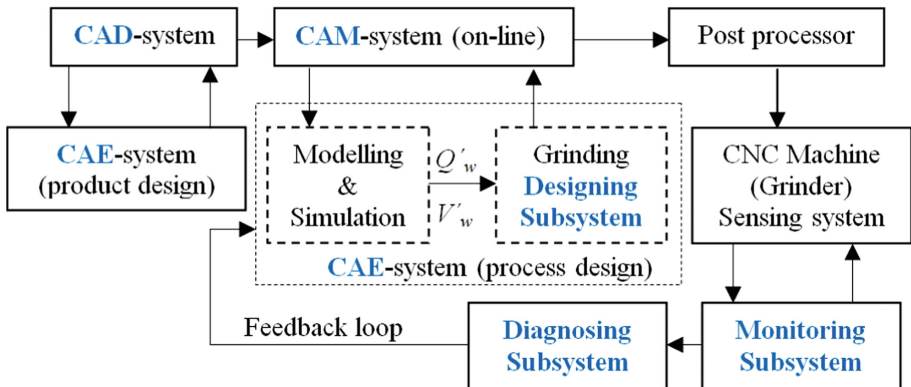


Fig. 3. Integrated CAD/CAM/CAE system shows novel feedback introduced to implement the grinding system’s online self-training.

Self-learning of the gear grinding system presented in Fig. 3 is carried out in a closed (through negative feedback) loop. Three additional subsystems are directly involved in this: designing, monitoring, and diagnosing ones (Fig. 3).

4 Results

The choice of the grinding parameters for roughing, semi-finishing, and finishing operation stages is performed according to the following method. The value of specific grinding work of $e_s = 50 \text{ J/mm}^3$ is previously set (further, this value can be corrected in the online mode of self-training of the gear grinding system). For this, the following steps are performed.

Table 1. The Q'_w – parameter assigned for gear grinding operation stages.

Parameter	Rough stage	Semifinish stage	Finish stage
$Q'_w, \text{ mm}^3/(\text{mm}\cdot\text{s})$	8.6–5.0	5.0–1.0	1.00–0.25

1. Set the specific material removal rate Q'_w depending on the stage of grinding following Table 1. For example, set for the grinding first stage $Q'_w = 8.6 \text{ mm}^3/(\text{mm}\cdot\text{s})$.
2. Choose the maximum possible axial feed V_f . For example, for the first grinding stage, it is $V_f = 116.667 \text{ mm/s}$, i.e., 7000 mm/min.
3. According to the nomogram (not given here), determine the relative temperature, which corresponds to the specific grinding unit. For example, in this case, the relative temperature is $T_H/e_s = 10.478 \text{ [}^\circ\text{C} \cdot \text{mm}^3\text{)]/J}$. The absolute grinding temperature is obtained as the product of the relative temperature of 10.478 $[(^\circ\text{C} \cdot \text{mm}^3)/\text{J}]$ by a specific work of $e_s = 50 \text{ J/mm}^3$. In this case, the grinding temperature is $T_H = 10.478 \cdot 50 = 523.9 \text{ }^\circ\text{C}$. Thus, we have $T_H = T_H(V_f, Q'_w) = 523.9 \text{ }^\circ\text{C}$.
4. Compare the obtained temperature T_H with the critical level of the grinding burn temperature, e.g., with $T_{CR} = 550 \text{ }^\circ\text{C}$. Because $523.911 \text{ }^\circ\text{C} < 550 \text{ }^\circ\text{C}$, the found value of the axial feed is fixed. If it would be $T_H > T_{CR}$, the parameter value Q'_w is reduced.
5. For a given value of the indicator $Q'_w = 8.6 \text{ mm}^3/(\text{mm}\cdot\text{s})$ and the fixed value of the axial feed 116.667 mm/s (7000 mm/min), the link is determined by the formula $Q'_w = t_v V_f$. That is $t_v = Q'_w/V_f$. In this case, we have $t_v = 8.6/116.667 = 0.07371 \text{ mm}$. Because the grinding stock allowance is calculated in the normal direction to the workpiece surface, it is necessary to determine the normal grinding depth when determining the number of strokes. You can use the following simplified relationship between these cutting depths: $t_n = t_v \sin \alpha$, where α is the pressure angle of the basic rack. In this case, at $\alpha = 20^\circ$, the normal grinding depth is $t_n = 0.02521 \text{ mm}$. Thus, the gear grinding parameters for the rough grinding stage are as follows: $t_n = 0.02521 \text{ mm}$, $t_v = 0.07371 \text{ mm}$, and $V_f = 7000 \text{ mm/min}$. For example,

the grinding stock allowance of 0.77 mm is removed sequentially in three stages of grinding: in the first stage, $z_1 = 0.5$ mm; in the second stage $z_2 = 0.25$ mm; in the third stage, $z_3 = 0.02$ mm (the allowance is measured in the normal direction to the workpiece surface).

6. Determine the number of strokes for the first stage of grinding, i.e., $i_1 = z_1/t_{n1}$. In this case, we have $i_1 = 0.5/0.02521 = 19.832$. Round the number of strokes found to the nearest whole number. In this case, we have $i_1 = 19$. Recalculate the normal grinding depth of $t_{n1} = 0.026$ mm (instead of $t_n = 0.02521$ mm). Recalculate the grinding temperature taking into account the adjusted value of the vertical depth of 0.077 mm. The grinding temperature will be $T_H = 541,025$ °C (instead of $T_H = T_H(V_f, Q'_w) = 523.9$ °C).
7. Determine the specific material removal V'_w (the volume of material to be removed per unit of the grinding wheel active width B) according to the formula $V'_w = Bt_v$. For example, for the first gear grinding stage, it will be $V'_w = 24 \cdot 0.077 = 1.848$ mm³/mm.
8. Generate the initial data for the CNC machine with the indication of the calculated grinding temperature.

Similarly, choose the grinding parameters for the second (Table 2) and third stages to remove the grinding stock allowance ($z_2 = 0.25$ mm, $z_3 = 0.02$ mm).

Table 2. Gear grinding parameters were calculated for the second (semifinish) operation stage.

Number of stroke	t_n , mm	t_v , mm	V_f , mm/min	Q'_w , mm ³ /(mm·s)	V'_w , mm ³ /mm	T_H , °C
1	0.015	0.043	7000	5.016	1.032	349.68
2	0.015	0.043	7000	5.016	1.032	349.68
3	0.015	0.043	7000	5.016	1.032	349.68
...
17	0.015	0.043	7000	5.016	1.032	349.68

Within the final grinding stage, the axial feed V_f can be reduced to obtain the required roughness, reducing the roughness if the roughness requirements are high. For high accuracy classes of gears, the values of axial feed V_f are chosen based on the required cooling of the workpiece as its final size is formed to eliminate the effect of thermal deformation on machining accuracy, including changing the grinding cycle structure. Namely, omission of the working stroke means the only up or the only down grinding, sector grinding, etc.

The specific material removal rate Q'_w (Fig. 4) and the specific material removal V'_w (Fig. 5) are also used as grinding system state parameters in the computer-aided gear grinding designing, monitoring, and diagnosing.

The found distribution of parameters Q'_w and V'_w over the gear grinding passes is the initial technological information for a CNC machine’s control program, in this case for the gear grinding CNC machine Höfler Rapid 1250. Besides, the data in Fig. 5 is used to determine the grinding wheel dressing moments. When changing the grinding

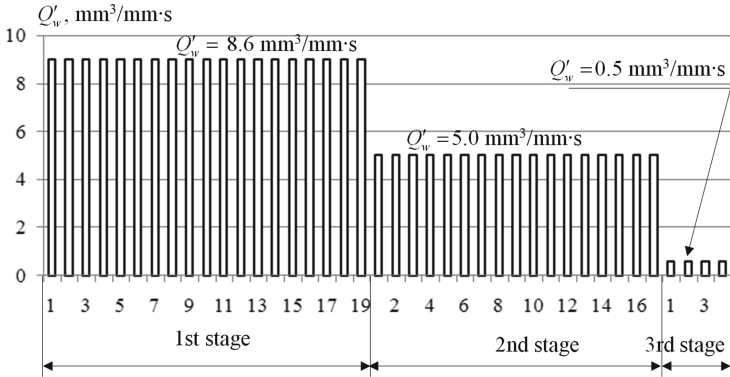


Fig. 4. Program changing the Q'_w parameter vs. gear grinding stages and strokes.

conditions (e.g., grinding allowance value, specific grinding energy), the found grinding parameters are recalculated and, as a consequence, the control program changes. Also, there is a possibility to control the actual engagement between a grinding wheel and a gear being ground to increase the axial feed V_f when the so-called “air grinding”. The latter occurs at the rough stage of gear grinding with an uneven distribution of the grinding allowance along the gear wheel’s periphery.

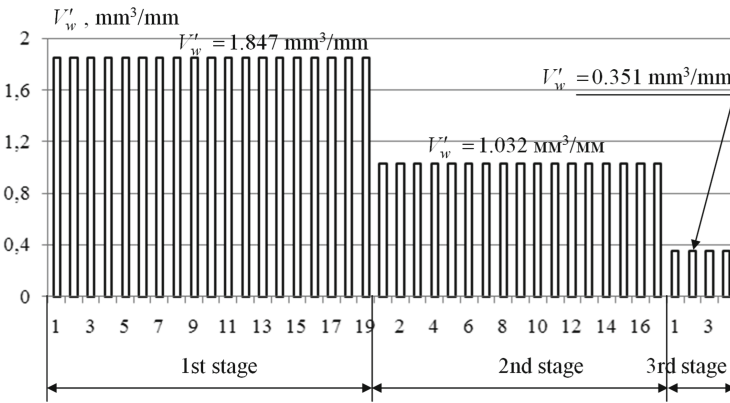


Fig. 5. Program changing the V'_w parameter vs. gear grinding stages and strokes.

5 Conclusions

The introduction of negative feedback from the built-in online sensors of technological (process) information (when such sensors are available) allows, based on monitoring the grinding system state and output parameters, to correct the setting of the CAE system, which is used not only offline but also in the online mode.

Given as an example, the step-by-step sequence of actions to determine the parameters of grinding the complex-shaped machine parts on the example of gears makes it possible to understand the algorithm of operation of an intelligent self-training grinding system.

The new provisions for the automation of technical systems (both processes and constructs) developed in the paper are universal in nature, regardless of the specifics of production processes.

Acknowledgement. This work was carried out under the state (Ukraine) budget theme of the Odessa National Polytechnic University (2018–2021, registration number: 0118U004400).

References

1. Horst, J., Hedberg, T., Feeney A.B.: On-machine measurement use cases and information for machining operations. National Institute of Standards and Technology, USA (2019)
2. Kyratsis, P., Kakoulis, K., Markopoulos, A.P.: Advances in CAD/CAM/CAE. *Technol./Mach.* **8**(1), 13 (2020)
3. Wang, L., Chen, Z.C.: A new CAD/CAM/CAE integration approach to predicting tool deflection of end mills. *Int. J. Adv. Manuf. Technol.* **72**(9–12), 1677–1686 (2014)
4. Wagner, E.: A new optimization CAD/CAM/CAE techniques for the processing of the complex 3D surfaces on 5 axes CNC machines. *Procedia Technol.* **19**, 34–39 (2015)
5. Wang, J., et al.: A CAD/CAE-integrated structural design framework for machine tools. *Int. J. Adv. Manuf. Technol.* **91**(1–4), 545–568 (2016)
6. Larshin, V., Lishchenko, N.: Complex-shaped parts grinding technology information ensuring. *Appl. Aspects Inf. Technol.* **3**(4), 246–262 (2020). <https://doi.org/10.15276/aait.04.2020.3>
7. Petrakov, Y., Shuplietsov, D.: Programming of adaptive machining for end milling. *Mech. Adv. Technol.* **1**(79), 34–40 (2017)
8. Lima, P.U., Saridis, G.N.: Design of intelligent control systems based on hierarchical stochastic automata. World Scientific Publishing Co. Pte. Ltd., Singapore (1996)
9. Nam, S., Kim, B.: Design of material removal rate to reduce machining time of dental crown. *J. Mech. Sci. Technol.* **33**, 3423–3434 (2019)
10. Klocke, F.: Manufacturing Process 2. Grinding, honning, lapping. Translated by Kuchle, A. Springer, Heidelberg (2009)
11. González-Santander, J.L.: Maximum temperature in dry surface grinding for high pecklet number and arbitrary heat flux profile. *Math. Prob. Eng.* 1–9 (2016)
12. Prashant, P., Chandrakant, P.: FEM simulation and analysis of temperature field of environmental friendly MQL grinding. In: Proceedings of the International Conference on Communication and Signal Processing, vol. 137, pp. 182–186 (2017)
13. Jin, T., Yi, J., Li, P.: Temperature distributions in form grinding of involute gears. *Int. J. Adv. Manuf. Technol.* **88**(9–12), 2609–2620 (2016)
14. Lishchenko, N.V., Larshin, V.P.: Gear-grinding temperature modeling and simulation. In: Radionov, A.A., Kravchenko, O.A., Guzeev, V.I., Rozhdestvenskiy, Y.V. (eds.) ICIE 2019. LNME, pp. 289–297. Springer, Cham (2020). https://doi.org/10.1007/978-3-030-22063-1_32
15. Jin, T., Yi, J., Peng, S.: Determination of burn thresholds of precision gears in form grinding based on complex thermal modelling and Barkhausen noise measurements. *Int. J. Adv. Manuf. Technol.* **88**(1–4), 789–800 (2016)

16. Yi, J., Zhou, W., Deng, Z.: Experimental study and numerical simulation of the intermittent feed high-speed grinding of TC4 titanium alloy. *Metals* **9**(7), 802 (2019)
17. Lan, S., Jiao, F.: Modeling of heat source in grinding zone and numerical simulation for grinding temperature field. *Int. J. Adv. Manuf. Technol.* **103**(5–8), 3077–3086 (2019). <https://doi.org/10.1007/s00170-019-03662-w>
18. Malkin, S., Guo, C.: Thermal analysis of grinding. *CIRP Ann. Manuf. Technol.* **56**(2), 760–782 (2007)
19. Kountanya, R., Guo, C.: Specific material removal rate calculation in five-axis grinding. *J. Manuf. Sci. Eng.-Trans. Asme* **139**, 121010-1–121010-6 (2017)
20. Alexandre, F.A., Lopes, W.N., Dotto, F.R.L., et al.: Tool condition monitoring of aluminum oxide grinding wheel using AE and fuzzy model. *Int. J. Adv. Manuf. Technol.* **96**, 67–79 (2018)
21. Liu, C.-S., Ou, Y.-J.: Grinding wheel loading evaluation by using acoustic emission signals and digital image processing. *Sensors* **20**(15), 4092 (2020)
22. Tian, Y.B., Liu, F., Y. Wang, Y., Wu, H.: Development of portable power monitoring system and grinding analytical tool. *J. Manuf. Process.* **27**, 188–197 (2017)
23. Alberro, N.A., Rojas, H.A.G., Egea, A.J.S., Hameed, S., Aguilar, R.M.P.: Model based on an effective material-removal rate to evaluate specific energy consumption in grinding. *Materials* **12**(6), 939 (2019)



Choice of Carrier Behavior Strategy According to Industry 4.0

Dmitriy Muzylyov¹ , Natalya Shramenko^{1,2} , and Mykola Karnaukh¹ 

¹ Kharkiv Petro Vasylenko National Technical University of Agriculture, 44, Alchevskyyh Street, Kharkiv 61002, Ukraine
murza_1@ukr.net

² Sumy National Agrarian University, 160, Herasyima Kondratieva Street, Sumy 40000, Ukraine

Abstract. The research aims to choose a strategy for transport companies' behavior in the context of the development of Industry 4.0. It is proposed to use a mini-maximum model as an optimization function. This model proposes to make a management decision based on the accounting of primary capital investments for trucks purchase and costs associated with rolling stock operations. The article presents an initial algorithm for accelerating decision-making by creating your software product for specific transportation conditions. This approach allows managers to search faster for the optimal transport option of any production, which is necessary for the concept of industry 4.0. The article provides an example of calculating the creation of a rolling stock fleet for goods transportation into the retail chain of supermarkets in Kharkiv. This approach is universal and can be used to choose the best option for delivering goods between enterprises when transporting raw materials, agricultural goods, mail, etc. The approach is universal for making a correct management decision for different types of routes and allows managers to form the necessary fleet of vehicles with minimal investment and the highest productivity.

Keywords: Route · Costs · Model · Transportation · Risk

1 Introduction

Building and organizing a reliable transportation system is important for the success of any production process in the era of Industry 4.0. In particular, the transportation management system (TMS) should be based on the concept of smart transport and intelligent transport systems (ITS) [1]. Of particular note is the key role in the transport process and logistics of the Internet of Things (IoT) [2].

When transport process organizing that corresponds to Industry 4.0 concept, it is necessary to consider main costs that are associated with capital investments in the purchase of rolling stock, as well as the cost of transporting goods, taking into account changing conditions of supply processes: exchange of information between delivery subjects, creation a flexible route taking into account changes in delivery conditions (weather, restrictions, risk) [3]. Simultaneously, the important point is to consider possible risks

for carriers, which are expressed in increased costs with an incorrectly chosen behavior strategy. Now transport services, which logistics operators introduce, should be organized with minimal losses and, if possible, use robotics [4] or autonomous vehicles [5]. Logistics processes for smart transport should be organized based on behavioral strategies using data obtained by a specialized software product and the physical Internet [6].

Therefore, information support when choosing a strategy for the carrier's behavior in servicing the customer should allow for the prompt adoption of a correct decision considering the risk factors of increased costs. The research aims to present an initial mathematical tool for estimates risk factors during transport process planning.

2 Literature Review

The Industry 4.0 concept [7] provides flexibility in choosing a transport company's market behavior strategy. This is evidenced by the latest opinions of experts [8] in the field of modern transport logistics, who are convinced that the concepts of IoT [9] and blockchain technologies [10] give opportunities to make more flexible management decisions.

Smart approaches for building efficient supply chains are based on the carrier's design of a risk structure [11], which allows the best strategy to be chosen because of minimal losses. Thus, the implementation of transport company capabilities using investment and risk accounting in the supply chain is shown in the example of the Australian courier firms. The described concept is based on using the partial least squares' method used to build a mathematical model [12].

The choice of enterprise behavior strategy can be based on simulation results using modern software products. The study [13] shows the flexibility of the manufacturing process using simulation in the FlexSim environment. This concept allows managers to increase productivity and reduce losses from possible risks significantly.

The strategy of transport companies' behavior-based recently on neuro-network modeling [14–17] or for organizing routes based on results obtained by Petri networks (PN) has been widely applied [18]. However, the last research (PN) practically does not consider various risks [19, 20]. Problems associated generally with the use of mathematical modeling in logistics processes are described in studies [21, 22].

The author shows how using the Monte-Carlo method to optimize a fleet of rolling stock [23]. A carrier must first proceed from its production capacity when choosing a behavior strategy. Create a structure of the vehicle fleet that corresponds to transport conditions and fully satisfies the demand for transport service [24–26].

Integrated criteria are often used to select a carrier or industrial production strategy, which involves minimizing the financial performance associated with fleet operation [27–29] or optimizing production processes [30]. Cost savings are possible by effectively planning the entire supply chain [31]. In particular, to reduce idle time of trucks in anticipation of reverse loading [32].

Researchers are increasingly focusing on risk management in the Industry 4.0 era [33]. The logistics principles presented by the authors in solving problems in heavy

production (metallurgy) [34, 35] can be transferred to some extent to solve issues in transport [36].

It is especially difficult to choose a correct behavior strategy in conditions of considerable uncertainty. The number of random factors influencing the transport process is usually more when delivering bulk cargo (cereals, products of heavy metallurgy, coal, or ore materials) [37–39]. Operations of transport companies characterize a slightly lower uncertainty level during goods delivery with small batches [40, 41].

Application and initial implementation of innovative technologies into transportation systems (Petri networks, neuro-network models, IoT, as well as blockchain technologies) are based on a good mathematical apparatus that allows researchers to establish the necessary patterns [42–44], as can be seen from the literature review in most cases. This allows the carrier to take a more flexible approach to its customer service strategy [45, 46]. At the same time, the risk of unjustified losses is reduced.

3 Research Methodology

The choice of the most effective strategy of the carrier's behavior is made considering the invested capital for the purchase of trucks, which are necessary to satisfy customers' orders in freight transportation in conditions of complete uncertainty. This takes into account possible risk situations arising in the transport services market.

This approach is based on applying the indicator of guaranteed costs that the carrier can incur from the implementation of a particular investment project, that is, the chosen behavior strategy. Therefore, management decisions take into account the minimum cost indicator:

$$C_{strategy} = \min_i \max_j C_{ij}, \quad (1)$$

where C_{ij} - value of specific annual costs for transport service by i -type of the truck on the j^{th} route, UAH.

Each strategy corresponds to a specific value of the transportation prime cost of planned volumes based on transportation prime cost per one ton of cargo. The set of values of transport service prime cost during transportation annual volume of cargo is determined by:

$$Pr C = \{Pr C_{ij}\}, i = \overline{1, m} \dots j = \overline{1, n}, \quad (2)$$

where $Pr C_{ij}$ - the prime cost of transport service when transporting the annual volume of cargo by the i^{th} type of truck on the j^{th} route, UAH. where $Pr C_{ij}$ - the prime cost of transport service when transporting the annual volume of cargo by the i^{th} type of truck on the j^{th} route, UAH.

Values cannot be determined at the first stage of choosing a strategy because they are considered unmanaged factors. Therefore, when calculating, the carrier will use the prime cost of transporting one ton of cargo based on the standard operation of trucks on routes:

$$Pr C_{ij} = Pr C_{ij}^t \cdot V_{an}, \quad (3)$$

where $Pr C_{ij}^t$ - the prime cost of transport service when transporting one ton of cargo by the i^{th} type of truck on the j^{th} route, UAH/ton; V_{an} - annual value of the transporting, ton.

The prime cost of transportation per one tone is calculated according to classical dependencies considering possible technical and operational indicators of rolling stock operation on planned service routes.

Calculation results can be presented as a table of the following template (Table 1).

Table 1. Transportation service prime costing matrix.

Truck type	Route		
	1-th	...	n-th
1-th	PrC_{11}	...	PrC_{1n}
...
m-th	PrC_{m1}	...	PrC_{mn}

Each pair of K_i and C_{ij} corresponds to a certain value of the specific annual costs, which are calculated according to the formula:

$$C_{ij} = NORM \cdot K_i + Pr C_{ij}, \tag{4}$$

where $NORM$ - standard capital investment efficiency ratio, $NORM = 0.1$; K_i - capital investment for buying an i^{th} type of truck, UAH.

Matrix of specific costs (formula 5) can be composed based on having sets $\{K_i\}$ and $\{Pr C_{ij}\}$ (Table 2)

$$C_{strategy} = ||C(K_i, Pr C_{ij})|| = ||C_{ij}||. \tag{5}$$

Table 2. Matrix of specific costs (criteria for the choice of carrier behavior strategy).

Capital investment for buying a truck	Prime cost of transport service on the route			$\max_i C_{ij}$
	PrC_{11}	...	PrC_{1n}	
K_1	C_{11}	...	C_{1n}	$\max(K_1, C_{1n})$
...
K_m	C_{m1}	...	C_{mn}	$\max(K_m, C_{mn})$

The final choice of carrier behavior strategy during transport service must be made by criterion (1) and according to Table 2 (last column).

Carrier can create a software product using the following algorithm to faster choosing a rational strategy (Fig. 1).

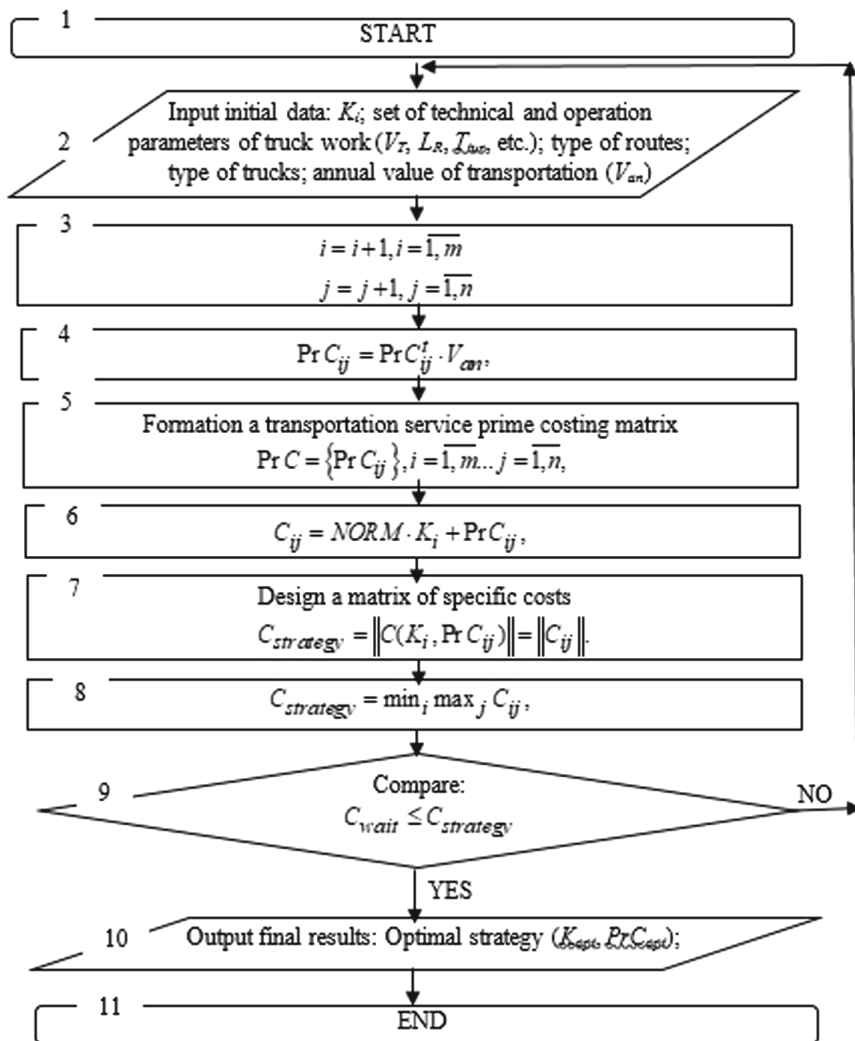


Fig. 1. Algorithm of software to choose a rational carrier behavior strategy.

This algorithm allows managers to compare the expected costs of carrying out the transportation process with the results obtained according to the minimax model (1). If carriers do not receive the required value, they can quickly set new conditions for selecting a strategy. Simultaneously, both values of capital investments and information on rolling stock operation on each route can change. Information about the external environment parameters is altered, which corresponds to the concept of Industry 4.0 and allows organizing the provision of transport services (production) more flexibly.

4 Results

This approach was tested when choosing a strategy for transport services for supermarkets. According to Google Maps, Kharkiv has one of the most extensive retail chains in Ukraine [47] (Fig. 2).

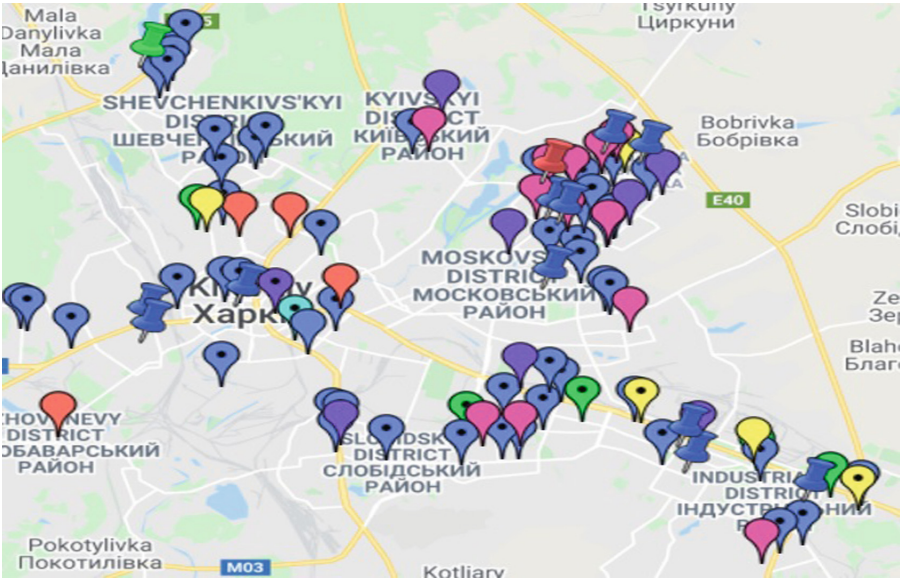


Fig. 2. Grocery Supermarkets in Kharkiv.

‘Silpo’ grocery network was chosen for evaluating the best strategy. Results of simulation are given in matrix for selection of rational strategy (Table 3).

Table 3. Matrix of specific costs to choose transportation strategy for ‘Silpo’ grocery network.

Capital investment for buying a truck, UAH	Prime cost of transport service on the route, UAH					$\max_i C_{ij}$
	7000000	7500000	6900000	7400000		
6000000	7600000	8100000	7500000	8000000		8100000
4500000	7250000	7150000	7750000	7650000		7750000
4200000	7920000	7420000	7320000	7820000		7920000
3500000	7350000	7750000	7250000	7850000		7850000

Four modes of carrier conduct were considered as a condition:

1. Acquisition of domestic on-board vehicles (type I);
2. Purchase of foreign-made on-board vehicles (type II);
3. Purchase of vans of the domestic manufacturer (type III);
4. Purchase of foreign vans (type IV).

The maximum value is selected for each row (Table 3). The last column specifies the best behavior strategy based on the minimum value.

In this case, it is preferable to organize transport services for groceries 'Silpo' trading network using second-type trucks with the third type's routes.

The main parameter based on which carrier chose an own behavior strategy is a prime cost. The factors influencing prime cost belong to the group of technical and operation parameters of vehicles that work on a route. These factors can take values randomly. This is due to the conditions for the operation of rolling stock. Such external factors as environment and weather are considered in the model not directly. The proposed mathematical approach considers these factors due to road conditions that influence the values of vehicle speed.

The proposed model gives a flexible tool to make rational decisions in different and very quickly changing market conditions because of considering such factors as type and brand of trucks, type of fuel using for transportation, a risk to receive the minimal value of profit, and some others. But the model didn't use a self-learning algorithm. This task for the next researches.

5 Conclusions

The presented approach allows managers to quickly choosing carriers' behavior strategy during the transport service of any production processes. Simultaneously, the ability to quickly take into account changing environmental factors guarantees flexibility in decision-making. This fully complies with the concept of Industry 4.0 when organizing production or providing transport services.

This approach is universal and can be used to choose the best option for delivering goods between enterprises when transporting raw materials, agricultural goods, mail, etc. The approach is universal for making a correct management decision for different types of routes and allows managers to form the necessary fleet of vehicles with minimal investment and the highest productivity.

Further research is considering additional factors in the study algorithm that reduce the level of uncertainty in the transport process.

References

1. Barreto, L., Amarala, A., Pereira, T.: Industry 4.0 implications in logistics: an overview. In: Manufacturing Engineering Society International Conference 2017, MESIC 2017, 28–30 June 2017, Procedia Manufacturing, vol. 13, pp. 1245–1252. Vigo (Pontevedra), Spain (2017)
2. Atzori, L., Iera, A., Morabito, G.: The internet of things: a survey. *Comput. Netw.* **54**(15), 2787–2805 (2010). <https://doi.org/10.1016/j.comnet.2010.05.010>

3. Hoey, B.: Transport Logistics in the Era of Industry 4.0. <https://blog.flexis.com/transport-logistics-in-the-era-of-industry-4.0>. Accessed 28 Oct 2020
4. Karabegović, I., Turmanidze, R., Dašić, P.: Robotics and automation as a foundation of the fourth industrial revolution - industry 4.0. In: Tonkonogyi, V., et al. (eds.) *InterPartner 2019*. LNME, pp. 128–136. Springer, Cham (2020). https://doi.org/10.1007/978-3-030-40724-7_13
5. Paprocki, W.: How transport and logistics operators can implement the solutions of “industry 4.0”. In: Suchanek, M. (eds.) *Sustainable Transport Development, Innovation and Technology*. TranSopot 2016. Springer Proceedings in Business and Economics, pp. 185–196. Springer, Cham (2017)
6. Maslarić, M., Nikoličić, S., Mirčetić, D.: Logistics response to the industry 4.0: the physical internet. *Open Eng.* **6**, 511–517 (2016)
7. Rauch, E.: Industry 4.0+: the next level of intelligent and self-optimizing factories. In: Ivanov, V., Trojanowska, J., Pavlenko, I., Zajac, J., Peraković, D. (eds.) *Advances in Design, Simulation and Manufacturing III*. DSMIE-2020. Lecture Notes in Mechanical Engineering, pp. 176–186. Springer, Cham (2020)
8. *Revolutions in Transport and Logistics: New Technologies for Industry 4.0*. Automotive World. <https://www.automotiveworld.com/news-releases/revolutions-in-transport-and-logistics-new-technologies-for-industry-4-0-2/>. Accessed 30 Oct 2020
9. Saniuk, S., Saniuk, A., Čagaňová, D.: Cyber industry networks as an environment of the industry 4.0 implementation. *Wirel. Netw.* (2019)
10. Muzylyov, D., Shramenko, N.: Blockchain technology in transportation as a part of the efficiency in industry 4.0 strategy. In: Tonkonogyi, V., et al. (eds.) *Advanced Manufacturing Processes*. InterPartner-2019. Lecture Notes in Mechanical Engineering, pp. 216–225. Springer, Cham (2020)
11. Birkel, H.S., Veile, J.W., Müller, J.M., Hartmann, E., Voigt, K.-I.: Development of a risk framework for industry 4.0 in the context of sustainability for established manufacturers. *Sustainability* **11**(2), 384 (2019)
12. Wang, M., Asian, S., Wood, L.C., Wang, B.: Logistics innovation capability and its impacts on the supply chain risks in the industry 4.0 era. *Mod. Supply Chain Res. Appl.* **2**(2), 83–98 (2020)
13. Luscinski, S., Ivanov, V.: A simulation study of industry 4.0 factories based on the ontology on flexibility with using FlexSim software. *Manag. Prod. Eng. Rev.* **11**(3), 74–83 (2020)
14. Medvediev, Ie., Muzylyov, D., Shramenko, N., Nosko, P., Eliseyev, P., Ivanov, V.: Design logical linguistic models to calculate necessity in trucks during agricultural cargoes logistics using fuzzy logic. *Acta Logistica – Int. Sci. J. Logistics* **7**(30), 155–166 (2020)
15. Andrade, K., Uchida, K., Kagaya, S.: Development of transport mode choice model by using adaptive neuro-fuzzy inference system. *Transp. Res. Res. Board* **1977**(1) (2006). <https://doi.org/10.1177/0361198106197700102>
16. Al Ghamdi, A.S., Eren, H., Mansour, A.: Application of fuzzy logic control in automated transport systems. In: *2010 IEEE Sensors Applications Symposium (SAS)* (2010)
17. Das, R.D., Winter, S.: A neuro-fuzzy based hybrid intelligent framework for transport mode detection. In: *MELT 2016 in conjunction to ACM SIGSPATIALat*, Burlingame, CA, USA (2016)
18. Pavlenko, O., Shramenko, N., Muzylyov, D.: logistics optimization of agricultural products supply to the european union based on modeling by petri nets. In: Karabegović, I. (ed.) *NT 2020*. LNNS, vol. 128, pp. 596–604. Springer, Cham (2020). https://doi.org/10.1007/978-3-030-46817-0_69
19. Morrison, M.: Risk management in automation of the accounting process. In: Linsley, P., Shrivs, P., Wiczorek-Kosmala, M. (eds.) *Multiple Perspectives in Risk and Risk Management*. SPBE, pp. 231–239. Springer, Cham (2019). https://doi.org/10.1007/978-3-030-16045-6_11

20. Gordon, R.: Cost effective design processes. In: *Intelligent Transportation Systems*, pp. 7–18. Springer, Cham (2016)
21. Lozhkin, A.: In the issues of mathematical modelling logistics processes. *Acta Logistica Int. Sci. J. Logistics* **6**(1), 15–18 (2019)
22. Buttazzo, G., De Pascale, L.: Optimal shapes and masses, and optimal transportation problems. In: *Optimal Transportation and Applications. Lecture Notes in Mathematics (Fondazione C.I.M.E., Firenze)*, vol. 1813, pp. 11–51. Springer, Heidelberg (2003)
23. Lampa, M., Samolejová, A.: Fleet optimization based on the monte carlo algorithm. *Acta Logistica Int. Sci. J. Logistics* **7**(1), 17–21 (2020)
24. Thakuriah, P., Geers, D.G.: Technology systems for transportation system management and personal use. In: *Transportation and Information. Springer Briefs in Computer Science*, pp. 35–71. Springer, New York (2013)
25. Gordon, R.: Transportation management centers. In: *Intelligent Transportation Systems*, pp. 157–176. Springer, Cham (2016)
26. Gordon, R.: Corridor management. In: *Intelligent Transportation Systems*, pp. 207–219. Springer, Cham (2016)
27. Muzylyov, D., Shramenko, N., Shramenko, V.: Integrated business-criterion to choose a rational supply chain for perishable agricultural goods at automobile transportations. *Int. J. Bus. Perform. Manag.* **21**(1/2), 166–183 (2020)
28. Ambrosio, L., Pratelli, A.: Existence and stability results in the L1 theory of optimal transportation. In: *Optimal Transportation and Applications. Lecture Notes in Mathematics (Fondazione C.I.M.E., Firenze)*, vol. 1813, pp. 123–160. Springer, Heidelberg (2003)
29. Gudmundsson, H., Hall, R.P., Marsden, G., Zietsman, J.: Planning for transportation. In: *Sustainable Transportation. Springer Texts in Business and Economics*, pp. 51–80. Springer, Heidelberg (2016)
30. Kotliar, A., Basova, Y., Ivanov, V., Murzabulatova, O., Vasylytsova, S., Litvynenko, M., Zinchenko, O.: Ensuring the economic efficiency of enterprises by multi-criteria selection of the optimal manufacturing process. *Manag. Prod. Eng. Rev.* **11**(1), 52–61 (2020)
31. Aulin, V., Pavlenko, O., Velikodnyy, D., Kalinichenko, O., Zielinska, A., Hrinkiv, A., Diyachenko, V., Dzyura, V.: Methodological approach to estimating the efficiency of the stock complex facing of transport and logistic centers in Ukraine. In: *1st International Scientific Conference on Current Problems of Transport, ICCPT 2019: Current Problems of Transport, Ternopil, Ukraine*, pp. 120–132 (2019)
32. Muzylyov, D., Shramenko, N.: Mathematical model of reverse loading advisability for trucks considering idle times. In: Karabegović, I. (ed.) *NT 2020. LNNS*, vol. 128, pp. 612–620. Springer, Cham (2020). https://doi.org/10.1007/978-3-030-46817-0_71
33. Ivanov, D., Dolgui, A., Sokolov, B.: The impact of digital technology and industry 4.0 on the ripple effect and supply chain risk analytics. *Int. J. Prod. Res.* **57**(3) (2019)
34. Kiyko, S., Druzhinin, E., Prokhorov, O., Ivanov, V., Haidabrus, B., Grabis, J.: Logistics control of the resources flow in energysaving projects: case study for metallurgical industry. *Acta Logistica Int. Sci. J. Logistics* **7**(1), 49–60 (2020)
35. Turpak, S.M., Taran, I.O., Fomin, O.V., Tretiak, O.O.: Logistic technology to deliver raw material for metallurgical production. *Sci. Bull. National Mining Univ.* **1**(1), 162–169 (2018)
36. van Dongen, L.A.M., Frunt, L., Rajabalinejad, M.: Issues and challenges in transportation. In: Singh, S., Martinetti, A., Majumdar, A., van Dongen, L.A.M. (eds.) *Transportation Systems. AA*, pp. 3–17. Springer, Singapore (2019). https://doi.org/10.1007/978-981-32-9323-6_1
37. Tryhuba, A., Bashynskiy, O., Medvediev, Ye., Slobodian, S., Skorobogatov, D.: Justification of models of changing project environment for harvesting grain, oilseed and legume crops. *Independent J. Manag. Prod. (IJM&P)* **10**(7), 658–672 (2019)

38. Gudmundsson, H., Hall, R.P., Marsden, G., Zietsman, J.: European union transport white paper. In: Sustainable Transportation. Springer Texts in Business and Economics, pp. 209–232. Springer, Heidelberg (2016)
39. Yunianto, I.T., Lazuardi, S.D., Hadi, F.: Freight calculation model: a case study of coal distribution. In: IOP Conference Series: Earth and Environmental Science, vol. 135, p. 012013 (2018). <https://doi.org/10.1088/1755-1315/135/1/012013>
40. Tang, L., Gong, H.: The coordination of transportation and batching scheduling. *Appl. Math. Model.* **33**(10), 3854–3862 (2009)
41. Juremalani, J., Chauhan, K.A.: Assessment of accessibility for mixed land use neighborhoods through travel behavior pattern. In: Pulugurtha, S., Ghosh, I., Biswas, S. (eds.) *Advances in Transportation Engineering. Lecture Notes in Civil Engineering*, vol. 34, pp. 13–20. Springer, Singapore (2019)
42. Lewis, S.: Transporting cargo from A to B. *Nat. Rev. Neurosci.* **14**, 589 (2013)
43. Matveeva, T.V., Belyaev, M.Y.: Control of the progress transport cargo vehicles during the experiments. In: 24th Saint Petersburg International Conference on Integrated Navigation Systems (ICINS), St. Petersburg, pp. 1–4 (2017)
44. Kang, K., Qi, H., Lu, J., Zhao, J.: Dual-channel supply chain disruption model and analysis under cargo transportation insurance. *IEEE Access* **8**, 114953–114967 (2020)
45. Vilko, J., Lättilä, L.: Analyzing supply chain vulnerability through simulation. In: Khojasteh, Y. (ed.) *Supply Chain Risk Management*, pp. 107–122. Springer, Singapore (2018). https://doi.org/10.1007/978-981-10-4106-8_7
46. Rehman Khan, S.A., Yu, Z.: IT in supply chain management. In: *Strategic Supply Chain Management. EAI/Springer Innovations in Communication and Computing*, pp. 249–260. Springer, Cham (2019)
47. Grocery Supermarkets in Kharkiv (Kharkov) – Ukraine. Google maps. <https://www.google.com/maps/d/u/0/embed?mid=1kGDZxZAKqRSYSfifc9zvCv84v-g&msa=0&hl=en&ie=UTF8&ll=49.99913293423344%2C36.27410863476561&spn=0.211886%2C0.439453&z=11&output=embed>. Accessed 30 Oct 2020



Autonomous Data-Driven Integration into ERP Systems

Janis Peksa^(✉) 

Riga Technical University, 1, Kalku Street, Riga 1658, Latvia
Janis.Peksa@rtu.lv

Abstract. The following article makes a case study with an SAP ERP system, which integrates with an external Web Service using API access. Algorithm implementation is demonstrated with all transactions used in SAP ERP. However, it should be noted that a limited version of SAP ERP S/4HANA version release 2.00.044. It was pointing to the capabilities test between the external system and the ERP system. During the experiment, the ABAP programming language and the built-in SAP ERP background job are used and configured as needed. The received data is stored in the SAP ERP data warehouse, modified to save the new data. The main result is to provide integration capabilities. Utility to use the Web Service and the ERP system's integration technique to enable the capability's regular use. The experiment shows that the SAP ERP system can be integrated from an external source and store data to improve future business processes and increase its business values. The approach allows for the development of future frameworks and the expansion of ERP systems between external systems.

Keywords: Enterprise resource planning systems · Algorithm implementation

1 Introduction

The global success of enterprise resource planning systems (ERP) has attracted researchers from the IT discipline and all major business research disciplines, including accounting, logistics, and manufacturing. The advent of ERP systems has increasingly moved computerized business information systems from the IT domain to the business realm, from systems design and programming to business configuration, process mapping, and engineering. The efforts and weight of critical success factors in the ERP systems have shifted from system design to system implementation, and implementation teams are now typically led and dominated by traditional business roles rather than IT staff. ERP systems put their logic on organizations and often make employees think about integrated processes and change accounting, production planning, and control [1, 2].

ERP systems are often confused with other used solutions and software products that help solve various business problems. For example, due to ignorance, ERP systems are considered analogies or alternatives to a CRM system for accounting and tax programs. ERP systems' main difference allows us to manage all of a company's resources, not individual parts [3, 4]. ERP systems have available data that is evenly distributed and

available throughout the system in one place. This data is mostly transaction data containing various information about the customer's order about suppliers. In various analyzes, this data is used and is very important to make predictions in support of business goal achievements. Mostly, performing additional analyzes requires different other data not available in ERP systems. There is a need for an integrated approach that would allow the insertion of external data into ERP systems. As it is already known today, the data is extensive, and a lot of it immediately means that this data is needed in an automated way because, with manual work, it is no longer possible to process it nowadays. Here also appears one of the main processes autonomous, used everywhere, from uploading images to social networks and automatically publishing on other social networks. Using data available from social networks to prepare a suitable advertising offer for a potential customer interested in purchasing a product [5].

In this article, an experiment with autonomous data-driven integration into ERP systems is performed, and the SAP ERP system is chosen for ERP systems, based on preview proposals [6]. Initially, a BPMN business process is created that explains what data and what business processes are going on in the X company from the company's point of view. As a next step, a flowchart explains the algorithm's actions and the parties involved. Then the solution in the UML diagram is discussed in more detail. These steps are followed by explaining the ABAP programming solution and the experiment, at the end of which autonomous data-driven integration into the SAP ERP system is obtained. SAP ERP transactions are also marked, which are used in the development process. Integration is performed between Web Service API access from the outside of SAP ERP systems. The received data is stored in the SAP ERP data warehouse, and the experiment runs in SAP ERP S/4HANA version release 2.00.044.

Research questions are raised:

1. Is it possible to connect the existing algorithm to the ERP system?
2. Does the existing algorithm indicate the existence of autonomy?

The rest of the paper is organized as follows: Sect. 2 discusses the algorithm, Sect. 3 autonomous data synchronization solution, and Sect. 4 provides conclusions.

2 Literature Review

When developing an algorithm, the problem that the created algorithm has to deal with is always considered, and by logically arranging each step, one can understand the essence of the algorithm and how the specific problem is solved. In this case, several issues affecting data-driven integration of ERP systems are evaluated, called data synchronization shortcomings [7]. Some of the common problems with data synchronization are:

- The complexity of data formats – from the very beginning, with the advent of the system. The data is presented in a relatively pure form that changes over time, and the organization grows, leading to problems such as the relationship between the target system and the source system, as well as data conversion problems during transmission between systems [8];

- Work in real-time – now is the real-time era where users want to know the current status of the system, customers want to see the current status of the order in the online store, track the current status of the package by its tracking number, monitor current account balances, and so on. Accordingly, there is a need for real-time interaction and system synchronization and post-construction, which could not only be updated but also ensure a continuous real-time production process [9];
- Data security – security rules and policies may vary depending on the system used. However, even if data security (storage, access rights) is ensured in the source system correctly, this policy should be transposed into the target systems as well as attention to information flows (e.g., enter one or the other encryption during data transfer between systems) to prevent possible misuse of information. This issue is crucial when working with stamped information and personal data [10];
- Data quality – another major obstacle is data quality. The data must not be inconsistent, and the integrity property must be satisfied. It is good practice to store data in one place and then redirects it to target systems, which helps to eliminate inconsistencies in the data and ultimately leads to more efficient management and maintenance of helpful quality data [11];
- Performances – measured against preset established standards of accuracy, completeness, expense, and speed, performing a given task [12]. Today, one of the most significant challenges facing the IT sector.

The following algorithm solution deals with real-time work, performance, and data quality; other problems are not considered.

3 Research Methodology

3.1 BPMN

BPMN is an essential part of an organization's overall architecture; by integrating it with several aspects of ERP systems used to run a business, a coherent and effective mechanism for documenting the relationship between people and processes and methods can be achieved, facilitating both deployment and ongoing operations. For example, Fig. 1 represents the organization's business process model.

It can be seen that the delivery of the product is carried out with the help of several parties involved. The manager identifies that the company is missing a specific product. The manager selects the quantity of the product and orders the request from the warehouse manager. The second, in turn, receives a request notification and checks the availability of the product. If the product is in stock, the employee closes the process, enters it into the data system, and delivers it to the manager. If the product is not in the warehouse, the warehouse manager sends a product request to the logistics worker. The logistics worker enters the required product information into the database using an autonomous data synchronization tool and delivers it to the product manager within two weeks via its channel. Whether the product came from the company's warehouse or the logistics manager, the manager checks it. If the correct product is delivered (manufacturer, product type, expiration date, certificate), the manager credits the assembly and delivery payment. If something is wrong after testing the product, the manager finds

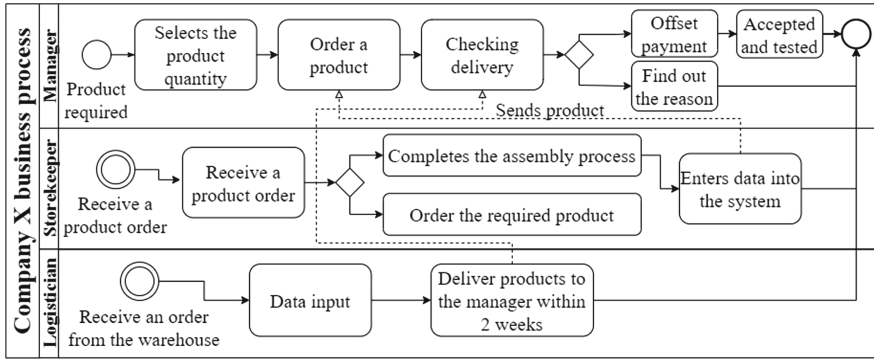


Fig. 1. Company X business process.

out the reason for the uncertainty and makes the necessary adjustments. As a result, a company that has aligned its operations with its strategy is agile, controls its processes, operates efficiently, and with well-trained staff can play alongside large companies.

It then receives the data at a specific URL that is sewn into the programming code. The URL is from an external Web Service with access to external data useful and used in the SAP ERP system. It is checked whether the data has been restored so that no data duplication is found if the data is not restored, the algorithm terminates. However, if the information is available and updated, it is collected and then forwarded to verify that it is structured correctly. If the data is incorrectly structured or uneven, it is pre-processed through the subprocess and sent back to the data validation. If the information is correct, it is forwarded to the data warehouse where it is stored. Once the data is stored in the data warehouse, the SAP ERP system generates reports on the database's changes, and the algorithm terminates. The corresponding algorithm is developed as an automated process that executes every day at noon.

3.2 UML

In Fig. 2, the UML diagram shows the supplier, products, delivery, employee, and customer. As well as an example of the data types of each object that are used, it is relatively simple, but the complexity starts the moment the orders reach a large quantity. It is necessary to execute the existing algorithm synchronously to check and store the data correctly to be in the right and specific amount. As an example, it can mention the correct use of data types according to stored values.

3.3 Integration

In Fig. 3, the main task of this ZAA_BAKA is to create an autonomous data synchronization solution. The ERP system from SAP was chosen for this purpose.

The challenge was to find approaches to implementing autonomy and synchronization with external platforms, sites, or files. It was determined that the most suitable experiment would take place with an external Web Service API [4] from which the data was

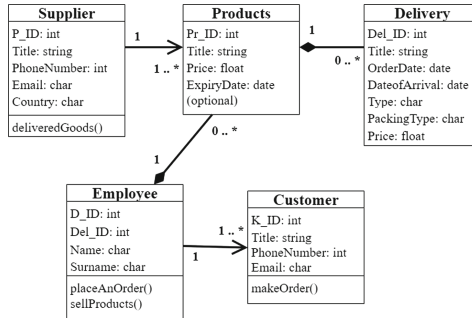


Fig. 2. UML of the SAP ERP integration example, data warehouse representation.

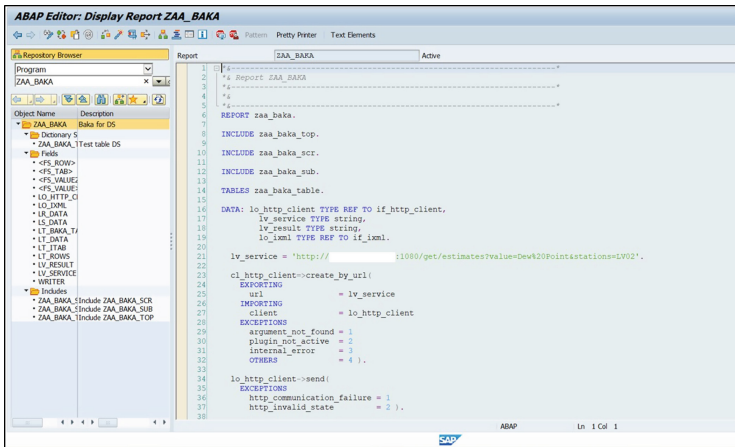


Fig. 3. SAP ERP integration ABAP editor report ZAA_BAKA.

decided to transfer to the SAP ERP system. There are many different options, devices, ready-made software in this SAP ERP system that are needed to use and customize different parts of the system. The system uses so-called transaction codes or transactions that can be used to move and edit the necessary details; for example, in transaction SE38 programs are created, in SE11, everything related to databases is created. The programming code is available in Fig. 4.

There are several privileges to use SAP ERP reports, and of course, there are also some disadvantages, see Table 1.

As a first advantage, it can seamlessly access data directly from the source to get up-to-date information. It is always pointing out the original data source. In this way, without distorting the data and preventing them from disappearing during the process. The second is a cost-effective application because the reports are already available in the SAP ERP system, and there are many different instructions on how to handle them. The third advantage is that it can merge the resulting information with other SAP and non-SAP data sources. In this case, the integration process is vital to be able to do it at

```

1 REPORT zaa_baka.
2 INCLUDE zaa_baka_top.
3 INCLUDE zaa_baka_scr.
4 INCLUDE zaa_baka_sub.
5 TABLES zaa_baka_table.
6 DATA: lo_http_client TYPE REF TO if_http_client,
7         lv_service TYPE string,
8         lv_result TYPE string,
9         lo_ixml TYPE REF TO if_ixml.
10
11
12
13 lv_service = 'http://xxx.xxx.xxx.xxx:1080/gst/
14 cl_http_client=>create_by_url(
15     EXPORTING
16         url = lv_service
17     IMPORTING
18         client = lo_http_client
19     EXCEPTIONS
20         argument_not_found = 1
21         plugin_not_active = 2
22         internal_error = 3
23         OTHERS = 4 ).
24
25 lo_http_client->send(
26     EXCEPTIONS
27         http_communication_failure = 1
28         http_invalid_state = 2 ).
29
30 lo_http_client->receive(

```

Fig. 4. ABAP programming code.

Table 1. SAP ERP reports advantages and disadvantages.

Capabilities	Possess
Up-to-date information	+
Cost-effective	+
Merge the result	+
No need to replicate data	+
Available in SAP ERP system	+
Performance issues	-
Depends on the report design and volume of data	-
Transactional data is not aggregated	-
Data format complexity	-

all. This capability also indicates that the SAP ERP system is not a completely closed system that cannot be accessed and accessed from other data sources. A fourth privilege capability is that there is no need to replicate data in different non-SAP relational tables. All data is available in one place, one of the best features of the SAP ERP system. As an absolute privilege, this report option is already available in the SAP ERP system and is ready to use and with a unique configuration and modification options. However, marking disadvantages that are available in the SAP ERP system reports. There are encountering performance issues when there are not enough resources to operate with large amounts of data from other information systems, which is also not rational to place them in the SAP ERP systems' data warehouse. The second drawback depends on the report design and the volume of data, limited to a certain amount. The next drawback is that transactional data is not aggregated, which is only logical that they need to be done manually according to a particular business process's needs. The latter is the data format

complexity, which complicates the data storage capability, but it would be an irrational duplication of information from external resources.

As already mentioned, several advantages and disadvantages should be noted that three disadvantages have an explanation that justifies why such capabilities are not fully used in the SAP ERP system. Performing an autonomous data synchronization solution solves problems like real-time, performance, and data quality. The solution can eliminate all three problems in real-time, reduce ERP systems' performance by placing an external service and ensure data quality with ERP systems' help before data storage. The following section explains the autonomous data synchronization solution that is integrated into the SAP ERP system.

4 Results

Before explaining the solution step by step, initially familiar with SAP ERP transactions that will be used:

- SM36 – SAP ERP systems background job processing (create, schedule, and reschedule). A background job is a mechanism that runs behind the usual digital operations. It is run in parallel, and dynamic processes and activities are not interrupted. The advantages of background jobs are that it reduces manual work; it can be scheduled as per each user and scheduled in the night. Background jobs are classified into 3 categories - high/medium/low priority [13];
- SM37 – SAP ERP systems background job monitoring. Monitoring background work is critical because it can be canceled due to any mistake once schedule the job [14];
- SE38 – ABAP editor is the standard SAP ERP systems transaction code available inside R/3 SAP systems. It helps developers to handle and execute reports (programs), versions, attributes, metadata, or text elements (with or without debugger) [15];
- SE11 – SAP ERP database tables are generated using transaction SE11 in the data dictionary and stored data inside the SAP ERP program. It includes master data, transaction data, configuration data. When a database table is formed, any data entered must remain until it is physically extracted or altered by something [16].

The synchronization was performed using the programs created in transaction SE38; the transaction exists to create and view various programs. The operation is written in a closed programming language called ABAP. Autonomy was realized through a built-in program called a background job. A background job is not an interactive process that is performed in addition to the usual interactive activities. It works in parallel and does not interfere with interactive processes and operations, and it is configured in transaction SM36. It can be analyzed using transaction SM37 by reviewing the activity log and status. The experiment started with an established program transaction, SE38. The application needs to be activated and run before it can be used in the future. No data may be output to the program but to display part of the result. It can be said that the data synchronization from the external API has been successful, and it is possible to work with the data already on the SAP ERP systems side. The main goal is to move all the data in the database to further keep them there for the future and further use it for various tasks. To move them

in a table, first need to create them, which can be done in transaction SE11. Accordingly, a table called ZARA_BAKU_TABLE is created. It consists of two columns, ID and ZAADATA. The first to store identification records and the second to store the data itself. Columns are defined in a unique way to avoid type conflicts. From the add-on program's startup results, 10,366 records were imported with the external Web Service API, which was successfully added to the database. To better understand the process, it is depicted in the concept in Fig. 5.

Autonomous data synchronization solution

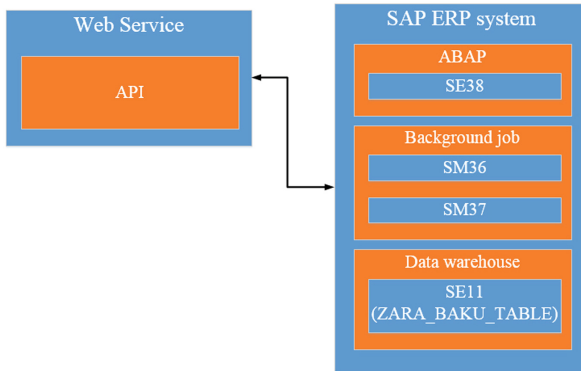


Fig. 5. The autonomous data synchronization solution between SAP ERP system and Web Service.

Once the program is created and the tests are completed, it can be started working with the standalone part. Since the background job is a built-in device that allows us to perform the necessary part of the experiment, there is no more programming. There is a small configuration where needs to specify the settings that will be made as required. The background job configuration occurs after transaction SM36, and all the necessary settings must be made there. The settings are not over; the next step is time and how often the program is started. Background job definition with scheduling the start date, the time at which the application is running, and the frequency were added. In this case, the program was updated daily at 12.00. Next, to check how the configuration went and whether the program started at all, check its status. It is necessary to refer to transaction SM37. In the work menu making this transaction, it needs to be select a job that is already created. Then pick the criteria by which needed to be applied a summary of the work. After checking the job overview form, it can be seen that the work exists with status *Released*. The job is ready to work according to the configurations.

The following example describes in great detail how an SAP ERP system can provide application development that can connect to an external Web Service and set up that application's background job so that it can work independently. Over time, this option allows management to increase business value.

5 Conclusions

The SAP ERP system's synchronization approach is implemented with an integrated approach, which contains a connection between the SAP ERP system and an external Web Service that uses API access. The solution uses the ABAP programming language and tests the code with standard output during the experiment to show that it is accepted from the Web Service to the SAP ERP system. As a result, information is obtained, and data integration reflects the experiment's progress and implementation. As mentioned above, this answers the first research question. Yes, it is possible to connect the existing algorithm to the ERP system.

The SAP ERP system's automation approach is already built-in into the system and was configured to meet the existing solution's needs. After configuration, the autonomy took place synchronously; data was read from the web service at a specific time each day. Is the answer to the second research question, "Does the existing algorithm indicate the existence of autonomy" found? Answers should be marked as yes, but automation should occur every minute, not once a day. Since this was designed as an experiment, then it can be assumed that autonomy has worked appropriately.

The implementation of the solution has been carried out according to the planned plan; it can be further used in several cases where it is necessary to integrate the systems and obtain various data. This solution can be supplemented and modified; it can work with complex data, create documents at once in the program, and save everything in several database tables. Autonomous data-driven integration into ERP systems is done with gloss showing excellent performance when working with an external Web Service that uses API access. In future work, integration with other ERP systems will be developed to compare the integration's complexity using the same Web Service.

Acknowledgment. This publication was supported by the Riga Technical University's Doctoral Grant program.

References

1. Magal, S.R., Word, J.: Integrated business processes with ERP systems. Wiley, Hoboken (2011)
2. Gronwald, K.D.: Integrated Business Information Systems. Springer, Heidelberg (2020). <https://doi.org/10.1007/978-3-662-59811-5>
3. Dechow, N., Mouritsen, J.: Enterprise resource planning systems, management control and the quest for integration. *Acc. Organ. Soc.* **30**(7–8), 691–733 (2005)
4. Viriyasitavat, W., Hoonsoapon, D.: Blockchain characteristics and consensus in modern business processes. *J. Ind. Inf. Integr.* **13**, 32–39 (2019)
5. Schubert, P.: Joint work and information sharing in the modern digital workplace: how the introduction of "social" features shaped enterprise collaboration systems. In: Riemer, K., Schellhammer, S., Meinert, M. (eds.) *Collaboration in the Digital Age*, pp. 45–59. Springer, Cham (2019). https://doi.org/10.1007/978-3-319-94487-6_3
6. Peksa, J.: Prediction framework integration into ERP systems. In: 2020 61st International Scientific Conference on Information Technology and Management Science of Riga Technical University (ITMS), pp. 1–6. IEEE (2020)

7. Nakatani, K., Chuang, T.T., Zhou, D.: Data synchronization technology: standards, business values and implications. *Commun. Assoc. Inf. Syst.* **17**(1), 44 (2006)
8. Gupta, S., Qian, X., Bhushan, B., Luo, Z.: Role of cloud ERP and big data on firm performance: a dynamic capability view theory perspective. *Management Decision* (2019)
9. Shafi, K., et al.: Measuring performance through enterprise resource planning system implementation. *IEEE Access* **7**, 6691–6702 (2019)
10. Mandal, S., Khan, D.A.: A dynamic programming approach to secure user image data in cloud based ERP systems. In: 2019 Fifth International Conference on Image Information Processing (ICIIP), pp. 91–96. IEEE (2019)
11. O’Leary, D.E.: Technology life cycle and data quality: action and triangulation. *Decis. Support Syst.* **126**, 113–139 (2019)
12. Hasan, N., Miah, S.J., Bao, Y., Hoque, M.R.: Factors affecting post-implementation success of enterprise resource planning systems: a perspective of business process performance. *Enterpr. Inf. Syst.* **13**(9), 1217–1244 (2019)
13. Dickersbach, J.T., Passon, M.F.: Master data, services and basis functions. In: *Service Parts Planning with SAP SCM™*, pp. 13–48. Springer, Heidelberg (2015). https://doi.org/10.1007/978-3-662-45433-6_2
14. Okungbowa, A.: Processing periodic programs. In: *Asset Accounting Configuration in SAP ERP*, pp. 269–294. Apress, Berkeley (2016)
15. Chuprunov, M.: IT general controls in SAP ERP. In: *Auditing and GRC Automation in SAP*, pp. 131–163. Springer, Heidelberg (2013). https://doi.org/10.1007/978-3-642-35302-4_6
16. Markandeya, S., Roy, K.: ERP and SAP overview. In: *SAP ABAP*, pp. 1–20. Apress, Berkeley (2014)



Three Dimensional Technology Radar Model to Evaluate Emerging Industry 4.0 Technologies

Erwin Rauch^(✉)  and Eugenio Vinante

Industrial Engineering and Automation (IEA), Faculty of Science and Technology,
Free University of Bolzano, Universitätsplatz 1, 39100 Bolzano, Italy
erwin.rauch@unibz.it

Abstract. Emerging Industry 4.0 technologies are changing very fast, and in few years, technologies reach a new level of maturity, or new technologies are introduced. This makes it difficult for manufacturing companies to keep track of the fast development and evaluate a future introduction of new technologies related to the Fourth Industrial Revolution. Therefore this work aims to realize an Industry 4.0 technology radar for industrial organizations based on the Gartner Hype Cycle Curve. This tool aims to analyze new emerging technologies that could affect manufacturing firms, enabling selecting the most suitable ones. The technology evaluation considers three parameters: a technology maturity level, enterprise value, and deployment risk of technologies. The application of such a tool highlights which technologies to include in the company's future technology strategy. The developed technology radar was applied in a real industrial case study to prove its applicability and limitations.

Keywords: Industry 4.0 · Technology radar · Evaluation model · Maturity model · Gartner hype cycle; emerging technologies

1 Introduction

After the era of lean management with many innovative organizational approaches [1], the fourth industrial revolution introduced new technologies that enable the development of new products and services, a more efficient manufacturing process, and better product quality. Industry 4.0 is characterized by nine key technologies [2]: advanced manufacturing, additive manufacturing, simulation, augmented reality, horizontal/vertical data integration, industrial internet of things, cloud computing, cybersecurity, and big data analytics. However, in this new era, a lot of new technologies are actually developed and implemented. Staying abreast of technological advances with solutions that ensure efficient manufacturing processes and resource consumption, flexibility, and accurate monitoring and corporate data analysis is part of many companies' corporate strategy [3]. With continuous progress across the entire spectrum of technologies used in manufacturing, a key factor in the practical implementation of the most modern systems is the availability of measurement and testing solutions that keep pace with technological

evolution. Identifying and successfully implementing a promising technology before the competitors could lead to finding a competitive advantage [4].

Several studies and research in the scientific literature focused on forecasting which technologies will be adopted or implemented in the future [5]. Forecasting the promising technological trends is not simple also due to the number of new technologies that are developed and because it is not always known the real impact that those technologies will have in practice. With continuous technological progress, choosing the most promising technology is not always the best solution and does not guarantee an advantage. For this reason, being able to identify new technologies is only one step to being able to achieve a competitive advantage. Selecting, assessing, and adopting the most appropriate technology suitable for a specific company is the real challenge that companies face right now [6]. The newest inventions usually look “shiny” and incredible but are not necessarily the best solution.

This work aims to develop a tool for supporting companies in identifying the most advantageous technologies and obtaining a competitive advantage over their competitors. This tool aims to assist the top management team in identifying, selecting, and assessing emerging technologies based on their maturity level, deployment risk, and the value they would provide to the company if implemented.

2 Literature Review

Today, companies face several challenges, such as rising competition, new competitors' entrance, shortening of the product life cycle, market uncertainty, and increasing complexity of the supply chain. Besides, the pace of technological improvements is growing exponentially, which means that having and maintaining a high technological competence is a key factor for gaining and maintaining a competitive advantage [7]. For this reason, many companies are investing a lot of time and resources for monitoring, researching, and identifying emerging technologies, which could be key factors for improving and innovating their business [8]. The absence and lack of exact information about organizations, activities, and events outside your company's business create an environmental uncertainty, making it difficult to predict future changes [9].

Companies started performing studies to predict future changes called strategic foresight for dealing with environmental uncertainty. It consists of understanding future trends and adopting future-oriented insights for strategic operations and decision making [10]. Strategic foresight is a systematic approach aimed to learn and understand the future to guide the present day, an approach that could also be applied for scouting emerging technologies [10]. For reaching a technological competence which consists of knowing relevant technological innovation and emerging trends, the result crucial, and for doing this, technological foresight results essential. More specifically, it is meant to monitor the entire technological spectrum carefully for identifying technologies that represent disruptive innovations [11].

One of the models regarding technology management and analyzes the evolution of the technology's performance over time. It is the so-called "S curve" model developed in 1986 by Richard Foster [12]. Technology scouting results to be a fundamental practice for gaining and maintaining technological competence achieving a competitive advantage. For performing this, "technology radars" are tools that permit identifying technological development in an early stage. Due to the constant growth of new technology, companies must continuously review their technological competence to remain informed and not lose any chance of implementing emerging technologies [7]. Technology radars substitute regular, occasional technology reviews made by external consultants or from the internal research and development department. A technology radar is a complex tool, and its contribution to innovation management goes beyond technological briefings and analysis of a technology potential [13]. Technology radar results in being above all a strategic instrument because they allow them to discover new promising technologies or trends from their initial stage of life cycle and determine their strengths, weaknesses, threats, and opportunities [13]. Rohrbeck and Heinrich identify the process of technology radar as a procedure of four steps: (i) technology identification, (ii) selection, (iii) assessment, and (iv) dissemination [13].

Scientific and consequently technology innovations are strictly related to many factors like scientific research, new ideas, effective communication of technological findings and scientific knowledge, availability of new resources, and the introduction of new technology in the market [14]. This means that since every emerging technology is affected by all these factors forecasting technological development is not a simple task. Forecasting which technologies will be developed and will be successful will strongly influence the formulation of corporate marketing strategies and offer strategical support for creating a technology strategy [15]. In this regard, Gartner Inc. introduced the "hype cycle model," proclaiming its ability to forecast technological development. The Gartner hype cycle curve shows the common advancement of innovation, from excessive enthusiasm through the disillusionment period to a possible understanding of its relevance and role in a market or domain. More specifically, it shows the expectation or visibility and value of technology concerning time [16]. Gartner Inc. publishes once a year an updated hype cycle curve where they place emerging technologies that they believe have the potential for becoming relevant in the future in their respective stage of maturity.

This work aims to develop a technology radar to enable companies to identify and assess the potential of emerging technologies in the context of Industry 4.0. Up to now, few works are showing a practice-oriented way for companies to do this.

3 Research Methodology

In this section, we present the research methodology used for this study. A model has been developed to identify, select, and evaluate new emerging technologies so that organizations can identify potential technologies to improve their operations and their manufacturing process. This means that our method focuses only on manufacturing or other manufacturing-related (operational) processes and not on technologies mainly addressing organizational processes or similar. Figure 1 illustrates the five steps of our technology radar model.

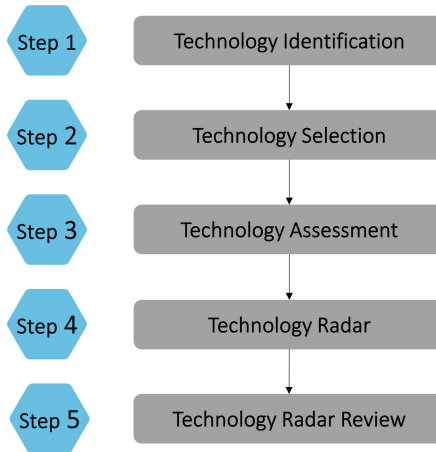


Fig. 1. Steps of the applied methodology.

The first part of the model focuses on identifying emerging technologies, while the second one is selecting the technologies that impact the manufacturing process. The third step deals with the assessment of the identified technologies considering three key parameters: (i) the maturity level, (ii) the deployment risk, and (iii) the enterprise value of each technology selected. Based on this evaluation, the technologies can be classified in a 3-dimensional technology radar into eight categories considering their level of high or low maturity, value, and risk in three axes. Thanks to this classification, an organization can then decide which technology might have strategic relevance for its business and consequently decide to adopt it or start a pilot program to understand if that technology positively affects the manufacturing process.

The following section shows more detailed information regarding each step of the above-illustrated technology radar model. The proposed model has been tested and applied in an industrial case study at a large device manufacturer for the printing industry.

4 Results

4.1 Step 1 - Technology Identification

The first section of the technology radar focuses on identifying new emerging technologies that will be considered for the evaluation. This part aims to create a list of technologies to give the users a wide choice for the next step.

Since the research focuses on emerging technologies, it was necessary to identify technologies that are not widely implemented for developing a long-term strategy to gain a business advantage concerning the competitors. The technologies listed in the Gartner hype cycle curve of the last three years have been used as a basis to make efficient research and obtain valid results. Reporting only the emerging technologies of the last year would be reductive since this phase's goal, as explained before, is to create a comprehensive list of technologies. Technologies are constantly changing, increasing

their maturity level and improving their performances, but new technologies will also be created and developed with time. For this reason, the process of technology scouting needs to constantly scan the technological environment and continue after the first technology radar evaluation to guarantee that when this process of assessment will be repeated, all new technologies will be included in the analysis.

4.2 Step 2 - Technology Selection

While the first step of the technology radar is equal for every organization, starting from the second one, the technology selection, every section will be different. In this phase, we select the technologies that could affect the individual organization's manufacturing process from the list of identified technologies. This means that an assessment group in the company must go through all the technologies identified and select only the ones that impact the firms' operation. Since the model was developed for being used by companies from different sectors, not all technologies will be relevant to all organizations. In this step, it is important to define assessment groups composed of at three to five persons from top management, research, development, manufacturing, logistics, and maintenance department.

The assessment group should report what technology could be used for manufacturing and how it could affect the process, providing the users a better understanding of each technology's application scenario. It is important to notice that there is no information about the requirements for implementing any technology for avoiding prevention in the selection in this section. The more technologies are selected in this phase, the wider the technology spectrum will be considered in the further analysis. This section aims to encourage users to choose as many technologies as possible but excludes obvious irrelevant technologies.

4.3 Step 3 – Technology Assessment

The phase of technology assessment is the most important and the most difficult and crucial step of the entire technology radar analysis. In this section, the technologies selected in the previous section are evaluated for quantifying their potential. For performing the evaluation are considered three main attributes of every single technology:

- maturity level,
- enterprise value,
- deployment risk.

To each of these attributes is assigned a numeric value between one and five. For achieving the final evaluation, both for enterprise value and deployment risk are identified four parameters that the user should evaluate and give the final results.

Every technology's maturity level evaluation is made based on the score assigned to each technology's corresponding position in the Gartner Hype Cycle Curve. As described before, the hype cycle curve released every year by Gartner Inc. identifies new emerging technologies and for each one determines the maturity phase (1 – innovation trigger,

2 – the peak of inflated expectations, 3 – thought of disillusionment, 4 – a slope of enlightenment, 5 – plateau of productivity).

The second parameter, which is considered for the assessment of technologies, is the enterprise value based on four indicators' evaluation.

1. Manufacturing impact,
2. Operational impact,
3. Organizational impact
4. Digitalization impact.

They take into consideration different aspects of how technology affects and consequently improves a company.

The last parameter considered for the technology assessment is the deployment risk. This parameter considers four indicators for obtaining a final score:

1. Resource allocation,
2. Integrability,
3. Applicability,
4. Time to reach the plateau of productivity.

The first indicator considers the time, effort, and economic investment required for the implementation of technology. The second indicator is integrability which refers to how easily a technology could be implemented in the existing system manufacturing process. The third indicator is applicability and refers to successful applications of the technology and best practice examples. The last indicator considered is the time to reach the plateau of productivity. This indicator's assessment can be done based on Gartner's forecast of the last three years, serving as a guideline for users to evaluate this indicator.

The assessment tool has been developed as a Microsoft Excel spreadsheet to support and facilitate the evaluation procedure. The scoring algorithm is automated and uses the manually encoded values for the three above-mentioned parameters for maturity level, enterprise value, and deployment risk.

4.4 Step 4 – Technology Radar

After assessing all the selected technologies, building the 3-dimensional technology radar (Fig. 2). Most of the assessment models and technology radars in literature are based on a two-dimensional structure. In this case, since the model developed considers three parameters, for an effective and clear representation of the results, was adopted a 3D structure. Depending on the level of each parameter, we can classify the technologies in eight quadrants. Every quadrant has the same dimension (every parameter can assume a maximum value of 5 and a minimum of 1). Based on the position of technology in these eight quadrants, a company is assisted in defining a strategy for handling each of the technologies (Table 1).

Building the sum of all three parameters, we can obtain a single assessment value for each technology, making it possible to compare all of those taken into consideration for the assessment and thus create a ranking (see an example of the industrial case study application in Table 2).

Table 1. Quadrants of the technology radar.

No	Quadrant	Maturity level	Enterprise value	Deployment risk
1	Gather Information	Low	Low	Low
2	Growth & Development	Low	High	Low
3	Limited Growth	High	Low	Low
4	Growth	High	High	Low
5	Divestment	Low	Low	High
6	Selection	Low	High	High
7	Limited Growth & Investment	High	Low	High
8	Growth & Investment	High	High	High

Figure 2 finally shows the technology radar chart illustrating the results.

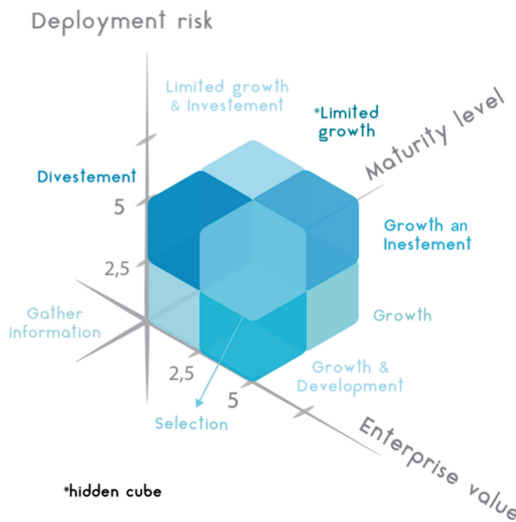


Fig. 2. Three-dimensional technology radar.

4.5 Step 5 – Technology Review

As it was the first time at the case study company that the Industry 4.0 technology radar tool was implemented, it was impossible to compare the results of this assessment with previous data. Gartner Inc. releases a new Hype Cycle every year to identify the most relevant new emerging technologies and positions them on the curve to determine the maturity phase. When the next Hype Cycle will be released, the company should repeat the analysis and compare the “old” and the “new” radar results.

Table 2. Results of case study application - Technology Ranking.

Pos.	Technology	Maturity level	Enterprise value	Deployment risk	Total score
1	Digital twin	2	4.25	3	9.25
2	Augmented reality	3	3	2.75	8.75
3	Autonomous mobile robots	1	3.75	3.75	8.5
4	Enterprise taxonomy	3	2.5	3	8.5
5	Smart robots	1	4	3.5	8.5
6	4D printing	1	3.25	4	8.25
7	Mixed reality	3	3	2.25	8.25
8	Nanoscale 3D printing	1	3	4.25	8.25
9	Virtual reality	4	2.25	2	8.25
10	3D sensing cameras	3	2.5	2.5	8
11	IoT platform	2	3.25	2.75	8
12	Flying autonomous vehicles	1	2.25	4.25	7.5
13	DigitalOps	1	2.75	3.5	7.25
14	Blockchain	2	2	3	7
15	Decentralized autonomous organizations	1	2.25	3.75	7

4.6 Discussion and Limitations

This research aimed to build a tool for evaluating emerging Industry 4.0 technologies with a strong focus on manufacturing companies and processes. Even if it considers

many information-based technologies, its implementation would not be effective in other industries, e.g., software companies.

The first section of the model that focuses on the technology identification is crucial because if this initial phase of scouting a technology is neglected, it will not be considered in the following phases of the analysis. Besides, since the model is based on the Gartner Hype Cycle and every year a new one is released, the list of technologies, the value of maturity level, and forecast time for reaching the plateau of productivity must be manually updated.

The most significant limitation of this model is the assessment methodology because, except for the maturity level, the other two parameters considered for the assessment are evaluated subjectively. This means that there is no objective evaluation method for evaluating both the enterprise value and the deployment risk. Furthermore, the assessment strongly depends on the evaluator's knowledge about the individual technologies. If a user of this tool is not an expert in a given field, e.g., Augmented reality, it is not easy to assess individual attributes. The authors recommend evaluating an interdisciplinary group with experts from different company and external technology experts' functions to mitigate this risk.

Finally, this model aims not to make an exact and precise evaluation of emerging technology but to support organizations in identifying promising technologies providing an approach to encircle the most promising technologies as a basis for continuously updating the own corporate technology strategy.

5 Conclusions

This work aimed to develop, apply, and validate a Technology Radar-based evaluation model of emerging Industry 4.0 technologies. Through the developed model, we can guide companies in a structured and systematic way through the identification, selection, and evaluation of promising technologies.

The fact that the developed model is not completely based on members of an assessment group's subjective opinions but partly also on reliable results from renowned models like the Gartner hype cycle curve is encouraging to use this model in practice.

The application of the technology radar model in the case study has shown that users appreciate a structured guideline and framework that they can follow. Although there are limitations based on subjective evaluations during the assessment, this can be tackled by preparing, training, and adequately selecting the assessment group members.

Further research is still needed as the model should be applied in multiple case studies and different industrial sectors and enterprise sizes. In addition, other researchers should further develop the proposed model to reduce the limitations mentioned above.

Acknowledgment. This project has received funding from the European Union's Horizon 2020 research and innovation program under the Marie Skłodowska-Curie grant agreement No. 734713 (SME 4.0 – Industry 4.0 for SMEs).

References

1. Dallasega, P., Rauch, E., Matt, D.T., Fronk, A.: Increasing productivity in ETO construction projects through a lean methodology for demand predictability. In: Proceedings of 2015 International Conference on Industrial Engineering and Operations Management IEOM, Dubai, UAE, pp. 1–11. IEEE (2015)
2. Alcácer, V., Cruz-Machado, V.: Scanning the industry 4.0: a literature review on technologies for manufacturing systems. *Eng. Sci. Technol. Int. J.* **22**(3), 899–919 (2019)
3. Bonilla, S.H., Silva, H.R., Terra da Silva, M., Franco Gonçalves, R., Sacomano, J.B.: Industry 4.0 and sustainability implications: a scenario-based analysis of the impacts and challenges. *Sustainability* **10**(10), 3740 (2018)
4. Ciffolilli, A., Muscio, A.: Industry 4.0: national and regional comparative advantages in key enabling technologies. *Eur. Plan. Stud.* **26**(12), 2323–2343 (2018)
5. Gordon, A.V., Ramic, M., Rohrbeck, R., Spaniol, M.J.: 50 Years of corporate and organizational foresight: looking back and going forward. *Technol. Forecast. Soc. Chang.* **154**, 119966 (2020)
6. Boe-Lillegraven, S., Monterde, S.: Exploring the cognitive value of technology foresight: the case of the Cisco Technology Radar. *Technol. Forecast. Soc. Chang.* **101**, 62–82 (2015)
7. Rohrbeck, R.: Technology Scouting—a case study on the Deutsche Telekom Laboratories. In: Proceedings of International Society for Professional Innovation Management Connects ISPIM-Asia Conference, Singapore, Malaysia, pp. 1–14 (2007)
8. Vecchiato, R., Roveda, C.: Strategic foresight in corporate organizations: handling the effect and response uncertainty of technology and social drivers of change. *Technol. Forecast. Soc. Chang.* **77**(9), 1527–1539 (2010)
9. Duncan, R.B.: Characteristics of organizational environments and perceived environmental uncertainty. *Adm. Sci. Quar.* 313–327 (1972)
10. Iden, J., Methlie, L.B., Christensen, G.E.: The nature of strategic foresight research: a systematic literature review. *Technol. Forecast. Soc. Chang.* **116**, 87–97 (2017)
11. Arnold, H.M.: *Technology Shocks: Origins, Managerial Responses, and Firm Performance*. Springer, Berlin (2012)
12. Foster, R.N.: *Innovation: The Attacker's Advantage*. Summit Books (1986)
13. Rohrbeck, R., Heuer, J., Arnold, H.: The technology radar—an instrument of technology intelligence and innovation strategy. In: Proceedings of 2006 IEEE International Conference on Management of Innovation and Technology, vol. 2, pp. 978–983 (2006)
14. Silvestrini, P., Amato, U., Vettoliere, A., Silvestrini, S., Ruggiero, B.: Rate equation leading to hype-type evolution curves: a mathematical approach in view of analysing technology development. *Technol. Forecast. Soc. Chang.* **116**, 1–12 (2020)
15. Dedehayir, O., Steinert, M.: The hype cycle model: a review and future directions. *Technol. Forecast. Soc. Chang.* **108**, 28–41 (2016)
16. Linden, A., Fenn, J.: Understanding Gartner's hype cycles. <http://www.ask-force.org/web/Discourse/Linden-HypeCycle-2003.pdf>. Accessed 01 Oct 2020



Applicability of Traditional Project Closeout Approaches in Agile Developed IT Projects

Philipp Rosenberger¹  and Jozsef Tick² 

¹ University of Applied Science FH Campus Wien, Favoritenstr. 226, 1100 Vienna, Austria
philipp.rosenberger@fh-campuswien.ac.at

² J. Neumann Faculty of Informatics, Obuda University, Bécsi út 96b, Budapest 1034, Hungary

Abstract. This article investigates the applicability and compatibility of project closeout processes defined in traditional project management frameworks in cases of agile-developed IT projects. Based on a literature review analysis of three project management frameworks, the hypothesis is formed that traditional project closeout processes are critical in agile developed IT projects. The developed hypothesis suggests an unclear indication of how to trigger a project closeout, the inapplicability of scope fulfillment for closeout trigger, and critical transitions between closed projects and ongoing agile software improvement and maintenance. All three parts of the hypothesis are then individually evaluated by an online survey with 85 participants. As a result of this survey, all three hypotheses are falsified. For most project management practitioners in agile projects, closeout processes are not critical, scope fulfillment is still the most relevant closeout trigger, and the transition to a continues-improvement and maintenance process is seen as principally uncritical.

Keywords: Agile project management · Tailoring · Project closeout; SCRUM · IT project management

1 Introduction

IT project management is a profession shaped by, on the one hand, project management frameworks, best practices, and supporting Information Management Systems for the project manager and on the other hand, by agile trends that emerged since 2001 by the publishing of the agile manifesto [1] and the abstraction of the SCRUM methodology. Since agile approaches spread into all IT-related industries. One very specific phase in traditional project management is the project closeout, which is clearly defined in different project management frameworks.

This end of the projects is at the same time completely not a part of agile approaches. Agile development is an iterative process to develop software features as efficiently as possible and does not consider any rules or definitions of a traditional project [2]. It was introduced in the form of the agile manifesto to ease software developers' lives and increase their productivity by using short-term iterations, flexible product backlogs, and a focus on "people and running code" over processes and documentation [1]. So two worlds

related in a single project may collide because one framework has clear expectations and rules, and the other one does not consider the closeout at all. The gap between these different but in IT projects coexisting frameworks is analyzed regarding the phase of project closeout. This research and its result support the bigger goal of harmonizing agile development using agile approaches and traditional project management according to long-established project management frameworks. In addition to that, this bigger goal is targeting to build up a basis of integrating such tailored project management framework in industry-specific information management systems, eventually even supported by the application of big data and data science approaches [3] optimizing project management frameworks.

2 Literature Review

Based on an analysis of three different project management frameworks especially used in the IT development industry, the definition of project closeout processes is analyzed in the form of brief literature research. Based on this analysis and by putting these results in contrast to agile mindsets, tools and methods, an assumption is postulated, whether traditional project closeouts are a critical process in agile developed IT projects or not. This hypothesis consists of three sub-hypothesis. These are then individually verified or falsified by a quantitative survey with 85 participants.

2.1 Project Management Institute

The project management body of knowledge, also called PM-BOK, in its sixth version is a 700-page guideline describing 49 project processes structured into 5 phases and 10 knowledge areas. [4] Within the knowledge area of “Integration Management”, the process “Project Closeout” is defined as “...to formally complete the project, phase, or contractual obligation...” and described in a six-page analysis containing input factors, tools, and expected outputs. Advantages of using the described process are defined in archiving proper information, finalizing the project work, and setting project-related resources free for other tasks. Jung [5] recommends summarizing all these tasks in the form of a workshop with all project participants and stakeholders. In a second part of the PM-BOK, structured in process groups, the closeout process group is described in three pages, also focusing on archiving of information and detailing output documents like:

- Closeout protocol
- Change protocols
- Milestone lists
- Quality reports
- Risk matrix

All the available elements are based on highly traditional project set-ups and structured in strict phases with end-to-end planning activities in the project’s initiation phase. Of course, this contradicts the iterative nature of agile approaches. To cope with this

lack of agile applicability, the PMI organization, in cooperation with Agile Alliance [6], integrated an “Agile Guideline” handbook within the latest version of the PM-BOK, including a “PM-BOK Guide Mapping” overview, which tries to map the 10 knowledge areas toward agile approaches [7]. In his evaluation, Clayton gives a poor evaluation of the Agile Guideline Handbook”, even calling it “non-helpful” because it fails to close the gap between agile and traditional project management approaches.

As a conclusion, it can be summarized that the current PM-BOK project management framework, even supported by the Agile Handbook does not incorporate agile needs but only serves the purpose of providing information about traditional project closeout requirements.

2.2 International Project Management Association

The International Project Management Association (IPMA) also provides a project management framework called Individual Competence Baseline (ICB) [8]. The IPMA framework differs regarding its approach towards a framework. When PMI focuses on the methods, processes, and tools, the IPMA structures skillsets of project managers, divided into three domains: Project-, Program- and Portfolio Management. Although Agility is a needed skill to act sustainably within a project in ICB’s latest version, there are no further references about integrations of agile development frameworks, cultures, or methods.

Based on an analysis of the ICB framework defines a project closeout as “...*formally complete the project, phase, or contractual obligations*” [8]. Kuster et al. [9] describes ten tasks as needed for successful project closeouts and mentions the transformation and handover of resources as highly important.

As the basic guideline of IPMA does not cover agile approaches in detail, the organization also developed a short and, with its 60 pages very superficial document, called ICB4 in an Agile World [10] describing agile needs and adaptations.

As with PMI, the IPMA framework provides traditional tasks and skillset descriptions for project closeouts, not covering agile needs. Its Agile Handbook does not provide deep insights into agile project closeouts.

2.3 CAMMP

In contrast to the above described widespread project management frameworks, let us also include a more specific and adaptable project management framework into this analysis. The “Customizable and Adaptable Methodology for Managing Projects” or CAMMP developed by the Company SUKAD in 2004 [11] is not a real framework but more like a loose methodical approach or collection of best practices [12], available for organization-specific tailoring and adaptation. The CAMMP approach details project closeout activities at the end of the “Delivery Phase” of projects. The main result of the closeout is only defined as a closeout report. This should include lessons learned, performance- and success evaluations, and plan deviations. As an additional metric for success, besides cost, time, and scope fulfillment, CAMMP also includes the success of the project management approach for consideration. Such evaluation of project management readiness could also be incorporated into the larger goal of data-based optimization

[13] and integration into Information Management Systems. Pfleger [14] even extracted a checklist of closeout requirements for CAMMP projects.

Although the scope of closeout activities is quite large in CAMMP projects, there seem to be not agile-specific requirements in place.

3 Research Methodology

3.1 Development of Hypothesis Based on Literature Research

After providing insights into the most common and also one very specific project management framework regarding the requirements and processes of project closeout activities, we will conclude a hypothesis, whether these frameworks in their entirety are suitable for the management of project closeouts of agile developed IT projects or not?

The first basis for this hypothesis is the highlighted fact that none of the frameworks explicitly targets agile developed projects. PMI and IPMA created side documents to move with the trend of agile approaches. Still, even after publishing new versions of their frameworks, the basic elements and contents of the project management processes and requirements did not change. So let us conclude as a first step that none of the existing frameworks focusses on agile-developed projects.

To evaluate if these existing “non-agile” frameworks are still applicable for agile projects, we will summarize agile needs and compare them with the current frameworks.

Agile and SCRUM-based development only describes a way of incremental software development and, by being a process description, does not give any indication about “how to stop” or how the end a project. Agile is, per definition, not a project management framework but just a process description of how to program effectively. Nevertheless, it has strict cultural rules, meeting structures, and roles that can conflict with traditional project management approaches. So the fact that these two elements need to work together, but in their definition as such do not take care of each other, is the basis of the first part of our hypothesis:

1. As agile development is a process and not a project, there is no indication of ending it. Therefore, it is unclear for involved agile developed projects, how to stop the project, and which criteria to stop it.

The second fact of agile development that contradicts rigid traditional project plans focuses on flexible product backlogs. Therefore, the scope of agile projects can vary from one day to another. [1] So as the second part of the hypothesis, it can be argued:

2. Traditional “Scope Fulfillment” does not work anymore for agile developed projects because of its constant change and flexibility.

The third part of the hypothesis again takes the closeout of a traditional project and the transformation towards an ongoing maintenance and feature integration and improvement process into consideration. In agile frameworks like SCRUM, the end of projects does not impact agile approaches at all. However, in traditional projects, the release of project resources and management stops is an integral part of project closeout. That is why the third part of the hypothesis suggests that:

3. The transition between traditional projects towards an ongoing agile improvement and maintenance process can often be unclear and critical.

An online survey will now validate these hypotheses.

3.2 Survey Structure

Chapter one of the Online Survey captured brief demographic information ensuring a correspondence of the participants to IT industry-specific demographic structure. This chapter covers:

- Age distribution
- Experience in project management

Chapter two evaluates the impressions and satisfaction of participants working in agile developed IT projects regarding project closeout phases and practices by covering the following questions:

- Are project closeout criteria clearly defined right from the project starting phase?
- Which factor is most relevant in triggering project closeouts? Budget, Time, or Scope fulfillment?
- Do you support the agile trend of fixing budget and time and adding flexibility regarding scope fulfillment as long as a “product vision” is achieved?

The third chapter of the survey directly evaluates the need to adapt the established closeout phases and approaches in agile developed IT projects using one very specific choice question to evaluate the developed hypothesis and its alternatives. This rating is enriched by the possibility to add a voluntary statement by the participant.

- Rate the clarity of the transition process in your projects from the closed project towards ongoing maintenance and ongoing feature development.

4 Results

4.1 Representability of Survey Participants

85 persons participated in the online survey. With 35%, most of the participants actually work within the Austrian IT industry. 21% represent the banking and financial sector, 10% cover Consulting and training. The other participant spread through different sectors like logistics, engineering, science, and teaching and sales. As nowadays many banking-related activities cover IT-related tasks and challenges, it can be concluded that a high percentage of the survey participants work in IT-related professions or at least deal with IT professionals.

The age distribution, presented in Fig. 1 below, shows that the age distribution of the survey participants only poorly matches the actual industry age distribution [15]. Many of the participants are young professionals in the IT sector who recently finished their Master's Program.

Regarding experience and expertise in project management, the survey participants have been asked to evaluate themselves according to a Lickert-Scale from 1 = “very low expertise” to 5 = “very high expertise”.

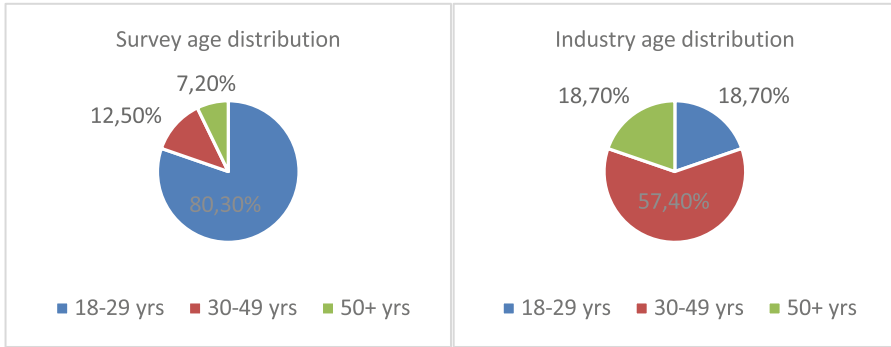


Fig. 1. Age distribution of survey participants.

The result, presented in Fig. 2 shows, that although participants are younger than usual in the industry, most of them evaluate their project management knowledge and experience as sufficient. This positive fact balances the weakness of differing age distribution of participants compared to the industry in general.

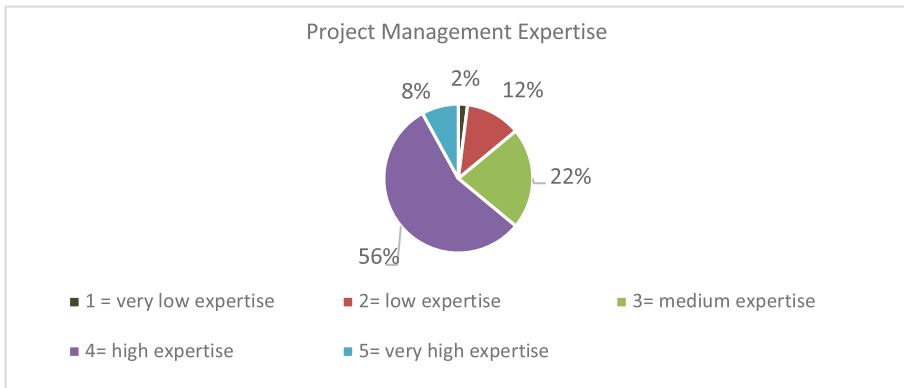


Fig. 2. Self-evaluation of project management expertise.

Considering all influences, it can be concluded that a high percentage of the research participants are fit for answering questions of such specific IT project management-related survey.

4.2 Project Closeout Success and Satisfaction

To evaluate the current situation regarding project closeouts in agile-developed IT projects, the problem statement was verified by investigating if it is clear from the start of the development project how and when a project closeout will happen. To keep the survey complexity as low as possible for participants, a simple yes/no answer was

chosen for verification. As seen in Fig. 3, 66% defined this closeout criterion as available from the beginning. This can be interpreted as a not perfect, however quite good situation. The definition of how and when the closeout will happen is not a big issue in the IT industry. This proves the first part of the hypothesis wrong.

As the trigger of closeouts seems to exist in agile-developed IT projects, it is investigated which element of project fulfillment is responsible for starting a project closeout phase? Presented in the second diagram of Fig. 3, the fulfillment of scope is the biggest trigger of project closeouts. This again falsifies the second part of the hypothesis defining scope as flexible in agile developed projects based on a limited budget and/or time. An additional yes/no question, including a possibility of personal statements, provides input to the second hypothesis. In this question, the second hypothesis is directly stated, and the question of agreement or disagreement is asked. The result of this question presents itself as indifferent. 55% agree with the statement, and 42% disagree. The other 3% used the personal statement. Using the personal statement mentioned that a clear project vision is enough to define a clear scope of a project and therefore reach the vision as a trigger of a project closeout phase. This unclear result again more or less supports the falsification of the second hypothesis.

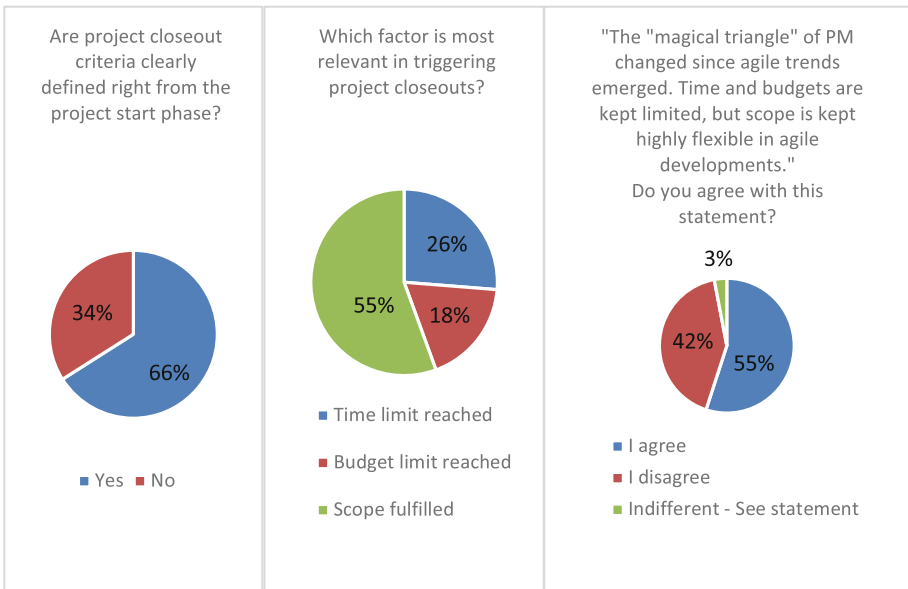


Fig. 3. Closeout triggers and success.

4.3 Need of Project Management Framework Adaption in Agile Developed IT Projects

To finally investigate the formulated hypothesis, that due to an ongoing sprint-based update process, project closeout processes of traditional project management frameworks are outdated, the participants needed to rate the clarity of the switch from the traditional project into ongoing software maintenance and improvement. A low rate of clarity would then indicate the correctness of the hypothesis and the need for project closeout adaptation in agile-developed IT projects.

As shown below and highlighted with a red box, 75 out of 85 participants indicated that the transition process is clear or at least uncritical for the success of the and/or the quality of the project outcome. This falsifies the third part of the hypothesis (Fig. 4).

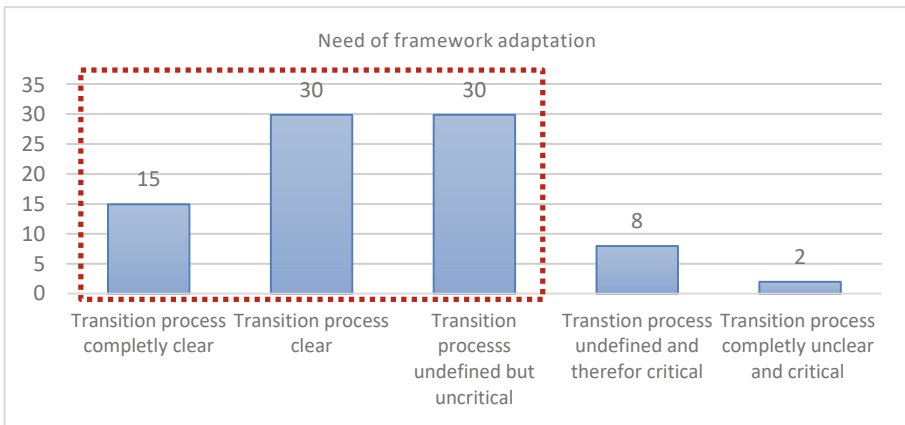


Fig. 4. Need of framework adaptation.

In addition to this evaluation, the possibility of voluntary statements showed a specific proposal for adaptation. Eight of the twelve voluntary statements mentioned a possibility to clarify the transition by officially adding an “Ongoing maintenance phase” to the project, recognizing that this process is by definition not part of the traditional project anymore.

Examples of such statements are: (translated from the German language)

- “I don’t care how many phases a project has; I just need a point to close it and continue with an ongoing process of improvement...”
- “After the last phase of the project, another phase of “Maintenance Process” could be defined.”
- “If an ongoing development phase is added as after the project closeout, the long-term success of projects will be increased, and valuable project resources could be made available for other tasks.”

4.4 Limitations

A total amount of participants of 85 persons could be seen as a weakness of this research. Especially because of the different age distribution in contrast to the industry-specific distribution, highlighted in Fig. 1. Many survey participants come from a part-time student background. Although exact numbers are not available due to the anonymous character of the survey, a large portion of the participants relates to the University of Applied Science FH Campus Wien. This is a weakness of the representability of the survey. However, at the same time, it also can be suggested that agile practitioners may be on average younger than the industry median because agile approaches and the issues of combining agile with traditional project frameworks is a new and trending topic. This assumption could at the same time support the representability of the survey participants.

5 Conclusions

Based on a literature review analyzing three project management frameworks and implications in contrast to agile development approaches, the hypothesis has been postulated that classical project closeout criteria are not perfectly suitable for agile developed IT projects. This hypothesis has been investigated using an online survey targeting agile project practitioners. As a result of this survey, the hypotheses can be falsified due to the following results.

The project closeout seems to be not a real issue for practitioners in agile-developed IT projects. 66% of the survey participants know the specific closeout criteria from the project start.

Triggers of such project closeouts are also different than expected in the hypotheses. More than half of the participants mentioned “Scope fulfillment” as the most relevant trigger. This also contradicts the hypothesis that in agile projects, the scope is highly flexible, and therefore project closeouts are mainly triggered by limited time or budget. The direct question about the need for change in nature of the “magical triangle of project management” has been answered indifferently.

The last part of the problem statement is based on unclear transitions from the project end towards ongoing agile improvement and maintenance processes. This part can also be seen as falsified as 88% of survey participants mention this transition as “uncritical”.

The falsification of all three parts of the hypothesis clearly shows that traditional project management closeout processes and approaches also work in agile developed IT projects. There seems to be no need for agile tailoring. One reason is that project managers are experienced and flexible enough to understand and accept agile characteristics but still manage to integrate them into rigid project management frameworks. The other reason could be that although “labeled” as agile, many IT projects still follow very traditional development structures. Like developing in sprints, but with a completely defined product backlog. As agile development is not a black or white approach, this variance in the “amount of agility” could also be why expected complications seem not to exist.

The closeout phase is just a short single phase in traditional project frameworks. Due to the high amount of failing projects in the IT industry which is rated as high as 64% in agile developed projects [16] and the realization that the closeout phase is less

of a concern, it needs to be evaluated in which project processes the most critical task are hidden. Further, it could be investigated whether an optimization approach based on large amounts of project data could highlight if the usage of certain project processes is useful or maybe even detrimental for project success in agile-developed IT projects.

References

1. Beck, K.: Agile Manifesto (2001). <http://www.agilemanifesto.org/>. Accessed 30 Oct 2020
2. Slinger, M.: Agile Project Management with SCRUM. PMI Global Congress, USA (2011)
3. Grabis, J., Haidabrus, B., Protsenko, S., Protsenko, I., Rovna, A.: Data science approach for IT project management. In: Proceedings of the 12th International Scientific and Practical Conference «Environment, Technology, Resources», pp. 51–55. Rezekne, Latvia (2019)
4. Project Management Institute: A guide to the project management body of knowledge – sixth version. Project Management Institute, Inc., Pennsylvania, USA (2017)
5. Jung, S.: Projektabschluss: Sechs Tipps für wirkungsvolle Projekt Nachbereitung. <https://www.societybyte.swiss/2017/09/29/projektabschluss-sechs-tipps-fuer-wirkungsvolle-projekt-nachbereitung/>. Accessed 30 Oct 2020
6. Homepage of Agile Alliance. <https://www.agilealliance.org>. Accessed 30 Oct 2020
7. Clayton, M.: PMI's Agile Practice Guide: What You Need to Know, Online PM Courses. <https://onlinepmcourses.com/pmi-agile-practice-guide/>. Accessed 30 Oct 2020
8. International Project Management Association. Individual competence baseline, for project, programme portfolio management, GPM Deutsche Gesellschaft für Projektmanagement e.V., Germany (2015)
9. Kuster, J., Bachmann, C., Huber, E.: Handbuch Projektmanagement: Agil -klassisch – hybrid. Springer Gabler, Germany (2019)
10. International Project Management Association. IPMA Reference Guide ICCB in an Agile World Version 2.2, Deutsche Gesellschaft für Projektmanagement e.V., Germany (2018)
11. Homepage of SUKAD Corp. <http://sukad.com/>. Accessed 30 Oct 2020
12. Ajam, M.A.: Project Management Beyond Waterfall and Agile. CRC Press/Taylor & Francis Group, Boca Raton (2017)
13. Haidabrus, B., Protsenko, S., Rosenberger, P., Grabis, J.: Data analysis of readiness programs of machine-building enterprises. In: Ivanov, V., Trojanowska, J., Pavlenko, I., Zajac, J., Peraković, D. (eds.) DSMIE 2020. LNME, pp. 128–136. Springer, Cham (2020). https://doi.org/10.1007/978-3-030-50794-7_13
14. Pflieger, S.: Checkliste: Projektabschluss, InLoox Blog. <https://www.inloox.de/unternehmen/blog/artikel/checkliste-projektabschluss/>. Accessed 30 Oct 2020
15. Homepage of Austrian Chamber of Commerce. Demographic Excel Download. https://news.wko.at/news/oesterreich/Demografische_Entwicklung_in_Unternehmen.html. Accessed 21 Oct 2020
16. StandishGroup, Chaos Report 2018. The Standish Group International Inc. (2018)



Reliability of Road Transport Means as a Factor Affecting the Risk of Failure – The Transport Problem Case Study

Piotr Trojanowski¹  and Justyna Trojanowska² 

¹ West Pomeranian University of Technology in Szczecin, 17, Piastów Avenue, 70-310 Szczecin, Poland

piotr.trojanowski@zut.edu.pl

² Poznan Univeristy of Technology, 3, Piotrowo Street, 61-138 Poznan, Poland

Abstract. The article's objective was to develop a method for analyzing the operational reliability of means of transport, emphasizing destructive factors affecting the disruptions in the continuity of supply. The introduction contains a diagram of the occurrence of adverse events in the transport system. The concept of reliability analysis of rolling stock based on two conditions (its fitness and unfitness) was presented. We describe the proposed method in three stages. The first one is related to activities aimed at extending the fitness condition of the rolling stock. As part of this stage, destructive factors were classified, depending on the rolling stock life cycle phase, with degradation parameters identified and characterized. The second stage concerns diagnostic activities. An approach to assessing damage based on the diagnostic indicator, which resulted in the so-called diagnostic matrix's suggestion, was developed. The last stage of the presented method includes repair activities, based on which the concept of applying risk measures, including the risk measure of rolling stock unavailability, was introduced. The results acquired based on the presented method are designed to provide data enriching the decision-making process in transport activities, aimed at reducing the risk of failure to perform the transport task. The method of analyzing the reliability of means of transport presented in our work forms part of the author's work on developing a comprehensive analysis of the operational reliability of transport systems.

Keywords: Transport engineering · Car stock · Transport systems · Mechanical engineering

1 Introduction

Road transport plays a dominant role in cargo transport in many different countries. It is largely implemented by lorries in the form of road sets consisting of a tractor unit and a semi-trailer. It should be noted that the road rolling stock is one of the elements of the transport system, the reliability of which is of crucial importance for the correct functioning of national economies. There exist many different approaches to reliability concerning transport systems. One of them assumes that the reliability of the system

equals the probability of performing the transport task. Transport disruptions may occur in all parts of the transport system, i.e., road infrastructure, rolling stock, technical facilities, organizational division, etc. However, issues related to infrastructure and road rolling stock play a crucial role here. In connection in addition to that, the reliability models were identified, which include:

- infrastructure failure models,
- rolling stock failure models,
- rolling stock reliability models,
- models taking into account the time and operating cycles of the rolling stock,
- load-endurance models of vehicle structures and infrastructure.

All these models can be either analytical, stochastic, or combined. If the system fails to operate as intended, there has been a loss of reliability. It can adopt different forms, including the partial loss of reliability, e.g., due to a failure of a subsystem of a vehicle, which allows, although with some limitations, to continue the transport, or the total loss of reliability that renders further transport impossible, e.g., due to destruction of means of transportation in consequence of an adverse event. Figure 1 presents the diagram of the occurrence of adverse events in the transport system.

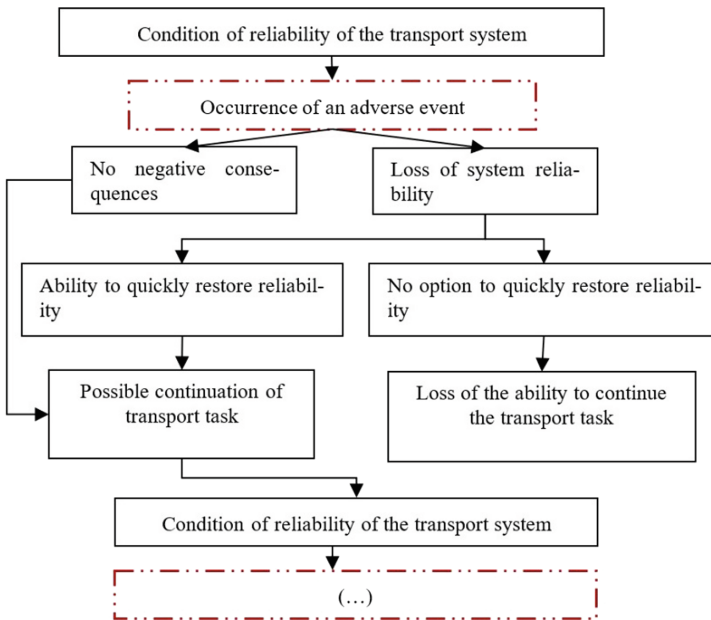


Fig. 1. Diagram of occurrence of adverse events in the transport system.

The presented diagram shows the cyclicity of adverse events occurring during the operation of the transport system. Most of them are left without consequences. Nevertheless, some of them lead to a loss of system reliability of a long-term nature.

In these situations, the inability to continue the transport task may lead to its complete non-performance and the loss of the transported load. To prevent this, on the one hand, research is carried out to prevent the occurrence of adverse events and, on the other hand, to alleviate negative effects, e.g., by quickly restoring the system's reliability they occur. In the case of heavy goods vehicles, it is important to research both to increase their operational reliability and restore this condition as quickly as possible in the event of its loss, both of which are the present article's objective.

2 Literature Review

Transport systems in the context of their reliability are a frequent topic of scientific research. In some cases, the transport system is considered [1–5], and on other occasions, it is divided. This division includes such elements as infrastructure, means of transport, traffic control systems, organizational, legal, and institutional divisions. The important issue from the viewpoint of the present publication, at least as far as road infrastructure reliability is considered, is the occurrence of disturbances discussed, among other things, in [6–9]. Furthermore, the concept of road infrastructure reliability inevitably links us with the concepts of the durability of technical structures, such as bridges [10, 11]. Due to the proposed analysis of the reliability of the transport system narrowed down to one of its elements, i.e., means of transport, our review of subject literature focused primarily on issues related to diagnostic and repair activities and the risk of failure to perform the transport task related to rolling stock's loss of reliability. The diagnostics issues as an activity impacting the reliability of technical structures [12, 13] may include both individual elements and entire systems present in means of transport [14–16]. Particularly noteworthy are the onboard and remote diagnostics mentioned below in the present article, which were the research subjects [17–20] in the last few years. Carrying out diagnostics and repair activities forms the starting point for determining the risk of non-performance of the transport task [21, 22], which was the final part of the author's research. Based on the conducted analysis of the subject literature on the methods of determining risk measures [23–25], we elaborated a concept of measuring the risk of failure to perform the transport task.

3 Research Methodology

Maintaining the operational reliability of means of transport plays a crucial role in maintaining the continuity of supplies. In reality, we observe certain operating cycles, and we can simulate their course. These cycles typically include several conditions, i.e.:

- fitness condition and connected reliability of the means of transport,
- condition of partial unfitness in which it is possible to perform transport tasks, albeit after taking certain limitations into account,
- condition of unfitness, preventing the implementation of tasks.

Different tasks are performed, depending on the current cycle of the means of transport. In the first of them - the condition of fitness - measures are taken to extend it. These

activities include, among others use of the means of transport according to their purpose, ensuring structural strength and efficiency of systems at the production stage, servicing.

The second condition, partial failure, has the most complex characteristics and is also the most common practice condition. What can be related to the complexity of a technical structure in the form of means of transport? Partial unfitness adopts many different forms, from a mild scenario to an extremely destructive one. Damage to parts increasing the comfort of the driver, such as the radio, is of marginal importance in the context of the possibility of performing the transport task, otherwise, when there is damage, for example, to a refrigeration unit when transporting perishable cargo, the vehicle can, at least physically, continue to perform the transport, but there is a serious risk of loss cargo properties, which may lead to failure to perform the transport task. Therefore this particular condition has a non-uniform structure, requiring us to introduce a classification for different failures.

The ultimate condition - the condition of total unfitness - adopts two different forms. The first one concerns the condition in which the means of transport cannot be restored to fitness, or at least such actions are not economically justified, and the vehicle is permanently excluded from further operation. The second form assumes the possibility (and economic justification) for restoring the condition of fitness. For this purpose, diagnostic activities are carried out.

Figure 2 presents a general outline of the transitions of means of transport between the conditions of fitness and unfitness, along with an attempt to restore the desired condition. Based on the presented diagram, we elaborated a method for analyzing the rolling stock's operational reliability, consisting of three stages, with particular emphasis on destructive factors affecting the disruptions in the continuity of supplies and diagnostic and corrective actions aimed at eliminating the disruptions as mentioned above.

Stage I: Activities Aimed at Extending the Roadworthiness of the Rolling Stock

Analysis and classification of factors that impact the possible transition to the condition of unfitness:

- factors of a violent nature, e.g., road collisions, causing a sudden transition to the condition of unfitness in the result of one or more features of the means of transport transferring beyond acceptable standards,
- factors of a reversible nature, e.g., tire wear, predictable and characterized by the ease with which they can be counteracted,
- factors of a slow nature, i.e., aging processes, wear processes, etc., in which case, despite the awareness of their occurrence, it is difficult to determine the moment of transition to the condition of unfitness.

At this stage, the classification of possible degradation factors was also proposed within the adopted classification parameters and types of damage. This classification was based on seven parameters:

1. occurrence of failure, types: rapid, gradual, cascade;
2. connection with other damages, types: dependent, independent;

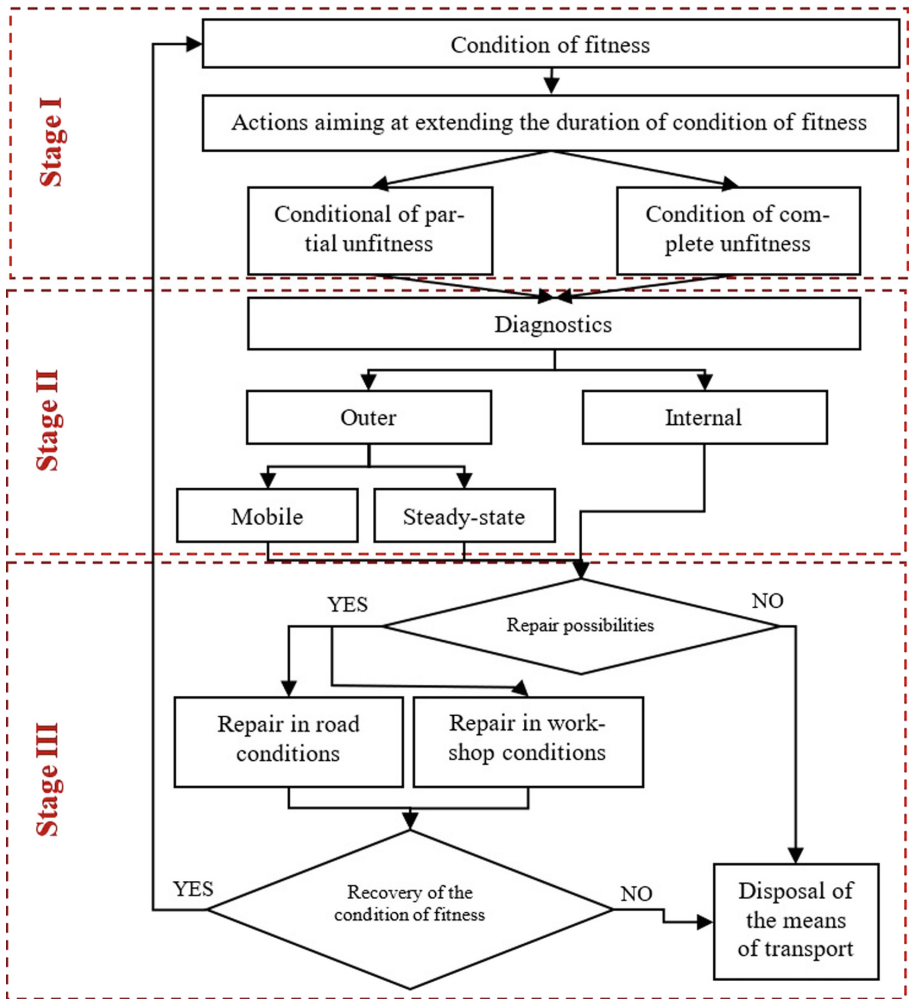


Fig. 2. Diagram of transition of the means of transport to the condition of their fitness/unfitness.

3. repairability, types: full, partial, impossible;
4. necessity to perform repair, types: immediate, recommended, optional;
5. detectability, types: high, low;
6. causes of occurrence, types: natural, artificial;
7. time-consuming repair, types: high, low.

The analysis and classification aimed to provide tools supporting the decision-making process aimed at extending the fitness of the means of transport.

Stage II: Diagnostic Activities

Diagnostics are used to examine the current condition and identify possible faults. Defects occurring in means of transport can be very diverse, and therefore there exists a

wide variety of diagnostic tools. Based on the literature review, we identified the diagnostic methods. These methods can be divided into traditional ones, i.e., functional control, condition control, fault location, and mathematical methods, i.e., deterministic, stochastic, and simulation models. The comparative analysis of the measured parameters and their comparison to theoretical values is also a frequently applied method.

Diagnostics also supports the decision-making process related to servicing the operated rolling stock and allows us to assess whether the rolling stock's condition was restored.

Diagnostic systems should be considered according to two categories. Internal, concerning onboard equipment and decision support systems, and external, i.e., stationary (workshop-installed) and mobile (which can be performed in road conditions) diagnostics. An important part of diagnostics is the tests of accident-damaged means of transport. On their basis, parameters such as the roadworthiness/unfitness of the vehicle, the damage and the mechanisms of its occurrence, the possibility of repair, etc., are all determined.

Stage III: Repair Activities

Repair activities are directly related to diagnostics. Their implementation is possible only after the identification of damaged parts. As was the case in stage II, repair activities can be divided into those performed in road conditions (mobile) and those performed in workshop conditions (stationary). In the case of cargo transport, especially in the context of perishable cargo, ad hoc repairs play an important role, enabling the continuation of transport, taking into account the limitations resulting from less repair possibilities under road conditions. Nevertheless, there are economic reasons for this, because the disruption of the continuity of transport is often associated with failure to meet delivery terms, which results in contractual penalties. The recent development of services in the just-in-time system further strengthens the requirement to create a network of mobile diagnostic and repair centers.

The methodology of analysis of operational reliability of means of transport and its restoration methods presented in our work forms one of the elements of the author's work on the creation of a comprehensive assessment of operational reliability of transport systems.

4 Results

The results will be discussed in stages proposed in the methodology. Stage I: What is important is that not every defect leads to permanent damage to the vehicle. Therefore, cyclical reliability assessments should be carried out by analyzing changes occurring in the used vehicle. In addition, it is recommended to prepare forecasts of the impact of individual factors, depending on environmental conditions. The impact assessment of individual factors on the fitness of the rolling stock was classified according to the phases of the life cycle of the means of transport and presented in Table 1.

Stage II: Damage assessment can be performed using a comparative analysis of functional parameters $f(x)$. According to the theory, each of the parameters can take values within the defined min-max range. Moreover, the so-called diagnostic indicator

Table 1. Assessment of the impact on the fitness in particular phases of the rolling stock life cycle.

Stage	The phase of the rolling stock life cycle	Assessment factors
I	Novelty phase - post-production	Manufacturing defects
II	The main phase	Natural wear of a predictable nature
III	Aging period	Unpredictable aging and wear processes
I–III	Following restoration to fitness	Repair activities and their impact on the means of transport

λ , which determines whether the parameter has exceeded the permissible values, may adopt the value 0 or 1. In the case of fault diagnosis, it is assumed that the diagnostic indicator $\lambda = 1$, when:

$$f(x)_{min} > f(x) \wedge f(x)_{max} < f(x) \tag{1}$$

In the case of no failure, when the diagnostic indicator $\lambda = 0$, the following relationship is satisfied:

$$f(x)_{min} < f(x) \wedge f(x)_{max} > f(x) \tag{2}$$

The application of the above method enables the creation of a matrix of diagnostic results, as presented in Table 2.

Table 2. Diagnostic matrix.

No.	Diagnostic indicator λ	Damages					
		f1	f2	...	f _i	...	f _n
1.	λ_1	0	1		0		0
2.	λ_2	1	1		0		1
3.
4.	λ_i	1	0		1		0
5.
6.	λ_m	0	1		0		0

Stage III: We developed risk measures to obtain indicators enabling the assessment of the risk of failure to perform the transport task. These measures were divided into several issues. One of them is the calculation of the risk measure of the rolling stock unavailability MR_{RSU} , calculated as the ratio of the average rolling stock availability time to the sum total of this time and the duration of diagnostic and repair activities, i.e.:

$$MR_{NT} = 1 - \frac{T(z)}{[T(z) + T_{DN}]}, \tag{3}$$

where: $T(z)$ - the average service life of the rolling stock, T_{DN} - average time of diagnostic and repair activities.

The comprehensive analysis of the risk of failure to perform the transport task will be further enriched with the risk measure of an undesirable event, as developed by the author.

5 Conclusions

Developing an effective strategy to extend the roadworthiness of road rolling stock requires in-depth knowledge of the phases of the life cycle of vehicles and the factors contributing to the formation of degradation processes in technical systems.

The conducted research on car diagnostics allowed us for their division into stationary and mobile diagnostic activities. The latter is particularly important in terms of maintaining continuity of supplies. One of the most common reasons necessitating diagnostic operations is the occurrence of damage, e.g., due to a collision. It is connected with the intensive exploitation of these vehicles. The proposed diagnostic indicator enables the assessment of the tested object's suitability based on a comparative analysis of its functional parameters. In the event of a condition of unfitness, it is necessary to carry out corrective actions. Whenever possible, it is recommended to perform the repair in road conditions, but if this proves impossible, there is a need to send a replacement unit, which contributes to delays and, consequently, to failure to perform the transport task. Considering the issues mentioned earlier, a measure of the risk of failure to perform the transport task was elaborated, based on the average time the means of transport remain in a fit condition and the average duration of diagnostic and repair activities.

Based on the method for assessing the reliability of means of transport presented in the paper, we can conclude that it is justified to develop a comprehensive methodology for evaluating the reliability of transport systems with a holistic approach, applying system analysis.

References

1. Soltani-Sobh, A., Heaslip, K., Stevanovic, A., El Khoury, J., Song, Z.: Evaluation of transportation network reliability during unexpected events with multiple uncertainties. *Int. J. Disaster Risk Reduct.* **17**, 128–136 (2016)
2. Walther, C., Niemeier, E.: Reliability in transport systems: what do we really know? In: 26th World Road Congress World Road Association (PIARC) (2019)
3. Gidebo, F.A., Szytko, J.: Reliability assessment of the transport system, Addis Ababa case study. *J. KONBiN* **49**(4), 27–36 (2019)
4. Shramenko, N., Muzylyov, D.: Forecasting of overloading volumes in transport systems based on the fuzzy-neural model. In: Ivanov, V., et al. (eds.) *DSMIE 2019. LNME*, pp. 311–320. Springer, Cham (2020). https://doi.org/10.1007/978-3-030-22365-6_31
5. Semenov, I.N., Filina-Dawidowicz, L.: Topology-based approach to the modernization of transport and logistics systems with hybrid architecture. Part 1. Proof-of-concept study. *Arch. Transp.* **43**, 105–124 (2017)
6. Jacyna, M., Żak, J.: Simulation models in testing reliability of transport process. *J. KONBiN* **37**(1), 203–230 (2016)

7. Islam, M.R., Kalevela, S.A., Rivera, J.A., Rashid, T.B.: Dynamic modulus and field performance of cold-in-place recycled asphalt pavement. *J. Eng. Sci.* **6**(2), B1–B7 (2019). [https://doi.org/10.21272/jes.2019.6\(2\).b1](https://doi.org/10.21272/jes.2019.6(2).b1)
8. Kawa, A., Anholcer, M.: Exclusionary constraints in transport-results of quantitative research. *LogForum* **16**(4), 573–592 (2020)
9. Kim, H., Kim, C., Chun, Y.: Network reliability and resilience of rapid transit systems. *Prof. Geogr.* **68**(1), 53–65 (2016)
10. Teichgraeber, M., Hawryszków, P.: The SHM system as a data source for durability assessment. Case study of Rędzński Bridge stay cable system. *MATEC Web Conf. EDP Sci.* **219**, 03012 (2018)
11. Soltani-Sobh, A., Heaslip, K., Scarlatos, P., Kaiser, E.: Reliability based pre-positioning of recovery centers for resilient transportation infrastructure. *Int. J. Disaster Risk Reducti.* **19**, 324–333 (2016)
12. Pavlenko, I., Ivanov, V., Kuric, I., Gusak, O., Liaposhchenko, O.: Ensuring vibration reliability of turbopump units using artificial neural networks. In: Trojanowska, J., Ciszak, O., Machado, J.M., Pavlenko, I. (eds.) *MANUFACTURING 2019. LNME*, pp. 165–175. Springer, Cham (2019). https://doi.org/10.1007/978-3-030-18715-6_14
13. Pavlenko, I., Trojanowska, J., Ivanov, V., Liaposhchenko, O.: Parameter identification of hydro-mechanical processes using artificial intelligence systems. *Int. J. Mechatron. Appl. Mech.* **2019**(5), 19–26 (2019)
14. Goncharov, A.E., Bondarenko, E.V., Krasnoshtanov, S.Y.: Theoretical aspects of diagnostics of car as mechatronic system. *MS&E* **327**(4), 042037 (2018)
15. Fedotov, A.I., Kuznetsov, N.Y., Lysenko, A.V., Vlasov, V.G.: Car suspension system monitoring under road conditions. In: *AIP Conference Proceedings*, vol. 1915, no. 1, p. 040014. AIP Publishing LLC. (2017)
16. Komorska, I., Wólczyński, Z.: Fault diagnostics of air intake system of the internal combustion engine. In: Timofiejczuk, A., Łazarz, B.E., Chaari, F., Burdzik, R. (ed.S.) *ICDT 2016. ACM*, vol. 10, pp. 91–100. Springer, Cham (2018). https://doi.org/10.1007/978-3-319-62042-8_8
17. Dragojević, M., Stević, S., Stupar, G., Živkov, D.: Utilizing IoT technologies for remote diagnostics of next generation vehicles. In: 2018 IEEE 8th International Conference on Consumer Electronics-Berlin (ICCE-Berlin), pp. 1–4. IEEE (2018)
18. Kalmeshwar, M., Prasad, K.N.: Development of on-board diagnostics for car and it's integration with Android mobile. In: 2017 2nd International Conference on Computational Systems and Information Technology for Sustainable Solution (CSITSS), pp. 1–6. IEEE (2017)
19. Naik, P., Kumbi, A., Telkar, N., Kotin, K., Katti, K.C.: An automotive diagnostics, fuel efficiency and emission monitoring system using CAN. In: 2017 International Conference on Big Data, IoT and Data Science (BIGDATA), pp. 14–17. IEEE (2017)
20. Kirthika, V., Vecraraghavatr, A.K.: Design and development of flexible onboard diagnostics and mobile communication for internet of vehicles. In: 2018 International Conference on Computer, Communication, and Signal Processing (ICCCSP), pp. 1–6. IEEE (2018)
21. Vilko, J., Ritala, P., Hallikas, J.: Risk management abilities in multimodal maritime supply chains: visibility and control perspectives. *Accid. Anal. Prev.* **123**, 469–481 (2019)
22. Goloshchapova, L., Plaskova, N., Prodanova, N., Yusupova, S., Pozdeeva, S.: Analytical review of risks of loss of profits in cargo transportation. *Int. J. Mech. Eng. Technol.* **9**(11), 1897–1902 (2018)
23. Filina-Dawidowicz, L., Iwańkiewicz, R., Rosochacki, W.: Risk measures of load loss during service of refrigerated containers in seaports. *Archiv. Transp.* **34**, 19–27 (2015)
24. Antosz, K., Stadnicka, D.: Evaluation measures of machine operation effectiveness in large enterprises: study results. *Maint. Reliab.* **17**, 107–117 (2015)
25. Świdorski, A., Józwiak, A., Jachimowski, R.: Operational quality measures of vehicles applied for the transport services evaluation using artificial neural networks. *Maint. Reliab.* **20**, 292–299 (2018)



An Intelligent Scheduling System Architecture for Manufacturing Systems Based on I4.0 Requirements

Leonilde Varela , Vaibhav Shah , Aurélio Lucamba , Adriana Araújo ,
and José Machado 

University of Minho, Campus de Azurém, 4804-533 Guimarães, Portugal
jmachado@dem.uminho.pt

Abstract. In this paper, an Industry 4.0 oriented architecture of a manufacturing scheduling decision support system is provided. This proposal is based on an analysis performed about some other decision support systems architectures found in the literature and based on another analysis that was carried out regarding the results obtained through a questionnaire distributed through a wide set of enterprises in the Iberian Peninsula. This analysis did enable us to realize that the main characteristics considered fundamental to be integrated into the proposed manufacturing scheduling decision support system were, in fact, of utmost importance, within the current Industry 4.0 requirements. Moreover, the main characteristics proposed for integrating the manufacturing scheduling decision support system's architecture presented were also used to establish a comparative analysis between the proposed system's architecture and the ones analyzed from the literature. Besides, through this analysis, it was possible to realize that none of the architectures analyzed from the literature covered the whole set of important I4.0 oriented characteristics proposed.

Keywords: Intelligent manufacturing scheduling · Decision support system architectures · Industry 4.0

1 Introduction

Manufacturing scheduling (MS) decision support systems (DSS) are of utmost importance for companies, namely the industrial ones, and several types of systems have been put forward and used over the last decades, based on different types of underlying approaches and methods for solving the MS problems. MS DSS, either in their more traditional or conventional form, or web-based systems or platforms, aim currently, in the context of Industry 4.0 or I4.0 [1], to fulfill the associated general recommendations [2], by making use of exponential technologies [3], and satisfying digital workplace requisites [4] for reaching the expected readiness stage [5], for solving complex and dynamically changing manufacturing problems occurring in the cyber-physical systems [6, 7]. Thus, further integrating robots and other automated resources and devices [8, 9] and enabling simultaneous modeling and other I4.0 requisites [9, 10]. Furthermore, it is now of utmost

importance to follow some I4.0 architecture [11, 12] regarding the current need for digitalization [13, 14], based on the internet, and remote processing capabilities [15, 16], along with other general I4.0 purposes [17].

Therefore, regarding manufacturing management functions [18, 19], combined with sustainable practices [20], it is essential to apply proper optimization approaches [21, 22], further applicable in other contexts [23].

Therefore, in this work, an MS DSS architecture is put forward to contribute to the state-of-the-art and achieve the I4.0 requisites. For accomplishing this objective, one of the fundamental tasks underlying this work consisted of a study to survey architectures of existing DSS, namely to support MS, such as [21, 22]. It also turned out to be essential to obtain a set of main characteristics considered fundamental ones in MS DSS currently oriented to I4.0. Thus, several sources related to I4.0 main pillars or dimensions were analyzed, for instance [1, 2].

In order to validate the importance of the fundamental characteristics identified through the developed study, an additional study was also carried out, based on the results of a survey that was put available through a widened range of companies in Portugal and Spain, for which a set of 198 valid results were obtained.

The results obtained through the surveys allowed to give consistency to a proposal of an architecture of an MS DSS, based on Artificial Intelligence (AI), along with other I4.0 oriented features to respond to the current requirements imposed by the I4.0 [1, 2].

For exposing the main contributions of the work underlying this paper, it is structured as follows: In Sect. 2, a brief description of some of the main DSS architectures directed to I4.0 issues, and with a particular focus on MS, are presented. In Sect. 3, the proposed I4.0 oriented MS DSS architecture is briefly described. In Sect. 4, an analysis and evaluation of main characteristics underlying I4.0 oriented DSS are presented, and a comparative analysis with the proposed architecture is performed, based on the related systems analyzed and on the validation that was performed through the analysis of the results obtained through the questionnaire. Finally, in Sect. 5, the main conclusions reached through this work are summarised, and some open issues for future work.

2 Literature Review

In this section, a set of DSS, mainly for supporting MS, will be briefly presented, with particular emphasis on proposals for more recent systems' architectures and with different types of interactions with other peripheral devices and systems, in order to allow further integration of scheduling with other management functions, such as master production, and orders and process planning, along with lot sizing, and materials management and its acquisition, besides layout optimization, among other manufacturing management functions, which may range from the product design phase to products distribution, through complete and integrated logistic networks, along with reverse and reengineering processes [18].

2.1 Integrated Networked Process Planning and Scheduling System

Integrated process planning and scheduling systems are described in [22, 23] and extended in [24]. In the paper [24], a network system architecture for integrating process

planning functions with production scheduling is proposed. In that, the integration of these two functions with several additional modules and functions is also considered, which allows, from the automatic acquisition of data from the production system to access to a set of services, dispersed across the network, through the Cloud, to fully accomplish production scheduling integrated with process planning [24].

2.2 Decision System for Setups Scheduling Based on Multivariate Data Analysis

In [25] an Interoperable DSS is presented based on multivariate time series for processing and visualizing data related to production scheduling with setups. In this system, the authors included three main modules for data pre-processing and its acquisition from the manufacturing system through various technologies, such as PLC/Smart object, RFID, and a set of sensors. Also included in the system were user interfaces with pre-processing of the data, to subsequently feed a scheduling module, based on an MS knowledge base, available on the Cloud, which integrates an ontology to support the selection of appropriate MS algorithms for each type of MS problem [24, 25]. Moreover, this module connects to another module that enables post-processing of MS data, namely about machines setups, along with other data, such as processing, waiting, machine stoppages, and their causes, which are processed, analyzed, and visualized based on a multivariate data analysis software [25].

2.3 Hybrid System to Support Scheduling in Distributed Environments

An architecture of a hybrid system to support MS in complex extended or distributed production environments, based on a knowledge-based system (KBS), is presented in [26]. In this paper, the distributed KBS includes helpful information to select MS methods in complex and distributed companies, including virtual enterprises. Collaboration between the various companies and the sharing of MS problems and methods is an important asset. In the system's architecture, a main central component includes an inference mechanism based on two indexes to help classify the usefulness of the various types of information related to problems, solve methods and the alternative solutions given by applying different types of MS algorithms.

2.4 I4.0 Oriented Scheduling System Based on Dynamic Selection of Dispatching Rules and the Kano Model

Another MS DSS, oriented towards I4.0 and based on a dynamic selection mechanism for dispatching rules supported by the Kano model, is presented in [27]. Through this system, a user can specify the MS problem's characteristics to solve [26, 27], including a set of one or more performance measures to be optimised, and an automatic solution will be generated dynamically by the system. This whole automatic process and the ability to refine solutions obtained for a given type of MS problem are controlled by implementing the Kano method that provides this MS support system an essential and differentiating value in the current I4.0 context [27].

2.5 Hybrid Scheduling System Based on Multi-agents and Meta-heuristics

In [28], a hybrid system supporting production scheduling and adjustments to the production systems' configuration centered on the human and based on multi-agents and meta-heuristics is presented. The system allows quick and adjusted responses, in real-time, based on the multi-agent system, and combined with a PSO (Particle Swarm Optimization) algorithm, to solve both kinds of problems [28] jointly. Although this may be minimal and thus, the system allows for human intervention to obtain optimized solutions, being a system that adapts easily to unexpected events, adjusting itself according to the priorities established by the human through a user-friendly interface. The system also allows evaluating the performance of the developed algorithms and the decentralized response capacity in case of several interruptions or failures [28].

2.6 Scheduling System Based on Self-organized Negotiation Mechanism and Collective Intelligence

The authors in [29] propose an MS DSS based on a self-organized negotiation mechanism and collective intelligence (swarm intelligence). Under the negotiation, mechanism agents interact and collaborate to improve a global production program. Through this system, several agents can reach an agreement on the exchange of operations on competitive resources, using approaches based on artificial bee colony (ABC), to minimize the total production time of a set of jobs to be processed in a given production system, and which also aims at maximizing the occupation of the corresponding machines.

2.7 Road Anomaly Detection System

Another system, which, although not being an MS DSS, is also an interesting I4.0 oriented DSS or recommendation system, based on AI approach, for instance on Machine Learning, with an architecture projected to detect and plan information about road anomalies [30]. In this system, the difference between the implementation of detection and identification of system road anomalies in a "conditioned" configuration and the real world is analyzed, based on training data sets and analysis of the complexity of the attributes, through the application of PCA techniques, and analyzing the attributes in the context of each type of anomaly, using the standard deviation of acceleration to observe how different classes of anomalies are distributed in the Cartesian coordinate system. In this system, the road anomaly and vehicle data are collected during condition activities using smartphones and a web application to identify anomalies on the roads [30].

3 Research Methodology

In this, the authors propose an architecture of an MS DSS based on a set of characteristics that were proposed as being fundamental ones, based on a study carried out through the literature about fundamental I4.0 pillars or dimensions, along with the analysis of some existing DSS architectures, as previously briefly described.

3.1 Main I4.0 Oriented DSS Characteristics

From the analysis previously carried out and synthesized in the previous section about some existing DSS, along with the study about main I4.0 pillars and dimensions, it was possible to verify that there is a set of general characteristics that appear to be fundamental and transversal to the various types of DSS architectures [31], namely to support MS [32] in the currently I4.0 oriented context [33], and that are related to:

1. Horizontal and vertical integration of systems and processes [34, 35];
2. Storage, processing, and analysis of large volumes of diversified data (Big Data) [36, 37];
3. Use of AI-based technologies and approaches, e.g., based on Machine Learning [38, 39];
4. Use of diverse digital technologies, such as IoT/ IIoT, RFID, and Cloud [40, 41];
5. Use of augmented reality (AR) technologies [42, 43];
6. Development of human-centered decision support systems (HC-DSS) [44, 45].

3.2 Proposed Architecture

A proposed MS DSS architecture is briefly described in this section, based on six main I4.0 oriented characteristics previously identified (Fig. 1).

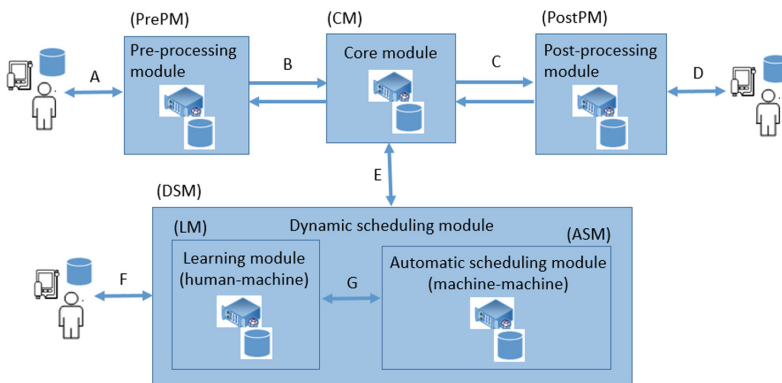


Fig. 1. Proposed manufacturing scheduling decision support system’s architecture.

As can be seen from the analysis of Fig. 1, the proposed architecture of an MS DSS is based on 4 main modules or components: 1. PrePM - Data Pre-processing Module; 2. CM - Central Module; 3. PosPM - Data post-processing module; and 4. DSM - Dynamic Scheduling Module, which, in turn, is subdivided into modules LM - Learning Module and ASM - Automatic Scheduling Module.

Besides, the following main interactions are also presented in this figure: A: User - PrePM; B: PrePM - CM; C: CM - PosPM; D: PosPM - User; E: CM - DSM; F: User - DSM; and G: LM – ASM.

Through the MS DSS's proposed architecture, the possibility of pre-processing data related to MS problems, through a human-machine interaction ('A') is based on the PrepPM module for data pre-processing. This module is considered a fundamental one, as it intends to allow pre-filtering, analysis and validation of MS data, through an experienced user, which is considered very relevant, in order to allow the entire integrated DSS, consisting of the various interconnected modules, to work effectively, and also as efficiently as possible.

The central module (CM), as the name refers, is a central one, which communicates with the remaining modules of pre and post-processing (PrePM and PostPM) and with the dynamic scheduling module (DSM). Through the interaction with the other modules, the CM allows to ensure the smooth functioning of the MS DSS, as a whole, as it is responsible for several interconnections and interfaces between the various modules. As well as for controlling the operation of the system as a whole, both in terms of processes and subsystems linked internally in a company, plus, in order to allow interaction and integration of processes at a more general level, namely with other business partners, through of various digital technologies, such as IoT/ IIoT, RFID, Cloud, and the like, which are considered fundamental not only to ensure proper integration, horizontally and vertically, within a company but also at a broader level, for collaboration with other business partners, for instance, at the level of integration and remote order processing, which may also further imply Augmented Reality technology integration.

The DSM, composed of the learning module (LM) and automatic scheduling module (ASM), is responsible for the entire MS process. The module executes, locally or remotely, MS algorithms specific for solving each MS problem instance. Therefore, this module is also of utmost importance and enables an interaction ('E') with the CM, which interacts and exchanges information and processes with the PrepPM and PostPM through the corresponding interactions 'B' and 'C', respectively.

Through the LM, the system allows learning the most appropriate way to solve an MS problem, based on stored historical information, regarding the previous solutions of related problems or with some degree of similarity, as well as through help from an experienced user who interacts ('F') with this module, which incorporates a set of ML algorithms for that purpose. In this way, this user works as an 'oracle', whose primary function is to provide 'positive' or 'good' examples, and 'negative', 'bad' or 'invalid' ones, which allow the LM to learn to solve MS problems effectively.

The other module that integrates the DSM, the ASM, further aims to solve, autonomously and automatically, instances that belong to different types of MS problems that are already known by the DSS, as they have already been solved by the system before.

Another module considered of fundamental importance to integrate the MS DSS is the PostPM, which also communicates ('C') with the CM and interaction with an experienced user ('D'), in order to enable post-filtering, analysis, and validation of solutions provided for MS problems, through the DSM. This module is also extremely important, not just to pass valid final information or decision to the production system that will produce the works according to the production program found, in a dynamic way. However, also due to the importance it has regarding the feedback for the CM, and subsequently to the DSM, constantly provided with new information, which is crucial

for the good functioning of the MS DSS, as a whole, and concretely in what it refers to the provision of “historical” data to enrich and improve the learning process, which occurs in the corresponding LM.

4 Results

In this section, the set of fundamental characteristics considered for being incorporated in the proposed I4.0 oriented MS DSS were subject to a validation of their effective importance based on the results of a survey that was distributed through a wide and diversified group of companies of the Iberian Peninsula (Portugal and Spain).

Moreover, based on this set of main I4.0 oriented characteristics, a comparative analysis between the proposed MS DSS and the other DSS analyzed is performed.

4.1 Validation of the Importance of the Main I4.0 Oriented Characteristics

Following the literature review and study carried out on MS DSS architectures, as summarized in the previous Sect. 2, and once performing a deep analysis of each one of the main characteristics underlying the intended I4.0 main DSS architectures’ characteristics, a questionnaire was developed and distributed through a widened set of companies in the Iberian Peninsula (Portugal and Spain), based on the set of fundamental questions related to the main characteristics identified as corresponding to the most relevant ones to be met regarding the current requirements imposed by the I4.0, and the obtained main results reached are presented next, in Tables 1 and 2, and in Fig. 2.

Table 1 shows the number of responses obtained for each degree of agreement regarding the set of questions Q1 to Q6 posed through the survey distributed through a set of 256 companies from the Iberian Peninsula, from which a total of 198 valid questionnaires were obtained. In this questionnaire, “1” corresponds to an answer in which the respondent is entirely at odds with the statement and “6”, the case in which it is entirely in agreement with the statement, with the case of “3” being indifferent, that is, he or she does not agree or disagree with the corresponding statement or has no opinion about the statement.

Regarding the identification of the minimum and maximum values in the results obtained for each question (Q1 to Q6) it is possible to verify, for example, that there was no answer, among the 198 obtained, that corresponded to answer “1” (1 - Completely disagree), in question 5 (Q5).

On the other hand, this same question 5 (Q5) was also the one that obtained the highest number of responses of the type “3” - Indifferent, neither in agreement nor disagreement, in a total of 91 valid responses.

Besides, some more values were determined regarding the descriptive statistical analysis of the results obtained by the respondents, in order to clarify better the analysis of these results obtained, by calculating the value of the responses’ weighted average (RWA), and also of the responses’ range of variations (RRV), expressed in Table 2.

Table 1. Number of valid responses obtained for questions Q1 to Q6, for each degree of agreement from 1 to 5.

Response		1	2	3	4	5
Question	Q6 (Human-centred decisions)	3	15	71	56	44
	Q5 (Augmented Reality)	0	27	91	45	35
	Q4 (IoT/IIoT, RFID, Cloud)	3	12	59	69	55
	Q3 (Machine Learning)	19	14	69	68	28
	Q2 (Big Data)	12	28	67	66	25
	Q1 (Integration)	2	10	59	75	52

Through the analysis of the results presented in Table 2, regarding the values obtained for the range of variation of the survey results, it is possible to verify that the questions Q5 ('Augmented Reality'), Q1 ('Integration'), and Q6 ('Human-cantered decisions') were the ones that presented a greater range of variation in the response values, respectively.

Table 2. Responses' weighted average (RWA) and range of variations (RRV).

Question	RRV	RWA
Q6 (Human-centred decisions)	68	46,0
Q5 (Augmented Reality)	91	45,5
Q4 (IoT/ IIoT, RFID, Cloud)	66	50,3
Q3 (Machine Learning)	55	44,4
Q2 (Big Data)	55	43,9
Q1 (Integration)	73	50,6

In Fig. 1 it is also possible to see these distributions of the numbers of responses obtained. Regarding the values obtained for the weighted averages of the survey results, it is possible to verify that the answers that obtained the highest score, therefore, a more consistent validation, were the questions Q1 ('Integration'), Q4 ('IoT/ IIoT, RFID, Cloud'), and Q6 ('Human-cantered decisions'), respectively, although the rest did also receive positive and good validation scores, with relatively close values.

From the analysis of the results obtained to the distributed survey, it is possible to verify, regarding the mode identified for each of the groups of results underlying the questions from Q1 to Q6, that:

1. In question 1 (Q1 – ‘Integration’), there was a greater concentration of responses of type “4” (‘Agreement’).
2. In question 2 (Q2 – ‘Big Data’), there was a greater concentration and practically the same number for responses of type “3” (‘Neither agreement nor disagreement’) and type “4” (‘Agreement’).
3. In question 3 (Q3 – ‘Machine Learning’), there was a greater concentration and also practically the same number for responses of type “3” (‘Neither agreement nor disagreement’) and type “4” (‘Agreement’).
4. In question 4 (Q4 – ‘IoT/ IIoT, RFID, Cloud’), there was a greater concentration of responses of type “4” (‘Agreement’).
5. In question 5 (Q5 – ‘Augmented Reality’), there was a greater concentration of responses of type “3” (‘Neither agreement nor disagreement’), with no response of type “1” (‘Completely disagree’).
6. In question 6 (Q6 – ‘Human-centred decision-making or Oracle’), there was a greater response of type “3” (‘Neither agreement nor disagreement’), although it did also occur a high number of responses of types “4” (‘Agreement’), and “5” (‘Completely in agreement’).

Therefore, through the analysis of the responses obtained to the survey, it is possible to conclude that, in general, it was noticed that there was no doubt, on the part of the respondents, that all these characteristics considered when designing architectures of MS DSS are important ones to be considered.

Additionally, it was possible to verify that the questions Q1 (‘Integration’), and Q4 (‘IoT, IIoT, RFID, Cloud, and similar technologies’) were those in which the respondents most clearly agreed, in general (“4” – ‘Agreement’), as well as regarding the importance of having a person at the center of the decision-making process (Q6 – ‘Human-centered decisions’), which did also reach a very good level of agreement.

Regarding the other two questions (Q2 – ‘Big Data’, Q3 – ‘Machine Learning’, and Q5 – ‘Augmented Reality’), although all of them were also considered essential issues, that is, essential characteristics to be considered in the architectures of MS DSS, the Q5 (‘Augmented Reality’) was the one that obtained a relatively greater importance confirmation, followed by questions Q3 (‘Machine Learning’) and Q2 (‘Big Data’).

4.2 Comparative Analysis of the Proposed Architecture with Similar Ones

In this section, the results obtained about the comparative analysis carried out between the various architectures of DSS from the literature with the proposed one are briefly described, and the main result obtained is shown in Table 3.

Based on the results expressed in Table 3, it is possible to verify that although, in general, all the fundamental characteristics, which were analyzed, through the questions Q1 to Q6 considered through the distributed questionnaire. There is no existing architecture of DSS that focuses on all 6 underlying issues or characteristics. Those that focus on a more significant number of characteristics are the architectures underlying the S1 [24] and S3 [26] systems, which focused on 5 characteristics, followed by the architectures of the systems S2 [25], and S7 [30], with 4 characteristics and followed by

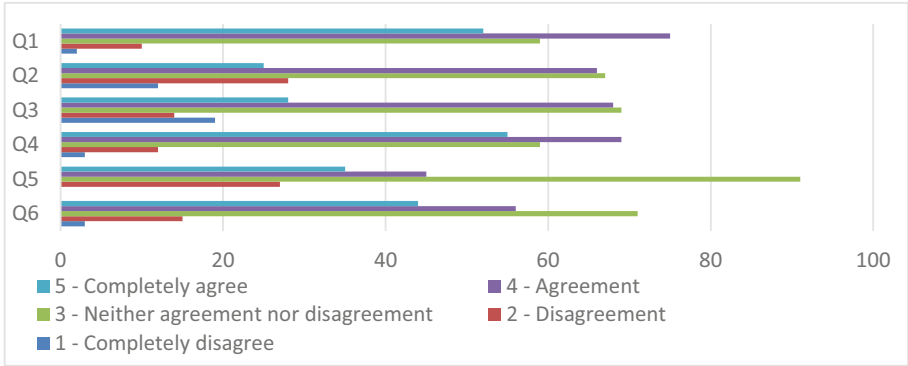


Fig. 2. Histogram of frequencies about the number of responses by a degree of agreement in questions Q1 to Q6.

the S4 [27], and the S6 [29], with 3 characteristics and, finally, by the S5 system [28], with 2 characteristics.

Therefore, it can be concluded that just the DSS proposed (S8) focuses on the 6 characteristics considered relevant for supporting MS in the current I4.0 context.

Table 3. Synthesis of comparison of the proposed architecture with similar ones.

Characteristic System	Integration (Q1)	Big Data (Q2)	AI/Machine Learning (Q3)	IoT/IIoT, RFID, Cloud (Q4)	Augmented Reality (Q5)	Human-centered decisions (Q6)	Number of focused characteristics
S1 [24]	X	X	X	X	X		5
S2 [25]	X	X		X		X	4
S3 [26]	X	X	X	X		X	5
S4 [27]	X		X			X	3
S5 [28]			X			X	2
S6 [29]		X	X			X	3
S7 [30]	X	X	X	X		X	4
S8 [Proposed]	X	X	X	X	X	X	6

5 Conclusion

In this paper, an analysis and evaluation of some existing DSS architectures, along with a proposal of an architecture of a DSS to support manufacturing scheduling (MS) was provided, based on a study carried out for identifying a set of main characteristics that are fundamental in the current I4.0 context.

Moreover, based on the study accomplished, it was also possible to validate the importance of the set of characteristics considered in the scope of I4.0 through the results obtained from 198 valid questionnaires that were put available to Portuguese and Spanish Companies.

Additionally, the main characteristics underlying the proposed MS DSS architecture were further analyzed through a study that was performed to establish a comparative analysis between the proposed architecture and the ones underlying the other system's architectures that were explored. This comparative analysis realized that no other existing DSS architecture, among the ones analyzed, besides the one proposed in this paper, refers to the whole set of 6 main I4.0 oriented characteristics considered.

It will be essential to develop the proposed MS DSS architecture to be implemented and used in different industrial companies in terms of future work.

Acknowledgment. This work has been supported by FCT – Fundação para a Ciência e Tecnologia within the R&D Units Project Scope: UIDB/00319/2020, and UIDP/04077/2020.

References

1. Xu, L.D., Xu, E.L., Li, L.: Industry 4.0: state of the art and future trends. *Int. J. Prod. Res.* **56**(8), 2941–2962 (2018)
2. Kagermann, H., Hellbig, J., Hellinger, A., Wahlster, W.: Recommendations for implementing the strategic initiative INDUSTRIE 4.0: securing the future of German manufacturing industry; final report of the Industrie 4.0 Working Group. Forschungunion (2013)
3. I4.0 technologies. <https://www.intechopen.com/books/digital-transformation-in-smart-manufacturing/fourth-industrial-revolution-current-practices-challenges-and-opportunities>. Accessed 16 Oct 2020
4. 5C Architecture. <https://www.avvanz.com/skills-for-digital-workplace/>. Accessed 16 Oct 2020.
5. Smart Industry readiness index. <https://www.humanresourcesonline.net/edb-launches-new-tool-to-prepare-singapore-manufacturers-for-industry-4-0/>. Accessed 16 Oct 2020
6. Putnik, G.D., Ferreira, L.G.M.: Industry 4.0: models, tools and cyber-physical systems for manufacturing (Editorial). *FME Trans.* **47**(4), 659–662 (2019)
7. Lee, J., Bagheri, B., Kao, H.A.: A cyber-physical systems architecture for industry 4.0-based manufacturing systems. *Manuf. Lett.* **3**, 18–23 (2015)
8. Monostori, L.: Cyber-physical production systems: roots, expectations and R&D challenges. *Procedia Cirp* **17**, 9–13 (2014)
9. Rodič, B.: I4.0 and the simulation modelling paradigm. *Organizacija* **50**(3), 193–207 (2017)
10. Smit, J., Kreutzer, S., Moeller, C., Carlberg, M.: Policy Department A: Economic and Scientific Policy—Industry 4.0. European Parliament, EU, pp. 1–94 (2016)
11. Gotze, J.: Reference Architectures for Industry 4.0 (2016)
12. RealPars. <https://realpars.com/automation-pyramid/>. Accessed 16 Oct 2020
13. Deloitte: I4.0 Challenges and solutions for digital transf. and use of exp. technologies (2014)
14. Hankel, M., Rexroth, B.: The Ref. Architectural Model I4.0 (RAMI 4.0). ZVEI (2015)
15. IIC: The Industrial Internet Reference Architecture (2017)
16. IIRA v1.7. http://www.iiconsortium.org/IIC_PUB_G1_V1.80_2017-01-31.pdf. Accessed 16 Oct 2020
17. I4. <https://www.i-scoop.eu/industry-4-0/>. Accessed 16 Oct 2020
18. Pinedo, M.L.: *Scheduling Theory, Algorithms, and Systems*. Springer, Heidelberg (2012)
19. Aytug, H., Bhattacharyya, S., Koehler, G.J., Snowdon, J.L.: A review of machine learning in scheduling. *IEEE Trans. Eng. Manag.* **41**, 165–171 (1994)

20. Berral, J.L., Goiri, Í., Nou, R., Julià, F., Guitart, J., Gavaldà, R., Torres, J.: Towards energy-aware scheduling in data centers using machine learning. In: Proceedings of the 1st International Conference on Energy-Efficient Computing and Networking, pp. 215–224 (2010)
21. Cunha, B., Madureira, A.M., Fonseca, B., Coelho, D.: Deep reinforcement learning as a job shop scheduling solver: a literature review. In: Madureira, A.M., Abraham, A., Gandhi, N., Varela, M.L. (eds.) HIS 2018. AISC, vol. 923, pp. 350–359. Springer, Cham (2020). https://doi.org/10.1007/978-3-030-14347-3_34
22. Leite, M., Pinto, T.P., Alves, C.: A real-time optimization algorithm for the integrated planning and scheduling problem towards the context of Industry 4.0. *FME Trans.* **47**(4), 775–781 (2019)
23. Alves, F., Rocha, A.M.A., Pereira, A.I., Leitão, P.: Automatic nurse allocation based on a population algorithm for home health care. In: 9th International Conference on Operations Research and Enterprise Systems, pp. 395–402. SciTePress (2020)
24. Varela, M.L., Putnik, G.D., Manupati, V.K., Rajyalakshmi, G., Trojanowska, J., Machado, J.: Integrated process planning and scheduling in networked manufacturing systems for I4. 0: a review and framework proposal. *Wireless Netw.* 1–13 (2019)
25. Varela, L., et al.: Decision support visualization approach in textile manufacturing a case study from operational control in textile industry. *Int. J. Qual. Res.* **13**(4) (2019)
26. Santos, A.S., Madureira, A.M., Varela, M.L.R., Putnik, G.D., Abraham, A.: A hybrid framework for supporting scheduling in extended manufacturing environments. In: The 14th International Conference on Hybrid Intelligent Systems, pp. 213–218. IEEE (2014)
27. Ferreirinha, L., et al.: An Industry 4.0 oriented tool for supporting dynamic selection of dispatching rules based on Kano model satisfaction scheduling. *FME Trans.* **47**(4), 757–764 (2019)
28. Alves, F., Varela, M.L.R., Rocha, A.M.A., Pereira, A.I., Leitão, P.: A human centered hybrid MAS and meta-heuristics based system for simultaneously supporting scheduling and plant layout adjustment. *FME Trans.* **47**(4), 699–710 (2019)
29. Madureira, A., Pereira, I., Pereira, P., Abraham, A.: Negotiation mechanism for self-organized scheduling with collective intelligence. *Neurocomputing* **132**, 97–110 (2014)
30. Silva, N., Shah, V., Soares, J., Rodrigues, H.: Road anomalies detection system evaluation. *Sensors* **18**(7), 1984 (2018)
31. Rao, H.R., Sridhar, R., Narain, S.: An active intelligent decision support system—architecture and simulation. *Decis. Support Syst.* **12**(1), 79–91 (1994)
32. Guo, Z., Ngai, E., Yang, C., Liang, X.: An RFID-based intelligent decision support system architecture for production monitoring and scheduling in a distributed manufacturing environment. *Int. J. Prod. Econ.* **159**, 16–28 (2015)
33. Raptis, T.P., Passarella, A., Conti, M.: Data management in industry 4.0: State of the art and open challenges. *IEEE Access* **7**, 97052–97093 (2019)
34. Wangler, B., Paheerathan, S.J.: Horizontal and vertical integration of organizational IT systems. *Inf. Syst. Eng.* (2000)
35. Liu, Q., Chen, J., Liao, Y., Mueller, E., Jentsch, D., Boerner, F., She, M.: An application of horizontal and vertical integration in cyber-physical production systems. In: 2015 International Conference on Cyber-Enabled Distributed Computing and Knowledge Discovery, pp. 110–113. IEEE (2015)
36. O'Donovan, P., Leahy, K., Bruton, K., O'Sullivan, D.T.J.: Big data in manufacturing: a systematic mapping study. *J. Big Data* **2**(1), 1–22 (2015). <https://doi.org/10.1186/s40537-015-0028-x>
37. Lee, J., Lapira, E., Bagheri, B., Kao, H.A.: Recent advances and trends in predictive manufacturing systems in big data environment. *Manuf. Lett.* **1**(1), 38–41 (2013)

38. Aggour, K.S., et al.: Artificial intelligence/machine learning in manufacturing and inspection: A GE perspective. *MRS Bull.* **44**(7), 545–558 (2019). <https://doi.org/10.1557/mrs.2019.157>
39. Monostori, L., Márkus, A., Van Brussel, H., Westkämpfer, E.: Machine learning approaches to manufacturing. *CIRP Ann.* **45**(2), 675–712 (1996)
40. Tao, F., Cheng, Y., Da Xu, L., Zhang, L., Li, B.H.: CCIoT-CMfg: cloud computing and internet of things-based cloud manufacturing service system. *IEEE Trans. Industr. Inf.* **10**(2), 1435–1442 (2014)
41. Zhong, R.Y., Wang, L., Xu, X.: An IoT-enabled real-time machine status monitoring approach for cloud manufacturing. *Procedia CIRP* **63**, 709–714 (2017)
42. Doil, F., Schreiber, W., Alt, T., Patron, C.: Augmented reality for manufacturing planning. In: *Proceedings of the Workshop on Virtual Environments*, pp. 71–76 (2003)
43. Novak-Marcincin, J., Barna, J., Janak, M., Novakova-Marcincinova, L.: Augmented reality aided manufacturing. *Procedia Comput. Sci.* **25**, 23–31 (2013)
44. Jasiulewicz-Kaczmarek, M., Saniuk, A.: Human factor in sustainable manufacturing. In: Antona, M., Stephanidis, C. (eds.) *UAHCI 2015. LNCS*, vol. 9178, pp. 444–455. Springer, Cham (2015). https://doi.org/10.1007/978-3-319-20687-5_43
45. Mattsson, S., Salunke, O., Fast-Berglund, Å., Li, D., Skoogh, A.: Design concept towards a human-centered learning factory. *Procedia Manuf.* **25**, 526–534 (2018)



A New Approach for the Evaluation of Internal Logistics Processes and Their Readiness for the Industry 4.0 Concept

Michal Zoubek^(✉) , Michaela Koubovská, and Michal Šimon 

University of West Bohemia, 8, Univerzitní, 301 00 Pilsen, Czech Republic
zoubekm@kpv.zcu.cz

Abstract. The concept of Industry 4.0 is inflected in many areas with the introduction of automation, robotics, or modern storage systems with a key element of digitization. An important area for implementing the elements of Industry 4.0 is internal logistics because the supply of production lines and material storage are among the company's key processes. The complexity and irregularity of processes can be automated and changed into an autonomous form based on the concept. The article deals with internal logistics and describes new approaches to the evaluation of logistics processes based on the developed methodology. The methodology design is based on theoretical foundations, and therefore the main part of the article describes the main areas entering the new methodology. Internal logistics is structured into five main dimensions, which completely cover it. According to the company maturity, dimensions are divided into six levels, where the highest level corresponds to Industry 4.0 principles. The evaluation is based on maximizing the criterion function and point evaluation from structured interviews with company members. After partial results from each dimension, it is possible to evaluate the current company level in internal logistics, which is the primary goal. The methodology is therefore mainly of a diagnostic nature.

Keywords: Industry 4.0 · Internal logistics · Logistics audit · Readiness model · Manipulation

1 Introduction

Industry 4.0 has a wide scope and is not only about the implementation of new technologies in industrial enterprises and gradual automation replacing human power. Due to its scope, there are definitions and views from academics, companies, consulting companies, and practical associations. However, the respondents agree that the essence of Industry 4.0 is digitization, expansion of high-speed Internet, development of smart technologies, communications, and many other topics. Businesses that want to maintain their competitiveness and market position must take their first steps towards digitization today. Digitization promises lower costs, higher production quality, flexibility, and efficiency. Investment in digitization is crucial for the growth of all industrial companies, regardless of their size or industry. Industry and the whole economy are undergoing

fundamental changes caused by information technology, cyber-physical artificial intelligence systems in production, services, and all economic sectors. The impact of these changes is so fundamental that they are referred to as the 4th Industrial Revolution. The main historical milestones are: the main definition of Industry 4.0 is based on a document presented at a trade fair in Hanover in 2013. The basic vision of this concept was created in 2011.

Developments for Industry 4.0 based on digitization and automation present enormous challenges for logistics and opportunities for further growth and development. The field of logistics, therefore, has great potential within this concept. However, it is essential and necessary to be more specific because this field is very broad. We focus on other areas of internal logistics in the following sections. The maturity of companies for Industry 4.0 is evaluated according to readiness models, which divide the company into several areas and assess the readiness of the relevant processes into several levels. The highest level corresponds to Industry 4.0.

2 Literature Review

The newly proposed methodology for internal logistics processes evaluation includes fundamental topics such as Industry 4.0, internal logistics within the Industry 4.0 concept, logistics evaluation audit, and readiness models assessing the readiness of companies for the concept of Industry 4.0. An overview and knowledge of each area play an essential role in the new methodology.

2.1 Internal Logistics and Evaluation According to the Logistics Audit

Logistics can be divided according to its application within the logistics chain and the focus of material flows, where internal logistics focuses on logistics processes within the company [1]. The internal logistics system is responsible for supply, production, and distribution logistics [2]. Internal logistics takes over the cross-sectional function and is fully responsible for the internal flow of material and information from incoming goods, warehouse, order picking, production, assembly to outgoing goods, thus connecting internal systems. The primary operational functions of internal logistics are manipulation, storage, transport within the company, product picking, and packaging [3].

Internal logistics processes are evaluated based on a logistics audit. According to the evaluated areas' scope, it is divided into internal and external [4]. A logistics audit is a standardized analytical and design process. It provides a detailed overview and diagnostics of the current state of logistics in the company, points out the potential of logistics changes, helps to find bottlenecks in the logistics system, and offers suggestions for their elimination. The project character of this program makes it possible to implement both immediate organizational interventions leading to rapid effects and fundamental conceptual changes in logistics processes [5]. The logistics audit aims to provide management with comparative material on its state in the company and show the potential for changes in logistics activities to achieve more efficient performance [6].

Logistics audit methodologies were analyzed in detail, and this is the input for determining the internal logistics dimensions evaluation proposal with the integration of Industry 4.0. According to the Chamber of Logistics Auditors, the methodology evaluates logistics in 25 key areas based on the auditor's questions and subjectivity [7]. VDA 6.3 is a methodology for industrial companies where internal logistics is evaluated in manipulation, transport, storage, and packaging [8]. The MMOG/LE methodology is used mainly in the automotive field to evaluate manipulation, supply, packaging, and material identification [9].

2.2 Models of Readiness for the Industry 4.0 Concept

Readiness models in the context of Industry 4.0 are used to measure the maturity of an organization or business process related to a specific target state. Characteristic for them is their use because based on the model application, it is possible to identify the current state and readiness for the concept of Industry 4.0 comprehensively in the entire company or various business areas [10]. Maturity models come in many modifications, and these complex models should equip companies with practical knowledge, such as:

- what is Industry 4.0, and how it can effectively affect society,
- what is the level of readiness of the company and subbusiness areas,
- how the company can gradually and purposefully improve and increase the level,
- how to start implementing modern technologies, and where are the opportunities.

Capability Maturity Model Integration (CMMI) is a key model concept on which most analyzed maturity models are based [11]. CMMI is a model that aims to help an organization plan, define, implement, develop, evaluate, and improve processes [12]. CMMI models come in various modifications and include a graded evaluation principle that defines five levels of maturity from the lowest Initial, through Managed, Defined, Quantitatively Managed to the highest fifth level of Optimizing [13]. A similar inspiring model is the Software Process Improvement and Capability Determination (SPICE), which deals with process assessment, especially in the automotive field [14]. This model works with six maturity levels from zero levels in a similar sequence as CMMI [15]. For the maturity models within the Industry 4.0 concept, the analyzed dimensions are defined as the main parameter. The model and its scope determine dimensions because models can be macro or micro levels [16]. Within macro models, the level evaluation concerning countries, within micro models, the readiness of the subject itself - the enterprise is evaluated, and these models are focused on in the article [17]. An important aspect is the model intent, which can be descriptive, comparative, or prescriptive [18]. Models also differ in design and are categorized into roadmaps, readiness, maturity models, or evaluation frameworks [19]. The second key parameter for the models is the evaluation method and classification into appropriate levels, which are usually four to six and are ranked from the lowest level, including characteristics [20]. A total of thirty maturity models were analyzed and compared, then gradually selected and classified for further research [21]. Models that worked with dimensions of internal logistics were separated in the form of abstraction, and these models with their main attributes are shown in

Table 1. Although the main goal was to look up models designed for internal logistics, the others served as inspiration for further analysis.

Table 1. Maturity models with main attributes for analysis.

Maturity model	Source type	Analysis dimension	Method of assessing maturity	Model intention
The Logistics 4.0 maturity model [22]	Acad.	3	From 1 (ignoring) to 5 (integrated)	Comp.
Acatech Industrie 4.0 maturity index [23]	Acad. Pract. Asoc.	4	From 1 (computerisation) to 6 (adaptability)	Comp.
Intelligent logistics for production [24]	Acad.	7	Assessment into 5 levels (uses level 0)	Comp. Prescr.
Maturity levels for Logistics 4.0 [25]	Acad.	4	From 1 (unconnected) to 5 (completely)	Comp.
A maturity model for Logistics 4.0 [26]	Acad.	7	From 1 (ignoring) to 4 (integrated)	Comp.

2.3 Findings

The first part of the article deals with a search of the main areas, and it is, therefore, possible to summarize the main findings and concepts:

- Internal logistics deals with material and information flow within the company, i.e., especially in the warehouse, production and assembly areas.
- Principles and technologies based on Industry 4.0 will be applied to internal logistics as one of the suitable areas for implementation.
- Logistics audit systems do not reflect developments within the Industry 4.0 concept and do not evaluate internal logistics processes with this in mind.
- Internal logistics activities that evaluate some logistics audits, such as warehousing, and manipulation, are not evaluated comprehensively.
- Industry 4.0 readiness models have divided areas into different dimensions and are used for level assessment (usually 4–6).
- The minimum of models (six within the search) is generally designed for logistics, and if internal logistics is evaluated, levels are not described or characterized in detail.

3 Research Methodology

The proposed evaluating methodology for the readiness of companies for the concept of Industry 4.0 in the field of internal logistics is based primarily on a literature review

of logistics audits, readiness models, and internal logistics itself. This methodology was developed in several phases, where the main steps and their specific content were determined. The first and most important phase was studying and evaluating the literature and experts' opinions who deal with this field. It is possible to create a comprehensive view of its development and its activities in all areas. Even though this area has great potential for the modernization of most processes, there is no comprehensive methodology to evaluate internal logistics in detail. The already developed methodologies, which were analyzed and compared, served as inspiration and a concept for creating a new methodology focused on logistics.

In most cases, different dimensions were analyzed in specific areas, which were evaluated at several levels. Then the method of evaluation and its representation was always given. Another aspect influencing methodology design and form is the focus of the authors who specialize in industrial engineering at the Faculty. In addition to the academic area, the industrial area is also important, where professional interviews took place within the framework of cooperation and workshops. Based on these two aspects, the methodology was subsequently developed.

3.1 Description of Methodology and Its Main Parameters

The methodology is created mainly for medium-sized industrial companies that have logistics. It does not consider the type of production or complexity of logistics processes but the requirements and specifics of the company, including the current situation and logistics systems. For this reason, the initial phase was the analysis of the main activities in business logistics, which are manipulation, storage, supply, packaging, and material identification. These activities represent relatively general dimensions, and therefore they are further broken down into subdimensions and indicators. The application of subdimensions specifies which area of the dimension the methodology will focus on. By setting the main indicators, the methodology focuses directly on activity or technology essential for evaluating the company. Another parameter is the level, of which there are 6, and which describes the company's maturity depending on a specific indicator. Each level is complemented by logistical elements that make it easier to classify the company appropriately. An essential part of the methodology is formulating questions for a structured interview with a responsible person, which serves as an input parameter for company evaluation. Questions are based on indicators and their characteristics which are evaluated according to the answers. Based on its current status, a company is classified at the appropriate level and evaluated in terms of Industry 4.0 readiness in the field of internal logistics. The results are interpreted in an analytical and graphical form, for example, within a logistics audit.

3.2 Determining Readiness Levels

Immediately after determining the new model structure, the levels of readiness are determined. There is a total of six levels, and they describe company maturity depending on specific indicators. The set levels are evolving, and from their brief definition, it is understandable what the given level means. These six levels of readiness, i.e., levels from 0 to 5, are described in Table 2.

Table 2. Description of readiness levels.

Level	Level description
Level 0	Processes are not explicitly defined, and there is no connection between them. Information systems and simple software are not used at this level
Level 1	Certified process management takes place here, which is controlled by the human factor. It uses simple software and basic information systems
Level 2	Processes are fixed and controlled. The use of automated elements in standardized processes is beginning. Data collection is partially digitized, and information systems process data only within the company
Level 3	Most processes are automated with partial human cooperation. Digitized technologies and information systems are used for data collection, connected to external data sources, where mutual communication occurs
Level 4	Processes are digitized and automated, with limited human intervention. It uses smart information systems that connect all areas, including external sources
Level 5	Processes are fully automated and human-controlled. The control of all systems is autonomous. Online communication thanks to sophisticated information systems that connect all areas of the company, including external sources

3.3 Determination of Dimensions and Subdimensions

Internal logistics is a broad area that deals with material flow and accompanying information flow. The methodology has five primary dimensions: the main activities of internal logistics, and are further broken down into subdimensions and indicators. Below in Table 3 is an example of the manipulation dimension, including subdimensions and indicators. The second dimension is storage consisting of three subdimensions, which deal with storage technology, information security, and material receipt and dispatch system. The third is the supply dimension, which has three subdimensions, including supply technology

Table 3. Overview of the manipulation dimension.

Dimension	Subdimensions	Main indicators
Manipulation	Manipulation technology	Degree of automation
		Environmental aspects
		Guidance of manipulation technology
	Information security	Interconnection of systems
		Management and information assurance
		Data processing
	Manipulation units	Standardization
		Identifiable
		Degree of automation

and information provision of material recalls. The fourth dimension is packaging, which deals with packaging technologies and methods of packaging, types of packaging, and packaging material, including packaging management. The last dimension is material identification, which has two subdimensions: the identification method and information provision.

3.4 System of Evaluation and Determination of the Level of Internal Logistics

An essential phase is the part of the methodology that focuses on a structured interview with an authorized person from the company in logistics. Creating a structured questionnaire requires the data determined when creating dimensions, subdimensions, indicators, and levels. Questions are created using indicators, and answers correspond with appropriate levels. With the help of the created questions and answers, the interviewee can choose an answer from which it is possible to put the company on the appropriate level. This system aims to determine the final evaluation for each subdimension, its parent dimension, and overall evaluation for internal logistics. The maximization criterion function is used to assess the current state of the internal logistics level. This approach was chosen based on a structured interview evaluating heterogeneous areas that influence the overall level the most. The derived relationship is a function of values of individual dimensions, see Eq. (1).

$$F_{KRITmax} = f(d) \tag{1}$$

The index “i” indicates each of the five evaluated dimensions, the variable “di” indicates the point evaluation in the given dimension. Equation (2) shows the sum of the maximum of 225 points.

$$\sum_{i=1}^n d_i = 225 \text{ points} \tag{2}$$

4 Results

This subchapter provides an example of a final table, including questions for evaluating the manipulation dimension. It is a manipulation between the receipt and material

Table 4. Example question for automation indicator.

Question: What manipulation technique do you use in terms of controllability?	
Humans manually operate the manipulation technique.	<input type="checkbox"/>
The manipulation technique is mechanized.	<input type="checkbox"/>
It is partially automated with standard tasks.	<input type="checkbox"/>
The technique is more automated for defined tasks with human cooperation.	<input type="checkbox"/>
Technology is mostly automated, controlled by IS. Human is involved in decision making.	<input type="checkbox"/>
The technology is fully automated, controlled by IS. Human only supervises.	<input type="checkbox"/>

warehouse or between the warehouse and finished products dispatch. The manipulation dimension has subdimensions: manipulation technology, manipulation units, and information security during manipulation. Table 5 deals with the subdimension of the manipulation technique and includes three indicators that specify this area in more detail. Intersection with indicators is levels from 0 to 5, into which the company can be included according to its maturity. These levels are then used as answers when asking questions. Table 4 gives an example of a question, including its answers. The level of the answer is known only to the evaluator, who evaluates it according to Table 5.

Table 5. Example of subdimension of manipulation technique.

Level	Main indicators				
	Guidance of manipulation technology	Environmental aspects	Degree of automation		Logistic elements
0	Manipulation technology is not guided (without any system)	Use of non-ecological diesel engines	Basic manipulation technique controlled manually by man	0%	Order picker, hand pallet truck
1	The technology is guided by standard industrial methods	Implementation of hybrid propulsion units reducing CO ₂ , NO and airborne particles	Mechanized manipulation technique controlled manually by man	0%	Forklifts, reach trucks, platform trucks
2	Manipulation technology guided according to signaling and digital recording	Implementation of electric drive units and their partial automation	Manipulation technology switches to partially automated standard operations	0%–25%	Forklifts, belt conveyors, tractors
3	Manipulation technology guided according to the signaling of wireless technology with partial communication	Implementation of electric drive units and their majority automation	Manipulation technique is more automated for predefined tasks with human cooperation	25%–50%	Automated carts, tractors, trains
4	Manipulation technology guided according to IS with partial online communication	Implementation of manipulation equipment for electric drives from renewable sources	The technology is mostly automated and controlled by IS. One is involved in decision making	50%–75%	Automated forklifts, autonomous AGV

(continued)

Table 5. (continued)

Level	Main indicators				Logistic elements
	Guidance of manipulation technology	Environmental aspects	Degree of automation		
5	Manipulation technology is fully IS-guided according to available information, including online communication	Manipulation technology for alternative energy sources	Manipulation technology is fully automated, controlled by IS. Human only supervises, controls	75%–100%	Unattended autonomous manipulation technology (AGV), collaborative robots

5 Conclusions

Expansion of product variability, the pressure to reduce production times and optimize operating costs force companies to innovate established processes. Internal logistics is one of the active factors involved in increasing a factory’s overall production performance, as it has a direct impact on optimizing, reducing production time, utilization of inventory, and increasing quality. That is why a methodology was developed that assesses the current level and readiness of internal logistics for the Industry 4.0 concept. The breakdown of these five dimensions into subdimensions and their indicators creates a complex methodology with evaluation from the lowest zero levels to the highest fifth level. The evaluation is carried out based on a structured interview with thirty-nine questions for representatives from the company who should know the Industry 4.0 concept. The answers for calculating the readiness level are as follows. It is essential to mention that currently, the methodology has only been developed and tested in companies. The results and verification will be the subject of further articles, including a description of the mathematical processing of the results. The methodology output will be the final evaluation with graphical analysis.

Acknowledgment. This article was supported by the project SGS-2018-031 solved within the Internal Grant Agency of the University of West Bohemia in Pilsen: Optimizing sustainable production system parameters.

References

- Schmidtke, N., Behrendt, F., Thater, L., Meixner, S.: Technical potentials and challenges within internal Logistics 4.0. In: 4th International Conference on Logistics Operations Management (GOL), pp. 1–10, (2018)
- Fragapane, G., Ivanov, D., Peron, M., Sgarbosa, F.: Increasing flexibility and productivity in Industry 4.0 production networks with autonomous mobile robots and smart intralogistics. *Ann. Oper. Res.* (2020)

3. Pfohl, H.C.: Logistikmanagement. Springer, Heidelberg (2016). <https://doi.org/10.1007/978-3-662-48784-6>
4. Lambert, D.M., Stock, J.R., Ellram, L.M.: Fundamentals of Logistics Management. Irwin/McGraw-Hill, Boston (1998)
5. Chamber of Logistics Auditors: New methodology of logistic audit (2020). <http://www.kla.cz/cs/metodika>. Accessed 20 May 2020
6. Malindžák, D., Marková, Z.: Comprehensive logistics audit system. *Acta Montanistica Slovaca* **1**, 82–89 (2010). [in Slovak]
7. Tvrdouň, L., Bazala, J., David, R.: A new approach of the logistics audit. In: CLC 2012, pp. 66–71 (2012)
8. Der Automobilindustrie, V.V.: Quality management in the automotive industry. In: Quality Assurance in the Process Landscape, vol. 4. VDA (2009). [in German]
9. Butler, T., Williams, D., Yan, T.: MMOG/LE: improving supply chain delivery performance through buyer-supplier collaboration. *J. Transp. Manage.* **25**(2), 57–68 (2015)
10. Amaral, A., Jorge, D., Peças, P.: Small medium enterprises and Industry 4.0: current models' ineptitude and the proposal of a methodology to successfully implement Industry 4.0 in small medium enterprises. *Procedia Manuf.* **41**, 1103–1110 (2020)
11. Torrecilla Salinas, C.J., Sedano, J., Escalona Cuaresma, M.J., Mejías Risoto, M.: Agile, web engineering and capability maturity model integration: a systematic literature review. *Inf. Softw. Technol.* **71**, 92–107 (2016)
12. Kneuper, R.: CMMI: Improving Software and Systems Development Processes Using Capability Maturity Model Integration, 1st edn. Rocky Nook, San Rafael (2008)
13. Kim, D.Y., Grant, G.: E-government maturity model using the capability maturity model integration. *J. Syst. Inf. Technol.* **12**(3), 230–244 (2010)
14. Lami, G., Biscoglio, I., Falcini, F.: An empirical study on software testing practices in automotive. In: Clarke, P.M., O'Connor, R.V., Rout, T., Dorling, A. (eds.) SPICE 2016. CCIS, vol. 609, pp. 301–315. Springer, Cham (2016). https://doi.org/10.1007/978-3-319-38980-6_22
15. Falcini, F., Lami, G., Costanza, A.M.: Deep learning in automotive software. *IEEE Softw.* **34**(3), 56–63 (2017)
16. Viharos, Z. J., Soós, S., Nick, G., Várgedő, T., Beregi, R. J.: Non-comparative, Industry 4.0 readiness evaluation for manufacturing enterprises. In: 15th IMEKO TC10 Workshop on Technical Diagnostics Technical Diagnostics in Cyber-Physical Era, Budapest, Hungary, pp. 181–187 (2017)
17. Poór, P., Basl, J.: Readiness of companies in relation to Industry 4.0 implementation. In: Proceedings of The International Scientific Conference Hradec Economic Days 2019 Part II (2019)
18. De Carolis, A., Macchi, M., Kulvatunyou, B., Brundage, M.P., Terzi, S.: Maturity models and tools for enabling smart manufacturing systems: comparison and reflections for future developments. In: Ríos, J., Bernard, A., Bouras, A., Foufou, S. (eds.) PLM 2017. IAICT, vol. 517, pp. 23–35. Springer, Cham (2017). https://doi.org/10.1007/978-3-319-72905-3_3
19. Schmitt, P., Schmitt, J., Engelmann, B.: Evaluation of proceedings for SMEs to conduct I4.0 projects. *Procedia CIRP* **86**, 257–263 (2019)
20. Lichtblau, K., et al.: IMPULS-Industrie 4.0-Readiness. Impuls-Stiftung des VDMA, Aachen-Köln (2015)
21. Zoubek, M., Poor, P., Šimon, M.: A maturity model for evaluating and increasing the readiness of the company within the concept of Industry 4.0 with a focus on internal logistics processes. In: The International Conference on Science, Technology, Engineering and Management (ICSTEM), Moscow, Russia (2020)
22. Oleśków-Szłapka, J., Stachowiak, A.: The framework of Logistics 4.0 maturity model. In: Burduk, A., Chlebus, E., Nowakowski, T., Tubis, A. (eds.) ISPEM 2018. AISC, vol. 835, pp. 771–781. Springer, Cham (2019). https://doi.org/10.1007/978-3-319-97490-3_73

23. Zeller, V., Hocken, C., Stich, V.: Acatech Industrie 4.0 maturity index – a multidimensional maturity model. In: *Advances in Production Management Systems. Smart Manufacturing for Industry 4.0*, pp. 105–113 (2018)
24. Krajcovic, M., Grznar, P., Fusko, M., Skokan, R.: Intelligent Logistics for Intelligent Production Systems. *Commun. Sci. Lett. Univ. Zilina* **20**(4), 16–23 (2018)
25. Sternad, M., Lerher, T., Gajsek, B.: Maturity levels for Logistics 4.0 based on NRW's Industry 4.0 maturity model. In: *Business Logistics in Modern Management*, vol. 18, pp. 695–708 (2018)
26. Facchini, F., Oleśków-Szłapka, J., Ranieri, L., Urbinati, A.: A maturity model for Logistics 4.0: an empirical analysis and a roadmap for future research. *Sustainability* **12**, 86 (2020)

ICT for Engineering Education



Mobile Application for Test Control of Knowledge Among Mechanical Engineering Students

Alexander Alexeyev , Tetiana Malandii , and Alina Moshna 

Sumy State University, 2, Rymkogo-Korsakova Street, Sumy 40007, Ukraine
t.malandii@tmvi.sumdu.edu.ua

Abstract. The article analyzes mobile technologies that are the most widely used in a modern technical university's educational process. It is noted that under certain conditions for test control on mobile devices, technologies that are limited to the use of students' mobile devices will be preferred. It is emphasized that for the successful mobile devices use in the knowledge test control of students. It is necessary to consider the features of practical classes on professional and practical training of future engineers. Such features include the widespread use of graphic materials at all training stages and holding a part of the practical training in specialized classrooms without access to mobile Internet. The mobile application SSUquestionnaire-m is described, which allows one to consider the features of engineering training listed in the article and ensure participation of all students in the classroom in control activities at the same time.

Keywords: Engineering education · Mobile technologies · Fuzzy logic · Mobile learning

1 Introduction

In a technical university, the educational process's rational organization is impossible without the correct setting of control over students' readiness to solve educational and professional problems. Knowledge control results are one of the most significant means of regulating many indicators of the educational process and, at the same time, a means of controlling the education quality. Quick and accurate assessment of students' knowledge is an urgent problem of the educational process both in the long-standing full-time and correspondence learning and in the relatively recently appeared mobile learning form or with the partial introduction of mobile learning technologies in traditionally held classes.

By far, among the knowledge control methods, the most intensive growth of interest is observed in knowledge test control systems. Actively using mobile and computer technologies, test control successfully supplements and improves existing traditional forms and control methods.

The paper notes [1] that testing on computers implements essential pedagogical functions. Using the example of conducting training sessions in using the virtual environment MOODLE, which has recently become widespread, the advantages of computerized test

control have been identified and described. Interactive simulators [2], and 3D laboratories [3], according to the authors, not only make it possible to organize better the process of studying new educational material on the theory of machine parts interchangeability but can also be an effective tool in summing up the results of students' educational activities. The approaches to introducing simulators and virtual laboratories into the educational process outlined in these works can be applied when performing most types of training sessions at all stages of control, from entrance testing to a comprehensive summing up of training results.

With the massive use of smartphones, smartwatches, fitness bracelets, and other mobile devices with all the essential computing characteristics of a computer by modern youth, there is a noticeable trend towards the widespread use of the entire mobile devices functions in the educational process. Already today, to solve most of the tasks that students face, there are high-quality applications that are freely available for mobile devices or installed by default on the gadget.

Everything indicates that, according to the results of the rapid development of mobile technologies and their introduction into the educational process, a symbiosis of test control and mobile gadgets should take place. However, few examples of test control on mobile devices are known that can confirm the success of the implementation of these trends. Especially noticeable is the lack of such examples in the organization and conduction of knowledge test control, skills in professional and practical engineering students' training.

The purpose of the article is to describe the experience of designing mobile applications, the use of which will take into account the peculiarities of future engineers training - mechanical engineers when conducting testing on mobile devices. For achieving this purpose, the following tasks were stated: to analyze the existing technologies of using mobile devices in the educational process; to highlight and summarize the main features of teaching engineering specialties students; to develop on this basis a mobile application that allows pedagogically correct combine the new teaching technologies with the specifics of engineering training at a technical university.

2 Literature Review

2.1 Technologies for the Application of Mobile Devices in the Educational Process

Domestic and foreign literature has recently seen an increase in the number of publications reflecting scientific research results and mobile technologies' practical use to solve pedagogical problems. They examined many theoretical issues and developed guidelines to improve mobile devices' implementation in the educational process [4].

The collection [5] has combined articles that analyze various aspects of mobile technologies application for learning. They describe mobile learning's current state, provide research results in improving mobile learning, describe the experience of implementing mobile learning in different countries, and provide recommendations on the mobile technologies used to improve teachers' qualifications. A number of articles in the collection offer their approaches to forming the functionality and design of mobile applications intended for higher education. Particular emphasis is placed on the use of VR and AR technologies in the educational process.

The work [6] proposes the author's approaches to introducing mobile learning in the education system. The broad possibilities of using mobile gadgets during training are described, and the restrictions that hinder their introduction into the educational process are noted. It is shown that the use of mobile devices does not lead to substantial changes in the main structural and pedagogical components of the learning system but makes it possible to supplement the existing e-learning model with the main components of mobile learning.

The reference book [7] contains works that consider mobile device application's admissible spheres in the educational process, particularly for a control knowledge test. Attention is paid to the testing method and questionnaires on mobile devices. The shortcomings of personal computers, the expediency of their replacing for students with their gadgets for university studies, and mobile devices' functions are listed, which allow them to recommend them for implementation in the educational process.

The authors of a number of works distinguish certain types of mobile technologies. Particularly, in the research papers [8, 9], authors applied the technologies of augmented and virtual reality for training engineering students. Additionally, Rafael Ballagas, speaking at the UbiComp 2004 conference [10], listed a set of features that allow you to define BYOD (bring your device) technology as a separate type. This technology began to advance especially actively after its introduction by Intel in 2009. Scientists in work [11] presented the possibilities and limitations of BYOD technology based on this technology's practical application throughout the year for various pedagogical practices in higher educational institutions. At present, such varieties are known as BYOP (bring your phone), BYOT (bring your technology), and (BYOPC: bring your own PC) [12].

In parallel with BYOD technology, GYOD (give your device) technology has been actively developed recently. It also has several varieties: become popular CYOD (Choose Your Own Device) [13], COPE (Corporate-Owned Personally Enabled) [14], and some others. Their common feature is that the university acquires mobile devices for educational classes. For GYOD technology, mobile devices' uniformity, achieved through centralized procurement and service, is one of its main advantages.

The main difference between the basic BYOD and GYOD technologies is who owns the mobile devices that students use when completing learning tasks. A common drawback for both technologies is not always the sufficient providing of students with mobile devices. For BYOD technology, this is because some students may not have technical devices with specified characteristics. GYOD technology limitation may be the educational institution's budget, which will have to be increased to provide mobile devices to all students. In the conditions of a domestic technical university, an obstacle may also be that mobile devices are issued to students only for their stay at the educational institution. When completing diploma and course projects, controlling knowledge, and other independent work types, problems will arise associated with the unequal characteristics of technical training aids.

The review shows that all the considered mobile technologies have advantages and disadvantages. BYOD technology involves the use of students' existing gadgets. The effectiveness of the implementation will be higher if measures are taken aimed at improving the security of the use of mobile devices. The ability to involve all students of the

study group in solving educational problems regardless of what gadgets they possess is also essential.

The purpose of the article is to describe the experience of designing mobile applications, the use of which will take into account the peculiarities of future engineers training - mechanical engineers when conducting testing on mobile devices. For achieving this purpose, the following tasks were set: to analyze the existing technologies of using mobile devices in the educational process; to highlight and summarize the main features of teaching engineering specialties students; to develop on this basis a mobile application that allows pedagogically correct combine the new teaching technologies with the specifics of engineering training at a technical university.

2.2 Features of Mobile Devices Use in the Classes of the Engineering Disciplines

A feature of mobile education for engineering specialties students is that the starting point for the assimilation of educational material in engineering disciplines is various kinds of three-dimensional graphic models, plane projection drawings, diagrams, models, graphs, and other graphic elements. As a result, graphic images, including large ones, are used as the initial data and results of implementing educational tasks. They introduce students to a wide range of professional knowledge about how structures work. Standardization in graphic design and a close connection between students’ information in the technical university are then applied. Therefore, it is essential that, during control events, students also have access to graphic information about the object, similar to that used at the training stage. Otherwise, the tested students will not fully familiarize themselves with the test items’ contents and correctly formulate their answers.

According to the standard [15], which regulates technical documentation formats in Ukraine, graphic information can be drawn upon drawings of different sizes (Table 1). The standard is based on the A0 format with a surface area of 1 square meter. Other formats are its derivatives.

Table 1. Formats of technical documentation

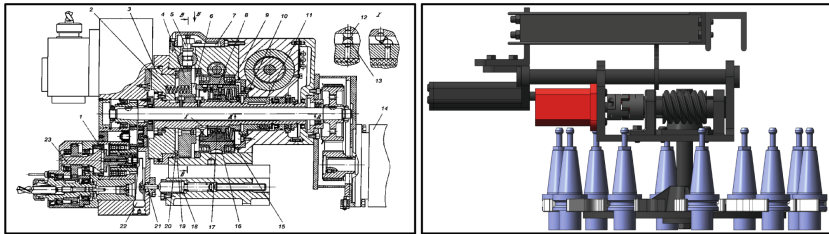
Formats					
	A0	A1	A2	A3	A4
Sheet size, mm	1189 × 841	841 × 594	594 × 420	420 × 297	297 × 210
File sizes, MB					
1 figure	75	35	17	9	5
3 figures	220	100	50	27	10

It is often difficult to view images in A0 format or those close to them in the area on the screen of mobile devices. Mobile devices’ resources are limited here and are inferior in functionality to personal computers with a screen diagonal from 15" to 25" or more. The screens of most laptops, netbooks, tablets, or e-book readers are, as a rule, significantly smaller than the monitors of personal computers (screen diagonal no

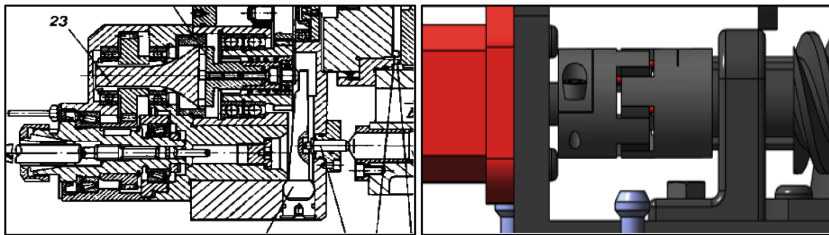
more than 15"–17"). At the same time, students for various reasons but rarely use these gadgets in the classroom. Unfortunately, when planning a lesson, you cannot focus on such devices.

Our observations show that engineering specialties students have smartphones more often than other students. MOVR research data [16] show that the share of sales of smartphones with screen sizes from 5.5 to 6 in. increased from 7.5% in 2015 to 43.3% in 2017, and more than 59% of the volume of Internet traffic falls on devices with a screen larger than 5". However, in the case of smartphones, when planning work with graphic materials, you need to focus primarily on mobile devices with the worst screen settings. Today, these are smartphones with a diagonal screen size of 3.5"–4".

It is difficult for a student to view an image of even a relatively small A3 format on a smartphone screen with a diagonal size of 3.5"–4". For example, Fig. 1 shows illustrations for the educational material that students of specialty 133 "Industrial Engineering" study. It explains the design of two technical devices: a turret and a tool changer, which are part of a metal cutting machine's technological system.



(a) reduced drawing and computer model



(b) enlarged fragments of the drawing and computer model

Fig. 1. The smartphone screen displays a drawing of a turret [17] and a computer model of the tool change mechanism of a metal cutting machine.

In Fig. 1 a, their images were reduced to fully fit on the screen of a smartphone with a diagonal of 4". Obviously, from such reduced illustrations, it is impossible to understand the design and operation principle of the devices shown. The only way to complete the training task, in this case, is to enlarge the image to such a size that you can distinguish between individual, even the smallest details. Figure 1 b shows enlarged fragments of nodes images of a metal cutting machine. The selected scale, in this case, allows you to see all the necessary elements, including the symbols on the drawing. However, to see

other sections of either of the two illustrations, the student must either change the scale or constantly move the picture, making some fragments visible and hiding the others. This manipulation makes it difficult to understand what is displayed on the screen and makes the whole perception unrealizable.

The problem also lies in the fact that graphic format files are usually significant. Table 1 shows the approximate sizes of graphic files that advise drawings printed on sheets of standard-size paper. If you load several such files into the memory of a smartphone or tablet, then the requirements for the mobile device's resources increase sharply, which is not always permissible since such high-tech devices may not be available to students will become critical during classes. Reducing the size of files by reducing the image's resolution leads to a loss of visibility and the inability to zoom in to consider small details.

Another significant feature that should be considered when planning classes in the disciplines of professional and practical training of students of engineering specialties is performing practical tasks in specialized educational laboratories or industrial premises. Students need to learn how to design, operate and produce engineering products.

It is possible that when holding classes in specialized rooms, it will be technically difficult to provide reliable mobile telephony, for example, due to interference caused by the operation of laboratory or industrial equipment. Additional measures will likely be required, in particular, to make mobile communication free of charge for students. As a result, in the absence of a connection to the mobile network, the network resources use will be limited or completely blocked. A partial solution may be the separate study of theoretical and practical training material. For example, to hold classes in different rooms: the practical part – in the training laboratory or the workplace, the study of theoretical material and test control – in the classroom with access to the network through mobile operators or Wi-Fi. If this is impractical or unrealizable, then the teaching materials should be changed to consider mobile applications' specifics when working offline.

3 Research Methodology

This goal was achieved through the following research methods: theoretical - analysis of psychological and pedagogical, scientific, technical, and methodological literature on the research problem, educational literature analysis, educational standards and programs of professional and practical training of engineering students to summarize theoretical issues, functions, features of mobile devices use to study engineering disciplines; empirical - observations, interviews, questionnaires, teachers and students analysis, expert assessment to collect data on the practical state of the problem.

The transition from an oral exam to test control changes the nature of the interaction between the instructor and the student in testing knowledge procedures. The student needs to formulate a unique answer from a limited set of words, letters, numbers or graphic symbols during the test tasks. In most well-known testing methods, the answer's correctness is determined only by its coincidence with the reference. The student has no tools at his disposal that allow him to express difficulties in formulating the answer. Depersonalization in assessing knowledge does not make it possible to establish how confident the student is in the answer but how much he guessed it, relying only on luck.

As a result, it is not excluded that a mistake will be added to the control result due to the student's need to think out the answer, going beyond the limits of his own knowledge.

For minimizing such a mistake, it is proposed to use an expert system based on the apparatus of fuzzy logic when creating an application for modular control of engineering students' knowledge [18]. In terms of ordinary logic, the student's answers can be linked to the test control results only with the help of two extreme statements: 1) "if the student's answer does not coincide with the reference answer, then the student does not have the necessary knowledge", 2) "if the student's and reference answers coincide, then knowledge is sufficient". For fuzzy logic, in addition to such limiting theses, any other intermediate statements are allowed that can relate a certain degree of coincidence of the student's answer with the answer that is set in the test as correct.

When doing a test task using the SSUquestionnaire-m mobile application, the student can additionally report how confident he is of the correct answer. The expert system transforms the student's decision and gives an assessment depending on whether this answer coincides with the reference or not. If the answer is correct and the student expressed maximum confidence, he is affixed with the highest possible points. When, with the correct answer, the student expressed considerable doubt, then points are not added to his assessment. In other cases, the final assessment depends on whether the answer was correct, and what degree of doubt the student expressed. If the answer is correct, the number of points will be higher, the lower the level of doubt indicated.

Conversely, if the answer is incorrect, the number of points increases if the student shows more doubt. Expressing the degree of confidence in the answer, the student thereby provides the expert system with data to mathematically accurately differentiate his academic achievements and give an assessment that does not allow other interpretations. Ultimately, the use of fuzzy logic eliminates from the assessment the guessing error associated with the need for the student to give unambiguous answers, even if they cannot be formulated based on his knowledge.

4 Results

4.1 Application Interface

SSUquestionnaire-m mobile application allows you to consider a number of training features in the disciplines of professional and practical training of engineering specialties students. The application use requires mobile devices with the Android operating system. The interface language is determined by the settings of the operating system installed on the mobile device. Depending on the selected system language, the program interface will automatically be installed in Ukrainian, English, or Russian. The application is multi-screen.

1. The start screen (Fig. 2, left figure). It has two input fields: "ID" and "Digital code". In the field "ID" indicates the user ID. If you set the instructor's password in it, then the next buttons will be available: "Results", "Coding" and "Refusal,". When you click the "Results" button, the "Test Results" screen (Fig. 2, the central figure) opens to view and edit the records of the remote database. Pressing the "Coding" button will open another screen (Fig. 2, the right figure) and it will be possible to

start developing the test. If a different identifier is entered instead of the instructor's password or the "Refusal" button is pressed, it is assumed that the student data has been entered in the "ID" field.

The digital test code contains encrypted information on the rating scale, the correct answers, and a decoding key. You can enter the code manually using the virtual keyboard or camera (optical sensor) of a mobile device. To do this, point the camera at the QR code (a two-dimensional matrix representation of the digital code printed on the test form). Click the "Scan" button – the QR code will be recognized programmatically and the received digital code will be automatically put in the input field.

This completes the input of the initial data necessary for passing the test. After clicking the "Continue" button at the bottom of the screen, the "ID" and "Digital code" fields are checked. If they contain valid values, the next screen will open, and the application will go into test control mode.



Fig. 2. Application screens (from left to right): "Start", "Test results", "Coding".

2. Testing screen (Fig. 3). When passing the test, the student must answer the questions, marking with a finger those that he considers correct. To express doubt during the test task, it is enough to move the "slider" pointer to any of the positions: from the far left – not sure, to the far right – pretty sure. The fuzzy-logic expert system built into the application will adjust the score based on the slider pointer's selected position. After completing all the test tasks and clicking the "Show result" button, a new screen opens (no figure). It displays the student's mark obtained from the test. Identification data is also provided here: student ID, digital code, and test variant. If

the test control is carried out in the room, there is access to the mobile network, then the control results are also recorded in a remote database.

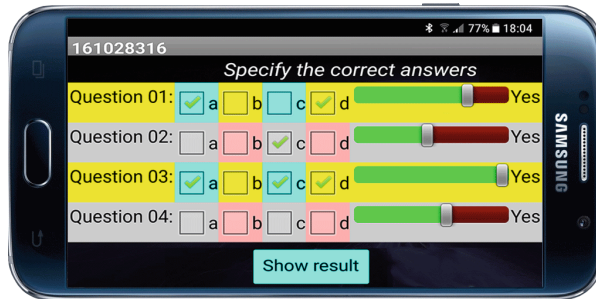


Fig. 3. Screen “testing”.

3. Screen test results. It displays information from a remote database of test control result and navigation buttons. The screen displays date of control, student ID, digital test code, assessment, numbers of correct and incorrect answers for each database record. To navigate through the records, the buttons “Forward”, “Back”, “Start”, “End” are provided. The selected record can be deleted from the database or saved to a mobile device.
4. Coding screen. It makes it possible to design a test that includes from 3 to 15 test tasks. The screen contains 15 input fields for coding reference responses. The number 1 here means that the answer is correct, and the number 0 – the answer is incorrect. The combination of zeros and ones determines the reference response of the task. The number of test tasks is determined by the number of correctly filled coding fields. For selecting a rating scale, an additional input field is provided. It is required to indicate the maximum mark that the student will receive for all correctly completed test tasks (according to a 100-point system). After the initial data for designing the test is entered, you need to click the “Get a digital code” button – the code will be automatically generated, displayed on the screen, and saved in a text file on the mobile device. The “Get QR code” button allows you to generate a matrix representation of a digital code and record it on a mobile device as a graphic file in.png format. If the device does not support this function, then you should use any of the known QR code generators, for example.

4.2 Carrying Out the Test Control

Before starting testing using the SSUquestionnaire-m mobile application, the instructor must have a set of tests at his disposal, the composition of which is determined by the tasks assigned to testing.

Based on the engineering education peculiarities (Sect. 3), the text of the assignment and illustrations revealing their contents are proposed to be written in a standard paper

format (if the image does not fit on a sheet of A4 format paper, it is allowed to reproduce it separately, for example, using multimedia). The digital and QR code can be included in the descriptive part and printed at the beginning of the test form along with the information about the subject of controlled educational material, type of control, variant of the assignment.

A barcode scanner application should be installed first to scan a QR code on a mobile device. If the first scan is not on the device, then a link for downloading from the Google Play store will be automatically offered.

Figure 4 shows a diagram of a mobile test control using the SSUquestionnaire-m application. The application features allow you to carry out all control activities in rooms without access to Wi-Fi or the mobile web. Simultaneously, the presence of the Internet can be considered an option, expanding the application’s capabilities in terms of remote control of students’ knowledge and simplifying the statistical processing of test results.

Students passing control remotely must be clients of the mobile network and have a mobile device installed with the Android operating system. Forms with test items are delivered to them in electronic form, for example, as a pdf-document. The control results are stored in a remote database and available to the instructor both on his mobile device and on a personal computer with access to the Internet.

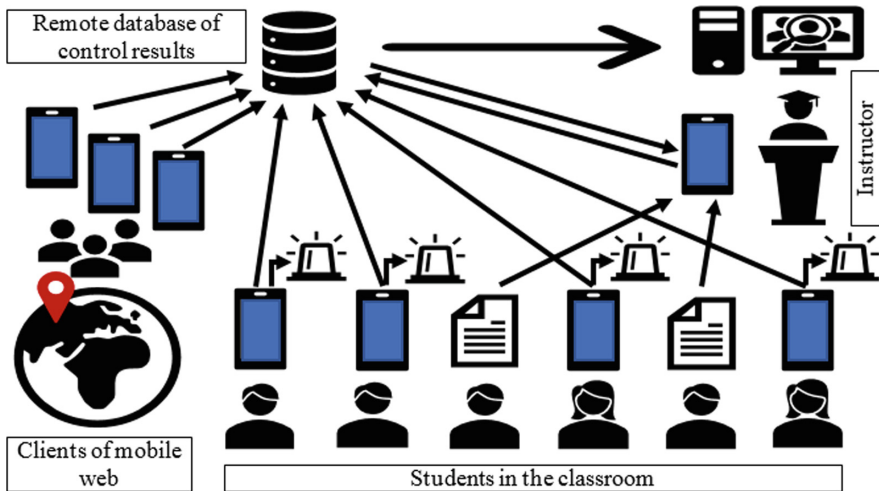


Fig. 4. Mobile test control scheme.

Students who do not have the necessary technical devices can participate in testing along with everyone in the classroom. To do this, it is enough for such students to write down their answers on a piece of paper and indicate the confidence degree in them (for example, in numbers ranging from 0 to 9). After completing the control common to all, the instructor checks the answers on his mobile device. Checking does not require much time but allows you to stay within the BYOD technology and at the same time carry out test control in one session.

If control is carried out in an audience without access to a mobile network, control is performed. However, the control results are not recorded in the remote database. After the received mark is visible on the mobile device screen, the student must show it to the instructor, for example, raising a hand with the device held and turning it with the screen towards the instructor. Further, the instructor records the mark received by the student and, at the same time, checks the compliance of the completed assignment with the given option (according to the last four characters of the digital code that appear on the same screen).

5 Conclusions

In the educational process of modern technical universities, mobile technologies are widely used. The most widely used technologies are BYOD, GYOD, and some of their varieties. All of them have both advantages and disadvantages. When introducing test control on mobile devices, BYOD technologies require lower initial financial costs for the education classrooms' technical equipment. They will be preferable if you ensure simultaneous participation in all the students' control activities in the classroom.

The developed SSUquestionnaire-m mobile application allows one to consider some specific features of holding classes in the professional and computer training disciplines of engineering specialties students. It is not required to restrict the number and size of graphic illustrations in test tasks when using it. It is also allowed to hold test control entirely offline. The advantage of the application is the integrated fuzzy-logical system. It allows the student to answer with a certain degree of confidence in their answer's correctness, and with that, receive a more accurate grade on the test. The application's properties allow one to organize test control in such a way as to ensure that all students in the classroom participate in a test at the same time. However, to stay within the BYOD technology, the acquisition of additional training equipment will not be required.

The introduction of the SSUquestionnaire-m application removes only part of the mobile devices' restrictions in the knowledge test control of mechanical engineering students. Therefore, work in the direction of its development and control methodology improvement should be continued. As priority tasks, it is planned to develop automation tools for statistical processing of control results and expand the application's capabilities to develop tasks that reduce the probability of guessing.

References

1. Vaganova, O., Smirnova, Z., Mukhina, M., Kutepov, M., Kutepova, L., Chernysheva, T.: The organization of the test control of students' knowledge in a virtual learning environment moodle. *J. Entrep. Educ.* **20**(3) (2017)
2. Korotun, M., Denysenko, Y., Malovana, N., Dutchenko, O.: Improvement of the effectiveness of general engineering courses using trainers. In: Ivanov, V., Trojanowska, J., Pavlenko, I., Zajac, J., Peraković, D. (eds.) *DSMIE 2020. LNME*, pp. 23–34. Springer, Cham (2020). https://doi.org/10.1007/978-3-030-50794-7_3
3. Hu, W., et al.: Plug-in free web-based 3-D interactive laboratory for control engineering education. *IEEE Trans. Industr. Electron.* **64**(5), 3308–3318 (2017)

4. Kuznekoff, J., Munz, S., Titsworth, S.: *Mobile Devices and Technology in Higher Education*. Routledge, New York (2020)
5. Zhang, Y.: (Aimee): *Handbook of Mobile Teaching and Learning*. Springer, Heidelberg (2015)
6. Tkachuk, G.: Features of mobile learning implementation: prospects, advantages and disadvantages. *Inf. Technol. Teach. Aids* **64**(2), 13–22 (2018)
7. Information Resources Management Association: *Mobile devices in education*. Information Science Reference, Hershey, PA (2020)
8. Ivanov, V., Pavlenko, I., Trojanowska, J., Zuban, Y., Samokhvalov, D., Bun, P.: Using the augmented reality for training engineering students. In: 4th International Conference of the Virtual and Augmented Reality in Education, VARE 2018, pp. 57–64 (2018)
9. Bun, P., Trojanowska, J., Ivanov, V., Pavlenko, I.: The use of virtual reality training application to increase the effectiveness of workshops in the field of lean manufacturing. In: 4th International Conference of the Virtual and Augmented Reality in Education, VARE 2018, pp. 65–71 (2018)
10. Ballagas, R., Rohs, M., Sheridan, J., Borchers, J.: BYOD: Bring Your Own Device. In: *Proceedings of the Workshop on Ubiquitous Display Environments, Ubicomp* (2004)
11. Song, Y., Kong, S.: Affordances and constraints of BYOD (Bring Your Own Device) for learning and teaching in higher education: teachers' perspectives. *Internet High. Educ.* **32**, 39–46 (2017)
12. Beginner's Guide to BYOD. <https://www.arkgroup.com/thought-leadership/beginners-guide-to-byod>. Accessed 12 Sep 2020
13. Zrinscak, S., Perl, A., Robra-Bissantz, S.: Choose your own devices. *HMD Praxis Der Wirtschaftsinformatik* **54**(6), 887–899 (2017)
14. Paskova, A.: Mobile education in higher education: BYOD technologies. *Bull. Maykop State Technol. Univ.* **4**, 98–105 (2018)
15. Technical documentation for products. Drawings. Dimensions and formats. DSTU ISO 5457: 2006. State Committee for Technical Regulation and Consumer Policy, Kyiv (2008). [in Ukrainian]
16. Smartphone screen size trend. <https://www.scientiamobile.com/smartphone-screen-size-trend/>. Accessed 20 Sep 2020
17. Solomentsev, Y., Zhukov, K., Pavlov, Y., et al.: *Robotic technological complexes and flexible production systems in mechanical engineering: album of diagrams and drawings*. Mechanical Engineering, Moscow (1989)
18. Alekseev, A., Aleksieieva, M., Lozova, K., Nahorna, T.: Using fuzzy logic in knowledge tests. In: 11th International Conference on ICT in Education, Research, and Industrial Applications (ICTERI 2015), pp. 51–61. Lviv (2015)



Institutional Aspects of Integrated Quality Assurance of Engineering Study Programs at HEI Using ICT

Vitaliy Kobets¹  , Vira Liubchenko² , Ihor Popovych¹ , and Svitlana Koval³ 

¹ Kherson State University, 27, Universitetska Street, Kherson 73003, Ukraine
vkobets@kse.org.ua

² Odessa National Polytechnic University, 1, Shevchenko Avenue, Odessa 65044, Ukraine

³ Kherson State Agrarian University, 23, Stritenskaya Street, Kherson 73006, Ukraine

Abstract. Informatization of Ukrainian higher education institutions is a key priority of the state education policy, one of the directions to improve HEI's IT infrastructure. The paper aims to develop an integrated quality assurance information system to enhance institutional aspects of higher education institutions' study programs. Therefore, there is an urgent need for all stakeholders to develop, at the university level, a service-oriented architecture to assure the quality of higher education with mandatory elements, for example, student survey results, student ratings, university teachers' rating, educational programs, results of uniqueness verification for scientific research and qualifying papers, review of educational programs for higher education applicants etc. It will allow to unify the approaches to electronic resource management and accelerate the integration of multi-level HEI quality assurance resources into a single portal. The paper presents a quality assurance information system, which allows processing students' feedback to provide HEI's authorities' decision making.

Keywords: Quality assurance management in HEI · Students' feedback · Engineering study programs

1 Introduction

The primary purpose of using IT in Quality Assurance (QA) management in higher education institutions is to increase the applicants' satisfaction with their learning process by using management information systems (IS).

The use of IT in management is aiming to ensure the quality of HEI education, and it should guarantee:

1. In the area of education: developing innovative distributed learning and methodological environment at the university; using service-oriented systems in the educational process; implementing an e-learning management system for all students.

2. In the area of science: presenting scientific research capacity of a University in a global information space using open source databases; providing access for researchers and students to the scientific information resources; managing the implementation of joint research projects as part and parcel of an international consortium.
3. In the area of university management: gathering, storing, and processing information about the participants in the learning process, data collection and analysis; providing the automated follow-up to the decision taken; improving planning process to guarantee quality in education at HEI.

These issues include governmental authority versus institutional autonomy, lack of an internal quality assurance mechanism for individual institutions as performance evaluation [1]. Many Ukrainian and foreign HEIs are trying to solve the problems of implementing the educational process's quality assurance management by using certain computer programs that allow scheduling classes, checking scientific articles for uniqueness, determining the applicants' satisfaction with their learning process. Nevertheless, the techniques are not efficient enough; there is currently still no single system approach to management in the HEI strategy. Integrated information systems have affected how both students and universities perceive education that focuses on management and learning [2]. Different types of software development make it impossible to exchange data accurately, effectively, and consistently. That is the reason why HEIs, as a rule, buy or create an integrated management system that allows synchronization at different levels of quality assurance in HEI. To achieve the goal of successful implementation of an internal quality assurance system at the university, it is necessary to solve the following issues:

- to develop the models of management activities and learning strategies to support the quality of university education using information database;
- to establish and maintain IS architecture for student ratings, curriculum, degree qualifications profile, study programs;
- to create and introduce new techniques and methods of quality assurance management at the university based on integrated IS;
- to reduce the time of information assessment and processing in decision making;
- to create a system to predict the university development using key performance indicators (KPI).

The researchers' data gathering instrument is the Graduate Tracer Study developed by the Commission on Higher Education [3]. To decide on the architecture of integrated IS (buy or develop), it is necessary to reveal all the required business processes for quality assurance of education [4].

The paper aims to develop an integrated quality assurance information system to enhance institutional aspects of engineering study programs at HEI.

The paper has the following structure. Part 2 describes a comparison of institutional quality assurance systems; part 3 investigates research methodology for QA using information system; part 4 examines the development, monitoring, and revision of the SP using QA information system; the conclusions is the last part.

2 Literature Review

The change of higher education structure, development of quality assurance systems and mechanisms enabling the dimension of study program flexibility related to the necessary specific subject competencies [5] represent arguments for the development of institutional design (ID) models, which based on the relationship between institutional rules, learning process, and learning outcomes. As a process, ID is a curriculum development cycle; a needs assessment, labor market analysis, design, development, implementation, and results.

“Institutional designer” is a person who designs educational courses to fulfill the needs and requirements of external and internal stakeholders. A needs assessment focuses on determining the current state and the desired state, and the type of business process to bridge that gap [6].

The European Foundation for Quality Management (EFQM) was founded to promote self-evaluation as a key business process improvement. The EFQM Excellence Model is a diagnostic tool, with a set of criteria generally accepted across Europe, which can be used by HEI to evaluate their strengths, weaknesses, opportunities, and threats and to monitor the progress of strategic actions [7–9]. For HEI, it provides a framework for continuous improvement (Fig. 1).

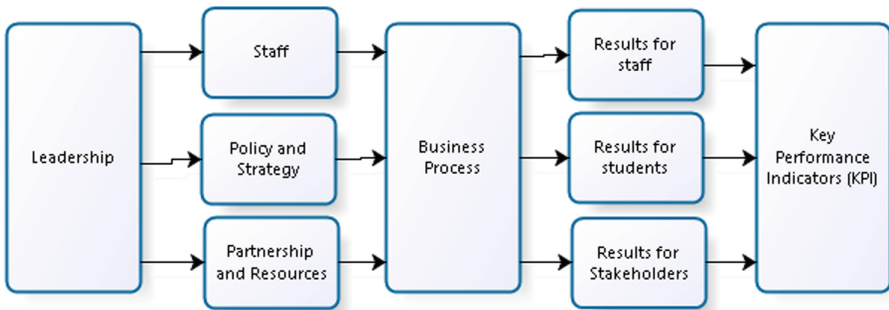


Fig. 1. EFQM excellence model.

Criterion 1. Leadership: How top management of HEI creates additional values for students who are personally involved in the QA management system and motivate students to increase their capitalization.

Criterion 2. Policy and Strategy: The systems guarantee that the needs of stakeholders (employers, students, alumni, academic staff, local authority, parents, etc.) are incorporated in the strategy. The strategy tasks should be developed, deployed, and communicated.

Criterion 3. People: academic staff, a guarantor, a support team are engaged in the student learning process.

Criterion 4. Partnership and Resources: Interconnection of information (databases, e-library, e-repository), material (labs, equipment, technology), and financial resources.

Criterion 5. Business Processes: The methods are used for managing and improving processes, including learning, teaching, R&D process, revising of SP, implementation process of SP.

Criterion 6. Student Results: The KPI of students’ perceptions of the organization and other HEI performance indicators for external stakeholders, including image and the reputation of the HEI’s educational services.

Criterion 7. Staff Results: The measures of staffs’ perceptions of HEI and other indicators of HEI performance, such as satisfaction, motivation, recognition, involvement, and achievement.

Criterion 8. Stakeholders Results: The measures of the organization’s performance to satisfy the expectations and society’s needs (local, national, or international community, accreditation bodies).

USA BQA (Baldrige Quality Award) Criteria Framework is a tool intended to be used by organizations to evaluate their performance and monitor the strategy progress and process changes (Fig. 2).

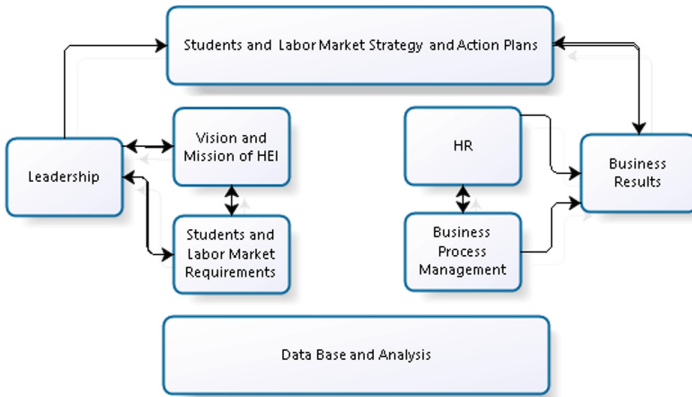


Fig. 2. BQA criteria framework.

HEI has to continuously improve its study programs to stay competitive in the dynamic and changing education and labor market environment. Quality Assurance (QA) is defined as planned and systematic actions implemented within the quality system to provide adequate confidence that educational services will satisfy given requirements for quality (National Qualification Framework and/or Standards of High Education). Quality Management (QA) provides a systematic approach or a QA model linked with educational quality improvement [10]. An example of a systems approach is a definition of quality of education as an “ability of students’ knowledge to satisfy specified requirements of accreditation bodies, professional societies, employers, etc.” [10].

Process input-output satisfaction model with goal and specification clarifies what HEI are required to do and what students and stakeholders can expect in the future. QA protects the interests of all students. QA is required to meet all the expectations of Study Programs. QA indicators are intended to help HEI demonstrate that SP’s expectations are being met using regulations, procedures, and practices of HEI.

The institutional design of the Process input-output satisfaction model with goal and specification is based on the system approach and includes several elements (Fig. 3):

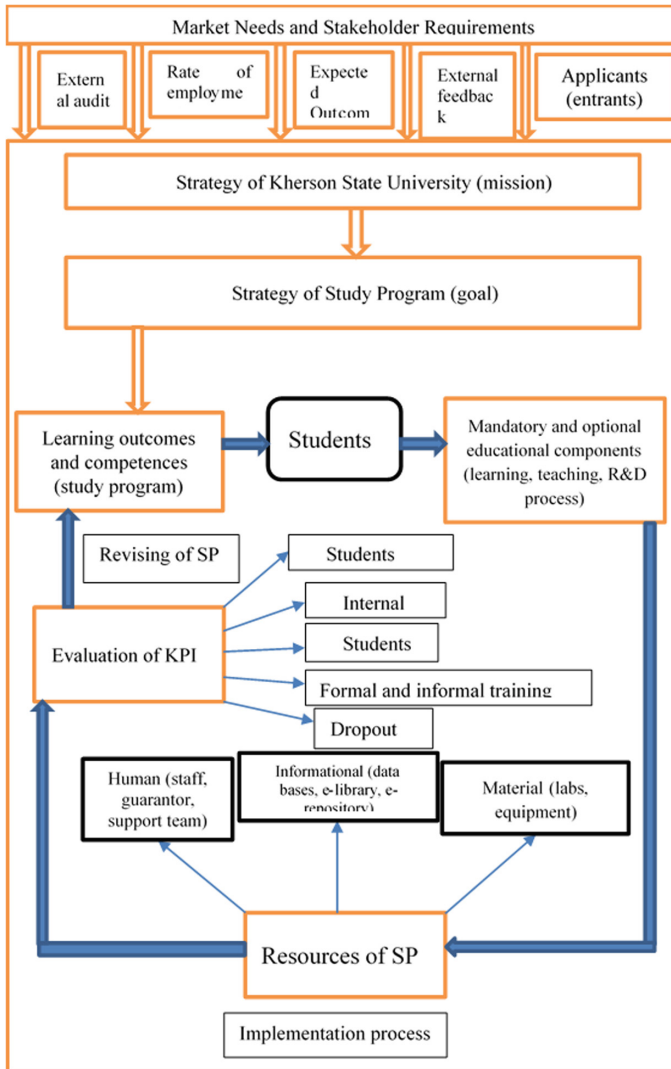


Fig. 3. Institutional design of quality assurance procedures at Kherson State University.

1. goals and specifications of the study program of HEI represent its expected outcomes;
2. to achieve these goals, HEI needs to provide all necessary resources, including human, material, information, and infrastructural resources;
3. the resources need to be accumulated to manage and improve the academic and business processes of the study program;

4. the management and improvement of educational processes and achievement of goals can bring satisfaction for the stakeholders under regular monitoring of the SP with the intent of continual improvement.

The evaluation and monitoring of SP can use multiple methods or their combinations; among them are audit, self-assessment, benchmarking, etc.

Learning analytics (LA) and tools for intelligent analysis of data accumulated in the IS used by HEIs provide an opportunity to increase the effectiveness of monitoring, management, quality assurance, and evaluation of training for each study program and decision-making. LA tools help managers of HEIs identify courses and programs that more closely match the students' needs and preferences, considering the requirement of the labor market and feedbacks of all stakeholders [11]. Some of the tools are standalone software tools, while the others are modules included in LMS. Each LA tool is based on a model with a set of indicators, the data of which is extracted from the LMS used at the university.

3 Research Methodology

The development of feedback evaluation is a complementary tool towards heightening the comprehensiveness of existing quality assurance mechanisms [12]. Focus groups help ensure that multiculturalism, diversity, and inclusion are central to the HEI's discussion agendas. A strong correlation between technical/engineering SPs and good quality assurance results was found by authors [13], probably because quality expertise is particularly developed in these disciplines.

The key stage of development, monitoring, and revision of the SP includes the following steps (Fig. 4):

1. **Initiation** – project team (PT).
2. Determining the needs for a study program SP (project team, employers, graduates, Google surveys).
3. **Analysis of requirements and requests**, Professional Standard (PT, specialist profile regarding the employers and graduates' views – list of competencies: LinkedIn electronic competency platform, etc.).
4. **Determining a list of program competencies for graduates** of SP – PT, an occupation profile.
5. Compiling a list of learning outcomes (LO) – PT, list of LO.
6. Compiling a list of educational components (EC) – PT, a draft list of the EC.
7. Defining an educational certificate attestation type – PT, attestation types.
8. **Determination of the internal quality assurance system features in higher education** (PT, rating, polls, revising of SP, checking for plagiarism).
9. Consultations on the institutional capacity to provide the SP (scientific, financial, academic, logistical base) – PT, HEI administration, management decisions.
10. Development of educational components – PT, staff, descriptions of EC (syllabus, etc.).
11. Feedback of students, teachers, graduates after educational activities – types of educational activities, learning outcomes at ECTS.

12. **Revision of SP** (program competencies, program learning outcomes, educational components).

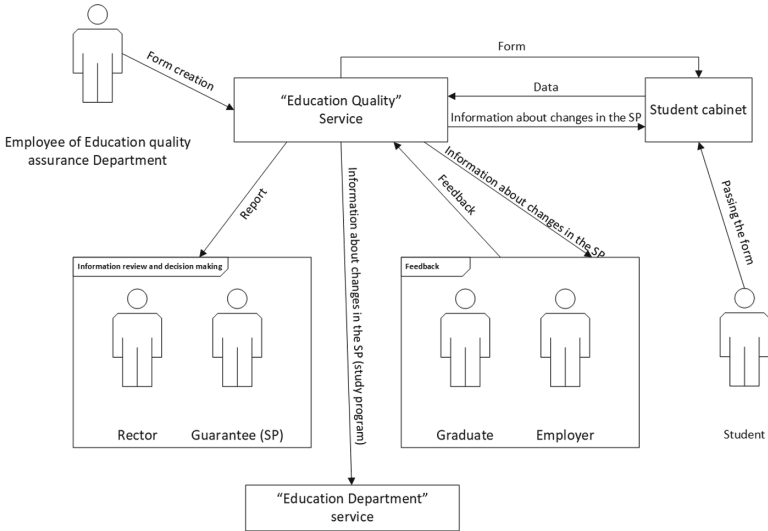


Fig. 4. The procedure of development, monitoring, and revision of the SP.

4 Results

ESG 2015 Standard means that Institutions should monitor and periodically review their programs to ensure that they achieve the objectives set for them and respond to students and society’s needs. These reviews should lead to the continuous improvement of the program [14]. Any action planned or taken as a result should be communicated to all those concerned. Programs are reviewed and revised regularly, involving students and other stakeholders. The information collected is analyzed, and the program is adapted to ensure that it is up-to-date. Revised program specifications are published [15].

Measures/procedures

1.1. Monitoring at the level of an individual study component (study program in whole) which provides for:

1. Formation of KPI of quality of study component of the study program:
 - quantitative (student achievement results, the average quality of education, the number of expelled students);
 - qualitative (feedback from students, teachers, etc.).

2. Determination of indicators' threshold values for which, if achieved (for example, a low percentage of students' quality of education), make it mandatory to monitor the study component at the higher education institutional level.
3. Preparation of a report dealing with the results of course revision.
4. Monitoring the implementation of an action plan to improve the training component.

Informing all stakeholders about changes to the study program based on the results of the review:

- informing students, staff, educational service departments, and external stakeholders about study program monitoring;
- getting feedback after reviewing the annual monitoring reports on a study program;
- publication information about monitoring of study programs.

The relationship between students' satisfaction with the learning process and the quality of their education for students of mathematical and engineering study programs at Kherson State University is determined using Google forms. Data are obtained according to the results of processing 432 questionnaires of applicants for the higher education of Computer Science, Physics and Mathematics Faculty (Table 1).

Table 1. Feedback of students (1 semester 2019–2020), Kherson State University.

Code	Study program	Rating of disciplines (RateDisc) min = 1 max = 5	Rating of staff (RateStaff) min = 1 max = 5	Quality of education of bachelors (QE) min = 0 max = 100
121	Software engineering	4,04	4,29	40,5
122	Computer science	3,67	4,03	37,9
126	Information systems and technology	4,30	4,58	42,9
014	Secondary education (mathematics)	4,42	4,44	46,2
014	Secondary education (physics)	3,83	4,19	37,5
014	Secondary education (Informatics)	4,39	4,55	46,7
014	Secondary education (labor training and technology)	3,60	3,61	21,7

Let's consider dependency between the rating of disciplines (dependent variable *RD*) and the rating of staff (explanatory variable *RS*) $RD = b_0 + b_1 \cdot RS + u$ using Table 1 data:

$$RD = 0.177 + 0.909 \cdot RS + u \left(R^2 = 82\% \right) \tag{1}$$

Each unit of RateStaff increases by 0.909 RateDisc (statistically significant, $t(b_1) = 4.74 > t_{cr} = 2.57$). These dependencies are presented in Fig. 5. R^2 means that the variation of RS determines 82% variation of RD.

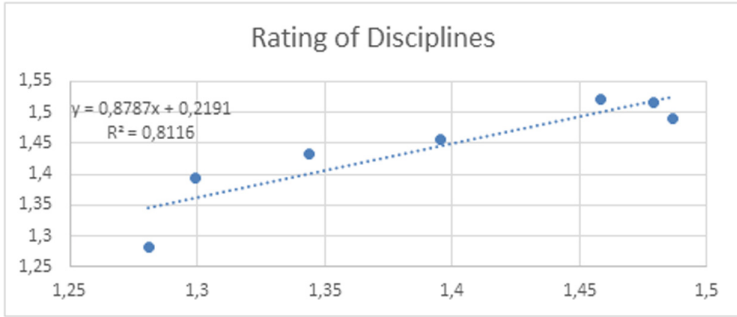


Fig. 5. Quality assurance for SP.

If we transform absolute values (Table 1) in the relative index, we can get regression of the following form

$$\ln RD = 0.06 + 0.92 \cdot \ln RS + u \quad (R^2 = 81.2\%) \tag{2}$$

It means that each 1% increase in staff rating will increase by 0.92% rating of disciplines.

At the same time quality of education of bachelors (only good and excellent grades) as a rule depends only on a rating of staff:

$$QE = -60.27 - 1.74 \cdot RD + 25,07 \cdot RS + u \quad (R^2 = 89.9\%) \tag{3}$$

Each unit of RateStaff increases by 25,07 quality education for Bachelor of Computer Science, Physics, and Mathematics. In our opinion, students’ motivation to study courses, which cover specific subject competencies, is determined by the teacher’s personality. Based on the feedback results at KSU in 2020–2021, it is planned to make more optional disciplines.

A key role of IAS and Google forms: collect, store and visualize all the data related to students and their achievements, study programs and individual courses (especially learning outcomes), schedule of classes, and statistics important for university management, financial and quality assurance.

5 Conclusions

The key stage of development, monitoring, and revision of the SP includes initiation, analysis of requirements and requests, determination of the program competencies for the graduates, determination of the internal quality assurance system features in higher

education, study program review, and revision. Programs are reviewed and revised regularly, engaging students and stakeholders. The information collected is analyzed, and the program is adapted to ensure that it is up-to-date.

Using our developed quality assurance information system, we got that each unit of staff rating increases on a rating of staff increases on 0.91 rating of disciplines. The rating of staff directly impacts the rating of courses, which cover specific subject competencies. The teacher's personality determines students' motivation to study field. Based on the feedback results at KSU in 2020–2021, it is planned to make more optional disciplines.

References

1. Ko, J.W.: Quality assurance system in Korean higher education: development and challenges. In: *The Rise of Quality Assurance in Asian Higher Education*, vol. 7, pp. 109–125 (2017)
2. Martins, J., Branco, F., Gonçalves, R., et al.: Assessing the success behind the use of education management information systems in higher education. *Telematics Inform.* **38**, 182–193 (2019)
3. Albina, A.C., Sumagaysay, L.P.: Employability tracer study of Information Technology Education graduates from a state university in the Philippines. *Soc. Sci. Humanit. Open* **2**(1), 100055 (2020)
4. Eilouti, B.: Reinventing the wheel: a tool for design quality evaluation in architecture. *Front. Archit. Res.* **9**(1), 148–168 (2020)
5. Sanchez-Puchol, F., Pastor-Collado, J.A., Borrell, B.: Towards an unified information systems reference model for higher education institutions. *Procedia Comput. Sci.* **121**, 542–553 (2017)
6. Kravtsov, H., Kobets, V.: Model of the curriculum revision system in computer science. In: Ermolayev, V., et al. (eds.) *Proceedings of 14th International Conference on ICTERI*, 2104, pp. 488–500. CEUR-WS, Aachen University (2018)
7. Suárez, E., et al.: Quantitative research on the EFQM excellence model: a systematic literature review (1991–2015). *Eur. Res. Manag. Bus. Econ.* **23**(3), 147–156 (2017)
8. European Foundation for Quality Management. <https://www.efqm.org/index.php/efqm-model/download-your-free-short-copy-of-the-efqm-model/>. Accessed 21 Nov 2020
9. National Institute of Standards and Technology. <https://www.nist.gov/baldrige>. Accessed 21 Nov 2020
10. Hota, P., Nayaka, B., Sarangi, P.: Integration of total quality management principles to enhance quality education in management institutions of Odisha. *Mater. Today Proc.* (2020). <https://doi.org/10.1016/j.matpr.2020.10.129>
11. Doneva, R., Gaftandzhieva, S., Bliznakov, M., Bandeva, S.: Learning analytics software tool supporting decision making in higher education. *Int. J. Inf. Technol. Secur.* **12**(2), 37–46 (2020)
12. Endut, A.S.: Enhancing internal quality assurance mechanism at HEI through responsive program evaluation. *Procedia Soc. Behav. Sci.* **123**, 5–11 (2014)
13. Marra, M., McCullagh, C.: Feeling able to say it like it is: a case for using focus groups in programme evaluation with international cohorts. *Int. J. Manage. Educ.* **16**(1), 63–79 (2018)
14. Kooli, C.: Governing and managing higher education institutions: the quality audit contributions. *Eval. Program Plann.* **77**, 101713 (2019)
15. Tiziana, I.S., Migliaretti, G.G., Vesce, E.: Accreditation in higher education: does disciplinary matter? *Stud. Educ. Eval.* **63**, 41–47 (2019)



An Android Application for Explaining Form Deviations Using 3D Models

Grigore Marian Pop^(✉) , Radu Comes , and Liviu Adrian Crisan 

Technical University of Cluj-Napoca, 103-105 Muncii Street, Cluj-Napoca, Romania
grigore.pop@muri.utcluj.ro

Abstract. The research aims to develop a mobile learning engineering application, presenting the form deviations according to ISO 1101. This application aims to improve the quality of tolerances and dimensional control and 3D Modelling courses for engineering students, covering the following lines of studies: design, robotics, industrial and mechanical engineering. The previous studies focused on mobile learning's impact on student achievement show that the method could be one of the promising educational technologies. The educational applications used on mobile devices develop a friendly environment and generate a positive effect on learning. The authors conducted a detailed analysis of the educational applications presenting geometrical tolerances available in Google Play. This paper also presents the advantages and disadvantages of the published applications. In 2018 we published the educational android application ISO Checker. They are using this mobile application integrated into the engineering courses students transmitted positive feedback. Students are hi-tech learners, and they are in trend with current technological innovations in education.

Keywords: Mobile learning · Geometrical tolerancing (GD&T) · Form deviations · Geometrical product specification (GPS) · Educational application

1 Introduction

The purpose of the research is to implement and design a mobile learning application to improve the quality of the teaching dimensional and tolerances control and 3D Modelling courses for engineering students, covering the following lines of studies: design, robotics, industrial and mechanical engineering. The developed application will provide information regarding the indication and interpretation of the geometrical tolerances according to the latest ISO GPS standards, using 3D interactive models to highlight the tolerance zones. The authors aim is to develop the application to be available in three different languages: English, German and Romanian.

The shape of the real workpiece surface in the geometrical meaning conforms with the nominal surface's shape only approximately. For example, a cylindrical shaft's surface may have the shape of a cone or a barrel, and a section in the plane perpendicular to the axis can look like an ellipse. These differences from nominal shape are called form deviations (see Fig. 1).

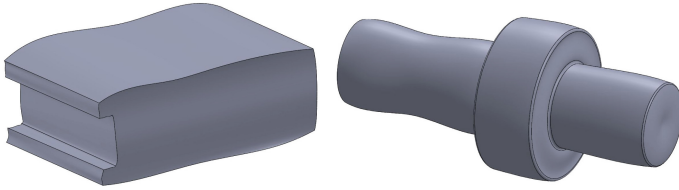


Fig. 1. Real surface non-ideal.

The actual workpieces have elementary form only rarely, e.g., cylinder or sphere, as in pins or balls of bearings. The geometrical shape of a workpiece is usually more complex, e.g., a stepped shaft consists of a few cylindrical surfaces, a gearbox is solid with several holes. In these cases, apart from keeping the proper dimensions and form, there is a necessity for proper orientation and location of individual elements. For example, the two-stepped shaft surfaces should be cylinders having a common axis, and the holes in the gearbox should have parallel axes. Due to manufacturing circumstances, this cannot be achieved readily. To set the permissible limits of form location and orientation, geometrical tolerances are defined [1]. Depending on the characteristic to be specified and the way it is specified, the tolerance zone is one of the following, according to EN ISO 1101:2017:

- the space within a circle,
- the space between two concentric circles,
- the space between two parallel circles on a conical surface,
- the space between two parallel circles of the same diameter,
- the space between two parallel straight lines,
- the space between two non-equidistant complex lines,
- the space within a cylinder,
- the space between two coaxial cylinders,
- the space within a cone,
- the space within a single complex surface,
- the space between two parallel planes,
- the space within a sphere,
- the space between two non-equidistant complex surfaces.

Since geometry and 3D space are still considered a complicated subject area for students, learning innovation requirements arise to overcome the problems faced while understanding geometry [2].

The awareness that plus/minus tolerances is not sufficient for the unique definition of the part's geometry was raised in the industry in the middle of the 20th century. Finally, in 1969 recommendation ISO/R 1101-1: Tolerances of form and position – Part 1 Generalities, symbols, indications on drawings was published. It was replaced in 1983 by the 1st edition of the standard ISO 1101 Technical drawings – Geometrical tolerancing – Tolerancing form, orientation, location, and run-out – Generalities, definitions, symbols, and drawings. Similar needs in the USA drove to publish standard USASI Y14.5-1966 Geometric dimensioning and tolerances preceded by three editions of military standard

MIL-STD-8. Currently, the 4th edition of International Standard ISO 1101:2017 and 6th edition of American Standard ASME Y14.5-2018 is valid [3].

Although researchers are still exploring the implications of m-learning in all educational fields, and there are different views on the matter, Adriana Teodorescu shows in her study that traditional teaching strategies corroborated with m-learning practice have paved the way to an effective improvement of students' skills [4]. Thanks to smartphones, people can search very fast and provide information, cultural activities, learning tools, economic activities, and social communication. A number of studies focus on mobile learning's influence on student achievement and show that the method can be a promising educational technology for developing an educational environment. The use of mobile devices as tools for educational purposes has a positive effect [5]. Various studies have explored the educational advantages and the potential of mobile learning (virtual reality) [6, 7], showing that students engage with their learning materials more effectively when using their own devices [8, 9].

An education strategy should be adopted to the needs of students. Considering the recent innovations, students are now hi-tech learners. So, we consider that using mobile applications integrated into the study of technical courses stimulates student's involvement, considering the positive feedback we had during the first semester of the academic year 2018–2019 after publishing the android application ISO Checker.

2 Literature Review

As presented by other researchers, the field of metrology has constantly evolved, being driven by two essential elements: hardware and software development [10]. The authors analyzed all the available android applications before developing the GD&T application and noticed the following:



Fig. 2. Print screens from Mechanical Design and Gd&T – Offline App [11].

1. According to its description, the app presented in Fig. 2 covers all basic mechanical engineering-related topics, basic interview questions, notes, lecturer materials, news & blogs, college notes for the mechanical engineering course. Related to geometrical

tolerances, it only presents some examples of 2D annotations and definitions of the tolerance zones without any graphical representations.

- The next application found on google play is MechTab Werder AG, presented in Fig. 3, which has in its menu also some explanations regarding Geometrical Tolerances, such as Symbols, 2D drawings, and explanations (Fig. 4).

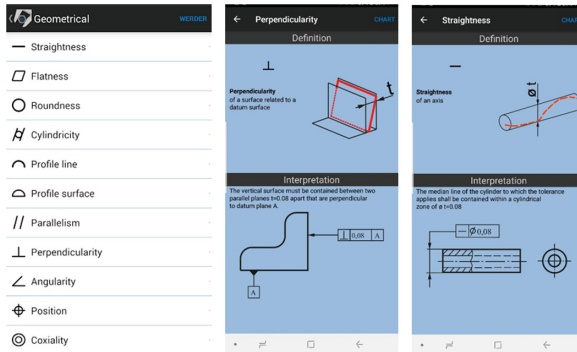


Fig. 3. Print screens from MechTab Werder AG [12].



Fig. 4. Print screens from EasyGDT Guide [13].

- EasyGDT Guide Free (Early Access) is a quick reference for GDT and Drawings symbols, meaning according to ASME Y14.5-1994, but it does not present the free version's geometrical tolerances (Fig. 5).
- According to the authors, this is an App version of their best-selling printed pocket guide on Geometric Dimensioning and Tolerancing (GD&T). In its 77 pages, it describes the GD&T symbols and their use on engineering drawings. Standard inspection techniques and reporting methods are also included in the descriptions.

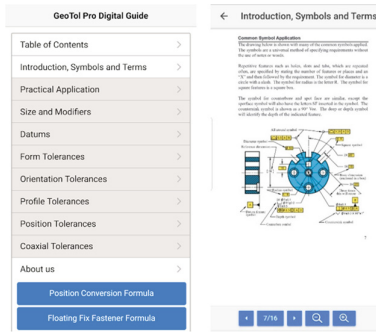


Fig. 5. Print screens from GeoTol Pro GD&T Guide [14].

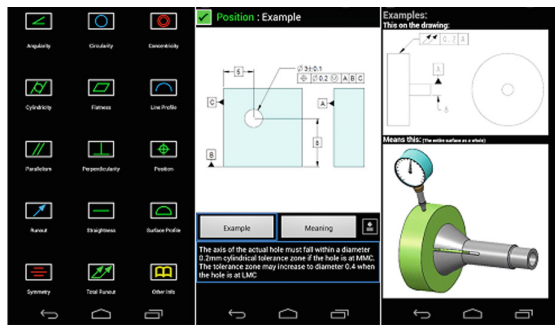


Fig. 6. Print screens from GeoTol Pro GD&T Guide [15].

- GDT app presented in Fig. 6 is the online reference application according to the ASME Y14.5-2009 “Geometric Dimensioning and Tolerancing” standard. It is intended only for a brief introduction to GD&T (Fig. 7).

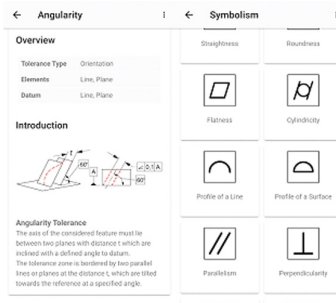


Fig. 7. Print screens from GD&T from ZEISS [16].

- GD&T from ZEISS available in English and German (Form und Lage Pro), but only some examples are explained in the free version. It presents the GD&T according to ISO 1101 and describes the definitions of geometric dimensioning and tolerancing in order to support the engineers and technical employees as a multimedia reference book. This app explains the definitions of GD&T and its interpretation using video animations with examples for all the geometrical tolerances.

3 Research Methodology

Based on the analysis and reviews of the relevant mobile applications in the field of tolerances and dimensional control, the authors are willing to develop a free android application to be used by the engineering students when studying Tolerances' courses Design. Further, we present some examples included in the android application, 2D, 3D annotations, and animations for explaining the tolerance zones for form tolerances according to ISO 1101:2017.

The developed application integrates 3D models that were defined using Solidworks 2018 software. The ideal CAD models have been defined using the traditional sketching and modelling workflow, while de deform models have additional free form cuts that make use of spline profiles [10]. The 3D models have then been exported using the standardized AP 214 step file format defined by ISO-10303-24-2. This file format has multiple advantages over the AP203 (defined by ISO-10303-21), such as adding color, layers, design intent, and most importantly, geometric dimensioning and tolerances while having the other common interoperability features such as geometry topology and individual solid models for part elements and assemblies (Fig. 8).

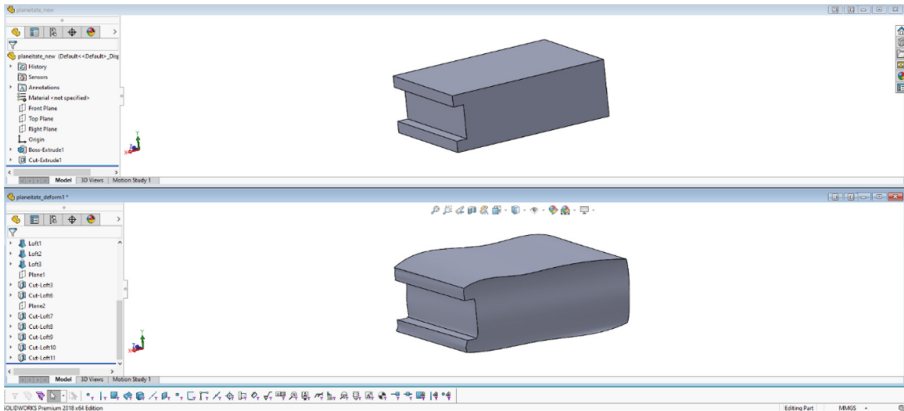


Fig. 8. The definition of the ideal and deformed model in SolidWorks for the Flatness tolerance.

The AP214 STEP files have been imported to Autodesk 3ds Max 2020 software which was used to define individual 3D models for the annotations, axes, leaders, arrows, tolerances elements. This step was essential to ensure that all these elements can be properly converted to 3D elements that can then be visualized on the mobile application.

Autodesk 3ds Max software has been used to define various animations of the 3D models such as section cutting and interactive annotation appearance to define better digital learning material (Fig. 9).

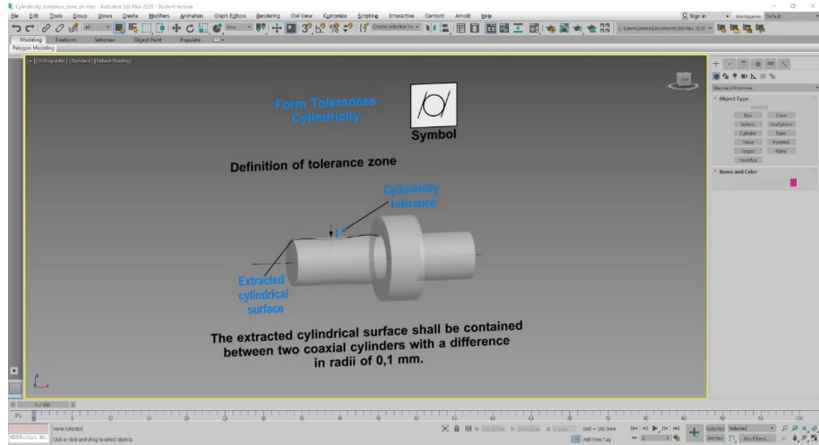


Fig. 9. The definition of axes, leaders, arrows, annotations, and tolerance elements as 3D representations of the non-ideal features.

The mobile device application has been created using Unity software (Fig. 10). The 3D models defined both in SolidWorks and 3ds Max have been integrated within a tiles user interface that enable the user to enable individual annotations, either the 2D, 3D or the explaining tolerance zones.

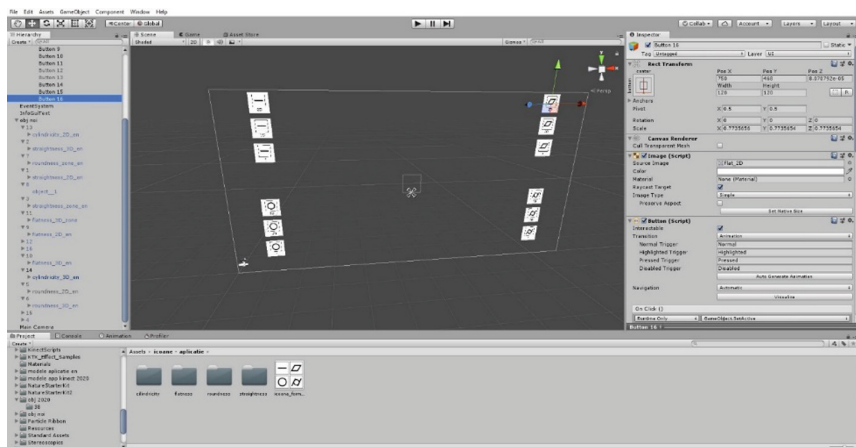


Fig. 10. The development of the mobile application within Unity.

4 Results

These elements are positioned in the center of the screen, and the user can rotate and scale the objects. The Android version application interface is presented in Fig. 11.

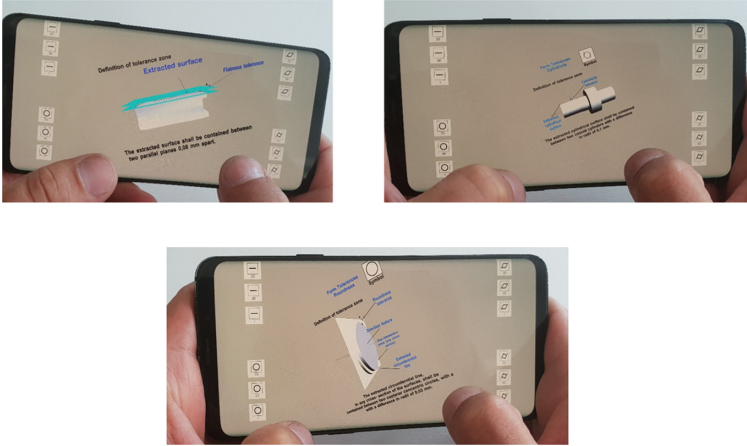


Fig. 11. Explanations of geometrical tolerances presented in the developed android application.

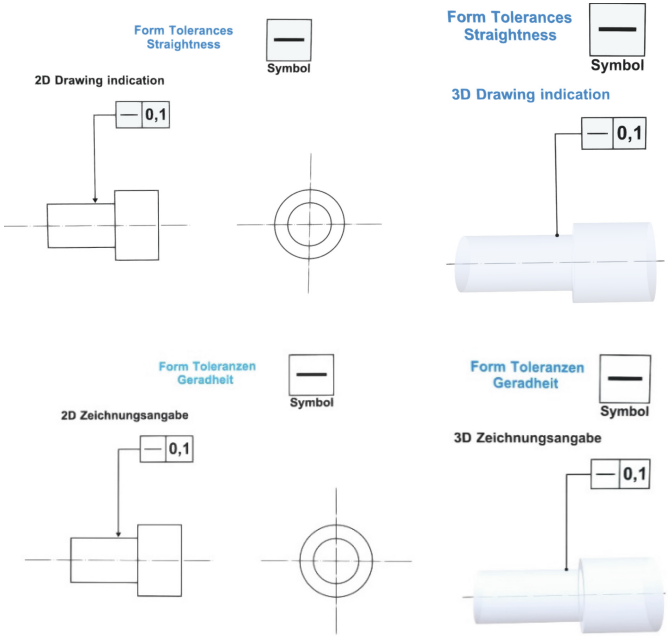


Fig. 12. 2D and 3D drawing indication for Straightness tolerance [17, 18].

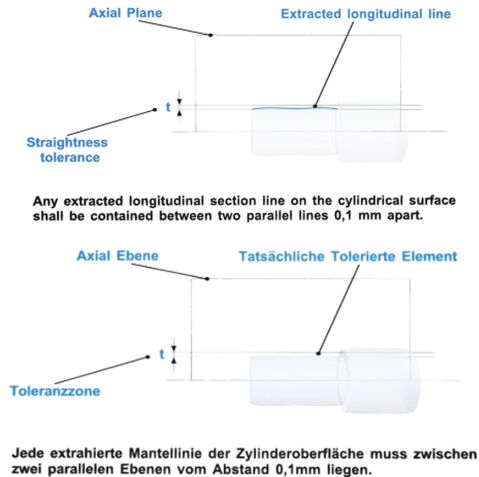


Fig. 13. Print of the 3D definition of the tolerance zone for Straightness tolerance [19].

Figures 12 and 13 present the explanations given by the developed android applications for straightness tolerance in English and German.

5 Conclusions

The previous studies focused on mobile learning's impact on student achievement show that the method could be one of the promising educational technologies. The educational applications used on mobile devices develop a friendly environment and generate a positive effect on learning. In 2018 the authors published the educational android application ISO Checker. They are using this mobile application integrated into the engineering courses students transmitted positive feedback. Using mobile learning allows students to access the information round the clock. This is one of the reasons why mobile devices are being used intensively, and they have increased the effectiveness of learning environments.

Students can easily download these didactic resources to their smartphones or tablets, making the learning experience more dynamic and engaging than traditional teaching methods.

The developed Android application presented in this paper uses 3D animations presenting four geometrical tolerances (straightness, flatness, roundness, and cylindricity).

After using the developed application, the students will be able to:

- understand what a geometrical feature is,
- be aware of the relationships between geometrical features (ideal and non-ideal),
- have a general knowledge on geometrical tolerances,
- interpret the ISO geometrical tolerances,

- recognize symbols of geometrical tolerances,
- know the rules of indication of geometrical tolerances.

Further features that will be added to the presented application:

- represent and explain all geometrical tolerances according to iso 1101 with explanations in 3 different languages (English, German, and Romanian);
- explanations regarding the 3d measurements of the explained geometrical tolerances using POWERINSPECT form AutoCAD;
- indications regarding the use of GDT in the design of different machine parts,
- the application will also be developed to be compatible with MS Windows.

References

1. Plowucha, W., Jakubiec, W., Humienny, Z., Hausotte, T., Savio, E., Dragomir, M., Bills, P.J., Marxer, M., Wisla, N., Mathieu, L.: Geometrical product specification and verification as toolbox to meet up-to-date technical requirements. In: The 11th International Scientific Conference “Coordinate Measuring Technique” CMT 2014, Bielsko-Biala, Poland (2014)
2. Gargrish, S., Mantri, A., Kaur, D.P.: Augmented reality-based learning environment to enhance teaching-learning experience in geometry education. In: 9th World Engineering Education Forum, WEEF. *Procedia Comput. Sci.* **172**, 1039–1046 (2019)
3. Humienny, Z.: New ISO geometrical product specification standards as a response to industry 4.0 needs. In: Wang, L., Majstorovic, V.D., Mourtzis, D., Carpanzano, E., Moroni, G., Galantucci, L.M. (eds.) *Proceedings of 5th International Conference on the Industry 4.0 Model for Advanced Manufacturing. LNME*, pp. 306–312. Springer, Cham (2020). https://doi.org/10.1007/978-3-030-46212-3_23
4. Crompton, H., Burke, D.: The use of mobile learning in higher education: a systematic review. *Comput. Educ.* **123**, 53–64 (2018)
5. Teodorescu, A.: Mobile learning and its impact on business English learning. In: The 6th International Conference Edu World 2014 “Education Facing Contemporary World Issues”. *Soc. Behavioral Sci.* **180**, 1535–1540 (2014)
6. Buń, P., Trojanowska, J., Ivanov, V., Pavlenko, I.: The use of virtual reality training application to increase the effectiveness of workshops in the field of lean manufacturing. In: 4th International Conference of the Virtual and Augmented Reality in Education, VARE 2018, pp. 65–71 (2018)
7. Salaimeh, S.A., Hjouj, A.A.: Visual object-oriented technology and case-tools of developing the internet/intranet-oriented training courses. *J. Eng. Sci.* **4**(2), H9–H11 (2017). [https://doi.org/10.21272/jes.2017.4\(2\).h9](https://doi.org/10.21272/jes.2017.4(2).h9)
8. Chen, Y.-L., Hsu, C.-C.: Self-regulated mobile game-based English learning in a virtual reality environment. *Comput. Educ.* **154**, 103910 (2020)
9. Ivanov, V., Pavlenko, I., Trojanowska, J., Zuban, Y., Samokhvalov, D., Bun, P.: Using the augmented reality for training engineering students. In: 4th International Conference of the Virtual and Augmented Reality in Education, VARE 2018, pp. 57–64 (2018)
10. Neamtu, C., Hurgoiu, D., Popescu, S., Dragomir, M., Osanna, H.: Training in coordinate measurement using 3D virtual instruments. *Measurement* **45**(2012), 2346–2358 (2012)
11. Mechanical Design and GD&T. <https://play.google.com/store/apps/details?id=com.eazyon.tech.mechanicalengineeringdesign&hl=en>. Accessed 21 Nov 2020

12. MechTab Werder AG. <https://play.google.com/store/apps/details?id=ch.samuelwerder.newmechtab&hl=en>. Accessed 21 Nov 2020
13. EasyGDT Guide Free (Early Access). <https://play.google.com/store/apps/details?id=com.easygdt.free&hl=en>. Accessed 21 Nov 2020
14. GeoTol Pro GD&T Guide. <https://play.google.com/store/apps/details?id=alliancetek.pocketguide.pro&hl=en>. Accessed 21 Nov 2020
15. <https://play.google.com/store/apps/details?id=com.peterkanold.www.gdt&hl=en>. Accessed 21 Nov 2020
16. <https://play.google.com/store/apps/details?id=de.zeiss.imt.fulpro&hl=en>. Accessed 21 Nov 2020
17. Pop, G.M., Crişan, L.A., Tripa, M.: Toleranzen und Passungen. PRESS, Cluj-Napoca (2019)
18. Zhongyu, J.L.: Learning with mobile technologies, handheld devices, and smart phones: innovative methods. University of Huddersfield, IGI-Global (2012)
19. Sung, Y.-T., Chang, K.-E., Liu, T.-C.: The effects of integrating mobile devices with teaching and learning on students' learning performance: a meta-analysis and research synthesis. *Comput. Educ.* **94**, 252–275 (2016)



In-campus Way of the Insight Transfer Technology

Lesya Shkitsa^(✉) , Volodymyr Kornuta , Olena Kornuta , Vasyl Bui ,
and Iryna Bekish 

Ivano-Frankivsk National Technical University of Oil and Gas, Institute of Engineering Mechanics, 15, Karpatska St., Ivano-Frankivsk 76019, Ukraine
lshkitsa@nung.edu.ua

Abstract. The version of solving the relevant problem of increasing the innovative activity of engineering specialties students by organizing the academic environment is proposed. The purpose of the activity is to update future engineers and working citizens' professional competencies and ensure transparent conditions for evaluating instructional designing results. The ways of implementing the project-oriented training principles in the technical university are presented, which will allow to actively involve students in scientific and innovative activities within the educational process and the performance of qualification work. The authors have proposed a model of the information system based on the use of electronic document flow, implemented, at this stage, for the organization of the activity process. The proposed approaches to engineering education will allow to use of student youth's potential for the development of innovations by scientific-educational project teams and minimize the costs of ensuring the functioning of single information space of innovation-project activity.

Keywords: Citizens innovation development · Innovation infrastructure · Information system

1 Introduction

The decrease in the number of the employed/engaged in innovation activities in Ukraine indicates the urgency of the problem of modifying the workflow of technical higher educational institutions. This problem is also commonly found in other countries, even those considered to belong to a group of developed economic leaders [1].

The cycle of return of investments in the re-equipment of educational institutions is long and does not guarantee the result for a particular enterprise; therefore, entrepreneurs tend to buy ready-made solutions of more advanced economies. Novelties are expensive. Respectively, the technical level lags behind several years (nevertheless, it is ahead of the average technological level in the region). Solving the problem by technology imports leads to a lack of skills of workers and graduates of the universities in innovation activities, which in the long run leads to a deepening of the crisis phenomena. Thus, the low level of commercialization of innovative developments is the general problem.

A new EU Framework Programme for Research and Innovation should bring research and innovation even more closely together [2]. For the future, the goal is to succeed in translating knowledge in marketable products and services because now each student, research and teaching staff, SME, and innovator must develop solutions on their own to the same problems with access to modern, personalized production equipment. Together with regulatory restrictions, this increases the entry threshold on the R&D market or makes it unavailable due to limited resources and virtually no investment potential (relatively small investments in high-tech and innovative R&D projects, insufficient number of RTSs possessing the skills of such work).

It is necessary to improve universities' technology transfer systems to facilitate (financially and organizationally) potential entrepreneurs overcoming the "death valley" between innovative developments and launching commercial or social production, preferably while increasing the willingness of academic and urban communities to engage in science, production. The early involvement of university researchers in industry needs along the value chain is of key importance to bridge the "valley of death" between the idea and the market. This should also enable breakthrough innovations.

2 Literature Review

The education should foster innovation by putting curiosity, critical thinking, deep understanding, the rules, and inquiry tools. The teachers can offer students the tools and experiences that spur an innovative mindset. Innovation now emerges from teams and networks—and we can teach students to work collectively and become better collective thinkers. Group work is common, but teamwork is rare [3].

The difficult task of education is to teach and encourage students to ask new questions, solve new problems and create new knowledge. Consequently, the triunity of knowledge, skills, and motivation should be the basis of education in the modern century. Internal motivation, new skills, learning new material throughout life is the basis of success in innovation [4, 5].

An important task of the system of higher technical education is the training of specialists for innovation and projects. The analysis of pedagogical practice and theoretical research allows determining the project activity as means of developing competence, in the course of which the evolution of professionally important qualities of a specialist, formation of his key competencies takes place [6, 7].

Therefore, to ensure the goals of sustainable development in the conditions of accelerated evolution of the industrial and economic system, higher education of Ukraine should be sufficiently dynamic, and the experience and achievements of the best educational systems of the world should be used as a roadmap of change [8, 9].

Universities of Ukraine traditionally apply the approach to the management of training, which suggests that students acquire skills during individual work in the study of disciplines. A student can get a solid knowledge of each discipline, which, however, does not provide the ability to integrate tools to solve real-life problems. Leading universities and associations have proposed applying the project-oriented approach and the involvement of students in innovation activity as a method of solving similar problems. The use of virtualization (3d visualization) in the classrooms for better understanding

by future engineers design and models of work objects with which they will work in professional activities is also known [10, 11]. The concurrence of the subject-oriented (skill-oriented) and project-oriented management of the educational process in higher education institutions is a separate problem [4].

In the future, the university campus will become a precinct that interfaces university and society, with start-ups, community organizations, and social enterprise intermingling with the students: there will be full integration with society and industry [12]. Universities will remain vital places for the development of global citizens; a university thinks internationally, is based in the local economy, but works for the purpose of national and regional development [13].

Educational systems might increase the economic, innovative, and business potential of the regional centers and contribute to sustainable economic development. Rapidly growing economies are marked by social fragmentation and economic divisions but can become the drivers for shrinking social divisions and creating opportunities for all the citizens [14]. The level to which the technological environment is developed has a major impact on society's development overall. The technological environment encompasses the quality of education, support for science, and use of scientific knowledge in practice [15].

Project-based learning is undoubtedly one of the best instructional methods for developing students' broad learning capabilities beyond teaching specific subject matter [16, 17]. The results show that the intervention's implementation significantly improved higher-order cognitive skills, self-efficacy, teamwork, and communication skills [18]. Observed benefits of teaching in the new environment include increased faculty ability to visually explain complex problems, increased ability of students to conceptualize engineering problems, and increased engagement of students in after-class collaboration [10].

Research and innovation create investment opportunities for new and better products and services and increase competitiveness and employment [18].

The modern technological system leads to the need to reform the traditional system of education and scientific activity. The reform process takes place around the world [8, 19, 20].

3 Research Methodology

In the course of the research, the system's principles and complex and process approaches; methods of analysis and synthesis, logical generalization, analogies, comparative comparison; techniques of grouping, and schematic representation of data were used to solve the set tasks. In particular, a comparative analysis of diagrams of subject learning processes and processes specific to project-based learning was performed. Processes were broken down into constituent components in individual user actions with artifacts/materials/documents. For further analysis, the method of graphical analysis (construction of UML diagrams) was used. Methods of logical generalization, comparative comparison were used to study the features of information flows and the corresponding documentary support of project and process learning activities. Generalization and synthesis of the center of innovative development work's scheme were carried out using

grouping techniques based on semantic and visual reflections. The analogies method was used to assess the effectiveness of the proposed approaches to accelerate and enhance the impact of research and private development on the economics of innovation development.

4 Results

Ivano-Frankivsk National Technical University of Oil and Gas (Ukraine), together with the Technical University of Cluj Napoca - North University Center of Baia Mare (Romania) and NGO «Association Academic Organization for Research, Innovation and Professional Development» (Romania), implement the project “Ro-Ua Trans-border Academic Development for Research and Innovations” (Ro-Ua TADRI) aimed at creating pre-conditions for sustained cooperation in the fields of research and innovation under the Joint Operational Programme Romania - Ukraine 2014–2020.

This project makes possible further academic development for research and innovation of actual project implementation for the relevant regional production plants. The created Innovation Development Centers (CIDs) will increase researchers’ and students’ competence in modern equipment usage and produce real prototypes of innovative products. The project achievement and distinguished feature will be the preparation of human potential to solve the actual challenges of society and production to strengthen innovation development.

It should be noted that the CID further expands the existing innovation infrastructure. The general objective of Ro-Ua TADRI is to increase the potential of development, research, and innovation in mechanic, electronic, environment protection domains to reduce technological differences and contribute to the economic development of the trans-border region. The achievement of this goal involves the accomplishment of at least the following objectives: to establish a communication environment between universities and regional companies to joint academic research and innovation potential with companies’ real needs; to support researchers and students in developing new competencies in modern technologies; to create for the students new competencies for innovation and involve them in research and innovation projects, increasing the quality of students projects by their materialization in competition premises.

The WEB-interface information system is accepted as the technological basis of interaction [21, 22]. The European Strategy for Innovation Development predetermines the need to develop a separate information system. The strategy envisages the creation of national and regional units of the modern research infrastructure of the EU and the provision of access to open data and knowledge in the single digital European market.

The information system serves to provide documentary support to Innovators and Researchers activities and become a testing ground for developing the model of electronic document circulation of the university. The information system based on the use of electronic document flow realized for the organization’s organization is realized.

The introduction of innovations in real production involves the development of existing prototypes. This, in turn, requires design work. International practices show that such a system works more effectively with the introduction of a single information space based on the use of electronic document flow. The implementation of design and development currently supports a specialized class of corporate information systems - technical document flow systems, which requires more thorough research.

In the development process, it is necessary to determine the set of actions for users of the basic scientific and educational space information system to ensure innovation and design activities. A set of user scenarios defines the required set of information system functionality.

The industry-specific higher educational institution (HEI) has been chosen as the institutional basis for ensuring the scientific and educational information space's functioning. An analysis of the existing HEI business processes has been carried out using the approach of creating classifiers and time budgeting based on map tables [23]. A conceptual model of combining educational work and research with CID's help has been developed, the schematic representation of which is shown in Fig. 1. The model of work is based on the information system of CID (IS of CID).

The model is based on the search for a solution by intellectual storming, where the questions are the priority research areas, the answers are formulated in the form of project proposals. The proposal can be based on known technical solutions [23] or proposed as an innovative idea for further commercial implementation, e.g., in the form of a start-up. Proposals are formulated by stakeholders, who can act as entrepreneurs or potential start-ups, students, scientific and pedagogical workers, or anyone interested.

To submit a project proposal, a person registers as a stakeholder in the information system by filling out the appropriate form. Each stakeholder can submit a project proposal. The project proposal should contain a list of tasks to be performed with an analysis of the existing logistics and the equipment park of the HEI or laboratories of common use (reference or contractual, possibly sectoral). To do so, a list of all available equipment, its layout, a use planning tool, and an ordering tool for educational services to acquire skills and access to it should be available (at least within the internal information space available to employees with appropriate disclosure restrictions). An additional parameter of the project proposal may be the productivity within the HEI's license conditions requirements. The project proposal should provide an opportunity to obtain scientific results at the level of advanced worldwide developments.

The project is considered by the CID management and approved or rejected. Project rejection can be conditional or unconditional. Of course, projects that contain signs of illegality are rejected. Projects that cannot be implemented on existing CID equipment are conditionally rejected. The stakeholder may propose changes to the conditionally rejected project, which will allow its implementation in the CID or contribute to the CID's additional equipment to ensure the possibility of the initial project. Use Case diagram of the laboratory management system is shown in Fig. 2.

The stakeholder, whose project is approved, acquires the rights of a CID user. The CID user can form a team for the project implementation, book the time of using the equipment necessary for the project implementation.

The CID information system provides everyone with a list of equipment, a description of its capabilities, and the skills needed to access the equipment. The system's tools are used to control the existence of users' skills required to access the equipment. In the absence of skills, the user can offer to join the user's team with the necessary skills or acquire them by completing the necessary training tasks (by taking the appropriate course in the CID). The CID offers different (standard and individual) training, depending on the user's skills. Minimum training – 3 academic hours (0.1 credits) – on the safety and basic

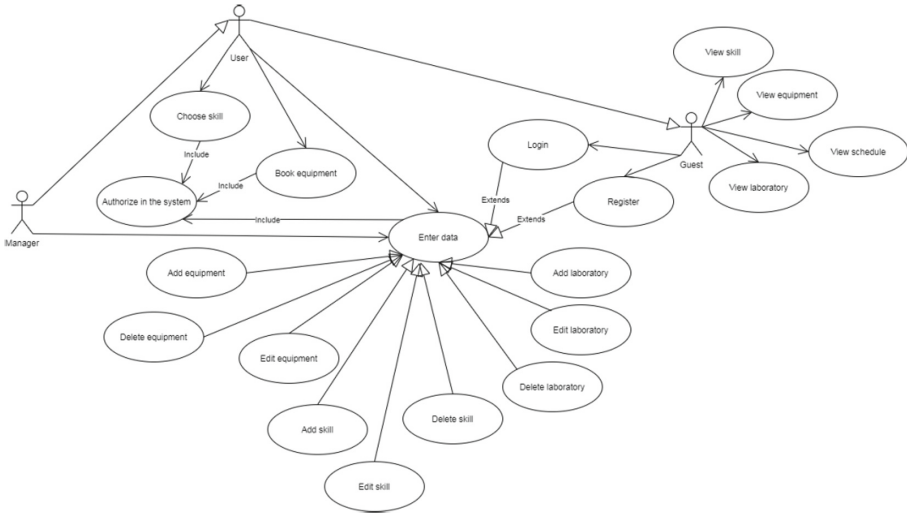


Fig. 2. Use Case diagram of the laboratory management system.

The CID equipment list is based on the basic assumption that the center should implement projects in various industries (currently except the development of the microelectronic components). However, all these projects would have a material implementation, e.g., in the form of a model or mockup that the researcher/developer or their group would be able to do by themselves (to acquire relevant skills and to deepen the knowledge of potential difficulties, methods of overcoming them, advantages and disadvantages of using single production technologies). Among the equipment: a variety of hand tools (both manual and mechanized, e.g., power tools), milling machines, laser engraver, plasma cutter, lathe (all equipped with CNC), vertical drilling machines, 3D printers (FDM and SLA), welding inverter, locksmith workbenches and assembly table, soldering stations, etc. All equipment, except for the laser engraver, plasma cutter, and lathe, was purchased in several units to provide opportunities for group work on the project.

The proposal for the implementation of projects, proposed by potential employers or through own challenges/problems of potential students, the availability of infrastructure for the projects, the availability of supplies, spare parts, contacts with suppliers, the executed projects (portfolio) is the basis for the increase of the interest in technical education. The modern university has to be a sort of business incubator and the “first job” for its graduates. As a result of the implemented in the CID project, the student will acquire knowledge, skills, and possibly equipment suitable for immediate use in the labor market or to implement their own projects.

The CID will provide the functioning of the information and reference system. The system includes the following modules: registration of tasks; formation of project groups; organization of the distribution of time and material resources during the implementation of a specific project and between projects; an electronic directory of implemented projects and a database of documents for the verification of project results.

The module of the formation of project groups provides the implementation of several role functions: a student who joins the task performance; a teacher who assesses the task for compliance with a particular discipline and offers the number of points a student can gain upon completion of the assignment; a representative of the stakeholders, who proposes tasks and evaluates their solutions.

The database will contain registration of companies' needs of development and innovation and connect universities with economic actors, growing the involvement of researchers and students in regional companies' future growth and the responsibilities of highly qualified human resources in regional development. Joint projects that ensure the learning through projects are developed. The tutor for the company-end coordinator for the university is conducting the project development guaranteeing the quality of the results. Along with the project's theoretical development, the main component is the practical result obtained using CID's equipment.

Since the CID's equipment is valuable, it must be equipped with access control and video surveillance systems. Such equipment, besides the direct use, also allows realizing two things (as part of the methodology of activity analysis): to confirm the independence of project implementation; to use CID as a base for implementing the practical part of the qualification tasks.

Video files along with other documents form the case of the project. We offer the information system, constructed based on the new concept [23], as one of the possible technological support alternatives for academic integrity.

5 Conclusion

The ways of increasing the innovative activity of engineering specialties students, which are proposed, include: Center for Innovation and Development, equipped with modern technologies machine and tools, the researchers and students, who can create mockups and prototypes of their projects; database, which contains the registration of companies needs of development and innovation, connects universities with economical actors; the information system, which provides documentary support to researchers and students' activities. This will help achieve the following results: increased amount of information about companies' development, research & innovation needs; improved researchers and students' competencies in modern technologies; developed infrastructure enabling researchers to create the experimental model in minimum time after registration and selection of ideas; increased number of joint research activities, researchers and students involved in the development of innovative projects; increased number of students' projects involving new technologies determining improved students' projects quality. CID's main function is similar to one of the FabLab network functions - ensuring equal access to modern technologies on both sides of the border. Although in FabLab, this feature contributes to a simple transfer of technical developments, in the context of CID, it promotes joint development of innovation and transfer of developed technologies through the equalization of technological capabilities.

References

1. Glaesser, J.: Competence in educational theory and practice: a critical discussion. *Oxf. Rev. Educ.* **45**(1), 70–85 (2018). <https://doi.org/10.1080/03054985.2018.1493987>
2. Guidelines for the new EU Framework Programme for Research and Innovation Federal Government Position Paper (2017). https://www.bmbf.de/files/Federal_government_FP9_guidelines_September_2017.pdf. Accessed 29 Oct 2020
3. Markham, T.: *Project Based Learning*. HeartIQ Press, San Rafael (2012)
4. Wagner, T., Dintersmith, T.: *Most Likely to Succeed: Preparing Our Kids for the Innovation Era*. Scribner (2016)
5. Halimatun, A., Zul, A., Shaharudin, I., Mohd, Z.: BYOD implementation in university: balancing accessibility and security. In: *Proceedings of 2nd International Conference on Education, Business, Islamic and Technology (ICEBIT 2018)*, pp. 145–154 (2018)
6. Gozalo-Delgado, M., León-Del-Barco, B., Mendo-Lázaro, S.: Good practices and learning strategies of undergraduate university students. *Int. J. Environ. Res. Public Health* **17**(6), 1849 (2020). <https://doi.org/10.3390/ijerph17061849>
7. van Stijn, N., van Rijnsoever, F.J., van Veelen, M.: Exploring the motives and practices of university–start-up interaction: evidence from route 128. *J. Technol. Transf.* **43**(3), 674–713 (2017). <https://doi.org/10.1007/s10961-017-9625-5>
8. Volchik, V., Oganessian, A., Olejarz, T.: Higher education as a factor of socio-economic performance and development. *J. Int. Stud.* **11**(4), 326–340 (2018). <https://doi.org/10.14254/2071-8330.2018/11-4/23>
9. Volchik, V., Zhuk, A., Oganessian, A., Abrhám, J.: Analysis of the institutional building and sustainable development of higher education in transition economies. *Entrepr. Sustain. Issues* **7**(2), 1413–1423 (2019). [https://doi.org/10.9770/jesi.2019.7.2\(43\)](https://doi.org/10.9770/jesi.2019.7.2(43))
10. Koh, C., Tan, H.S., Tan, K.C., Fang, L., Fong, F.M., Kan, D., Lye, S.L., Wee, M.L.: Investigating the effect of 3D simulation based learning on the motivation and performance of engineering students. *J. Eng. Educ.* **99**(3), 237–251 (2010). <https://doi.org/10.1002/j.2168-9830.2010.tb01059.x>
11. Pasyeka, N., Pasyeka, M.: Construction of multidimensional data warehouse for processing students' knowledge evaluation in universities. In: *Proceedings of the 13th International Conference on Modern Problems of Radio Engineering, Telecommunications and Computer Science (TCSET)*, pp. 822–824 (2016). <https://doi.org/10.1109/TCSET.2016.7452195>
12. de Wit-de Vries, E., Dolfsma, W.A., van der Windt, H.J., Gerkema, M.P.: Knowledge transfer in university–industry research partnerships: a review. *J. Technol. Transf.* **44**(4), 1236–1255 (2018). <https://doi.org/10.1007/s10961-018-9660-x>
13. Halloran, L., Friday, C.: *Can the universities of today lead learning for tomorrow? The University of the Future* (2018). <https://cdn.ey.com/echannel/au/en/industries/government--public-sector/ey-university-of-the-future-2030/EY-university-of-the-future-2030.pdf>. Accessed 29 Oct 2020
14. Tvaronavičienė, M., Tarkhanova, E., Durglishvili, N.: Sustainable economic growth and innovative development of educational systems. *J. Int. Stud.* **11**(1), 248–256 (2018). <https://doi.org/10.14254/2071-8330.2018/11-1/19>
15. Kořiová, E., Grmanová, E., Habánik, J.: Regional disparities in financing innovations in small and medium-sized enterprises. *J. Int. Stud.* **11**(3), 124–136 (2018). <https://doi.org/10.14254/2071-8330.2018/11-3/11>
16. Barak, M.: From 'doing' to 'doing with learning': Reflection on an effort to promote self-regulated in technological projects in high school. *Eur. J. Eng. Educ.* **37**(1), 105–116 (2012). <https://doi.org/10.1080/03043797.2012.658759>

17. Silva, F.B., Sabbatini, F.H., de Barros, M.: Project-based learning in civil engineering education: an experience at the University of São Paulo. In: International Symposium on Project Approaches in Engineering Education, São Paulo (2012)
18. Ford, M.: Rise of the Robots: Technology and the Threat of a Jobless Future. Basic Books, New York (2015)
19. Bhatnagar, R., Kumar, A., Gupta, S.: Role of Information systems in an university setup – a case study. *Int. J. Comput. Sci. Electron. Eng. (IJCSEE)* **4**, 151–156 (2016)
20. Shkitsa, L., Kornuta, V., Kornuta, O., Bekish, I.: The model of informational space for innovation and design activities in the university. *Sci. Innov.* **15**(6), 14–22 (2019). <https://doi.org/10.15407/scin15.06.014>
21. Htwe, T., Aung, M.: Development of information system for a university. *Int. J. Sci. Res. Publ.* **9**(6), 494–499 (2019). <https://doi.org/10.29322/IJSRP.9.06.2019.p9071>
22. Romanyshyn, Y., Sheketa, V., Pikh, V., Poteriailo, L., Kalambet, Y., Pasioka, N.: Social-communication web technologies in the higher education as means of knowledge transfer. In: Proceedings of 14th International Conference on Computer Sciences and Information Technologies (CSIT), pp. 35–38 (2019). <https://doi.org/10.1109/STC-CSIT.2019.8929753>
23. Shkitsa, L., Kornuta, V., Kornuta, O., Bekish, I., Bui, V.: Information support of design innovation activity of the technical university. *Manag. Syst. Prod. Eng.* **28**(2), 127–132 (2020). <https://doi.org/10.2478/mspe-2020-0019>



Information and Communication Technology Tools for Enhancing Engineering Students' Creativity

Olena Titova¹ (✉) , Petro Luzan² , Natalia Sosnytska¹ , Serhii Kulieshov¹ ,
and Olena Suprun¹

¹ Tavia State Agrotechnological University, 18, B. Khmelnytskyi Ave.,
Melitopol 72310, Ukraine
olena.titova@tsatu.edu.ua

² Institute of Vocational Education of the National Academy of Pedagogical Sciences of
Ukraine, 98a, Vito-Lithuanian Lane, Kyiv 03045, Ukraine

Abstract. Nowadays, students naturally prefer using information and communication technologies in various situations. That led to their different attitude to information and the way they perceive and process information. On the other hand, engineers' widespread use of information and communication technologies in their job has changed the goals, learning content, methods, forms, teaching aids, methods, and teachers and students' interaction. The article's purpose was to analyze a range of tools in terms of didactic tasks that could be successfully solved. The paper deals with the review of resources enabled revealing some learning areas which the information technologies can support: activation of various external senses through the use of multimedia, automation of calculations, improve graphic part of the design, organization of a creative educational environment, optimization of the time-consuming processes of learning outcomes control. The ideas for the organization of students' cognitive activities of higher levels and learning software for implementing the ideas are presented in the article. The conclusion about the necessity of the educational process updating under the information technologies application was made. Being oriented on the development of the creative potential of engineering students, the information and communication technologies influence goals, learning content, teaching forms and methods as well as cooperation of teachers and students providing development of students' information literacy, skills of processing information, creation and joining ideas into new combinations and transferring them to different situations to provide engineering students' preparedness for the innovative engineering activity.

Keywords: Engineering education · Engineering students' creativity · Creative potential of engineering students · Creative educational environment · Software

1 Introduction

The educators at higher engineering schools deal with the generation of students that grew up in the creative educational environment of information and communication

technologies (ICT). Nowadays, students consider it completely natural to use ICT in any life, an academic or professional situation, not excluding other ways but preferring ICT [1]. That condition has influenced students' attitude to information, the means of its processing, and even the way of thinking. The current generation of engineering students easily and efficiently operates information searching, processing, storage, and transmission [2, 3]. Widespread use of ICT by engineers to solve any problem requires modernization of the goals, learning content, methods, forms, teaching aids, methods of control, and teacher's and student's activities and cooperation. Students can build different research approaches, knowledge acquisition, formation of own experience in critical evaluation of information, and prediction of consequences of their professional activity, and development of responsibility. All this, in turn, leads to the development of critical and figurative thinking, the search for alternative skills of learning, the ability to build causal relationships, etc.

Thus, the support of the educational process at universities with information and communication technologies is expedient and natural as it is based on the growing provision of educational institutions with Internet communication, computers, interactive whiteboards, electron microscopes, webcams, etc. The learning process is supported by cloud technologies, educational platforms, video conference tools, messengers, social networks to organize access to the university site with students' and teachers' accounts where the learning process, progress, and results are presented.

2 Literature Review

The research results indicate that the ICT application's effectiveness in an engineering classroom depends on many factors. The first is the quality of ICT tools and technologies used in learning. Research on the issue, for example, at EU engineering schools, has shown that teachers are sometimes not satisfied with ICT quality [4]. On the other hand, educators are often not ready for the wide use of ICT in their practice limiting them to applying certain functions in addition to traditional methods [5, 6]. For example, despite the benefits of interactive whiteboards that can replace traditional whiteboards, PowerPoint presentations, and textbook content, teachers do not have the skills to use them to organize student-centered learning and creativity development. That naturally raises the question of cost-effectiveness as interactive whiteboards are quite expensive.

The application of information and communication technologies in the engineering education process is supposed to involve students to solve various engineering problems, so the learning goals must be focused on higher productive levels of students' cognitive activity, including creation, application, evaluation of information, development of ideas, models, etc. [4, 7, 8].

The analysis of the latest publications [4, 6, 9–11] allowed to reveal some directions in the learning process which ICT applications currently covers:

- activation of various external senses through multimedia (visualization of processes, phenomena, events) based on materials prepared by both a teacher and a student. That opens new opportunities for students' creativity. For example, a video illustrating the operation of a device or its node can be found on the Internet. Otherwise, the teacher

can prepare it themselves or can offer students to make the video as an individual creative task or a group project [12, 13];

- support of calculations and graphic part of a design through automation of actions using standard and specially developed software. Moreover, involving students in the design of appropriate software is effective in fostering their creative potential, as the process provides the entire design cycle: from identifying the customer needs and the problem up to testing and working out the shortcomings. For instance, the tools for modeling dynamic systems can be used by students during their research work. The engineering aspect and the procedure itself have been already analyzed and published [14, 15];
- organization of a creative educational environment, which can support and provide necessary means (including methodological) for personal learning trajectory. On the other hand, it is effective for keeping academic and professional communication, mutual exchange, support, cooperation between students and teachers [12, 16];
- providing diagnostics for the learning process, when the ICT allows to automate the time-consuming processes of control, evaluation, analysis of learning outcomes, and accumulation of statistic data. Also, students can be provided with the tools for examining their mechanical comprehension, learning abilities, or level of their creative potential as it has been considered in [17].

Thus, the introduction of information and communication technologies in the educational process looks promising. In respect of that, the article's purpose was to analyze and understand a wide range of tools in terms of didactic tasks that could be successfully solved. We predicted that the findings could be the base for further scientific substantiation of ICT use in the engineering education process.

3 Research Methodology

The methodology was based on synergetic, personality-oriented, activity, information, and technological approaches that made it possible to consider the specifics of engineering both as a professional and learning spheres. The complex of approaches corresponded to the directions of solving the problem of ICT use for education purposes. The synergetic and personality-oriented methodological approaches allowed to study the dynamics of personality development from the standpoint of self-determination, self-development, joint creativity, freedom of choice of one's educational trajectory due to self-organization, self-reflection, and development of nonlinear thinking under ICT tools application in the classroom. The information and technological approaches enabled a conclusion about the specific educational process that should consider methodological principles and combine in harmony education and personal development under the conditions of trust, mutual respect, cooperation, and partnership. The activity approach helped to reveal the necessity to attract students to intensive intellectual and creative activities. That provided conditions for productive self-learning and self-control by students of their goals, opportunities, and results. Based on the activity approach requirements, it was established that to enhance students' creativity, appropriate tasks (real problems, open tasks, etc.) should be developed and offered to students. While working with the

tasks and searching for the solutions, the students were supposed to be involved in various professional-oriented learning activities. That consistently prepared students for performing innovative engineering activities.

4 Results

ICT tools allow an engineer to develop an idea from the beginning in the form of notes or drawings through modeling with spreadsheets and computer-aided design systems, further digital image processing, animation, or video preparation that would demonstrate the idea in action. When the idea is developed in an interdisciplinary project, for example, with the involvement of experts from different spheres, ICT enables the further exchange of ideas, critical evaluation, consultation, discussion, analysis, selection, transformation, and rapid presentation of results. That accelerates communication and supports the creative process. Thus, the active introduction of information and communication technologies to solve educational and production problems radically changes the paradigm of engineering education, bringing learning situations closer to real problems and stimulating the students' creative potential.

ICT in this context introduces both *ideas* for students' cognitive activities towards their tasks and *tools* for implementation of the ideas and solutions to these problems. Students use numerous technologies outside the classroom in everyday life, not usually to require additional training. Considering the results of the latest research on ICT application for educational purposes and on student's creative potential development gave grounds to make a deep analysis of the areas for the effective use of information and communication technologies in the engineering education process (Fig. 1). It was offered to introduce specific ICT tools at different learning levels (from reproductive to creative activities). That enabled the consecutive development of students' creative skills, starting from the abilities to find and process necessary information leading the student to the confidence in using engineering applications (apps) and Computer-Aided Design (CAD) systems.

Thus, the replacement or addition of ICT to traditional forms, methods, and teaching tools will not contribute to the development of the student's creative potential. For these purposes, the combination of tools must be justified with clearly defined goals, predictable results, expected benefits, and so on. With the advent and adaptation of *Web 2.0* and *Cloud Technologies* and *Services*, educational technologies are shifting towards the prevalence, publicity, and multimodality.

ICT makes students creative and responsible in choosing different styles and formats of information processing and joining educational and professional resources, networks, and projects due to the development of skills of critical thinking, problem-solving, and new ideas generating. Social media (*Facebook*, *MySpace*, *LinkedIn*), multimedia (*YouTube*), online games, and blogs offer wide opportunities to create ideas, share results and get quick feedback.

Video and animation tools are very effective for creativity development. The use of these tools to perform tasks increases the interest and motivates students to work independently. Creating videos and animations illustrating the phenomenon or process under consideration involves students in an in-depth study of different questions. The variety

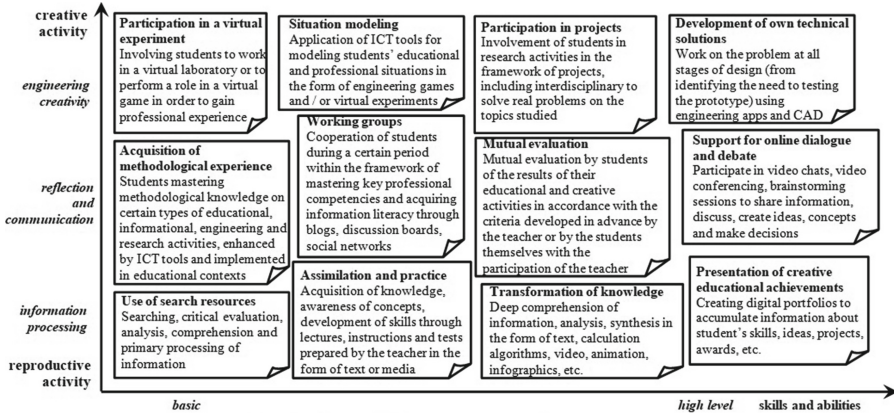


Fig. 1. Areas of application of ICT in the engineering educational process.

of resources and programs for professionals and beginners allows students with different backgrounds to test and develop their creativity. For video editing, experts recommend *Movavi, AdobePremierePro, FinalCutPro, SonyVegas, DaVinciResolve*, and available for smartphones *PowerDirector, KineMaster*. Programs like *3ds Max, AdobeAfterEffects, Dragonframe, StopMotionPro* are recommended for creating animation.

Resources for enhancing thinking through the use of brainstorming techniques help increase students' creativity and give them different ways of interconnecting thoughts. Using ICT, students can receive many simple and free tools to develop visual and effective mind maps, graphs, and diagrams to illustrate the topic, concept, sequence of operations, procedures, decisions, etc. The most common tools for online brainstorming are *MindMapping software, SpiderScribe, WiseMapping, ChartTool, Creately*.

Games are one of the leading means of promoting cooperation and creative development. Educational games allow students to acquire knowledge in an atypical way combining interactive and figurative elements in their minds. Games help to develop risk-taking skills revealing freedom for creativity. Among the professionally-oriented games [18], we can name *RoboRush* (the essence of the game is to develop and sell robots and modernize their production), *TheEISSimulation* (developed by the Center for Advanced Learning Technologies, involves players in teamwork to introduce innovation and persuade managers to accept development), *PowerUp* (aimed at developing knowledge of different sciences in terms of environmental impact), *ElectroCity* (allows students to understand power energy and the environment as well as design their city).

We also tested games and game resources for the improvement of technical creativity. For example, *TrussMe* was developed by missile designer, professor of aerospace technology at Georgia Institute of Technology, USA [19]. The game implements real algorithms and simulation techniques used in the aerospace, engineering, and construction industries. The game's task, which aims to develop engineering skills, is to design and test various structures.

The *Edheads* resource offers a series of games for engineering students. They allow mastering the forces that operate in simple and complex mechanisms (*SimpleMachines*

and *TheCompoundMachine*). Students can become virtual technicians in production, master and practice routine skills, measurements, quality assessment, equipment debugging, troubleshooting, production decision making (*Manufacturing Technician*). Engineering students can participate in the development of a mobile phone for special needs and master the tools and basics of the design process (*Design a cellphone*).

An additional resource, which can be offered to students, is the software provided by the International Organization of Electrical and Electronics Engineers (IEEE). The application of *TRYEngineering* allows students to foster technical creativity due to the deepening of engineering knowledge and developing design skills. That is enabled by many methods realized in the games, *The Transformer* (introduces future engineers to materials and their properties), *Energy Flows* (provides basic knowledge about the production and transmission of energy), *Bionic Arm Design Challenge* (guides future designers through all stages of bioelectronic prosthesis development and introduces the basics of robotics, biotechnology, and electronics), etc.

Virtual reality technology is a global industry currently with powerful investments that have significant potential for education [20]. Virtual Labs in the form of a website or software designed to simulate and reproduce real phenomena and processes allow students to explore issues, change conditions, scenarios, compare and contrast results, interrupt and resume the experiment, reproduce it again, take notes, etc. Some resources for virtual reality that can be used in the development of engineering students' creative potential are freely available: *Vitlab* (a virtual chemistry laboratory that offers experimental and demonstration resources, tasks, and tools for creating their experiments by students and teachers of colleges and universities), *VirtualLabs* (laboratory experiments to study the microstructures and resistance of materials, mechanics, thermodynamics, hydraulics, robotics, automatic mechanical systems, fault diagnosis, etc.).

Another group of online resources and software was offered to students to automate design, calculations, and modeling processes. One example is the *Altair Solid Thinking Package*, which is focused on modeling informed design solutions in production and design training, engineering model development, prototyping, and testing. Students mastering design were involved in the full life cycle of the product from concept development to operation. The software covers various disciplines, including statics, dynamics, fluid physics, thermal energy management, electromagnetic systems, etc., as well as provides data analysis and reliable simulation and visualization of processes. Another tool for modeling dynamic systems is *Solid Thinking Embed (VisSim)* software. The software allows designing control systems and digital signal processing for multi-domain modeling. The package is used for modeling aeronautical, biological, or medical systems, energy systems, electric motors, hydraulic, mechanical, electrical, technological, thermal, and econometric systems by building models as a visual way to describe the situation. The advantage of using this method by students is that they do not need to deal directly with the solution's mathematical expressions, which can be quite difficult to understand and solve. Also, visual modeling, which employs a hierarchical composition to create nested flowcharts, facilitates the data's perception and processing. That significantly improves students' skills of analysis, evaluation, comparison, making conclusions, etc.

It was stated that the software products for automatic design could be successfully used to solve some didactic tasks on the creative development through the influence on intellectual, motivational, and productivity spheres, as they allow to:

- design and analyze machines and units that have moving parts or several interacting mechanisms, cams, gears, etc. (*MechDesigner*);
- develop mechanisms with effective kinematic equations that provide accurate solutions; create digital and 3D models of physical objects with their preparation for 3D printing; create flexible designs that can be reused and customized using global parameters (*Geomagic Design*);
- perform structural, static and dynamic calculations, thermal analysis, weight optimization, analysis of vibration modes and modeling of safety and reliability of structures using extended numerical methods for solving nonlinear problems with the possibility to prepare relevant documentation (*ANSYS DesignSpace*);
- model electrical, mechanical circuits, fluid flows and chemical reactions based on physics of the process (*COMSOL Multiphysics*);
- research previously developed models and create libraries of special components that are integrated into other modeling programs (*MapleSim*);
- a model with application of ready-made standard components and units from libraries; the model based on the mock-ups or kinematic diagrams; model solids and surfaces including intuitive creation of new geometry (*KOMPAS-3D*);
- perform parametric modeling; program tools for CNC machines; develop and export STL models for 3D printers (*Fusion 360*);
- design, identify problems and defects of development; analyze by dividing complex systems into subsystems and research of each subsystem using special tools (*RecurDyn Professional*);
- to convert measurement units (*Engineering Unit Converter*);
- perform multi-level calculations in all disciplines using mathematical functions; perform vector and matrix calculations (*MATLAB, TechCalc100*);
- develop electrical circuits using intelligent technology *Smart Wires* (*CircuitLab, Engineering Power Tools, TinkerCAD*).

Considering our practical experience we can claim that the application of educational software increases the efficiency of student's independent work, so the optimal learning organization employs ICT as dominant. This allows organizing the educational process as a technological one when an engineering student passing every subsequent stage develops his approaches and activity from reproductive to creative.

There is a possibility to diagnose interim learning outcomes, identify inconsistencies with the planned results, refine and master the material in the optimal mode, and consider each student's abilities. Diagnostics in the learning process involves timely detection, evaluation, and analysis of the learning outcomes. It includes control, evaluation, accumulation of statistics, analysis, clarification of dynamics, trends, forecasting further developments and results with application ICT, allowing automating the time-consuming process of educational results control.

To provide a purposeful character of the educational process, the presented resources and applications could be reasonably included in a syllabus supported by a specially

designed distance course. That could provide students with constantly available learning content and methodological support, which, also, could be used by students and teachers beyond the university developer. Some free resources like *MOODLE* enable creating both full-fledged distance courses and designing a test base with different types of test tasks (multiple-choice, matching, alternative, open tasks, essays, etc.) could provide control at all the stages of learning. There is also an opportunity to organize a technological process with diagnostics of the students' entrance level, choice of forms, methods, and means of teaching, systematic step-by-step implementation of cognitive activities of higher levels (from recognition to implementation and evaluation, up to creation), control and correction of learning outcomes that do not meet the established requirements.

5 Conclusions

Thus, the introduction of information and communication technologies into the educational process for the development of the engineering students' creative potential is one of the current requirements which engineering universities tend to meet to prepare their graduates for effective professional activity under the conditions of total informatization and automation of all spheres of life. The ICT is introduced with interactive whiteboards, webcams, cloud technologies, educational platforms, video conference tools, messengers, social networks, software for video and animation, resources for brainstorming, games, virtual reality technology, applications for automated design, calculations, and modeling. A deep analysis was made in the article to define the areas for the effective use of information and communication technologies in the engineering education process and introduce specific ICT tools at different learning levels to develop students' creative skills and abilities consecutively.

Further research should be devoted to updating the educational goals, learning content, teaching forms and methods, teacher's and student's activities oriented on the students' creativity development through the ICT application.

References

1. Prensky, M.: Digital natives, digital immigrants part 2: do they really think differently? On Horizon **9**(6), 1–6 (2013). <https://doi.org/10.1108/10748120110424843>
2. Tapscott, D.: Grown up digital: how the net generation is changing the world. Int. J. Market Res. **52**(1) (2010). <https://doi.org/10.2501/S1470785310201119>
3. Cachia, R., Ferrari, A., Ala-Mutka, K., Punie, Y.: Creative Learning and Innovative Teaching. Final Report on the Study on Creativity and Innovation in Education in the EU Member States. Publications Office of the European Union, Luxembourg (2010). <https://doi.org/10.2791/52913>
4. Hadgraft, R.G., Kolmos, A.: Emerging learning environments in engineering education. Australas. J. Eng. Educ. **25**(1), 3–16 (2020). <https://doi.org/10.1080/22054952.2020.1713522>
5. Onuiri, E., Sunday, A.I., Patricia, E.C.: IT evolution: opportunities for personal and national development. Int. J. Comput. Appl. **115**(19), 37–42 (2015). <https://doi.org/10.5120/20262-2665>
6. Abdulla, M., Motamedi, Z., Majeed, A.: Redesigning telecommunication engineering courses with CDIO geared for polytechnic education. In: 10th Conference on Canadian Engineering Education Association Proceedings (2019). <https://doi.org/10.24908/PCEEA.VI0.13855>

7. Hernandez-de-Menendez, M., Morales-Menendez, R.: Technological innovations and practices in engineering education: a review. *Int. J. Interact. Des. Manuf. (IJIDeM)* **13**(2), 713–728 (2019). <https://doi.org/10.1007/s12008-019-00550-1>
8. James, M.A.: Managing the classroom for creativity. *Creat. Educ.* **6**, 1032–1043 (2015). <https://doi.org/10.4236/ce.2015.610102>
9. Haldorai, A., Murugan, S., Ramu, A.: Evolution, challenges, and application of intelligent ICT education: an overview (2020). <https://doi.org/10.1002/cae.22217>
10. Țirziu, A.M., Vrabie, C.I.: NET Generation. Thinking outside the box by using online learning methods. In: *New Trends and Issues Proceedings on Humanities and Social Sciences*, vol. 8, pp. 41–47 (2016)
11. Vries, P., Klaassen, R., Kamp, A.: Emerging technologies in engineering education: can we make it work? In: *13th International CDIO Conference Proceedings*. University of Calgary (2017)
12. Kim, H., Choi, H., Han, J., So, H.-J.: Enhancing teachers' ICT capacity for the 21st century learning environment: three cases of teacher education in Korea. In: Lim, C.P., Chai, C.S. (eds.) *Building the ICT Capacity of the Next Generation of Teachers in Asia*. Australas. J. Educ. Technol. **28**(6), 965–982 (2012)
13. Majumdar, S.: *Emerging Trends in ICT for Education & Training* (2015)
14. Panchenko, A., Voloshina, A., Titova, O.: Development of the universal model of mechatronic system with a hydraulic drive. *Eastern-Eur. J. Enterp. Technol.* **4**(7(94)), 51–60 (2018). <https://doi.org/10.15587/1729-4061.2018.139577>
15. Panchenko, A., Voloshina, A., Boltiansky, O., Milaeva, I., Grechka, I., Khovansky, S., Svyrenenko, M., Glibko, O., Maksimova, M., Paranyak, N.: Designing the flow-through parts of distribution systems for the PRG series planetary hydraulic motors. *Eastern-Eur. J. Enterp. Technol.* **3**(1(93)), 67–77 (2018). <https://doi.org/10.15587/1729-4061.2018.132504>
16. Ala-Mutka, K., et al.: *ICT for Learning, Innovation and Creativity* (2015). <https://citeseerx.ist.psu.edu/viewdoc/download?doi=10.1.1.424.1525&rep=rep1&type=pdf>. Accessed 15 Dec 2020
17. Sosnytska, N., Titova, O., Symonenko, S., Kravets, O.: Examining the creative potential of engineering students. In: Nadykto, V. (ed.) *Modern Development Paths of Agricultural Production*, pp. 299–306. Springer, Cham (2019). https://doi.org/10.1007/978-3-030-14918-5_31
18. Jensen, R.: 50 Great Sites for Serious, Educational Games. <https://www.onlinecolleges.net/50-great-sites-for-serious-educational-games/>. Accessed 15 Dec 2020
19. McFadden, C.: 8 Awesome Engineering-Based Paid and Free Games for Kids. <https://interestingengineering.com/8-awesome-engineering-based-paid-and-free-games-for-kids>. Accessed 15 Dec 2020
20. Kamińska, D., Sapiński, T., Aitken, N., Della Rocca, A., Barańska, M., Wietsma, R.: Virtual reality as a new trend in mechanical and electrical engineering education. *Cent. Eur. J. Phys.* **15**(1), 936–941 (2017). <https://doi.org/10.1515/phys-2017-0114>

Numerical Simulation and Experimental Studies



Development of Optimum Thin-Walled Parts Milling Parameters Calculation Technique

Sergey Dobrotvorskiy¹ , Serhii Kononenko¹ , Yevheniia Basova¹  ,
Ludmila Dobrovolska¹ , and Milan Edl² 

¹ National Technical University “Kharkiv Polytechnic Institute”,
2, Kyrpychova St., Kharkiv 61002, Ukraine

² University of West Bohemia, Univerzitni 2732/8, Pilsen 30100, Czech Republic

Abstract. In machining thin-walled parts, determining the optimum machining strategy and the criterion selection of milling parameters is highly relevant. This study addresses the gap in the variety of computer-aided machining parameters calculation solutions. Thin-walled parts are broadly used in many industries due to their efficiency and lightweight. But there are many barriers to surface formation processes. Therefore, the features of thin-walled parts in modern manufacturing preparation have to be taken into account. Furthermore, to provide machining parameters information in a wide range, an intelligent selection method of parameters is essential for a robust basis in the progressive Industry 4.0 concept. The research is laid down in the context of production digitalization in Industry 4.0 thus represents linkage of data, analytics, and interface interaction. The software solution interface is a calculation application consisting of modules of thin-walled part geometrical and material properties, machine, tool, removal, cut parameters, and the area of computed results. The solution database is based on the resultant values collected from mechanical engineering literature, static and dynamic finite element modeling of thin-walled part response under applied loads.

Keywords: Thin-walled parts · Milling parameters · Variable stiffness · Part deflection · High-speed milling

1 Introduction

Thin-walled parts are broadly used in many industries due to their efficiency and lightweight. But there are many barriers to surface formation processes. The deflection of thin-walled parts is one of the major problems that appear during the process of machining. The deflections critically limit material removal performance and lead to geometrical deviations. Existing calculation solutions mostly consider only the tool's flexibility, while the part is supposed to be rigid. Generally, deflections are solved by additionally designed devices or techniques, which raises the cost of the product. However, the problem should be considered comprehensively. Depending on the technical requirements for the surface quality, it is often necessary to use both - as additional equipment as intelligent systems in production preparation.

Several milling parameters selection methods: tabular, analytical, graph-analytical, using CAM software, and special calculation solutions. The demand for developing this software is the fact that the traditional data search in the reference books, literature, accompanying tool guides significantly slows down the technological preparation for production. Also, during the manual calculations, tables search a lot of routine work is performed, which significantly increases the possibility of errors and increases the human factor.

The principal goal of the study is to scientifically facilitate the process of milling parameters selection, considering the features of thin-walled parts.

2 Literature Review

The Industry 4.0 concept has a set of modern technologies, the use of which is aimed to create a new generation of manufacturing systems [1]. The central problem of implementing the Industry 4.0 concept for a small machinery manufacturing enterprise has also been registered in the paper's contexts: the digitizing of all stages of manufacturing production (CAD/CAM/CAE/CAPP), management (PDM, PLM), marketing and customer relationship management (CRM), overall coordination (ERP) and full product life cycle (PLC) with a single information and software platform. Critical for small machinery manufacturing enterprises are the costs of vertical integration [2], which can be reduced through open and free information management. Deep learning application in CNC monitoring is observed in paper [3].

Studying the problem of processing thin-walled parts, we have analyzed domestic and foreign scientists [4–6]. The quality of critical machine parts and assemblies (for example, the rotor of a steam turbine [7]) depends on the manufacturing of thin-walled parts. Some authors in their researches suggest special software solutions to ensure the best quality of the part. The solution [8] represents the method based on applying a software system that predicts technological deformations during processing. Using the system, a technologist can pick rational cutting modes taking into consideration the deformation predictions.

Another research [9] touches upon the issues of the development of engineering methods of calculating a thin-walled part for valve and flange sealing joints, followed by the formulation of tasks using modern automated calculation software based on Parametric Technology Corporation MathCAD with subroutines for the search for an extremum of functions and the computational block 'Given-minimize'.

In paper [10], problems related to thin-walled parts processing have been considered. Emphasis was placed on "soft" cutting parameters method automation. Solutions using modern software libraries and techniques have been suggested.

Also, the work [11] in which the integration method for error prediction and compensation was established to deal with force-induced errors in NC machining of thin-walled parts has been analyzed. In this research, the mathematical iterative algorithm of errors was built.

The ultrasonic on-machine scanning technique for automatic thickness measurement of large thin-walled parts was proposed in this article [12].

Such technical solutions are relevant because the thin-walled parts are easily distorted in processing each layer of the material. Modeling of distortion due to the processing of thin-walled components depicts that the distortion of the structure is extremely related to the residual stress induced by manufacturing processes like heat treatment, forming, or machining [13, 14].

One of the studies represents a digital solution for milling force determination with optional mill material combinations. The solution involved light scanning in detecting the cutting tool edge geometry, scanning to measure the edge of the tool sectional rake and profiles, FEM analysis of orthogonal cutting to evaluate the force, the simulation with inputs that involved the recognized cut edge geometry, FEM force model, and measured dynamics [15].

It should be noted that a significant part of even the most interesting and advanced ideas are of little use in the real practice of manufacturing thin-walled parts. This can be partially explained by the lack of early product information [16]. As a greater homogenization of information management and software in various small machinery manufacturing enterprises, the approach developed in JavaMach Cluster [17] can be used when information technology and software are developed on a single basis of the programming language Java and Web technologies.

3 Research Methodology

The research methodology utilizes tabular data collected from mechanical engineering literature [18], analytical calculations, and finite element analysis to verify the adequacy of certain parameters. The following research aspects are defined: formulation of the mathematical model, the methods of determining the cutting parameters, main modules of the program solution to develop Fig. 1, implementation of solution algorithm, required technologies for development, and calculations to test the reliability of the results.

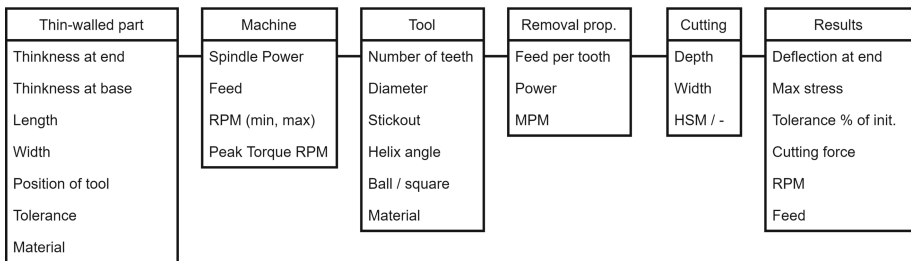


Fig. 1. Main modules and parameters of the program.

The developed software solution should allow: to evaluate the value of the thin-walled part deflection and obtain the maximum stress in the milling of the free end of the part. Have to be implemented the mechanism of validation whether the deflection of the element at the calculated feeds and speeds lies within the initially specified tolerance zone.

The utilization of additionally designed devices or techniques may change the cutting force indicators. Therefore, the software solution should make manual adjustments of the calculated cutting force to evaluate the change in the resulting parameters.

3.1 Model of Thin-Walled Part Deflection

In the process of thin-walled part machining, undesirable deflections occur in the direction of force impact of end mill tool on the surface Fig. 2.

It leads to non-compliance with the technical requirements as the deflection value exceeds the acceptable tolerance zone. It is caused by the decrease in the performance of the machining process since the portion of the cutting energy is spent on the elastic deformation of the thin-walled part.

In the research, the sample geometry of a thin-walled element is a simplified representation of the turbine blade that is commonly applied in many mechanical solutions. The feature of these parts is that the distribution of stiffness in each section significantly varies. Therefore, the developing solution should calculate the deflections for a flat wall with constant thickness and tapering one.

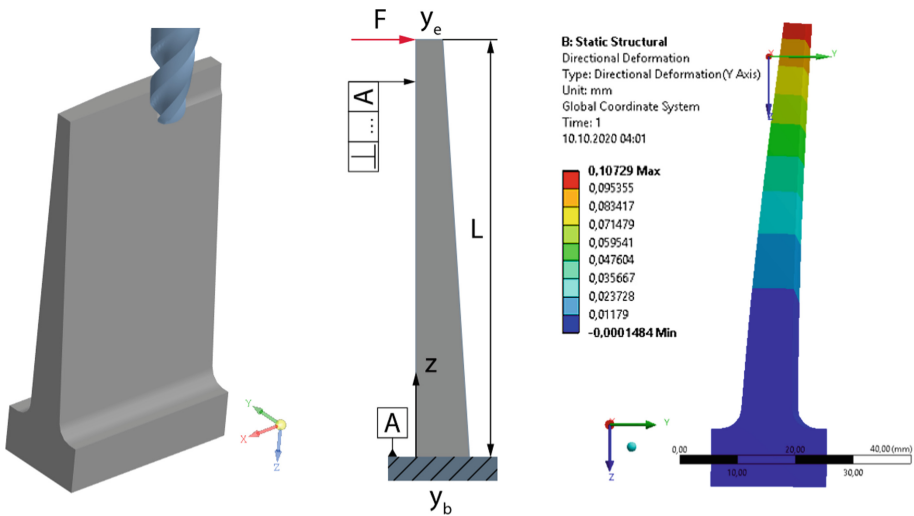


Fig. 2. Model of thin-walled part and FE deflection analysis.

As an entry point for the calculation solution development, the only static behavior of thin-walled structures during machining is presented in this research.

The following deflection equation is used in the development of the proposed calculation solution:

$$\Delta = \frac{12F}{bE} \left(\frac{y_e - y_b}{2m^3 y_b} - \frac{\ln(y_e/y_b)}{m^3} - \frac{L(2y_b - y_e)}{2m^2 y_b^2} \right), \tag{1}$$

where F – generalized force, acting in the y direction to the surface, y_e – the thickness at free end, y_b – the thickness at the base, E – Young’s modulus, is a measure of the material stiffness, L – length of the part, m – the increasing measure of thickness, and represented as $(y_b - y_e)/L$, b – the width of the part.

The sample thickness of the free end $y_e = 3.7$ mm, and the base thickness $y_b = 8.7$ mm. Length of the sample $L = 70$ mm, width $b = 40$ mm. The material is aluminum alloy 1100.

The maximum stress at the base of the part in case of applied force at the free end of the part:

$$\sigma_{\max} = \frac{6FL}{by_b^2}. \quad (2)$$

To check the adequacy of the model, a finite element analysis is performed Fig. 2, and the calculated value practically matches the simulated one $\Delta_{\text{calc}} = \Delta_{\text{fea}} = 0.107$ mm.

3.2 Finite Element Machining Analysis

To fill the database with predefined parameters requires performing the finite element analysis for different materials Fig. 3.

For preliminary analysis, an orthogonal cutting model was selected. It accurately describes the mechanics of machining - speed, depth of cut, material parameters, and applied to obtain raw preliminary data to build dependencies in the database. Although such implementation is useful for quick process modeling, it is impractical for the real machining preparation to obtain accurate results.

The material of the thin-walled sample to represent the calculation solution is aluminum alloy 1100. To perform a high strain analysis, the Johnson-Cook plasticity and damage model are used. Experimental values of the model in Table 1 are obtained from [19]. A , B , n , C , and m are specific material constants that can be obtained experimentally. The Johnson-Cook model is empirical and is widely utilized in metal-cutting simulations.

In the Abaqus Explicit, the chip formation is simulated by a progressive damage model. After the beginning of the damage, the material’s stiffness degrades progressively, corresponding to the applied response of damage evolution. The material’s stiffness degrades smoothly in the advanced model, which is suitable for dynamic and static cases.

The analyzed sample consists of a chip, separation, and machined layers. The thickness of the chip layer (depth of cut) equals 0.1 mm. The thickness of the separation layer is 0.01 mm; the plasticity and damage models are applied, as this thin layer facilitates the separation and further chip formation. For the rest chip and machined layers, only the plasticity model is used. The tool was specified as a non-deformable rigid body.

The analysis allows getting the force acting in the x and y directions. From the point of view of the deflection of the thin-walled part, F_y that directed perpendicular to the wall is essential to consider. Filtering forces output the median of $F_y = 122$ N.

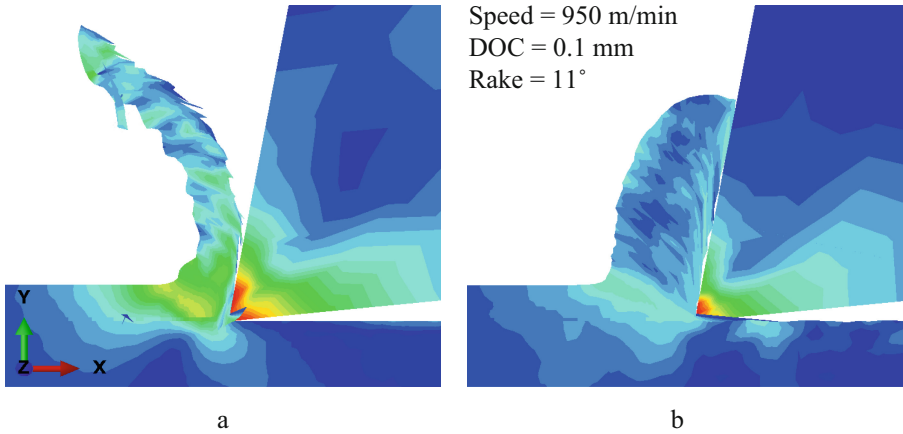


Fig. 3. Finite element analysis of high-speed machining of stainless steel 2Cr13 (a) and aluminum alloy 1100 (b).

Table 1. Aluminum alloy 1100 Johnson-Cook model material constants.

Model	Material constants				
J.C. plasticity model	A, MPa	B, MPa	n	C	m
	148	361	0.183	0.001	0.859
J.C. damage model	d1	d2	d3	d4	d5
	0.071	1.248	-1.142	0.147	0.0

4 Results

4.1 Algorithmic Representation of the Developed Solution

Generally, after analyzing requirements, the direct development of a software product begins with developing program logic, i.e., a set of components interacting with each other according to certain rules and in a certain sequence.

The program starts with reading parameters of thin-walled part geometry Fig. 4, including expected tolerance value and material. The position of the tool (point of applied force) is chosen along the z-axis. The input of its specification parameters selects the machine: RPM, RPM at peak load, maximum available spindle power, and feed ranges.

The next step is the tool (diameter, material, number of teeth, stick out, helix angle, ball/square) and cuts parameters (DOC, WOC, whether HSM is applied) selection. Based on the input, the speed and feeds are calculated and compared to the table values in the database. Depending on the calculation, the right cutting force is applied in the thin-walled part deflection component. The values of forces are obtained as the result of finite element analysis. If an additional impact factor could change the cutting force, the ability to insert value manually is available.

At every stage set of functions perform validations. Thus, in the part deflection component, the verification executes whether the deflection value exceeds the acceptable tolerance zone. The error indicated in the results area, and milling parameters have to be revised if it is. The results are stored in the database and represent the reports that subsequently allow the implementation of an intelligent system of recommendations. The in-development solution is open to access at GitHub Pages [20].

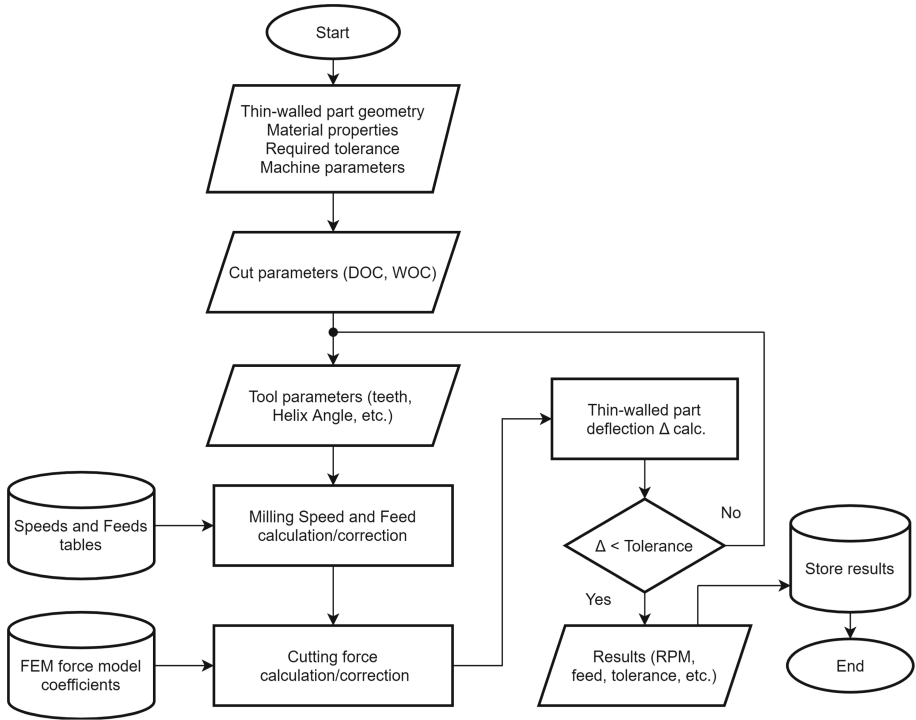


Fig. 4. Block diagram of the program algorithm.

4.2 Development and General Interface of the Calculation Program

The program is implemented as a web application. JavaScript language was used for development. The choice is explained by the possibility of instant access to the application from any platform; there is no need to download the installation files, etc.

The server side is made in Node.js. The interaction between the client and the server is based on the REST API. Data transfer is performed in JSON format. The input and output of the program are stored in the database at the end of calculations.

The general view of the program interface is shown in Fig. 5 and Fig. 6.

The order of common use:

- selection of the machining material expected tolerance, and the geometry of thin-walled part (flat wall/tapering);
- the input of the machine specification parameters;
- selection of the tool material and parameters;
- removal parameters (feed per tooth, unit power, MPM);
- cutting parameters (width, depth of cut, tool deflection);
- calculate button in the result area;
- evaluation of the results depending on the color indicators (red – error, machining cannot be performed, or invalid input value; yellow – the parameter is near its maximum; green – the deflection is in the tolerance zone).

Part		Machine	
	Thickness at end y_e mm	<input type="text" value="4.8"/>	
	Thickness at base y_b mm	<input type="text" value="9.8"/>	
	Length L mm	<input type="text" value="70"/>	
	Width b mm	<input type="text" value="40"/>	
	Pos. of tool ($z=L$ - end) z mm	<input type="text" value="70"/>	
	Tolerance \perp mm	<input type="text" value="0.2"/>	
	Cutting force (auto) F_y N <input checked="" type="checkbox"/>	<input type="text"/>	
	Material:	<input type="text" value="Aluminum"/>	
Tool		Removal prop.	
<input type="text" value="High speed steel"/>			
Diameter mm	<input type="text" value="8.5"/>	Unit power (kW/cm ³)/s	<input type="text" value="0.9"/>
Teeth	<input type="text" value="3"/>	MPM (min, max)	<input type="text" value="30"/> <input type="text" value="190.0"/>
Tool stickout mm	<input type="text" value="22.86"/>	Feed per tooth mm (min, max)	<input type="text" value="0.02032"/> <input type="text" value="0.0531"/>
Helix angle	<input type="text" value="30"/>		
Ballnose <input checked="" type="checkbox"/>			

Fig. 5. The input interface of the program.

Cutting		Results	Calculate
High-speed milling <input checked="" type="checkbox"/>		Deflection at part end mm 0.10685	
Depth mm (min, max)	<input type="text" value="0.1"/> <input type="text" value="0.1"/>	Max stress (z=L at yb) N/mm² 13.33819	
Width mm (min, max)	<input type="text" value="4.899"/> <input type="text" value="4.899"/>	Tolerance perc. of initial % 53.42336	
Tool deflection mm (max)	<input type="text" value="0.01"/>	RPM 11830 (77%)	
		Feed mm/min 4999 (100%)	
		Depth mm 0.1 (100%)	
		Width mm 4.9 (100%)	
		MPM 68.09 (37%)	

Fig. 6. The cutting parameters input and results area.

5 Conclusion

Based on the literature review, there are many solutions to automate machining parameter selection, but many of them are aimed at interaction with the rigid body. In this research, the preliminary development of the solution took into account the basic features of thin-walled parts.

The approach consists of an analytical and practical implementation in the form of a calculation program. The reliability of the static deflection model was proven by finite element analysis. The simplified simulation of machining of the thin-walled sample was performed.

The solution represents the frame that is necessary for extension and its modules modification. Accordingly, the solution requires further improvements and development. The main areas: the complication of the milling process modeling of a thin-walled sample, including complex tool geometry into the calculation; addition of new geometry parameters to the thin-walled element sample model; solution extension by the introduction of dynamic behavior consideration.

The ability to perform Python scripts for Abaqus lets accomplish time-consuming tasks, automates repetitive tasks, and operates with information from databases. Thus there is an ability to further integrate the improved solution as an additional software layer in the production preparation of thin-walled parts machining.

References

1. Jimeno-Morenilla, A., Azariadis, P., Molina-Carmona, R., Kyratzi, S., Moulianitis, V.: Technology enablers for the implementation of Industry 4.0 to traditional manufacturing sectors: a review. *Comput. Ind.* **125**, 103390 (2021)
2. Kűfner, T., Schőnig, S., Jasinski, R., Ermer, A.: Vertical data continuity with lean edge analytics for industry 4.0 production. *Comput. Ind.* **125**, 103389 (2021)

3. Żabiński, T., Mączka, T., Kluska, J., Madera, M., Sęp, J.: Condition monitoring in Industry 4.0 production systems - the idea of computational intelligence methods application. *Procedia CIRP* **79**, 63–67 (2019)
4. Kononenko, S., Dobrotvorskiy, S., Basova, Y., Gasanov, M., Dobrovolska, L.: Deflections and frequency analysis in the milling of thin-walled parts with variable low stiffness. *Acta Polytechnica* **59**, 283–291 (2019). <https://doi.org/10.14311/ap.2019.59.0283>
5. Liu, C., Sun, J., Li, Y., Li, J.: Investigation on the milling performance of titanium alloy thin-walled part with air jet assistance. *Int. J. Adv. Manuf. Technol.* **95**(5–8), 2865–2874 (2017). <https://doi.org/10.1007/s00170-017-1420-9>
6. Vukman, J., Lukić, D., Milošević, M., Borojević, S., Antić, A., Đurđev, M.: Fundamentals of the optimization of machining process planning for the thin-walled aluminium parts. *J. Prod. Eng.* **19**(2), 53–56 (2016)
7. Avdieieva, O., Usatyi, O., Vodka, O.: Development of the typical design of the high-pressure stage of a steam turbine. In: Ivanov, V., Pavlenko, I., Liaposhchenko, O., Machado, J., Edl, M. (eds.) *DSMIE 2020. LNME*, pp. 271–281. Springer, Cham (2020). https://doi.org/10.1007/978-3-030-50491-5_26
8. Eremeykin, P.A., Zhargalova, A.D., Gavriushin, S.S.: Experimental substantiation of soft cutting modes method. In: *AIMEE 2018*, pp. 539–547. Springer, Cham (2019)
9. Gozbenko, V.E., Belogolov, Y.I., Kargapol'tsev, S.K.: Calculation of sealing joints with elastic edge in PTC MathCAD. In: *International Conference on HIRM 2019. J. Phys. Conf. Ser.* **1353**(1), 012027 (2019)
10. Eremeykin, P.A., Zhargalova, A.D., Gavriushin, S.S.: A software system for thin-walled parts deformation analysis. In: *1st International Conference of AIMEE 2017. Advances in Intelligent Systems and Computing*, vol. 658, pp. 259–265 (2018)
11. Qiao, K., Shu, X.: Integration of machining error prediction and compensation for thin-walled workpieces. *Zhongguo Jixie Gongcheng/China Mech. Eng.* **26**(21), 2895–2900 (2015)
12. Lian, M., Liu, H., Zhang, T., Bo, Q., Li, T., Wang, Y.: Ultrasonic on-machine scanning for thickness measurement of thin-walled parts: modeling and experiments. *Int. J. Adv. Manuf. Technol.* **104**(5–8), 2061–2072 (2019). <https://doi.org/10.1007/s00170-019-04021-5>
13. Schulze, V., Arrazola, P., Zanger, F., Osterried, J.: Simulation of distortion due to machining of thin-walled components. *Procedia CIRP* **8**, 45–50 (2013)
14. Kononenko, S., Dobrotvorskiy, S., Basova, Y., Dobrovolska, L., Yepifanov, V.: Simulation of thin-walled parts end milling with fluid jet support. In: Ivanov, V., Trojanowska, J., Pavlenko, I., Zajac, J., Peraković, D. (eds.) *DSMIE 2020. LNME*, pp. 380–389. Springer, Cham (2020). https://doi.org/10.1007/978-3-030-50794-7_37
15. Gomez, M., No, T., Schmitz, T.: Digital force prediction for milling. *Procedia Manuf.* **48**, 873–881 (2020)
16. Sinnwell, C., Krenkel, N., Aurich, J.C.: Conceptual manufacturing system design based on early product information. *CIRP Ann.* **68**, 121–124 (2019)
17. JavaMach Cluster. <https://jmcluster.herokuapp.com/>. Accessed 21 Oct 2020
18. Oberg, E., Jones, F., Horton, H., Ryffel, H.: *Machinery's Handbook*, 29th edn. Industrial Press, New York (2012)
19. Fathipour, M., Zoghipour, P., Tarighi, J., Yousefi, R.: Investigation of reinforced sic particles percentage on machining force of metal matrix composite. *MAS* **6**(8), 9–20 (2012)
20. TW milling. <https://jmcldev.github.io/t-w-calc/>. Accessed 23 Oct 2020



Measurement of Contact Pressure for Conical Honing

Eshreb Dzhemilov  and Ruslan Dzhemalyadinov  

Crimean Engineering and Pedagogical University, 8, Uchebnyi Side Street, Simferopol 29501, Republic of Crimea, Ukraine

Abstract. One of the promising directions for increasing the efficiency of parts processing with diamond tools is studying the mechanics of contact interaction based on the theory of elastic-plastic contact interaction of rough surfaces. The contact interaction theory allows you to establish the optimal requirements for diamond tools, processing modes, and the workpiece's initial parameters. This study discusses a method for determining the contact pressures directly in the honing process of conical holes. The existing methods are based on theoretical calculations or require significant equipment modernization with subsequent analysis of the obtained data. The proposed method is simple and considers the distribution of the linear contact load of the honing bar along the generatrix of the conical hole in the workpiece. The method is based on the usage of strain gauges which are characterized by small dimensions, low cost, and high measurement accuracy at any stage of the technological operation. The results of static and machine experiments showed the qualitative characteristics of the tool-workpiece contact.

Keywords: Honing · Contact pressure · Method of measurement

1 Introduction

Making precise tapered bores is a complex process. Known operations that create tapered holes do not provide consistent surface quality.

Internal grinding of a tapered hole is carried out with a preliminary check of the surface runout, which leads to a decrease in the productivity of the process. The occurrence of errors in the conical hole's shape is associated with vibration and the grinding wheel's elastic extrusion mounted on a cantilever. High speeds during grinding and high temperatures in the cutting zone lead to burns on the processed surface and changes in the structure of the material's surface layer, reducing the processing quality.

When countersinking tapered holes, the shape of the tool is copied to the work surface. The main reasons for machining errors are low tool life due to chipping and chips on the countersink's cutting part.

One of the high-performance operations that ensure the quality of the tapered holes is diamond honing. A characteristic feature of honing tools is the large length of the diamond bar compared to its width. This causes a linear distribution of contact load. To optimize the machining process's design and technological parameters, it is important to

know the nature of the linear contact load distribution in any phase of the honing process. To do this, it is necessary to have a practically convenient and engineering accurate experimental method for determining contact pressures in the real honing process at any time.

2 Literature Review

Nowadays, there are methods for determining contact deformations based on the laws of elasticity, and these methods are uniquely related to the contact pressures. Most of these methods are based on analytical calculations. In the work of K.R. Muratov et al., the modeling of contact when honing cylindrical holes is considered. Analysis of the results shows non-linear behavior of the average contact pressure and transmission coefficient. These factors depend on the applied force and surface profile and the materials used in the tool and workpiece [1]. In work [2], the authors provide an analytical calculation of the contact pressure by introducing simplifications into Lamé's equation. Abbasov et al. were performed an analytical calculation of the nature of the distribution of contractual pressure between the outer surface of the sealing material and the rigid wall of the cylinder, depending on the geometric dimensions and mechanical properties of the seal during its one-sided compression [3]. In paper [4], the authors briefly review the most important contact mechanics theories [5] between randomly rough surfaces. In particular, the relation between the applied load and separation is fundamental in many engineering applications as seals, lubrication, and wear. In work [6], the displacement function of the external contour points of a hub and the friction surface microgeometry that correspond to the uniform distribution of the contact pressure over a friction surface are theoretically determined. The authors in [7] carried out an analysis of variance, which showed that the most important parameters for the maximum depth of roughness are cutting speed and specific pressure of final honing.

One of the most common methods for practical control of contact pressures is the acoustic emission method. In works [8, 9], developing a new probing method to inspect the inner diameter of micro-scale holes is presented. This was accomplished by contact detection using acoustic emission with a rotating wire probe tip. Contact is detected when the rotating probe approaches and influences the whole inner surface. Authors in [10] show that the acoustic emission method has a high probability of detecting probable defects in pressure vessels before their failure. This method must be applied under pressure. These pressure loads create stresses in the vessel. During increasing pressure loads, AE signals are obtained from inhomogeneities and other places of stress concentration. In [11], the authors propose a technique for acoustic emission monitoring under dynamic loading. It proposes a method for separating the total flow of acoustic emission signals into stationary groups that are typical for different acoustic emission sources.

In industrial applications, optoelectronic methods have also been used for non-contact deformation measurements. In work [12] showed the developed laser interferometry for measurements of the small dynamic displacements. The optoelectronic method of the signal registration from the laser interferometer and the signal processing method is presented. This technique allows determining the among and from of the dynamic

displacements with high sensitivity and accuracy. Work [13] showed a technique for smoothing continuous optically rough surfaces to allow successful application of the ray method for deformation measurement. Detailed analysis of the measurement and evaluation process concerning the most important measurement factors is performed.

Researchers have not practically considered the measurement of the contact pressures directly in the conical holes' honing process, although the contact pressures directly affect the formed surfaces' quality. In work [14] influence of different parameters of the rough honing process on surface roughness and material removal rate were studied. While considered grain size, the density of abrasive, tangential speed of cylinders, the linear speed of honing head, and pressure of abrasive stones on an internal surface of cylinders. The influence of these parameters on the obtained surface roughness in terms of Ra and Rt parameters and the material removal rate Qm is shown. The authors of the study [15] show that the surface roughness during honing depends on five investigated variables (grain size, density, pressure, linear velocity, and tangential velocity) in both cases, the most important factors being grain size and pressure. In [16, 17], indirect models based on neural networks are presented to model the technological processes. This model allows obtaining values to be set for different process variables (linear speed, tangential speed, pressure of abrasive stones, grain size of abrasive, and density of abrasive) as a function of required average roughness Ra.

The existing experimental methods for determining the contact pressures are distinguished by the complexity of their structures and distortion of contact interaction conditions between tool and workpiece. Therefore, the development of a fundamentally new method for the experimental determination of the contact pressures during the honing process is relevant not only from a practical but also from a scientific point of view.

3 Research Methodology

The distribution of contact pressures q (MPa) on the bar's surface is determined from geometric considerations by the nature of the change in the depth of cutting δ . Let us consider the tool's position when the radius of the hole of the workpiece r_w is greater than the radius of the circle passing through the tops of the diamond grains of the bar r_b Fig. 1.

The figure shows that the penetration depth of diamond grains varies smoothly from zero (at the ends of the contact width b_c) to a maximum - δ_{max} (at its middle). Contact pressures can be described by a symmetric function:

$$q = q_{max} \cdot f(\varphi) \tag{1}$$

Following the diagram of contact pressures, we bring q to a linear distributed load p , N/m:

$$p = 2 \int_0^{\varphi_{max}} q(\varphi) r \cos \varphi d\varphi = 2q_{max} \int_0^{\varphi_{max}} f(\varphi) d\varphi = 2q_{max} \psi(\varphi_{max}) \tag{2}$$

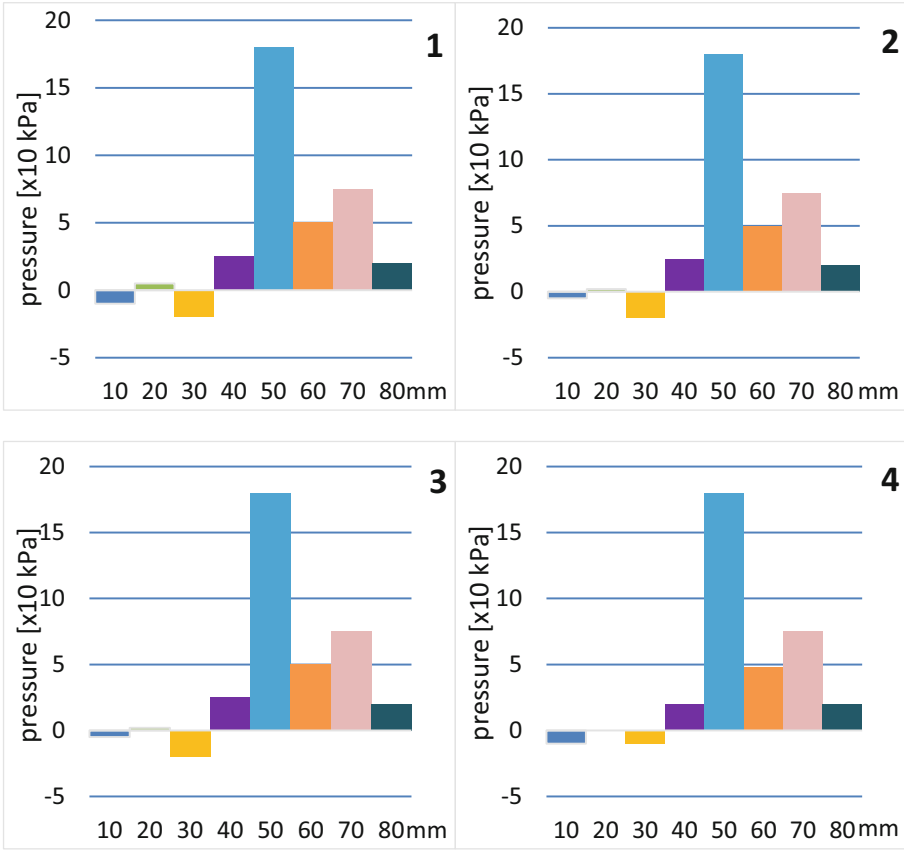


Fig. 3. The distribution of the contact pressures at a load of 392.3 kPa and the exit of a bar at 1/3L from a small hole.

The diamond bar would self-align concerning the hole’s generatrix to better distribute the contact pressures along the entire length of the workpiece. For this purpose, a steel ball was installed in the center of the bar’s lower plane. Simultaneously, the diamond block was in full contact with the workpiece along its entire length. Based on the results of the experiment, the pressure distributions are shown in Fig. 4 (Fig. 5).

Figure 6 shows a setup for measuring contact pressure using a steel ball and a compensator.

Another set-up was created to carry out experiments in dynamics, and its general view is given in Fig. 7. A radial drilling machine model 2K522 was used as equipment.

Based on the results, the distribution of the contact pressures was obtained a given in Fig. 8.

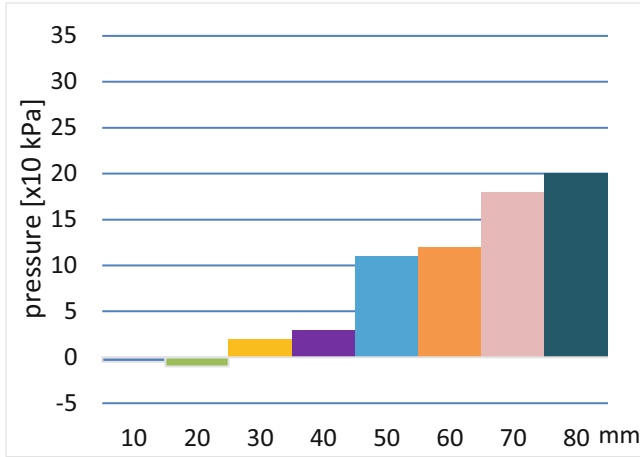


Fig. 4. The contact pressure distribution at a load of 392.3 kPa with self-alignment of the bar and its exit to 1/3 L from a small hole workpiece.

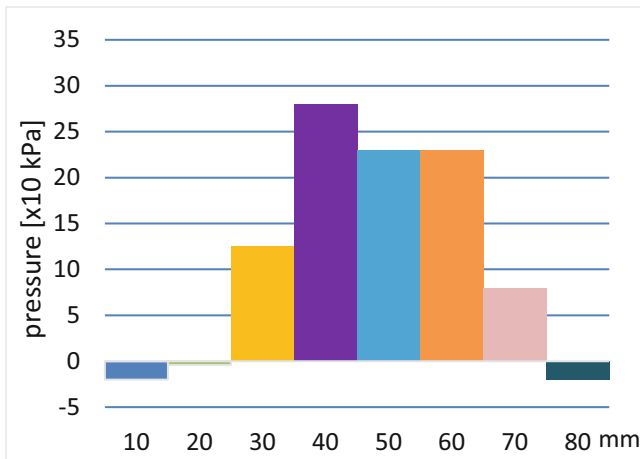


Fig. 5. Diagram of the distribution of contact pressures at a load of 40 kg using a compensator during self-alignment of the bar and its full contact with the workpiece.

The performed experiments' obtained results show that the values of contact pressures change along the length during honing. This is because there is a resilient release of the honing head's pads in the middle of the contact length. This happens due to the tool's design features and a change in the contact area of the diamond grains of the pad with the treated surface. In this regard, it is necessary to create a new design of the pad, which will allow equalizing the contact pressures along the entire length of the bar.



Fig. 6. Stand for measuring the contact pressure during self-alignment of the bar and the use of a compensator.

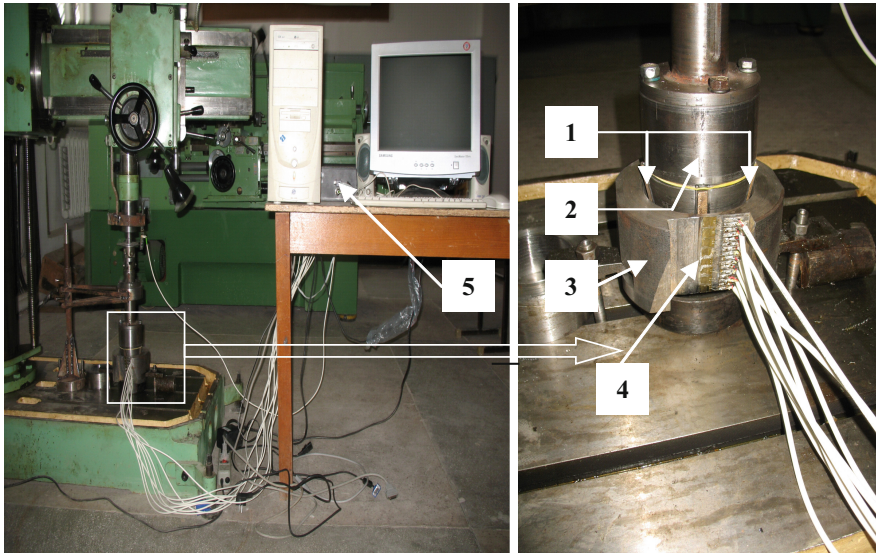


Fig. 7. General view of the installation. 1- diamond bars; 2 - conical honing head; 3 - workpiece; 4 - strain gauges; 5 - 8 channel strain gauge station.

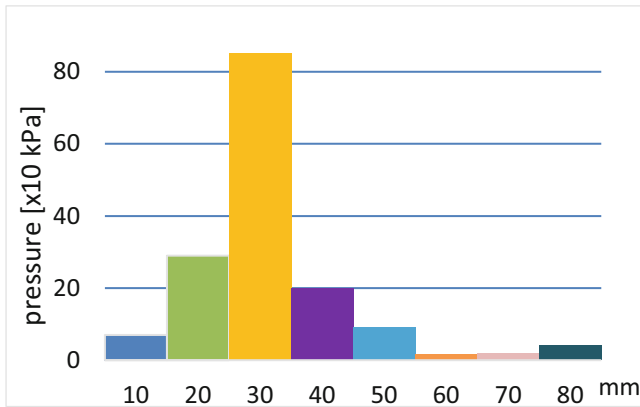


Fig. 8. The distribution of the contact pressures between the tool and the workpiece in dynamics.

5 Conclusion

Creating an experimental setup as close as possible to the conical honing process allows obtaining objective results for the nature of the distribution of the contact pressures on the working surface of a diamond bar. A strain gauge station with special software was used for the first time to investigate the contact pressures in the honing of conical holes.

Further research is planned to be directed to the complex diagnostics of the parameters affecting the hole's accuracy in the conical honing process.

References

1. Muratov, K.R., Ablyaz, T.R., Gashev, E.A.: Contact pressure in honing. *Russ. Eng. Res.* **40**(10), 859–861 (2020). <https://doi.org/10.3103/S1068798X20100160>
2. Campos, U., Hall, D.: Simplified Lamé's equations to determine contact pressure and hoop stress in thin-walled press-fits. *Thin-Walled Struct.* **138**, 199–207 (2019)
3. Abbasov, S.D.E.M., Rustamova, K.O., Rustamova, A.O.: Contact pressure between the outside surface of the sealer and cylinder wall. *J. Appl. Math. Phys.* **08**(02), 349–366 (2020)
4. Carbone, G., Bottiglione, F.: Contact mechanics of rough surfaces: a comparison between theories. *Meccanica* **46**, 557–565 (2011)
5. Yavtushenko, A.V., Protsenko, V.M., Bondarenko, Y.V., Kirichenko, A.G., Ping, F.Y.: Numerical experiment for the calculation of normal contact stress in the deformation center when rolling a metal strip. *J. Eng. Sci.* **6**(2), E31–E35 (2019). [https://doi.org/10.21272/jes.2019.6\(2\).e5](https://doi.org/10.21272/jes.2019.6(2).e5)
6. Mirsalimov, V.M., Akhundova, P.E.: The optimal design of a friction unit with uniform contact pressure. *J. Friction Wear* **40**(6), 562–568 (2019). <https://doi.org/10.3103/S1068366619060187>
7. Vrac, D.S., Sidjanin, L.P., Kovac, P.P., Balos, S.S.: The influence of honing process parameters on surface quality, productivity, cutting angle and coefficients of friction. *Ind. Lubr. Tribol.* **64**(2), 77–83 (2012)
8. Maršálek, O., Vopařil, J., Novotny, P.: Validation of analytical calculation of contact pressure. *Adv. Mech. Sol.* **393**, 495–500 (2016)

9. Elfurjani, E., Ko, J., Jun, M.B.G.: Micro-scale hole profile measurement using rotating wire probe and acoustic emission contact detection. *Measurement* **89**, 215–222 (2016)
10. Wuriti, G.S., Chattopadhyaya, S., Tessa, T.: Acoustic emission examination of high strength steel M250 pressure vessels for aerospace applications. *IOP Conf. Ser. Mater. Sci. Eng.* **998**, 012037 (2020)
11. Popkov, A., Kochetkov, A.: Dynamic loading in monitoring of brittle objects by acoustic emission method. In: X International Scientific and Technical Conference “Polytransport Systems” 2018, MATEC Web Conference, vol. 216, p. 03006 (2018)
12. Osipov, M., Grebennikov, S.K.: Optoelectronic method for measurement of small dynamic displacements. *Proc. SPIE Int. Soc. Opt. Eng.* **4317**, 616–620 (2001)
13. Novak, J., Miks, A.: Modern optoelectronic methods for non-contact deformation measurement in industry. *J. Opt. A: Pure Appl. Opt.* **4**(6), 413–420 (2002)
14. Buj-Corral, I., Vivancos-Calvet, J., Salcedo, M.F.C.: Modelling of surface finish and material removal rate in rough honing. *Precis. Eng.* **38**(1), 100–108 (2014)
15. Buj-Corral, I., Vivancos-Calvet, J., Rodero-de-Lamo, L., Marco-Almagro, L.: Comparison between mathematical models for roughness obtained in test machine and in industrial machine in semifinish honing processes. *Precis. Eng.* **132**, 545–552 (2015)
16. Pavlenko, I., et al.: Parameter identification of cutting forces in crankshaft grinding using artificial neural networks. *Materials* **13**(23), 5357 (2020). <https://doi.org/10.3390/ma13235357>
17. Sivatte-Adroer, M., Llanas-Parra, X., Buj, I., Vivancos-Calvet, J.: Indirect model for roughness in rough honing processes based on artificial neural networks. *Precis. Eng.* **43**, 505–513 (2015)



Simulation Methodology of Diamond Burnishing

Vladimir Fedorovich¹ , Ivan Pyzhov¹ , Janos Kundrak² , Larisa Pupan¹  ,
and Irina Voloshkina¹ 

¹ National Technical University «Kharkiv Polytechnic Institute», 2,
Kyrpychova Street, Kharkiv 61002, Ukraine

² Institute of Manufacturing Science, University of Miskolc, C/1 108, Miskolc-Egyetemváros,
Miskolc 3515, Hungary

Abstract. The paper presents computer simulation results of the equivalent stress distribution in the surface layer of the diamond burnishing and ultrasonic burnishing products. Finite element analysis was carried out using Third Wave AdvantEdge (TWA) and Solid Works CAE systems. The simulation considered the physical and mechanical properties of both processed and tool materials. The elastic modulus of the processed material E_{pm} was found to have the most significant influence on equivalent stresses in the surface layer of the processed materials, which predetermines the operational properties of products. The E_{pm} values served as a basis in simulation experiments to study the effect of the technological parameters (burnishing force P , burnishing speed V , burnishing depth t , and the burnisher radius r) on equivalent stresses σ_{eq} in the surface layer of the burnished material. The primary influencing technological factors in the analysis of the equivalent stress distribution during diamond ultrasonic burnishing were the vibration frequency of the tool f , the radius of its working surface r , and the elastic modulus of the solder E_{sol} . As a result of the simulation, rational values of the technological parameters of the diamond burnishing and ultrasonic burnishing were determined. The study showed that the optimal choice of the technological parameters should consider both the equivalent stress distribution in the surface layer of the products and the factors influencing the tool wear observed under a particular processing mode.

Keywords: Burnished products · Surface quality · Finite element method · Equivalent stress

1 Introduction

One of the trends in mechanical engineering technologies is to increase the reliability and service life of manufactured products. The operational properties of products are formed throughout all the stages of their manufacturing, particularly during finishing. Finishing machining methods largely determine the surface layer quality of parts and, accordingly, their operational properties.

The traditional abrasive methods (grinding, honing, and polishing) provide the required geometric accuracy. The necessary quality indicators of the surface layer, as

a rule, require additional methods, for example, surface plastic deformation of products. One of the promising methods of this technology is diamond burnishing (DB). The advantages of the DB process include high surface quality of the parts, high productivity, versatility, relative simplicity of implementation, and stability.

Combined technologies can improve the efficiency of the diamond burnishing, for example, additional ultrasonic action on the used burnishing tool (ultrasonic burnishing).

2 Literature Review

The diamond burnishing method has proven itself well in the manufacture of a wide range of critical products made from different materials – parts of aircraft engines and units, turbine blades, mechanical engineering components, and tools [1, 2].

Diamond burnishing is appealing due to its broad technological capabilities and significant technical and economic advantages. DB process combines the effects of finishing and hardening.

Particular attention is paid to the experimental study of mechanical and micro-geometric parameters of the surface quality of the burnished products – roughness, microhardness, degree and depth of hardening, and their effect on performance properties [3, 4].

One of the basic characteristics of the surface layer is its stress-strain state as a consequence of elastic-plastic deformation in the process of DB. The process usually results in a favorable residual stress distribution, which determines the strengthening of the near-surface layers and significantly increases wear resistance, fatigue resistance, reliability, and other operational properties of products [5]. Despite the positive role of compressive residual stresses, their appearance requires adjusting the processing modes of DB and their setting, considering the specified technological tolerances for geometric dimensions, the shape of critical surfaces, and the tool wear.

Studies indicate the dependence of the surface layer quality of DB products and the productivity of the method on the technological parameters: pressing force, burnishing feed and speed, geometric parameters of the tool. In particular, pressing force and feed have a significant impact. The number of passes and burnishing speed affect the roughness and microhardness of the processed surface to a much lesser extent [6]. However, high-speed values, providing high productivity of the DB process, can cause vibrations, which degrade the processing quality and reduce the tool life. One of the basic speed limitations is the relatively low heat resistance of diamond and increased tool wear due to graphitization and diffusion. This is especially important for iron-carbon alloys [7].

The combined finishing processes, such as ultrasonic vibration-assisted burnishing, are quite promising in increasing efficiency and improving parts [8, 9]. These processes provide a decrease in the acting forces and also reduce the deformation resistance of the metal.

The main tasks in the diamond burnishing practical implementation, including the ultrasonic burnishing technique, are mainly related to the search for optimal processing modes [2, 6]. Optimization of finishing and hardening processing of DB should be based on the relationship of technological parameters with a set of quality indicators – ensuring

the necessary performance properties of products, high productivity, minimal tool wear, and cost-effectiveness.

The possible solution to this problem is using the methodology of analytical calculation [10] or computer simulation, some features of which concerning finishing processes are considered in works [11, 12].

It can be concluded that there is no literature data on the use of the finite element method (FEM) for the DB modeling.

This work deals with developing a diamond burnishing computer simulation methodology based on FEM to study the distribution of equivalent stresses in the surface layer of the machined parts to optimize the processing modes.

3 Research Methodology

To simulate the diamond burnishing process Third Wave AdvantEdge (TWA) package, based on the finite element method and providing 2D/3D simulation of dynamic machining processes [13, 14] selected.

Adding to the model the physical and mechanical properties of the machined and tool materials and processing modes allows calculating the equivalent and residual stresses, strain energy, strain energy density, principal stresses, forces, and temperature in the plastic deformation zone during diamond burnishing.

The tasks were solved using TWA according to the following algorithm.

1. Construction of a geometric model.
2. Setting material properties for each element of the system using a standard database. The elastic modulus (Young's modulus) E_{pm} , Poisson's ratio μ , mass density ρ , coefficient of thermal expansion α , thermal conductivity q , specific heat c , and others were used as material properties. The workpiece materials are carbon steel C45, wrought aluminum alloy EN AW 2024-T4, nickel-aluminum bronze C95500 (Table 1).

Table 1. Physical and mechanical properties of the workpiece materials.

Material	Property					
	Young's modulus E_{pm} , GPa	Poisson's ratio μ	Mass density ρ , kg/m ³	Coefficient of thermal expansion α , 10 ⁻⁶ /K	Thermal conductivity q , W/(m·K)	Specific heat c , J/(kg·K)
C45	201	0.27	7700	12	48	460
EN AW 2024-T4	69	0.33	2770	23	121	875
C95500	135	0.34	7530	17	42	419

3. Partitioning the geometric model into finite elements, consisting of nodes (nd) and elements (el) (Fig. 1, a). The parameters of dynamic change of the finite element mesh were also set: a mesh with significantly reduced element sizes was generated in the deformation zone.
4. Fixing the finite element model at the nodes (Fig. 1, a), and setting the motion of the burnisher (Fig. 1, b).

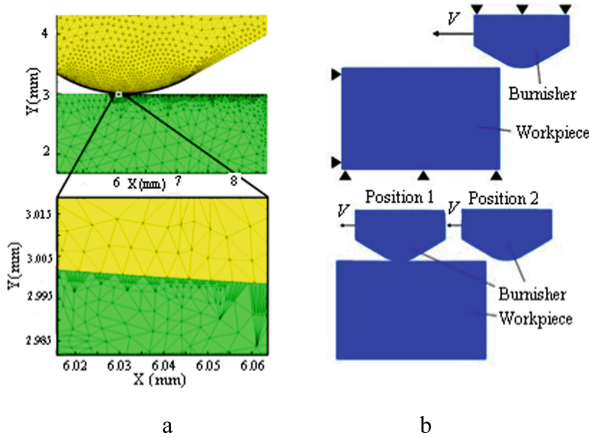


Fig. 1. Partitioning the original model into finite elements (a); schematic view of the model fixing and setting the burnisher motion (b).

As burnishing is a complex dynamic system, which is influenced by many parameters, a multivariate experiment plan was used to numerical study the process in TWA APP. Four basic parameters were chosen as the key ones: elastic modulus of the processed material E_{pm} , burnishing speed V , burnishing depth t , and the working surface radius of the burnisher r .

FEM-based Solid Works, containing the Simulation CAE plug-in, was determined as the most optimal system to simulate the combined process of ultrasonic vibration-assisted burnishing [15].

The effect of the ultrasonic vibrations frequency f on the stress-strain state of the “diamond burnisher – processed material” system was determined. As the tool is subjected to additional dynamic load, this requires considering the solder properties and properties of the tool metal coating and metal phase in the diamond burnisher. A finite element mesh model was created with a corresponding thickening in the area of contact of the diamond with the processed material based on the adopted “holder body – solder – metal coating – diamond – metal phase – processed material” 3D system (Fig. 2).

The computational experiment performed using a uniformly distributed load applied to the upper surface of the tool (the simulated pressing force of a diamond burnisher) and the side surface (feed simulation). The ultrasonic burnishing was simulated by sinusoidal vertical loading with frequencies of 10, 30, and 50 kHz and amplitude of ± 2 MPa.

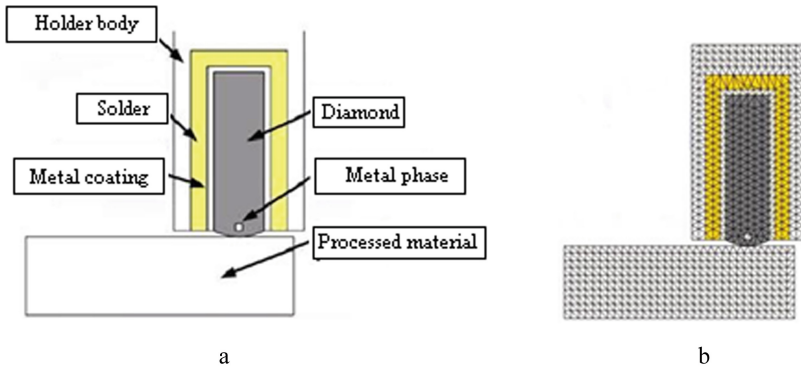


Fig. 2. Initial “holder body – solder – metal coating – diamond – metal phase – processed material” 3D-system (a) and finite element mesh model (b).

4 Results

4.1 Results of Diamond Burnishing Simulation

The simulation revealed a significant difference in the equivalent stress distribution depending on the elastic modulus of the processed material E_{pm} , the effect of which turned out to be the most significant in comparison with the rest of the investigated factors.

The calculations showed a significant equivalent stresses σ_{eq} decrease in the surface layer of the part with the elastic modulus E_{pm} decreasing. With an increase in E_{pm} , the part’s material has a greater resistance to deformation, which leads to a substantial increase in the equivalent stresses both in the surface layer of the workpiece and in the tool material. Thus, DB ensures better indicators of surface layer hardening in materials with a higher elastic modulus.

Further simulation procedures mainly used E_{pm} to optimize the processing modes.

Changes in the projections of the burnishing force P showed that its component in the direction opposite to the speed direction for all the elastic moduli of the studied materials invariably amounts to 50...60 N. At the same time, the force acting in the axial direction of the tool increases significantly as E_{pm} increases. For example, for the aluminum alloy EN AW 2024-T4 ($E = 69$ GPa), the force was $P = 160$ N, for nickel-aluminum bronze C95500 ($E = 135$ GPa) – $P = 192$ N, and for steel C45 ($E = 201$ GPa) – $P = 311$ N.

The processing of materials with high E_{pm} causes an increase in mechanical loads on the tool and, accordingly, an increase in equivalent stresses in the surface layer of the diamond burnisher (Fig. 3).

For revealing the dependence of the equivalent stresses in diamond burnisher on the elastic modulus of the PM, a one-factor experiment was carried out, with the initial data selected from the practical experience: $r = 2$ mm; $V = 100$ m/min; $t = 8$ μ m. With the above E_{pm} values of the studied materials and the selected processing mode, the values of the equivalent stresses were $\sigma_{eq} = 794, 978,$ and 1374 MPa, respectively. The data obtained for the specified processing mode are comparable with the ultimate strength of

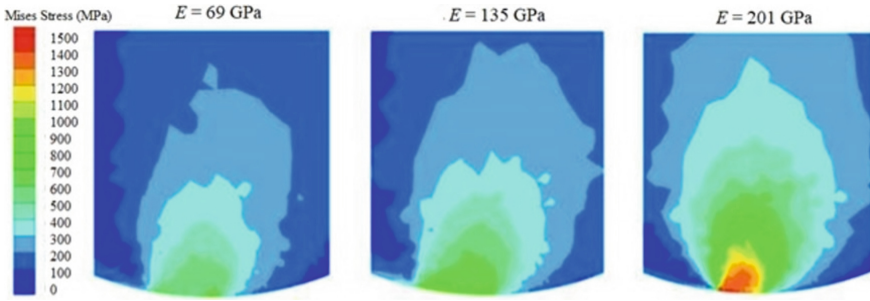


Fig. 3. Dependence of stresses in a diamond burnisher on the elastic modulus of the processed materials E_{pm} .

diamond and can cause damage of the working surface of the crystal with falling out of the mandrel and, ultimately, failure of the tool.

In this regard, the influence of the DB mode parameters on the level of equivalent stresses in the surface layer of the PM was studied, considering the required tool life.

The results showed that an increase V from 60 to 140 m/min led to a change in σ_{eq} in part by only 3...4%. Thus, the burnishing speed has practically no effect on the surface hardening of the part. For achieving the maximum productivity of the process, it is necessary to set the maximum possible values of the burnishing speed, which do not cause an excess of critical temperatures in the contact zone and intensive wear of the burnishing tool.

The calculation for steel C45 ($r = 2$ mm, $V = 100$ m/min, $t = 8$ μ m), showed that the maximum tool temperature was 146.9 °C. For increasing the DB productivity and reduce the tool wear, it is advisable to use various methods for heat removal from the processing zone. For example, the use of cutting fluids and optimization of the tool in order to increase its heat dissipation (heat-conducting material of the burnisher and the solder that fixes the diamond in the tool; the maximum possible contact area of the solder with the diamond surface; optimization of the tool shape due to cooling fins).

The simulation results indicated the insignificant effect of the burnishing depth t on the equivalent stresses σ_{eq} in the surface layer of the part. For ensuring an optimal processing result, the burnishing depth should be sufficient to get the specified roughness of the processed surface. The burnishing depth must not exceed the values of vibrations that appear, and the surface quality deteriorates.

Tool geometry has an ambiguous effect on equivalent stresses in the surface layer of the parts made of different materials (Fig. 4). At a relatively low value of E_{pm} (aluminum alloy), the radius r of the tool working surface has practically no effect on σ_{eq} . With the growth of E_{pm} , the influence of the tool geometry becomes more significant. For steel C45, a change in radius from 3 to 1 mm causes an increase in stress. This factor has a positive effect on the process, improving the hardening performance and increasing the residual compressive stresses of the part surface. The optimal choice of r should be corrected by the value of stresses in the tool surface layer, preventing its catastrophic wear.

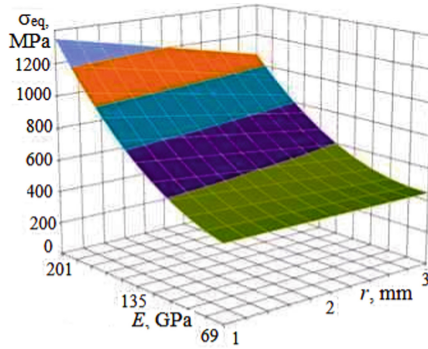


Fig. 4. Influence of the burnisher radius on the surface layer equivalent stresses of materials with different elastic moduli; $V = 140 \text{ m/min}$, $t = 6 \text{ }\mu\text{m}$.

4.2 Results of Ultrasonic Diamond Burnishing Simulation

During ultrasonic burnishing, the tool is subjected to an additional dynamic load. Thus, there is a danger of its destruction due to increased stresses in the zone of contact with the solder. This requires considering the properties of the solder in the simulation.

The factors of the numerical experiment were taken as follows: elastic modulus of the solder E_{sol} (X_1); vibration frequency of the burnisher f (X_2); the radius of the burnisher r (X_3); elastic modulus of the processed material E_{pm} (X_4). Values of the factors are given in Table 2. Three levels of variation correspond to the code values +1 (upper), 0 (basic), -1 (lower). Copper, bronze, and brass were used as possible solder materials.

Table 2. Variable factors of the ultrasonic burnishing modeling.

Variable factors							
E_{sol}, MPa	X_1	f, kHz	X_2	r, mm	X_3	E_{pm}, MPa	X_4
1,05E+5 (bronze)	+1	50E+3	+1	3	+1	6,9E+5	+1
9,8E+4 (copper)	0	30E+3	0	2	0	4,4E+5	0
9,1E+4 (brass)	-1	10E+3	-1	1	-1	1,9E+5	-1

As a result of multivariate numerical modeling, 24 values of the equivalent stresses in the PM at its contact with the diamond burnisher were obtained. Some examples are shown in Fig. 5 in the form of isolines σ_{eq} for individual values of the variable parameters.

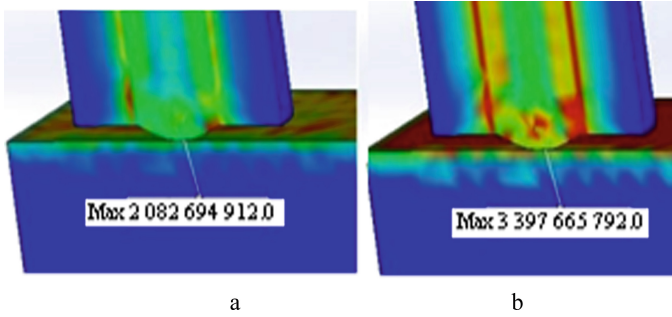


Fig. 5. Visualization of the simulation results of the stress-strain state in the «diamond burnisher – processed material» zone: a – $E_{pm} = 1.9E + 5$ MPa; $r = 1$ mm; $E_{sol} = 9.1E+4$ MPa; $f = 10$ kHz; b – $E_{pm} = 4.4E+5$ MPa; $r = 2$ mm; $E_{sol} = 9.1E+4$ MPa; $f = 25$ kHz

Based on the study performed, the regression equation was as follows.

$$\begin{aligned}
 Y = & 2.484 + 0.134X_1 + 0.244X_2 + 0.327X_3 + 0.463X_4 + 0.805X_1^2 + 0.366X_2^2 \\
 & - 0.412X_3^2 - 0.291X_4^2 - 0.014X_1X_2 + 0.001X_1X_3 - 0.014X_1X_4 \\
 & + 0.016X_2X_3 - 0.014X_2X_4 + 0.045X_3X_4
 \end{aligned}$$

Solving this equation revealed the influence of the above factors on the equivalent stresses arising in the contact patch of the “diamond burnisher – processed material” system.

For the analysis clarity and convenience, two-parameter relationships are presented as $\sigma_{eq} = f(X_i)$ (Fig. 6).

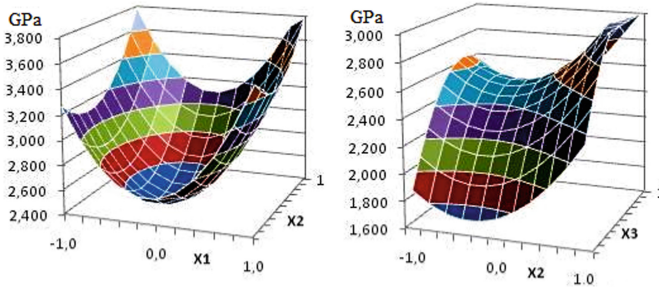


Fig. 6. Dependence of the equivalent stresses in the contact zone on the parameters X_1, X_2, X_3 .

Analysis of the equivalent stresses dependences on the vibration frequency at various elastic moduli of the solder justified using copper as a solder at a periodic load form.

The optimization of ultrasonic burnishing was carried out in Maple 14. As a result of modeling for the considered case, the following values of the factors were founded: $X_{1\text{opt}} = -0.09$; $X_{2\text{opt}} = -0.33$; $X_{3\text{opt}} = 1$; $X_{4\text{opt}} = -1$. The maximum stress is $Y_{\text{max}} = 0.99$. These values correspond to the following optimal parameters, subject to a high level of compressive stresses in the surface layer: $E_{sol} = 9.8E+4$ MPa (i.e., the value is close to that of copper solder), $f = 25$ kHz, $r = 1$ mm, $E_{pm} = 1.9E+5$ MPa.

5 Conclusions

The simulation showed a significant difference in the distribution of equivalent stresses σ_{eq} in the surface layer of the studied materials and the material of the diamond burnisher, depending on the elastic modulus of the processed materials E_{pm} . Processing materials with $E_{pm} > 200$ MPa causes stresses (e.g., that exceeds the ultimate strength of the burnisher material), leading to tool failure due to its destruction and falling out of the mandrel.

Increasing the burnishing speed V from 60 to 140 m/min insignificantly changes the σ_{eq} value in the part's material.

The maximum possible speed is optimal to achieve the highest performance, considering the heat removal to reduce the critical temperatures in the contact zone and prevent intensive wear of the diamond burnisher.

For ensuring a high degree of the surface layer hardening of materials with a relatively high elastic modulus (steel), it is advisable to use a burnisher with a smaller radius of the working surface ($r = 1$ mm). The value of r has practically no effect on σ_{eq} in the surface layer of aluminum and copper alloys.

Analysis of the dependence of equivalent stresses in the surface layer of parts on the ultrasonic diamond burnishing technological parameters made it possible, along with ensuring a high level of equivalent stresses in the surface layer of the processed part, to provide an optimal choice of solder. This allows avoiding the catastrophic destruction of the tool (falling out of the solder) caused by an unacceptable stress concentration in the diamond burnisher at the contact area with the solder.

The studied modeling methodology of the diamond burnishing and ultrasonic diamond burnishing allows establishing the optimal (rational) combinations of the primary process parameters of the “diamond burnisher – processed material” system at the technological process development with minimal costs. This ensures predicting the specified characteristics of critical parts of the product at the design stage, which improves their quality and ensures high resource indicators.

Further research will focus on establishing the optimal combination of physical and mechanical properties of the superhard tool materials and the processed materials to increase the efficiency of diamond burnishing and obtain products with desired properties.

References

1. Klimenko, S.A., etc., under total ed. Chizhik, S.A., Kheifets, M.L.: Finishing of surfaces in the production of parts. Belaruskaya Navuka, Minsk (2017). (in Russian)
2. Maximov, J.T., Duncheva, G.V., Anchev, A.P., Ichkova, M.D.: Slide burnishing – review and prospects. *Int. J. Adv. Manuf. Technol.* **104**(9), 1–17 (2019)
3. Sachin, B., Narendranath, S., Chakradhar, D.: Sustainable diamond burnishing of 17–4 PH stainless steel for enhanced surface integrity and product performance by using a novel modified tool. *Mat. Res. Express* **6**(4) (2019)
4. Ferencsik, V., Varga, G.: Analysis of surface microhardness on diamond burnished cylindrical components. *Cutting Tools Technol. Syst.* **90**, 151–157 (2019)

5. Huuki, J., Laakso, S.V.A.: Surface improvement of shafts by the diamond burnishing and ultrasonic burnishing techniques. *Int. J. Mach. Machinabil. Mater.* **19**(3), 246–259 (2017)
6. Shirsat, U., Ahuja, B., Dhuttargaon, M.: Effect of burnishing parameters on surface finish. *J. Inst. Eng. (India)* **98**, 431–436 (2017)
7. Li, Z.J., Fang, F.Z., Gong, H., Zhang, X.D.: Review of diamond-cutting ferrous metals. *Int. J. Adv. Manuf. Technol.* **68**(5–8), 1717–1731 (2013). <https://doi.org/10.1007/s00170-013-4970-5>
8. Li, C., Zhang, F., Meng, B., Liu, L., Rao, X.: Material removal mechanism and grinding force modeling of ultrasonic vibration assisted grinding for SiC ceramics. *Ceram. Int.* **43**(3), 2981–2993 (2017)
9. Emmer, T., Welzel, F., Borysenko, D., Voropai, V., Nguyen, D.T.: Development of the mathematical model smoothing while using FEA. *Cutting Tools Technol. Syst.* **91**, 58–68 (2019)
10. Hiegemann, L., Weddeling, C., Tekkaya, A.E.: Analytical contact pressure model for predicting roughness of ball burnished surfaces. *J. Mat. Process. Tech.* **232**, 63–77 (2016)
11. Teimouri, R., Amin, S., Bami, A.: Evaluation of optimized surface properties and residual stress in ultrasonic assisted ball burnishing of AA6061-T6. *Measurement* **116**, 129–139 (2018)
12. Grabchenko, A., Dobroskok, V., Ostroverkh, Y., Fedorovich, V., Pupan, L.: Features of using metal coatings on diamond grains in electrically conductive grinding wheels when machining polycrystalline superhard materials. In: Tonkonogyi, V., et al. (eds.) *InterPartner 2019. LNME*, pp. 44–52. Springer, Cham (2020). https://doi.org/10.1007/978-3-030-40724-7_5
13. Kunderák, J., Karpuschewski, B., Pálmai, Z., Felhő, C., Makkai, T., Borysenko, D.: The energetic characteristics of milling with changing cross-section in the definition of specific cutting force by FEM method. *CIRP J. Manuf. Sci. Technol.* **32**, 61–69 (2021)
14. Papazoglou, E.L., Karkalos, N.E., Markopoulos, A.P.: A comprehensive study on thermal modeling of SLM process under conduction mode using FEM. *Int. J. Adv. Manuf. Technol.* **111**(9–10), 2939–2955 (2020). <https://doi.org/10.1007/s00170-020-06294-7>
15. Skondras-Giousios, D., Karkalos, N.E., Markopoulos, A.P.: Finite element simulation of friction and adhesion attributed contact of bio-inspired gecko-mimetic PDMS micro-flaps with SiO₂ spherical surface. *Bioinspir. Biomimet.* **15**(6) (2020).



Optimal Milling Conditions for Complex Shaped Thin-Walled Components

Anton Germashev¹ , Yuri Vnukov¹ , Mark Kuchuhurov¹ ,
Viktor Logominov¹  , and Bert Lauwers² 

¹ National University «Zaporizhzhia Polytechnic»,
64, Zhukovs'koho Street, Zaporizhzhia 69063, Ukraine

² KU Leuven, 13, Oude Markt, 3000 Leuven, Belgium

Abstract. This paper investigates the dynamic behavior of the milling of complex shaped thin-walled components. As an interrupted cutting characterizes the milling process, a detailed study of the tool entrance point in relation to the vibration of the part is performed. Milling tests were performed on two thin-walled workpieces with different static and dynamic characteristics. The rigidity of the milling tool was much higher than the rigidity of the workpiece. End milling of thin-walled components deals with short cutting lengths, contributing to a decrease in the number of regenerative waves on the cutting surface. As a result, there is less than one regenerative wave beginning from relatively low spindle speed. Therefore, vibrations in high-speed milling of thin-walled structures are rather caused by resonance phenomenon than by self-excited oscillation. These findings have been supported by experimental validation where two thin-walled structures have been machined. The worst processing conditions occur when the tool impacts the workpiece when its amplitude of vibration is high.

Keywords: Thin-walled structures · Chatter · Surface quality · Vibrations

1 Introduction

The trend of modern production requires the fabrication of complex shaped and high-quality parts. Considering the manufactures of aircraft and space components, where most of the produced parts are thin-walled products, made from hard and resistant (temperature, chemical,...) materials, the occurrence of chatter is one of the most difficult manufacturing issues [1]. Since these thin-walled products often have small dimensions and low stiffness, it is very hard to avoid vibrations within the machining process.

Understanding the kinematics of the milling of thin-walled components is important to clarify the process behavior. Milling of complex-shaped thin-walled workpieces parts (e.g., turbine blades, blisks, impellers, etc.) is often performed using ball-shaped or toroidal cutters, with a small radial (a_c) and axial depths of cut (a_p). Due to low cutting depths, these machining conditions impose that only one tooth is in contact (Fig. 1), resulting in a periodical loss of contact between the tool and the part. It is logical to assume that the milling of complex shaped thin-walled components always encounters interrupted machining conditions, making the process different from classical milling.

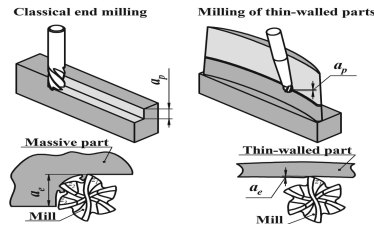


Fig. 1. Features of classical and thin-walled end milling.

Due to the intermittent character, the cutting force behaves periodically (Fig. 2b), causing a large level of forced vibration. The tooth passing frequency determines the frequency of this vibration/excitation. While cutting forces almost does not exist, the thin-walled features vibrate following the law of a free damped oscillation.

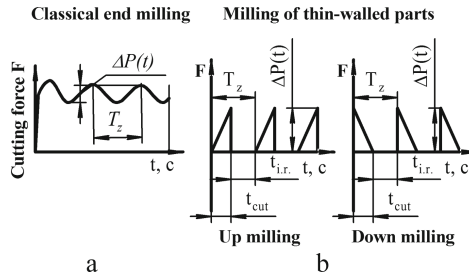


Fig. 2. Fluctuation of cutting forces during classical and thin-walled end milling.

2 Literature Review

Chatter and/or vibration problems in machining processes is well known and has been studied by many researchers [2]. Theoretical approaches of chatter prediction, based on regenerative theory, have been developed [3, 4] and has been applied for the last 40 year [5], which consists in building stability lobe diagrams. These diagrams show spindle speed zones with stable and unstable regions. Initially, theories and approaches were developed for turning operations, but it has been further extended for milling process [6, 7].

Compared to turning, chatter prediction in milling operations is much more complex since it is characterized by more complicated kinematic movements and the intermittence of the cutting process. In high-speed milling, where the cutting time is very small, chatter suppression is the most difficult problem [8]. It often requires experimental testing, providing knowledge about the dynamics of the milling process to eliminate vibrations and provide stable machining processes. Also, high-speed milling of complex shaped thin-walled components occurs with low immersion, meaning that often not no more than one tooth of the mill is involved in cutting. In this case, interrupted cutting imposes additional difficulties to find stability.

Therefore, research on the milling of thin-walled structures attracted a lot of attention from a scientific perspective. Significant steps in the dynamic investigation of the milling of flexible parts were made by Budak [9], Altintas and Tuysuz [10], Shtehin [11], Wang [12].

Davies and Balachandran [13] noticed that numerous types of nonlinearities could affect the dynamic behavior of milling processes. However, the effect of nonlinearities associated with intermittency has been virtually ignored in the literature. They showed that impact dynamics are likely to dominate vibrations in milling operations where the cutter rotation can excite flexible modes in the workpiece. Further, Davies et al. [14, 15] concluded that the assumptions of the traditional regenerative stability theory become invalid for highly interrupted machining, and they proposed a first direct analytical solution to the problem.

Investigation of the stability of interrupted machining proposed by Stepan and Inspurger [16], based on a semi-discretization method, showed that a new unstable domain that arises in high-speed cutting could also be the reason for a new kind of machine tool chatter. This additional stability problem or unstable phenomena is related to the time periodicity of the milling process. In further research [17] they concluded, that as the number of active teeth decreases and the cutting becomes more and more interrupted, the amplitudes related to the lower and higher frequency peaks get larger.

Budak and Altintas [18] and Merdol and Altintas [19] presented a multi frequency solution of chatter stability prediction. Such approach is well appropriate for low immersion milling and showed that only when the harmonics of the tooth passing frequency shifts the transfer function to the region of natural modes, additional narrow stability pockets are created, which differ from the lobes predicted by the single frequency or classical solutions.

Although, as mentioned above, the milling of thin-walled structures shows a number of significant differences compared to the turning operation, for which stability lobe diagrams have been developed, vibration elimination in milling of thin-walled structures is still based on the same principle.

A very important limitation of the milling process due to forced vibrations, causing geometric inaccuracies of the detailed part features, was noticed by Kline et al. [20], Tlustý [21], Montgomery and Altintas [22], Smith et al. [23], Tarn et al. [24], Schmitz et al. [25–27] and other. Therefore, even under seemingly stable cutting conditions, the thin-walled structures experience forced vibrations, which depend on the workpiece/tool natural frequency and excitation frequency (or tooth passing frequency), causing big fluctuations of the weakest parts of the machined component (or in combination with the machine tool structure). As a result of these vibrations, surface location errors take place and are visible. Although it is important to take this additional behavior into account, only a limited number of researchers propose investigating the surface errors to reduce vibration in milling.

This paper aims to investigate the main source of vibration at milling of complex shaped thin-walled components limiting productivity and production of high-quality parts. The paper shows that in the case of interrupted machining, forced oscillations have a bigger influence on machine-tool structure than chatter.

The paper is organized as follows. In Sect. 2, the characteristics of the milling of thin-walled structures and the main differences to classical end milling are presented. The experimental setup and the applied research methodology are described in Sect. 3. Kinematics behavior of a thin-walled structure at low and high spindle speed is also included in this section. Experimental results, analysis, and discussion of the results are presented in Sect. 4. Conclusions are given in Sect. 5.

3 Research Methodology

3.1 Experimental Setup

Studying the vibration behavior of the milling of thin-walled structures requires the simultaneous consideration of both the external force (thrust force F_{th}), which deflects the workpiece from its equilibrium position, and the internal - elastic force (F_{elast}) which restores it to its equilibrium position. In addition, there is the friction force (F_{fr}) (depending on the workpiece motion speed) and the inertial force (F_{in}), depending on the workpiece mass and acceleration. Since the workpiece motion has a vibrating character, forces constantly change in magnitude and direction.

An experimental setup for investigating the vibration behavior of thin-walled structure machining has been developed earlier by the authors [28] (Fig. 3). It consists of a thin plate, cantilevered by clamping one end in a rigid body, on which the test workpiece is mounted. The part vibration is monitored by an Eddy-Current sensor clamped on the rigid holder, making an independent part vibration measurement possible. The dielectric platform allows using a milling tool as a switcher that provides an electric connection when contact workpiece and milling tool exist. The contact signal (tool in contact or not) is simultaneously recorded with the displacement of the thin plate. This makes it possible to divide the signal (movement) during the cutting process and free workpiece movement.

In this investigation, the tool is considered rigid. The experimental setup makes it possible to independently change the conditions of material removal in the cutting zone (material of workpiece, cutting conditions, tool geometry, dry or wet cutting), defining the value of external force (F_{th}) as well as the characteristics of the part elastic system (stiffness, damping, mass), specifying the importance of internal forces (F_{elast}).

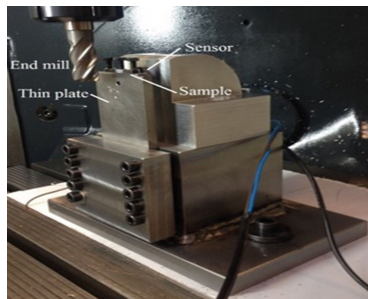


Fig. 3. Experimental setup.

3.2 Theoretical Explanation, Initial Experiments

A large number of experiments were obtained at different milling conditions, resulting in different dynamic process characteristics. It is proposed to analyze the process in a time horizon of one tooth passage. This allows evaluating all kinds of oscillations during the milling process (forced, self-excited (chatter), and free damped oscillations).

Figure 4 shows a fragment (time segment) of the workpiece vibration, indicating the tooth passage sector (= tool in contact). The “cutting time” indicates the time while cutting, while the other indicates free movements (cutting in the air). It is clear from Fig. 4 that there is a workpiece deflection. Due to relatively low cutting speed, the chance of self-excited oscillation is high, although the low cutting length contributes to the small number of chatter waves.

The cutting conditions, as shown in Fig. 4, are rather artificial due to the low spindle speed. However, it allows observing different types of oscillations contributing to movements of the thin-walled feature. At high spindle speeds, typical for the machining of thin-walled parts, the tooth passage time is very short. Therefore, the system is even not able to make a self-excited oscillation during the cutting process. Moreover, the impact of the chatter wave is relatively small, so the regenerative effect has little influence on the process stability. The thin-walled workpiece in a vibrational state after cutting, and the time of its free movement is not enough to damp it down before the next tooth entrance. Therefore, the next tooth cuts into the workpiece when it is still in a free damped oscillation. At high-speed milling, free movement of the part is so small that it can make just one free oscillation or less. Therefore, the surface quality is determined by the locations (state of movement) of the part where the cut starts. Thus, the surface quality mostly depends on the surface location error, but not from a self-excited oscillation [28]. Moreover, the vibration in such conditions might be bigger (up to 1 mm or even more depending on the structural characteristic of the part) than due to self-excited oscillation.

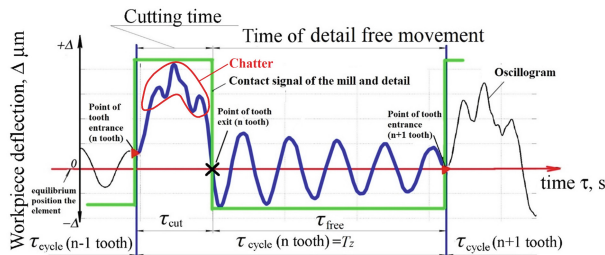


Fig. 4. Workpiece vibration (movement) at low spindle speed ($n = 710$ rpm, $h = 6$, $D_{\text{mill}} = 20$, $z = 3$).

Figure 5 shows a fragment of the workpiece vibration at high-speed milling. The cutting time is less than the period of one regenerative wave. The workpiece movement depends on its initial position when the tool impacts (P_1), the modal properties of the part structure, and the cutting time. When the tooth exits from the part (point P_2), it starts to have a free oscillation until the next tooth entrance. Its modal properties determine the

movement of the workpiece at this time, the position of the workpiece when the cutting process ends (point of tooth exit), and the idle running time.

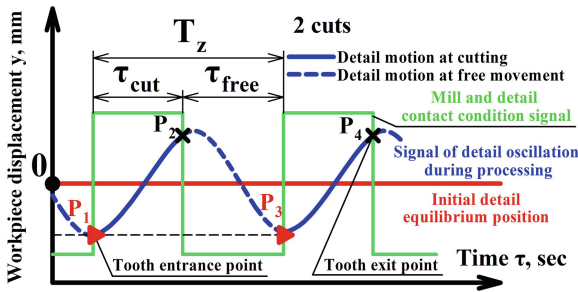


Fig. 5. Principle scheme of the workpiece deflection at high-speed milling of thin-walled details and parameters affecting the motion of the part (for variables description, see Table 1).

Table 1. Variables are shown in Fig. 5.

During cutting time:	During free movement:
- Point of tooth entrance – P_1, P_3 (distance from equilibrium position along workpiece displacement Y)	- Point of tooth exit – P_2, P_4
Natural frequency - f_n	Natural frequency - f_n
Damping ratio - ξ_{cut}	Damping ratio – ξ
Cutting time - τ_{cut}	Idle running time $\tau_{i.r.}$

A good state of the cutting process is guaranteed if the part l when the tool tooth starts to cut P_1, P_3 along y -direction (Fig. 5) has more or less the same range. In this case, the radial depth of cut is more or less constant during the whole machining process. The proposed figure describes the ideal situation when the workpiece displacement at point P_1 and P_3 is equal.

Suppose the part deflection (point of measurement) changes at the location of tooth entrance (P_1, P_3) from cutting to cutting. In that case, it is not possible to obtain a good surface finish because the radial depth of cut and, hence, chip thickness is different for every cut (P_1, P_3). The larger the difference between positions of the workpiece at the place of tooth entrance, the larger the fluctuation of the radial depth, resulting in bad surface quality.

From Fig. 6, it can be seen that if the workpiece (point of measurement) has a big fluctuation (upper figure) at the time of tooth entrance/exit, a poor surface finish is generated. In case the tool enters/exits at the same value of workpiece positions (Fig. 6, below), then a high-quality surface finish is achieved. The parameter characterizing the fluctuation at the tooth entrance point and the cutting condition is the peak-to-peak value of the workpiece deflections when the tool tooth starts to cut ($P_{entrance}$).

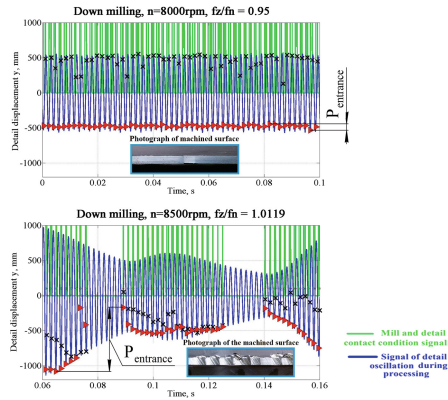


Fig. 6. Workpiece vibration at thin-walled end milling at different cutting states (experimental results, obtained with 6 mm thick plate).

4 Results

Down-milling experiments (dry machining) were performed at different spindle speeds ranging from 500 to 10000 rpm, with steps of 100 rpm. Other cutting parameters were kept constant: feed per tooth (ft) 0.05 mm, axial depth of cut (ap) 2 mm, radial depth of cut (ae) 0.5 mm, tool diameter (D_{mill}) 19mm, number of the teeth (Nt) 4.

Two thin plates, steel: S235, length: 80 mm, width: 60 mm with different thickness (h), were applied as the workpiece. Table 2 gives the modal parameters (measured experimentally by impact test) of the part.

Milling test results show that the peak-to-peak value of point of tooth entrance significantly changes within the observed spindle speed range (Fig. 7, Fig. 8). It was chosen 100 cuts at the center of the workpiece and the distance of 10mm for analyzing. It should be noted that part behavior shows typical cases valid along the whole tool path.

Table 2. Modal properties of the part.

The thickness of the plate (mm)	$f_n(\text{Hz})$	ξ	$k(\text{N/m})$
6	560	0,01	992×10^3
8	787	0,012	2398×10^3

Minimum workpiece deviation (deflection) when the tool inserts the workpiece guarantees optimal cutting conditions and good surface quality.

The ideal cutting parameters for the 6 mm thick plate (Fig. 7) was observed within the following spindle speed regions $\Omega = 2300\text{--}2700$ rpm; $\Omega = 3200\text{--}3700$ rpm; $\Omega = 4800\text{--}8000$ rpm and $\Omega = 9700\text{--}10000$ rpm.

For a spindle speed $\Omega = 8400$ rpm, a large amplitude at the natural frequency of the part system and tooth passing frequency is observed. Because the frequencies are

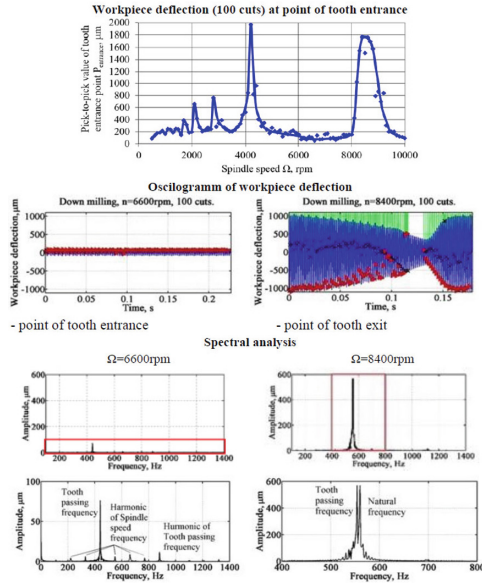


Fig. 7. Tooth entrance position vs. spindle speed, oscillogram of workpiece deflection, and spectral analysis ($h = 6$ mm).

within the same range, the “beat” phenomenon took place, meaning that the position of the workpiece (point of measurement) is different at every consecutive cutting. Such behavior of the vibrating system (thin-walled detail) is typical in large workpiece fluctuations at the time of tooth entrance. The spectra are dominated only at a tooth passing frequency when low tooth entrance point fluctuation is achieved ($\Omega = 6600$ rpm). We deal with low amplitude in such cases.

The stability lobe diagram, calculated for the 6mm plate, is shown in Fig. 8. The stability chart has been calculated with 100 points discretized the delay period, and the stability charts were computed on a 400×300 grid. Obtained results claim that most of the milling tests should be conducted under unstable cutting conditions. Moreover, at the spindle speed ranges where stable cutting conditions are defined, milling tests show high vibrations.

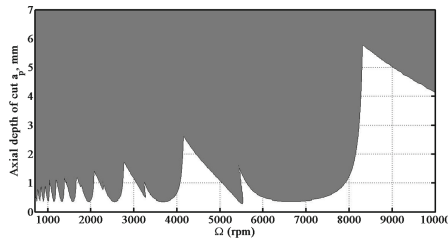


Fig. 8. Stability lobe diagram ($h = 6$ mm).

The most ideal cutting parameters for the 8 mm thick plate (Fig. 9) was observed within the following spindle speed regions: $\Omega = 2300\text{--}2400$ rpm, $\Omega = 2800\text{--}3000$ rpm, $\Omega = 3700\text{--}3900$ rpm, $\Omega = 4900\text{--}5700$ rpm and $\Omega = 7400\text{--}10000$ rpm.

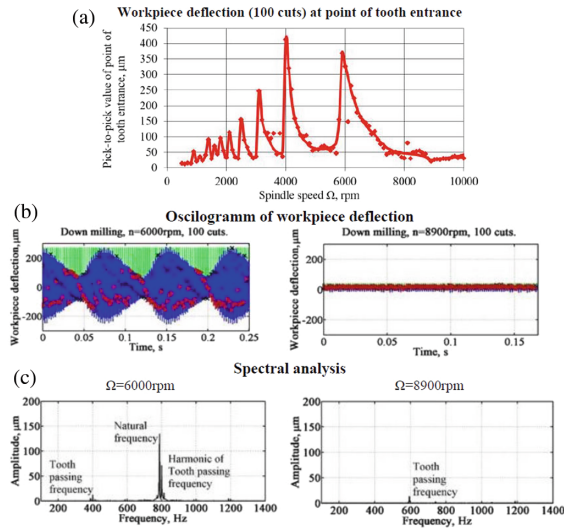


Fig. 9. Tooth entrance position vs. spindle speed (a), oscillogram of workpiece deflection (b), and spectral analysis (c) ($h = 8$ mm).

When bad cutting conditions occur ($\Omega = 6000$ rpm), a large amplitude at the natural frequency, tooth passing frequency, and sub-harmonic was observed. Due to the vicinity of the natural frequency and the sub-harmonic of the tooth passing frequency, the “beat” phenomenon took place, and cutting occurs with high fluctuation of the part when the tooth starts to cut. The spectra have low amplitude for the 6mm thick plate and are dominated only at a tooth passing frequency when the cutting process occurs at good cutting conditions ($\Omega = 8900$ rpm).

The stability lobe chart for the 8mm plate (Fig. 10) and fluctuation of part position when the tooth starts to cut (Fig. 9) show that at spindle speed ranges where stable condition should be observed, a high vibration level was detected.

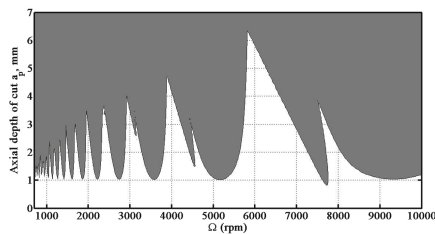


Fig. 10. Stability lobe diagram ($h = 8$ mm).

The character of the curves for both plates (Fig. 7, Fig. 9) is the same, but the regions of maximum and minimum workpiece vibrations take place at different spindle speed ranges. However, considering the workpiece vibration as a function of the ratio of the tooth passing frequency (f_z) and the natural of the part, l (f_n), it becomes clear that the same regularities determine the state of processing for both workpieces (Fig. 11). The worst processing condition was observed in spindle speed regions when the tooth passing frequency is close to the natural frequency of the detail ($f_z/f_n = 1$). The same is seen for frequency ratios (f_z/f_n) of 0,5; 0,33; 0,25; but with decreasing trend. When the ratio was lower than 0,2, then the system has time to make one or more self-excited oscillations during the cutting process, e.g., for observed modal properties of the system and milling condition, the period of one cutting has become more than chatter period. In that case, the stability of the process should/can be analyzed and evaluated using classical stability theories.

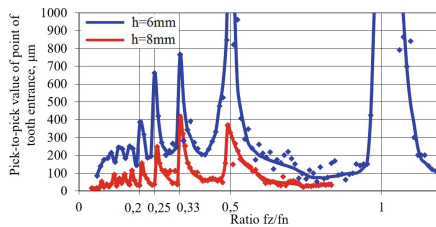


Fig. 11. Pick-to-pick value of point of tooth entrance vs. ratio of tooth passing frequency and natural frequency of the detail.

It can be concluded that vibrations during machining of thin-walled parts are related to resonance phenomena. Due to the infinite number of higher harmonics of the tooth passing frequency, spindle speed regions with large workpiece vibrations might be endless when the tooth passing frequency is equal or in integer number times lower than the natural frequency thin-walled structure. However, at low spindle speed, when one or more regenerative waves are placed on the cutting surface, regularities are not dominated based on the resonance phenomenon. In such a case, chatter determines the quality of the machining. Moreover, at low spindle speeds, the oscillation is significantly damped during the free workpiece movements between cuttings, resulting in soft workpiece amplitudes when the tooth enters the workpiece.

5 Conclusions

Milling of complex shaped thin-walled components always occurs under interrupted machining conditions, which is an important difference from classical end milling. Experimental results show that the worst processing conditions occur in a spindle speed range where the natural frequency of the part is in the vicinity of the tooth passing frequency or its sub-harmonics. Such conditions should be avoided. Simultaneously, the best milling conditions and good surface quality are achieved when the natural frequency

of the part feature to be machined is lower or between sub-harmonics of tooth passing frequency.

Milling of thin-walled components deals with short cutting lengths, contributing to a decrease in the number of regenerative waves on the cutting surface. As a result, there is less than one regenerative wave beginning from relatively low spindle speed. Therefore, vibrations in high-speed milling of thin-walled structures are rather caused by resonance phenomenon than by self-excited oscillation.

These findings have been supported by experimental validation where two thin-walled structures have been machined. The worst processing conditions occur when the tool impacts the workpiece when its amplitude of vibration is high.

Acknowledgments. The authors are grateful to the Erasmus exchange program KA1, which supported the stay in Belgium of Ph.D. students Anton Germashev (Contract 000000076839) and Mark Kuchuhurov and their research at KU Leuven.

References

1. Altintas, Y., Stepan, G., Budak, E., Schmitz, T., Kilic, Z.M.: Chatter Stability of Machining Operations. *J. Manuf. Sci. Eng.* **142**(11), 1–46 (2020)
2. Cheng, K.: *Machining Dynamics. Fundamental, applications and practices.* Springer Series in Advanced Manufacturing. Springer-Verlag London, Brunel University (2009).
3. Tobias, S.A., Fishwick, W.: Theory of regenerative machine tool chatter. *Engineer* **205**(199–203), 238–239 (1958)
4. Tlustý, J., Poláček, M.: The stability of the machine tool against self-excited vibration in machining. In: *Proceedings of the International Research in Production Engineering Conference*, pp. 465–474. ASME, Pittsburgh (1963).
5. Schmitz, T.L., Smith, K.S.: *Machining Dynamics. Frequency Response to Improve productivity.* Springer, Heidelberg (2019)
6. Altintas, Y., Budak, E.: Analytical prediction of stability lobes in milling. *Ann CIRP* **44**, 357–362 (1995)
7. Altintas, Y.: *Manufacturing automation.* Cambridge University, Cambridge (2012)
8. Weremczuk, A., Rusinek, R., Warminski, J.: Bifurcation and stability analysis of a nonlinear milling process. In: *AIP conference proceedings*, vol. 1922, No. 1, p. 100008. AIP Publishing LLC (2018)
9. Budak, E.: *Mechanics and dynamics of milling thin-walled structures.* The University of British Columbia (1994)
10. Tuysuz, O., Altintas, Y.: Frequency domain updating of thin-walled workpiece dynamics using reduced-order substructure methods in machining. *J. Manuf. Sci. Eng.* **139**, 1–16 (2017)
11. Shtehin, O.O., Wagner, V., Seguy, S., Landon, Y., Dessein, G., Mousseigne, M.: Stability of ball-end milling on a warped surface: semi-analytical and experimental analysis. *Int. J. Adv. Manuf. Technol.* **89**, 2557–2569 (2017). <https://link.springer.com/article/10.1007/s00170-016-9656-3>
12. Wang, T., Ning, H., Liang, L.: Milling stability analysis considers process damping and mode shapes of in-process thin-walled workpiece. *Int. J. Mech. Sci.* **159**, 382–397 (2019)
13. Davies, M., Balachandran, B.: Impact dynamics in the milling of thin-walled structures. In: *Proceedings of the Nonlinear Dynamic Control Symposium*, pp. 12–22 (1996)
14. Davies, M., Pratt, J., Dutterer, B., Burns, T.: Stability prediction for low radial immersion milling. *J. Manuf. Sci. Eng.* **124**, 217–225 (2002)

15. Davies, M., Pratt, J., Dutterer, B., Burns, T.: The stability of low radial immersion milling. *CIRP Ann. Technol.* **49**, 37–40 (2000)
16. Insperger, T., Stépán, G.: Stability of the milling process. *Period Polytech. Eng. Mech. Eng.* **44**, 47–57 (2000)
17. Totis, G., Insperger, T., Sortino, M., Stépán, G.: Symmetry breaking in milling dynamics. *Int. J. Mach. Tools Manuf.* **139**, 37–59 (2000)
18. Altintas, Y., Budak, E.: Analytical prediction of chatter stability in milling - Part I: general formulation. *J. Dyn. Syst. Meas. Control* **120**, 22–30 (1998)
19. Merdol, S.D., Altintas, Y.: Multi frequency solution of chatter stability for low immersion milling. *Trans. Soc. Mech. Eng. J. Manuf. Sci. Eng.* **126**, 459–466 (2004)
20. Kline, W., DeVor, R., Shareef, I.: The prediction of surface accuracy in end milling. *J. Eng. Ind.* **104**, 272–278 (1982)
21. Tlustý, J.: Effect of end milling deflections on accuracy. In: King, R.I. (ed.) *Handbook of High Speed Machining Technology*, pp. 140–153. Chapman and Hall, New York (1985)
22. Montgomery, D., Altintas, Y.: Mechanism of Cutting Force and Surface Generation in Dynamic Milling. *Journal of Engineering for Industry* **113**(2), 160–168 (1991)
23. Smith, S., Tlustý, J.: An overview of modeling and simulation of the milling process. *J. Eng. Ind.* **113**(2), 169–175 (1991)
24. Targ, Y., Liao, C., Li, H.: A mechanistic model for prediction of the dynamics of cutting forces in helical end milling. *Int. J. Model. Simul.* **14**(2), 92–97 (1994)
25. Honeycutt, A., Schmitz, T.L.: A study of milling surface quality during period-2 bifurcations. *Procedia Manuf.* **10**, 183–193 (2017)
26. Kiran, K., Rubeo, M., Kayacan, M.C., Schmitz, T.: Two degree of freedom frequency domain surface location error prediction. *Precis. Eng.* **48**, 234–242 (2017)
27. Honeycutt, A., Schmitz, T.L.: Surface location error and surface roughness for period-n milling bifurcations. *J. Manuf. Sci. Eng.* **139**, 1–18 (2017)
28. Germashev, A., Logominov, V., Khristal, V., Kozlova, E.: Methodology of determination of the optimal cutting condition for milling of thin-walled components. In: *UTIS 9th International Congress on Machining*, pp. 349–360 (2018).



Study of Dynamic and Power Parameters of the Screw Workpieces with a Curved Profile Turning

Ivan Hevko , Andrii Diachun , Oleg Lyashuk  , Yuriy Vovk ,
and Andriy Hupka 

Ternopil Ivan Puluj National Technical University, 56, Ruska Street, Ternopil 46001, Ukraine
oleglashuk@ukr.net

Abstract. A dynamic model of the external turning of the screw workpiece outer edge is worked out. The differential equations of the system motion to determine the torsional and linear vibrations of a screw workpiece, a mandrel, and a cutter are deduced. Based on research analyses, the analytical dependences for determining the dynamic loads on the system are developed. The graphic dependences of variation value of cutting force in time are developed, as well as the angle change of screw workpiece deformation in time, and the linear deformation while turning the screw workpiece outer edge. The cutting conditions for turning the screw workpiece outer edge are experimentally specified. According to the results of the experimental study of turning L-shaped auger spirals, outer edges made of 30 Steel (eq. C 30), 20 Steel (eq. C 22), and Steel 08kp (eq. St14), the increase in cutting speed reduces the cutting force. The increase of cutting depth and feed leads to increased cutting force.

Keywords: Curved profile · Turning · Cutting · L-shaped · Screw

1 Introduction

Screw machine parts and mechanisms are widely used in various technical systems, as well as their sub-type - the L-shaped auger spirals (LSASs), due to the peculiarities of their geometric structure. They are used as the working bodies of screw conveyors, mixers, grinders, granulators, separators, screw conveyors, and spiral descents in the construction, food processing industry, powder metallurgy, agricultural machinery, ventilation, and heat exchange systems. Nowadays, the production of advanced technology systems with screw workpieces must meet the higher requirements for their quality and accuracy. Screw workpieces (SWs) manufactured by deforming the tape or sheet workpieces do not always provide the required accuracy of external and internal diameters. Dimensional deviations are 2 mm or more, the ovality and eccentricity - approximately 1 mm. For modern machines and mechanisms, these deviations are not acceptable. According to analysis, the dimensional and shape tolerance for the surface should be less than 0.5 mm. Therefore, the challenge is to introduce the turning operations in SW manufacturing processes, and in some cases – the grinding operations.

2 Literature Review

The use of augers with inclined turns set at a certain angle to the axis provides a significant increase of efficiency in transportation [1], compared to augers with spirals set horizontally to the axis. The firms in many countries manufacture screw workpieces with a curved profile; however, they face a problem providing the accuracy of geometrical dimensions. In the article [2] designed experiment procedure, the model's reliability is validated by comparing predicted and measured results. Study [3], based on the model for the cutting process concerning the delayed argument, proposes to employ a heuristic criterion for selecting the frequency of change in speed considering a minimum of power consumption for the process of cutting. Further studies [4–6] determining the optimum relationships between the amplitude and frequency of spindle speed variation. This paper proposes an algorithm that can significantly improve the part machining accuracy without increasing the machining time, organized in the form of the model by state variables and the Runge-Kutta procedure of integration [7, 8]. The authors propose a solution to the problem of increasing dimensional accuracy in turning equipment by replacing the original geometric model of the workpiece in the model, taking into account elastic deformation force occurring in the technological system under the action of cutting forces [9–11]. In this model, the impacts of cutting parameters on energy are fully considered, and the MATLAB optimization toolbox is used for the solution [12]. The paper [13, 14] discusses custom systems for hi-tech production complexes in studying the principal steps and influence factors. The article [15] considers innovative methods in modeling and designing machining systems drives and machine processes. Therefore, the challenge is to develop the progressive methods of manufacturing augers and their sub-type - L-shaped auger spirals with high precision geometrical dimensions. The feature of this turning is the occurrence of shock loads and the screw workpiece's deformation during cutting.

3 Research Methodology

The features of SW geometry significantly affect the dynamics of SW turning and the development of the necessary equipment and tools. The passable cutters can be used to turn both the internal and external SW diameters and the typical cylindrical surfaces. However, there are some significant differences. First, SWs possess relatively low stiffness, and second, they belong to discontinuous surfaces. Therefore, the process of SW turning is associated with extremely complex shock and shaping processes; it especially concerns the turning of an LSAS curved profile.

Consequently, there is a need to develop a mathematical model to study the nature of load changes on the system' LSAS, mandrel, cutter' when turning. Turning the LSAS discontinuous surfaces is considered the transient dynamic process. The study of the dynamic system details by taking them off the chain cannot provide a sufficiently accurate picture of actual stresses in constituent parts of the system' LSAS, mandrel, cutter'. Therefore, the system of interrelated parts should be calculated considering the elasticity of links and the vibration motions of all elements.

The schemes of turning the screw workpiece are shown in Fig. 1 and Fig. 2. The feature of this scheme is the diameter of the LSAS after formation. It varies along the

axis of the mandrel. The LSAS surface is cone-shaped with an angle α . After turning, the LSAS gains the form of a cylinder. The value of moments of elasticity forces for the system shown in Fig. 1 can be found by solving differential equations of motion - dynamics equations that describe transients in the system' LSAS, mandrel, cutter'.

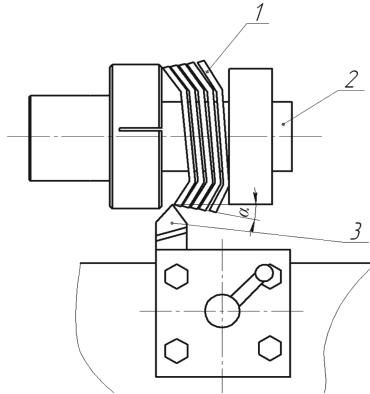


Fig. 1. Scheme of turning the SW with a curved profile: 1 - screw workpiece; 2 - mandrel; 3 - cutter.



Fig. 2. General view of the process of turning the outer edges of an SW curved profile.

To study the actual process of turning with all constituents, it is necessary to create a complex system of differential equations. Therefore, to determine the basic nature of LSAS turning, the secondary factors should be neglected.

The system' LSAS, mandrel, cutter' is considered a mechanical model consisting of lumped masses connected by elastic links. Elastic links are permissible weightless and are characterized by constant stiffness coefficients. Local stresses and strains in the joints of individual elements of the system can be neglected. We should choose such transients and natures of the applied forces changes that allow obtaining in a transient process the maximum possible values of moments and elasticity forces in individual elements of the system.

According to the above, the system' LSAS, mandrel, cutter' can be generalized to an equivalent multi-mass system shown in Fig. 3. The concentrated masses, shown in Fig. 3,

include I_1, I_2 are LSAS and mandrel generalized moments of inertia correspondingly; m_1, m_2, m_3, m_4, m_5 is LSAS, mandrel, cutter, cutter carrier, carriage masses correspondingly. Screw workpiece turns are compressed together and do not boarder tightly to each other. During SW turning, the deformation of LSAS sheet materials occurs. This deformation negatively affects the quality of a finished surface. In addition, in (Fig. 3), are marked: C_{12}, C_2 are LSAS, and mandrel generalized stiffnesses. The generalized coefficients of linear stiffness are marked as well: k_{12z}, k_{12y} are generalized LSAS linear stiffnesses in the direction of axes z and y ; k_{2z}, k_{2y} are generalized linear stiffnesses of a mandrel in the direction of axes z and y ; k_{34z}, k_{34y} are generalized linear stiffnesses of a cutter in the direction of axes z and y ; k_{45z}, k_{45y} are generalized linear stiffnesses of a tool carrier in the direction of axes z and y ; k_{5z}, k_{5y} are generalized linear stiffnesses of a carriage in the directions of axes z and y . Besides, the damping coefficients are marked: $\beta_{12\varphi}$ is the coefficient of damping the torsional modes between the mandrel and LSAS; $\beta_{2\varphi}$ is the coefficient of damping the torsional modes between a mandrel and a spindle; β_{12z}, β_{12y} are coefficients of damping the linear oscillations between the mandrel and LSAS in the direction of axes z and y ; β_{2z}, β_{2y} are coefficients of damping the linear oscillations between a mandrel and a spindle in the direction of axes z and y ; β_{34z}, β_{34y} are coefficients of damping the linear oscillations between a cutter and a tool carrier in the direction of axes z and y ; β_{45z}, β_{45y} are coefficients of damping the linear oscillations between a tool carrier and a carriage in the direction of axes z and y ; β_{5z}, β_{5y} are coefficients of damping the linear oscillations between a carriage and a bedplate in the direction of axes z and y .

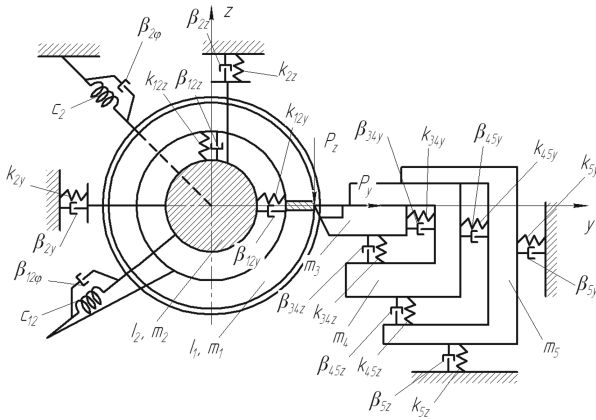


Fig. 3. Scheme of the dynamic model of turning the screw workpiece with a curved profile.

The cutting force (metal chips formation) affects the mass I_1, m_1 , an LSAS, and a cutter m_3 . This force is composed of shock loads and the resistance force of cutter movement along the back surface. It is decomposed into tangential component P_z and a radial component P_y . LSAS turning may be considered as the intersection of two surfaces: the LSAS external diameter and the screw surface of finishing from a cutter feed. The law of changing the loads on LSASs can be considered as a function from the

time t or the value of relative motion of the cutter top and an LSAS along the length l of the tool contact line with the LSAS body in fixed coordinates.

The contact time of the cutter and an LSAS equals:

$$t_k = \frac{H + \delta}{2 \sin(\gamma_1 \pm \gamma_2) \pi \cdot R \cdot n} \quad (1)$$

where H is the thickness of LSAS material, mm; δ is LSAS surface deflection along the normal to the contact point, mm; γ_1 is the inclination angle of the midline of LSAS outer radius, grad; γ_2 is the inclination angle of the screw line of cutter feed, grad, n is a number of spindle revolutions per second, R is the radius of turning.

The formula (1) + sign refers to the processing of right spirals using the right cutter, and the sign – to the processing of left spirals. The angular displacements of inertial masses φ_1, φ_2 and the linear displacements of masses in the direction of axes z and y are chosen as the generalized coordinates: $z_1, z_2, z_3, z_4, z_5, y_1, y_2, y_3, y_4, y_5$.

At the beginning and the end of the cutting area, the value of cutting depth t_p and feed S is changed. Therefore, in these areas, the cutting forces $P_z(t)$ and $P_y(t)$ are presented by increasing and decreasing linear dependencies. In the area with the constant cutting depth and feed, the cutting forces $P_z(t)$ and $P_y(t)$ are assumed constant with sufficient accuracy and can be determined by empirical dependencies.

The differential equations of motion of the system for forced torsional vibrations and linear displacements using Lagrange equations of the second kind are deduced:

$$I_1 \cdot \ddot{\phi}_1 + C_{12} \cdot (\phi_1 - \phi_2) + \beta_{12}(\dot{\phi}_1 - \dot{\phi}_2) - k_{12z}(z_2 - R\phi_1 - z_1)R - \beta_{12z}(\dot{z}_2 - R\dot{\phi}_1 - \dot{z}_1)R = P_z(t) \cdot R;$$

$$I_2 \cdot \ddot{\phi}_2 + C_2 \cdot \phi_2 + C_{12} \cdot (\phi_2 - \phi_1) + \beta_2 \cdot \dot{\phi}_2 + \beta_{12}(\dot{\phi}_2 - \dot{\phi}_1) = 0;$$

$$m_1 \cdot \ddot{z}_1 - k_{12z}(z_2 - R\phi_1 - z_1) - \beta_{12z}(\dot{z}_2 - R\dot{\phi}_1 - \dot{z}_1) = P_z(t);$$

$$m_2 \cdot \ddot{z}_2 + k_{12z}(z_2 - R\phi_1 - z_1) + \beta_{12z}(\dot{z}_2 - R\dot{\phi}_1 - \dot{z}_1) + k_{2z}z_2 + \beta_{2z}\dot{z}_2 = 0;$$

$$m_3 \cdot \ddot{z}_3 - k_{34z}(z_4 - z_3) - \beta_{34z}(\dot{z}_4 - \dot{z}_3) + k_{2z}z_2 = P_z(t);$$

$$m_4 \cdot \ddot{z}_4 + k_{34z}(z_4 - z_3) + \beta_{34z}(\dot{z}_4 - \dot{z}_3) - k_{45z}(z_5 - z_4) - \beta_{45z}(\dot{z}_5 - \dot{z}_4) = 0;$$

$$m_5 \cdot \ddot{z}_5 + k_{45z}(z_5 - z_4) + \beta_{45z}(\dot{z}_5 - \dot{z}_4) + k_{5z}z_5 + \beta_{5z}\dot{z}_5 = 0$$

$$m_1 \cdot \ddot{y}_1 - k_{12y}(y_2 - y_1) - \beta_{12y}(\dot{y}_2 - \dot{y}_1) = P_y(t);$$

$$m_2 \cdot \ddot{y}_2 + k_{12y}(y_2 - y_1) + \beta_{12y}(\dot{y}_2 - \dot{y}_1) + k_{2y}y_2 + \beta_{2y}\dot{y}_2 = 0;$$

$$m_3 \cdot \ddot{y}_3 - k_{34y}(y_4 - y_3) - \beta_{34y}(\dot{y}_4 - \dot{y}_3) = P_y(t);$$

$$m_4 \cdot \ddot{y}_4 + k_{34y}(y_4 - y_3) + \beta_{34y}(\dot{y}_4 - \dot{y}_3) - k_{45y}(y_5 - y_4) - \beta_{45y}(\dot{y}_5 - \dot{y}_4) = 0;$$

$$m_5 \cdot \ddot{y}_5 + k_{45y}(y_5 - y_4) + \beta_{45z}(\dot{y}_5 - \dot{y}_4) + k_{5y}y_5 + \beta_{5y}\dot{y}_5 = 0. \tag{2}$$

An example of the cutting force change while turning screw elements with variable cutting depth during the periodic cutting is shown in Fig. 4, obtained based on experimental data.

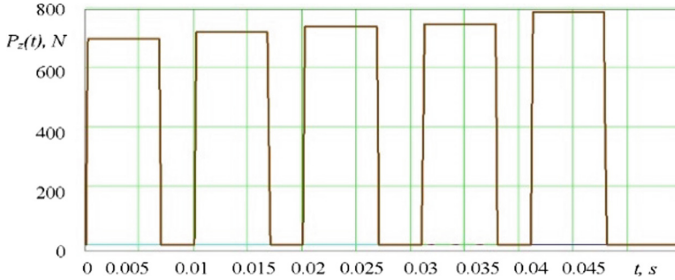


Fig. 4. Graph of changes of cutting force $P_z(t)$ in time.

The deformation of elastic elements of the system during the turning of the LSAS occurs when the interaction of a cutter and a turn occurs. This moment is considered a time-reference point. Therefore, the initial relative coordinates and rates are assumed equal to zero. Further deformation occurs due to external forces. Differential equations (2) should be solved on the computer by applying a standard sub-program of the Runge-Kutta numerical method.

4 Results

Based on the research results, the following graphic dependences are developed during the turning of an LSAS made of steel and with a radius of 100 mm: the angle change of LSAS deformation in time (Fig. 5) and linear deformation of an LSAS in time (Fig. 6).

To test the adequacy of the proposed system of differential equations, all its components were determined experimentally. The developed graphic dependences prove that the angle of LSAS deformation in time increases when the cutting depth increases to 0.15° . Then it gradually decreases with damped vibrations to zero during the exit of a cutter from the cutting area. The study technique for turning the outer edge of LSAS by a tight package (Fig. 2) is as follows. The mandrel is set in a spindle of the lathe 16K20; a cutter is set in a cutter carrier. The turning process, accompanied by collecting the necessary data using the frequency converter Altivar and the software PowerSuite v.2.5.0, is carried out.

The technological process of turning the outer edge of an SW curved profile is applied to the original SW with an outer diameter of 90 mm. A spiral turn width of 2 mm (material is Steel 08kp (equivalent St14).

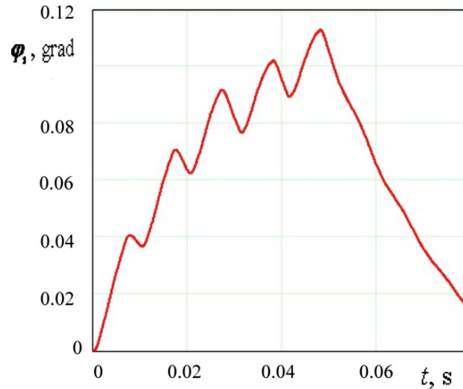


Fig. 5. Graph of the angle change of deformation of the screw workpiece in time.

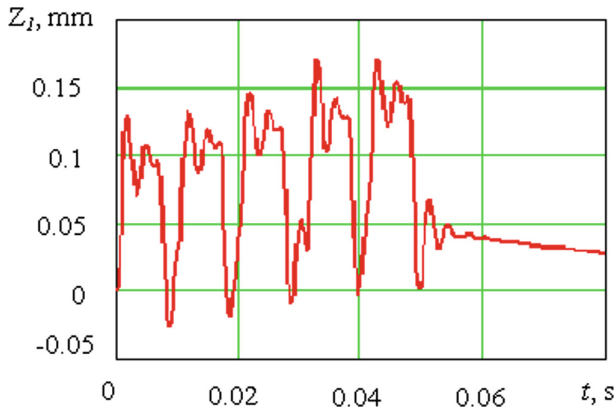


Fig. 6. Graph of changes of linear deformation of a screw workpiece in time.

In the process of shelf formation by a forming roller at the initial corner of the first spiral 45 grades, an angle of each next turn of a screw workpiece is reduced by 0.35° – 0.45° . Under such conditions, the last turn of a screw workpiece (for 10 turns) is from 44° to 43° . Therefore, if the angle of an inclined shelf is reduced, the obliquity in all cases is created in the external outline of a formed workpiece (Fig. 1). Therefore, after one-step calibration of a screw workpiece, the diameter along the whole length of a working body is non-uniform. Experimental studies were conducted to determine the maximum values of cutting forces that occur during the turning.

The parameters of the screw workpiece under study were as follows: material - Steel 08kp, 20 Steel (equivalent C 22) and 30 Steel (equivalent C 30), the range of external diameters – from 90 to 130 mm; the thickness of the outer edge – from 1 to 3 mm and the shelf inclination angle from 30° to 60° . According to experimental researches, the cutting speed should possess certain values. Otherwise, the external screw surface can be deformed. The range of cutting speeds was determined experimentally. Thus, to achieve

sufficient surface quality, particularly the surface roughness $Ra = 4.2\text{--}7.5 \mu\text{m}$ and IT10, the cutting speed should be approximately 300 m/min.

If the thickness of a screw surface increases by more than 0.5 mm, the screw speed can be reduced to 100–200 m/min. However, the quality of finishing is one to two orders of magnitude smaller. The pulsing nature of the cutting force dependence in time can be traced in oscillograms. Based on experimental data, graphical dependencies of the angle change of shelf inclination on cutting force (Fig. 7) and the change of cutting force on the cutting depth are developed (Fig. 8). If the cutting force ranges from 500 to 550 N, the angle of shelf inclination remains unchanged. If the cutting force increases to 550... 900 N, the angle of shelf inclination increases to 1.6° . For steels with higher yield strength, greater cutting forces occur.

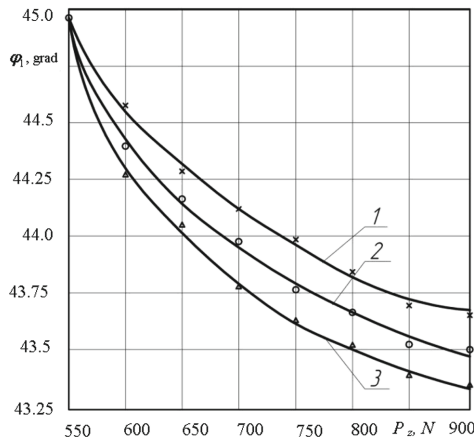


Fig. 7. Dependences of the angle change of shelf inclination of cutting force during turning: 1) 30 Steel; 2) 20 Steel; 3) Steel 08kp.

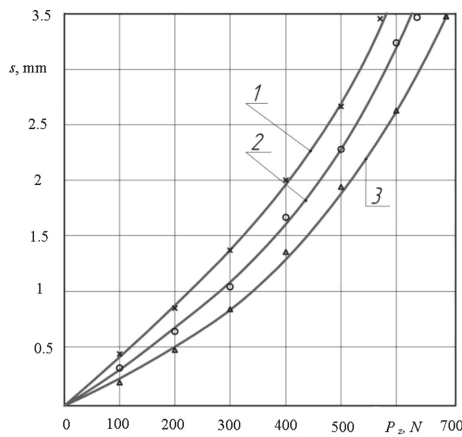


Fig. 8. Dependence of the cutting force change on the cutting depth: 1) 30 Steel; 2) 20 Steel; 3) Steel 08kp.

5 Conclusions

Based on research analyses, the analytical dependences for determining the dynamic loads on the system are developed. The graphic dependences of variation value of cutting force in time are developed, as well as the angle change of screw workpiece deformation in time, and the linear deformation while turning the screw workpiece outer edge.

The graphic dependences of variation value of cutting force in time, the angle of LSAS deformation in time during the cutting an LSAS with a radius of 100 mm and made of Steel 08kp are developed. The graphic dependences of linear deformation changes of an LSAS in time are developed as well. Based on the research results, the nature of changes of cutting forces in a range from 690 to 780 N per 0.5 s was defined. The cutter vibrations within 0.02–0.07 mm and SW vibrations within 0.03–0.17 mm per 0.07 s were studied. When the cutting force is less than 550 N, the angle of shelf inclination is virtually unchanged. When the cutting force increases, the angle of shelf inclination reaches 1.6°.

References

1. Korolev, A.V., Korolev, A.A.: Friction machine for accelerated wear tests of frictional rolling elements. *J. Frict. Wear* **38**, 77–81 (2017)
2. Yao, Q., Luo, M., Zhang, D., Wu, B.: Identification of cutting force coefficients in machining process considering cutter vibration. *Mech. Syst. Sign. Process.* **103**, 39–59 (2018)
3. Changlin, L., Xiao, C., Jianguo, Z., Junjie, Z., Jianning, C., Junfeng, X., Jianfeng, X.: Molecular dynamic simulation of tool groove wear in nanoscale cutting of silicon. *AIP Adv.* **10**, 015327 (2020). <https://doi.org/10.1063/1.5133855>
4. Zhang, S.J., To, S., Zhang, G.Q.: Diamond tool wear in ultra-precision machining. *Int. J. Adv. Manuf. Technol.* **88**, 613–641 (2017)
5. Al-Regib, E., Lee, J., Ni, S.-H.: Programming spindle speed variation for machine tool chatter suppression. *Int. J. Mach. Tools Manuf.* **43**(12), 1229–1240 (2003). [https://doi.org/10.1016/S0890-6955\(03\)00126-3](https://doi.org/10.1016/S0890-6955(03)00126-3)
6. Albertelli, P., Musletti, S., Leonesio, M., Bianchi, G., Monno, M.: Spindle speed variation in turning: technological effectiveness and applicability to real industrial cases. *Int. J. Adv. Manuf. Technol.* **62**(1–4), 59–67 (2012). <https://doi.org/10.1007/s00170-011-3790-8>
7. Yang, J., Aslan, D., Altintas, Y.: A feedrate scheduling algorithm to constrain tool tip position and tool orientation errors of five-axis CNC machining under cutting load disturbances. *CIRP J. Manufact. Sci. Technol.* **23**, 78–90 (2018)
8. Petrakov, Y., Danylchenko, M., Petryshyn, A.: Programming spindle speed variation in turning. *East.-Eur. J. Enterp. Technol.* **2**(1), 4–9 (2017)
9. Nekrasov, R.Y., Solovyov, I.V., Starikov, A.I., Bekareva, O.V.: Improving dimensional accuracy of turning on CNC equipment. *Key Eng. Mater.* **736**, 95–100 (2017)
10. Nekrasov, R.Y., Solovyov, I.V., Starikov, A.I., Tempel, Y.A., Tempel, O.A.: Numerical studies to determine spatial deviations of a workpiece that occur when machining on CNC machines. In: *MATEC Web of Conferences*, vol. 129 (2017)
11. Nekrasov, R., Putilova, U., Tempel, Y.: Precision CNC machining and ways to achieve it. In: *MATEC Web of Conferences*, p. 01048. EDP Sciences (2018)
12. Ma, F., Zhang, H., Cao, H., Hon, K.K.B.: An energy consumption optimization strategy for CNC milling. *Int. J. Adv. Manuf. Technol.* **90**(5-8), 1715–1726 (2017)

13. Martinov, G.M., Kozak, N.V., Nezhmetdinov, R.A., Grigoriev, A.S., Obukhov, A.I., Martinova, L.I.: Method of decomposition and synthesis of the custom CNC systems. *Autom. Remote Control* **78**(3), 525–536 (2017)
14. Aguado, S.: Improving a real milling machine accuracy through an indirect measurement of its geometric errors. *J. Manuf. Syst.* **40**, 26–36 (2016)
15. Yemelyanov, N.V., Yemelyanova, I.V., Zubenko, V.L.: Improving machining accuracy of CNC machines with innovative design methods. In: *IOP Conference Series: Materials Science and Engineering*, p. 042028. IOP Publishing (2018)



Effect of Abrasive Finishing on the Electrical Parameters of S-B and Rectangular Waveguides

Natalia Honchar^(✉) , Pavlo Tryshyn , Dmytro Stepanov , and Olena Khavkina 

National University “Zaporizhzhia Polytechnic”, 64,
Zhukovsky Street, Zaporizhzhia 69063, Ukraine
gonchar@zntu.edu.ua

Abstract. Most S-band waveguides are manufactured from a calibrated rectangular tube supplied with the required channel surface accuracy and quality. However, for the compactness of the transmission line, waveguides are made with corner bends and variable cross-sections, which are made by welding or soldering. During manufacturing, defects and deformations occur in the weld zone, which are eliminated by finishing. The main problem here is the assurance of required characteristics of current-carrying surface in weld zones. Several methods for machining waveguide channels provide the necessary roughness, although not all of them apply to rectangular cross-sections and, for machining, corner bends. Previously, the influence of the micro roughness height on the waveguide electrical characteristics was studied, but different finishing methods create their characteristic micro-relief, the direction of micro roughness, a certain degree of work hardening; all these factors also affect the electrical characteristics of working surfaces and require further research. In this work, comprehensive studies have been carried out to study various methods and tools for finishing, making it possible to machine hard-to-reach places of waveguide corner bends, including ensuring the waveguide electrical parameters. Based on the work results, rotating polymer abrasive tools are recommended to finish the weld-affected zones of waveguide corner bends, which provide a favorable surface micro-relief and improved electrical parameters. A model is proposed that makes it possible to predict the attenuation coefficient taking into account the presence of areas with inhomogeneous roughness.

Keywords: Rectangular waveguide · Attenuation coefficient · Conductivity · Finishing · Roughness · Texture direction · Work hardening · Tube brush · Polymer-abrasive filament

1 Introduction

Most radar stations operate in the S-frequency range ($f = 2...4$ GHz) of H_{10} type electromagnetic waves. The basis of the transmission line of these devices are waveguides, which are a construction welded or soldered of flanges and sections of a thin-walled rectangular pipe, which in the delivery state meets necessary standards of accuracy and quality of the channel surface. The waveguides are made of aluminum and brass.

For compactness of transmission lines, waveguides have corner bends, variable cross-section, which increases the number of welds (Fig. 1). During welding and soldering, waveguide section deformations and surface defects (penetrations, lapping, steps) appear in the seam zone; they are eliminated by subsequent finishing, while the rest of the section does not require machining. The inner working surfaces of the weld-affected zone are polished with tight tolerances $(3...15) \cdot 10^{-7} / f$ mm and roughness of less than Ra 0.8 μm .



Fig. 1. The appearance of corner waveguides.

It is known that the real electrical parameters of a waveguide often differ from the expected values depending on the level of electrical conductivity of the material and the height of the working surface micro roughness [1]. In turn, the control of the values of electrical parameters is the main and final in the waveguide manufacturing, as it gives an objective characteristic of their functionality. The main electrical parameters of waveguides include:

1. Voltage standing-wave ratio (VSWR);
2. Attenuation coefficient;
3. Electrical strength.

The most significant electrical parameter in assessing the waveguide quality is the attenuation coefficient, which characterizes the amount of energy loss in the waveguide channel. It is known that the roughness increases the currents path length in the metal (Fig. 2). With the value of microroughness (h_A) equal to the current penetration depth (δ), the losses increase about 1.6 times compared to the expected values. Therefore, to not have losses related to roughness, the microroughness height should be less than half of the current penetration depth in a given range (for aluminum 1.1...1.9 μm ; for brass 1.9...2.8 μm) [2].

The waveguide electrical parameters are also related to the nature of the high-frequency currents movement in the surface layer of the channel. The current motion vectors J_B and J_C in the waveguide walls (Fig. 3) are directed perpendicular to the magnetic field vector H : on a narrow wall, they have only a transverse direction, and on a wide one – both longitudinal and transverse directions [3, 4].

In addition, the transverse currents on the narrow walls do not depend on the y coordinate and remain constant along the entire length. In contrast, the longitudinal currents are equal to zero. On a wide wall, the currents depend on the z coordinate and

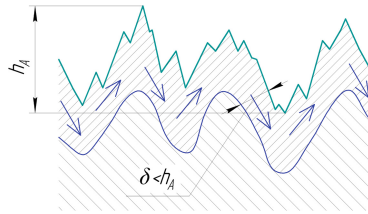


Fig. 2. Influence of microroughness on the current path in the waveguide channel if the current penetration depth (δ) is less than the microroughness height (h_A).

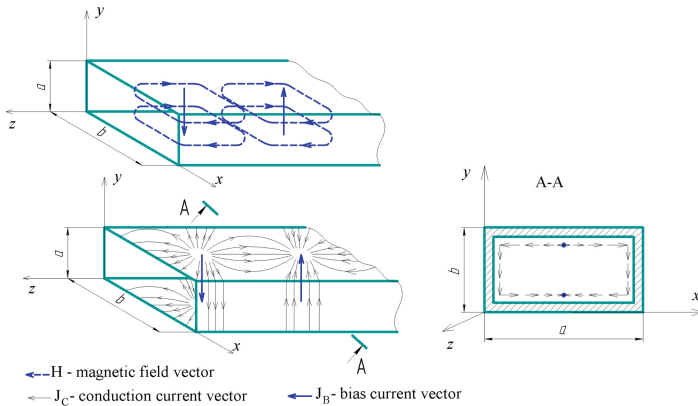


Fig. 3. The current line structure in the walls of a rectangular waveguide for the H_{10} wave.

take a value from zero to a maximum distance of half of the wavelength. When finishing, it is necessary to ensure that steps and grooves of micro roughness occurred due to the machining neither cross the current movement lines nor increase their path length in the metal.

It should be taken into consideration that the investigated waveguide is a thin-walled aluminum complex spatial structure; its processing is carried out on a step-by-step basis, often manually, using tools with low durability, which complicates the process of automation or mechanization. Moreover, not all methods for finishing waveguide channels that provide the necessary roughness apply to rectangular cross-sections and machining corner bends. Often, the polishing of these places, due to difficult access to them, is carried out with hand-held power tools (using sandpaper, cones) and does not even provide the necessary roughness. Various methods of finishing waveguide create on the surface their characteristic micro-relief, the direction of microroughness, a certain degree of work hardening, which directly affects the electrical characteristics of current-carrying surfaces. Therefore, the search and study of finishing methods, from the point of view of providing a favorable micro-relief and the surface layer properties to ensure high electrical parameters of bent rectangular waveguides of aluminum alloys, is of some interest.

2 Literature Review

Many studies [5, 6] on the influence of channel roughness parameters on losses in waveguides, attenuation coefficient, and electric field distribution. In these studies [6, 7], the computational models of real waveguides are based on the use of correction coefficients that consider the microroughness value and the ratio of the true length of rough channel walls to the length of ideally smooth ones. It was found that the waveguide surface roughness is random, and the microroughness height corresponds to the Gaussian random process. It was shown in [8] that the presence of the waveguides surfaces roughness is equivalent to a decrease in these surfaces' specific conductivity compared with the values included in the Shchukin-Leontovich boundary conditions for smooth surfaces. Surface microroughness located along or across the current paths can affect the wavefield structure in different ways and change the electrical parameters of the waveguides. Therefore, when finishing the waveguide working surfaces, attention should be paid to the direction of the microroughness induced by it.

Analysis of various methods for calculating the attenuation coefficient [9, 10] for a rectangular waveguide with an ideally smooth inner surface has shown that the results obtained with the same initial conditions differ significantly. Also, mathematical models give significant deviations from real values.

Presently, to achieve the required surface roughness of the waveguide channel, different finishing methods can be used, for example, anodic-abrasive polishing [11], abrasive-extrusion processing [12], processing with polishing tools on special machines [13], electrochemical polishing, and water jet machining [14]. However, these methods are laborious and inefficient. The disadvantages of these methods are the need to prevent deformation of thin walls during the tool movement under pressure, applicability only to straight waveguides, or smooth, rather than angular, turns, the need to wash the machined surfaces, sometimes disposing of waste. As a result, the finishing of corner waveguides is performed mainly using small-scale mechanization; sandpaper, bit rotary burrs, polymer-abrasive brushes [15] are used as tools.

During machining, each of the finishing methods also induces a certain degree of work hardening of the surface layer. In this case, work hardening can change the electrical conductivity of the waveguide wall surface layer. For example, the electrical conductivity of copper first increases slightly after work hardening to 35% and then begins to fall again with an increase in the deformation level [16]; at the same time, the electrical conductivity of the nickel-based alloy IN718 [17] first decreases and then rises with an increase of hardness. In some cases, the deformation processing of the surface layer can be accompanied by a decrease in the area of coherent scattering of the material and redistribution of alloying elements [18]. Such changes can also affect both its mechanical and physical properties, such as modulus of elasticity and electrical resistance. This shows the need to choose a rational method and processing modes in which a favorable combination of surface properties is achieved in terms of reducing signal attenuation. The higher the electrical resistance of the conductive layer is, the greater part of the power passing through the waveguide is converted into heat. Since for the waveguides under the investigation, the penetration depth of the high-frequency current is less than the work hardening depth. Therefore, the study of the work hardening effect on the electrical parameters is relevant.

The purpose of this research was to determine experimentally the optimal method for finishing hard-to-reach zones of waveguides corner bends, which ensures high quality, favorable micro-relief, and minimal additional work hardening of the waveguide working surfaces, and as a result, the optimal electrical parameters in general.

3 Research Methodology

To study the influence of the finishing methods of the channel, full-scale aluminum (AD0 material) waveguides with a corner bend and channel cross-section of 72×34 mm (Fig. 4) were used. Different tools were used to polish the inner channel at the seams after straightening and mechanical processing of the flanges. The tools used are sandpaper on a mandrel, a grinding flap wheel with a polymer on a flaring tool, an abrasive grinding brush, a grinding head made of non-woven abrasive material, an endless grinding head with an abrasive belt, and a belt made of non-woven abrasive tape. Polishing in the seam zone was performed until defects were eliminated from a smooth transition to the channel's main surface. The instrument rotation was carried out following their design features, inducing microroughness of a certain direction.



Fig. 4. The appearance of the test waveguides.

The grain size of the instruments was varied (F80; F120; F180) to obtain different microroughness height. The equipment used was a *Metabo GE710 Plus* electric polishing machine, a *Makita HP1630* electric drill, and a *Makita 9032* electric band file, providing a polishing speed of 2...25 m/s. The electrical parameters measured on the ready waveguides were carried out in the S-frequency range of the H_{10} wave. During the measurements, the values of VSWR, attenuation coefficient, and electrical strength were determined. A workstation was assembled from a *P2-56* panoramic meter, matched load, and the waveguide to be measured to check the VSWR. The workstation for testing the attenuation coefficient consisted of a *Rohde & Schwarz ZVH8* cable and antenna analyzer, coaxial-waveguide junctions, and the waveguide to be tested. The electrical strength of the waveguides was tested on a high-power stand, which included a *P-604* power meter and an *SI-65* oscilloscope; the waveguide to be tested was fixed using adapters with an eyepiece. During the electrical strength test, the criteria for waveguide conformity were the absence of arcing and breakdown in the test waveguide and the absence of visible changes in the oscilloscope signal.

To determine the surface roughness obtained by each specific finishing method, the waveguides were cut after checking the electrical parameters. At the polishing zones, samples of 30 × 30 mm in size were cut out. The roughness was studied using a 171621-profiler in the longitudinal and transverse directions. The amount of work hardening formed by finishing was determined on the same samples as the roughness by measuring the microhardness on a PMT-3 device at a load of 50 g and 100 g.

4 Results

All finishing methods gave a different quality of the conductive surface of the waveguides, which in turn affected their electrical parameters. Polishing with a non-woven abrasive wheel and a polymer-abrasive brush showed the results in roughness (Fig. 5, 6), a class higher than processing with abrasive paper (sandpaper on a mandrel, an endless abrasive belt, and a non-woven abrasive belt) and with an abrasive flap wheel. Furthermore, it showed 2 times less labor intensity.

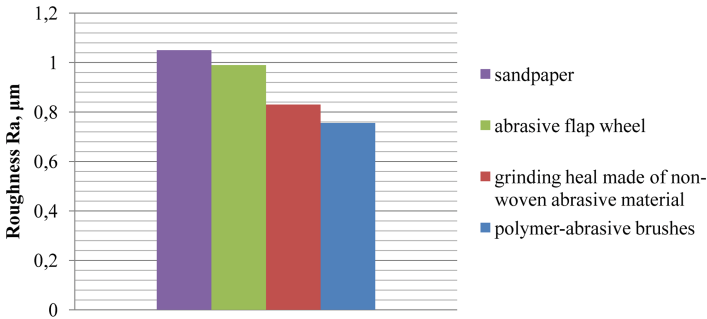


Fig. 5. Surface roughness in the cross-section of the waveguide when polished with tools (F180 grain size).

Also, these methods have advantages when machining “soft” materials:

- The material of the tool support is “elastic”, which does not allow abrasive grains to penetrate deeply into the material being machined;

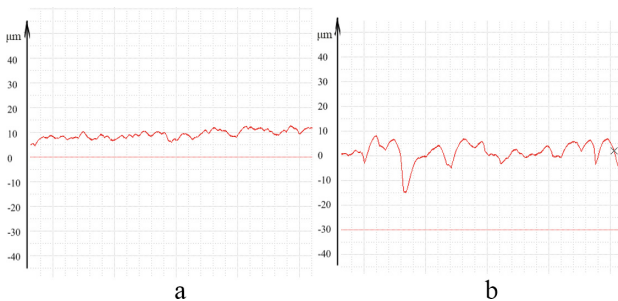


Fig. 6. Surface profilogram after processing with polymer-abrasive brushes (a); sandpaper (b).

- A low thermal and force effect is applied to the part surface;
- When a blunt, abrasive grain falls out, the base is erased, revealing new grains;
- The tool has a low tendency to load.

When polishing, the roughness measured in the direction of the tool movement (rotation) was on average one class higher than the transverse one.

When machining by all methods, the influence of the value and different directions of the obtained roughness on VSWR and electrical strength in the investigated frequency range was negligible. For all investigated waveguides, the VSWR was less than the acceptable values and the electrical strength corresponded to the technical requirements. A significant change in the values of these parameters, including going beyond the permissible limits, is usually observed in the presence of homogeneities of the channel surface (penetrations, solder beads, burrs, etc.). During the experiments, these defects were not allowed. Therefore, stable results were obtained, and no significant difference was observed in them.

A simultaneous study of local surface hardening due to processing with the above-mentioned tools showed that the amount of surface work hardening during processing with a polymer-abrasive brush was minimal and represented 1...3% (due to thinned-out fibers and their little extension), while during processing with sandpaper on the mandrel the maximum work hardening of 5...20% was obtained. Therefore, the machining with a brush did not cause a significant change in the electrical conductivity of the surface layer and, as a result, in the attenuation coefficient.

It was experimentally proved that with a decrease in roughness, the value of the attenuation coefficient decreased. The attenuation coefficient at a channel surface roughness R_a of 1.6 μm for this waveguide design was 3...3.5 times higher than at R_a 0.8 μm . Different attenuation values were obtained when machining with varying tools of finishing with the same grain size. This is primarily because tools of different hardness form different microroughness height on the surface (Fig. 7).

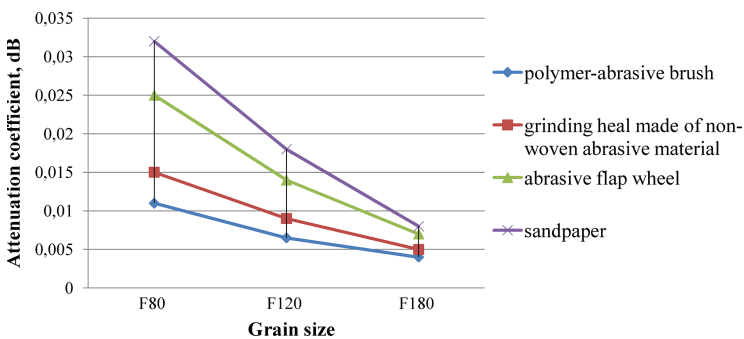


Fig. 7. Influence of processing method on attenuation coefficient for type 2 waveguide.

When machining with the same tool material, in the same modes, but with a different direction of tool rotation, another direction of microroughness was obtained: along and across the channel. It was found that the attenuation coefficient was less by 25...40% in

the case when directional lines of the surface microroughness run across the waveguide channel (Fig. 8).

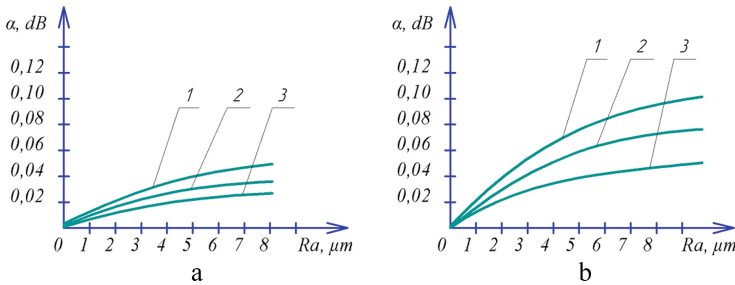


Fig. 8. Influence of roughness on the attenuation coefficient when polishing waveguides of three types (1–3) with sandpaper across the channel (a); along the channel (b).

The channel of the investigated waveguides has dissimilar roughness: the weld zones differ after finishing while the main surface of the waveguide tube remains in the as-delivered state.

Therefore, the measured attenuation coefficient is significantly different from the calculated one obtained without considering the heterogeneous roughness (Fig. 9). The range of experimental values can be explained by the influence of additional factors of hand-processed waveguides; the waveguides machined with polymer-abrasive brushes gave stable results.

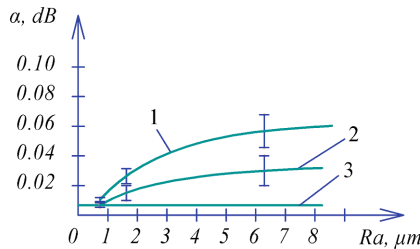


Fig. 9. Comparison of the experimentally measured attenuation coefficient for polishing along (1) and across (2) the waveguide channel and the attenuation coefficient calculated for ideally smooth walls (3).

Therefore, based on the experiments and analysis of existing dependencies, the following formula was proposed for the attenuation coefficient of the H_{10} wave of a rectangular S-band waveguide, where the roughness was taken into account:

$$\alpha = \alpha_E + \alpha_R \tag{1}$$

where α_E is an attenuation coefficient, calculated according to the well-known formula for a perfectly smooth surface [19, 20]; α_R is an attenuation coefficient depending on

the roughness of the current-carrying surfaces.

$$\alpha_R = \left(2.02 \cdot \frac{S_1}{S_2} \right)^{\frac{4 \cdot Ra_T}{\delta}} - 1 \quad (2)$$

where δ is the penetration depth of the high-frequency current, μm ;

Ra_T is the roughness of the current-carrying surfaces measured across the channel, μm ;

S_1 is the area of the polished surface, m^2 ;

S_2 is the area of the initial channel surface, m^2 .

The formula has been tested on angular waveguides having surfaces with different roughness and made by this method for the H_{10} wave. It takes into account the ratio of areas with different roughness instead of a correction factor used before.

The calculation error does not exceed 8%.

Since the attenuation coefficient is a frequency-dependent characteristic, then for waveguides with a different cross-section, operating frequency, and wave type, it is necessary to conduct similar experiments and derive an updated attenuation coefficient based on these results. The general formula for the entire frequency range from 300 MHz to 30 GHz, even for a certain (specific) wave type, has a big margin of errors due to different penetration depths and different roughness requirements.

5 Conclusions

Polymer-abrasive brushes were also used for finishing operations on other aluminum and brass rectangular waveguides with corner bends; they provided a favorable micro-relief of the working surfaces of hard-to-reach places, minimal additional work hardening, and optimal electrical parameters for all the researched waveguides.

Compared with other types of tools with similar processing modes and grain size of the abrasive tool, the attenuation coefficient values were 1.5...2 times lower, and the productivity of the polishing process was 2...3 times higher.

The mathematical dependence of the attenuation coefficient was developed where the inhomogeneous roughness of the channel of the S-band rectangular waveguide was taken into account.

Based on the results obtained, it is necessary to automate or mechanize the processing with polymer-abrasive brushes since they have high predictable durability [21].

References

1. Binke, H., Qi, J.: Accurate modeling of rough conductor surfaces in waveguide devices. *Electronics* **8**(3), 269 (2019)
2. Skin effect Homepage. https://en.wikipedia.org/wiki/Skin_effect. Accessed 22 Oct 2020
3. Nickelson, L.: Rectangular hollow metallic waveguides and resonators. In: *Electromagnetic Theory and Plasmonics for Engineers*. Springer, Singapore (2019)
4. Sudhakar, M.: *Microwave Engineering*. S. Chand & Co Ltd., New Delhi (2017)
5. Chen, J., Binke, H.: Effects of surface roughness on lossy rectangular waveguide. *Appl. Comput. Electromagnet. Soc. J.* **27**(7), 610–619 (2012)

6. Binke, H., Chen, J., Jiang, W.: Effects of surface roughness on TM modes in rectangular waveguide. *J. Infrared Millimeter Terahertz Waves* **30**, 717–726 (2009)
7. Lomakin, K., Gold, G., Helmreich, K.: Analytical waveguide model precisely predicting loss and delay including surface roughness. *IEEE Trans. Microw. Theor. Tech.* **66**(6), 2649–2662 (2018)
8. Biryukov, V., Grachev, V., Karakozova, E., Lobin, S., Shcherbakov, V.: Estimation of losses per unit length in a rectangular waveguide with rough screening surfaces based on the concept of partial waves. *ITM Web Conf.* **30**, 07001 (2019)
9. Yeap, K.H., Tham, C.Y., Yassin, G., Yeong, K.C.: Attenuation in rectangular waveguides with finite conductivity walls. *Radioengineering* **20**(2), 472–478 (2011)
10. Yeap, K.H., Wong, E.V.S., Nisar, H., Lai, K.C., Ng, C.A.: Attenuation in circular and rectangular waveguides. *Electromagnetics* **37**(3), 171–184 (2017)
11. Trifanov, V., Melkozerov, M., Sukhanova, O., Trifanov, I., Mednikov, D.: The study of the light section canal anodic-abrasive polishing mechanism. In: *IOP Conference Series: Materials Science and Engineering* 2020, vol. 822, no. 1, p. 012022. IOP Publishing (2020)
12. Baraiya, R., Babbar, A., Jain, V., Gupta, D.: In-situ simultaneous surface finishing using abrasive flow machining via novel fixture. *J. Manuf. Process.* **50**, 266–278 (2020)
13. Deaconescu, A., Deaconescu, T.: Improving the quality of surfaces finished by lapping by robust parameter design. *J. Econ. Bus. Manag.* **2**(1), 1–4 (2014)
14. Vaporblast Homepage. <http://vaporblast.ru/>. Accessed 22 Act 2020
15. Tryshyn, P., Honchar, N., Semeryuk T., Tereshchenko, K.: Research of quality of a current conductive surface of aluminum waveguides at polishing with various methods. In: *International Scientific and Practical Conference “Sciences: History, The Present Time, The Future, Eu Experience”* 2019, pp. 140–143. Baltija Publishing, Wroclaw (2019)
16. Muzibur Rahman, M., Reaz Ahmed, S., Salim Kaiser, M.: On the investigation of reuse potential of SnPb-solder affected copper subjected to work-hardening and thermal ageing. *Mater. Charact.* **172**, 110878 (2021)
17. Nagy, P.B.: Non-destructive methods for materials’ state awareness monitoring. *OR Insight* **52**(2), 61–71 (2010)
18. Vasylyev, M., Mordyuk, B., Pavlenko, D., Yatsenko, L.: Ultrasonic impact processing of surface layer of the BT1-0 titanium in a submicrocrystalline state. *Metallofiz. Noveishie Tekhnol.* **37**, 121–134 (2015)
19. Pozar, D.M.: *Microwave Engineering*. Wiley, New Jersey (2011)
20. Rao, R.S.: *Microwave Engineering*. PHI Learning Pvt Ltd., Delhi (2015)
21. Tryshyn, P., Honchar, N., Kondratiuk, E., Stepanov, D.: Development of technological restrictions when operating disc polymer-abrasive brushes. *East.-Eur. J. Enterp. Technol.* **6**(1), 27–33 (2020)



Prediction the Durability of Hobs Based on Contact and Friction Analysis on the Faces for Cutting Teeth and Edges During Hobbing

Ihor Hrytsay^(✉)  and Vadym Stupnytskyi 

Lviv Polytechnic National University, 12, Bandera Street, Lviv 79000, Ukraine
i.gryc@i.ua

Abstract. A method for determining the most dangerous zones of the hob cutter to develop the fastest wear of teeth and edges by the criterion of maximum friction on the contact surfaces has been developed. The geometric model of 3D undeformed chips, which is the basis for determining the force and tribological load, considers the actual shape of the transition surface in each gap, considering the shape and size of the inner surface of the chips, which is formed during the previous axial position of the hob. The cutting force was investigated as a function of the cross-sectional area and the chip compression ratio. This value is set depending on the variable thickness of the cross-sections and is determined using the Deform 2D software. The effect of changing the actual geometry of the cutting wedge of the hob's teeth on friction and contact conditions on the flank face of the trailing edges ultimately determines the maximum wear of the hob cutter.

Keywords: Hobbing · Cutting forces · Dynamic process · Gear wheel · Cutting simulation · Friction process

1 Introduction

Many practical problems are possible at the present stage of scientific research development based on complex simulations of cutting processes. Hobbing is one of the most complex cutting processes because multi-toothed, multi-edge, intermittent and helical tool is used, with non-free triangular cutting on most teeth. This is the complexity of its modeling and predicting of the wear rate.

The main factor in the loss of cutting properties of teeth and edges is the heat generated in the working area and the change in mechanical properties of the cutting wedge due to the high temperature, particularly reducing hardness and wear resistance. In turn, the main factor and heating of the teeth of the hob cutter is the friction on its contact faces during the machining process. Based on this, information about the areas of maximum friction and patterns of its distribution on work faces can serve as a basis for predicting the intensity of wear of teeth and cutter edges and develop measures to prevent wear of these zones by various measures- design and technology.

2 Literature Review

Numerous scientific works are devoted to solving this problem by computer modeling. Thus, in [1], developed methods for approximating wear on the geometry of chips and its parameters – thickness and length and the chip compression ratio, are determined geometrically. The method for estimating wear on tooth angles depending on chip thickness, deposition intensities, and chip length found graphically the parameters used in these mathematical relations are explained graphically is described in the article [2].

A partial task - the study of the influence of the geometry of the tooth and the radius of rounding of the top edges of the hob teeth on the total wear rate of tool profile and workpiece geometry is described in articles [3, 4].

Numerous works determine the cutting force during milling and its components in the frame of reference of the tool and machine [1, 5–7]. A similar problem was solved in [8, 9], where the calculation of the deformation load on the tops of the teeth is given, which is considered as one of the criteria for wear. Wear prediction is based on modeling of chip formation and load on the rail by the finite element method chip formation, and the load on the rake face was FEM-simulated for the generating position with the largest chip volume in the full cut is described. A partial task - the study of the influence of the geometry of the tooth and the radius of rounding of the top edges of the hob teeth on the total wear rate of tool profile and workpiece geometry is described in articles [3, 4]. However, the cutting force and its components can be used to evaluate the cutting performance, which reflects the load on the cutting elements of the hob cutter, but this parameter does not take into account friction in the hobbing process and only indirectly corresponds to wear teeth and edges.

More accurate methods of predicting wear are based on simulation of stress-strain state, cutting temperature, and contact pressure on every tool face location, and the relative sliding velocity at the tool-workpiece interface by the FEM-based methods for predicting tool wear progress [11–13]. However, computer visualization of the studied parameters in such systems does not allow to fully take into account the conditions of contact and friction on the teeth and edges of the worm cutter, taking into account all possible options for chips and the possibility of cutting by one, two or three edges simultaneously with different distribution of cut layers between leading, trailing and head edges of hob cutter.

From the above, it follows that the task of developing theoretical foundations and modeling friction on the contact faces of hob cutters in the process of gear machining remains relevant. There is a need for a methodology based on the basic principles of cutting theory and uses scientific developments in this field to analytically describe deformation, tribological and thermal processes during hobbing, takes into account all conditions, allowing more fully, accurately predicting wear zones, and values.

The purpose of this work is to study and analytically describe the friction on the contact faces of the hob cutter to predict zones of most intense wear of its teeth and edges and identify the possibility of reducing the negative influence of technological factors on the durability of hob cutters.

3 Research Methodology

In [14, 15], the power load on the tooth and the edges of the hob cutter was simulated and studied. The mathematical model of the cutting force of hobbing is presented in a three-dimensional force field and is used for specific initial conditions. According to this method, the force is considered as a result of solving a number of interrelated problems: geometric modeling of 3D undeformed chips, shear intensity, friction on the head, and side edges on the sequence of all active teeth of the hob on the helical surface and the rails. In contrast to the existing methods of modeling cutting sections, the developed technique considers the traces of all teeth that formed gaps in the previous position of the cutter on the axial feed, which provides higher accuracy of three-dimensional structure and size of chips.

As an example of geometric modeling, Fig. 1 shows the shape of a three-dimensional undeformed chip, which is cut by one of the teeth of the helical line of the hob cutter in three angles, designed in the AutoCAD. In the same system, the calculation of quantitative parameters of each cut layer is carried out: the cross-sectional area, thickness, and width, and length of edges cutting.



Fig. 1. 3D model of undeformed chips cut by one of the hob cutter teeth.

Using the experience of these works and the basic provisions of the theory of cutting, the friction on the working faces and edges of the tool can be simulated. Besides, it is essential to investigate the kinematic angles on the side edges and the change in the conditions of deformation and friction because this factor is not taken into account in the known scientific works on this topic.

3.1 Methods for Determining the Actual Geometric Parameters of the Hob Cutter and Their Effect on Contact Loading and Friction

The hob must be pre-installed at an angle to the end of the wheel to be machined. For the spur wheels, this angle is equal to the angle of the rise of the screw surface of the cutter. As a result, the actual geometric parameters of the cutter will be different from the static ones, i.e., those obtained by the hob during manufacture. The top edges of the hob cutter teeth due to backing-off have a significant positive flank angle (about 4–7°) depending on the outer diameter of the cutter. The rake angle for the standard hob cutters is zero. Changing these angles after installing the hob has no significant effect on the cutting process.

However, the installation of the cutter at an angle to the plane of the cutting speed vector changes the operating conditions of the side edges, and the cutting process becomes oblique. In the process of hobbing, the rake face of the tooth is inclined relative to the plane of cutter rotation, as shown in Fig. 2, and the actual or kinematic angles on the side edges differ from the static ones. Thus, for a suitable cutter with a helix angle λ , the kinematic rake angle on the side leading edge becomes negative, equal to $(-\lambda)$, and the kinematic rake angle on the trailing edge becomes positive by the same value, i.e. $(+\lambda)$. The actual flank angles change oppositely: the leading edge receives a positive flank angle λ , and the trailing receives a negative flank angle equal to $(-\lambda)$. The change in the actual geometry on the cutting edge of a single tooth is shown in the right corner of Fig. 2 and Fig. 3.

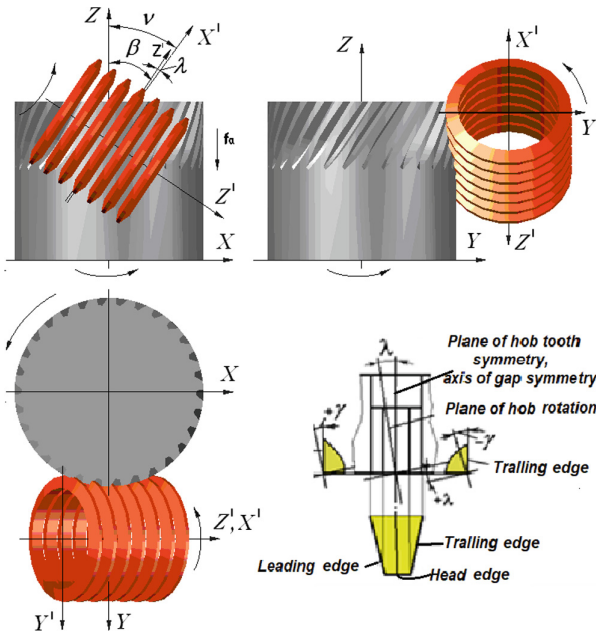


Fig. 2. Kinematic scheme of the hobbing process and the change of the actual angles on the cutting wedges due to the inclined installation of the cutter.

From the above, it follows that the forces of friction on the cutting faces on the top and side edges, where the flank kinematic angles are positive, can be neglected, but it is necessary to take into account the friction between the relief face and the workpiece on the trailing edge, where the flank kinematic angle is negative. Therefore, the flank face of the trailing edges is exposed to increased contact pressure and friction load.

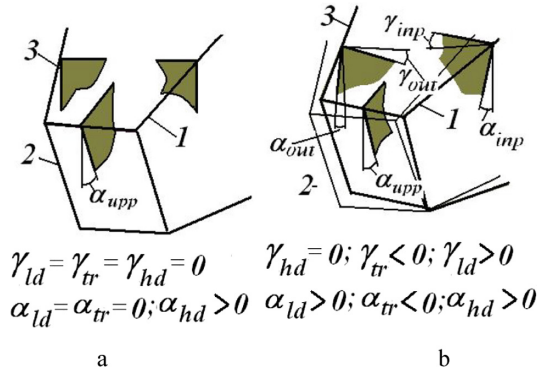


Fig. 3. Static angles of edges of the hob cutter tooth (a) and actual (kinematic) angles of cutting edges (b) of hob: 1 - leading, 2 - head, 3 - trailing.

3.2 Method of Calculating the Friction Load on the Rake Face of the Hob’s Teeth, Taking into Account the Kinematic Angles

As is known, the friction load on the rake face is determined by the intensity of contact between the chips and this surface, depends on the intensity of chip compression ratio due to shear (in the primary zone of plastic deformation) and causes deformation of chips in the zone of secondary deformation. To calculation the desired parameters, we use the fundamental laws of the cutting theory and the relationships between the components of the forces acting on the cutting wedge.

The coefficient of friction μ and, accordingly, the friction angle ρ , which determine the friction force on the rake face of the hob cutter, depending on the angle ω , defined in the cutting theory as the angle of the action. This angle characterizes the cutting force vector R (shaving) relative to the cutting speed vector. The direction of force R changes at different values of the rake angle (Fig. 4).

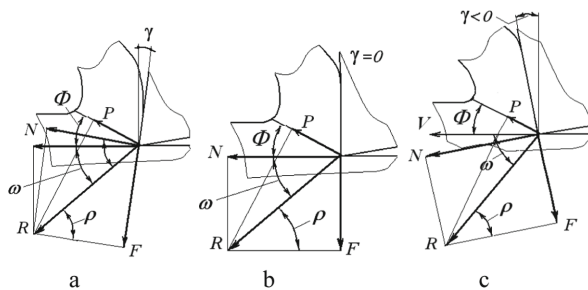


Fig. 4. The angle of action and forces acting on the cutting edge when the tool’s rake angle $\gamma > 0$ (a), $\gamma = 0$ (b), and $\gamma < 0$ (c).

To calculate the value of the angle ω used the relationship between this angle and the shear angle Φ [16]:

$$\omega = I - \Phi , \tag{1}$$

where angle:

$$I = (i_0 - 6) \cdot a^{-0.05} , \tag{2}$$

a – cut thickness.

4 Results

Initial data for calculations and simulation are as follows: right-handed involute helical work gear, workpiece material is high-carbon steel AISI 1045, normal modulus $m_n = 3$ mm, number of gear teeth $Z_g = 36$, gear helix angle $\beta = 350$; hob outside diameter $Da_h = 90$ mm and number of column (flank teeth) $q = 10$; the hob helix angle, right: $\lambda = 2,13$; up-cutting hobbing, axial feed $f_a = 3$ mm/rev; depth of cut - full teeth height.

The value of the shear angle was determined for these conditions based on rheological simulation depending on the variable thickness of the cut layer on the edges. The value of the parameter i_0 is calculated experimentally for a number of structural materials (for example, $i_0 = 50$ for steel AISI 1045) [16]. According to Eqs. (1) and (2), the value of the angle ω is calculated, and Fig. 5 shows graphs of changes in this angle by the angle of rotation of the cutter on its turns, marked by numbers “-3”, “-2”, ... “+2”. The average value of the angle ω between the cutting speed and the cutting force vector is equal: for the leading edge is 18° , for the head edge is 8° and for the trailing edge is 14° . Hereinafter, the graphs of the parameters that characterize the hobbing process are smoothed and continuous. Although the cutting process itself is determined in successive discrete relative positions of the hob cutter and wheel, multiples of turning the wheel at the angle of profiling and turning by one angular step, the continuity of graphs allows to represent better the general patterns of change of relevant parameters on the helical surface or teeth of individual rails.

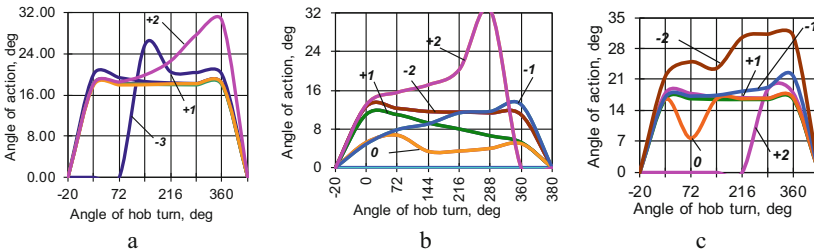


Fig. 5. The angle of action: a - trailing edges; b - head edges; c - leading edges.

Determining the angle of action ω , the value of the friction angle ρ and the coefficient of friction μ is found by the equation:

$$\rho = atg\mu = \omega + \gamma, \tag{3}$$

When $\gamma = 0$, the friction angle ρ is equal to the angle of action ω , and the friction coefficient is $\mu = tg\rho = tg\omega$.

The force N is a component of the cutting force R on each edge, which is equal to the geometric sum of the friction force F and the normal force N . In turn, the force R is a function of the shear force P (Fig. 3):

$$R = \frac{P}{\cos(\Phi + \omega)} \tag{4}$$

Taking into account the dependence (2), we obtain:

$$R = \frac{P}{\cos I}, \tag{5}$$

and the normal force is equal to:

$$N = R \cdot \cos \rho = \frac{P \cdot \cos \rho}{\cos I} = \frac{P \cdot \cos \rho}{\cos(\omega + \Phi)}. \tag{6}$$

Hence, the friction forces on the edges can be described by the following relationship:

$$F = N \cdot \mu = \frac{P \cdot \cos \rho}{\cos(\omega + \Phi)} \cdot \mu. \tag{7}$$

In [14, 15], the formula for the shear force calculation on a single edge is used:

$$P = S \cdot \bar{\tau} \cdot \xi, \tag{8}$$

where S is the cross-sectional area of the cut, mm^2 ; ξ is the chip compression ratio; $\bar{\tau}$ is the shear strength of the workpiece, MPa; p_c is the length of the cutting path, equal to the length of the arc of contact of the tool with the workpiece, mm.

For the above initial data, Fig. 6 shows the shear force on the hob teeth at the angle of its rotation, respectively, on the trailing, head, and leading edges on the turns of hob cutter with N° from (-3) to $(+3)$. The larger value of the angle ω on the leading edges is because the cross-sectional thickness of the sections is smaller, so the intensity of deformation of the cut layer is higher, respectively, and the part of the cutting force that depends on this factor will also be greater.

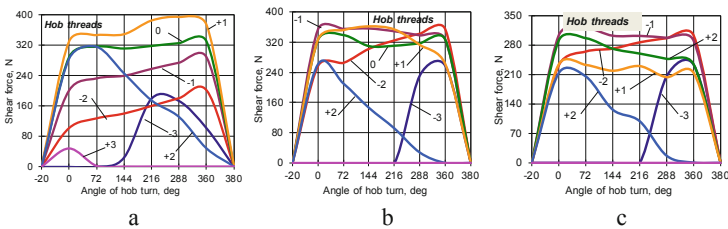


Fig. 6. Shear forces on the edges: a - trailing, b - head, c – leading.

As can be seen from Fig. 3, taking into account the actual rake angle, the friction angle also gets other values:

$$\rho = \omega \pm \gamma; \mu = \text{tg} \rho. \tag{9}$$

where the sign “+” corresponds to the positive rake angle on the trailing edge of the hob cutter tooth and the sign “-” for the negative rake angle on the leading edge (Fig. 3b). For the head edge $\gamma = 0$.

According to the data above, the actual coefficient of friction on the rake face of the hob’s tooth is described by the following equations:

- For the trailing edge: $\mu = tg(\omega - \gamma)$;
- For the head edge: $\mu = tg\omega$;
- For the leading edge: $\mu = tg(\omega + \gamma)$.

Under these dependencies and for the above data, Fig. 7 shows graphs of changes in the coefficient of friction on the rake face of the trailing, head, and leading edges of the hob’s teeth of the second (relative to the central tooth) turn of the hob cutter on the output part of the working zone.

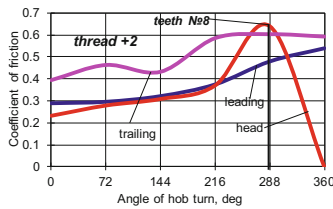


Fig. 7. Coefficient of friction on the trailing, head, and leading edges of the hob teeth on the turn № (+2).

The largest value of the coefficient μ on the trailing edges does not exceed 0.6, the largest value of μ on the head edges is 0.64, and on the leading edges not exceed 0.53.

Using the above data and the described methodic, Fig. 8 shows graphs of changes in the friction force on the rake face of the hob edges and relative to the angle of its rotation.

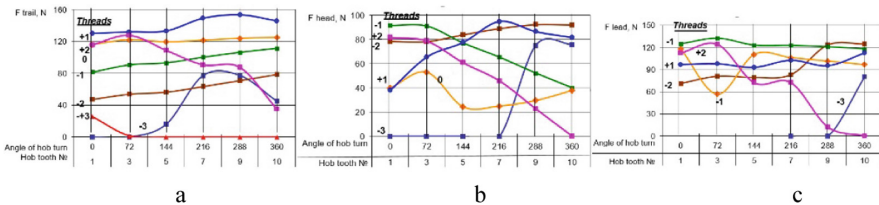


Fig. 8. Friction force on the rake face of the hob edges and relative to the angle of its rotation.

From the simulation results given in Fig. 8, it is clear that the most significant friction on the rake face occurs on the trailing edges of the turns marked by the numbers “0” and “+1” (teeth № 7 and № 9) and on the leading edge of the turn with № “-1” (tooth № 3).

5 Conclusions

1. A new methodic for predicting the dislocation of teeth and edges of a hob cutter has been developed, at which the wear rate will be maximum due to increased friction on the surfaces of their contact with chips and with the machined surface.
2. Accurate registration of the most loaded teeth on the helical surface of the hob cutter or rails, determined for specific initial conditions, allows preventing their intense wear and equalize the wear rate and loss of cutting properties of hob by the known design, technical or technological ways. In particular, fixation of the maximum friction zones can be used to develop measures to local hardening of precisely these most loaded teeth and edges, for the proposition to use an appropriate coating according to the composition and application technology to prevent premature softening of the substrate, or correction the geometry of these edges to compensate for the angular position of the hob cutter relative to the plane of its rotation during hobbing.
3. The developed technique and analytical apparatus for research can be used as the basis for further refined models of computer simulation of thermal and wear models taking into account the peculiarities of the processes of generative gear machining.

References

1. Bouzakis, K.-D., Lili, E., Michailidis, N., Friderikos, O.: Manufacturing of cylindrical gears by generating cutting processes. A critical synthesis of analysis methods. *CIRP Ann. Manuf. Technol.* **57**, 676–696 (2008)
2. Bouzakis, K.-D., Kompogiannis, S., Antoniadis, A., Vidakis, N.: Gear hobbing cutting process simulation and tool wear prediction models. *J. Manuf. Sci. Eng.* **124**(1), 42–51 (2002)
3. Karpuschewski, B., Knoche, H.J., Hipke, M., Beutner, M.: High performance gear hobbing with powder-metallurgical high-speed-steel. In: 5th CIRP Conference on High Performance Cutting, pp. 196–201. Elsevier, Zurich (2012)
4. Stachursk, W., Kruszyński, B.: Influence of cutting speed on the hob wear in hobbing with the minimum quantity lubrication. *Tehnički Vjesn.* **27**(2), 341–345 (2020)
5. Rech, J., Claudin, C.: Development of a new rapid characterization method of hob's wear resistance in gear manufacturing - application to the evaluation of various cutting edge preparations in high speed dry gear hobbing. *J. Mater. Process. Technol.* **209**, 5152–5160 (2009)
6. Stein, S., Lechthaler, M., Krassnitzer, S., Albrecht, K., Schindler, A., Arndt, M.: Gear hobbing: a contribution to analogy testing and its wear mechanisms. In: 5th CIRP Conference on High Performance Cutting, pp. 220–225. Elsevier, Zurich (2012)
7. Umezaki, Y., Ariura, Y.: An application of numerical analysis of hobbing to hob wear, cutting force and gear tooth topography. In: Proceedings of the 4th World Congress on Gearing and Power Transmission, pp. 43–51. Elsevier, Paris (1999)
8. Klocke, F., Gorgels, A., Stuckenberg, A., Schalaster, R.: Software-based process design in gear finish hobbing. *Gear Technol. Mag.* **27**(3), 48–52 (2010)
9. Brechera, C., Brumma, M., Krömera, M.: Design of gear hobbing processes using simulations and empirical data. In: *Procedia CIRP*, vol. 33, pp. 484–489. Elsevier (2015)
10. Liu, W., Ren, D., Usui, S., Wadell, J., Marusich, T.D.: A gear cutting predictive model using the finite element method. In: 14th CIRP Conference CMMO, vol. 8, pp. 51–56. Elsevier (2013)

11. Bouzakis, K.-D., Friderikos, O., Mirisidis, I., Tsiafis, I.: Determination of chip geometry and cutting forces in gear hobbing by a fem-based simulation of the cutting process. In: Proceedings of the 8th CIRP International Workshop on Modeling of Machining Operations, pp. 49–58. Elsevier, Chemnitz (2005)
12. Bouzakis, K.-D., Friderikos, O., Mirisidis, I., Tsiafis, I.: FEM-based simulation of the cutting process in gear hobbing with various kinematics. In: Proceedings of the 2nd International Conference on Manufacturing Engineering (ICMEN), pp. 97–110. Elsevier, Kallithea-Chalkidiki (2005)
13. Bouzakis, K.-D., Friderikos, O., Tsiafis, I.: FEM-supported simulation of chip formation and flow in gear hobbing of spur and helical gears. In: CIRP Journal of Manufacturing Science and Technology, vol. 1, pp. 18–26. Elsevier (2008)
14. Dong, X., Liao, C., Shin, Y., et al.: Machinability improvement of gear hobbing via process simulation and tool wear predictions. *Int. J. Adv. Manuf. Technol.* **86**, 2771–2779 (2016)
15. Hrytsay, I., Stupnytskyy, V., Topchii, V.: Improved method of gear hobbing computer aided simulation. *Arch. Mech. Eng.* **66**(4), 475–494 (2019)
16. Silin, S.S.: *Similarity Methods in Metal Cutting*. Mechanical Engineering, Moscow (1979)



Modelling of the Effect of Slide Burnishing on the Surface Roughness of 42CrMo4 Steel Shafts

Rafał Kluz , Tomasz Trzepiecinski , Magdalena Bucior ,
and Katarzyna Antosz  

Rzeszow University of Technology, 12, al. Powstancow Warszawy, 35-959 Rzeszow, Poland
katarzyna.antosz@prz.edu.pl

Abstract. Slide burnishing is one of the methods of metal processing that use the phenomenon of surface plastic cold deformation. This article presents the results of a study investigating the effect of slide burnishing on the surface roughness of 42CrMo4 steel shafts. The burnishing process was performed with the use of a polycrystalline diamond tip tool. Before burnishing, the samples were subjected to turning on the toolmaker's lathe. Investigations were conducted based on PS/DS-P:Ha3 Hartley's plan, which makes it possible to define the regression equation in the form of a second-degree polynomial. Moreover, the artificial neural network (ANN) models have been used to predict the surface roughness of shafts in the burnishing process. The input process parameters considered include the applied pressure, burnishing rate, and feed rate. In all analyzed burnishing cases, the value of the mean surface roughness was reduced. The differences between the experimental data and Hartley's model do not exceed 24%. The best representation of Hartley's model was obtained for the burnishing parameters: feed rate $f = 0.32$ mm/rev, applied pressure $P = 130$ N, and burnishing speed $v = 180$ rpm. ANN models were the best predictors of roller surface roughness of the shafts. With the Pearson's correlation R^2 coefficient = 0.99974, the values of prediction errors did not exceed 0.0016249.

Keywords: Artificial neural networks · Hartley's plan · Multilayer perceptron · Surface topography

1 Introduction

Burnishing is one of the methods of metal processing that use the phenomenon of surface plastic cold deformation. Machining ensures the necessary precision of the size and shape of components. Still, it is not too beneficial for assuring the surface stereometric structure obtained in the final phase of a component's production [1]. Due to the small dimensions of the tool tips, the plastic deformation zone of burnished parts is very small. According to the purpose of the treatment, burnishing can be classified as hardening, smoothing, or dimensional [2]. One of the smoothing treatments is slide burnishing. This process is a fine machining method used to improve mechanical properties, such as corrosion resistance, surface roughness, wear, coefficient of friction, and fatigue resistance [3].

Slide burnishing induces an intense and deep compressive layer [4]. Due to the small tool radius, slide burnishing is characterized by the presence of low forces, which enables the machining of low-rigidity parts [5]. The burnishing process makes it possible to achieve such advantages as [6]: increase of the surface hardness, an increase of resistance to fatigue, ability to produce the surfaces with high corner radius, ability to produce the surfaces characterized by a low coefficient of friction, ability to reach high surface smoothness, minimal heating of the surface layer during machining, ability to use burnish tools on universal lathes, high process efficiency, and durability, increase the corrosion resistance of the surface layer, the low energy consumption of the burnishing process.

2 Literature Review

Numerous researchers worldwide deal with burnishing technology and its impact on the properties of the surface layer. Luo et al. [7] examined slide diamond burnishing of copper alloys using a cylindrical polycrystalline diamond sliding tool. They found that the surface roughness values revealed a markedly reduction due to burnishing. Korzynski et al. [8] investigated slide diamond burnishing of a 42CrMo4 with a cylindrical sliding component made of polycrystalline diamond. The surface layer was characterized by an increased microhardness and compressive residual stresses. The surface roughness values were reduced significantly. Analysis of the ball-burnishing process in terms of the surface roughness reduction has been conducted by Shiou and Cheng [9]. They found that by applying the optimal flat surface ball burnishing and ball polishing parameters sequentially to NAK80 tool steel, the surface roughness R_a of the surface on the tested parts can be improved sequentially from about $1.0\ \mu\text{m}$ average to $0.020\ \mu\text{m}$ on average. The effect of input parameters of processes on surface roughness and residual stresses of the 42CrMo4 steel surface has been investigated by Dzierwa and Markopoulos [10]. It was found that it was possible to reduce the value of the S_q parameter from $0.522\ \mu\text{m}$ to $0.051\ \mu\text{m}$ and increase the wear resistance of specimens. El-Tayeb et al. [11] applied a roller burnishing process to 6061 aluminum alloy. They found that an increase in the roller contact width led to less improvement in the surface roughness. Gharbi et al. [12] applied the Taguchi technique to identify the effect of burnishing parameters on surface roughness and surface hardness of burnished surfaces. The mean surface roughness of AISI 1010 steel hot-rolled plates has been improved from $R_a = 2.48$ to $1.75\ \mu\text{m}$, while the hardness increases from 59 to 65.5 HRB. Maximov et al. [13] analyzed the slide burnishing process parameters on the residual stresses and wear resistance obtained in slide burnishing of AISI 316Ti steel. They found that the greater burnishing velocity increases the productivity of burnishing, but on the other hand, this velocity reduces the residual stresses. Moreover, that greater burnishing velocity reduced the fatigue life of specimens subjected to cyclic bending fatigue tests. A literature review of the publications devoted to slide burnishing has been conducted by Maximov et al. [14].

In this paper, the slide burnishing process on the surface topography of the 42CrMo4 steel shafts was investigated. The burnishing process was performed with the use of a polycrystalline diamond tip tool. Investigations were conducted based on PS/DS-P:Ha3 Hartley's plan, which makes it possible to define the regression equation in the form of a second-degree polynomial. Moreover, artificial neural networks (ANNs) were

applied to study the correlations between machining parameters and surface roughness of specimens.

3 Research Methodology

Shafts made of 42CrMo4 alloy steel with a 21–22 HRC hardness were used as a test material. The diameters of the shafts were equal to 50 mm 42CrMo4 steel is common chromium-molybdenum steel that is usually used after quenched and tempered, with high hardenability. Such 42CrMo4 steel is formulated for machine parts requiring high core plasticity for components subjected to changing loads. It is mainly used for crankshafts, high-loaded bolts, gears, axles as well disks. The chemical composition of steel tested is listed in Table 1.

Table 1. Chemical composition of the 42CrMo4 steel.

C	Mn	Si	P	S	Cr	Ni	Mo	W	V	Co	Cu
0.38–0.45	0.4–0.7	0.17–0.37	Max. 0.035	Max. 0.035	0.9–1.2	Max. 0.3	0.15–0.25	Max. 0.2	Max. 0.05	–	Max. 0.25

The shafts were machined to obtain a surface roughness of $Ra = 2.6 \mu\text{ms}$. Slide burnishing was carried out on a universal lathe LZ 360 (Fig. 1), appropriate for precise manufacturing of medium-size parts according to DIN8605 tool accuracy. The burnishing process was carried out on the test stand (Fig. 2a) using a DB-3 burnishing tool (Fig. 2b). A polycrystalline diamond (PCD) tool tip was used in the investigations.

Experimental investigations were realized according to the static polyselectional Hartley’s plan. It is a three-leveled plan of experiments that requires setting the input factors only on three equidistant levels. The input process parameters considered include the applied pressure, burnishing rate, and feed rate. The design matrix is given in Table 2.

The measurements of surface roughness of the specimens were carried out using the Taylor-Hobson Surtronic 2 profilometer according to EN ISO 4287:1999. Arithmetical average height Ra as a main surface roughness parameter was selected to characterize the tribological properties of the burnished surfaces. As a result of the experiments carried out according to Hartley’s plan, a regression equation of the slide burnishing process is received as:

$$y = b_0 + \sum b_k x_k + \sum b_{kk} x_k^2 + \sum b_{kj} x_k x_j \tag{1}$$

where b_k , b_{kk} , b_{kj} are coefficients of the regression equation, x_k and x_j are input parameters.



Fig. 1. Universal lathe LZ-360.

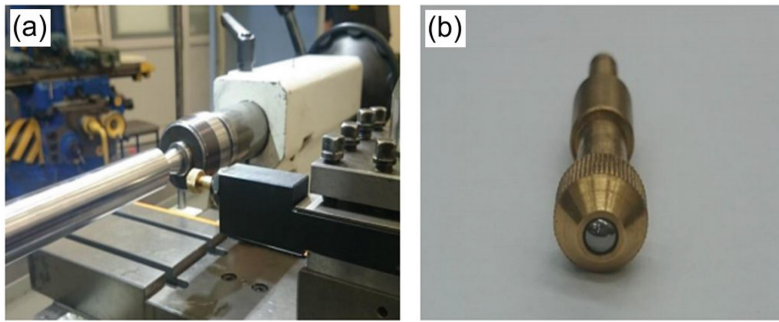


Fig. 2. (a) Test stand and (b) burnishing tool.

Table 2. Experimental design matrix.

No. of experiment	Feed rate f , mm/rev.	Applied pressure P , N	Burnishing speed v , rpm
1	0.094	130	360
2	0.094	30	180
3	0.032	130	180
4	0.032	30	360
5	0.094	80	270
6	0.032	80	270
7	0.063	130	270
8	0.063	30	270
9	0.063	80	360
10	0.063	80	180
11	0.063	80	270

ANNs are tools to build and analyze linear and nonlinear models of complex regression problems. There are many structures of the ANNs used to modeling the relation

between input and output parameters. In this paper, the multilayer perceptron (MLP) [15] is utilized. A MLP with a suitable number of hidden layers and neurons is theoretically sufficient to approximate any nonlinear function [16]. To calculate the output value of neuron of ANN, the hyperbolic tangent function (Eq. 2) is applied:

$$f(x) = \tanh(x) = \frac{e^x - e^{-x}}{e^x + e^{-x}} \quad (2)$$

In this study, the following input sets of variables were assigned as input signals: feed rate, applied pressure, and burnishing speed. As output variable, the value of arithmetical average height Ra was set.

All experimental sets of input data that correspond with the output signal were assigned as the training set. The back propagation algorithm with a learning rate equal to 0.1 was used to training the MLP. As a result of the training process, the neural network may acquire the ability to predict output signals based on the sequence of input signals and their corresponding output signals. The task of the training algorithm is to select weight values and threshold values of all neurons to minimize the MLP.

The architecture of the MLP was selected based on the many numerical experiments conducted in the Statistica program. The regression quality of the network was assessed based on the standard deviation ratio and Pearson-R correlation computed between the real values of the clarified variable and values calculated by the model. The model with the lowest values of standard deviation (SD) ratio connected with the highest value of Pearson-R correlation is network MLP 3:3-5-1:1 (Fig. 3).

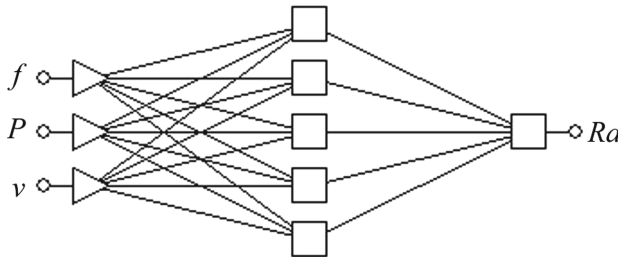


Fig. 3. Architecture of MLP 3:3-5-1:1.

4 Results

The burnishing process led to a significant reduction in the surface roughness of the shafts. The highest reduction in the Ra parameter was found after burnishing at feed rate $f = 0.032$ mm/rev., applied pressure $P = 130$ N, and burnishing speed $v = 180$ rpm. The highest surface roughness of shafts was observed after slide burnishing at feed rate $f = 0.063$ mm/rev., applied pressure $P = 30$ N, and burnishing speed $v = 270$ rpm (Table 3). The difference between values of the Ra parameter measured in two shaft surfaces is very similar. This confirms the high repeatability of the machining process.

The values of the coefficients in the regression equation and their critical values are presented in Table 4. Adequacy of the obtained regression equation

$$Ra = -0.42042 - 22.915 \cdot f + 0.00157 \cdot P + 0.00882 \cdot v - 120.83 \cdot f^2 - 0.00006 \cdot P^2 - 0.133 \cdot f \cdot v + 0.029 \cdot P \cdot f \quad (3)$$

was tested using the Fisher-Snedecor based on the adequacy variance

$$S_{ad}^2 = \frac{r \sum_{i=1}^{11} (\bar{y}_i - \hat{y}_i)^2}{N - k - 1} \quad (4)$$

and critical value of random variable F_{kr} :

$$F_{kr} = F_{(\alpha;f_1;f_2)} = F_{(0.05;7;11)} = 3.0123 \quad (5)$$

where y_i is the average value of the process factor in the i th experiment, r is the number of repetitions, k is the number of factors in the regression equation, and N is the number of experiments.

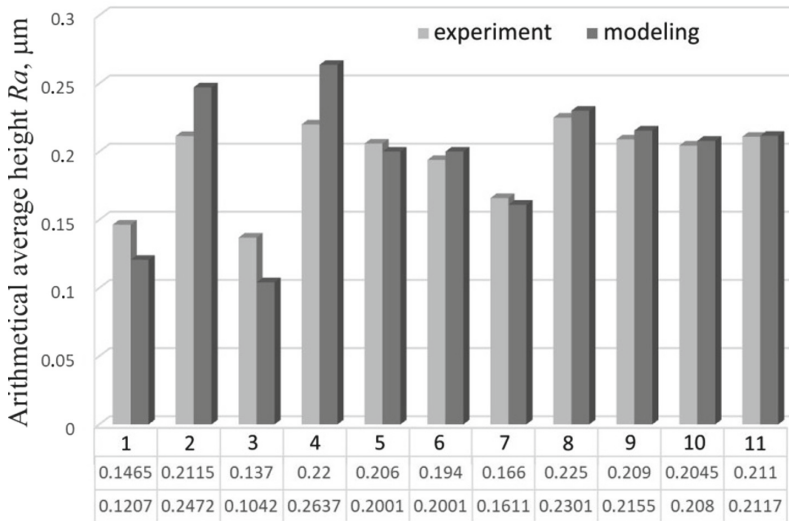
Table 3. Arithmetical average height Ra measured on the specimens burnished by PDC tool.

No. of experiment	Arithmetical average height Ra		
	Measurement 1	Measurement 2	Average
1	0.145	0.148	0.1465
2	0.216	0.207	0.2115
3	0.143	0.131	0.137
4	0.217	0.223	0.220
5	0.205	0.207	0.206
6	0.191	0.197	0.194
7	0.169	0.163	0.166
8	0.226	0.224	0.225
9	0.216	0.202	0.209
10	0.204	0.205	0.2045
11	0.208	0.214	0.211

The results of Hartley’s plan show that the obtained random factor F does not exceed the critical value F_{kr} for the adopted significance level $\alpha = 0.05$. Therefore, the regression equation (Eq. (3)) can be considered adequate. The Hartley’s function reaches a minimum of $Ra = 0.1042 \mu\text{m}$ corresponding to the experimental burnishing parameters ensuring the lowest value of the shaft surface roughness. In experiments no. 1–4, the relative error ranges from 18–24%, while in the remaining segments, the error value does not exceed 3% (Fig. 4).

Table 4. Significance of the parameters in the regression equation.

Coefficient	Coefficient value	Critical value	Significance
b_0	2.1171	0.0442	Significant
b_1	0.02171	0.03271	Non-significant
b_2	−0.3451	0.03271	Significant
b_3	0.03751	0.03271	Significant
b_{11}	−0.1161181	0.051492	Significant
b_{22}	−0.16112531	0.051492	Significant
b_{33}	−0.048621	0.051492	Non-significant
b_{12}	0.0451	0.04006	Significant
b_{13}	−0.371	0.04006	Significant
b_{23}	0.00251	0.04006	Non-significant

**Fig. 4.** Comparison of experimental R_a values and using Hartley's plan.

The learning process of the 3:3-5-1:1 network was interrupted after the neural network error stabilized at the level of 0.00862. The learning process was characterized by undisturbed convergence up to 1700 epochs. The value of Pearson's correlation coefficient R was 0.99974, and the value of the standard deviation ratio was 0.0225. The value of the SD ratio is much smaller than 1, so the MLP presents good performance. The predicted values of arithmetical average height R_a are listed in Table 5. For the 11th experiment, the prediction error of arithmetic average height R_a was greater than $0.0016 \mu\text{m}$. In other cases, this error does not exceed $0.0008 \mu\text{m}$ (Fig. 5).

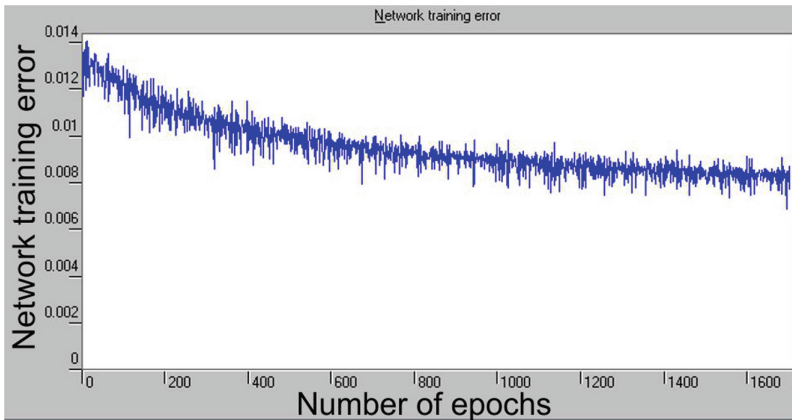


Fig. 5. Variation of the network error during training.

Table 5. Experimental and predicted values of arithmetical average height Ra (μm).

No. of experiment	Experiment	ANN	Error
1	0.1465	0.146524	0.0000244
2	0.2115	0.211545	0.0000450
3	0.137	0.136949	-0.0000513
4	0.22	0.219757	-0.0002432
5	0.206	0.205359	-0.0006410
6	0.194	0.193672	-0.0003282
7	0.166	0.165336	-0.0006636
8	0.225	0.224543	-0.0004574
9	0.209	0.208259	-0.0007415
10	0.2045	0.203729	-0.0007710
11	0.211	0.212625	0.0016249

Observation and closer analysis of response surfaces indicate that:

- for the burnishing speed in the range of 180–270 rpm, an increase of the parameter value causes the arithmetical average height Ra value to increase (Fig. 6a). After exceeding the value of 270 rpm, the arithmetical average height Ra starts to decrease,
- a decrease of feed rate value causes a reduction of the average arithmetical value Ra value (Fig. 6a),
- a decrease of applied pressure value causes a reduction of the arithmetical average height Ra value (Fig. 6b).

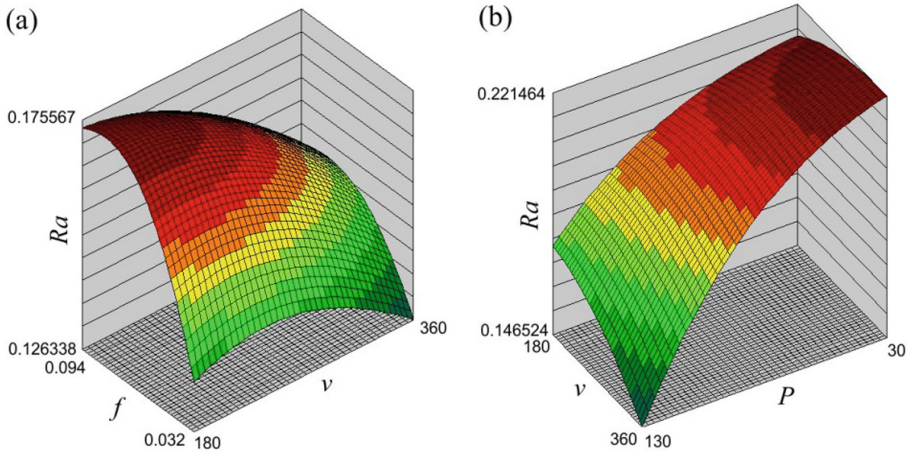


Fig. 6. Response surfaces presented the effect of (a) feed rate and applied pressure and (b) burnishing speed and applied pressure on the value of arithmetical average height Ra .

5 Conclusions

In this paper, the effect of the slide burnishing parameters on the surface roughness of 42CrMo4 steel shafts have been studied using Hartley's plan and artificial neural networks. The following conclusions are drawn from the research:

- Although the training set contained only 11 measurement data, the neural network perfectly built a regression model that is characterized by the value of Pearson's correlation coefficient $R = 0.99974$.
- Regression statistics and errors of prediction of shaft surface roughness by ANN model are considerably better than results of Hartley's plan.
- The regression equation allows for optimizing the slide burnishing parameters regarding the quality of the surface to be processed.

In future research, investigations of slide burnishing should be carried out on a wide range of changes in machining parameters. The next task is to consider the effect of tool roughness and lubrication conditions on the surface roughness of 42CrMo4 steel shafts. By increasing the data in the training set, the predictability of the neural network can be improved.

References

1. Korzynski, M., Zarski, T.: Slide diamond burnishing influence on of surface stereometric structure of an AZ91 alloy. *Surf. Coat. Technol.* **307**, 590–595 (2016)
2. Dzierwa, A., Gałda, L., Tupaj, M., Dudek, K.: Investigation of wear resistance of selected materials after slide burnishing process. *Eksploracja i Niezawodność – Maint. Reliab.* (3), 432–439 (2020)

3. Kumar, K., Prasad, K.E.: Application of roller burnishing process for final machining of cylindrical surface. *IOSR J. Mech. Civil Eng.* **12**(1), 1–7 (2015)
4. Chomienné, V., Valirgue, F., Rech, J., Vierdu, C.: Influence of ball burnishing on residual stress profile of a 15–5PH stainless steel. *CIRP J. Manuf. Sci. Technol.* **13**, 90–96 (2016)
5. Zaleski, K., Skoczylas, A.: Effect of slide burnishing on the surface layer and fatigue life of titanium alloy parts. *Adv. Mater. Sci.* **19**(4), 35–45 (2019)
6. Labuda, W., Starosta, R., Charchalis, A.: The analysis of the influence of the burnishing process on corrosion properties of steel applied to sea water pump shafts. *J. Kones Powertrain Transp.* **18**(4), 221–228 (2011)
7. Luo, H., Liu, J., Wang, L., Zhong, Q.: Investigation of the burnishing process with PCD tool on non-ferrous metals. *Int. J. Adv. Manuf. Technol.* **25**, 454–459 (2005)
8. Korzynski, M., Lubas, J., Swirad, J., Dudek, K.: Surface layer characteristics due to slide diamond burnishing with a cylindrical-ended tool. *J. Mater. Process. Technol.* **211**(1), 84–94 (2011)
9. Shiou, F.J., Cheng, C.H.: Ultra-precision surface finish of NAK80 mould tool steel using sequential ball burnishing and ball polishing processes. *J. Mater. Process. Technol.* **201**(1–3), 554–559 (2008)
10. Dzierwa, A., Markopoulous, A.P.: Influence of ball-burnishing process on surface topography parameters and tribological properties of hardened steel. *Machines* **7**, 11 (2019)
11. El-Tayeb, N.S.M., Low, K.O., Brevern, P.V.: Influence of roller burnishing contact width and burnishing orientation on surface quality and tribological behaviour of aluminium 6061. *J. Mater. Process. Technol.* **186**, 272–278 (2007)
12. Gharbi, F., Sghaier, S., Al-Fadhalah, K.J., Benameur, T.: Effect of ball burnishing process on the surface quality and microstructure properties of AISI 1010 steel plates. *J. Mater. Eng. Perform.* **20**, 903–910 (2011)
13. Maximov, J.T., Duncheva, G.V., Anchev, A.P., Ganev, N., Amudjev, I.M., Dunchev, V.P.: Effect of slide burnishing method on the surface integrity of AISI 316Ti chromium–nickel steel. *J. Brazilian Soc. Mech. Sci. Eng.* **40**(4), 1–14 (2018). <https://doi.org/10.1007/s40430-018-1135-3>
14. Maximov, J.T., Duncheva, G.V., Anchev, A.P., et al.: Slide burnishing – review and prospects. *Int. J. Adv. Manuf. Technol.* **104**, 785–801 (2019)
15. Rao, K.V., Murthy, B.S.N., Rao, M.: Prediction of cutting tool wear, surface roughness and vibration of work piece in boring of AISI 316 steel with artificial neural network. *Measurement* **51**, 63–70 (2014)
16. Altaf, S., Mehmood, M.S., Imran, M.: Implementation of efficient artificial neural network data fusion classification technique for induction motor fault detection. *J. Eng. Sci.* **5**(2), E16–E21 (2018)



Analytical Modelling of Crack Formation Potential in Thermomechanical Processing of Materials

Maksym Kunitsyn^(✉) , Anatoly Usov , and Yulia Sikirash 

Odessa National Polytechnic University, 1, Shevchenko Ave., Odessa 65044, Ukraine
m.v.kunitsyn@opu.ua

Abstract. Thermomechanical processes that accompany the processing of products made of structurally inhomogeneous materials are considered. The presence of stress concentrators in the surface layer of processed products in various types of heterogeneities of hereditary origin introduced in obtaining the workpiece and subsequent mechanical processing types are the leading indicators of working surfaces' bearing capacity. The lack of research on the influence of inhomogeneities formed in the surface layer of products during mechanical processing on their functional properties and, in particular, on the bearing capacity or wear resistance, their optimization determines the relevance of constructing a mathematical model of defect formation in the physical and technical processing of structural elements using optimal criteria of fracture mechanics. A numerical and analytical model is developed to determine the thermomechanical state of structurally inhomogeneous materials containing inhomogeneities such as interfacial cracks and inclusions during mechanical processing. Based on this model, the crack resistance criterion's functional relationships with the technological control parameters are determined to ensure products' processed surfaces' quality characteristics.

Keywords: Temperature · Heat · Defect formation · Cracks · Surface layer · Stress state

1 Introduction

The quality of the surface layer of structural elements during their manufacture is formed under the influence of thermomechanical phenomena accompanying mechanical processing [1, 2]. In various types of heterogeneities of hereditary origin, the presence of stress concentrators, introduced in obtaining the workpiece and subsequent types of mechanical processing, are the leading indicators of working surfaces' bearing capacity. The formation of technological origin defects occurs because of heat stress during structural elements [3]. Based on models of temperature fields, stress fields, and fracture mechanics, we study the regularities of the formation of defects such as structural changes, micro-cracks, and technological possibilities for their elimination, depending on the thermophysical properties of the processed materials, processing modes, design, and characteristics of the tools used [3, 4]. The problem of stress concentration in defects

is solved using the mechanics of materials, which considers micro-heterogeneities and their materials' defects when calculating structural elements' load-bearing capacity. Taking into account defects allows it to represent the mechanism of loss of products' functional properties more adequately during their machining.

2 Literature Review

Currently, available models of thermomechanical processing processes are obtained under the assumption of uniformity of materials of structural elements and do not consider defects in the technological inheritance of products [5]. Some studies investigate the effect of structural transformations in steel during machining on the formation of cracks. According to these studies, the presence of a large amount of austenite in the subsurface layer leads to the formation of tensile stresses, which are realized in the form of brittle cracks [6, 7]. Structural transformations cannot be an "independent" cause of cracks since structural stresses that reach destructive values are formed over a significant period. In some cases, structural elements' physical and technical processing is characterized by short duration, high heating and cooling rates, at which structural changes are insignificant, and thermomechanical stresses reach the limit values [8].

Models of the stress-strain state of parts with coatings are developed that consider the piecewise heterogeneity of products "coating-matrix" [9, 10]. However, the lack of research into the effects of inhomogeneities on functional properties on the bearing capacity or durability, and optimization of thermomechanical processes that accompany the processing, determine the relevance of a mathematical model of defect formation physical and technical treatment of structural elements using the optimum criteria of fracture mechanics. The simulation results allow us to effectively assess the effect of structural inhomogeneities formed during machining in the working surfaces of products, their optimal state on the loss of the required properties.

3 Research Methodology

To develop a numerical and analytical model for determining and optimizing the thermomechanical state of products made of functionally graded materials that contain inhomogeneities such as interfacial cracks and inclusions during machining. This model determines the functional relationships of the optimal crack resistance criterion with the control of technological parameters to ensure the quality characteristics of products' processed surfaces.

The development of mathematical models describing thermomechanical processes in the surface layer of structural elements in their manufacture from materials and alloys, taking into account their inhomogeneities that affect the formation of crack-type defects, allows us to determine the criteria for their equilibrium state during the operation of such elements, taking into account their functional purpose.

When choosing and justifying the mathematical model, it was taken into account that both thermal and mechanical phenomena accompany the process of manufacturing parts. However, the overall effect on the stress-strain state of the surface layer is exerted by temperature fields. Given that the bulk of the surface layer of metal during physical

and technical processing is in an elastic state, we can use a thermoelastic body model that reflects the relationship between mechanical and thermal phenomena at finite values of heat fluxes. For studies of the optimal thermomechanical state of the working surfaces of structural elements, information about the propagation of temperatures and stresses and the material's depth, taking into account the inhomogeneities present in it, is essential.

For further studies of the kinetics of the formation of thermomechanical processes in the processed material, we use the following system of differential equations [11, 12] as the main theoretical prerequisite, describing the interaction of the strain field and the temperature field:

$$G\Delta\vec{U}_j + (\lambda_t + G) \text{grad div } \vec{U}_j - \rho \frac{\partial^2 U_j}{\partial \tau^2} + P_j = \alpha_t \beta_t \text{grad } T \quad (1)$$

$$\Delta T - \frac{1}{\alpha} \frac{\partial T}{\partial \tau} - \eta l \frac{\partial}{\partial \tau} \text{div } \vec{U}_j = -\frac{W}{\lambda} + C_q^{-2} \frac{\partial^2 T}{\partial t^2} \quad (2)$$

where λ_t , G are Lamé constants; $\beta_t = 3\lambda_t + 2G$ is the density of the processed material; α_t is the temperature coefficient of linear expansion of metal; $\alpha = \frac{\lambda}{C_v}$ is the thermal diffusivity; λ is the thermal conductivity; C_v is the volume heat capacity; $U(\Phi, \tau)$ is the total displacement vector of the inner point $\Phi(x, y, z)$ of the surface layer under the action of thermomechanical forces accompanying the processing process; $l = \frac{1+\tau_r\delta}{\delta}$ (τ is the relaxation time); $\eta = \frac{\alpha_t \beta_t T(\Phi, \tau)}{\lambda}$; W is the power of the heat source; C_q is the speed of heat propagation in the processed material; τ is the time; P_j is the cutting force; $\text{grad } T(x, y, z) = \frac{\partial T}{\partial x} \vec{i} + \frac{\partial T}{\partial y} \vec{j} + \frac{\partial T}{\partial z} \vec{k}$; $\text{div } \vec{U}_j = \frac{\partial U_x}{\partial x} + \frac{\partial U_y}{\partial y} + \frac{\partial U_z}{\partial z}$ ($j \leftrightarrow x, y, z$).

Since thermal phenomena prevail over force phenomena in finishing processing methods, we can neglect the term in the heat equation that considers the conversion of mechanical energy into heat, and we will come to the parabolic type heat equation. For the specified system (1)–(2), we will neglect the influence of inertial terms and the heat propagation velocity's boundedness. Moreover, to overcome the analytical difficulties associated with solving spatial problems of thermoelasticity, we will consider the planar problem. This transition is justified because to study the thermomechanical state of the treated surfaces and optimize it, information about the propagation of temperatures and deformations and the source movement's depth and direction are essential.

For an extensive range of grinding products, accompanied by thermomechanical processes in the surface to be processed, the choice of temperature fields and power load distribution is required. For ensuring an optimally low level of the thermomechanical state, it is natural to take the measure of the stress state as a function of the goal – the functional of the elastic strain energy (3):

$$W = \frac{1}{2} \int_0^\tau \int_{\vartheta} (\sigma_x e_{11} + \sigma_y e_{22} + 2\tau_{xy} e_{12}) d\nu d\tau \rightarrow \min \quad (3)$$

where $e_{ij} = e_{ij}^{(m)} - e_{ij}^t$ and $e_{ij}^t = \delta_{ij} \alpha_t$ are components of elastic and thermal deformation; $\sigma_x, \sigma_y, \tau_{xy}$ are the stress components.

When drawing up the design scheme, we assume that the processed product can be modeled as a piecewise homogeneous half-plane, which allows us to study thermomechanical processes in it with several types of coatings with a thickness of Δa_k applied

to the main matrix. This scheme determines the thermal and deformation conditions for the interface of layers along the boundaries of their section a_k .

The influence of structural inhomogeneities that occur in the material both during smelting and during the technological process will be taken into account in the model by inclusions and defects such as microcracks in the surface layer.

For a complete understanding of the role of material defects in the mechanism of strength reduction, consider the following problem. Let us assume that non-interacting pores are scattered in the surface layer of the coating with a depth much less than their length, and they are within the thickness of the material removal in one pass. Let the contact zone S of the tool with the part contain a defect of the air pore type, the length of which is $2l$. Let us choose the XOY coordinate system so that this defect is located along the x axis with the center at the origin. The defect direction's accepted choice corresponds to the most likely development of this defect into a crack.

Determination of the temperature field on the coating surface is reduced to solving the following boundary value problem [13, 14]:

$$\frac{\partial T}{\partial \tau} = a \left(\frac{\partial^2 T}{\partial x^2} + \frac{\partial^2 T}{\partial y^2} \right) \tag{4}$$

$$\begin{cases} T_k, x, y \in S_k \\ 0, x, y \notin S_k \end{cases} \tag{5}$$

where $T(x, y, \tau)$ is the temperature of the product at point (x, y) at time τ ; T_k is the contact temperature on the surface of the product formed during machining.

Using the method of integral transformations, it can obtain a solution to the problem in the form:

$$T(x, y, \tau) = \frac{T_k}{4} \left[\operatorname{erf} \left(\frac{x + b_0}{2\sqrt{a\tau}} \right) + \operatorname{erf} \left(\frac{x - b_0}{2\sqrt{a\tau}} \right) \right] \times \left[\operatorname{erf} \left(\frac{y + b_0}{2\sqrt{a\tau}} \right) + \operatorname{erf} \left(\frac{y - b_0}{2\sqrt{a\tau}} \right) \right] \tag{6}$$

where $\operatorname{erf}(z) = \frac{2}{\sqrt{\pi}} \int_0^z \exp(-u^2) du$; a is the coefficient of thermal diffusivity of the coating material or the base material, if its tendency to crack formation is considered.

The components of the stress tensor $\sigma_x, \sigma_y, \tau_{xy}$ are expressed in terms of the thermoelastic displacement potential Ψ in the form [15]:

$$\sigma_x = -2G \frac{\partial^2 \Psi}{\partial y^2}, \sigma_y = -2G \frac{\partial^2 \Psi}{\partial x^2}, \tau_{xy} = -2G \frac{\partial^2 \Psi}{\partial x \partial y} \tag{7}$$

$$\Delta \Psi = (1 + \nu) \alpha_t T(x, y, \tau) \tag{8}$$

where G is the shear modulus; ν is the Poisson ratio; α_t temperature coefficient of linear expansion.

Differentiating (8) by τ and taking into account (4)–(5):

$$\Delta \left[\frac{\partial \Psi}{\partial \tau} - (1 + \nu) \alpha_t a T(x, y, \tau) \right] = 0 \tag{9}$$

From the last expression, it can be seen that the function $\frac{\partial \Psi}{\partial \tau} - (1 + \nu)\alpha_t a T$ is harmonic over the entire plane and, therefore, can be either a constant or some function of time $g(\tau)$. We introduce its derivative instead of the potential Ψ : $\Psi' = \Psi \int_0^\tau g(\tau) d\tau$.

Thus, for the potential Ψ , we have the equation:

$$\frac{\partial \Psi}{\partial \tau} = (1 + \nu)\alpha_t a T \quad (10)$$

Integrating (10), we obtain the following relation for the thermoelastic potential:

$$\Psi = (1 + \nu)\alpha_t a T \int_0^\tau T(x, y, \tau) d\tau + \Psi_0(x, y) \quad (11)$$

where $\Psi_0(x, y)$ is the displacement potential corresponding to the initial temperature.

From here:

$$\Psi_0(x, y) = -\frac{(1 + \nu)\alpha T_0}{2\pi} \iint \ln\left(\frac{1}{R}\right) d\xi d\eta \quad (12)$$

where $R = \sqrt{(x - \xi)^2 + (y - \eta)^2}$.

Substituting in (7) the expression for $T(x, y)$ from (6) and considering that outside the contact zone of the tool with the part $\Delta\Psi_0 = 0$:

$$\begin{aligned} \sigma_y = & -\frac{G(1 + \nu)\alpha_t T_k}{4\sqrt{\pi}} \left\{ 4\sqrt{\pi} \delta(x, y) + \frac{4}{\sqrt{\pi}} \left[\operatorname{arctg}\left(\frac{y + \sqrt{\frac{Dh}{4}}}{x + b}\right) \right. \right. \\ & + \operatorname{arctg}\left(\frac{\sqrt{\frac{Dh}{4}} - y}{x - b}\right) + \operatorname{arctg}\left(\frac{\sqrt{\frac{Dh}{4}} - y}{x + b}\right) + \operatorname{arctg}\left(\frac{\sqrt{\frac{Dh}{4}} + y}{x - b}\right) \left. \right] \\ & - \int_0^{\tau k} \frac{1}{\tau\sqrt{a\tau}} \left[(x + b)e^{-\frac{(x+b)^2}{4a\tau}} + (x - b)e^{-\frac{(x-b)^2}{4a\tau}} \right] \\ & \times \left[\operatorname{erf}\left(\frac{y + \sqrt{\frac{Dh}{4}}}{2\sqrt{a\tau}}\right) + \operatorname{erf}\left(\frac{\sqrt{\frac{Dh}{4}} - y}{2\sqrt{a\tau}}\right) \right] d\tau \left. \right\} \quad (13) \end{aligned}$$

where $\delta(x, y) = \begin{cases} 1, & (x, y) \in S_k \\ 0, & (x, y) \notin S_k \end{cases}$.

Since the singular integral equation determines the stress intensity factor for an isolated defect with the Cauchy kernel [16]:

$$K_1 = -\frac{1}{\sqrt{\pi l}} \int_{-l}^l \sigma_y(x, 0, \tau) \sqrt{\frac{l+x}{l-x}} dx$$

then, using (13):

$$K_1 = \frac{GT_k(1+\nu)\alpha_t}{\sqrt{\pi l}} \left\{ \pi l + \frac{2}{\pi} \left[\arctg \left(\frac{\sqrt{\frac{Dh}{4}}}{2(\pi+b)} \right) + \arctg \left(\frac{\sqrt{\frac{Dh}{4}}}{2(b-\pi)} \right) \right] \sqrt{\frac{l+\xi}{l-\xi}} d\xi \right. \\ \left. - \frac{1}{2\sqrt{\pi}} \int_{-l}^l \int_0^{\tau_k} \frac{1}{\tau\sqrt{a\tau}} \left[(\xi+b)e^{-\frac{(\xi+b)^2}{4a\tau}} + (b-\xi)e^{-\frac{(b-\xi)^2}{4a\tau}} \right] \operatorname{erf} \left(\frac{\sqrt{\frac{Dh}{4}}}{4\sqrt{a\tau}} \right) \sqrt{\frac{l+\xi}{l-\xi}} d\xi \right\} \quad (14)$$

In the case when the stress intensity coefficient approaches the local fracture criterion K_c [17] of the material of the processed product, a crack-like defect begins to develop into a crack. Thus, from the last relation, we obtain optimal conditions for the equilibrium of defects of length $2l$ in the form:

$$l_0 = \frac{K_c^2}{\pi[GT_k(1+\nu)\alpha_t]^2} \quad (15)$$

In this formula, the value of the contact temperature T_k in the processing zone depends on the technological parameters of the tool characteristics and properties of the processed material and can be determined by the formula [17]:

$$T_k = \frac{CV_{kp}}{\lambda\sqrt{Dh}V_g^2} \sqrt{\frac{\pi}{a_n}} \left[1 - e^{-\frac{v_0\sqrt{Dh}}{a\tau}} \right] \quad (16)$$

where V_{kp} , V_g , h are the processing mode; D , C are the tool parameters; λ , a_n are the thermophysical characteristics of the processed material.

4 Results

The adequacy of the constructed model was tested experimentally on samples made of 17CrNiMo6 (Germany) steel. Using a scanning electron microscope, it was found that the surface layer of the processed product has structural defects with a length of $2l = 40$ microns (Fig. 1). Physical and mechanical characteristics of steel: $K_{c} = 2.0 \text{ MPa} \cdot \text{m}^{1/2}$, $\alpha = 8.58 \text{ K}^{-1}$, $G = 168 \text{ GPa}$. The machining parameters were selected so that the contact temperature in the processing zone reached $T_k = 800 \text{ }^\circ\text{C}$. The grid of cracks formed on the surface. For structural defects not to develop into prominent cracks, that is, to remain in an equilibrium state, when performing inequality (15), it is necessary to select the optimal processing modes and tool characteristics in such a way that $T_k \leq 600 \text{ }^\circ\text{C}$. A highly porous circle with evenly distributed pores was used as a tool (Fig. 2). These circles allow for a lower temperature level in the cutting zone and increase the grinding operation's productivity.

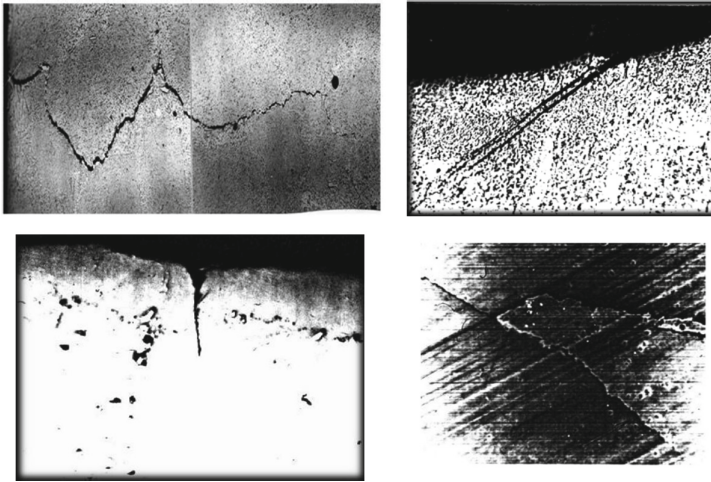


Fig. 1. Formation of grinding cracks during sample processing when optimal processing modes are violated.

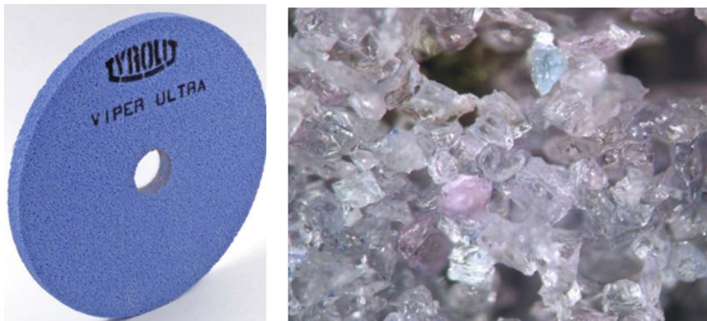


Fig. 2. Appearance and structure of high-porous circles of the company “Tyrolit” (Austria).

5 Conclusions

The developed model allows us to consider the influence of technological origin’s inhomogeneities (starting from the workpiece and ending with the finished product) that occur in the surface layer during the manufacture of structural elements on its destruction.

The solution of the problem of thermoelasticity describing the thermomechanical state of the surface layer of the treated surface allows us to determine the stress intensity in the vicinity of the vertices of defects of the crack type and, by comparing it with the optimal criterion of crack resistance for the material of a structural element, we can determine its state. If this criterion is violated, the defect develops into the main crack.

The intensity of crack formation in the surface layer of products at finishing operations is determined mainly by their materials’ crack resistance, formed during the workpiece and subsequent operations.

Modeling thermomechanical processes allows us to obtain optimal criterion relations of the defect's equilibrium state condition depending on the contact temperature gradients.

The mechanism of formation and development of crack-type defects in functionally graded materials of the inhomogeneous structure under the influence of optimal thermo-mechanical phenomena accompanying the manufacturing technology and operation of structural elements is studied.

The developed model allows us to consider the influence of technological origin's inhomogeneities (starting with the workpiece and ending with the finished product) that occur in the surface layer during the manufacture of structural elements on its destruction.

The solution of the singular integral equation with the Cauchy kernel allows us to determine the stress intensity in the vicinity of the vertices of structural defects that are formed in the surface layer of products during their machining and by comparing it with the crack resistance criterion for the material of a structural element, we can determine its state.

If this criterion is violated, the defect develops into the main crack. Modeling thermo-mechanical processes during the mechanical processing of structural elements allows us to obtain a criterion ratio of the balanced state of defects in the surface layer of products, depending on the technological parameters.

References

1. Jannot, Y., Degiovanni, A.: *Thermal Properties Measurement of Materials*. Wiley, Hoboken (2018)
2. Marinescu, I.D., Hitchiner, M.P., Uhlmann, E., Rowe, W.B., Inasaki, I.: *Handbook of Machining with Grinding Wheels*. CRC Press, Boca Raton (2016)
3. Pramanik, A., Islam, M.N., Davies, I.J., Boswell, B., Dong, Y., Basak, A.K.: Contribution of machining to the fatigue behaviour of metal matrix composites (MMCs) of varying reinforcement size. *Int. J. Fatigue* **2**, 9–17 (2017)
4. Frómeta, D., Cuadrado, N., Rehr, J., Suppan, C., Dieudonné, T., Dietsch, P.: Microstructural effects on fracture toughness of ultra-high strength dual phase sheet steels. *Mater. Sci. Eng. A* (804), 140631 (2021)
5. Shen, S., Song, X., Li, Q., Li, X., Zhu, R., Yang, G.: A study on stress corrosion cracking and hydrogen embrittlement of Jethete M152 martensitic stainless steel. *Mater. Sci. Eng. A* **740–741**, 243–251 (2019)
6. Doi, T., Uhlmann, E., Marinescu, I.D.: *Handbook of Ceramics Grinding and Polishing*. Elsevier Science, Amsterdam (2015)
7. Shi, Y., Chen, L., Xin, H., Yu, T., Sun, Z.: Investigation on the grinding properties of high thermal conductivity vitrified bond CBN grinding wheel for titanium alloy. *Int. J. Adv. Manuf. Technol.* **107**(3–4), 1539–1549 (2020). <https://doi.org/10.1007/s00170-020-05134-y>
8. Shin, Y.C., Xu, C.: *Intelligent Systems: Modeling, Optimization, and Control*. CRC Press, Boca Raton (2017)
9. Zhou, T., Yi, M.: Microscopic cracking simulation of nanocomposite ceramic tool materials under the consideration of residual stress. *Int. J. Adv. Manuf. Technol.* **94**(9–12), 3485–3502 (2016). <https://doi.org/10.1007/s00170-016-9663-4>
10. Nowacki, W.: *Thermoelasticity*. Elsevier Science, Amsterdam (2013)
11. Povstenko, Y.: *Fractional Thermoelasticity*. Springer (2015)

12. Hertzberg, R.W., Vinci, R.P., Hertzberg, J.L.: *Deformation and Fracture Mechanics of Engineering Materials*. Wiley, New York (2020)
13. Pasternak, I.M., Sulym, H.T., Ilchuk, N.I.: Interaction of physicommechanical fields in bodies with thin structural inhomogeneities: a survey. *J. Math. Sci.* **253**(1), 63–83 (2021). <https://doi.org/10.1007/s10958-021-05213-9>
14. Noda, N., Sumi, N., Ohmichi, M.: Analysis of transient plane thermal stresses in functionally graded orthotropic strip. *J. Therm. Stresses* **41**(10–12), 1225–1243 (2018)
15. Muskhelishvili, N.I.: *Singular Integral Equations: Boundary Problems of Function Theory and Their Application to Mathematical Physics*. Dover Publications (2013)
16. Lifanov, I.K.: *Singular Integral Equations and Discrete Vortices*. Walter de Gruyter GmbH & Co KG, Berlin (2018)
17. Oborskiy, G.A., Daschenko, A.F., Usov, A.V., Dmitrishin, D.V.: *System modeling*. Astroprint, Odessa (2013)



The Influence of Grinding Modes on the Quality of the Surface Layer

Maksym Kurin^(✉) , Serhii Nyshnyk , and Anatolii Dolmatov 

National Aerospace University “Kharkiv Aviation Institute”, 17,
Chkalova Street, Kharkiv 61070, Ukraine
m.kurin@khai.edu

Abstract. The analysis shows that one of the most rational ways to increase the efficiency of the grinding process is the choice of rational processing modes because, in this case, occur a comprehensive solution to the problem: first, the need to use expensive lubricant-cooling agent reduced, and second, the need for special grinding wheels and their frequent trueing was reduced. The structure of comprehensive theoretical and experimental studies of energy-power parameters for the technological processes was considered. A system of equations developed based on the hyperbola method was presented, which describes spatial fields of the velocities of particle displacements around the abrasive grain. The order of mathematical operations is expounded, which allows finding important physical quantities characterizing the chip material’s deformed state. The deformed state of the cut layer is analyzed – the flow around abrasive grain during plunge grinding. The velocities and dislocation density fields were constructed for a specific example of processing. In the experimental part of the work, the research of the influence of technological regimes and the abrasive tool’s characteristics on the quality of the hard-working materials’ grinded surface was carried out.

Keywords: Grinding process · Velocity fields · Dislocations density · Quality of grinded surface · Surface roughness · Abrasive grain · Recommendations for technological modes

1 Introduction

The grinding process is one of the most heat-intensive [1] and energy-intensive cutting processes [2], the output indicators of which depend on both the processing modes [3, 4] and many other technological and other factors [5]. The accompanying thermal processes have a decisive influence on the processing process itself [6] and the ground surfaces’ quality [7].

One of the most important indicators of the grinding process is productivity [8], precision, and processing quality. Simultaneously, the regimes of maximum productivity usually do not coincide with the regimes ensuring high quality of the machined surface. Therefore, grinding modes’ purpose and choice are always a search for a compromise between productivity and machining quality, especially when it comes to parts made

of complex alloyed hard-to-machine alloys prone to burns and burns cracking [9]. The efficiency and quality of processing during grinding, which is a mass high-speed micro-cutting process and is based on plastic deformation and destruction of materials, are mainly determined by the process's energy-power parameters [10]. It is established that the main factors influencing the efficiency of processing while maintaining quality parameters of the surface and surface layer are cutting modes [11], characteristics of abrasive wheel [12, 13], lubricating [14], and cooling technologies [15]. In this case, all these factors indirectly affect the efficiency of processing due to operation, blunting, and salinization of the grinding wheel [16].

The analysis shows that one of the most rational ways to increase the efficiency of the grinding process is the choice of rational processing modes [17, 18] because in this case, occur a comprehensive solution to the problem: first, the need to use expensive lubricant-cooling agent reduced [19], and second, the need for special grinding wheels [20, 21] and their frequent truing is reduced [22]. Thus the theory of grinding is imperfect and needs further development.

The work goal is to develop a conveniently engineering technique for predicting material deformed state in the cutting zone. It will make it possible to determine the energy-power characteristics of the process and develop effective technological recommendations. The scientific novelty of investigation consists in further hyperbole method development and a new approach to a visual representation of deformed state main parameters of the material chip.

2 Literature Review

2.1 Structure of Investigation of Energy-Power Parameters of Machining Processes

A theoretical analysis of the majority of technological processes along with the conducted experiments allows us to determine the nature of dependence velocity of particles plastic deformable metal on coordinates. The velocity of particles in four-dimensional space can be represented through a velocity vector [23]:

$$\mathbf{V} = v_x \mathbf{i} + v_y \mathbf{j} + v_z \mathbf{k} + v_t \mathbf{n}. \quad (1)$$

The continuity equation expresses the law constancy of a volume during the deformation:

$$\operatorname{div} \mathbf{V} = 0. \quad (2)$$

Using Eqs. (1)–(2), we can determine the form of functional dependence of speed on coordinates. Thus, the particles velocity field of material is determined, which makes it possible to calculate the strain rates and their intensity using the formulas:

where $q_1, q_2,$ and q_3 are orthogonal curvilinear coordinates.

$$\varepsilon_{q_1q_1} = \frac{1}{H_1} \frac{\partial \mathbf{V}_{q_1}}{\partial q_1} + \frac{\mathbf{V}_{q_2}}{H_1 H_2} \frac{\partial H_1}{\partial q_2} + \frac{\mathbf{V}_{q_3}}{H_1 H_3} \frac{\partial H_1}{\partial q_3}, \tag{3}$$

$$\varepsilon_{q_1q_2} = \frac{1}{H_2} \frac{\partial \mathbf{V}_{q_1}}{\partial q_2} + \frac{1}{H_1} \frac{\partial \mathbf{V}_{q_2}}{\partial q_1} - \frac{\mathbf{V}_{q_1}}{H_1 H_2} \frac{\partial H_1}{\partial q_1} - \frac{\mathbf{V}_{q_2}}{H_1 H_2} \frac{\partial H_2}{\partial q_1},$$

$$H_k = \sqrt{\sum_{i=1}^3 \left(\frac{\partial x_i}{\partial q_k} \right)^2} \tag{4}$$

here, H_k are Lamé parameters.

Then, it is necessary to determine components of deformation to find the energy-power process parameters,

$$\mathbf{e}_{11} = \int \varepsilon_{11} dt, \quad \mathbf{e}_{22} = \int \varepsilon_{22} dt \tag{5}$$

and deformation intensity,

$$\mathbf{e}_i = \frac{\sqrt{3}}{2} \sqrt{(\mathbf{e}_{11} - \mathbf{e}_{22})^2 + (\mathbf{e}_{22} - \mathbf{e}_{33})^2 + (\mathbf{e}_{33} - \mathbf{e}_{11})^2 + \frac{3}{2}(\mathbf{e}_{12}^2 + \mathbf{e}_{23}^2 + \mathbf{e}_{31}^2)}. \tag{6}$$

The dislocations density in the removed chips is determined through the intensity of deformations [23, 24]:

$$\rho(x, y, z) = \left[\frac{2\pi}{Gb} \cdot \sigma_{0.2/T} (m \cdot e_i^n - 1) \right]^2 \tag{7}$$

where G is shear modulus, Pa; b is Burgers vector, m; n is strain hardening index; m – coefficient taking into account change the yield stress of material; σ_T is yield stress of the material, Pa.

The efficiency of investigation energy-energy characteristics has been proved by the hyperbole method [23]. We have researched deformable chip material for specific machining cases.

To simplify calculations constructing a picture of changes in dislocations density as well as more convenient assessment and comparison simulation results, we will propose that the flow stress does not depend on deformations intensity. This will allow us to take $m = 1$ in formula (7).

3 Research Methodology

The velocity field of particle displacements wrapping around elliptical grain has been developed using the hyperbole method. A distinctive feature of obtained equations is the presence of the third independent variable [24]:

$$\left. \begin{aligned}
 & \left[\begin{aligned}
 & V_x(x, y, z) = V_0(\omega(x, y, z))^{-1/2} \\
 & \times \left[\begin{aligned}
 & \frac{\left(x \sin(\alpha) + y \cdot \cos(\alpha) \sqrt{1 - z^2/B^2} \right) \cdot \cos(\alpha)}{\sqrt{1 - z^2/B^2} \cdot \sqrt{e^2 - 1}} \\
 & + \frac{(e^2 - 1) \sin(\alpha) \left(x \cos(\alpha) - y \sin(\alpha) \sqrt{1 - z^2/B^2} \right)}{\sqrt{1 - z^2/B^2} \cdot \sqrt{e^2 - 1}}
 \end{aligned} \right] \times \sqrt{1 - z^2/B^2}; \\
 & V_y(x, y, z) = -V_0(\omega(x, y, z))^{-1/2} \\
 & \times \left[\begin{aligned}
 & \frac{\left(x \sin(\alpha) + y \cdot \cos(\alpha) \sqrt{1 - z^2/B^2} \right) \cdot \sin(\alpha)}{\sqrt{1 - z^2/B^2} \cdot \sqrt{e^2 - 1}} \\
 & - \frac{(e^2 - 1) \cos(\alpha) \left(x \cos(\alpha) - y \sin(\alpha) \sqrt{1 - z^2/B^2} \right)}{\sqrt{1 - z^2/B^2} \cdot \sqrt{e^2 - 1}}
 \end{aligned} \right]; \\
 & \omega(x, y, z) = a^2(x, y, z) \left[1 - \frac{z^2}{B^2} (1 - e^2 \sin^2(\alpha)) \right] - \frac{x_0^2 z^2}{B^2 - z^2} + e^2 \zeta^2(x, y, z); \\
 & \zeta(x, y, z) = \frac{\frac{x_0 B}{\sqrt{B^2 - z^2}} \cos(\alpha)}{1 - e^2 \sin^2(\alpha)} \\
 & + \frac{\sqrt{\sin^2(\alpha) (1 - e^2) \left(a^2(x, y, z) (e^2 \sin^2(\alpha) - 1) - \frac{x_0^2 B^2}{B^2 - z^2} \right)}}{1 - e^2 \sin^2(\alpha)}; \\
 & \left\{ \begin{aligned}
 & a(x, y, z) = \sqrt{\frac{x^2 + y^2 \left(1 - z^2/B^2 \right) - e^2 \left(x \cos(\alpha) - y \sin(\alpha) \sqrt{1 - z^2/B^2} \right)^2}{(e^2 - 1) \left(1 - z^2/B^2 \right)}};
 \end{aligned} \right.
 \end{aligned} \right. \tag{8}$$

where V_0 is a cutting speed; coordinate x_0 determines the plastic flow beginning; e is an eccentricity of hyperbola; α is an angle of rotation ($\alpha = -\gamma/2$, γ – cutting angle); B – grain half-width.

An example is considered: the operation of grinding a part of an alloy OT-4; the speed of rotation of the abrasive wheel $V_{wh} = 35$ m/s; the speed of rotation of the workpiece $V_w = 30$ m/min; cutting depth $t = 2 \cdot 10^{-5}$ m. Parts were machined with an abrasive wheel 63C40CM2K with geometry $\gamma = \alpha = 101.6^\circ$. (Figs. 1, 2).

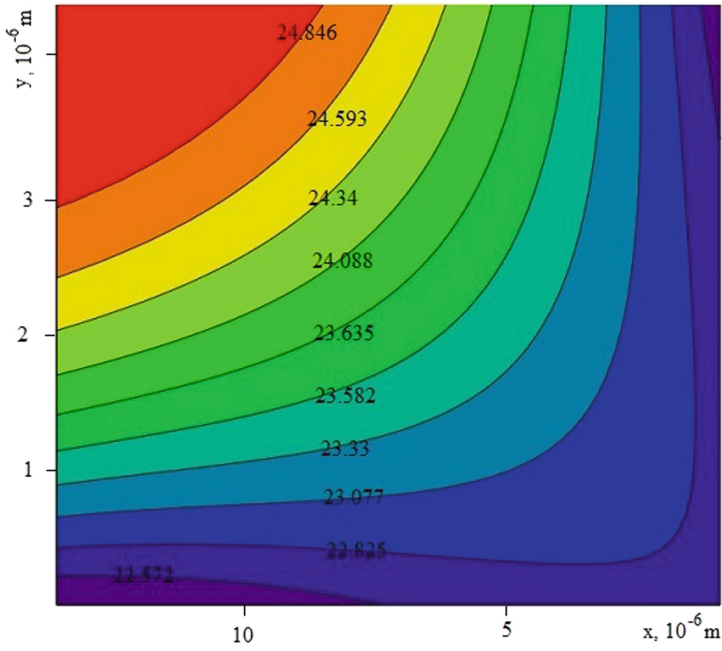


Fig. 1. The deformation intensity wrapping around the elliptical grain.

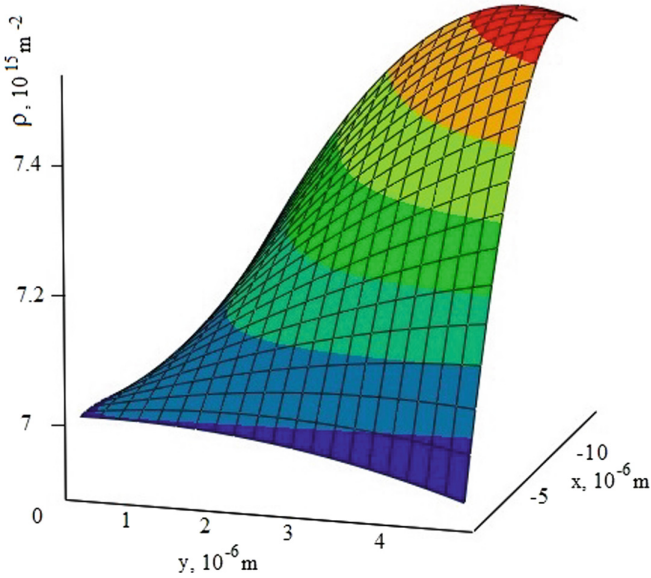


Fig. 2. The dislocations density wrapping around the elliptical grain.

4 Results

4.1 Investigation of Power-Strength Parameters of Grinding Process

Most researchers usually mean a whole set of indicators by the quality of the grinded surface. There are geometric (roughness, waviness, shape, and direction of microroughness) and physicomechanical, characterizing the state of the metal in the surface layer (cauterization, microcracks, structural transformations) [12, 13]. As we know, all of the above indicators are determined by processing modes, characteristics, and quality of abrasive tools, as well as coolant lubricants. The surface layer of metal is exposed to force and heat factors, leading to change in the surface layer's physical and mechanical parameters, which are essential during processing. Since grinding is the final operation of the technological process, it should be borne in mind that all changes that occur in the surface layer at this stage remain in the finished product. Thus, designing technological grinding operation, a decisive choice for processing modes, makes it possible to provide the best indicators state of surface layer simultaneously with maximum productivity. In this work, samples were made from steel DIN X6Cr17 stainless steel of ferrite class, steel 30HGSA of pearlite class, high-temperature alloy CrNi65CoMoWAlTi, and titanium ($\alpha + \beta$)-alloys up to Ti3Al15V3Cr3Sn1 and α -alloys Ti0.8Al0.8Mn. These materials are of most significant interest. These materials are often used to manufacture reliable gas turbine engines, which tend to the dull grinding wheel and occurrence grinding cracks and cauterization.

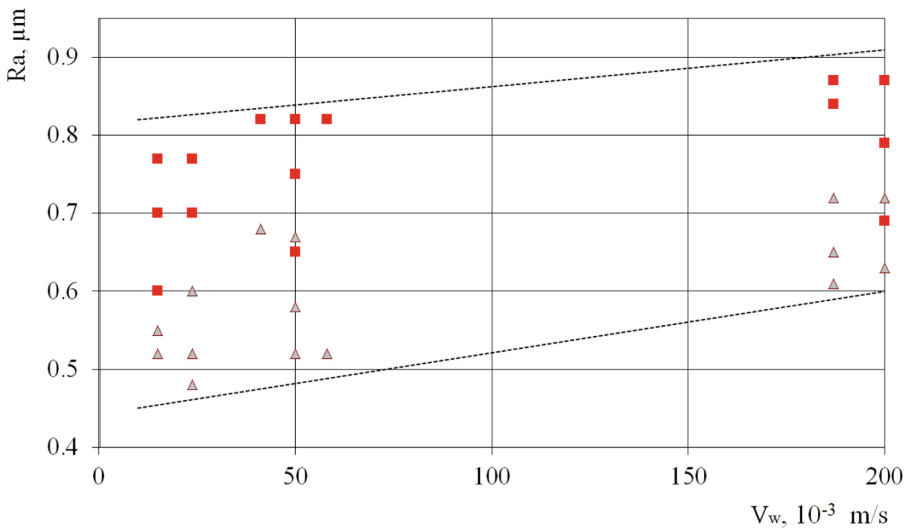
Increasing the rotation speed of the part leads to a deterioration surface roughness of all investigated materials. With a grinding depth $t = 5 \cdot 10^{-5}$ m and part rotation speed change within $V_w = 0.015\text{--}0.200$ m/s in abrasive wheel 24A 25P CM1 6K 6 for all materials, the surface roughness was $R_a = 0.28\text{--}0.85$ μm (Fig. 3). This is because increasing the part rotation speed, the distance contact increases between adjacent grains points of the abrasive wheel with the workpiece surface. Other things being equal, the surface roughness almost did not change when decreasing the wheel diameter after dressing. However, with increasing depth of cut from 0.01 to 0.05 mm, the roughness also increased in the R_a range 0.31–0.80 μm . The grain size of the grinding wheel affects the surface roughness. It grows with increasing grain size. However, the difference in grain size does not significantly affect roughness with an increase in cutting speed. The surface roughness remains almost unchanged with an increase in the number of ground samples without wheels dressing, indicating the stability of cutting properties.

Surface roughness investigation shows:

- increasing cutting speed has the maximum effect on a decrease in processed surface roughness. A longitudinal feed and part rotation speed change have little effect on roughness. With their increasing, the roughness also increases;
- the roughness almost does not change during long-term grinding, which confirms the stability cutting properties of abrasive wheels.

During metallographic studies, no changes were observed in the surface microstructure of all the treated samples (Fig. 4).

The surface temperature of treated areas was measured in a zone located directly in front of the grinding wheel using an IR-1000L pyrometer to compare its value in



■ – for the material Ti3Al15V3Cr3Sn1; Δ – for the material Ti0.8Al0.8Mn

Fig. 3. The dependence surface roughness on the part rotation speed

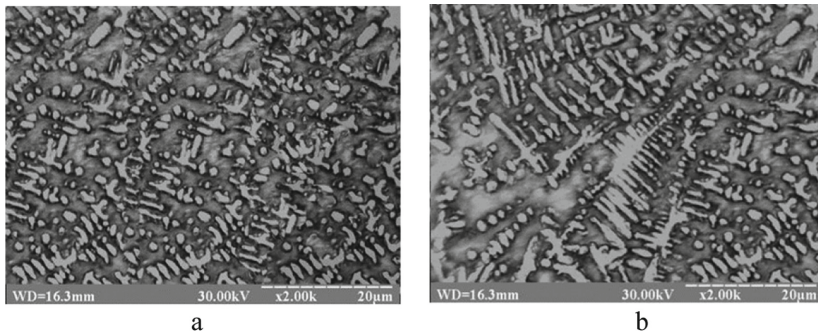


Fig. 4. The structure of the Ti0.8Al0.8Mn material at different depths.

different modes. It was found that with an increase of speed rotation part, a decrease in contact temperature is observed.

4.2 Recommendations for Technological Modes of Processing Appointment

Processing is performed with cycles to increase maximum grinding performance when accuracy specified parameters and surface roughness are achieved. The cycle is formed in such a way as to remove allowance most intensively at machining beginning, moderately at the end of machining, and to reduce the error of previous stages grinding during nursing, which is performed without feeding wheel to grinding depth.

Three-stage (full) is recommended to use a processing cycle when forming sizes 7–5 of accuracy and surface roughness $R_a = 0.2\text{--}0.6\ \mu\text{m}$. In this case, the most considerable value of the grinding allowance is divided into two parts: a large (0.8–0.9) Z_{max} is removed by increasing the longitudinal speed $V_{lon} = 0.14\text{--}0.2\ \text{m/s}$ and with maximum $V_d = 0.6\text{--}0.8\ \text{m/s}$ to increase productivity, as well as increase cutting ability and stability of the abrasive wheel.

A two-stage processing cycle is recommended to use formation sizes 8–7 of accuracy and surface roughness $R_a = 0.6\text{--}0.9\ \mu\text{m}$. The grinding allowance is removed with an average longitudinal speed $V_{lon} = 0.04\text{--}0.14\ \text{m/s}$ and maximum rotation speed of part $V_d = 0.6\text{--}0.8\ \text{m/s}$ to increase productivity and increase cutting ability and abrasive wheel stability. Nursing increases the accuracy of geometric shapes and reduces treated surface roughness. Therefore it should be carried out at $V_{lon} = 0.02\text{--}0.04\ \text{m/s}$ and $V_d = 0.2\text{--}0.3\ \text{m/s}$. In this case, the finishing stage is longer. The specified processing conditions allow achieving high values of surface quality and the material surface layer, reduce the cauterization on treated surface, and increase the abrasive wheel's durability.

5 Conclusions

The hyperbole method and a new approach to the visual representation of deformed state main material chip parameters were further developed. It will make it possible to determine the energy-power characteristics of the process and develop effective technological recommendations.

Based on one, the velocity field of particle displacements wrapping around elliptical grain was determined when flowing around an abrasive grain in conditions of non-free cutting. A distinctive feature of obtained equations is a third independent variable, which allows one to research the cut layer's deformed state in space. The investigation results can be used to construct a metal flow picture and analyze the deformed state of the cut layer for various schemes and types of non-free cutting. It can be used as to complex-profile tool by dividing the shaped cutting edge into parts.

The recommendations on improvement and expansion of the technological modes of grinding are given.

References

1. Stachurski, W., Sawicki, J., Krupanek, K., Nadolny, K.: Numerical analysis of coolant flow in the grinding zone. *Int. J. Adv. Manuf. Technol.* **104**(5–8), 1999–2012 (2019). <https://doi.org/10.1007/s00170-019-03966-x>
2. Grzesik, W.: *Advanced Machining Processes of Metallic Materials: Theory, Modelling, and Applications*, 2nd ed. Elsevier (2017)
3. Baumgart, C., Radziwill, J.J., Kustera, Fr., Wegener K.: A study of the interaction between coolant jet nozzle flow and the airflow around a grinding wheel in cylindrical grinding. In: Outeiro, J., Poulachon, G. (eds.) *16th CIRP Conference on Modelling of Machining Operations*, vol. 58, pp. 517–522. Elsevier Ltd. (2017). <https://doi.org/10.1016/j.procir.2017.03.261>

4. Jamshidia, H., Budak, E.: Grinding temperature modeling based on a time dependent heat source. In: Monostori, L. (eds.) 8th CIRP Conference on High Performance, pp. 299–302. Elsevier Ltd. (2018). <https://doi.org/10.1016/j.procir.2018.09.020>
5. Gear Tooth Profile Grinding. https://www.atlantic-grinding-wheels.com/fileadmin/redaktion/bilder/downloads/kurzinformationen/EN_Zahnflankenprofil schleifen_01.pdf. Accessed 11 Oct 2020
6. Stepanov, M., Ivanova, L., Litovchenko, P., Ivanova, M., Basova, Y.: Model of thermal state of the system of application of coolant in grinding machine. In: Ivanov, V., et al. (eds.) DSMIE 2018. LNME, pp. 156–165. Springer, Cham (2019). https://doi.org/10.1007/978-3-319-93587-4_17
7. Zaborowski, T., Ochenduszeko, R.: Grinding burns in the technological surface of the gear teeth of the cylindrical gears. *Mechanik* **10**, 135–139 (2017)
8. Larshin, V., Lishchenko, N.: Adaptive profile gear grinding boosts productivity of this operation on the CNC machine tools. In: Ivanov, V., Rong, Y., Trojanowska, J., Venus, J., Liaposhchenko, O., Zajac, J., Pavlenko, I., Edl, M., Perakovic, D. (eds.) DSMIE 2018. LNME, pp. 79–88. Springer, Cham (2019). https://doi.org/10.1007/978-3-319-93587-4_9
9. Stepanov, M., Litovchenko, P., et al.: Coolant supply device. Patent of Ukraine № 136095 (2019)
10. Tyuhta, A.V., et al.: Ways to enhance environmental flat grinding by improving the technology of the coolant supply. In: Radionov, A.A. (eds.) 2nd International Conference on Industrial Engineering, ICIE 2016, vol. 150, pp. 1073–1080. Elsevier Ltd. (2016). <https://doi.org/10.1016/j.proeng.2016.07.217>
11. Lishchenko, N., Larshin, V.: Temperature models for grinding system state monitoring. *Appl. Aspects Inf. Technol.* **2**(3), 216–229 (2019)
12. Lishchenko, N., Larshin, V.: Comparison of measured surface layer quality parameters with simulated results. *Appl. Aspects Inf. Technol.* **2**(4), 304–316 (2019)
13. Rowe, W.B.: Towards high productivity in precision grinding. *Inventions* **3**(2), 1–16 (2018)
14. Rowe, W.B.: Temperatures in grinding - a review. *J. Manuf. Sci. Eng.* **139**(12), 1–6 (2017)
15. Jun, Y., Tan, J., Wei, Z., Zhaohui, D.: Theoretical and experimental analysis of temperature distribution during full tooth groove form grinding. *J. Manuf. Process.* **58**, 101–115 (2020). <https://doi.org/10.1016/j.jmapro.2020.08.011>
16. Lishchenko, N.V., Larshin, V.P.: Gear-grinding temperature modeling and simulation. In: Radionov, A.A., Kravchenko, O.A., Guzeev, V.I., Rozhdestvenskiy, Y.V. (eds.) ICIE 2019. LNME, pp. 289–297. Springer, Cham (2020). https://doi.org/10.1007/978-3-030-22063-1_32
17. Badger, J., Murphy, S., O'Donnell, G.E.: Acoustic emission in dressing of grinding wheels: AE intensity, dressing energy, and quantification of dressing sharpness and increase in diamond wear-flat size. *Int. J. Mach. Tools Manuf.* **125**, 11–19 (2018)
18. Jin, T., Yi, J., Li, P.: Temperature distributions in form grinding of involute gears. *Int. J. Adv. Manuf. Technol.* **88**(9–12), 2609–2620 (2016). <https://doi.org/10.1007/s00170-016-8971-z>
19. Patil, P., Patil, C.: FEM simulation and analysis of temperature field of environmental friendly MQL grinding. In: Proceedings of the International Conference on Communication and Signal Processing 2016 (ICCASP 2016), pp. 182–186 (2017)
20. Novikov, F.V., Riabenkov, I.A.: Improved gear grinding gears. *Bull. Natl. Tech. Univ. “KhPI” Technol. Mech. Eng.* **33**(1205), 138–144 (2016)
21. Li Hao, N., Axinte, D.: On a stochastically grain-discretised model for 2D/3D temperature mapping prediction in grinding. *Int. J. Mach. Tools Manuf.* **116**, 1–27 (2017)
22. Tkachuk, A., Zablotskiy, V., Kononenko, A., Moroz, S., Prystupa, S.: Directed formation of quality, as a way of improving the durability of conjugated parts of friction pairs. In: Ivanov, V., Trojanowska, J., Machado, J., Liaposhchenko, O., Zajac, J., Pavlenko, I., Edl, M., Perakovic, D. (eds.) DSMIE 2019. LNME, pp. 370–377. Springer, Cham (2020). https://doi.org/10.1007/978-3-030-22365-6_37

23. Kurin, M.O.: Determination of the boundaries of plastic zone of metal deformation during the cutting. *Progress Phys. Metals* **21**(2), 249–273 (2020). <https://doi.org/10.15407/ufm.21.02.249>
24. Kurin, M.O.: Analysis the process of plastic deformation metal chip at non-free cutting. *Metallofiz. Noveishie Tekhnol.* **42**(3), 433–449 (2020). <https://doi.org/10.15407/mfint.42.03.0433>



Improvement of the Gear Shaping Effectiveness for Bimetal Gears of Internal Gearing with a Friction Coating

Mykola Korotun¹ , Yuliia Denysenko¹  , Olaf Ciszak² ,
and Oleksandr Ivchenko¹ 

¹ Sumy State University, 2, Rymskogo-Korsakova St., Sumy 40007, Ukraine

² Poznan University of Technology, 3, Piotrowo, 61-138 Poznan, Poland

Abstract. This paper presents an experimental study of the gear shaping process of the internal gearing with a friction coating. It is known that this process is characterized by the occurrence of significant vibrations, the decrease in the stability of the cutting tool, and the ambiguity of the technological parameters. These factors limit the ability to process bimetallic discs with friction coatings on gear-shaping machines. Therefore, the dependence of the amplitude of oscillations of the ram and the table with the fixture for clamping the package of parts on different machining modes are investigated in the paper. The experiment was performed on a gear-shaping machine model TOS OHO 50 and using an accelerometer 7290A-2. To register the vibration acceleration, the Information Collection System “National instruments mod. NI-9234” was used. Also, during the experiment, the analysis of the period of stability of the cutting tool depending on the number of double runs of the shaper-type cutter and circular feed. The tool’s stability was analyzed by the chamfer wear on the rear surface, which was checked by a microscope. According to the experiment results, the optimal processing mode, according to the tool’s maximum productivity and stability, is proposed in the paper. The application of the proposed processing mode reduces the self-excited vibrations of the technological system, increases the cutting tool’s stability, stabilizes the surface roughness parameters, and increases the gear-shaping process’s efficiency of the package of friction discs.

Keywords: Bimetal gears · Gear shaping · Friction discs · Vibrations

1 Introduction

The bimetal gears of internal gearing with a friction coating (Fig. 1) are used in onboard frictions of caterpillar equipment of both civil and military function. It is known that such equipment is widely used and works in difficult operating conditions; that is why their especially stressed components are susceptible to increased wear and require repair. The parts of these units include bimetallic gear disks with friction coatings. One of the problematic technological operations in the manufacture of internal gears with friction coating is to obtain an internal gear ring. As usual, the processing of an internal gear

ring is carried out by broaching, gear hobbing, or gear shaping. Broaching and push broaching are quite productive processes. However, taking into account the diameter of 400–450 mm of the internal gear ring, there are significant limitations both in the tool (broaches and push broaching of such diameter are not possible in principle) and in machines that require dividing fixture, if the processing is carried out with a tool that copies the treated surface, which limits productivity and complicates the operational capabilities of the process. Obtaining internal gears by hobbing is also limited by the presence of a special carriage, the possibility of its placement inside the part, and a special cutting tool. In particular, the issue of finishing the internal gear ring is exacerbated during the repair of friction discs due to the limited technological capabilities of repair services. Therefore, given the above, it is most appropriate to study gear shaping, but the peculiarity of this work is the study of the gear-shaping process of the package of friction discs.

Our preliminary test of the gearing process of the internal gear ring (Fig. 1) revealed significant vibrations that occur during processing, the decrease in the stability of the cutting tool, and the ambiguity of the technological parameters of the gear shaping process.



Fig. 1. Bimetallic gear disk of internal gearing with a frictional coating.

The gear ring is made with a diameter of $348^{+0.26}$ mm, a module of 3 mm, the number of teeth 91, and surface roughness of $Ra\ 3.2\ \mu\text{m}$. The basis of modern friction discs is spring steels (steel 65G, 60C2, etc.), which provide high elastic properties of the disk and the ability of the toothed surfaces of the disk to resist crushing during operation. The friction coating of the working disks is made of a graphitized composite alloy based on copper, which can withstand high temperatures and has a high stable coefficient of friction. Material of the cutting tool - high-speed steel P6M5.

It should be noted that any of the mentioned technological processes for increasing productivity should be carried out not on a single part but a package of them due to the small thickness (6 mm) of the bimetallic disk. Therefore, processing and researching the efficiency improvements of gear shaping were performed on a package of 9 disks.

2 Literature Review

D. Ershov etc. [1], V. Maksarov [2], I. Wolfson [3], and I. Zharkov [4] researched the vibrations of technological systems. Analysis of their works showed that oscillations in the technological system (hereinafter TS) occur due to dynamic forces. Depending on the nature of fluctuations in the technological system, they are divided into:

1. Free vibrations of the system occur due to the gravel impact of external forces. As a rule, these oscillations are quickly damped due to energy dissipation in the TS.
2. Forced vibrations (of the first kind), emerging due to the occasionally acting external force not related to the process of cutting the allowance. These oscillations may occur due to an imbalance in the machine's drive or under the action of some external dynamic load. Oscillations of this type usually do not reach the resonant frequencies of the TS.
3. Forced vibrations (of the second kind) occur during the cutting process. The cutting process has its inherent periodicity, which leads to the appearance of forced oscillations (for example, the process of formation of intermittent elemental chips or periodic incision of the teeth of the circular shaper-type cutter). Oscillations of this type also usually do not reach the resonant frequencies of the TS.
4. Self-excited vibrations, a phenomenon in which oscillating motion occurs and is maintained in the process of cutting by energy sources that do not have oscillating properties. Self-excited vibrations are inextinguishable oscillations of the system, which themselves are the source of these oscillations, and the amplitude and period are determined by the system's properties and do not depend on the exciting external force [5]. However, the research of vibrations during milling machines in these works was carried out, and the modeling of machining of thin disks and with friction coating [6, 7] was not considered. Even for well-adjusted machines with high stiffness, under certain operating conditions in the cutting process, self-excited vibrations can occur, limiting the allowable cutting modes, reducing the quality of products, and sometimes leading to premature wear and destruction of the cutting tool (hereinafter CT). In contradistinction to forced vibrations, the frequency of self-excited vibrations usually remains constant in a wide range of cutting speeds, which is the most distinctive feature by which forced oscillations can be distinguished from self-excited vibrations [8, 9]. In these works, one of the main parameters of vibration - vibration acceleration was not considered. The causes of self-excited vibrations can be the phenomena of rivet and build-up, the variable speed of the chips, the variable thickness of the cut layer, and other factors. To eliminate self-excited vibrations, it is necessary to change the properties of the system itself.

Thus, when gear shaping a package with the variable hardness of the material, both forced and self-excited vibrations can occur. Oscillations in metal cutting have long been considered forced vibrations. This interpretation was first refuted by N. Drozdov [10]. He stated that the oscillation frequency in the TS remains virtually unchanged over a wide range of cutting speeds in his work. Based on this fact, he concluded that the oscillations generated by the cutting process should be considered self-excited vibrations.

Several fundamental studies [4, 5, 10, 11] and many research works [12–21] have been devoted to studying oscillations, including self-excited vibrations of the TS during

metal cutting. In the paper [14], the vibrations on bearing housings of turning machines were investigated, and experimental values of the acceleration amplitude of mechanical vibrations (vibration acceleration) were measured. We consider these measurements to be important for our research. In [15], the issues of roughness prediction during turning based on vibration analysis considered the processing modes and geometric parameters of the tool. The study of the end milling of stamped steel is presented in [16]. Edge (initial) tool wear is considered in [17], but the process was considered only for turning cutters. The stabilization of vibrating systems was studied in [18]. It is indicated that stabilization is possible using random parametric excitations. The issue of stabilization of vibrating systems is quite important, but it is individual for each machining process and therefore requires additional research for a particular type of processing. In [19], the surface roughness was also predicted, but in our case, the roughness of lateral surfaces of internal gearing teeth is not a limiting factor, although it is related to the quality of the product. The study of the influence of self-excited vibrations on various main mechanical characteristics of the system “workpiece – tool – material” was carried out, where measurements were performed on a six-component dynamometer [20]. The studies [21, 22] propose different vibration analysis methods for ensuring the reliability of technological processes.

Thus, the investigated works’ analysis shows that researches of various vibration parameters, including vibration acceleration, were considered. However, studies did not concern the gear shaping process in general, not to mention gear shaping the gear ring in bimetallic gear disks with friction coatings personally. The instantaneous magnitude of vibration acceleration can be used to assess the nature of vibration processes occurring during processing and the magnitude of the load on the machine’s main mechanisms. But in the absence of equipment, registration sensors, particularly vibration acceleration, were not considered by researchers, especially when gearing. Therefore, one of the tasks of examining the issue of improving the efficiency of gear shaping of bimetallic disks was the consideration, registration, and analysis of vibration acceleration.

3 Research Methodology

To study gear-shaping gear in bimetallic gear disks with friction coatings, a machine model TOS OHO 50 was used. The main cutting force of gear shaping is directed along the axis of the machine ram. To estimate the load’s magnitude on the machine components, accelerometers 7290A-2 were used, placed, and fixed on the ram and the machine table. The layout of the accelerometers on the machine is given in Fig. 2.

To register the vibration acceleration, the Information Collection System “National instruments mod. NI-9234” was used, which is designed for vibroacoustic research.

The system reads data from the sensors in real-time and transfers it to a personal computer that records and processes data using the program. The NI 9234 is a four-channel dynamic signal acquisition module for highly accurate measurements from IEPE sensors. NI 9234 provides a dynamic range of 102 dB and includes built-in electronics of piezoelectric (IEPE) signal conditioning at a direct current of 2 mA for accelerometers and microphones. Simultaneously, we get four input channels at speeds up to 51.2 Kbyte/s. In addition to that, the module contains built-in anti-aliasing filters, which are

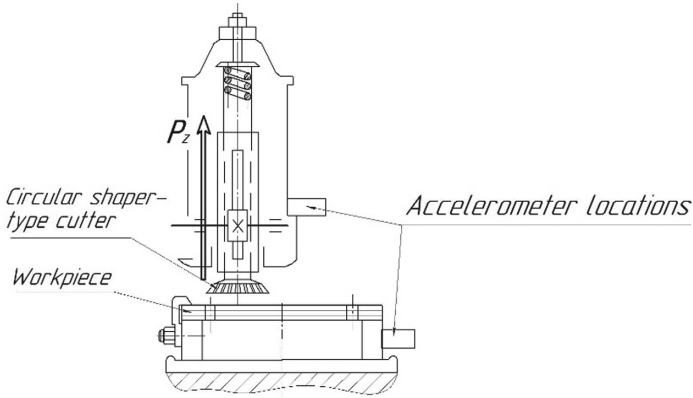


Fig. 2. The layout of accelerometers on a gear-shaping machine.

automatically adjusted to the sampling frequency. Compatible with NI CompactDAQ and CompactRIO single-module USB media, the NI 9234 is used for a wide range of mobile or portable applications, such as industrial machine monitoring, noise, vibration, and stiffness testing. The general view of the experimental installation is shown in Fig. 3.



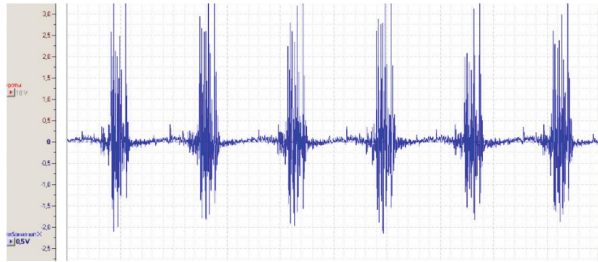
Fig. 3. General view of the experimental installation on the machine model TOS OHO 50.

4 Results

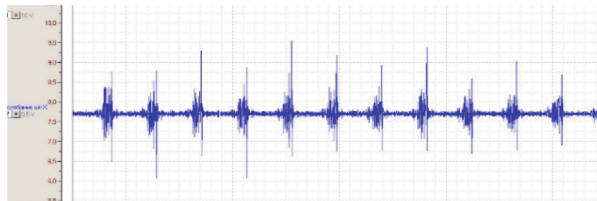
The following cutting modes were selected for the experimental processing of the batch of parts: the number of double runs per minute – 56, 71, 90, 112, 140, 180, 224, circular feed – 0.16, 0.2, 0.25, 0.31, 0.4 mm/dbl.runs/min. According to the experimental processing results, the period of stability of the tool was determined by the following criterion – chamfer wear on the rear surface doesn't exceed 0.3 mm, which was checked by a microscope with the eyepiece division value of 0.1 mm per full rotation of the part.

The amplitudes of the ram vibrations and the table with the fixture for clamping the package of parts were also determined. The research results are presented in Fig. 4 in

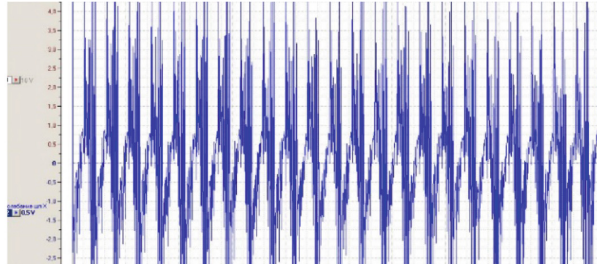
the form of records of the amplitudes of vibration acceleration of the ram for different values of double runs.



a)



b)



c)

Fig. 4. Experimental data of vibration acceleration of the ram: a – at 56 dbl.runs/min.; b – at 112 dbl.runs/min.; c – at 224 dbl.runs/min.

The amplitudes of the ram vibrations depending on the number of dbl.runs/min are given in Table 1.

Table 1. The value of the ram vibrations' amplitudes depends on the number of dbl.runs/min.

Number of double runs, min^{-1}	The amplitude of oscillations of vibration acceleration of the ram, m/s^2
56	3.53
71	2.97
90	1.5
112	1.07
140	3.09

According to the results of experimental data, the minimum amplitude of the ram vibrations is in the range of 5.53 m/s^2 at 56 dbl runs/min of the ram, then it decreases to 1.07 m/s^2 at 112 dbl runs/min, and then increases again to 3.09 m/s^2 at 140 dbl runs/min, i. e. the ram vibrations pass through the conditional minimum of the ram vibration acceleration. In our studies, this minimum was observed at 112 dbl runs/min, with the minimum amplitude of vibrations of the ram equal to 1.07 m/s^2 . With the increasing number of double runs, the machining process occurs with signs of self-exciting vibrations, as evidenced by the deterioration of roughness from 1.6 to 3.2 Ra and roughness of the processed surface of a package of details. It is possible to reduce self-excited vibrations by increasing the mass of moving parts, but such studies are expected to be performed in the future.

An experiment to study the tool stability shows that the main factor influencing stability is the cutting speed, which depends on double runs per minute.

In Table 2, the results of the study of the stability of the shaper-type cutter are given. The circular feed has almost no effect on the stability; however, there is a slight increase of the chamfer wear at minimum and maximum circular feed values.

Table 2. The tool stability (tool life, min) depending on the circular feed of processing in the number of full turns of part with the maximum admissible chamfer wear of 0.3 mm.

Number of double runs, min^{-1}	Circular feed, mm/dbl.runs/min				
	0.16	0.2	0.25	0.31	0.4
Tool stability, min					
56	2	2	2	2	2
71	2	2	2	2	2
90	3	3	3	3	3
112	4	4	6	5	5
140	2	2	3	3	2
180	Less than 1	Less than 1	Less than 1	Less than 1	Less than 1
224	Less than 1	Less than 1	Less than 1	Less than 1	Less than 1

Thus, the most efficient processing mode was experimentally established in terms of the highest tool stability and the lowest value of the ram's vibration amplitude, which is one of the most important factors of the machine's working capacity and durability 112 double runs per minute. Since the tool's oscillation stability is practically independent from the circular feed, except for its minimum and maximum values, it is advisable to choose a value of 0.25 or 0.31 mm/dbl.run to obtain maximum productivity and reduce costs.

The increase of the vibration resistance of the gearing process is possible by expanding the mass of moving parts, which will increase the force of inertia as a force that can counteract the uneven cutting force; it will also increase the resonant frequency, which will ensure the growth of the number of double runs of the ram without self-excited vibrations. Therefore, it is planned to conduct additional research and develop a mathematical model of the studied process.

5 Conclusions

The paper identifies the factors that limit the possibility of processing bimetallic discs with friction coatings on gear shaping machines, i.e., the presence of a friction layer, the stability of the circular shaper-type cutter (within 4–6 min), the maximum cutting speed (up to 25 m/min), and circular feed (within 0.25–0.31 mm/dbl.run).

The industry results' practical significance is to increase the gearing process's efficiency by determining the optimal processing mode on the criterion of maximum productivity and stability of the tool, i.e., the optimal value of the number of double movements affecting vibration resistance of the machining surface roughness.

Efficient processing mode with the maximum number of discs in the package – 9 (disc thickness – 6mm), number of double runs – 112, circular feed – 0.31mm/dbl.run, a number of passes – 1.

To increase the gear shaping process's vibration resistance, it is necessary to ensure the maximum possible cutting speed. For this purpose, it is planned to conduct additional research and develop a mathematical model of the studied process. Also promising is the study of the influence of the mass of moving parts of the machine to increase the inertia force, which can compensate for oscillations in cutting force due to different hardness in the parts package and determine friction layer effect on the processing productivity of bimetallic discs.

References

1. Ershov, D.Y., Zlotnikov, E.G., Timofeev, D.Y.: Analysis of proper fluctuations of technological systems. IOP Conf. Ser. Mater. Sci. Eng. **560**, 012015 (2019). <https://doi.org/10.1088/1757-899X/560/1/012015>
2. Maksarov, V.V., Olt, J.: Dynamic stabilization of machining process based on local metastability in controlled robotic systems of CNC machines. Notes of the Mining Institute, 446–451 (2017). 10.25515. PMI.2017.4.446
3. Wolfson, I.I.: Dynamics of Machines. Fluctuations: Studies Textbook for Academic Undergraduate. Yurayt, Moscow (2017)

4. Zharkov, I.G.: Vibrations during machining with a blade tool. Mechanical engineering, Leningrad (1986). (In Russian)
5. Fojtů, P.: The issue of self-excited oscillations. CVUT, Prague (2009)
6. Babak, V.P., Bilchuk, Ye.Yu., Shchepetov, V.V.: Increased wear coatings due intrastructural self-correction. *J. Eng. Sci.* **6**(1), C11–C15 (2019). [https://doi.org/10.21272/jes.2019.6\(1\).c3](https://doi.org/10.21272/jes.2019.6(1).c3).
7. Doluk, E., Rudawska, A., Stančeková, D.: Effect of the surface treatment on the strength of the single-lap adhesive joints. *Technologia I Automatyzacja Montażu* **1**(2021), 18–22 (2021)
8. Kudinov, V.A.: Self-oscillations at low frequencies (stability of movements) during cutting. *STIN* **2**, 16–22 (1997). [In Russian]
9. Janáč, A., Lipa, Z., Peterka, J.: Theory of machining. Slovak University of Technology in Bratislava (2006)
10. Neslušán, M., Čiliková, M.: Theory of machining. EDIS Žilina (2007)
11. Drozdov, N.A.: On the question of machine vibration during turning. *Mach. Tools* **22**, 10–16 (1937)
12. Ivanov, V., Dehtiarov, I., Pavlenko, I., Liaposhchenko, O., Zaloga, V.: Parametric optimization of fixtures for multiaxis machining of parts. In: Hamrol, A., Kujawińska, A., Barraza, M.F.S. (eds.) *MANUFACTURING 2019. LNME*, pp. 335–347. Springer, Cham (2019). https://doi.org/10.1007/978-3-030-18789-7_28
13. Ivanov, V., Pavlenko, I., Liaposhchenko, O., Gusak, O., Pavlenko, V.: Determination of contact points between workpiece and fixture elements as a tool for augmented reality in fixture design. *Wireless Netw.* **27**(3), 1657–1664 (2019). <https://doi.org/10.1007/s11276-019-02026-2>
14. Panda, A., Olejárová, Š., Valíček, J., Harničárová, M.: Monitoring of the condition of turning machine bearing housing through vibrations. *Int. J. Adv. Manuf. Technol.* **97**(1–4), 401–411 (2018). <https://doi.org/10.1007/s00170-018-1871-7>
15. Salgado, D.R., Alonso, F.J., Cambero, I., et al.: In-process surface roughness prediction system using cutting vibrations in turning. *Int. J. Adv. Manuf. Technol.* **43**, 40–51 (2009). <https://doi.org/10.1007/s00170-008-1698-8>
16. Sonawane, S.A., Pawar, A.P.: Effect of cutting variables of end milling process on surface roughness and machining vibrations. In: Pawar, P.M., Ronge, B.P., Balasubramaniam, R., Vibhute, A.S., Apte, S.S. (eds.) *Techno-Societal 2018*, pp. 661–670. Springer, Cham (2020). https://doi.org/10.1007/978-3-030-16962-6_67
17. Fang, N., Pai, P.S., Mosquera, S.: Effect of tool edge wear on the cutting forces and vibrations in high-speed finish machining of Inconel 718: an experimental study and wavelet transform analysis. *Int. J. Adv. Manuf. Technol.* **52**, 65–77 (2011). <https://doi.org/10.1007/s00170-010-2703-6>
18. Bobryk, R.V., Yurchenko, D., Bratus, A.S.: Suppression of self-excited vibrations by a random parametric excitation. *Nonlinear Dyn.* **90**(3), 1671–1679 (2017). <https://doi.org/10.1007/s11071-017-3756-y>
19. Cahuc, O., K'nevez, J., Gérard, A., et al.: Self-excited vibrations in turning: cutting moment analysis. *Int. J. Adv. Manuf. Technol.* **47**, 217–225 (2010). <https://doi.org/10.1007/s00170-009-2189-2>
20. Bisu, C.F., Gérard, A., K'nevez, J.Y., Laheurte, R., Cahuc, O.: Self-excited vibrations in turning: forces torsor analysis. *Int. J. Adv. Manuf. Technol.* (2008). <https://doi.org/10.1007/s00170-008-1850-5>
21. Pavlenko, I., Trojanowska, J., Ivanov, V., Liaposhchenko, O.: Parameter identification of hydro-mechanical processes using artificial intelligence systems. *Int. J. Mech. Appl. Mech.* **2019**(5), 19–26 (2019)
22. Bisu, C.F., Zapciu, M., Cahuc, O., et al.: Envelope dynamic analysis: a new approach for milling process monitoring. *Int. J. Adv. Manuf. Technol.* **62**, 471–486 (2012). <https://doi.org/10.1007/s00170-011-3814-4>



Penetration Depth of the Critical Temperature into the Workpiece Material During Grinding

Vladimir Lebedev^(✉) , Tatiana Chumachenko , Nataliya Klymenko ,
Olga Frolenkova , and Serhii Yevtifieiev 

Odessa National Polytechnic University, 1, Shevchenko Ave., Odesa 65044, Ukraine

Abstract. The grinding process successfully ensures high accuracy of the part, microgeometry, and geometry, then very often grinding reduces such quality indicators as the phase-structure and stress composition of the processed surface. When grinding, high contact temperatures arise, some of which, called critical, have a negative effect on the part's material and can lead to a change in the phase-structural composition and the stress state. The grinding process must be carried out so that these temperatures do not penetrate to a greater depth than the value of the remaining machining allowance. In this case, negative phase-structural changes occur in the layer of material that is removed. The article describes a technique that calculates the depth of penetration of critical temperatures and adjusts the processing modes so that each subsequent pass does not exceed the metal layer that will be removed.

Keywords: Contact temperature · Critical temperature · Allowance for processing · Phase transformations · Structural transformations · Stress state · Surface layer

1 Introduction

The increasing requirements for the accuracy of machine parts, the use of new difficult-to-machine materials, and hardening technologies have raised effective pure processing of workpieces, giving them the final accuracy and the necessary complex of physical and mechanical characteristics. One of the types of such processing is finishing, in particular, grinding. Abrasive processing is characterized by high productivity and, at the same time, provides a solution to many problems that other technological methods cannot solve. Therefore it is widespread.

However, if grinding successfully ensures high accuracy of the part, microgeometry, and geometry, grinding reduces such quality indicators as the phase-structure and stress composition of the processed surface. The grinding process is characterized by significant temperatures in the zone of contact between the wheel and the workpiece, as a result of which the processed material is subjected to additional, very harmful heat treatment. Different steels and alloys react to additional heating in different ways, depending on the chemical composition, the temperature, and the duration of its exposure. Each steel and alloy has its critical temperature, which causes unwanted transformations.

The grinding operation task is to obtain a high-quality surface free from grinding defects, burns, high tensile stresses, and cracks.

In numerous well-known works, thermodynamic processes taking place during grinding are considered in detail. In particular, critical grinding temperatures have been determined for a wide range of machine-building materials of the “metal alloy” type.

The critical temperature at which hardening burns are formed can be determined from the following considerations [1].

With rapid heating by the grinding temperature of the surface of the hardened steel part above the Ac1 line, the martensitic structure of the surface layer transforms into an austenitic structure. That is, the reverse martensitic transformation takes place. This transformation is all the more facilitated by the fact that as a result of high specific pressures exerted by abrasive grains on the metal surface, the Ac1 point decreases to the region of low temperatures.

Rapid heating of the surface layer is followed by its rapid cooling at rates significantly exceeding the critical quenching rates. Most of the Mf points in these steels are below 20 °C, that is, below the temperature to which the metal is cooled during grinding. As a result, martensitic transformations do not occur completely, as a result of which the structure of austenite of secondary hardening is fixed in the surface layer, which is called the grinding hardening burn.

The final cooling of the austenite structure occurs in the temperature range from 100 to 20 °C, that is, the cooling process ends between the points Ms and Mf, thus, the temperature range until the end of the martensitic transformation do not overlap, which determines the incompleteness of this transformation and the fixation of a significant part of the austenite.

To determine the critical temperature for burns of quenching, it is necessary to clearly understand which transformations occur in hardened steel during heating [1].

Martensite is a non-equilibrium structure that remains due to the low mobility of atoms at room temperature. When this structure is heated (when it comes to carbon steel), four transformations occur in the metal, the essence of which is briefly reduced to the following.

In the temperature range 150–200 °C, two-phase or heterogeneous decomposition of martensite occurs. In this case, the thinnest carbide plates are precipitated in separate areas of the martensitic structure. The thickness of these plates is several atomic layers, and the length is several hundred angstroms. The carbide lattice is coherently connected with the martensite lattice. That is, there is a standard layer of atoms at their boundary. Near the carbide plates, the solid solution is depleted in carbon, as a result of which the tetragonality of martensite decreases. However, due to the low diffusion rate of carbon in this temperature range, the concentration over the grain does not have time to equalize, and in one grain, there are two solid solutions with the same type of lattice but with different carbon concentrations. It is because of this that this mechanism of decomposition of martensite is called two-phase. As a result of the first transformation of tempering, tetragonal martensite turns into cubic, which is called tempering. Thus, the tempered martensite is a heterogeneous mixture of a supersaturated carbon solution in α -iron of an inhomogeneous concentration with non-isolated carbides.

In the temperature range 200–300 °C, the second transformation occurs, characterized by the fact that retained austenite is transformed into tempered martensite. Due to a decrease in the tetragonality of martensite, the compressive stresses acting on the retained austenite decrease.

In the temperature range 300–400 °C, the third transformation of tempering occurs. The diffusion rate of carbon in this temperature range increases significantly, and all of it is released from the α -lattice, forming cementite. As a result of this transformation, a highly dispersed ferrite-cementite mixture is formed, called temper troostite.

In the temperature range 400–600 °C, the fourth transformation occurs, consisting of carbide particles' growth and coagulation. The result is temper sorbitol or temper perlite structure.

From the above, we can conclude that if we talk about the tempering temperature, it is necessary to indicate the type of transformation. If the tempering temperature during grinding is considered the temperature at which the surface layer's martensitic structure completely decomposes, this will be the third tempering transformation temperature. Thus, the critical temperature of burns of quenching is the temperature of the third quenching transformation.

When grinding coated parts, especially ceramic ones, the temperature at the "coating-substrate" interface is of great importance, since in this case, the temperature causes residual stresses that can tear the coating of the substrate. Thus, in this case, the critical temperature will be such that it does not cause residual stresses that can tear off the coating.

A healthy sanded surface can only be obtained if the propagation of the critical temperature from the surface into the part's depth does not exceed the machining allowance. In this case, all thermal defects are formed in the layer of material to be removed. On the first pass, a combination of processing modes is established in which the thermal field of the critical temperature reaches the border of the allowance for processing. Subsequent passes are also performed in modes that ensure that the critical temperature's thermal field is within the remaining allowance.

Purpose – Analytically determine the depth of penetration of the critical grinding temperature into the part from the known surface temperature. Develop a block diagram of a mathematical program for calculating processing modes at which the critical temperature does not go beyond the processing allowance.

2 Literature Review

Considerable literature is devoted to the propagation of the contact temperature thermal field. So in [2], the phase-structural composition of the surface layer of the workpiece being ground is considered, but the critical temperatures and the depth of their penetration, depending on the surface temperature, are not considered.

In [3], reducing the forces and cutting temperatures during grinding are considered, but there is no specific data on the critical temperatures.

In [4], mathematical and physical models for calculating grinding temperatures are given. However, no data is linking critical grinding temperatures with contact temperatures.

In [5], a solution of a two-dimensional heat conduction problem by a numerical method is given. The work describes the process adequately but does not concern the penetration depth of critical temperatures.

The work [6] shows the results of mathematical modeling of thermal processes during grinding. Temperatures on the surface and temperatures propagating deep into the workpiece are calculated. However, the work does not show the critical temperatures and their relationship with the workpiece's surface temperatures.

In [7], the simulation of the temperature field of grinding when ultrasound is applied. It is shown that the temperature and the depth of the thermal field decrease. However, a clear relationship between surface and critical temperatures has not been shown.

The work [8] shows the relationship between temperature and technological processing factors and developed a method for calculating grinding temperatures when using a cup wheel. Critical temperatures are not considered.

In [9], mathematical modeling of the process of grinding a thermal barrier coating is considered. Critical temperatures are shown, which must be avoided, but no analytical expressions are connecting critical temperatures with surface temperatures.

The work [10] shows the solution to the problem of thermal conductivity during grinding, taking into account the pulse nature of the heat flow. A method for calculating the contact and pulse temperatures is given. There is no talking about critical temperatures for various steels.

In [11], the influence of various elements of the grinding regime on temperature is considered. Ways to lower the temperature are recommended. Critical temperatures for different materials are not considered.

In [12], an analytical solution to the problem of calculating the spatio-temporal temperature field in workpieces for various types of grinding with wheels of arbitrary design, taking into account the convective heat exchange of the treated surface with the environment, as well as the results of theoretical and experimental studies of thermal phenomena and the dynamics of the process at round grinding. There are no data on critical temperatures in operation.

In works [14, 15, 20], heat generation's general issues during grinding are considered. However, there is no data on critical temperatures.

3 Research Methodology

In this work, we solve creating a relatively simple and sufficiently accurate analytical expression linking the value of the contact temperature and the depth of penetration of the critical temperature. A program and block diagram for determining the parameters of the grinding mode is developed.

At present, there is a multiply tested expression for determining the surface temperature during grinding under the action of a flat instantaneous source [12], which is quite simple and accurate.

$$T = \frac{1,12 \cdot \eta \cdot q \cdot \sqrt{\tau}}{F \cdot \varepsilon} \cdot \left[e^{\frac{-y^2}{4 \cdot a \cdot \tau}} + y \cdot \Phi \cdot \left[\frac{y}{2 \cdot \sqrt{a \cdot \tau}} \right] \right], \tag{1}$$

where η – the amount of heat transferred into the workpiece during grinding; q – the power of the heat source during grinding; τ – the operating time of the source; F – the area of the contact patch of the wheel with the workpiece, m^2 , ε is the coefficient of thermal activity of the material being ground, $J/(m^2 \cdot K \cdot s^{0.5})$; y – coordinate of the propagation of the thermal field deep into the workpiece, m; a – thermal diffusivity of the workpiece material m^2/s .

For calculating the penetration depth of a specific temperature into the workpiece material, this equation must be solved with respect to y . For obtaining a sufficiently accurate and straightforward solution, it is necessary to analyze the results of calculating the temperature according to Eq. (1) and according to it without the second term in parentheses. For example, let us take the following grinding mode: wheel 25A12SM2K; design No. 6; diameter of a wheel $D = 0.3$ m; longitudinal feed $V_{lf} = 0.15$ m/s; the speed of wheel $V_w = 35$ m/s; transverse feed $S = 0.0015$ m/stroke; depth of grinding $t = 0.03$ mm.

The results showing the surface contact temperature values and their propagation along Y -coordinate are shown in Fig. 1.

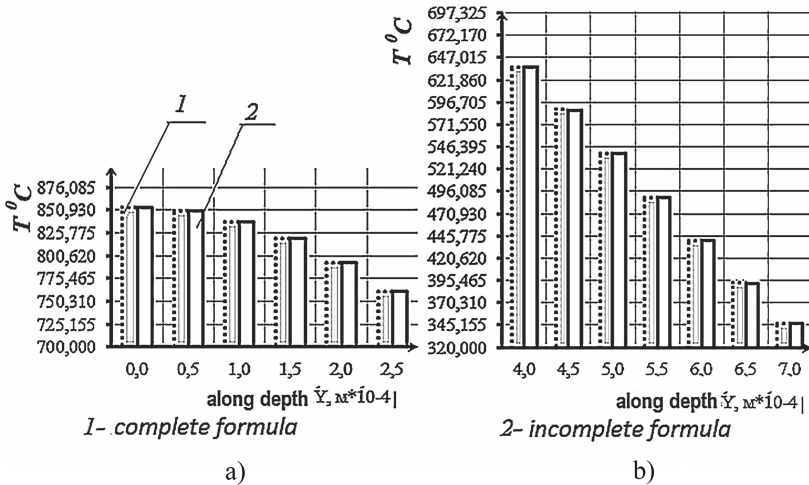


Fig. 1. The results of calculating the grinding temperature and its penetration into the depth of the workpiece 1– complete formula; 2 – incomplete formula without the right side.

As it can be seen, considering a small error, in tenths and hundreds of a degree, the depth of temperature penetration can be calculated using formula 2.

$$T(y) = \frac{1,12 \cdot \eta \cdot q \cdot \sqrt{\tau}}{F \cdot \varepsilon} \cdot e^{\frac{-y^2}{4 \cdot a \cdot \tau}} \tag{2}$$

By taking the logarithm of this expression and carrying out some transformations, it is possible to obtain a relatively accurate and straightforward expression that determines the depth of penetration of the critical temperature into the ground's workpiece. With an accuracy of about 99%, the depth of phase-structure transformations is determined by the expression:

$$y = 2 \cdot \sqrt{a \cdot \tau_{ef} \cdot \ln T_s/T_{cr}} = 2 \cdot \sqrt{a \cdot \tau \cdot \frac{T_s - T_{cr}}{T_s} \ln \frac{T_s + T_{cr}}{2 \cdot T_{cr}}} \tag{3}$$

where $\tau_{ef} = \tau \cdot \frac{T_s - T_{cr}}{T_s}$ is an effective time of thermal action on a given point of the surface; T_{cr} is the critical temperature at which phase or structural transformations begin; T_s is the surface temperature.

The effective time of thermal action is understood as when a temperature equal to or higher than the temperature T_{cr} acted on a given point of the surface. As can be seen from Fig. 2, this time can be determined directly from the heat impulse using the similarity of triangles ABC and DBE.

The effective time of the thermal effect of a temperature exceeding the temperature T_{cr} at which phase and structural transformations occur is somewhat less than the total time of the temperature's thermal effect on a given point. The value of the surface temperature acting during the time τ_{ef} is taken from Fig. 2.

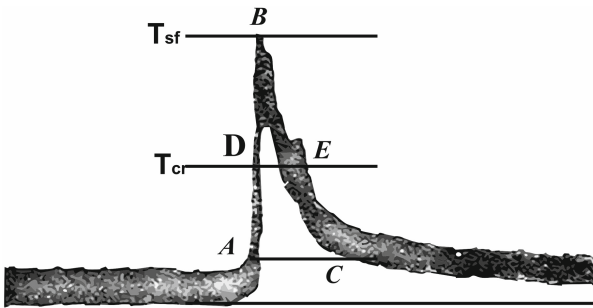


Fig. 2. View of a heat pulse recorded at a low sweep speed.

$$T_s = T_{cr} + (T_s - T_{cr})/2 \tag{4}$$

An estimate of the thermal field's penetration depths with a temperature corresponding to the temperature of structural transformations shows that with different combinations of temperatures and contact times of a given point of the metal with a wheel, the penetration depth of the thermal field will be different. Different modes allowed during processing provide, on the one hand, different temperatures, and on the other hand, different duration of these temperatures, which is reflected in the nature and depth of structural transformations.

The research carried out made it possible to create a program for calculating the processing modes in which thermal defects do not extend beyond the processing allowance. The block diagram of the program is shown in Fig. 3.

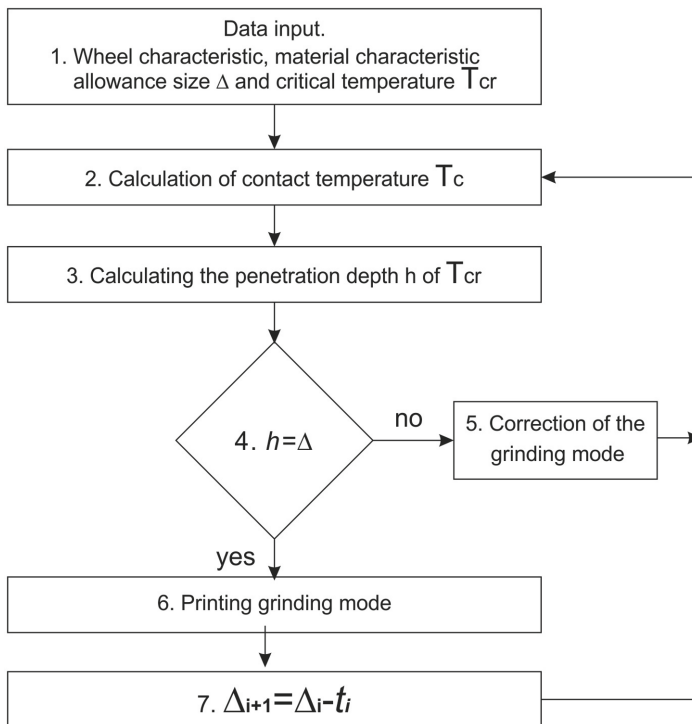


Fig. 3. The block diagram of the program for calculating grinding modes.

The second block is a block for calculating the contact temperature T_c .

The third block is a block for calculating the penetration depth of the critical temperature.

The fourth block is a block for comparing the penetration depth T_{cr} with the machining allowance value.

The fifth block works in the case of inequality h and Δ . In case when $h < \Delta$ the processing modes are tougher. In case when $h > \Delta$, the processing modes are reduced. After that, a new calculation cycle begins from block 2.

The sixth block works after receiving the result from block 4, with an error of 5%. It is used to memorize passage modes.

The seventh block corrects the allowance size taking into account the removed layer. After that, a new calculation cycle begins – block 2. The program runs until the entire allowance is removed.

4 Results

For determining the adequacy of the results obtained, direct experiments were carried out to determine the critical temperature's penetration depth. The research was carried out when grinding hardened steel DIN X12Ni5 – carburized at which hardening burns

(austenitic structure) and tempering burns (pearlite structure) are formed. The studies were carried out in such processing modes that ensure the formation of the above structures. The critical temperature's penetration depth was carried out by the metallographic method under the sources [20–22]. Thus, the thickness of the austenite layer corresponded to the critical burns of hardening temperature, and the thickness of the pearlite structure layer corresponded to the critical quenching burns temperature (Fig. 4).

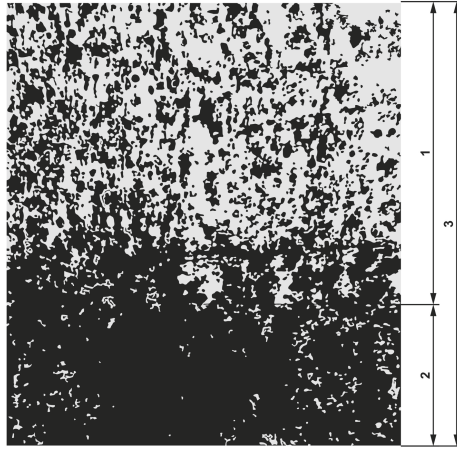


Fig. 4. Structures of hardening and quenching burns after grinding: 1 – hardening burn-in zone - austenite, 2 – quenching burn-out zone - pearlite, 3 – the defect layer's general zone, x150.

Statistical processing of experimental data made it possible to obtain an empirical dependence that links the defect layer's total depth, the processing mode, the thermophysical properties of the material, and the contact surface temperature.

$$y = 10^4 e^{0.03T_s} a^{0.5} v^{0.49} t^{0.25}, \quad (5)$$

where T_s – °C – surface temperature;
 a – coefficient of thermal diffusivity m^2/s ;
 v – longitudinal feed m/s ;
 t – grinding depth m .

Comparison of the calculated and experimental data showed their good convergence.

The results of calculating the processing modes for the case of grinding with pressure cooling are shown below. Treatment modes: wheel 25A12CM2K; No structure 6; $D_w = 0.3$ m; $V_{lf} = 0.15$ m/s; $V_w = 35$ m/s; $S = 0.0015$ m/stroke: cooling soda solution supplied by a pressure jet under a pressure of 6 at. The depth of cut t is distributed over the passes as follows – 0.055; 0.045; 0.045; 0.04; 0.035; 0.03; 0.03; 0.03; 0.025 mm. The contact temperature is equal to the third tempering transformation temperature at each pass, causing the tempering burn, which does not go beyond the remaining machining allowance. The polished parts were controlled by wiping the polished surface with a nitric acid solution in ethyl alcohol.

Quenching burns were not revealed.

5 Conclusions

The data given in the work allow us to assert that the proposed mathematical dependencies and the mathematical program for determining the processing modes adequately reflect the value and law of propagating the contact temperature of grinding into the depth of the workpiece.

The program for determining the grinding modes is implemented in the Math-Cad environment and can be used by engineering and technical departments and shop technologists when organizing production.

This method of calculating the depth of penetration of the critical temperature into the depth of the part can be recommended, first of all, when assigning the modes of grinding of hardened gear wheels, which are sensitive to hardening and quenching burns. The outlined material makes it possible to calculate such modes in which all thermal defects are closed in the machining allowance, which is removed.

When grinding coatings, the described material allows assigning such processing modes when a safe temperature acts on the coating and base metal boundary, causing residual stress that cannot tear the base's coating.

References

1. Gulyaev, A.P.: Metals Science. Alliance Publishing House, Moscow (2011). (in Russian)
2. Lebedev, V., Lugovskaya, E.: Phase-structural composition of the surface layers of parts during grinding. *Technol. Inf. Educ. Sci. Prod.* **3**(8), 204–212 (2015)
3. Novikov, F., Polyansky, V., Shkurupiy, V., Novikov, D., Hutorov, A., Ponomarenko, Y., Yermolenko, O., Yermolenko, O.: Determining the conditions for decreasing cutting force and temperature during machining. *Eastern-Eur. J. Enterpr. Technol.* **6**(1(102)), 41–50 (2019). <https://doi.org/10.15587/1729-4061.2019.183882>
4. Unyanin, A.: Analytical study of local temperatures during grinding. *Proc. Univ. Eng.* **6**, 41–49 (2006)
5. Smirnov, V.: A numerical method for solving a nonlinear two-dimensional problem of heat conduction during grinding. *Modern technologies, system analysis, modeling.* GTU, Irkutsk (2006)
6. Lomova, O.: Mathematical modeling of structural changes in the surfaces of workpieces under thermal disturbances in the process of grinding. *Omsk Sci. Bull.* **2**(120) (2013)
7. Unyanin, A., Sarainov, N.: Simulation of the temperature field during grinding with elbor wheels with the superposition of ultrasonic vibrations. *Bull. TulSU. Series "Tech. Sci."*, **8**(2), 112–120 (2017)
8. Ivanova, T.: Improving the efficiency of surface grinding with the end of the cup wheel based on the control of the heat-stressed state of the working zone. *Sci. Edn. Bauman MSTU Sci. Educ.* **9**, 43–56 (2013). <https://doi.org/10.7463/0913.0606036>
9. Lebedev, V., Frolenkova, O.: Imitation modeling of the grinding process of zro2 thermal barrier coating by circles of synthetic superhard materials. *Prospect. Technol. Devices* **12**, 97–104 (2018). (in Russian)
10. Smirnov, V.: Solution of the heat problem during grinding, taking into account the heat flux's impulsive nature. *Bull. Tomsk Polytech. Univ.* **319**(2), 46–49 (2011)
11. Khusainov, A.: The influence of the grinding mode's elements on the depth of penetration of the heat flux into the surface layer of the workpiece. *Bull. UISTU* **1**(17), 95–99 (2002)

12. Skuratov, D., Trusov, V.: Determination of rational processing conditions in the production of GTE parts. Samara Scientific Center of the Russian Academy of Sciences, Samara (2002)
13. Redko, S.: Heat generation processes when grinding metals. Ed. Saratov University, Saratov (1962)
14. Influence of heat generated during grinding. Library of technical literature. <http://delta-grup.ru/bibliot/39/76.html>. Accessed 10 Nov 2020
15. Kremen', Z.I., Yur'ev, V.G., Baboshkin, A.F.: Grinding technology in mechanical engineering. Polytechnic, St. Petersburg (2015)
16. Aleksandrova, M.Yu., Dobrynin, S.A., Firsov, G.I.: Simulation of the temperature field on the surface of the part during external centerless grinding. Sci. Tech. Dev. Bull. Nat. Technol. Group **10**(14), 46–53 (2008)
17. Kaluba, W., Kaluba, T., Zielinska-Lipiec, A.: Morphological evolutions in steels during continuous rapid heating. Mater. Sci. Forum **539–543**, 4669–4674 (2007)
18. Li, C.H., Ding, Y.C., Lu, B.H.: Innovative technology investigation into integrate the surface hardening process with the grinding precision finishing for cbn grinding crankshaft. In: 4th International Conference on Wireless Communications, Networking and Mobile Computing, Dalian, China, pp. 1–4 (2008). <https://doi.org/10.1109/wicom.2008.3039>
19. Xu, Y.: The role of retained austenite and residual stresses in rolling contact. Digital Commons University of Nebraska, Lincoln (1993)
20. Usov, A.V., Oborsky, G.A.: The effect of thermomechanical phenomena on the stability of cutting process and wear of cutting tools. J. Superhard Mater. **6**, 66–71 (2003)
21. Microsection preparation technique. <https://infourok.ru/laboratornaya-rabota-metodika-pri-gotovleniya-mikroshli-fa-852852.html>. Accessed 10 Nov 2020
22. Microscope MIM-7. <http://mikroskop-1.ru/?name=Mikroskopy~MIM-7&ref>. Accessed 10 Nov 2020



Justification of Technological Possibilities for Reducing Surface Roughness During Abrasive Processing

Fedir Novikov¹ , Dmytro Novikov¹ , Andrii Hutorov² ,
Yevhen Ponomarenko³ , and Oleksii Yermolenko¹ 

¹ Simon Kuznets Kharkiv National University of Economics, 9-A,
Nauky Ave., Kharkiv 61166, Ukraine

² NSC “Institute of Agrarian Economics”, 10, Heroiv Oborony St., Kyiv 03127, Ukraine

³ LTD Business Center “INGEK”, 4-A Bakulina St., Kharkiv 61166, Ukraine

Abstract. This work aims to determine the parameters of surface roughness during abrasive processing analytically and to substantiate the technological possibilities of its reduction in the conditions of transition from the micro-cutting process to the process of elastic-plastic deformation of the processed material. On this basis, the minimum possible values of surface roughness parameters during free abrasive treatment are analytically determined. It is shown that the main way to reduce the surface roughness is to reduce the grain size of the abrasive powder and increase the surface concentration of abrasive grains in the cutting zone. Based on the analysis of the graph of the relative supporting length of the micro-profile of the treated surface experimentally established during abrasive polishing, the significant effect of individual deep scratches on the surface roughness is shown. It is established that they occur as a result of the work of larger grains included in the considered grain fraction with a grain size of 1/0 and the different heights of the grains in the cutting zone. Therefore, it is recommended to use abrasive grains with a small range of their size spread during abrasive polishing and use ovalized abrasive grains, which prevent the formation of deep scratches. The obtained results can be effectively used for abrasive polishing of reflective surfaces of space products that operate under light conditions and require high surface roughness.

Keywords: Abrasive polishing · Micro-cutting process · Ovalized grains

1 Introduction

The essential condition for implementing high-quality mechanical processing of machine parts is to ensure high roughness of the treated surfaces. This is achieved by using effective methods of abrasive processing, including grinding, abrasive polishing, and others. Currently, considerable experience has been accumulated in their application. However, as practice shows, it is quite difficult to consistently achieve a significant reduction in the roughness parameter of the treated surface R_a to the level of $0.01 \mu\text{m}$ (microns) or less, even in conditions of abrasive polishing using an abrasive powder with

a grain size of $1/0$. As a rule, certain deep scratches are formed on the processed surfaces, leading to an increase in the R_a parameter and do not allow to meet the requirements for the quality of processing. This is especially true for the abrasive treatment of reflective surfaces (with minimal values of the R_a parameter) of space products that operate at high temperatures (more than 150 °C) and lose their performance properties due to significant temperature deformations. As practice shows, for their effective use, it is necessary to provide the roughness parameter of the treated surface R_a at a level of fewer than 0.05 μ . In this regard, it is essential to establish the maximum possibilities for reducing the roughness parameter of the treated surface R_a during abrasive processing and developing practical recommendations for their technological support, mainly when processing reflective surfaces of space products.

2 Literature Review

Unlike grinding processes [1, 2], high surface roughness can be achieved under free abrasive treatment conditions [3, 4] (especially during abrasive polishing [5, 6]) using fine-grained abrasive powder [7]. In this case, the processing efficiency is mainly related to ensuring the actual single-layer arrangement of abrasive grains in the cutting zone and excluding their different heights [8].

It is possible to reduce the surface roughness during abrasive polishing by smoothing the surface layer of the part [9, 10]. This is important for achieving high roughness of the treated surfaces during abrasive polishing and creating optical (reflective) properties [11, 12]. For a complete understanding of the possibilities of abrasive polishing in works [13, 14], the regularities of surface roughness formation during abrasive processing are described analytically from the standpoint of probability theory. This allowed us to theoretically justify the main conditions for surface roughness reduction and develop practical recommendations for their technological support [15, 16]. The possibility of reducing the roughness parameter of the treated surface R_a while simultaneously increasing the processing performance and reducing the cutting temperature under deep grinding conditions is shown [17], which is an essential factor in improving abrasive processing efficiency. Simultaneously, there are no theoretical solutions in the scientific and technical literature that allow us to estimate the maximum possibilities of reducing the R_a parameter during abrasive processing. As shown in work [18], they can be achieved under conditions of transition from the micro-cutting process to the process of elastic-plastic deformation of the processed material without chip formation. However, this requires further research to establish the regularities of surface roughness formation during abrasive processing – in the conditions of abrasive polishing.

3 Research Methodology

For solving this problem, it is necessary to set the minimum achievable values of the surface roughness parameter R_a , at which the micro-cutting process stops and the process of elastic-plastic deformation of the processed material begins. This requires an analytical determination of the surface roughness parameter R_a and establishing its relationship with the limit value of the ratio of the cut thickness a_z to the radius of rounding of

the abrasive grain R (i.e., the ratio a_z/R), at which there is a transition from the micro-cutting process to the process of elastic-plastic deformation of the processed material. It is also essential to establish the relationship between the height parameters of the surface roughness Ra and R_{max} under abrasive polishing conditions analytically. This will allow us to theoretically justify the main ways to reduce surface roughness and make an experimental assessment of the results' reliability. As an evaluation criterion, it is necessary to use the relative reference length of the micro profile of the treated surface, which is a comprehensive characteristic of the surface roughness parameters. The results will allow us to develop practical recommendations for choosing rational conditions for abrasive processing that provide the lowest values of the surface roughness height parameters.

4 Results

The calculation of the maximum height of the micro-roughness of the treated surface (the surface roughness parameter R_{max}) is based on the calculation scheme of the processing process with abrasive grains of the same size (radius R) with their single-layer arrangement and overlap by the value Δ (Fig. 1).

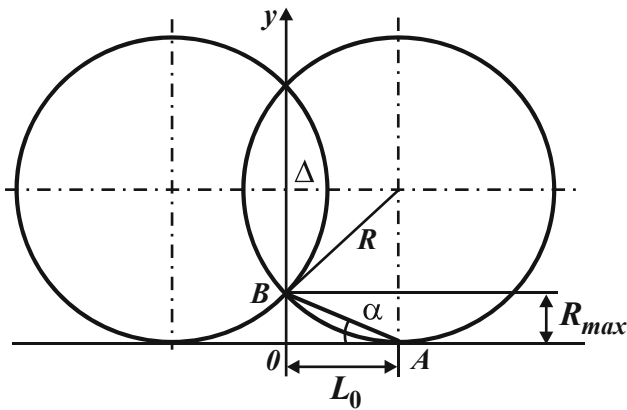


Fig. 1. Calculation scheme of the processing process with abrasive grains of the same size.

In this case, the surface roughness parameter R_{max} is determined by the segment of OB . For simplifications, the arc of the circle AB can be replaced with a straight-line AB due to the small value of the surface roughness parameter R_{max} .

Figure 2 shows a graph of changes in the reference length of the micro-profile of the treated surface $L(y)$, formed within half the distance between two adjacent abrasive grains $L_0 = R - \Delta$. The angle α is determined from the ratio: $tg\alpha = R_{max}/L_0$, where $L_0 = \sqrt{R^2 - (R - R_{max})^2} \approx \sqrt{2R \cdot R_{max}}$.

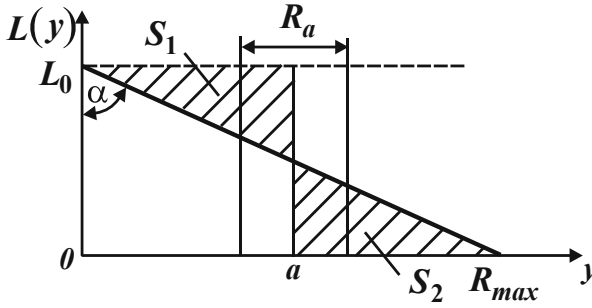


Fig. 2. Graph of changes in the reference length of the micro-profile of the treated surface $L(y)$.

To determine the surface roughness parameter R_a , at first, set the position $y = a$ of the midline of the micro profile of the treated surface from the condition that the areas S_1 and S_2 are equal (at Fig. 2, they are shaded):

$$S_1 = \frac{a^2}{2tg\alpha}, \tag{1}$$

$$S_2 = \frac{(R_{max} - a)^2}{2tg\alpha}. \tag{2}$$

Comparing the areas of S_1 and S_2 , we get $a = 0.5 \cdot R_{max}$.

The surface roughness parameter R_a is determined from the condition: $0.5 \cdot R_a = S_1/L_0$ (Fig. 2). Then $R_a = 0.25 \cdot R_{max}$.

As it can be seen, the surface roughness parameter R_a does not depend on the angle α and is 4 times less than the surface roughness parameter R_{max} . Accordingly, the ratio $R_{max}/R_a = 4$, which is consistent with the known experimental data given in the scientific and technical literature [15, 16], mainly when applied to the grinding processes.

Obviously, with an increase in the value of Δ (Fig. 1), the surface roughness parameters R_a and R_{max} will decrease, and their ratio will remain constant, equal to $R_{max}/R_a = 4$. The R_{max} parameter can be set from the condition:

$$(R - R_{max}) = \sqrt{R^2 - L_0^2}. \tag{3}$$

Then, after the conversions, it is obtained:

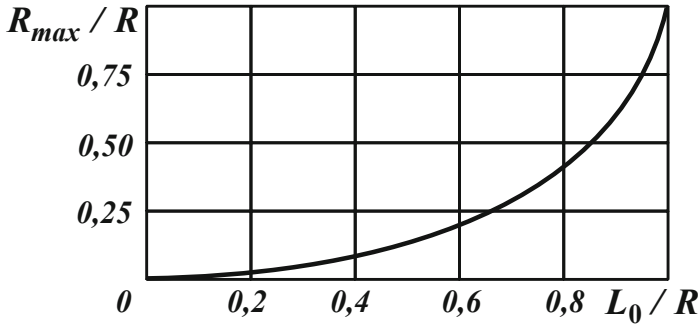
$$R_{max} = \frac{L_0^2}{\left(R + \sqrt{R^2 - L_0^2}\right)}. \tag{4}$$

In a generalized form, dependency (4) takes the form:

$$\frac{R_{max}}{R} = \left(\frac{L_0}{R}\right)^2 \cdot \frac{1}{\left[1 + \sqrt{1 - \left(\frac{L_0}{R}\right)^2}\right]}. \tag{5}$$

Table 1. The calculated values of the R_{max}/R ratio.

L_0/R	0.000	0.200	0.400	0.600	0.800	1.000
R_{max}/R	0.000	0.020	0.083	0.200	0.400	1.000

**Fig. 3.** The dependence of the ratio R_{max}/R from the ratio L_0/R .

As follows from dependency (5), Table 1 and Fig. 3, with a decrease in the L_0/R ratio, the R_{max}/R ratio decreases approximately in a parabolic relationship, i.e., quite intensively. Therefore, the primary condition for reducing the parameter R_{max} should be considered a decrease in the parameter L_0 by increasing the number of simultaneously working abrasive grains with their single-layer arrangement (Fig. 1), as well as by reducing the radius of the abrasive grain R . Due to this, the value $L_0 \rightarrow 0$ and, accordingly, $R_{max} \rightarrow 0$.

The surface roughness parameter R_{max} in the limit takes a value equal to the thickness of the cut with a separate abrasive grain (Fig. 1). Accordingly, the a_z/R ratio is analytically described by the dependence (5). According to the experimental data of professor I. Kragelsky, given in [19], the micro-cutting process is feasible under the condition $a_z/R = 0.14... 0.17$. At lower values of the a_z/R ratio, only elastic-plastic deformation of the processed material occurs without the formation of microarrays. Therefore, the lowest values of the R_{max} parameter can be achieved in the conditions of transition from the micro-cutting process to the process of elastic-plastic deformation of the processed material. Based on the conditions $R_{max}/R = 0.17$ and $R_{max}/R_a = 4$, we have $R_a = 0.0425 \cdot R$. If we take $R = 0.5 \mu$ (for a grain size of $1/0$), then $R_a = 0.021 \mu$.

If $a_z/R = 0.17$, the limit value of the ratio L_0/R , according to dependence (5), is 0.185 . Therefore, 5.4 times more abrasive grains should be involved in the micro-cutting process at the same time than in the case of $L_0/R = 1.0$. From this, you can set the required number of abrasive grains located on the unit area of the working part of the abrasive tool, which will provide processing with the specified values $a_z = R_{max}$ and $R_a = 0.25 \cdot R_{max}$.

Given the expression $L_0 = R - \Delta$, we have $L_0/R = 1 - \Delta/R$, from which the ratio is determined:

$$\frac{\Delta}{R} = 1 - \frac{L_0}{R} = 0,815. \tag{6}$$

According to the experimental data of Professor N. Bogomolov, given in [19], the limit values of a_z/R , at which the micro-cutting process is carried out, vary within 0.04–0.08. In this case, the surface roughness parameter R_{max} can take even lower limit values: $R_{max} = (0.04–0.08) \cdot R$. Accordingly, the surface roughness parameter

$R_a = (0.01–0.02) \cdot R$. If we take $R = 0.5 \mu$ (for a grain size of 1/0), then $R_a = 0.005–0.010 \mu$. To meet this condition, an even greater number of abrasive grains must participate in the micro-cutting process than in the previous case, established by professor I. Kragelsky. This is achieved by increasing the surface concentration of grains or reducing the processing performance (for example, reducing the pressure in the processing zone during abrasive polishing).

Figure 4 [19] shows experimentally established graphs of changes in the relative reference length of the micro-profile of the treated surface t_p of samples made of AMr4 alloy after their processing by various methods, including after abrasive polishing with ACM 1/0 paste (i.e., with a grain size of 1/0). Processing mode: the circumferential speed of the polisher is 50 m/s; the specific pressure is 500 kPa.

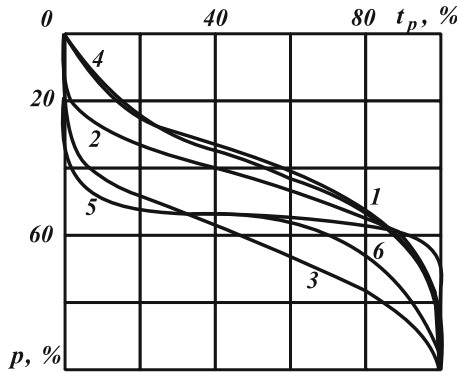


Fig. 4. Relative reference lengths of the micro profile of the treated surface of samples made of AMr4 alloy after different processing methods: 1 – rolled (initial surface); 2 – waterjet processing; 3 – fine turning; 4 – milling; 5 – abrasive polishing; 6 – diamond turning.

Figure 5 schematically shows a simplified view of this graph obtained after abrasive polishing, where $\bar{L}(y) = L(y)/L_0$ is the relative reference length of the micro – profile of the treated surface; L_0 is the base length of the micro profile of the treated surface, mm. it should be noted that AMr4 alloy is used for manufacturing products with reflective surfaces for space purposes.

From Fig. 5, it follows t_p that the function initially increases slightly along the Oy axis, and then when the $y = a$ position is reached (i.e., the midline of the micro profile of the treated surface), it increases intensively at an angle close to 90° to the Oy axis. In the

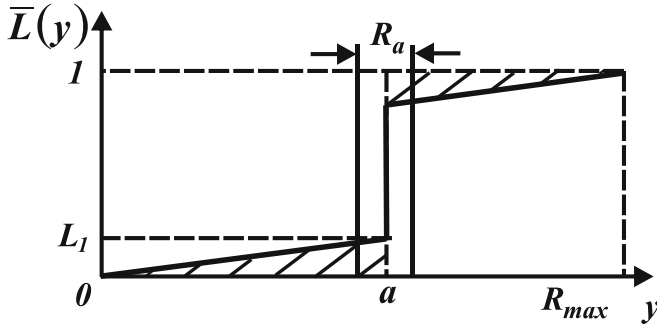


Fig. 5. The type of simplified function $L(y)$.

final section, the function t_p under consideration asymptotically tends to a single value. The surface roughness parameter R_a , in this case, is determined by the initial and final sections of the function t_p (in Fig. 5, they are shaded). Then from the condition $0.5 \cdot R_a = 0.5 R_{max} \cdot L_1$, we have:

$$\frac{R_{max}}{R_a} = \frac{1}{L_1}, \tag{7}$$

where L_1 is a dimensionless quantity ($L_1 \ll 1$).

As it can be seen, the ratio R_{max}/R_a , in this case, is much greater than one. This is confirmed by experimental data [19], according to which the ratio $R_{max}/R_a = 30.3$;

$R_a = 0.1 \mu$; $R_{max} = 3.03 \mu$. Accordingly, the dimensionless value.

$L_1 = 0.033$, i.e., $L_1 \ll 1$. This type of change in the R_{max}/R_a ratio is due to individual deep scratches on the treated surface, which are formed by larger grains that are part of the grain fraction. Second, the location of the abrasive grains at different heights. This is also consistent with the research results reported in the papers [20, 21].

Therefore, the spread of grain sizes and their different heights in the cutting zone is associated with the presence on the graph (Fig. 5) of two sufficiently extended sections characterized by a slight change in the function $\bar{L}(y)$ along the Oy axis. Obviously, by reducing the number of larger grains in the total mass of grains involved in the micro-cutting process, it can be significantly reduced the initial and final sections of the function $\bar{L}(y)$ in Fig. 5. Ideally, the function $\bar{L}(y)$ takes the form of a straight line that coincides with the middle line $y = a$. In this case, the ratio $R_{max}/R_a = 4$ (according to Fig. 2), and the surface roughness parameter $R_a \rightarrow 0$.

Thus, it is theoretically and experimentally established that during abrasive polishing, the surface roughness parameter R_a can be reduced to the lowest possible value by 1) reducing the range of variation in the size of the grain fraction used for processing; 2) ensuring the transition from the micro-cutting process to the process of elastic-plastic deformation of the processed material. In this regard, an essential condition for reducing the R_a parameter should be considered the use of oval-shaped abrasive grains that exclude the formation of deep scratches on the treated surfaces. In the course of experimental studies of abrasive polishing with the use of ovalized abrasive grains (1/0 grain size), it was found that the surface roughness parameter R_a decreases to a value of 0.01μ .

This is quite consistent with the above theoretical data for the considered case $a_z/R = 0.04-0.08$ (according to the experimental data of professor N. Bogomolov) as a result, as established experimentally, the light-reflecting properties of the treated surface of samples made of AMr4 alloy are provided, due to high surface roughness.

5 Conclusions

The paper presents analytical dependences for determining the parameters of surface roughness during abrasive processing. It is shown that when processing with a free abrasive, the main conditions for reducing surface roughness are: reducing the grain size of the abrasive and increasing the surface concentration of grains in the cutting zone. It is established that the lowest values of the height parameters of the surface roughness during abrasive polishing are achieved under the condition of transition from the micro-cutting process to the process of elastic-plastic deformation of the processed material. This is confirmed by the experimental studies of the relative reference length of the micro-profile of the treated surface of samples made of AMr4 alloy after their processing by abrasive polishing with ACM 1/0 paste.

The roughness of the treated surface mainly depends on the presence of individual deep scratches on it-scratches formed as a result of the work of larger grains present in the bulk of the grains and the different heights of the grains in the cutting zone. Therefore, it is necessary to reduce the range of grain size spread used for processing and use abrasive grains of ovalized shape to eliminate them. The research results are recommended for use in abrasive polishing of reflective surfaces of space products that reduce the light effect and the probability of temperature deformations of products by reducing the surface roughness.

References

1. Jeevanantham, S., Sivaram, N.M., Robinson Smart, D.S., Nallusamy, S.: Optimization of internal grinding process parameters on C40E steel using taguchi technique. *Int. J. Appl. Eng. Res.* **12**(19), 8660–8664 (2017)
2. Karkalos, N.E., Kundrák, J., Markopoulos, A.P.: Assessment of the performance of neural networks models for the prediction of surface roughness after grinding of steels. *Int. J. Artif. Intell.* **15**(1), 55–75 (2017)
3. Klocke, F.: *Manufacturing Processes 2. Grinding, Honing, Lapping*. Springer, Berlin (2009)
4. Zverintcev, V.V., Zavershinskaia, I., Tiaguseva, I., Zverintceva, L.V.: The physical nature of the abrasive polishing process. *Curr. Probl. Aviat. Cosmonaut.* **1**(10), 11–12 (2014)
5. Fu, G., Chandra, A.: A model for wafer scale variation of material removal rate in chemical mechanical polishing based on viscoelastic pad deformation. *J. Electron. Mater.* **31**(10), 1066–1073 (2002)
6. Wang, Y.G., Zhao, Y.W., Li, X.: Modeling the effects of abrasive size, surface oxidizer and binding energy on chemical mechanical polishing at molecular scale. *Tribol. Int.* **41**, 202–210 (2008)
7. Kim, J.-S., Lim, E.-S., Jung, Y.-G.: Determination of efficient superfinishing conditions for mirror surface finishing of titanium. *J. Central South Univ.* **19**, 155–162 (2012)

8. Serhieiev, O.S., Andilayah, O.O.: Theoretical analysis of technological possibilities of reducing surface roughness at abrasive processing. Reporter of the Priazovskiy State Technical University. Section: Technical Sciences, vol. 39, pp. 86–93 (2019)
9. Shkurupiy, V.G., Nazarov, I.: Smoothing of the surface layer of copper and aluminum parts during their abrasive polishing. *Prot. Metall. Mach. Breakdowns* **12**, 281–286 (2010)
10. Shkurupy, V.: Roughness of processed surfaces under abrasive polishing. *Rev. Fiabil. Durab.* **2**, 149–155 (2017)
11. Koroleva, L.F.: Nanoparticulate zirconia-modified solid solutions of aluminum-iron oxides for polishing titanium metal. *Diagn. Resour. Mech. Mater. Struct.* **1**, 90–102 (2015)
12. Kacalak, W., Szafraniec, F., Tandecka, K.: Analysis of the active abrasive grains in the films abrasive finishing process. *Mechanik* **90**(10), 885–887 (2017)
13. Novoselov, Y.: *Dynamics of Surface Shaping in Abrasive Processing*. LAP LAMBERT Academic Publishing, Saarbrücken (2017)
14. Korolev, A.A.: *Modern Technology of Shaping Superfinishing of Complex Profile Parts Surfaces*. Saratov State Technical University, Saratov (2001)
15. Sergeev, A.S.: Substantiation of efficiency of application of abrasive machining to reduce surface roughness. *Bull. Natl. Tech. Univ. “KhPI”. Ser. Tech. Mach. Ind.* **1**(1), 19–23 (2020)
16. Novikov, F., et al.: Determining the conditions for decreasing cutting force and temperature during machining. *Eastern-Eur. J. Enterp. Technol.* **6**(1), 41–50 (2019)
17. Matarneh, M.E.: Improvement of abrasive and edge cutting machining efficiency through theoretical analysis of physical conditions. *Int. J. Mech. Prod. Eng. Res. Dev.* **8**(2), 249–262 (2018)
18. Bratan, S., Kolesov A., Roshchupkin, S., Stadnik, T.: Theoretical-probabilistic model of the rotary belt grinding process. In: *MATEC Web Conference*, vol. 129, p. 01078 (2017)
19. Novikov, F.V., Shkurupiy, V.G.: *Fundamentals of Processing Metal Products with Optical Properties*. Simon Kuznets Kharkiv National University of Economics, Kharkiv (2015)
20. Dodok, T., Cubonova, N., Cisar, M., Kuric, I., Zajacko, I.: Utilization of strategies to generate and optimize machining sequences in CAD/CAM. *Procedia Eng.* **192**, 113–118 (2017)
21. Kuric, I., Cisar, M., Tlach, V., Zajačko, I., Gál, T., Więcek, D.: Technical diagnostics at the department of automation and production systems. In: Burduk, A., Chlebus, E., Nowakowski, T., Tubis, A. (eds.) *ISPEM 2018. AISC*, vol. 835, pp. 474–484. Springer, Cham (2019). https://doi.org/10.1007/978-3-319-97490-3_46



Geometric Modeling of Lathe Cutters for Turning High-Precision Stainless Steel Tapered Threads

Oleh Onysko¹ (✉) , Iulia Medvid¹ , Vitalii Panchuk¹ , Vesna Rodic²,
and Cristian Barz³ 

¹ Ivano-Frankivsk National Technical University of Oil and Gas, 15, Karpatska St.,
Ivano-Frankivsk 76019, Ukraine
o.onysko@nung.edu.ua

² Independent University of Banja Luka, 12, Veljka Mladenovica St., 7690 Banja Luka,
Bosnia and Herzegovina

³ Technical University of Cluj-Napoca, North University Center of Baia Mare, 62A,
Victor Babes St., 430083 Baia Mare, Romania

Abstract. The profiling of high-precision tool-joint tapered threads is performed according to an algorithm based on a convoluted screw model, which is functionally dependent on the cutter's geometric parameters and the size of the thread itself. It is proved based on visualization of algorithm that effective production of exact tapered thread from stainless steel is possible only using cutters with a specially calculated profile based on interpolation of a hyperbolic curve. There is created an acceptable geometric model for the cutting part of the thread cutter, the profile of which is a function of the back rake angle. Based on the visualization, it is confirmed that the axial profile of the sides of the tool-joint thread made by the cutter with a non-zero back rake angle is actually curved. On the example of algorithmic calculation of shaping by turning the tool-joint tapered thread size 2 7/8 Reg, it is determined that the use of the cutter model with a back rake angle of 12° and with a usual profile of the cutting edge causes the exceeding of the nominal thread profile side half profile angle by 3–10%, which gives grounds for the use of cutters without correction of their edge profile.

Keywords: Threading lathe tool · Rake angle · Drilling tool joint · Geometric modeling · Convoluted screw

1 Introduction

Tapered thread tool joints used for oil and gas drill-string and pipe casing are very offended with the aggressive carbon-dioxide gas environment. It imposes high requirements on the high-precision construction, anti-vibration protection, and anti-corrosion properties of the tool-joints material on the one hand and increased operational requirements for their tightness on the other. Nowadays, this has created many design problems

for the drill string tool joints themselves and actually for the cutting tool for their manufacturing. The most important issue is to ensure efficient turning of high-precision threads from hard-machined high-alloy steel with significant anti-corrosion properties. This problem is solved by using the appropriate materials of the cutting part of the lathe tool, which are made in the form of carbide inserts. However, manufacturers of inserts designed to form oil and gas tapered threads do not resort to the variability of their geometric parameters, though they are crucial for the cutting process. Obviously, this is due to the lack of a methodology and a convenient algorithm for calculating these cutting inserts' profiles, guaranteeing the resulting cut's high accuracy.

2 Literature Review

Many scientific researches in which the dependence of mechanical properties of threaded connections on their manufacturing accuracy are detected using theoretical [1] and experimental [2] approaches. Many works offer constructive solutions to increase the efficiency of drill-string connectors [3] and drilling tools in general [4, 5]. Vibration protection devices described in the articles [6–8] are designed to reduce the total load on the threaded connections of drill strings. The self-unscrewing threaded joint equipped with a spring-loaded collet is offered as a means of combating [9]. The surface strengthening of the thread surface with layered functional-gradient compositions characterized by high resistance to localized loads is also important [10–12]. The work [13] shows the negative impact of the leakages in the drill-string tool joints due to the tapered thread imperfection on their durability in aggressive environments. Among the studies, some prove the need for special methods and computer programs for the design of thread lathe tools for turning high-precision threads. Such analytical studies include the author's works of this study [14, 15]. However, the paper [14] describes the surface contact pressure in the dependence on the profile and the threading turning's geometric parameters. The analytical study of the kinematic rake angles distribution at the cutting edge of lathe tool for tapered thread manufacturing is represented in [15], but the thread accuracy is not investigated. Those investigations emphasize that the technology of turning difficult-to-machine materials requires cutters with a negative back rake angle. Simultaneously, the works [16] refer to using high-strength and stainless steel for manufacturing oil and gas pipes using a positive value rake angle.

The report [17] concerns a data acquisition system with the final idea of measuring the cutting force in the threading process done on a conventional lathe. But their analytical models are used to find the machining tool's depth of cut, not considering the conditions of different values of the back rake angle. Several stainless steel turning tests are conducted in the paper [18], but it mainly focuses on the lubrication method's influences on the thread precision. The analysis obtained in [19] defines that the thread profile precision could be essentially affected by the cutting tool's position active edges relative to the workpiece, but the back rake angle on the thread profile error isn't investigated in it. The work [20] aims to simulate a three-dimensional orthogonal cutting operation using FEM software to study the effects of rake angle on the cutting process. The results show the increase in the rake angle from negative (-15°) to positive angle ($+15^\circ$), causing the decrease in cutting force, effective stress, and total Von Mises strain.

But these studies do not aim at the accuracy of the thread. The paper [21] describes the machining of a thread with the desired lead, depth, undercut angle, and taper angle while also producing segmented chips, which is important for heavy machining stainless steel. But there is not any information about rake angle influence on the thread accuracy in it. Study of the measuring accuracy in terms of the thread parameters: profile angle and profile shape are provided in the article [22]. But monitoring algorithm does not include the values of the rake angle as input data.

The effect of the rake angle and the edge preparation of c-BN tools on the sub-surface displacement field, which has been experimentally investigated by using DIC, are presented in the paper [23], together with an analysis on the origins of the strains in hardened steel workpiece and chips. In work [24], a cutting energy-based tool wears geometrical model is proposed. Based on the cutting force’s prediction, the cutting energy consumption in the turning is estimated, but the offered geometrical model’s accuracy is absent.

The study [16] is about 13% Cr stainless steel has good comprehensive performance. This makes it suitable to work under the condition of high pressure, high temperature, and corrosive environment. It can be used as a material for petroleum pipes. The thread turning is heavy-load machining, which places a high requirement on the cutting equipment. The machinability of 13%Cr stainless steel was studied by turning experiments. Experimental results show that less cutting and longer tool life were acquired for the insert with a rake angle of $+12^\circ$ during the 13% Cr stainless steel buttress thread turning process [16].

2.1 The Geometry of a Regular Threading Tool

Therefore, it is necessary to analyze the current state of affairs with cutters for the production of threads in the oil and gas sector, particularly in drilling. Figure 1 schematically shows a lathe tool whose cutting edge profile corresponds to the drill-string thread profile. Therefore, it has a zero value of the back rake angle.

This approach is practiced by the vast majority of tool manufacturers [25], apparently because they do not calculate the cutting edge profile.

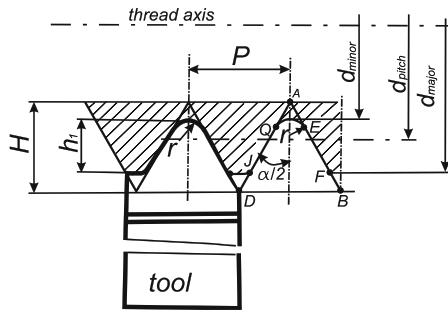


Fig. 1. Schema of the threading machining with a zero rake angle lathe tool: P – thread pitch, H – the height of a fundamental triangle, h_1 – thread height, d_{minor} – minor thread diameter, d_{pitch} – pitch diameter, d_{major} – major thread diameter, $\alpha/2$ – half profile angle, r – root radius.

Therefore, the work aims to create an acceptable geometric model for the cutting part of the thread cutter, the profile of which is a function of the back rake angle and basing on the model is to create a software interface that can be used to make high-precision tapered threads from different materials, including stainless steel.

3 Research Methodology

The thread’s accuracy is determined by its pitch (P) and profile angle (α). The cutter’s geometry determines them if its back rake angle is zero (Fig. 1). The standard API spec 7–2 states that the accuracy of the half profile angle of 30° is $\pm 40'$.

The lathe threading cutter has a non-zero value of the bake rake angle γ (Fig. 2a) that its cutting edge must be a hyperbolic profile or interpolated rectilinear profile based on the hyperbola (Fig. 2b). Therefore, the profile of such a cutting $gmjk$ does not coincide with the profile of the standard thread $dndb$ (Fig. 2b).

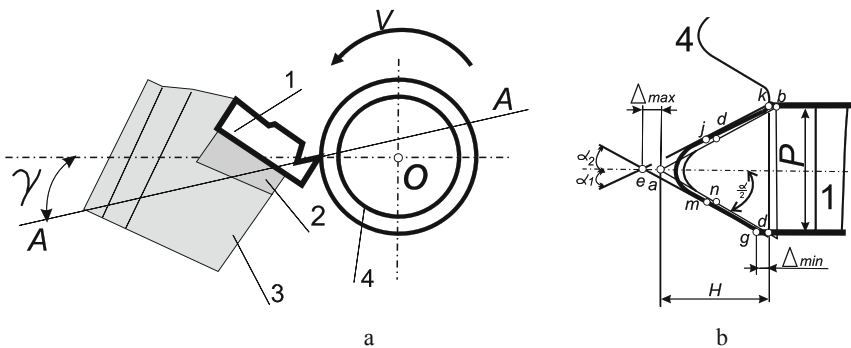


Fig. 2. Layouts for explaining the cutting keg profile interpolated based on hyperbola $kjemg$: 1 – carbon-cutting insert, 2 – anvil, 3 – lathe tool, 4 – workpiece, V – rotate vector.

The rectilinear interpolation is a necessary technological technique for easy making the cutting edge. So it is rectilinear profile keg in-plane A-A is of correct shape (Fig. 2). Therefore, the equation should be used to determine the profile of the cutting edge:

$$\alpha_1 = \alpha_2 = 2 \arctan\left(\frac{P}{2(\Delta_{min,max})}\right), \tag{1}$$

where:

$$\Delta_{max} = \frac{\left(\frac{d_{min.or}}{2} - b\right) \sin^2 \gamma}{2(1 + \cos \gamma)} ;$$

$$\Delta_{min} = \frac{\left(\frac{d_{min.or}}{2} - b\right)^2 \sin^2 \gamma}{\left(\frac{d_{major}}{2} + f\right) + \sqrt{\left(\frac{d_{major}}{2} + f\right)^2 - \left(\frac{d_{min.or}}{2} - b\right) \sin^2 \gamma}} ;$$

b, f – values from standard API spec 7-2.

To ensure the accuracy of the tapered threads during manufacturing with lathe tool, it suggests the following: In turning with a non-zero value of the rake angle, a convolute screw is formed. It means that not an Archimedean screw surface regulated by the standard *API spec 7-2* is received (Fig. 3).

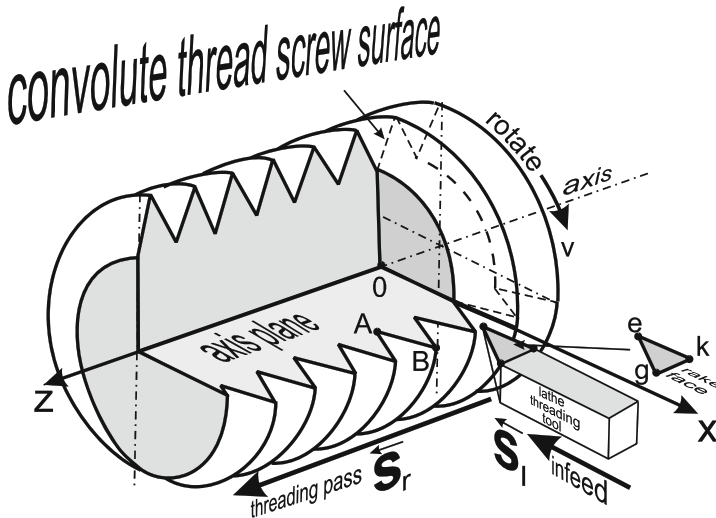


Fig. 3. The scheme of forming a convoluted surface is cut by a cutter with a positive back rake angle. The rake face includes a profile *keg*.

Figure 3 shows that the surface of the screw, which is formed due to the lathe tool infeed and workpiece rotation. Due to the axial displacement, that means the plate of the rake face *keg* does not parallel the screw axis plane; the convolute helical surface is formed.

The following expressions are the theoretical basis of the method of calculating the convoluted screw axial profile:

$$Z(x) = tg(\alpha_1)x \frac{\sin \tau}{\sin \gamma} - \frac{P\tau}{2\pi}, \tag{2}$$

where $\tau = \gamma - \arcsin\left(\frac{d_{min.or}}{2x} \sin \gamma\right)$.

α_1 – from Eq. (1).

Since expression (2) is not algebraic but transcendent, it is necessary to predict the behavior of the machined thread’s profile, i.e., with a given accuracy, to obtain the coordinates of a given number of its points. Figure 4 shows the threading scheme according to the standard with the inclusion of the Cartesian coordinate system. The X-axis (mm) is directed radially, and the Z-axis (mm) is along the thread axis (Fig. 4).

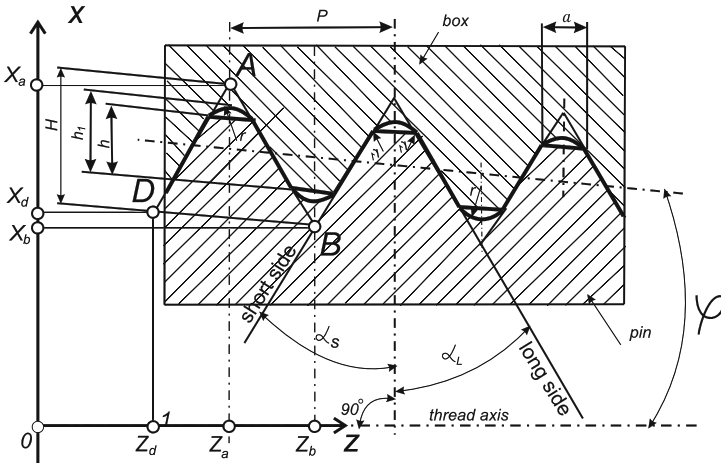


Fig. 4. Scheme of the standard tool-joint tapered thread with a Cartesian coordinate system.

4 Results

Figure 5 presents the compute program’s fragment for calculating the thread profile coordinates using formula (2). Input data: drill-string tapered thread of size 2 3/8 REG, X- iteration step of 0.25 mm. It includes the profile coordinate table (above) and profile diagram after them (below). The upper graph OZ_2 (green) corresponds to the thread profile, which is formed by the model of the cutter with a normal profile and back rake angle $\gamma = 70^\circ$. The bottom lines: the red line OZ_1 corresponds to the standard; the blue curve OZ corresponds to the profile made by the model of the cutter, which has the following geometric parameters: back rake angle $+12^\circ$, profile angles: $\alpha_1 = 12.56^\circ$, $\alpha_2 = 13.14^\circ$

As can be seen from the diagram for a large value of the rake angle, the thread’s axial profile is very different from the standard. However, the blue line corresponding to the modernized cutter’s profile with an angle of 12 is placed much closer to the standard (red). So, it is quite obvious to accept such a line as a straight line, and the formulas should, in this case, calculate the half-angle of the profile that it forms:

$$\alpha_s = \arctg\left(\frac{|z_a - z_d|}{|x_a - x_d|}\right). \tag{3}$$

$$\alpha_l = \arctg\left(\frac{|z_a - z_b|}{|x_a - x_b|}\right). \tag{4}$$

4.1 The Cutter-Model with Back Rake Angle 12°

Applying a computer program created based on formulas (1)–(4), we obtain the predicted values of the half profile angles of the tapered thread geometric model formed using cutters with a rake angle $+12^\circ$ (Tables 1 and 2).

X	Z	Z1	Z2	34,860	1,310	1,300	3,620
32,610	0,000	0,000	0,000	35,110	1,420	1,440	3,940
32,860	0,184	0,144	0,513	35,360	1,540	1,590	4,250
33,110	0,354	0,289	0,983	35,610	1,650	1,730	4,550
33,360	0,511	0,433	1,420	35,860	1,750	1,880	4,850
33,610	0,659	0,577	1,830	36,110	1,860	2,020	5,140
33,860	0,800	0,722	2,220	36,360	1,960	2,170	5,420
34,110	0,934	0,866	2,590	36,610	2,060	2,310	5,700
34,360	1,060	1,010	2,950	36,860	2,160	2,450	5,970
34,610	1,190	1,150	3,290	37,110	2,260	2,600	6,240

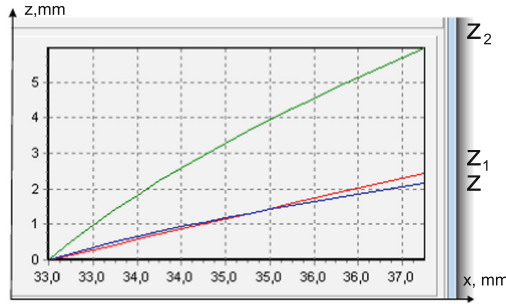


Fig. 5. Scheme of the thread profile size 2 3/8 REG made using cutter-model with back rake angle value 70° (green curve) and 12° (blue curve).

Table 1. Main results of the profile long side half profile angle α_1 calculation (size 2 7/8 Reg, Back Rake angle 12°).

X Coordinates $X_0 = 25,350$, mm		Z Coordinates, mm			Thread profile side half profile angle, °			Tolerance relative 30°	
x	Δx^*	Z	Z1	Z2	Adjusted	Usual	Non-adjusted	Adjusted	Non-adjusted
26.600	1.25	0.728	0.722	0.752	30.21	30.01	31.03	0.7%	3.4%
28.100	2.750	1.600	1.590	1.650	30.19	30.04	30.96	0.6%	3.2%
30.100	4.750	2.750	2.740	2.840	29.98	30.07	30.87	0.01%	2.9%

$\Delta x^* = x_a - x_b$ for long side, $\Delta x^* = x_a - x_d$ for short side. The short side inclination angle calculation shows that they are not so far from the nominal 30°, as the long side inclination angle.

The tables show that the cutter’s thread profile with adjusted edge profile is too close to nominal for the thread’s long side, but near 10% differ for the short side.

So, for practical thread manufacture, it can use the cutter with a non-adjusted edge profile because of the probable high price of a new one, and at the same time, sufficient accuracy of a profile is guaranteed.

Table 2. Main results of the profile short side half profile angle α_s calculation (size 2 7/8 Reg, Back Rake angle 12°).

X Coordinates (mm) X_0 = 25.350		Z Coordinates (mm)			Thread profile side half profile angle, $^\circ$		
x	Δx^*	Z	Z1	Z2	Adjusted	Usual	Non adjusted
25.700	0.35	0.201	0.202	0.204	29.87	29.99	30.24
26.100	0.750	0.430	0.433	0.437	29.83	30.00	30.23
27.300	1.950	1.12	1.13	1.14	29.87	30.1	30.31
27.700	2.350	1.35	1.36	1.37	29.88	30.06	30.24
29.400	4.050	2.320	2.340	2.360	29.81	30.02	30.23
29.750	4.400	2.520	2.540	2.560	29.80	30.00	30.19

5 Conclusions

Based on the visualization, it is confirmed that the axial profile of the sides of the tool-joint thread made by the cutter with a non-zero back rake angle is actually curved.

On the example of algorithmic calculation of shaping by turning the tool-joint tapered thread size 2 7/8 Reg, it is determined that the use of the cutter model with a back rake angle of 12° and with a usual profile of the cutting edge causes the exceeding of the nominal thread profile side half profile angle by 3–10%, which gives grounds for the use of cutters without correction of their edge profile.

The obtained geometric model predicts the precision of thread made from different steel sorts inclosing stainless steel.

The prospects for further study are related to other accuracy parameters of the thread.

References

1. Li, K., Jiang, L., Chen, M.: Experimental study on the influence of cutting parameters on thread precision of external thread turning. In: *Material Science Forum*, vol. 770, pp. 7–12. Trans Tech Publications, Switzerland (2014)
2. Pryhorovska, T., Ropyak, L.: Machining error influence on stress state of conical thread joint details. In: *Proceedings of the International Conference on Advanced Optoelectronics and Lasers*, 9019544, pp. 493–497. CAOL (2019)
3. Shats'kyi, I., Lyskanych, O., Kornuta, V.: Combined deformation conditions for fatigue damage indicator and well-drilling tool joint. *Strength Mater.* **48**, 469–472 (2016)
4. Ropyak, L.Ya., Pryhorovska, T.O., Levchuk, K.H.: Analysis of materials and modern technologies for PDC drill bit manufacturing. *Prog. Phys. Metals* **21**(2), 274–301 (2020)
5. Volchenko, N., et al.: Features of the estimation of the intensity of heat exchange in self-ventilated disk-shoe brakes of vehicles. *Eastern-Eur. J. Enterp. Technol.* **1**(5–97), 47–53 (2019)
6. Dutkiewicz, M., Gołębiewska, I., Shatskyi, I., Shopa, V., Velychkovych, A.: Some aspects of design and application of inertial dampers. In: *MATEC Web of Conferences 2018*, vol. 178, p. 06010 (2018). <https://doi.org/10.1051/mateconf/201817806010>

7. Shatskiy, I., Popadyuk, I., Velychkovych, A.: Hysteretic properties of shell dampers. In: Awrejcewicz, J. (ed.) DSTA 2017. SPMS, vol. 249, pp. 343–350. Springer, Cham (2018). https://doi.org/10.1007/978-3-319-96601-4_31
8. Velychkovych, A., Petryk, I., Ropyak, L.: Analytical study of operational properties of a plate shock absorber of a sucker-rod string. *Shock and Vibration* 2020 (2020)
9. Shatskiy, I., Ropyak, L., Velychkovych, A.: Model of contact interaction in threaded joint equipped with spring-loaded collet. *Eng. Solid Mech.* **8**(4), 301–312 (2020)
10. Shats'kyi, I.P., Ropyak, L.Ya., Makoviichuk, M.V.: Strength optimization of a two-layer coating for the particular local loading conditions. *Strength Mater.* **48**(5), 726–730 (2016)
11. Tatsiy, R.M., Pazen, O.Y., Vovk, S.Y., Ropyak, L.Y., Pryhorovska, T.O.: Numerical study on heat transfer in multilayered structures of main geometric forms made of different materials. *J. Serb. Soc. Comput. Mech.* **13**(2), 36–55 (2019)
12. Ropyak, L.Ya., Makoviichuk, M.V., Shatskiy, I.P., Prytula, I.M., Gryn, L.O., Belyakovskiy, V.O.: Stressed state of laminated interference-absorption filter under local loading. *Funct. Mater.* **27**(3), 638–642 (2020)
13. Shkitsa, L., Yatsyshyn, T., Liakh, M., Sydorenko, O.: Ways to improve safety of pumping-circulatory system of a drilling rig. *Mining Miner. Deposits* **12**(3), 71–79 (2018)
14. Onysko, O., Kopei, V., Panchuk, V.: Theoretical investigation of the tapered thread joint surface contact pressure in the dependence on the profile and the geometric parameters of the threading turning tool. In: IOP Conference Series: Materials Science and Engineering, vol. 749, p. 012007 (2020)
15. Onysko, O., Kopei, V., Panchuk, V., Medvid, I., Lukan, T.: Analytical study of kinematic rake angles of cutting edge of lathe tool for tapered thread manufacturing. In: Tonkonogyi, V., et al. (eds.) InterPartner 2019. LNME, pp. 236–245. Springer, Cham (2020). https://doi.org/10.1007/978-3-030-40724-7_24
16. An, Q.L., Guo, G.G., Zheng, X.H., Chen, M., Liu, G., Zhang, Y.S.: Experimental study on cutting characteristics for buttress thread turning of 13%Cr stainless steel. *KEM* **443**, 262–267 (2010). <https://doi.org/10.4028/www.scientific.net/kem.443.262>
17. Sineider, F.M., Reina-Muñoz, R., Lira, M.V.: System of cutting force data acquisition in mechanical lathes. *Dyna* **85**(207), 16–21 (2019)
18. Neshta, A., et al.: Technological assurance of high-efficiency machining of internal rope threads on computer numerical control milling machines. *ASME J. Manuf. Sci. Eng.* **140**(7), 071012 (2018). <https://doi.org/10.1115/1.4039062>
19. Slătineanu, L., Radovanovic, M., Coteață, M., Beșliu, I., Dodun, O., Coman, I., Olaru, S.C.: Requirements in designing a device for experimental investigation of threading accuracy. In: MATEC Web Conference, vol. 112, p. 01005 (2017)
20. Yanda, H., Ghani, J.A., Che Haron, C.H.: Effect of rake angle on stress, strain and temperature on the edge of carbide cutting tool in orthogonal cutting using FEM simulation. *ITB. J. Eng. Technol. Sci.* **42**(2), 179–194 (2010)
21. Berglind, L., Ziegert, J.: Modulated tool path (MTP) machining for threading applications. *Procedia Manuf.* **1**, 546–555 (2015)
22. Koleva, S., Enchev, M., Szecsi, T.: Compansation of the deviations caused by mechanical deformations during machining of threads. In: Manufacturing Engineering Society International Conference, pp. 480–486. Vigo (Pontevedra), NCTT (2017)
23. Baizeau, T., Campocasso, S., Fromentin G., Rossi, F., Poulachon, G.: Effect of rake angle on strain field during orthogonal cutting of hardened steel with c-BN tools. In: 15th CIRP, vol. 31, pp.166–171 (2015)
24. Zhang, G., Guo, C.: Modeling flank wear progression based on cutting force and energy prediction in turning process. *Procedia Manuf.* **5**, 536–545 (2016)
25. Tread turning tools. <https://www.sandvik.coromant.com/en-us/products/pages/thread-turning-tools.aspx>. Accessed 20 Dec 2020



Interaction of Flexural and Torsional Shapes Vibrations in Fine Boring with Cantilever Boring Bars

Alexandr Orgiyan¹ , Gennadiy Oborskyi¹ , Vitalii Ivanov² ,
Anna Balaniuk¹  , and Ruslan Matzey¹ 

¹ Odessa National Polytechnic University, 1, Shevchenko Ave., Odessa 65044, Ukraine

² Sumy State University, 2, Rymyskogo-Korsakova St., Sumy 40007, Ukraine

Abstract. In the process of fine boring of small-diameter holes ($d = 10\text{--}20$ mm), coupled flexural-and-torsional vibrations of boring cantilever bars are excited. It is of practical interest to study such vibrations during fine boring of long (or deeply located) holes with a ratio $l/d > 3$ (l – the length of a boring cantilever bar). In such cases, a coordinate relationship arises between the flexural and torsional forms. A number of experimental studies have been carried out to assess this relationship and the effect on the emergence of an increasing vibration level. The work studies the features of joint flexural-and-torsional vibrations, the relationship between amplitudes and frequencies, and vibration modes' effect on the loss of vibration resistance. The experiments were carried out on a test bench assembled based on a finishing-boring machine. Measurements were made by strain and piezometric sensors. Samples of steel and cast iron were bored. The criterion for the cutter resharpening was the relative radial wear and the machined surface roughness.

Keywords: Cantilever boring bar · Flexural-and-torsional vibrations · Vibration resistance · Dynamic model · Flexural rigidity

1 Introduction

Cantilever boring bars, mounted on the spindle head, provide high accuracy and productivity for fine finishing boring, maintaining the hole axis's straightness and eliminating the axis run-off. The rigidity and vibration resistance of boring cantilever bars depend on the cylindrical rod's diameter and are often characterized by l/d ratio, where l is the length of the rod, d – its diameter. At $l/d > 3$, the use of boring cantilever bars is limited by a decrease in flexural rigidity values. In this case, the cutter is undercut, the amplitudes of vibrations increase (the logarithmic vibrations decrement decreases), which leads to a loss of vibration resistance.

At the same time, when studying dynamic interactions, boring cantilever bars with a ratio $l/d > 3$ are often used in experiments. In this case, depending on the cutting conditions, the machine's closed dynamic system has a small stability margin. When using such boring bars with a long reach, the limiting processing conditions are easily determined, which ensures the tooling's operability [1, 2].

The accepted process flowsheets provide adjustment of finishing boring machines with a rotating boring bar and a stationary workpiece for fine boring and a rotating workpiece and a boring bar installed in a rigid fixture. Note that the vibration level during the cutting zone rotation is slightly higher than during boring with a boring stationary bar, although the patterns of variation in the vibration amplitudes in both flowsheets are preserved.

2 Literature Review

The complexity of the study of flexural-and-torsional vibrations is that both forms arise together and simultaneously in the cutting zone. Therefore, the problem of studying the features of each vibration mode in conditions of their joint excitation arises. On the other hand, the so-called ‘internal resonance’ should be realized when the natural frequencies of flexural and torsional vibrations coincide.

Cantilever boring bars ensure high performance when boring and, therefore, are widely used. However, their use generates increased flexural compliance at the cutter (technological compliance), and as a result, reduced vibration resistance. These features of boring cantilever bars have led to the fact that the study of their vibrations in the dynamics of machine tools occupy one of the leading places.

The use of vibration dampers to reduce the level of vibrations in small-diameter boring bars is limited due to the impossibility of placing them in the boring bars’ inner cavities. Therefore, it led to the impossibility of setting optimal parameters [3].

In [4], the influence of various internal cores on boring unit dynamics was studied. It is shown that the use of inner cores made of reinforced hydrocarbon fiber (carbon fiber) embedded in boring units with a large length-to-diameter ratio provides an effective reduction in the vibration level. CFRP is characterized by high rigidity and strength combined with low density [5, 6]. A decrease in forced vibrations’ amplitudes has been studied both experimentally and theoretically based on a combined approach: finite element analysis, experimental model analysis, and machining tests.

The ‘standard’ boring bar does not have an inner core and is a supporting tool. The other two boring bars have an inner core made of 31% carbon fiber by volume. Unlike the CFRP_1 inner core, the CFRP_2 inner core consists of two different carbon fiber materials. The bonding polymer used in the carbon fiber is an epoxy resin and a carbon fiber composite material (CFRP_1: Tenax HT 5631; CFRP_2: HS carbon 50K) (Fig. 1).

Amplitude-frequency characteristics, vibration spectra, and values of logarithmic vibration decrements have been obtained, making it possible to evaluate the efficiency of vibration damping and an increase in productivity.

The study [7] performed a theoretical analysis of the flexural characteristics of a rotating composite boring unit’s vibrations. The dynamic model of a boring composite unit is developed using Bernoulli-Euler beam theory. The dissipative properties of the viscoelastic composite material are considered. Changes in natural frequency, damping, and dynamic rigidity for variation in rotational speed, as well as the technology of composite manufacturing, have been studied [8].

The work [9] shows a vibration-resistant design of a boring unit for deep hole processing. For the efficient use of such a unit, a monitoring system (sensors), a drive system,

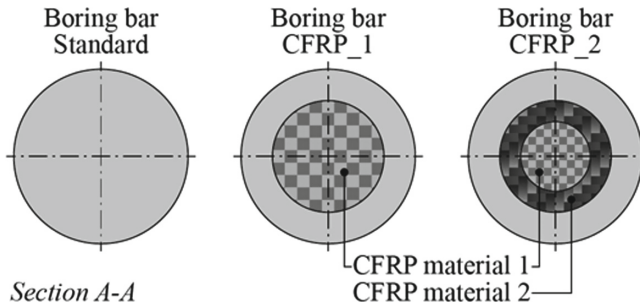


Fig. 1. Structure of boring units tested.

and a control logic have been developed. Optimal actuators have been developed that damp vibration in two respects: in radial when changing the cut depth and speed; drive for preloading under different operating conditions.

Actuators with integrated sensors and piezometric drives respond to increased dynamic tool responses and change either the feed rate or the cut depth.

In works [10, 11], dynamic interactions during bending and torsion of drilling boring bars, optimal setting of unit's vibration dampers are studied [12, 13]; the problems of vibrations damping are studied considering feedbacks [14, 15].

In conclusion, we should note that the study of coupled flexural-and-torsional vibrations during boring is presented insufficiently. In particular, their interactions and their influence on the accuracy of boring have not been studied.

3 Research Methodology

The study aims to expand the technological capabilities of thin edge boring when machining small diameter holes (10–20 mm) with a ratio of $l/d > 3$. Such machining conditions require the solution of particular problems aimed at studying the features and patterns of change in the amplitudes of joint flexural-and-torsional vibrations, as well as their ratios. A design model should also be developed, and the vibration resistance of long cantilever boring bars of small diameter is difficult. The boring conditions should be determined.

A number of experiments were carried out to study joint flexural-and-torsional vibrations. Samples of steel AISI 1045 and cast iron DIN GG-18 were machined. Boring bars with a diameter of 10, 12, 16, 20 mm with a length-to-diameter ratio $l/d = 3, 4, 6, 8$ were tested.

In carrying out these experiments, the following recommended geometry of the cutters was adopted [16]: - for steel boring $\varphi = 60^\circ$, $\varphi = 15^\circ$; for cast iron boring $\varphi = \varphi_1 = 45^\circ$.

Cutting modes: when boring steel AISI 1045 – $v = 125\text{--}150$ m/min, $s = 0.04$ mm/rev, $t = 0.05\text{--}0.1$ mm; when boring cast iron DIN GG-18 – $v = 100$ m/min, $s = 0.04$ mm/rev, $t = 0.05\text{--}0.1$ mm. Cutters material: TZ0K6 – for steel, VK3 – for cast iron.

In each experiment, boring was carried out with a set of 5 cutters having the same geometry. The criterion for regrinding with a cutter was the relative radial wear and the machined surface's roughness.

During the experiment, the boring bar was installed in the fixture, and the workpiece was attached to the spindle flange. The general view of the test benches and the diagram are shown in Figs. 2 and 3.

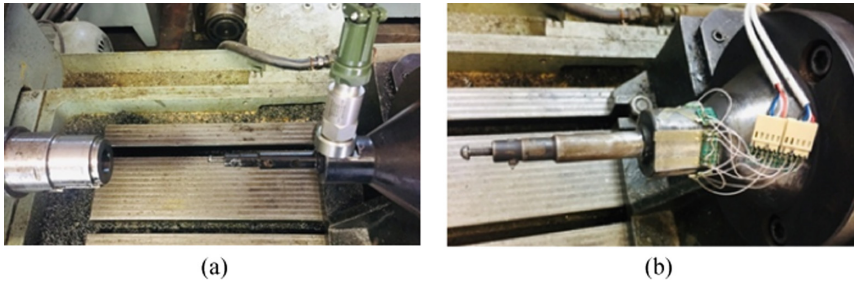


Fig. 2. Experimental test benches: a) with a piezoelectric sensor; b) with strain gauges.

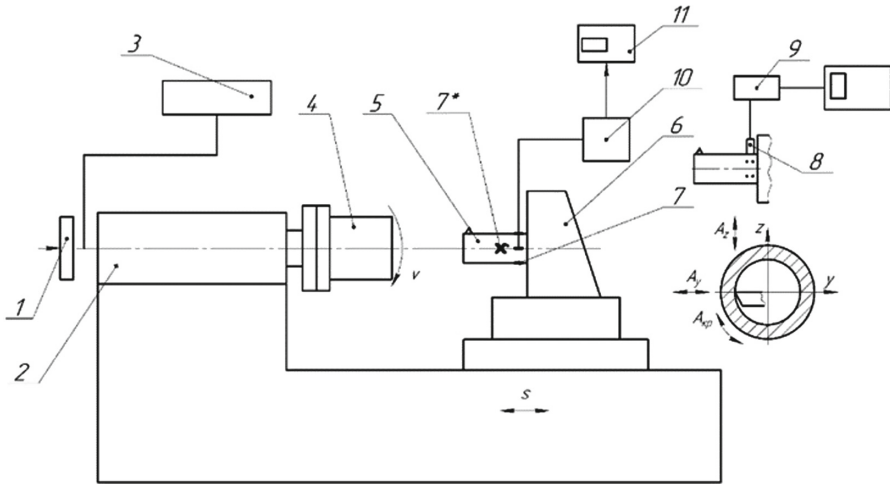


Fig. 3. Schemes of experimental stands for studying vibrations of boring bars: 1 – tachometer; 2 – spindle head; 3 – frequency converter; 4 – workpiece; 5 – boring bar; 6 – fixture; 7, 7* – strain sensors; 8 – piezoelectric sensor; 9 – vibration spectrum analyzer; 10 – vibration recording device (URK); 11 – personal computer (PC).

Measurements of flexural and torsional vibrations were carried out using strain sensors. Flexural vibrations were measured (Fig. 4):

- a) in the cutter plane y (along the normal to the machined surface – A_y);
- b) in a plane tangent to the machined surface z – A_z .

These vibrations were measured by two pairs of strain sensors glued to the flange of the boring bar (Fig. 3). Sensors 7 measured the amplitudes A_y and A_z . Torsional vibrations A_{tors} were measured by a pair of 7 strain sensors glued at an angle of 45° to the generatrix and perpendicular to each other. Each pair of strain sensors is included in two adjacent arms of the measuring bridge, i.e., a differential circuit is used for their inclusion. The amplifiers built into the URK allow measuring vibrations with a frequency in a range of 0–15 kHz.

In the experiments, the amplitudes of the vibrational displacements of the cutters were measured, where the displacements were caused by bending in the normal (A_y) and tangential (A_z) directions to the bored holes, as well as those caused by the torsion of the boring bar (A_{tors}). The total amplitude of flexural vibrations was calculated:

$$A = \sqrt{A_y^2 + A_z^2}.$$

4 Results

The cut depth affects the vibrations level significantly. Table 1 shows the experimental results reflecting the dependence of the amplitudes of the flexural and torsional vibration components of boring bars $d = 16$ mm on the cutting depth when boring, steel AISI 1045, and cast iron DIN GG-18. The amplitudes of flexural and torsional vibrations increase with increasing in cutting depth. The same regularity is observed for boring bars of other diameters and when boring samples from cast iron and other metals.

Table 1. Influence of the cutting depth on the amplitudes of flexural and torsional vibrations, μm , $d_b = 16$ mm, $l/d = 3$ when boring steel AISI 1045 and cast iron.

t, mm	A_y		A_z		A		A_{tors}	
	Steel	Cast iron	Steel	Cast iron	Steel	Cast iron	Steel	Cast iron
0.05	1	0.6	1.2	0.9	1.6	1.1	0.2	0.1
0.1	1.6	0.8	1.8	1.2	2.5	1.4	0.35	0.18
0.15	2	0.9	2.2	1.4	3	1.6	0.45	0.22
0.2	2.8	1	2.6	1.7	3.8	1.8	0.51	0.24

We should note that the amplitudes of flexural vibrations are significantly greater than the amplitudes of torsional vibrations, and when boring steel, all the components of the amplitudes are higher than when boring cast iron.

With an increase in the boring bars outreach (an increase in l/d), the intensity of the cutting depth's influence on the vibration amplitudes increases. It should be noted that vibrations cannot be fully characterized by l/d ratio. The vibration amplitudes at constant l/d and other equal conditions also depend on the boring bar's diameter. Figure 4 shows the boring bar diameter's influence on vibrations at constant $l/d = 3$ when boring steel samples.

With an increase in the boring bar's diameter, the amplitudes of the vibration components decrease, although l/d does not change.

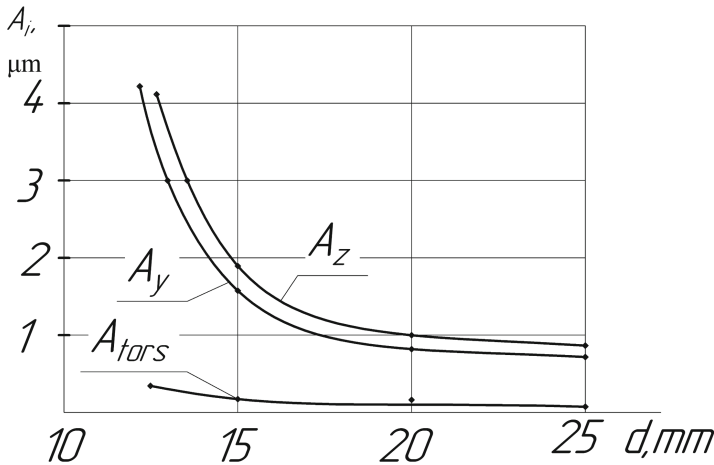


Fig. 4. Influence of the boring bar diameter on the amplitudes of flexural and torsional vibrations, when boring steel AISI 1045 ($l/d = 3$), ($v = 120$ m/min, $t = 0.05$ mm, $s = 0.03$ mm/rev).

Figure 5 shows the results of changes in flexural and torsional vibrations when changing the dimensions of the boring bar.

Since the amplitudes of torsional vibrations (A_{tors}) characterize the cutter movement in the tangential direction to the surface of the hole being machined due to the torsion of the boring bar, it makes sense to consider the tangential component of bending vibrations (A_z) to compare the vibration intensity, i.e., characterize these changes by A_z/A_{tors} ratio. Based on the results shown in Fig. 6, it can be concluded that with a decrease in the size of boring bars at $l/d = Const$, an increase in A_z occurs less intensively than an increase in A_{tors} . Figure 5 shows that for $l/d = 3$ with decreasing of the boring bar d , the amplitudes of flexural and torsional vibrations increase, and A_z/A_{tors} ratio decreases (Fig. 6) and is within 4–6 when boring steel, and for $d = 25$ mm – 8–12.

Therefore, a more informative term is the concept of 'ultimate yield'. In the experiments, the values of the limiting yield [K] were determined, which ensure the stability of the cutting process: for steel AISI 1045 [K] = 0.06–0.15 $\mu\text{m}/\text{n}$; for cast iron [K] = 0.2 $\mu\text{m}/\text{n}$.

Therefore, the limiting yield concept means that the system is in the stability threshold. The system transfers into an instability region for yield values exceeding [K]; in this case, the vibrations are increasing process system loses its operability. When the limiting yield is exceeded, the amplitudes of flexural and torsional vibrations increase sharply.

Generalization of experimental studies results led to the following ratios of the components of flexural-and-torsional vibrations: $A_z = (1.1-1.6) \cdot A_y$, $A_{tors} = (0.2-0.5) \cdot A_y$. The natural frequencies of torsional vibrations are 2–8 times higher than the flexural

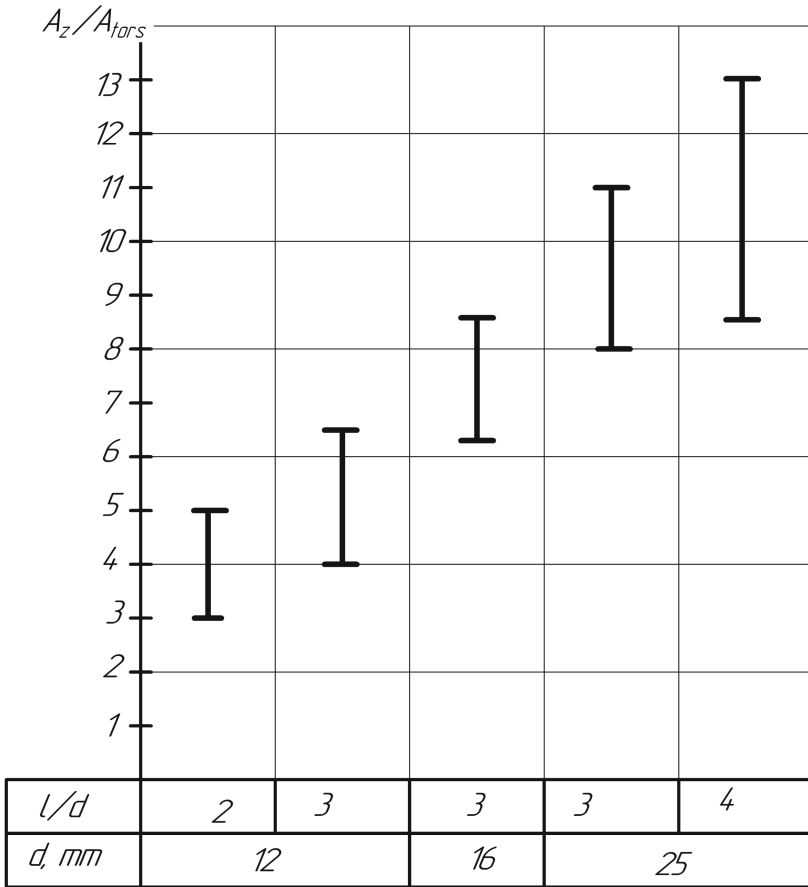
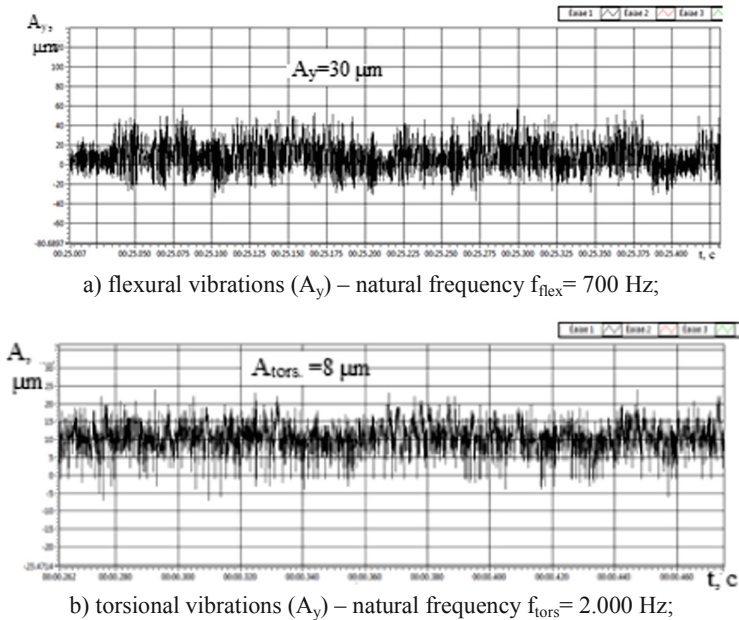


Fig. 5. Ratios of flexural and torsional vibrations components A_z/A_{tors} when boring bars diameter and outreach are changed (steel AISI 1045).

ones, which for boring bars with a diameter less than 20 mm are in the range of 0.4–1.5 kHz. Torsional vibrations are characterized by small amplitude, and their influence on flexural vibrations is manifested at small values of the boring bar diameter (less than 12 mm).

Figure 6 shows typical oscillograms of flexural and torsional vibrations during boring.

We should note that when treating cast iron, all the amplitudes' components are somewhat less than when treating steel, and the ratio of the amplitudes of the flexural and torsional vibrations is within 4.0–4.5.



a) flexural vibrations (A_y) – natural frequency $f_{flex} = 700$ Hz;

b) torsional vibrations (A_y) – natural frequency $f_{tors} = 2.000$ Hz;

Fig. 6. Oscillograms of flexural and torsional vibrations: $v = 125$ m/min, $d = 12$ mm, $l/d = 8$, $t = 0.15$ mm, $s = 0.03$ mm/rev, cast iron DIN GG-18, $R_a = 1.8$ μ m.

5 Conclusion

The features and regularities of the change in the amplitudes of the coupled flexural-and-torsional vibrations of small diameter (10–20 mm) cantilever boring bars when boring long holes $l/d > 3$ (4,6,7,8) have been studied. It was found in the experiments that the frequencies of flexural and torsional vibrations differ by 3–6 times when the outreaches of the boring bars change. The amplitudes of flexural vibrations are significantly greater than the amplitudes of torsional ones (up to 8 times) when boring steel with a change in cutting depth from 0.05 to 0.20 mm. The dependence of the amplitudes of flexural and torsional vibrations on the change in the boring bars' diameter has been established. Analysis of the experimental results revealed the following relationships between the components of the vibration amplitudes: $A_z = (1.1–1.6) A_y$, $A_{tors} = (0.2–0.5) A_y$.

In the following works, the developed computational model will be provided and calculations of vibration resistance of a closed dynamic system according to the Ross Hurwitz criterion. The methods of effective vibration damping will also be proposed with the study of boring accuracy indicators.

References

1. Oborskyi, G., Orgiyan, A., Tonkonogyi, V., Aymen, A., Balaniuk, A.: Study of dynamic impacts at combined operations of the thin turning and boring. In: Tonkonogyi, V., et al. (eds.) InterPartner 2019. LNME, pp. 226–235. Springer, Cham (2020). https://doi.org/10.1007/978-3-030-40724-7_23

2. Orgiyan, A., Kobelev, V., Ivanov, V., Balaniuk, A., Aymen, A.: Ensuring the bending stiffness of pre-compressed cantilever boring bars during fine boring. In: Ivanov, V., Trojanowska, J., Pavlenko, I., Zajac, J., Peraković, D. (eds.) DSMIE 2020. LNME, pp. 315–324. Springer, Cham (2020). https://doi.org/10.1007/978-3-030-50794-7_31
3. Chockalingam, S., Ramabalan, S., Govindan, K.: Chatter control and stability analysis in cantilever boring bar using FEA methods. *Mater. Today: Proc.* **33**(7), 2577–2580 (2020). <https://doi.org/10.1016/j.matpr.2019.12.166>
4. Thorenz, B., Friedrich, M., Westermann, H.-H., Döpfer, F.: Evaluation of the influence of different inner cores on the dynamic behavior of boring bars. *Procedia CIRP* **81**, 1171–1176 (2019)
5. Rajak, D., Pagar, D., Menezes, P., Linul, E.: Fiber-reinforced polymer composites: manufacturing, properties, and applications. *Polymers* **11**(10), 1667 (2019). <https://doi.org/10.3390/polym11101667>
6. Bruckner, W.: CFK: High costs block a breakthrough in the mass market (2018). (in German)
7. Ren, Y., Zhao, Q., Liu, Y., Ma, J.: Analysis of bending vibration characteristics of rotating composite boring bar. *J. Phys.: Conf. Ser.* **1303**(1), 012147 (2019)
8. Alammari, Y., Sanati, M., Freiheit, T., Park, S.S.: Investigation of boring bar dynamics for chatter suppression. *Procedia Manuf.* **1**, 768–778 (2015). <https://doi.org/10.1016/j.promfg.2015.09.059>
9. Grossi, N., Croppi, L., Scippa, A., Campatelli, G.: A dedicated design strategy for active boring bar. *Appl. Sci. (Switz.)* **9**(17), 3541 (2019)
10. Siddhpura, M., Paurobally, R.: A review of chatter vibration research in turning. *Int. J. Mach. Tools Manuf.* **61**, 27–47 (2012)
11. Bansal, A., Law, M.: A receptance coupling approach to optimally tune and place absorbers on boring bars for chatter suppression. *Procedia CIRP* **77**, 167–170 (2018)
12. Venter, G.S., Silva, L., Carneiro, M.B., da Silva, M.M.: Passive and active strategies using embedded piezoelectric layers to improve the stability limit in turning/boring operations. *Int. J. Adv. Manuf. Technol.* **89**(9–12), 2789–2801 (2016). <https://doi.org/10.1007/s00170-016-9620-2>
13. Gousskov, A.M., Voronov, S.A., Novikov, V.V., Ivanov, I.I.: Chatter suppression in boring with tool position feedback control. *J. Vibroeng.* **19**, 3512–3513 (2017)
14. Tanaka, H., Obata, F., Matsubara, T., Mizumoto, H.: Active chatter suppression of slender boring bar using piezoelectric actuators. *JSME Int. J. Ser. C Dyn. Control. Robot. Des. Manuf.* **37**, 601–606 (2012)
15. Saleh, M.K.A., Nejatpour, M., Yagci Acar, H., Lazoglu, I.: A new magnetorheological damper for chatter stability of boring tools. *J. Mater. Process. Technol.* **289**, 116931 (2021). <https://doi.org/10.1016/j.jmatprotec.2020.116931>
16. Mazur, N.P., Vnukov, Yu.N., Grabchenko, A.I., et al.: *Fundamentals of the Materials Cutting Theory*, 2nd end. NTU “KhPI”, Kharkiv (2013)



Heat Flows Affected on the Wheelhead of a Cylindrical Grinding Machine

Mykhaylo Stepanov¹ , Petro Litovchenko² , Larysa Ivanova² ,
Maryna Ivanova¹  , and Magomediemmin Gasanov¹ 

¹ National Technical University “Kharkiv Polytechnic Institute”,
2, Kyrpychova St., Kharkiv 61002, Ukraine

² National Academy of the National Guard of Ukraine, 3, Maidan Zahsnykyv Ukrainy,
Kharkiv 61001, Ukraine

Abstract. The paper focused on analyzing the scheme of the effect of heat (cooling) flows on the grinding wheelhead of a cylindrical grinding machine tool with an estimate of the power of heat sources to determine the influence of the temperature factor on the accuracy of machining. The most important sources of heat, which act on the wheelhead body, and were studied in the paper are heat released in the spindle bearings; heat released in guideways; heat released in the cutting zone; heat received by the grinding wheelhead body as a result of the action of heated liquid coolant on its front wall; heat from the airflow, removed by the ventilation system of the grinding wheel drive electric motor; heat (cooling flow) from the airflow arising from the rotation of the pulley and the movement of the drive belts of the grinding wheel drive; heat from the ventilation effect that occurs under the encasing of the grinding wheel as a result of its rotation at high peripheral speed; heat (cooling) supplied to the belt drive pulley of the grinding wheel drive, installed at the output end of the spindle. The mathematical models for determining the quantity of heat for each of the mentioned heat sources are given.

Keywords: Grinding wheelhead · Heat flow · Roller guideways · Coolant liquid · Cutting zone · Heat transfer

1 Introduction

The accuracy of machining parts on cylindrical grinding machines is determined by the total quantity of heat generated during machine tool elements and heat from the environment [1, 2].

This is because of the effect of thermal deformations, the relative position of parts and assemblies (including the grinding head - the most important element of the grinding machine structure) changes in space [3–5].

On the one side, the grinding wheelhead is one of the heat sources, and a higher temperature is observed in the areas where the bearings of the grinding wheel spindle are located [4]. On the other side, the wheelhead takes heat and cooling flows from other sources. Simultaneously, the heating rate of the grinding wheelhead in the first 4 h of work of the circular grinding machine is 2 times higher than the heating rate of the bed.

The temperature at different points of the wheelhead body of machine tools can vary within 10–50 °C. The spindle temperature can be 30–40% higher than the average temperature of the body part in which it is mounted.

All this affects the accuracy and quality of the part machined on the grinding machine tool.

In this regard, the purpose of the paper is to analyze the effect of heat flows acting on the grinding wheelhead of a cylindrical grinding machine and arising from various sources and evaluate the power of heat in these sources.

2 Literature Review

The study [6] on the thermal deformation of the spindle of the grinding machine depending on differences of temperatures of the front and rear bearings was done and confirmed that the temperature of the hydrostatic bearings is the main cause for the occurrence of the thermal deformation in all the cases of X, Y and Z axes.

The motorized spindle was modeled. Its thermal characteristics analysis by the finite element method was done using ANSYS software, which confirmed that the heat generation becomes severe when the spindle is at high speed. It will become a big heat source influencing temperature-rise [7].

The work is devoted to the design and analysis of wheelhead in tool grinding machine, consisting of various parts and units [8, 9].

For studying different phenomena in machine tools and three-dimensional modeling, mathematical modeling and numerical methods are also used [10, 11]. Analytical or numerical models are necessary to understand better the thermal behavior of machine tool parts and elements. For example, a new model for predicting the friction torque and mechanical efficiency of ball screws based on the empirical equations for the friction torque of rolling bearings has been presented [12].

It is noted [13] that thermal behaviors significantly affect the contact stiffness and position accuracy of the rolling linear guide, which worsens the performance of the precision machinery. Different approaches to modeling the thermo-mechanical behavior of ball screws have been analyzed [14].

Energy consumption and dissipation are discussed, leading to a thermal model for grinding, which provides a good estimation of contact temperature in the cutting zone and the finished surface [15].

Variations in the thermal state of machine tools spindle-bearing system can have a noticeable effect on the grinder's performance. The impact of different system parameters such as speed of rotation, type of bearing, ambient temperature, type of oil, initial preload on temperature output, and thermal growth within the system has been considered [16]. This impact can also be estimated using the parameter identification procedure [17, 18]. The issues related to the generation of working fluid temperature in the front and end spindle bearings are considered [19].

Although the study of temperature deformations of various elements of grinding machine has been devoted to many studies, the issue of the influence of heat flows generated by the work of multiple mechanisms surrounding and conjugate to the grinding wheelhead on it has not yet considered.

3 Research Methodology

3.1 The Balance Equation of Heat Flows Acting on the Grinding Wheelhead

Analysis of the heat flow diagram for heating and cooling (Fig. 1) shows that the most important sources of heat, which acts on the wheelhead body, are the following: heat released in the left (*LB*) and right (*RB*) spindle bearings; heat released in guideways *G*₁ and *G*₂; heat released in the cutting zone *CZ*; heat received by the grinding wheelhead body as a result of the action of heated liquid coolant on its front wall; heat from the airflow, removed by the ventilation system of the grinding wheel drive electric motor *V*_e; heat (cooling flow) from the airflow arising from the rotation of the pulley and the movement of the drive belts of the grinding wheel drive *PB*; heat from the ventilation effect that occurs under the encasing of the grinding wheel as a result of its rotation at high peripheral speed *W*; heat (cooling) supplied to the belt drive pulley of the grinding wheel drive, installed at the output end of the spindle, etc.

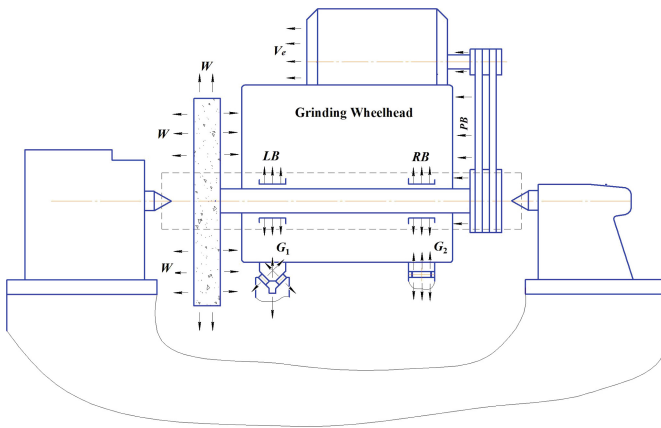


Fig. 1. The heating and cooling scheme flows on the grinding wheelhead in the technological system of a cylindrical grinding machine.

The balanced equation of heat flows acting on the grinding wheelhead has the form:

$$Q_{\Sigma} = Q_B + Q_{CL} + Q_{\Sigma AFW} + Q_{PB} + Q_G + Q_{Env}, \quad (1)$$

where Q_{Σ} - the total quantity of heat received by the grinding wheelhead; Q_B - heat flow entering the wheelhead from the working fluid of the lubrication subsystem of the bearings of the grinding wheel spindle; Q_{CL} The heat flow enters the wheelhead due to its contact with the heated coolant; $Q_{\Sigma AFW}$ - the flow of heat (cooling) generated by air flows resulting from the rotation of the grinding wheel; Q_{PB} - the flow of heat (cooling) generated by air flows arising from the operation of the belt drive of the grinding wheel drive; Q_G - the flow of heat (cooling) resulting from friction in the guideways; Q_{Env} - heat flow entering the wheelhead from the environment.

Analysis of the effect of heat sources in a cylindrical grinding machine shows that the most intense of them is the grinding process.

The quantity of heat released in the cutting zone Q_{CZ} during the grinding time t is determined by the formula

$$Q_{CZ} = 3600 \cdot P \cdot t, \quad (2)$$

where P - an effective grinding power, kW.

The accuracy parameters of machine tools are largely determined by the thermal state of the spindle assembly during processing, which depends on the temperature fields and the temperature deformations caused by them [20].

3.2 Determination of Heat Quantity Released in the Spindle Bearings

The highest temperature occurs in the spindle bearing areas. Heat generation in the grinding wheel spindle bearings depends on the intensity of heat exchange with adjacent elements of the technological system and the environment. Oil heating in the spindle bearings depends on the specific heat capacity and density of the oil, its consumption, and friction power losses.

The quantity of heat transferred from the bearings to the spindle and the wheelhead body depends, on the one side, on the heat capacity of the last, and the other side, on the operating conditions of the bearings and, especially, on the viscosity and thickness of the lubricant layer. It is generally accepted that 30% of the generated heat is transferred to the spindle and the rest to the wheelhead body. In connection with increasing the grinding wheel's speed, the most important criterion is the minimum power loss, which determines the heat generation in the spindle units.

Heat generation in sliding bearings per unit of time is determined by friction power losses and can be calculated [21] by the formula

$$Q_B = M_B \omega_s / 60, \quad (3)$$

where M_B - the total moment of friction in the lubricating layer of the bearings, Nm; ω_s - the angular speed of the spindle, sec^{-1} .

The formula determines oil heating in bearings

$$\Delta t = \frac{Q_B}{c \cdot \rho \cdot Q}, \quad (4)$$

where c, ρ - the specific heat and density of the working fluid, respectively, for mineral oil $c \cdot \rho = 1.7 \cdot 10^6 \text{ J}/(\text{m}^3 \cdot ^\circ\text{C})$; Q - required consumption of working fluid, m^3/sec .

3.3 Determination of Heat Quantity Released in the Guide Ways

The movement in the guideways of the kinematic pairs of machine tools is accompanied by friction, which is one of the reasons for the release of heat. It can be somehow tangible when using accelerated feeds. Preliminary calculations show that the quantity of heat generated in the rod and piston seals of the hydraulic cylinder of the table drive is much less than the heat generated due to friction in the table guideways.

It should be noted that the heat released in the rolling guideways of the grinding wheelhead is several times less than in the sliding guideways. It is important to consider the effect of joints in the guideways on the temperature field, which contributes to the uneven heating of the contacting surfaces.

The quantity of heat released due to friction in the guideways during the translational movement of the grinding wheelhead can be determined using a simplified formula

$$Q_G = F_f \cdot V_{WH}, \quad (5)$$

where F_f - frictional force (pulling force) in guideways, N; V_{WH} - speed of movement of the grinding wheelhead along with the guideways, m/sec.

In the general case, the friction force is determined by summing the friction forces on all edges of the guideways under reactions on each face. Pulling force is defined as the sum of the feed forces F_y and the total frictional force. The simplified formula for calculating the pulling force has the form [22]

$$F_p = F_y + 3F_{f0} + \frac{3f_k}{d} N_\Sigma, \quad (6)$$

where F_y - cutting force component, N; F_{f0} - initial frictional force on one edge of the guides (in the absence of external load), $F_{f0} = 4 \dots 5$ N; f_k - coefficient of friction in the rolling guideways, for steel guideways $f_k = 0.001$ cm for cast iron guideways, $f_k = 0.0025$ cm; d - the diameter of the rolling elements in contact with the edges of the guideways, $d = 0.07$ cm; N_Σ - total normal load on the guideways, N.

Total normal load on the guideways could be defined as

$$N_\Sigma = F_Z + G_Z, \quad (7)$$

where F_Z - tangential component of the cutting force, N; G_Z - the force of gravity of the headstock assembly, taking into account the weight of its body, spindle, pulleys, grinding wheel, faceplate and bearings, H.

3.4 Determination of Heat Quantity Released by the Airflow, Removed by the Ventilation System of the Grinding Wheel Drive Electric Motor

In an electric motor, energy losses arise in the active resistance of the windings, in steel when the magnetic flux in the magnetic circuit changes. Also, mechanical friction losses in bearings and air friction of rotating parts must be taken into account. These components are converted into heat energy, which is spent on heating the engine and the environment.

The quantity of heat generated by the electric motor during the time τ is determined

$$Q_{em} = 0,24 \sum P_{em} \tau, \quad (8)$$

where P_{em} - total power loss in the electric motor, W.

The V-belt pulley drive belt movement helps to cool the right-side wall of the wheelhead body, causing it to buckle.

The heat flow from the belt drive to the spindle pulley can be determined by knowing the relationship between the powers on the driven and driving shafts of the transmission, that is $P_{belt} = \eta_{belt} \cdot P_{em}$, where η_{belt} is the efficiency of the V-belt drive.

Then

$$Q_{belt} = \left(\frac{100 - \eta_{belt}}{100} \right) P_{belt} \cdot \tau, \quad (9)$$

where τ - belt drive running time.

When the sidewall of the grinding wheelhead is blown with air flows from the movement of the V-belt transmission elements (in particular, the pulley), the heat perceived (lost) by this surface can be determined by the formula:

$$Q = \alpha \cdot A \cdot (t_a - t_{air}), \quad (10)$$

where t_a - the average temperature of wall surface; t_{air} - air temperature away from the grinding wheelhead; A - the surface area of the wheelhead through which heat transfer occurs; α - heat-transfer coefficient by convection.

Heat transfer of the wall surface is intensified by increasing the speed of its blowing. To calculate formula (10), it's necessary to know the value of the coefficient α .

Using the research data [23] on the experimental determination of the parameters of blowing the surface (with an area comparable to the lateral surface of the grinding head) by a disk (with a diameter comparable to the diameter of the driven V-belt drive pulley), it's possible to obtain the formula

$$\alpha = 0,271 \lambda_a \left(\frac{\pi \omega_p}{\nu_a} \right)^{0,6} D_p^{0,2}, \quad (11)$$

where λ_a - thermal conductivity coefficient of the environment, W/(m·K); ω_p - angular speed of rotation of the pulley, sec^{-1} ; D_p - pulley outer diameter, m; ν_a - kinematic viscosity of the environment, m^2/sec .

Considering (10) and (11), a formula for calculating the quantity of heat dissipated by the lateral surface of the grinding head because of blowing air flows generated by the V-belt pulley can be obtained

$$Q = 0,271 \cdot A \cdot \lambda_a \cdot D_p^{0,2} \left(\frac{\pi \omega_p}{\nu_a} \right)^{0,6} \cdot (t_a - t_{air}). \quad (12)$$

3.5 Determination of Heat Quantity Released by the Airflow from the Ventilation Effect from the Rotating Grinding Wheel

The ventilating air flows inside the grinding wheel encasing can cool the encasing and the left side wall of the grinding wheelhead body.

The effect of heat flux (cooling) inside the grinding wheel encasing can be simulated depending on the stage of the grinding cycle.

When loading the workpiece (no grinding process), the liquid coolant does not enter the cutting zone, and the air flow generated by the wheel acts on the grinding wheelhead.

In the case of the rotation of the grinding wheel, it experiences resistance associated with the friction of the air against the surface of the wheel and the imparting of a rotational motion to the air, which forms air flows inside the encasing. In this case, the magnitude of the friction force depends on the design of the encasing. If the encasing walls are close to the ends of the grinding wheel, air movement can be minimized.

The work expended on rotating the wheel in the air (ventilation) varies in proportion to the quantity of air and the quantity of kinetic energy imparted to it.

Further, using formulas 12, it's possible to calculate the heat dissipated by the opposite wall of the grinding wheelhead due to blowing it with air flows generated by the grinding wheel at the stage of input and output workpieces.

However, this cooling process is partially neutralized by the ingress of heated liquid coolant into the encasing, which, on the contrary, heats this sidewall.

The quantity of heat transferred to the liquid coolant can be determined from the ratio

$$Q_{LC} = k \cdot Q_{CZ}, \quad (13)$$

where k - the coefficient determined by the grinding scheme.

The heated liquid coolant can also get on the front wall of the wheelhead body, heating it up. As a result of a change in the temperature of the walls under the action of the heated liquid coolant, their deformation occurs, which changes the spatial position of the entire grinding wheelhead, which, in turn, reduces the accuracy of the ground parts.

At the stage of grinding, the liquid coolant is supplied to the cutting zone and, in contact with the wheel, is sprayed in the form of an aerosol in the encasing of the grinding wheel on the side of the grinding wheelhead. Suppose the subsystem of use of liquid coolant ensures the stabilization of its temperature. In that case, the total heat is determined by the power spent on overcoming the friction force of the liquid coolant on the grinding wheel, the power spent on spraying the coolant, and the grinding time.

The heat transferred by the liquid coolant is estimated by expression (11), from which it can be seen that the amount of heat depends on the coolant temperature and heat transfer. It can be seen from formula (12) that the heat transfer coefficient is directly proportional to the coefficient of thermal conductivity of the medium washing the wall. At the grinding stage, this medium is a gas-air mixture (aerosol) with very different characteristics from those of the medium in air blowing. The coefficient of thermal conductivity of air $\lambda_a = 0.0257 \text{ W/(m}\cdot\text{K)}$, and of water - $\lambda_w = 0.598 \text{ W/(m}\cdot\text{K)}$, which is more than 20 times more. This greatly intensifies the heat transfer process compared to air blowing.

The grinding wheelhead is also deformed due to the airflow created by the cooling system (impeller) of the electric motor of the grinding wheel drive onto the upper plane of the grinding wheelhead, on which the electric motor is mounted.

4 Results

Based on the mathematical models obtained above, the analytical studies were carried out, the results of which are shown in Fig. 2, 3, 4 and 5.

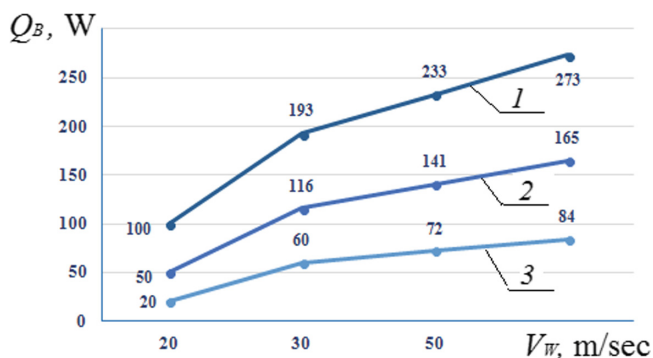


Fig. 2. Influence of grinding wheel speed and infeed on heat generation in the spindle bearing: 1, 2, 3 – infeed 2, 3, 4 mm/min respectively, grinding wheel characteristics - 14A2.5HC26B5, diameter $D_w = 300$ mm, height $H = 20$ mm.

Analysis of the graphs in Fig. 2 shows an increase in the cutting speed from 10 to 100 m/sec leads to increased heat generation in the bearings by more than 3 times. An increase in the wheel's speed from 50 to 100 m/sec (in 2 times) leads to an increase in the quantity of heat generated by 1.6 times. A 2-fold increase in infeed feed results in a 1.4-fold increase in the quantity of heat generated in the bearing.

Analysis of the graphs in Fig. 3 got according to the described method confirms the fact of minimal heat generation in the guideways of the grinding wheelhead.

Analysis of the graphs in Fig. 4 shows that the intensity of cooling by air flows from the grinding wheel increases by almost 8 times, increasing its speed and diameter.

As shown in the graphs in Fig. 5, the intensity of blowing the right wall of the wheelhead depends largely on the speed of rotation of the pulley of the V-belt transmission of the drive of rotation of the grinding wheel.

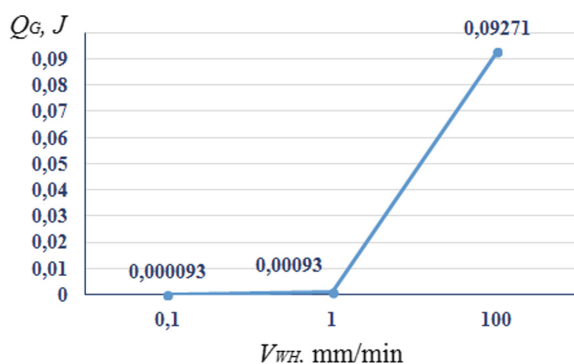


Fig. 3. Influence of the grinding wheel's movement speed along the guideways on the quantity of heat generated in them due to friction.

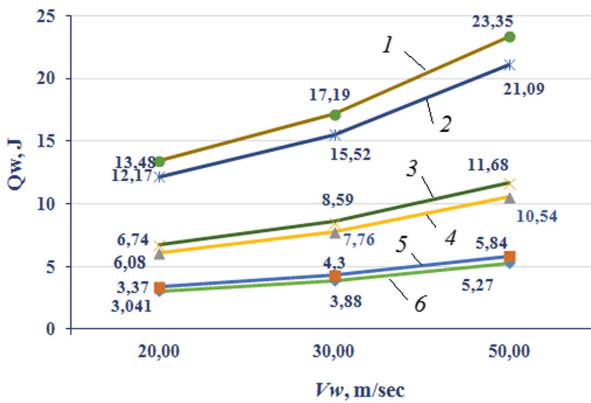


Fig. 4. Influence of the speed of the grinding wheel on the quantity of heat dissipated as a result of blowing air flows generated by the grinding wheel: 1, 3, 5 – grinding wheel diameter 300 mm; 2, 4, 6 – grinding wheel diameter 500 mm; 1, 4 - temperature difference is 0.5 °C; 2, 5 - temperature difference is 1.0 °C; 3, 6 - temperature difference is 2.0 °C.

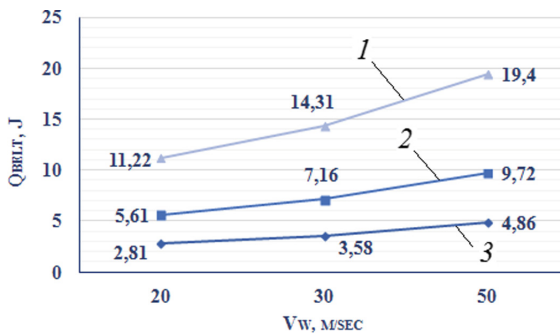


Fig. 5. Heat dissipated by the lateral surface of the grinding wheelhead as a result of blowing air flows generated by the V-belt pulley: 1, 2, 3 - the temperature difference between the wall and air is 0.5; 1.0; 2.0 °C, respectively; pulley diameter $D_p = 200$ mm.

5 Conclusions

At the present stage of the development of mechanical engineering, the accuracy of parts increases. Therefore, the study of thermal processes in the units and assemblies of machine tool equipment and the search for means and methods of controlling them are becoming increasingly important.

1. It was revealed that the most effective thermal effect is produced by the working fluid of the spindle bearing lubrication subsystem and coolant, acting on the outer surfaces of the grinding wheelhead.
2. The least perceptible factor of thermal impact is the heat released due to friction in the guides, which is several orders of magnitude less than the heat released by other sources.

3. The thermal effect of airflows generated by the moving elements of the machine tool has been analyzed. A dependence is obtained for calculating the heat dissipated by the side surface of the grinding headstock as a result of blowing with air flows generated by the grinding wheel and the V-belt drive pulley of the wheel rotation drive.

References

1. Malkin, S., Guo, C.: Grinding Technology: Theory & Application of Machining with Abrasives, 2nd edn. Industrial Press Inc., New York (2008)
2. Jamshidia, H., Budak, E.: Grinding temperature modeling based on a time dependent heat source. *Procedia CIRP* **77**, 299–302 (2018). <https://doi.org/10.1016/j.procir.2018.09.020>
3. Patil, P.J., Patil, C.R.: Analysis of process parameters in surface grinding using single objective Taguchi and multi-objective grey relational grade. *Perspect. Sci.* **8**, 367–369 (2016). <https://doi.org/10.1016/j.pisc.2016.04.077>
4. Stepanov, M., Ivanova, M., Litovchenko, P., Ivanova, L., Kotliar, A.: Improvement of the accuracy of grinding by means of coolant supply. In: Ivanov, V., Trojanowska, J., Pavlenko, I., Zajac, J., Peraković, D. (eds.) *DSMIE 2020. LNME*, pp. 325–335. Springer, Cham (2020). https://doi.org/10.1007/978-3-030-50794-7_32
5. Lupyr, O., Hovorun, T., Vorobiov, S., Burlaka, A., Khvostenko, R.: Influence of heat treatment technologies on the structure and properties of the corrosion-resistant martensitic steel type AISI 420. *J. Eng. Sci.* **7**(2), C10–C16 (2020). [https://doi.org/10.21272/jes.2020.7\(2\).c2](https://doi.org/10.21272/jes.2020.7(2).c2)
6. Bo-Sung, K., Gyeong-Tae, B., et al.: A study on the thermal characteristics of the grinding machine applied hydrostatic bearing. *Trans. Can. Soc. Mech. Eng.* **39**(3), 717–728 (2015). <https://doi.org/10.1139/tcsme-2015-0057>
7. Lu, Y., Yao, Y.X., Hong, R.H.: Finite element analysis of thermal characteristics of high-speed motorized spindle. *Appl. Mech. Mater.* **10–12**, 258–262 (2007). <https://doi.org/10.4028/www.scientific.net/amm.10-12.258>
8. Prasad, V.V.S.H., Labesh Kumar, C., Vanaja, T., Ashok Reddy, K.: Design and analysis of wheelhead in cutter and tool grinder. *Int. J. Mech. Prod. Eng. Res. Dev. (IJMPERD)* **7**(5), 175–182 (2017). <https://doi.org/10.24247/ijmperdoct201718>
9. Skoczylas, L., Belzo, A., Wdowik, R.: Application of CAD modelling in preparation of a grinding wheel used in shaping of a worm thread outline. *Technologia i Automatyizacja Montażu* **3**(2020), 53–57 (2020)
10. Krol, O., Sokolov, V., Tsankov, P.: Modeling of vertical spindle head for machining center. *J. Phys.: Conf. Ser.* **1553**, 012012 (2020). <https://doi.org/10.1088/1742-6596/1553/1/012012>
11. Tao, L., Wang, Y., He, Y., Feng, H., Ou, Y., Wang, X.: A numerical method for evaluating effects of installation errors of grinding wheel on rotor profile in screw rotor grinding. *Proc. Inst. Mech. Eng. Part B: J. Eng. Manuf.* **230**(8), 1381–1398 (2016). <https://doi.org/10.1177/0954405416654418>
12. Zhou, C.G., Feng, H.T., Yi, O.: A new model for predicting the mechanical efficiency of ball screws based on the empirical equations for the friction torque of rolling bearings. *Adv. Mech. Eng.* **10**(9), 1–8 (2018). <https://doi.org/10.1177/1687814018800173>
13. Wang, X.-Y., Feng, H.-T., Zhou, C.-G., Ye, K.-Q.: A thermal model for real-time temperature forecast of rolling linear guide considering loading working conditions. *Int. J. Adv. Manuf. Technol.* **109**(7–8), 2249–2271 (2020). <https://doi.org/10.1007/s00170-020-05723-x>
14. Oyanguren, A., Larrañaga, J., Ulacia, I.: Thermo-mechanical modelling of ball screw preload force variation in different working conditions. *Int. J. Adv. Manuf. Technol.* **97**(1–4), 723–739 (2018). <https://doi.org/10.1007/s00170-018-2008-8>

15. Rowe, W.B., Morgan, M.N., Batako, A., Jin, T.: Energy and Temperature Analysis in Grinding. *WIT Trans. Eng. Sci.* **44**(22), 1–22 (2003). <https://doi.org/10.2495/LAMDAMAP030011>
16. Alfares, M., Saleem, O., Majeed, M.: Analytical study of thermal variation impact on dynamics of a spindle bearing system. *Proc. Inst. Mech. Eng. Part K: J. Multi-Body Dyn.* **233**(4), 871–898 (2019). <https://doi.org/10.1177/1464419319841687>
17. Pavlenko, I., Trojanowska, J., Ivanov, V., Liaposhchenko, O.: Parameter identification of hydro-mechanical processes using artificial intelligence systems. *Int. J. Mechatron. Appl. Mech.* **2019**(5), 19–26 (2019)
18. Ivanov, V., Dehtiarov, I., Pavlenko, I., Liaposhchenko, O., Zaloga, V.: Parametric optimization of fixtures for multi-axis machining of parts. In: Hamrol, A., Kujawińska, A., Barraza, M.F.S. (eds.) *MANUFACTURING 2019. LNME*, pp. 335–347. Springer, Cham (2019). https://doi.org/10.1007/978-3-030-18789-7_28
19. Stepanov, M., Ivanova, M., Litovchenko, P., Ivanova, L., Tarasenko, O.: Study of thermal modes of working fluids in grinding machines. In: Tonkonogyi, V., et al. (eds.) *InterPartner 2019. LNME*, pp. 299–308. Springer, Cham (2020). https://doi.org/10.1007/978-3-030-40724-7_31
20. Dubrov, D., Dubrov, Yu., Syromyatnikov, D.: About the possibility of temperature stabilization of the spindle unit of a metal-cutting machine. *Sci. Internet Mag.* **9**(8) (2017). (in Russian)
21. Breev, B.G.: Modernization of high-speed grinding machines. *Machine Building, Moscow* (1982). (in Russian)
22. Galyuzhin, D.S.: Calculation and design of machine tools. Design of machines and automation equipment. Belarusian-Russian University, Mogilev (2019). (in Russian)
23. Zainullin, L., Kalganov, D., Spirin, N.: Investigation of the efficiency of cooling the rotating shaft of a furnace fan using single-disk devices. *Bull. Ferrous Metall.* **2**, 73–77 (2018). (in Russian)



Simulation Research of Machining-Induced Surface Layer Operational Characteristics

Vadym Stupnytsky^(✉) , Ihor Hrytsay , and She Xianning 

Lviv Polytechnic National University, 12, Bandera Street, Lviv 79000, Ukraine
stupn@i.ua

Abstract. The analysis of the rheological model, which formalizes the influence of the main technological factors on the formation of residual stresses and strains in the cutting process, is described in the article. An explanation of the physical phenomena of deformation processes during cutting and comparing theoretical conclusions with simulation studies results are given. The main task, the solution of which is proposed, is the generalization and system analysis of methodological studies of the influence of the technological factors and the cutting tool's geometry on the formation of the stress-strain and thermodynamic state of the surfaces of the workpieces during the cutting. Such problem-oriented modeling results are the basis for predicting the impact of technological process parameters on the formation of product's operational properties. An original scheme for determining the residual strains on top and in the machined surface depth is proposed. The analysis of the influence of technological operation data on residual strain formation was carried out using DEFORM 3D simulation.

Keywords: Functional-oriented process · Residual strain · Simulation study · Finite element analysis · Cutting parameters

1 Introduction

The lifecycle of mechanical engineering products depends on a large number of different factors [1]. Most scientific research usually focuses on the design and operation phases of a product. Undoubtedly, the macrogeometric shape of the part, material, quality of loaded surfaces of structural parts, conditions of their operation, the efficiency of scheduled repair, and service are of great importance for ensuring a machine's reliable and long-term operation or mechanism. However, a large number of properties of an engineering product are also formed at the manufacturing stage (machining and assembly). Additionally, in the process of machining, only the requirements that the designer assigned are met. However, this statement is only partially correct. For example, a given surface quality requirement can be achieved by different machining technologies. However, due to the use of some technologies, residual compressive stresses will appear in the processed layer of the workpiece (as a result of edge-tool cutting), and otherwise, residual tensile stresses appear on the surface layer (if abrasive processing technologies were used). The designer cannot influence the formation of these properties since they result

from the subsequent design stage of the product manufacturing technology. However, the sign of the residual stresses has a significant impact on ensuring the product's fatigue resistance. There are many examples of the importance of the impact of technological process performance on the operational properties of a machine.

Thus, for a comprehensive increase in the efficiency of the engineering products life cycle, the creation and implementation of scientific and applied foundations for the design of functionally oriented technologies are relevant [2]. The function of the goal in the formation of the optimal data of technological operations is to provide using concurrent engineering a complex of functional and operational properties of the product while observing the parameters of accuracy and quality of surfaces, service life, as well as organizational, technical and economic constraints specified by the designer [3].

2 Literature Review

The section of technological science, "Surface Integrity", is devoted to solving these issues. The most important studies were carried out by such scientists as J. Paulo Davim [3], Fritz Klocke [4], Viktor P. Astakhov [3], Wit Grzesik [5]. There are two aspects of surface integrity: topography characteristics and surface layer characteristics. The topography consists of surface roughness, waviness, shape errors, and imperfections. Characteristics of the surface layer can change during machining: plastic deformation, residual stresses, cracks, hardness, wear resistance, phase transitions, recrystallization, intergranular fracture, and hydrogen embrittlement. In traditional manufacturing processes (such as machining), the surface layer can withstand localized plastic deformation [6].

The chemical composition, mechanical properties, microstructure of the workpiece surface layer primarily affect the workability of the processed materials and thermal state in the cutting zone [7, 8]. Besides, there are intense processes in the chip-forming zone, accompanied by significant differences in force and stress-strain state of the machined layer and are a source of self-oscillations of the tool [9], loss of workpiece stability, various thermal deformation phenomena [10]. All this will affect the formation of the accuracy and other performance properties of the product.

It is known [7] that the cutting tool's forceful action causes the compaction of the crystal lattice of the processed surface layer of the workpiece. A layer of material with increased hardness is formed on the surface as a result of work hardening. However, the thermal state in the cutting zone within the range (0.25–0.30) of the processed material's melting temperature causes the tempering of the deformed metal of the surface layer, and the temperature above 0.4 of the melting temperature causes its recrystallization. A partial decrease in strain hardening accompanies this process. That is, in the process of cutting in the surface layer of the workpiece to be machined, two opposite processes simultaneously occur: strain hardening and thermodynamic softening. The physical state of the machined layer of the workpiece is determined by the ratio of these processes' intensity and velocity.

Furthermore, such a dynamic process's analytical description is extremely complicated and often inadequate [11, 12]. The decrease in the yield stress's actual value can be explained by the dominant influence of the thermal factor, which leads to the softening

of the material. An increase in the shear stress of the cut layer can be explained by the fact that a leading strain zone leads to an intensive increase in the dislocation density near the shear zone and, consequently, strengthening the material. This is explained by the fact that the layers of material from the main cutting edge, rounding the edge, and the auxiliary cutting edge are superimposed when they move along the corresponding shear planes. Therefore, there is a “self-locking” of the material layers [7].

The residual stresses imposed in this way from all these factors are diverse and opposite in signs. Establishing the dominant factor and not taking into account others is a difficult task that requires additional experimental research. Besides, in many cases, the actions of all these factors are approximately equivalent and interrelated. Therefore, the possibility of imitating rheological simulation of the cutting processes is the only way to quickly and adequately analyze the influence of cutting technological parameters (e.g., the structure of technological operation, machining parameters, tool coating, selection of an external technological environment) on the formation of residual stresses [13].

Another essential property of the machined layer is a residual strain (mechanical hardening). This deep inhomogeneity of properties is primarily due to the uneven distribution of the deformation accumulated due to cutting. Deformation anisotropy and the associated residual stresses can significantly reduce the product's strength when it is not subject to further heat treatment. In other cases, the machined layer's hardening has a positive effect on the wear resistance, as soon as an increase in corrosion resistance. A negative consequence of this phenomenon is a reduced oil-holding property of the surface layer, which is especially important for high-speed moving joints' efficiency. The calculation of residual stresses is performed according to the unloading theorem [14], according to which the residual stresses after plastic deformation are equal to the difference in stresses during plastic deformation and the so-called unloading stresses, which the material is deprived of during unloading. If during unloading, purely elastic deformations occur, then the unloading stress can be determined using the theory of elasticity [15]. The hardening of the surface layer of the machined surfaces is characterized by its microhardness and X-ray characteristics (expansion or blurring of interference lines), which is a consequence of the fragmentation of crystal blocks, an increase in crystal lattice distortions, and the development of dislocations. In the cutting process, the hardening of the surface layer increases with an increase in feed and depth of cut due to an increase in the cutting edge rounding and the transition from positive rake angles of the cutter to negative [16].

3 Research Methodology

The given research's primary purpose is to assess the mutual influence of the main technological parameters (cutting modes) on the formation of residual stresses and strains during the cutting process with an edge tool. The influence of cutting parameters on the formation of stress-strain state (including the residual) is usually presented in the form of statistic equations [17], based on conducting experiments using one- or multifactor experiments. Therefore, the main task, the solution of which is proposed in this article, is the generalization and system analysis of methodological studies of the influence of force, thermal factors and parameters of the tool geometry on the stress-strain and thermal

state of the workpiece surfaces during the cutting process. The analysis of such problem-oriented modeling is the basis for building predictive models of the technological process parameters' effect on the formation of product's operational properties.

The machined surface layer's mechanical state has mainly resulted from the after-effect of elastic-plastic strains, which occurs in the cutting zone, thermal exposure, and chemical reactions of the machined material with the cutting tool material and with the external technological environment (including coolant and lubricant). When the tool is cut-in into the metal being processed, the wave of plastic deformation, propagating in front of the tool's cutting edge, covers the chips and the metal located along the cut line. Therefore, machined material at the cutting edge itself is subjected to the normal force and the friction force acting in the shear line's direction. The normal force causes the compressive stress, and the friction force induces tensile stresses of the surface layer adjacent to the tool's flank face (Fig. 1). The surface layer of the part is subject to inhomogeneous plastic strain, monotonically damping, and cutting depth [13].

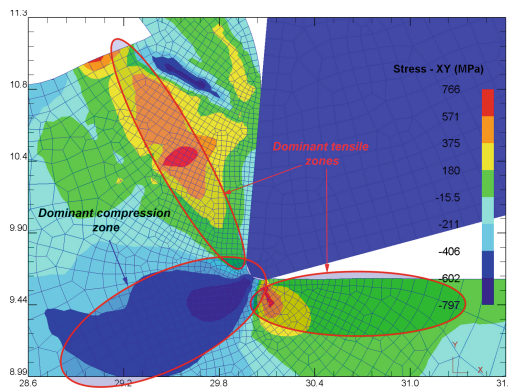


Fig. 1. Simulation pattern of residual stresses causal factors as interference of the compression and tension phenomena in the cutting zone.

Another reason for the occurrence of residual stresses is the thermal deep processes analysis [13]. The outer layer of the workpiece, heating up during the cutting process, tends to linear expansion. However, this is prevented by the cold inner layer, which is compressed. With intense heating, the current stresses on the surface exceed the yield stress, which causes plastic compression strain of the outer metal layer. The outer layer shrinks to a size less than the original by the value same as additional compression strain during subsequent cooling. This will be blocked by the stressed workpiece inner layer (Fig. 1). Therefore, either the mechanical factor can be dominant, and then the macrostress of compression prevails on the processed surface; or the heat factor, and then tensile stresses on the surface will become superior. However, this sequence will be violated if the cutting process is accompanied by significant phase transformations that are significant in intensity and depth. This phenomenon is sometimes a stronger source of stress formation in surface layers than mechanical and thermal factors.

The disadvantage of analytical modeling of the macrostress formation process is conventionality in the differentiated analysis of the influence of mechanical or temperature indicators, dependence on experimentally obtained correction factors, and the fact that it does not consider the force acting on the machined layer. This relativism does not correspond to the actual process of the temporary or residual stresses appearance. Until now, the only way of analysis was considered by the methods of experimental research: X-ray, experimental-mechanical, and the method of measuring microhardness [18]. The problem-oriented analysis of the corresponding simulation rheological modeling results will comprehensively and adequately assess the picture of the mutual influence of the force, mechanical and metallographic factors. This will contribute to implementing the optimal structure and parameters of the technological processing operation to minimize residual stress and strain.

One of the effective tools for the operational study of local characteristics of the stress-strain state in the chip's formation zone is the finite element analyses implemented in such well-known software products as DEFORM, ABAQUS, LS DYNA, AdvantEdge. These software products allow accurately calculating the cutting forces, chip thickness ratio, configuration, and area of the contact surface of the workpiece with the tool and the boundaries of the plastic zone, to make the distribution of force and deformation, obtain strain rates, and temperatures in the machined zone and the tool [2].

4 Results

The results of microhardness studies prove the presence of residual stresses and plastic deformations. The thin surface layer of machine parts has various mechanical, physical, chemical properties and stress than in the deep of the part. As noted above, the difference in the properties along the depth of the part is caused by a defect of mechanical, thermal, and physicochemical factors of different intensity and is obtained as a result of power and thermodynamic machining processes. This contributes to an increase in the free energy of the surface, increasing its adsorption activity and other changes that significantly impact the performance of the machined products [17].

The plastic strain must be accompanied by structural changes in the material of the machined layer. The number of dislocations, vacancies, and other defects in the crystal lattice increases sharply. During cutting, plastic deformation occurs, accompanied by fragmentation and drawing of crystal grains in the direction of deformation (texture formation), the curvature of sliding planes, and the appearance of fragments of crystal grains, the emergence of intercrystalline stresses. Besides, when processing plastic metals, the subsurface layer is deformed not only due to the force field of the rake face but also simultaneously deformed under the action of flowing chips. Due to the intensity of plastic strain of the metal chips is much higher than the intensity of deformation of the metal under the shear surface, the deformed particles under the influence of the upper layer of metal going into the chips are further stretched in the direction of chip's moving at the angle greater than 45° . This increases the specific volume of the metal and decreases its density, increases the strength, hardness, and brittleness, decreases ductility and viscosity, changes the magnetic and some other properties of the metal.

The cutting speed and feed have the most significant influence on the deformation of the surface layer because these parameters of the cutting mode determine mainly the

mechanical and thermal effects on the metal. As the cutting speed increases, the strain rates and the heating temperature increase, but the duration of stresses and the heating time of the surface layer of the workpiece decrease. Increasing heating of the deformed metal with increasing cutting speed increases the diffusion mobility of atoms, activates the softening processes due to recrystallization, reducing the intensity of deformation hardening of the surface layer. If the strain rate exceeds the recrystallization rate, only partial removal of the strain hardening is observed, despite the deformation will occur at a temperature exceeding the recrystallization temperature. The simulated rheological studies of technological transitions of machining of parts from the most representative machinery materials show that with increasing cutting speed, the thermal effect on the deformed metal of the surface layer increases and hardness decreases.

Compared with other parameters of the cutting parameters, the feed rate has the most significant effect on the deformation hardening of the surface layer. The values of the depth and hardening depending on the feed have extremes, i.e., there is an optimal feed, in which this hardening is the least important. The optimal feed for heat-resistant alloys is about 0.10–0.15 mm/rev. The increase in strain hardening with decreasing feed outside the optimal feed values is explained by the influence of the sliding process of the cutting edge, which creates additional deformation of the surface layer. The force load and the heating temperature of the metal in the cutting zone determine the nature of these dependencies. The feed has the most critical effect on the force acting on the surface layer. With an increase in cutting depth in turning, planning, and drawing, the main parameters of deformation hardening are increased. The rake angle of the tool cutter also affects the conditions of chip formation, which determine the formation of the surface layer. For example, when turning a NiCr20TiAl alloy with a change in the rake angle from $+15^\circ$ to -15° , the depth of hardening increases 3 times, which is associated with an increase in the resistance of the chips on the rake face of the cutter.

Rheological simulation of the heat-resistant alloy IN 718 turning, determined based on the analysis of the simulation model in Deform 2D, showed a decrease of the hardness by 55% compared with the processing of steel AISI 1045 in cutting parameters – feed $S = 0.25$ mm; cutting depth $t = 1$ mm; cutting speed $V = 120$ mm/min. The reduction of hardness, in this case, can help increase the strength and decrease the plastic properties of alloys and significantly reduce the coefficient of friction on the flank face of the cutter.

It is known [3] that the degree of hardening is defined as the ratio of the initial H_0 and the newly created (after machining) H hardness of the workpiece to its initial value:

$$N = \frac{H - H_0}{H_0}, \quad (1)$$

when turning heat-resistant alloys, the degree of hardening can be calculated according to the empirical equation [19]:

$$N = 40 h T_0^{-0.72}, \quad (2)$$

where h is the depth of hardening, which is determined by the results of rheological simulation of machining, μm ; T_0 - the temperature in the cutting zone when working with a carbide tool, which can also be determined by the results of rheological simulation.

Plastic strain and hardening of the surface layer of the metal occur in oppositely oriented grains of different compositions with different intensities; at that, ferrite grains

are deformed more intensely than pearlitic. This causes an uneven increase in energy and various changes in the electrode potential. During turning, more hardened ferrite grains and martensitic domains become anodes, less hardened pearlite grains are cathodes. For the same reasons, the distortion of atomic lattices in different crystal grains is different.

Hardening of the machined surface layer in most cases is harmful and reduces the performance of machine parts. Consequently, after the plastic deformation of the surface layer metal at room temperature, its specific volume increases, and the density decreases, promoting faster diffusion processes at high temperatures and thus accelerating the processes that reduce the resistance of the metal to dynamic destruction. Prolonged exposure to high temperatures on the hardened metal quickly leads to its intensive softening, which reduces the overall performance of the parts. The micro-hardness of the metal surface layer is responsible after its operation at high operating temperatures. Reducing the density of hardened metal facilitates the process of burning alloying elements of heat-resistant alloys, which leads to a decrease in the strength of alloys. A sign of burnout of alloying elements may be a change in the crystal lattice parameter of the heat-resistant alloys. With increasing degree and depth of hardening of heat-resistant alloys, their fatigue strength when working in an environment with high temperatures decreases significantly. Thus, at a hardening depth of $190\ \mu\text{m}$, which occurs during rough turning, the number of cycles before the destruction of the alloy at $700\ ^\circ\text{C}$ is approximately twice lower than after electropolishing, which does not cause hardening [4].

Scheme for determining residual strains on the basis of a 2D model of milling a workpiece made of steel AISI-N-13 by the CoroMill 300 cutter with a R300-1032E-PL S30T insert $\gamma = 8^\circ$, $\alpha = 15^\circ$ ($S = 0.1\ \text{mm}$; $t = 0.25\ \text{mm}$; $V = 120\ \text{m/min}$) is shown in Fig. 2. The total path of the tool along the length of the machined part of the part is separated into 22 ranges, and along with the depth - into 10 measurement ranges in order to analyze the dynamics of attenuation and studying the residual component of the stress-strain state as the aftereffect of the machining process.

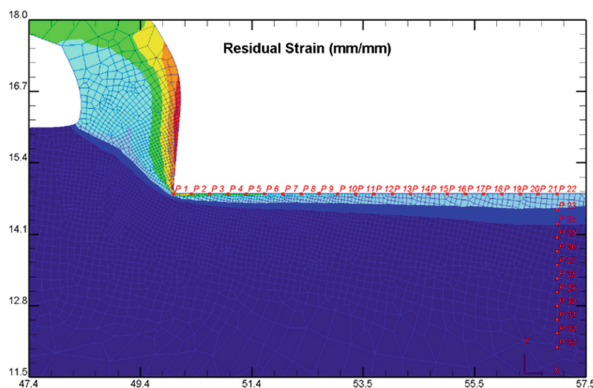


Fig. 2. Scheme for determining residual strains on the basis of a 2D model of milling a workpiece made of AISI-N-13 by the CoroMill 300 cutter with a R300-1032E-PL S30T insert $\gamma = 8^\circ$, $\alpha = 15^\circ$ ($S = 0.1\ \text{mm}$; $t = 0.25\ \text{mm}$; $V = 120\ \text{m/min}$).

The pattern of residual strains rheological simulation during milling a workpiece (material is alloyed steel X40CrMoV5) by the CoroMill 300 cutter with the R300-1032E-PL S30T insert ($\gamma = 8^\circ$, $\alpha = 15^\circ$; $S = 0.1$ mm; $t = 0.25$ mm; $V = 120$ m/min) is shown in Fig. 3. As a result of thermal relaxation with increasing distance from the head of the cutting wedge, these deformations exponentially decrease to some steady-state value in the zone of thermal deformation stabilization. It is this value that is the residual strain. The curve of residual strains (Fig. 3) shows the interference pattern of the fluctuations in thermal, load, and frictional processes arising in the cutting process. The average statistical value of residual strain in the zone of thermal stabilization (at a temperature of about 100°C) will be approximately $\varepsilon \approx 2.5$ (mm/mm).

The method for determining the depth of residual strains is similar, but the test points for measuring deformations are not located along the length of the processed surface but into the deep (Fig. 2). The modeling of the depth pattern should also be done in the zone of thermal stabilization of the machined surface. The simulation results are shown in Fig. 4.

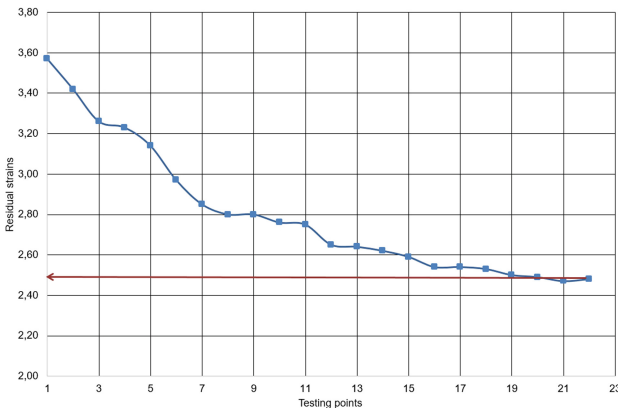


Fig. 3. Graph of surface residual strains obtained as a result of rheological simulation of milling a workpiece made of X40CrMoV5 ($S = 0.1$ mm; $t = 0.25$ mm; $V = 120$ m/min).

The presence of local traces of residual strains during the machining of plastic materials (for example, titanium alloys) is due to the complex nature of the dynamic load on the tool (Fig. 5). The sinusoidal and dissonant character of the longitudinal and transverse component of the cutting force causes local hardening zones of the surface layer's material and local softening zones. The most representative of this can be seen from modeling in Deform 3D (Fig. 6). The presence of alternating hardness zones significantly reduces the fatigue strength of the surface and the corrosion resistance of the machine part. Therefore, an essential step in assigning cutting parameters for such alloys is to reduce the dynamic component of the force action. The general recommendations of such a study are presented in [13].

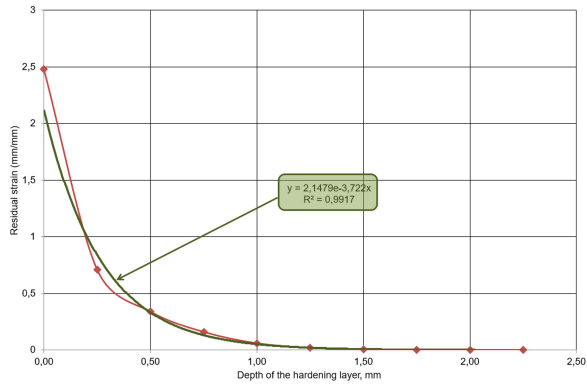


Fig. 4. Graph of residual strains into the deep obtained results from rheological simulation of milling a workpiece made of X40CrMoV5 ($S = 0.1$ mm; $t = 0.25$ mm; $V = 120$ m/min).

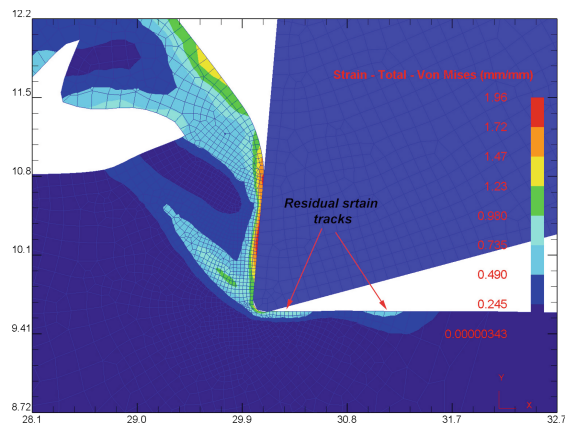


Fig. 5. Local traces of residual strains during the machining of titanium alloy Ti6Al4V.

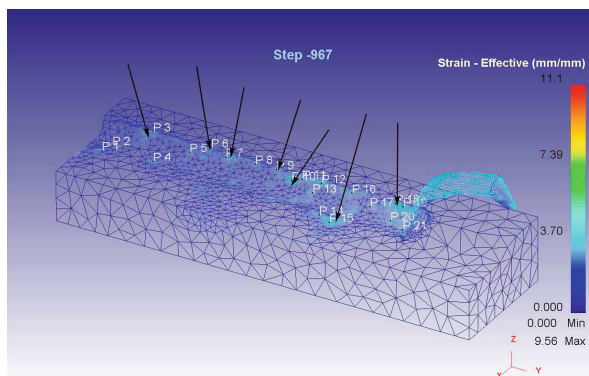


Fig. 6. Local traces of residual strains simulated in Deform 3D.

The analysis of the adequacy of modeling was carried out due to comparison with the results of experimental studies. Such comparative results were carried out using the method of measuring the microhardness of the surface layer before and after machining (Fig. 7). The analysis of the research results showed the comparability of the surface hardening value obtained from modeling and experimental research within 6–8%.



Fig. 7. Experimental study of the machined surface layer microhardness of the alloyed steel workpiece (X40CrMoV5).

5 Conclusions

Analysis of the influence of the technological operations data such as cutting parameters, tool's material, and the geometry of the cutting wedge on the residual strains, carried out based on rheological simulation in Deform 2D and 3D, allowed us to make the following conclusions.

Analysis of graphics (Figs. 3, 4) proves the exponential nature of the reduction of residual strains: if on the top of machined surface this value was $\varepsilon \approx 2.5$ (mm/mm), then for the depth of 0.25 mm, it is already $\varepsilon \approx 0.7$, and for the depth of 1.0 mm, the cutting-induced strain almost completely disappears and is only $\varepsilon \approx 0.06$ (mm/mm). The qualitative and quantitative nature of the distribution of strains proves the adequacy and effectiveness of the used methods for the formation of the analytical base in the functionally oriented technological process planning.

The influence of the cutting speed is declared, first, in the change in the duration of the thermal contact and force impact between the flowing chips, the treated surface, and the tool's cutting edge. Increasing the cutting speed contributes to the emergence of additional tensile strain, which increases the total residual tensile stress. When processing low-carbon steels (for example - AISI 1020), the increase in heat in the cutting zone,

associated with increasing the cutting speed, can harden the surface layer. The increase in the specific volume of the metal of the surface layer during its hardening leads to a decrease in residual tensile stresses formed at low speeds ($V = 40\text{--}80$ m/min) and their conversion into compressive stresses during machining at high cutting speeds ($V > 100$ m/min). Besides, when processing plastic metals, the subsurface layer is deformed not only under the influence of the force field of the cutter's rake face but also deformed under the influence of the flowing chips. Since the intensity of plastic strain of the metal chips is much higher than the intensity of deformation of the metal under the shear surface, the deformed particles under the influence of the upper layer of metal going into the chips are further stretched in the direction of chip's moving at the angle greater than 45° . This increases the specific volume of the metal and decreases its density, increases the strength, hardness, and brittleness, decreases ductility and viscosity, changes the magnetic and some other properties of the metal.

The presence of local traces of residual strains during the machining of plastic materials (for example, titanium alloys) is due to the complex nature of the dynamic load on the tool. The sinusoidal and dissonant character of the longitudinal and transverse component of the cutting force causes local hardening zones of the surface layer's material and local softening zones. The presence of alternating hardness zones significantly reduces the fatigue strength of the surface and the corrosion resistance of the machine part. Therefore, an essential step in assigning cutting parameters for such alloys is to reduce the dynamic component of the force action.

When processing carbon steels (for example, AISI 1045) and low-alloy steels (34CrNiMo6), increasing the heating of the surface layer by increasing the cutting speed above 120 m/min can cause the material's tempering. As a result, there are changes in the material structure associated with a decrease in the specific volume of the metal, which leads to a decrease in residual compressive stresses. Increased feed rate during the processing of hard-to-cut steels and alloys (for example, IN718), in which residual tensile stress is formed, leads to an increase in the plastic strain of the surface layer and a corresponding increase in residual tensile stresses. This leads to a significant reduction in the fatigue strength of the machined surface. Rheological simulation of the heat-resistant alloy IN 718 turning, determined based on the analysis of the simulation model in Deform 2D, showed a decrease of the hardness by 55% compared with the processing of steel AISI 1045 in cutting parameters - feed $S = 0.25$ mm; cutting depth $t = 1$ mm; cutting speed $V = 120$ mm/min. The reduction of hardness, in this case, can help increase the strength and decrease the plastic properties of alloys and significantly reduce the coefficient of friction on the flank face of the cutter.

References

1. Krueger, C.W.: Mechanical product lifecycle management meets product line engineering. In: Proceedings of the 19th International Conference on Software Product Line, vol. 1, pp. 316–320. Association for Computing Machinery, New York (2015)
2. Palagin, A.V.: Functionally oriented approach in research-related design. *Cybern. Syst. Anal.* **53**(6), 986–992 (2017). <https://doi.org/10.1007/s10559-017-0001-0>
3. Davim, J.P.: *Surface Integrity in Machining*. Springer, London (2010)

4. Klocke, F., Harst, S., Ehle, L., Zeis, M., Klink, A.: Surface integrity in electrochemical machining processes: an analysis on material modifications occurring during electrochemical machining. *Proc. Inst. Mech. Eng. Part B: J. Eng. Manuf.* **4**(232), 578–585 (2018)
5. Grzesik, W., Żak, K.: Characterization of surface integrity produced by sequential dry hard turning and ball burnishing operations. *J. Manuf. Sci. Eng.* **136**(3), 031017 (2014)
6. Degarmo, E.P., Black, J.T., Kohser, R.A.: *Materials and Processes in Manufacturing*, 9th edn. Wiley, Hoboken (2003)
7. Klocke, F.: *Manufacturing Processes 1: Cutting*. Springer, Heidelberg (2011). <https://doi.org/10.1007/978-3-642-11979-8>
8. Klocke, F.: *Manufacturing Processes 4: Forming*. Springer, Heidelberg (2013). <https://doi.org/10.1007/978-3-642-36772-4>
9. Astashev, V.K., Korendyasev, G.K.: Thermomechanical model of cutter self-oscillation in perpendicular free cutting. *J. Mach. Manuf. Reliab.* **41**, 435–440 (2012)
10. Abukhshim, N.A., Mativenga, P.T., Sheikh, M.A.: Heat generation and temperature prediction in metal cutting: A review and implications for high speed machining. *Int. J. Mach. Tools Manuf.* **46**(7–8), 782–800 (2006)
11. Gygax, P.E.: Cutting dynamics and process-structure interactions applied to milling. *Wear* **62**(1), 161–184 (1980)
12. Czán, A., Šajgalík, M., Martikán, A., Mrázik, J.: Dynamic process analysis in cutting zone during machining of nickel alloys. *Technol. Eng.* **12**(1), 15–20 (2015)
13. Stupnytskyy, V., Hrytsay, I.: Simulation study of cutting-induced residual stress. In: Ivanov, V., et al. (eds.) *DSMIE 2019. LNME*, pp. 341–350. Springer, Cham (2020). https://doi.org/10.1007/978-3-030-22365-6_34
14. Eraslan, A.N., Apatay, T.: Analytical solution to thermal loading and unloading of a cylinder subjected to periodic surface heating. *J. Therm. Stresses* **39**(8), 928–941 (2016)
15. Perez, N.: Theory of elasticity. In: Perez, N. (ed.) *Fracture Mechanics*. Springer, Cham (2017). https://doi.org/10.1007/978-3-319-24999-5_1
16. Shen, Q., Liu, Z., Hua, Y., Zhao, J., Mohsan, A.W.: Effects of cutting edge microgeometry on residual stress in orthogonal cutting of Inconel 718 by FEM. *Materials* **11**(6), 1015 (2018)
17. Stupnytskyy, V., Hrytsay, I.: Comprehensive analysis of the product's operational properties formation considering machining technology. *Arch. Mech. Eng.* **67**(2), 149–167 (2020)
18. Montanari, R., Fava, A., Barbieri, G.: Experimental techniques to investigate residual stress in joints. In: *Residual Stress Analysis on Welded Joints by Means of Numerical Simulation and Experiments* (2018).
19. Silin, S.: *Similarity Methods in Metal Cutting*. Mechanical Engineering, Moscow (1979)



An Experimental and Statistical Investigation on Cutting Forces in Turning of AISI 304 Stainless Steel Under Dry, MQL and Nanofluid MQL Conditions

Youssef Tougoui^{1,2} , Alper Uysal²  , Uğur Emiroglu² ,
and Eshreb Dzhemilov³ 

¹ Structures Research Laboratory (LS), University of Blida, Blida, Algeria

² Yildiz Technical University, Beşiktaş, 34349 Istanbul, Turkey
auysal@yildiz.edu.tr

³ Crimean Engineering and Pedagogical University, Simferopol, Republic of Crimea, Ukraine

Abstract. Machining AISI 304 austenitic stainless steel is well-known as it is very challenging due to its low thermal conductivity and hardening tendency. High-cutting forces are one of the common problems encountered during the machining of this kind of hard-to-cut materials. An attempt to improve its machinability while ensuring environmentally friendly conditions has been made. This experimental study was conducted from the perspective of performance assessment of machining parameters in turning AISI 304 under dry, minimum quantity lubrication (MQL), and nanofluid MQL conditions with consideration of the cutting forces. Additionally, as a methodology, the response surface methodology (RSM) and quantitative evaluation based on the primary effects plot were used. The study revealed that nanofluid MQL offered encouraging results compared to the MQL and dry conditions. Ultimately, the desirability function optimization method (DF) has been successfully executed to determine the best optimal machining responses under different cutting cooling conditions.

Keywords: Cutting forces · MQL · Nanofluid · Nano graphene · AISI 304 · Response surface methodology · ANOVA

1 Introduction

In recent years, the need to meet the machining field's ecological and environmentally friendly aspects has become an increasingly relevant theme in research trends. Researchers have attempted a number of sustainable machining methods, such as dry, minimum quantity lubrication (MQL), and nanofluid-MQL cooling. Therefore, some investigations have been undertaken on this issue, particularly in the machining of difficult-to-cut materials such as AISI 304 stainless steel, Ni-based alloys, and Ti-based alloys. Based on the previous studies, eco-friendly sustainable machining has greatly increased its importance in the metal-cutting industry, especially in difficult-to-cut materials. Apart from that, an experimental investigation was carried out in this paper on the

straight turning of AISI 304 stainless steel to statistically investigate the effect of cutting speed, feed, and cooling/lubricating conditions including dry, MQL, and nanofluid MQL on the main cutting and thrust forces.

2 Literature Review

Elbah et al. [1] performed AISI 4140 high-strength-low-alloy (HSLA) steel turning tests. Researchers studied the influence of cutting parameters such as cutting speed, feed, depth of cut and cutting radius, and dry, wet, and MQL machining environments on cutting force components. As a result, greater enhancement of the resulting cutting force was achieved under MQL machining compared to wet and dry machining environments. In their study, Rajmohan et al. [2] used a tow form of cutting fluids when turning of AISI 316L stainless steel. The authors observed that the cooling and lubricating properties of cutting fluid had been enhanced due to the inclusion of nano-particles, and the feed greatly impacted the cutting forces. Das et al. [3] carried out the hard turning experiments of HSLA steel using three different nanofluids and compared the results in terms of cutting force. The experimental findings concluded that copper oxide (CuO) nanofluid performed better than other nanofluids in terms of cutting force. Nouioua et al. [4] experimentally investigated the machinability issue of X210Cr12 steel under dry, wet, and MQL cooling conditions. It was achieved that better results in terms of cutting forces were observed for the MQL method than wet and dry machining. Bedi et al. [5] studied the effect of cutting speed on machining performance of AISI 304 under MQL conditions. Researchers examined the application potential of coconut oil and rice bran oil as cutting fluids.

Response surface methodology (RSM) -modeling method- has been widely used in the machining process. It has been proven to be effective for establishing productive models. For instance, in the study reported by Nouioua et al. [4], cutting force models were developed using the RSM approach. Based on the results, RSM models were found to be suitable for predicting cutting forces with accurate goodness of fit. In another investigation, Tebassi et al. [6] applied the RSM technique to predict cutting forces during the turning of Inconel 718. Researchers found out that RSM-generated models present a satisfactory agreement between actual values of cutting forces and estimated ones.

Likewise, finding the optimum cutting parameters has been considered a necessity in the machining process field to prevent poor quality characteristics. Therefore, various alternative computational methods such as Desirability Function (DF) have been applied successfully to optimize process parameters. Touggui et al. [7] optimized the cutting parameters during dry turning AISI 316L. The authors found that cutting speed of 212.84 m/min, feed of 0.08 mm/rev, and depth of cut of 0.1 mm were determined to minimize cutting force. Similarly, Selaimia et al. [8] experimentally explored the influence of design variables on cutting force in milling of AISI 304L and optimized the DF method's outcomes. From experimental results, a cutting force was impacted by the depth of cut followed by feed. In their study, Laghari et al. [9] used the DF approach to optimize cutting forces in turning hard-to-cut material. In literature [10, 11], it was reported that the DF technique was successfully implemented to determine the ideal

solutions under different nano-cutting cooling environments. Notably, Pavlenko et al. [12, 13] applied artificial neural networks for parameter identification of cutting forces. The influence of the contact zone's parameters on the turning of stainless steels was studied by Klimenko et al. [14]. Recently, the optimization of process parameters for reducing cutting forces while turning of AISI 316L was investigated by Tougui et al. [15].

3 Research Methodology

Straight turning experiments of AISI 304 with an axial length of 300 mm and diameter of 70 mm were carried out on a CNC lathe under dry, minimum quantity lubrication (MQL) nanofluid MQL cutting conditions. The cutting inserts were used as coated carbide inserts which are designated as ISO specification, namely TNMG 160408-MM 2025 supplied by Sandvik. In the MQL method, a commercial vegetable cutting fluid was used. In the nanofluid MQL method, graphene particles were added to the vegetable cutting fluid at 0.1% wt. During the turning operation, the metal-working lubricant was sprayed by a nozzle to the rake face at a flow rate of 30 ml/h and a pressure of 0.5 MPa using the MQL system. Cutting forces measurements were performed by utilizing Kistler piezoelectric dynamometer (type 9257B), which was attached to the charge amplifier, and LabVIEW software for measuring the sampling frequency and recording the force's database. The experimental set-up is given in Fig. 1. Twenty-seven experimental tests were conducted according to Taguchi's L27 orthogonal array. The parameters tested and their levels are given in Table 1.

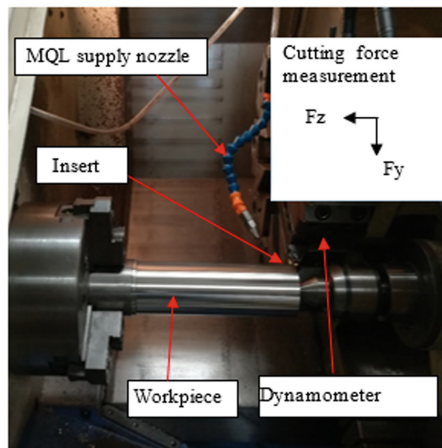


Fig. 1. Experimental set-up.

Table 1. The studied control factors and their levels.

Factors	Level 1	Level 2	Level 3
Cooling and lubricating conditions	Dry	MQL	Nanofluid MQL
Cutting speed (m/min)	160	190	220
Feed (mm/rev)	0.12	0.16	0.2

4 Results

Experimental findings associated with turning AISI 304 under various cutting conditions are discussed in this section. The first set of 9 experiments was conducted under dry conditions, the second set of 9 under MQL, and the next 9 under nanofluid MQL condition using nanographene as a cooling and lubricating agent. The results of main and thrust cutting forces are depicted in Figs. 2 and 3.

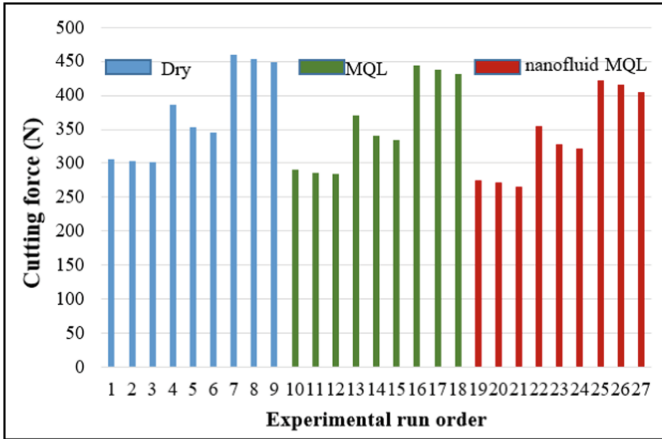


Fig. 2. Main cutting force in dry, MQL, and nanofluid MQL straight turning.

It can be observed that the nanofluid MQL condition provided the best results in terms of cutting forces (F_y and F_z) compared to dry and MQL approaches. In comparison, the MQL offered improved results than the dry machining tests. This is primarily due to the cooling and lubricating capabilities of both nanofluid MQL and MQL methods to significantly minimize the intense rubbing between the cutting and machined steel. In addition, the mist used tends to prevent the thermal shock process and therefore balances the thermal softening happening to the cutting tool [16, 17]. The lowest cutting force values were found in the cutting test No. 21, which was conducted at a cutting speed of 220 m/min and feed of 0.12 mm/rev when nanofluid MQL was used, compared to MQL and dry conditions with an improvement of 5.80% and 11.65%, respectively.

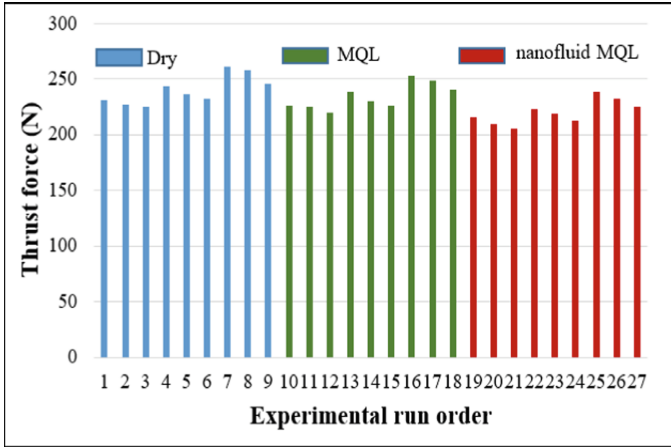


Fig. 3. Thrust force in dry, MQL, and nanofluid MQL straight turning.

In this study, the RSM was used to formulate a regression model between turning process responses and the design factors. The regression model for response parameters is expressed by Eq. 1:

$$\varphi = a_0 + \sum_{i=1}^k a_i X_i + \sum_{\substack{i=1 \\ i \neq j}}^k a_{ij} X_i X_j + \sum_{i=1}^k a_{ii} X_i^2 + \varepsilon \quad (1)$$

The established models for F_y (main cutting force) and F_z (thrust force) under dry, MQL, and nanofluid MQL are given in Eqs. 2–4 and 5–7. The correlation coefficients of all proposed models were greater than 0.98. Besides, these constructed models will be used in the multi-objective optimization process case.

$$F_{y_{\text{Dry}}} = + 438.05111 - 1.69222 * V_c - 465.15972 * f - 1.32153 * V_c * f + 4.18889E - 003 * V_c^2 + 8135.41667 * f^2 \quad (2)$$

$$F_{y_{\text{MQL}}} = + 422.64722 - 1.69017 * V_c - 465.40972 * f - 1.32153 * V_c * f + 4.18889E - 003 * V_c^2 + 8135.41667 * f^2 \quad (3)$$

$$F_{y_{\text{Nanofluid MQL}}} = + 425.29278 - 1.71206 * V_c - 565.32639 * f - 1.32153 * V_c * f + 4.18889E - 003 * V_c^2 + 8135.41667 * f^2 \quad (4)$$

$$F_{z_{\text{Dry}}} = + 217.98198 + 0.20170 * V_c - 106.04861 * f - 1.40069 * V_c * f - 4.26543E - 004 * V_c^2 + 2209.02778 * f^2 \quad (5)$$

$$F_{Z_{MQL}} = + 217.21698 + 0.20975 * V_c - 147.13194 * f - 1.40069 * V_c * f - 4.26543E - 004 * V_c^2 + 2209.02778 * f^2 \quad (6)$$

$$F_{Z_{Nanofluid\ MQL}} = + 208.31586 + 0.20364 * V_c - 173.34028 * f - 1.40069 * V_c * f - 4.26543E - 004 * V_c^2 + 2209.02778 * f^2 \quad (7)$$

The main effects plot shows each control factor's importance, such as cutting speed, feed, and cooling/lubricating condition on F_y and F_z . The effects of the studied turning process parameters on the main cutting and thrust forces are seen in Figs. 4 and 5 and discussed as follows:

The Effect of Cutting Speed

The cutting speed affects the cutting forces (F_y and F_z), particularly the main cutting force (F_y). The increase in cutting speed results in the reduction of F_y and F_z . It was observed that the lowest cutting forces could be attained by turning AISI 304 with the highest cutting speed (220 m/min). With the increase in cutting speed, a higher temperature is generated in the chip contact area. As a consequence of this, thermal softening takes place in the cutting area [18]. As a result, the chip becomes thinner and reduces the cutting forces [19].

The Effect of the Feed

The feed shows a strong effect on the cutting forces F_y and F_z . It is evident that, with the rise in feed, the cutting force tends to increase. This can be clarified as due to the long-chip contact region on the rake face [18]. Hence, an increase in the tool-chip section is a function of increased feed, leading to increased cutting forces. Other researchers have also outlined that feed is the most contributing parameter for cutting force [2, 20].

The Effect of Cooling and Lubricating Condition

The cooling and lubricating conditions also substantially affect cutting forces, especially on the thrust force (F_z) (shown in Figs. 6 and 7). Interestingly, the findings demonstrate that graphene-based nanofluid MQL exhibits efficiency in reducing main cutting and thrust forces. The explanation for this was attributed to the nanoscale structure (platelets) and lubrication properties of graphene, which could reduce friction between the tool and the workpiece [21], thus minimizing cutting forces and improving the dimensional accuracy of the workpiece.

Among the studied factors, including cutting speed, feed, and cutting condition, the feed has the most significant effect on F_y and F_z , followed by cooling and lubricating conditions.

The normal probability plots of RSM-derived F_y and F_z models were given in Fig. 6. It was clear that most data points were fallen close to the straight-line trend. It may also be suggested that the assumptions of normality have been verified [22]. The estimated RSM values were compared with the experimental values and obtained in good agreement, as shown in Fig. 7.

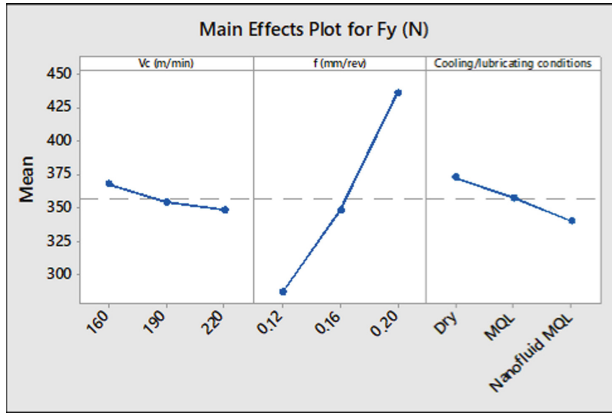


Fig. 4. Main effect plots for main cutting force (F_y).

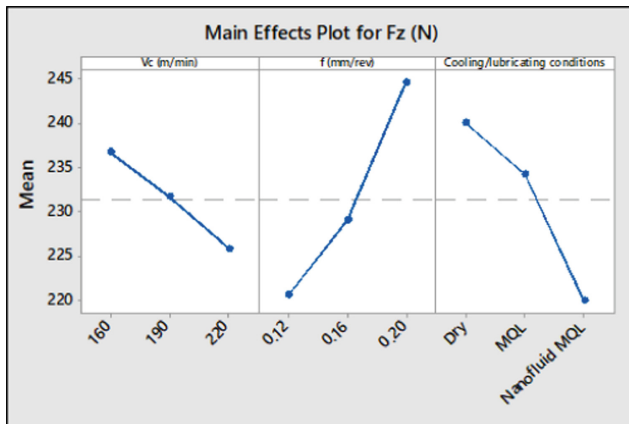


Fig. 5. Main effect plots for thrust force (F_z).

In this study, the desirability function (DF) is performed using Design-Expert (10) software to accomplish the multi-objective purpose.

The best optimum cutting setting determined by multi-objective optimization using DF to minimize F_y and F_z was also found to be similar to the cutting setting in cutting test No. 21, when the lowest F_y and F_z were achieved during turning with the highest cutting speed (220 m/min) and smallest feed (0.12 mm/rev) under nanofluid MQL condition as shown in Fig. 8. Thus, there is no need to do a confirmation test.

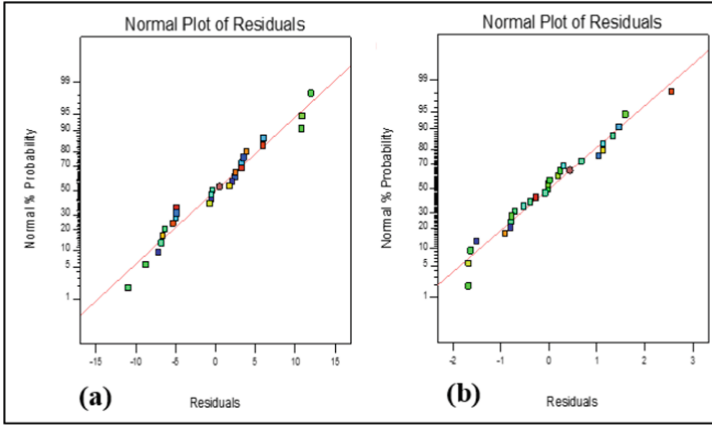


Fig. 6. Normal probability plots for a) F_y and b) F_z .

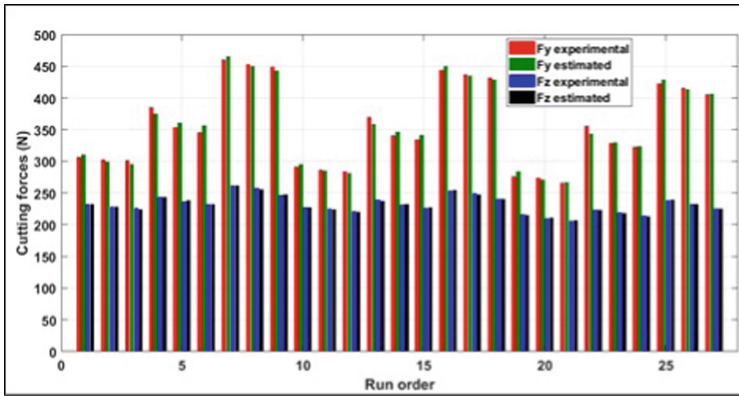


Fig. 7. Cutting force comparisons between experimental and RSM estimated values of F_y and F_z .

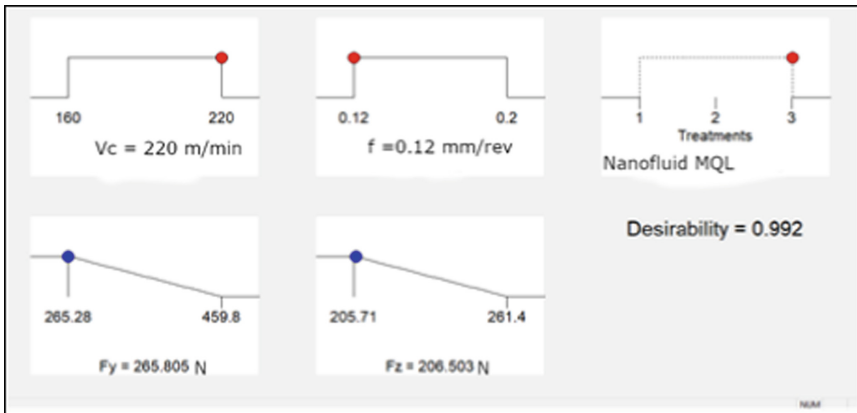


Fig. 8. Ramp function graph of the combined optimization.

5 Conclusions

In the current experimental research, an attempt was made to investigate the effects of turning process parameters on the main cutting and thrust forces when turning AISI 304 stainless steel. The considered turning process parameters were taken as cutting speed, feed, and cooling/lubricating condition. The RSM and main effects plots were used to develop the mathematical predictive models and assess the effect of various factor variables on responses. The desirability function was employed for the optimization of the responses. Based on the results, the following conclusions can be drawn:

- The nanofluid MQL gave promising results for the reduction of cutting forces relative to dry and MQL techniques. This is mainly accredited to the cooling/lubricating capability of the nanofluid MQL to reduce the intensity of the high heat produced in the shear plan region.
- The rise in cutting speed contributes to a decrease in cutting forces (F_y and F_z). This is due to the rise in cutting temperature in the cutting zone, which leads to the thermal softening of the manufactured material.
- The cutting forces (F_y and F_z) tend to increase with the increase in feed attributed to a large tool-chip contact area due to increased feed.
- The lowest F_y and F_z were obtained while turning at the highest cutting speed (220 m/min) and smallest feed (0.12 mm/rev) under nanofluid MQL.

In further research, more focus will be given to investigate and compare the effect of different solid lubricants concentration and their hybrids on machining AISI 304 stainless steel in terms of surface roughness, temperature, and chip morphology.

References

1. Elbah, M., Laouici, H., Benlahmidi, S., Nouioua, M., Yallese, M.A.: Comparative assessment of machining environments (dry, wet and MQL) in hard turning of AISI 4140 steel with CC6050 tools. *Int. J. Adv. Manuf. Technol.* **105**(5–6), 2581–2597 (2019). <https://doi.org/10.1007/s00170-019-04403-9>
2. Rajmohan, T., Sathishkumar, S.D., Palanikumar, K., Ranganathan, S.: Modeling and analysis of cutting force in turning of AISI 316L stainless steel under nano cutting environment. *Appl. Mech. Mater.* **766–767**, 949–955 (2015)
3. Das, A., Kumar Patel, S., Das, S.R.: Performance comparison of vegetable oil based nanofluids towards machinability improvement in hard turning of HSLA steel using minimum quantity lubrication. *Mech. Ind.* **20**, 506 (2019)
4. Nouioua, M., Yallese, M.A., Khettabi, R., Belhadi, S., Mabrouki, T.: Comparative assessment of cooling conditions, including MQL technology on machining factors in an environmentally friendly approach. *Int. J. Adv. Manuf. Technol.* **91**(9–12), 3079–3094 (2017). <https://doi.org/10.1007/s00170-016-9958-5>
5. Bedi, S.S., Behera, G.C., Datta, S.: Effects of cutting speed on MQL machining performance of AISI 304 stainless steel using uncoated carbide insert: application potential of coconut oil and rice bran oil as cutting fluids. *Arab. J. Sci. Eng.* **45**, 8877–8893 (2020)

6. Tebassi, H., Yallese, M.A., Meddour, I., Girardin, F., Mabrouki, T.: On the modeling of surface roughness and cutting force when turning of Inconel 718 using artificial neural network and response surface methodology: accuracy and benefit. *Period. Polytech. Mech. Eng.* **61**(1), 1–11 (2017)
7. Touggui, Y., Belhadi, S., Mechraoui, S.E., Yallese, M.A., Temmar, M.: Statistical study and multi-response optimization of cutting parameters for dry turning stainless steel AISI 316L using cermet tool. *Adv. Eng. Forum* **36**, 28–46 (2020)
8. Selaimia, A., Yallese, M.A., Bensouilah, H., Meddour, I.K., Khattabi, R., Mabrouki, T.: Modeling and optimization in dry face milling of X2CrNi18-9 austenitic stainless steel using RMS and Desirability approach. *Measurement* **107**(1), 53–67 (2017)
9. Laghari, R.A., Li, J., Mia, M.: Effects of turning parameters and Parametric optimization of the cutting forces in machining SiCp/Al 45 wt% composite. *Metals* **10**, 840 (2020)
10. Gupta, M.K., et al.: Performance evaluation of vegetable oil-based nano-cutting fluids in environmentally friendly machining of Inconel-800 alloy. *Materials* **12**, 2792 (2019)
11. Öndin, O., Kivak, T., Sarıkaya, M., Yıldırım, Ç.V.: Investigation of the influence of MWCNTs mixed nanofluid on the machinability characteristics of PH 13–8 Mo stainless steel. *Tribol. Int.* **148**, 106323 (2020)
12. Pavlenko, I., et al.: Parameter identification of cutting forces in crankshaft grinding using artificial neural networks. *Materials* **13**(23), 5357 (2020). <https://doi.org/10.3390/ma13235357>
13. Pavlenko, I., Trojanowska, J., Ivanov, V., Liaposhchenko, O.: Parameter identification of hydro-mechanical processes using artificial intelligence systems. *Int. J. Mechatron. Appl. Mech.* **2019**(5), 19–26 (2019)
14. Klimenko, S.A., Klimenko, S.An., Manokhin, A.S., Mel' nichuk, Yu.A., Kopieikina, M.Yu., Chumak, A.A.: Contact stresses on the rake face of cutting tools with PCBN in turning of hardened steel. *J. Eng. Sci.* **4**(1), F8–E14 (2017). [https://doi.org/10.21272/jes.2017.4\(1\).f2](https://doi.org/10.21272/jes.2017.4(1).f2)
15. Touggui, Y., Belhadi, S., Uysal, A., Temmar, M., Yallese, M.A.: A comparative study on performance of cermet and coated carbide inserts in straight turning AISI 316L austenitic stainless steel. *Int. J. Adv. Manuf. Technol.* **112**(1–2), 241–260 (2020). <https://doi.org/10.1007/s00170-020-06385-5>
16. Hegab, H., Umer, U., Deiab, I., Kishawy, H.: Performance evaluation of Ti-6Al-4V machining using nano-cutting fluids under minimum quantity lubrication. *Int. J. Adv. Manuf. Technol.* **95**, 4229–4241 (2018)
17. Hegab, H., Kishawy, H.A., Umer, U., Mohany, A.: A model for machining with nano-additives based minimum quantity lubrication. *Int. J. Adv. Manuf. Technol.* **102**(5–8), 2013–2028 (2019). <https://doi.org/10.1007/s00170-019-03294-0>
18. Sied Ahmed, Y., Youssef, H., El-Hofy, H., Ahmed, M.: Prediction and optimization of drilling parameters in drilling of AISI 304 and AISI 2205 steels with PVD monolayer and multilayer coated drills. *J. Manuf. Mater. Process.* **2**(1), 1–16 (2018)
19. Seid Ahmed, Y., Paiva, J., Covelli, D., Veldhuis, S.: Investigation of coated cutting tool performance during machining of super duplex stainless steels through 3D wear evaluations. *Coatings* **7**, 127 (2017)
20. Nur, R., Noordin, M.Y., Izman, S., Kurniawn, D.: Machining parameters effect in dry turning of AISI 316L stainless steel using coated carbide tools. *J. Process Mech. Eng.* **231**(1), 676–683 (2017)
21. Xu, Y., Peng, Y., Dearn, K.D., Zheng, X., Yao, L., Hu, X.: Synergistic lubricating behaviors of graphene and MoS₂ dispersed in esterified bio-oil for steel/steel contact. *Wear* **342–343**, 297–309 (2015)
22. Mia, M., et al.: Effect of time-controlled MQL pulsing on surface roughness in hard turning by statistical analysis and artificial neural network. *Int. J. Adv. Manuf. Technol.* **91**(9–12), 3211–3223 (2017). <https://doi.org/10.1007/s00170-016-9978-1>

Advanced Materials



Strengthening of the NKV Type Centrifugal Pump's Shaft by Chemical-Thermocycling Treatment

Kristina Berladir^(✉) , Tetiana Hovorun , and Oleksandr Gusak 

Sumy State University, 2, Rymyskogo-Korsakova Street, Sumy 40007, Ukraine
kr.berladir@pmtkm.sumdu.edu.ua

Abstract. The paper is devoted to studying the process of nitrocementation with cycling heating compared to nitrocementation with isothermal heating. The purpose of thermocycling nitrocementation is to grind the base's structure and the surface layer of steel type AISI 5140, which produces the centrifugal pump's shaft. The metallographic analysis showed that the grain score after isothermal and after thermocycling nitrocementation varies from № 5–6 to № 9 in the core and № 5–6 to № 10 in the diffusion layer (respectively). The thickness of the protective layer after thermocycling nitrocementation is 1.50 more than isothermal nitrocementation, which indicates a positive effect of thermal cycling on the saturation rate of the steel matrix. The depth of the protective layer obtained during nitrocementation and surface hardness are the criteria for assessing the shaft's serviceability. It is established that thermocycling nitrocementation in comparison with isothermal leads to increase cavitation resistance by 0.6–1.5 times. The use of chemical-thermocycling treatment leads to reduced time, grinding of grain, and improved mechanical properties of constructional steel.

Keywords: Pump · Shaft · Nitrocementation · Thermocycling treatment · Cavitation wear · Cavitation resistance

1 Introduction

Sumy is a powerful center of pump building, including a complex of leading manufacturers of pumps: JSC Nasosenergomash Sumy, SUMY ENGINEERING WORKS Ltd, JSC «VNIIAEN» etc. [1]. Departments of Sumy State University should be added to this complex because they are engaged in training students for further employment, development, and modernization of pumping equipment and modification of materials and technologies for strengthening the main parts of pump units.

The priority of Sumy pump manufacturers is the creation of responsible pumps for thermal and nuclear energy, oil production and pipeline transport of oil, and the complete supply of technological equipment for the oil, gas, and chemical industries.

Oil centrifugal pumps NK and NKV type and pumping units based on them ANK and ANKV type are used in technological installations of oil refining and petrochemical industries for pumping oil, petroleum products, liquefied hydrocarbon gases, and other

liquids, similar to those specified in the material properties and corrosive effects on the material of pump parts, with temperatures up to 360 °C [2].

Modernization of the pump design aims to reduce the metal content at the same parameters of the pumps, ensuring the greatest unification of pump parts, allowing to extend the range of pumps without significant additional costs for their production. Improving the quality and reliability of pumps, which saves energy resources and reduces the complexity of their operation and repair, is relevant and important.

1.1 Purpose and Operating Conditions of the Shaft of Centrifugal Pump

The main parts of the centrifugal pump are pump body, cover, bearing body, shaft, angular contact ball bearings, radial roller bearing of the shaft seal, impeller (Fig. 1) [3].

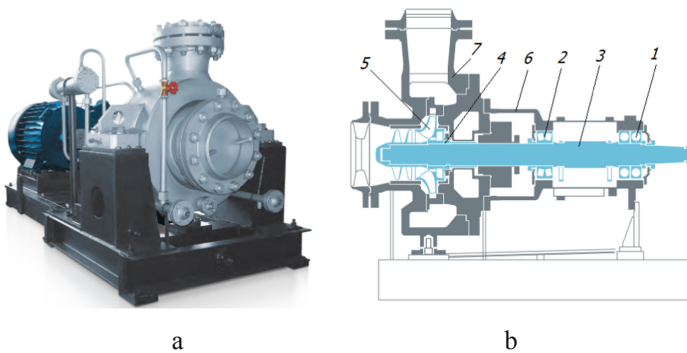


Fig. 1. Appearance (a) and a longitudinal section (b) of the pump NKV type: 1, 2 – bearings; 3 – shaft; 4 – stuffing box seal; 5 – impeller 6 – body; 7 – cover with the inlet pipe.

Shaft 3 of the pump (Fig. 1) is a cylindrical part with a step change of diameters and is used to transmit rotation to the impeller from the pump motor. The shaft of the multistage pump is the basic part of the pump rotor. Pumps NKV type are designed for pumping flammable and combustible liquids in the technological processes of the oil refining industry. They can be used to pump water in hazardous areas.

The shaft operates under conditions of intense alternating loads [4, 5]. This type of work requires a combination of high surface hardness and a sufficiently viscous core. When the material of the shaft interacts with the pumped environment (often inhomogeneous, containing abrasive particles), the processes of corrosion, cavitation, and abrasive wear occur. Significant wear can also occur during shaft operation in dry friction conditions in contact with bearings or directly with the impeller. Under such operating conditions, the surface layer must have high hardness and wear resistance, be inert to the material of bearings and impellers.

2 Literature Review

For improving the properties and characteristics of materials for the production of pumps, including shafts, extend their service life, increase reliability and durability, use various

technologies of thermal and chemical-thermal, as well as thermocycling and chemical-thermocycling treatment [6–8].

The author [9] developed and investigated the technology of local surface hardening of cylindrical gear of steel 45L. It was found that the higher the temperature of nitrocementation, the greater the depth of the diffusion layer and a more uniform difference in hardness over the thickness of the layer.

At the development of diffusion layers, it is necessary to observe a condition of the saturating atmosphere and conditions of heating of the material processed by chemical-thermal treatment, including to temperature of nitrocementation [10].

If in the process of heating and processing of the material the value of this potential remains above the ratio γ'/ϵ , the diffusion layers will consist of γ' - and ϵ -phases. However, if the potential value is lower than the above ratio during nitrocementation, the layers formed on the metal substrate during the diffusion saturation process will consist of only one γ' -phase [7]. The authors [11, 12] investigated the influence of laser heat treatment of nitrocementation steel on the phase composition, structure, and hardness of surface layers. It was shown that the combined heat treatment of steels (nitrocementation + laser hardening) allows providing high wear resistance of surface layers of steel.

Thermocycling treatment (TCT) is one of the promising types of hardening steels. Structural and phase transformations, in contrast to other types of heat treatment, repeatedly occur at a variable temperature «heating-cooling» during thermal cycling. The need for repeated processing at specified temperatures, as a rule, due to the desire to accumulate changes in the structure radically improves the quality of products and gives them properties that are unattainable with a single heat treatment [13].

In the paper [14], it was shown that cyclic heating and cooling significantly accelerate the kinetics of the process of chemical heat treatment of steel. The regularities of the formation of reinforced layers during thermocycling nitrocementation of steel 20H were considered. Production tests of machine parts after chemical thermal and chemical-thermocycling treatment were performed. The structure, phase composition, and intensity of the wear process depending on the number of cycles were studied.

TCT has the following main parameters: heating rate; cooling rate on each cycle; highest and lowest temperature; cooling rate on the final cycle; the number of cycles from 2 to hundreds.

The main schematic models, phase transformations, and mechanisms of structural change during thermocycling are described in detail in papers [13, 14].

The authors [15] were considered the processes occurring when the surface is saturated with various elements. Porous and high-density powder materials were subjected to chemical-thermal treatment. Various ways of technological processes have been developed. The dependences of the thickness of the nitrocemented layer on the total porosity at different temperatures of nitrocementation and the change in the proportion of open porosity on the granulometric composition of the powder were investigated. The optimal saturation modes and the parameters affecting the formation of the diffusion layer have been determined.

It was established that as a result of thermocycling processing, only a fine-grained structure up to nanometric is formed, which gives the steel product high operational properties [16].

In the paper [17], the influence of electrolytic-plasma carbonitration on the dislocation structure and field strength of low-carbon steel 18HN3MA-SH was studied. It was shown that after carbonitration in electrolytic plasma, the shape of the phase particles, their size, and relative position are different, and an α -matrix surrounds the particles of all phases. Compared with the initial state of the steel, the torque stresses were much lower, i.e., electrolyte-plasma carbonitration led to a decrease in internal stresses.

The paper [18] focused on creating a technology to improve the performance parts' properties due to the regularity of the structure of the core and surface of steels in thermocyclic modes of thermal and chemical-thermal treatment. Induction cyclic heating grinds steel grain to 12–14 points, and after cementation increases the number of carbides in the diffusion layer (hardness 66–68 HRC). Medium carbon steel after cementation, induction cyclic heating, quenching, and low tempering have a high toughness of 35–45 J/cm².

In article [19], the structure, morphology, and mechanical properties of carbon coatings were investigated. Also, the influence of heat treatment technologies on the structure and properties of corrosion-resistant steels was studied in the article [20].

Additionally, artificial neural networks for ensuring the reliability of pump shafts are applied in research works [21, 22]. Finally, TCT is a method of heat treatment based on constant accumulation from cycle to cycle of positive changes in the structure of metals [13, 23, 24].

3 Research Methodology

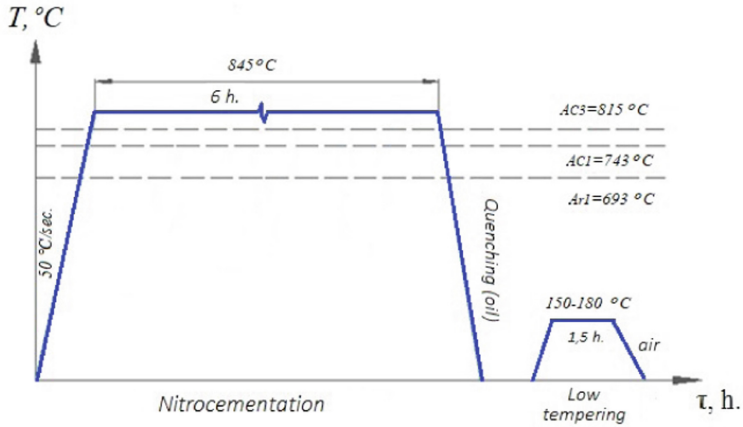
This paper presents the research results of structural alloy steel type AISI 5140 during nitrocementation with TCT.

For the experiment, samples measuring 10 × 10 × 20 mm were made, the surfaces of which were thoroughly cleaned of dirt, rust, and polished. The surface of the sample was decreased with alcohol. The process of saturating the surface of steel type AISI 5140 with nitrogen and carbon was combined with the process of thermal cycling and quenching. This technology aimed to obtain on the surface of the product a protective layer of high enough hardness and wear resistance.

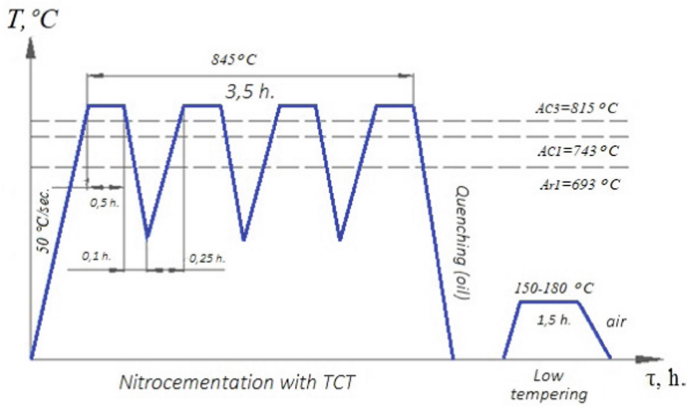
The process of nitrocementation with thermocyclic heating and subsequent quenching was performed in a furnace CИИОЖ 1.1.6/12. The maximum heating temperature was ($Ac_3 + (30-50)$) °C. The minimum temperature of thermal cycling is equal to 450 °C (Fig. 2). At the maximum temperature and minimum temperature of the thermal cycling used in this work, an isothermal exposure of 0,5 h. was performed. The total time of the chemical-thermocycling treatment process (Fig. 2, b) was 6 h.

Exposure at a temperature of 450 °C was realized by transferring the container from this furnace to the furnace CИИО 2.4/7. This furnace was also used for low tempering. Quenching was implemented in oil quenching tanks. Pincers were used to load and unload the container into the furnace.

Microstructure studies were performed on a metallographic microscope MIM-7. Identifying the steel structure was carried out by chemical etching with a 3–4% solution of nitric acid in ethyl alcohol.



a



b

Fig. 2. Graphics of heat treatment of steel type AISI 5140 during nitrocementation (a) and nitrocementation with TCT (b).

Wear tests in the conditions of dry friction-sliding were implemented on a friction machine SMT-1. Wear two methods performed resistance tests. The amount of wear was evaluated relative to the weight of the sample, before and after testing, on high-precision analytical balances VA-200.

Tests for cavitation resistance were carried out on a magnetostrictive ultrasonic disperser UZDN-2T of samples after nitrocementation, quenching, and low tempering for 8 h, measuring the weight loss every 30 min.

4 Results

The following structure was recorded by metallographic analysis of type AISI 5140 steel samples. The basis of steel type AISI 5140 after nitrocementation, quenching, and low tempering is fine-needle martensite and residual austenite. The surface layer of steel after nitrocementation coincides with the data of the authors [7, 11, 12, 25] and contains carbonitride ε -phase $(\text{Fe, Me})_{2-3}(\text{N, C})$ or oxycarbonitride $(\text{Fe, Me})_{2-3}(\text{N, C, O})$ phase. In some cases, the surface zone of the ε -phase contains a significant number of pores. The surface nitride zone located evenly on thickness makes 25–30 μ . Iron carbonitride $(\text{Fe, Me})_4\text{NC}$ (γ -phase) is also present in this zone.

One of the objectives of thermocycling nitrocementation is grinding the structure of the base and the surface layer of steel type AISI 5140, that used for the producing of the shaft of the centrifugal pump. It was established that the grain score of steel type AISI 5140 after isothermal and thermocycling nitrocementation varies from № 5–6 to № 9 in the core and from № 5–6 to № 10 in the diffusion layer respectively.

Two methods determined the thickness of the protective layer – metallographic visually and using a microhardness tester PMT-3. The thickness of the protective layer after thermocycling nitrocementation was 1.2–1.4 mm, which is more than with isothermal nitrocementation by 1.50. Comparing the thickness of the layer after thermocycling and isothermal nitrocementation, it can conclude the positive effect of thermal cycling on the saturation rate of the steel matrix. The depth of the protective layer obtained during nitrocementation and the surface hardness is the criteria for assessing the serviceability of the shaft. The distribution profile of microhardness corresponds to the distribution of nitrogen and carbon by depth.

The distribution of microhardness over the thickness of the layer is presented in Fig. 3. It is possible to conclude the positive influence of nitrocementation and gradual decrease in hardness from a surface to a basis of steel type AISI 5140. The hardness of the base is 36–40 HRC.

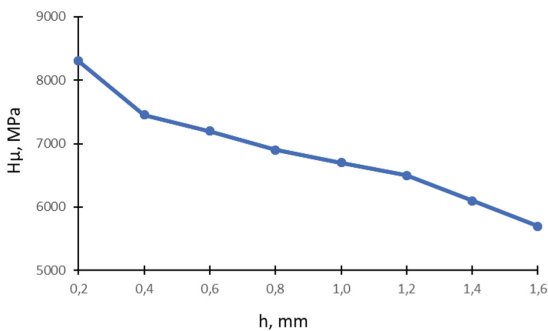


Fig. 3. Distribution of microhardness by the depth of nitrocemented layer of steel type AISI 5140, where h – distance from the surface, H_μ – microhardness.

Tests for wear of steel type AISI 5140 after nitrocementation with thermocycling heating, quenching, and tempering were carried out by sliding friction without lubrication

according to the liner-shaft scheme. The contact was realized on the side surface of the sample (liner). The amount of wear was determined by weight. The metallographic analysis of the wear holes gave information about the nature of wear. In wear holes of steel type AISI 5140, the lines of microcutting are observed after complex processing. They directed in the course of friction that is characteristic of the prevailing abrasive type of wear are observed. The abrasive is individual particles of the coating separated from the base during the test. The distance between the lines – traces of cutting are significant. It can be assumed that the abrasive nature of wear according to this test method will be decisive. If we take the coefficient of wear resistance of steel type AISI 5140 without treatment per unit, we obtained the following data of relative stability after different heat treatment (Table 1).

Table 1. Test results of steel type AISI 5140 for wear.

Type of processing	Mass of the sample before testing, g	Mass of the sample after testing, g	Weight loss of the sample during the test, g	Coefficient of wear resistance
Without processing	16.72896	16.47231	0.38664	1.00
Quenching, tempering	11.50561	11.29991	0.21951	1.77
Nitrocementation, quenching, tempering	7.162010	6.994210	0.16781	2.31
Nitrocementation + TCT, quenching, tempering	15.45821	15.23871	0.13809	2.82

The amount of wear was determined by measuring the area of the wear hole. As a result, the following data were obtained (Fig. 4). Steel type AISI 5140 after nitrocementation with thermocyclic heating, hardening, and low tempering is subject to the least wear.

Most authors point out that nitrocementation increases the cavitation resistance of steels [11, 26]. Figure 5 shows the curves of cavitation wear of the surface of steel type AISI 5140 after various types of processing.

As seen from Fig. 5, steel type AISI 5140 has the highest resistance after nitrocementation with TCT, quenching, and low tempering at cavitation for 8 h. The nitrocemented layer on steel type AISI 5140 has a lower cavitation resistance than the nitrocemented layer with thermocycling heating. During the cavitation of the sample after nitrocementation with ordinary heating, brittle fracture and cracking occurred after 2 h. This is due to the large grain size and lower microhardness of the layer than steel after complex processing. Comparing the surface layers, we can conclude that at first, the level of resistance of nitrocemented layers differs several times. After wear for 8 h, their cavitation resistance levels off, which can be associated with the same level of microhardness at a depth of 125–150 μ .

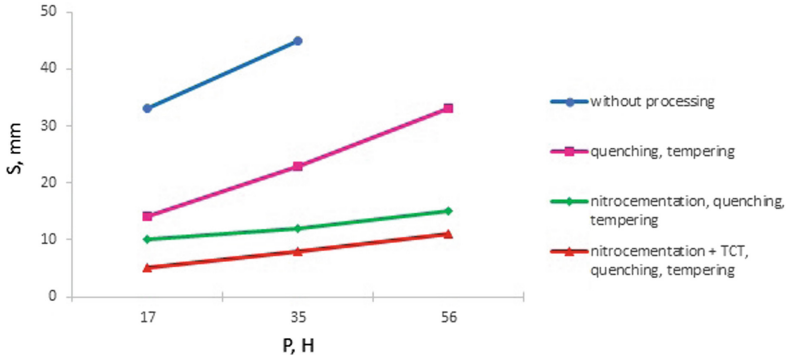


Fig. 4. Dependence of the amount of wear of steel 40H on the load, $t = 600$ min., $V = 0,36$ m/s, P – load, S – the amount of wear.

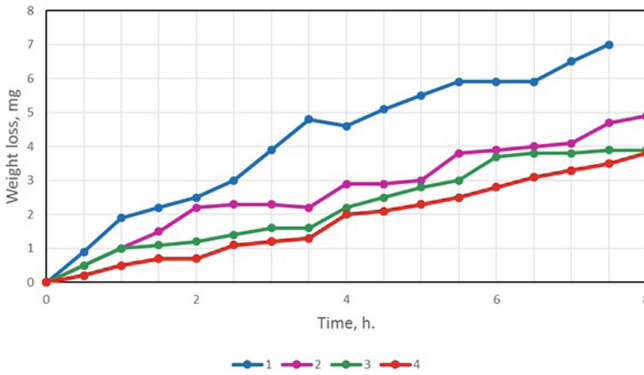


Fig. 5. Cavitation wear of steel type AISI 5140 after different types of processing: 1 – without processing, 2 – quenching, tempering, 3 – nitrocementation, quenching, tempering, 4 – nitrocementation + TCT, quenching, tempering.

The highest cavitation rate for steel type AISI 5140 samples without treatment and after heat treatment is observed during the first hour. In turn, the highest cavitation rate for samples after chemical-thermal treatment is observed in the interval of 3–4 h of testing. The increase in weight loss in the samples is associated with the acceleration of electrochemical reactions due to cavitation mixing of the liquid and the acceleration of diffusion. As a result of cavitation wear, uniform sloughing of the surface of the samples occurred. In Fig. 6, they are represented as light areas.

An explanation of this behavior of nitrocemented layers can be the initiation of subsurface (lateral) cracks. The formation of subsurface cracks is most likely at the interphase boundaries and the boundaries «coating – steel type AISI 5140».

The results of laboratory tests showed that thermocycling nitrocementation, in comparison with isothermal, leads to an increase in cavitation resistance by 0.6–1.5 times.

6. Berladir, K., Hovorun, T., Bondarenko, M., Shvetsov, D., Vorobiov, S.: Application of reinforcing thermocycling treatment for materials of stamps hot deformation. *J. Eng. Sci.* **6**(2), C6–C10 (2019). [https://doi.org/10.21272/jes.2019.6\(2\).c2](https://doi.org/10.21272/jes.2019.6(2).c2)
7. Nitriding. <http://www.uk-finishing.org.uk/N-COAT70/nitriding.htm>. Accessed 10 Oct 2020
8. Degula, A.I., et al.: Investigation of phase and chemical composition of complex carbide coatings. *Metallofiz. Noveishie Tekhnol.* **37**(11), 1461–1476 (2016). <https://doi.org/10.15407/mfint.37.11.1461>
9. Kostyk, K.O.: Development of technology for local surface hardening of cylindrical gear wheel of a centrifugal mixer. *Innov. Mater. Technol. Metall. Mech. Eng.* **2**, 39–43 (2015)
10. Gatey, A.M., Hosmani, S.S., Figueroa, C.A., Arya, S.B., Singh, R.P.: Role of surface mechanical attrition treatment and chemical etching on plasma nitriding behavior of AISI 304L steel. *Surf. Coat. Technol.* **304**, 413–424 (2016). <https://doi.org/10.1016/j.surfcoat.2016.07.020>
11. Bakhacheva, Yu.: Increase of steel surface operational properties by combined hardening. *J. Phys: Conf. Ser.* **1050**(1), 012006 (2018). <https://doi.org/10.1088/1742-6596/1050/1/012006>
12. Bakhacheva, Yu.: Combined methods of laser processing of steel. *Solid State Phenom.* **284**, 242–246 (2018). <https://doi.org/10.4028/www.scientific.net/SSP.284.242>
13. Cheiliakh, A.P., Cheiliakh, Ya.A., Samotugina, Yu.S.: Strengthening technologies of materials treatment. PSTU, Mariupol (2015)
14. Bakhacheva, Yu., Vasilyev, A.V., Petikova, T.N.: Solution to the diffusion problem in the thermocyclic nitro-cementation of steel. *Mater. Sci. Forum* **870**, 545–549 (2016). <https://doi.org/10.4028/www.scientific.net/MSF.870.545>
15. Prous, N., Korchagin, M., Sukhomlinov, V., Oleynikov, I.: Nitro-cementation of powder materials. *Mater. Sci.* (2018). <https://doi.org/10.23947/itno.2018.1.86-88>
16. Komolikhov, A.S., Kalinin, S.A., Kozyr, I.G., Kuzenkov, S.Ye.: Method of thermal cycling treatment of steels. Patent of Russia, No. 0002646180 (2018)
17. Bayatanoval, B., Rakhadilovb, K., Satbayeva, Z.A., Popovan, A.: Internal stresses and dislocation structure of low-carbon steel after electrolyte-plasma nitro-cementation. *Int. J. Mech. Prod. Eng. Res. Dev. (IJMPERD)* **10**(3), 14493–14502 (2020)
18. Tkachenko, G.A.: Features of induction thermal cycling treatment of structural steel parts. *Metall. Mech. Eng. Mater. Process. Technol.* **2**, 155–163 (2014)
19. Kulesh, E.A., Piliptsov, D.G., Rogachev, A.V., Hong, J.X., Fedosenko, N.N., Kolesnyk, V.: Boron-carbon coatings: structure, morphology and mechanical properties. *J. Eng. Sci.* **7**(1), C1–C9 (2020). [https://doi.org/10.21272/jes.2020.7\(2\).c1](https://doi.org/10.21272/jes.2020.7(2).c1)
20. Lupy, O., Hovorun, T., Vorobiov, S., Burlaka, A., Khvostenko, R.: Influence of heat treatment technologies on the structure and properties of the corrosion-resistant martensitic steel type AISI 420. *J. Eng. Sci.* **7**(2), C10–C16 (2020). [https://doi.org/10.21272/jes.2020.7\(2\).c2](https://doi.org/10.21272/jes.2020.7(2).c2)
21. Pavlenko, I., Ivanov, V., Kuric, I., Gusak, O., Liaposhchenko, O.: Ensuring vibration reliability of turbopump units using artificial neural networks. In: Trojanowska, J., Ciszak, O., Machado, J.M., Pavlenko, I. (eds.) *MANUFACTURING 2019. LNME*, pp. 165–175. Springer, Cham (2019). https://doi.org/10.1007/978-3-030-18715-6_14
22. Pavlenko, I., Trojanowska, J., Ivanov, V., Liaposhchenko, O.: Parameter identification of hydro-mechanical processes using artificial intelligence systems. *Int. J. Mechatron. Appl. Mech.* **2019**(5), 19–26 (2019)
23. Singh, J., Nath, S.K.: Improvement in mechanical properties and wear resistance of 13Cr–4Ni martensitic steel by cyclic heat treatment. *Trans. Indian Inst. Met.* **73**(10), 2519–2528 (2020). <https://doi.org/10.1007/s12666-020-02043-2>
24. Liu, C., Peng, Q., Xue, Z.: Microstructure and mechanical properties of Mo-Nb microalloyed medium manganese trip steel by cyclic quenching. *Metall. Mater. Eng.* **25**(2), 139–146 (2019). <https://doi.org/10.30544/426>

25. Khalaf, M.M., Kostyk, V., Demin, D., Kostyk, K.: Modeling of the case depth and surface hardness of steel during ion nitriding. *Eastern-Eur. J. Enterp. Technol.* **2/5**(80), 45–49 (2016). <https://doi.org/10.15587/1729-4061.2016.65454>
26. Fernandes, F.A.P., Heck, S.C., Picone, C.A., Casteletti, L.C.: On the wear and corrosion of plasma nitrided AISI H13. *J. Surface Coat. Technol.* **381**, 125216 (2020). <https://doi.org/10.1016/j.surfcoat.2019.125216>



The Influence of Synthesis Modes on Operational Properties of Oxide Ceramic Coatings on Aluminum Alloys

Nataliya Imbirovych¹ , Oleksandr Povstyanoy¹  , Olha Zaleta¹ ,
Sergey Shymchuk¹ , and Olga Priadko² 

¹ Lutsk National Technical University, 75, Lvivska St., Lutsk 43018, Ukraine
povstjanoj@ukr.net

² National University of Life and Environmental Sciences of Ukraine, 15, Heroyiv Oborony St.,
Kyiv 03041, Ukraine

Abstract. Electrophysical parameters of the process synthesis of oxide ceramic coatings in the plasma of spark discharge for electrolytes 1 g/l KOH (S1); 3 g/l KOH + 1 g/l of liquid glass and 5 g/l KOH + 6 g/l liquid glass, and distances between electrodes from 0.05 m to 4.5 m have been investigated in this work. The influence of synthesis regimes on the physic and mechanical properties of coatings has been researched too. Experiments helped us understand that the reduction in coating thickness at a critical distance between electrodes is dependent on the depletion of the electrolyte, and the maximum microhardness is dependent on the growing of the power in separate spark discharges and (or) the growing of the content of Al_2O_3 in this coating. The influence of the distance between electrodes on its meaning was found with the help of the study on wear resistance. It is experimentally set that the value of the synthesis voltage is influenced by the composition, electrolyte concentration, and the distance between the electrodes: an increase in the distance between the electrodes leads to an increase in the synthesis voltage.

Keywords: Oxide ceramic coating · Plasma and electrolyte synthesis · Forming · Microhardness · Thickness · Wear resistance

1 Introduction

Ensuring the reliability of elements in constructions of technological equipment operated under conditions of friction was and is at the center of engineering practice. Currently, this problem is of growing importance, and it gets new accents in connection with modern trends of technological development processes, which are characterized by more rigid operating modes of the equipment.

Today, aluminum alloys are widely used in aviation, automobile construction, and building constructions with the help of their properties [1]. The feature of duralumin is a combination of low density, high ductility, and specific strength. However, the rapid development of modern technologies requires increased functional properties of such

alloys. For solving this problem, work surfaces of details are applied with protective coatings with predictable properties [2]. According to widely used chemical and thermal analysis (methods) of the coatings creating, we must pay attention to possible environmental problems and other negative phenomena which are associated with intensive heating of the detail or its large part that leads to a change in its matrix structure, the scale formation, and surface curvature [3]. The existing competitive method of surface hardening is coating creations on valve metals by plasma electrolytic oxidation (PEO) as a new technology of intensive anode treatment of metal surfaces [4, 5].

The purpose of this work was to investigate the influence of mutual electrode arrangement on the properties of oxide ceramic coatings (OCC), which are synthesized in alkaline electrolytes and the plasma of spark discharges on the ENAW-2024 alloy.

2 Literature Review

At present, there is no generally accepted model of the process for the conversion of oxide-ceramic coatings on metals. The first attempt to briefly describe the stage of the process was made by such scholars as G.P. Wirtz, K.H. Dittrich, H.G. Schneider. The subsequent attempts of this process describing were made by J.C. Marchenoin and J.P. Masson, who used analogies with classical anodizing and saturation or surface phase formation in the vapor gas membrane [6, 7]. These work [8, 9] describe properties of oxide ceramic coatings synthesized in alkaline electrolytes on titanium alloy and their biological response. Snizhko, L.A, Kalinichenko, O.A., Misnyankin, D.A. investigated the influence of synthesis modes on properties of anodized Ti-15Mo alloy described in the works [10]. In most works related to the modeling process, there are only separate processes stages of the coating forming to be more or less deeply analyzed and described [11, 12]. In particular, there are analyzed and modified stages of electric breakdown in primary oxide film [13], the stage of the start development and ending of the spark discharge through the breakdown of the vapor gas bubble and the transfer of charge and substance in it into these works [14, 15].

There is used an electrochemical cell for the process realization of plasma electrolytic oxidation (PEO). This cell consists of the scheme “working electrode – electrolyte – auxiliary electrode” [16]. Exactly on the working electrode, the PEO process is carried out. There are used corrosion-resistant metal plates placed on one side or on the other side from the working electrode as an auxiliary electrode. However, in most cases, as the auxiliary electrode, we can use a corrosion-resistant metal bath. However, the influence of the distance between electrodes on properties of synthesized oxide ceramics on the aluminum alloy is interesting.

3 Researches Methodology

The plastic bath used the shape of the cutting in a high cylinder with a length of 5 m and a radius of 0.1 m. One of its butts was placed as an auxiliary electrode with stainless steel 1.4541 in size $10 \times 12 \times 1$ cm as the electrochemical cell for the research. The working electrode of the aluminum alloy ENAW-2024 with dimensions of $15 \times 20 \times 3$ mm was placed at a distance of 0.05 m–4.5 m from the working electrode. Electrical

impulses of anode and cathode stresses were filed on electrodes. Integral densities of anode and cathode currents and integral anode and cathode voltages, each, in particular, were measured by voltmeters of the magnetoelectric system of type M2044. The total voltage U_{Σ} between the electrodes was measured by the tester of the magnetoelectric system of type C4315 in the mode of voltage measuring. The general scheme of the feeling of electrical impulses to the electrochemical cell and the measurement of electrical parameters is presented in Fig. 1.

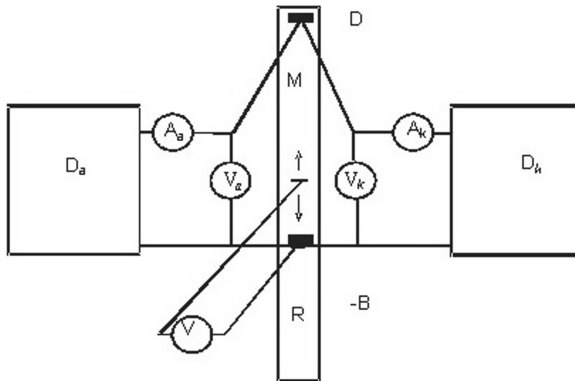


Fig. 1. Principle scheme for measuring of electric parameters in electrolyte bath: D_a – a source of source of anode tension; D_k – cathode tension; A_a, A_k – voltmeter M2044 for measuring of anode and cathode the currents accordingly; V_a, V_k – voltmeters for measuring of anode and cathode tensions; B – bath; D – auxiliary electrode, M – measuring electrode; R – working electrode.

The working electrolyte were solutions in distilled water such as 1 g/l KOH (S1); 3 g/l KOH + 1 g/l liquid glass (l.g.) with density 1.38 g/l and module 3 (S2); 5 g/l KOH + 6 g/l. g. (S3).

The work density of anode current I_a was 10 A/dm², and cathode – I_k 7.5 A/dm², namely – $I_k/I_a = 0.75$. Synthesis of oxide ceramic coatings was carried out for 120 min without stirring of the electrolyte (Fig. 2). Metallography researches were performed on micro-cuts, using microscope Microtech MMP - 14C. The microhardness of the coating was determined on micro-cuts using a stationary hardness tester micro Vickers NOVOTEST TC - MKB1. The microhardness was investigated under an indenter load of 0.001 g with a holding time under a load of 20 s.

Friction tests were carried out on a PTLK friction machine (f. p.). Speed of the slip friction was 0.3 m/s and was regularly supported. The roughness of a surface of the counter sample made of Steel 1.3505 was proved by diamond paste to a value of 0.02 μm by the parameter R_a , controlled by a laser microscope – profilometer LMP. The axial contact load was determined by the Hertz formula and was 400 N.

The criterion of linear wear was taken the average depth of the friction track on a static sample with the investigated coating, which was measured on the profilograph – profilometer “Caliber M - 201”. The friction path for the first, second, and third tracks was 500 m, for the fourth – 1000 m (Fig. 2). The total friction path was 2500 m.



Fig. 2. Samples synthesized on the 2024 alloy after a friction test.

4 Results

The PEO process occurs in the anode and cathode modes. Appropriate voltages measured by voltmeters V_a , V_c , stabilize in a few minutes (Fig. 3). The initial rapid growth of such voltages is due to the breakdown of the electrically conductive film on the metal, which is fixed by high voltages. Depending on the composition of the electrolyte and the distance between the electrodes in the synthesis of coatings, the values of the anode V_a and cathode V_c voltages vary. They are not significantly reduced for large distances between electrodes, and they are constant or slightly increasing for smaller distances. After the breakdown phase of the oxide film, the synthesis process proceeds evenly, as evidenced by a slight change in voltage at the anode over time, which is characteristic of all electrolytes.

For example, the initial value of the voltage at the anode is 280 V in an electrolyte S1 at a distance of 1 m between electrodes. It falls to a value of 250 V in the synthesis process. The decrease between the electrodes' distance to 0,5 m leads to a decrease in voltage to its first value of 185 V. In this case, a breakdown of the conductive films on the anode occurred in the first 10 min. After that, the PEO process was stabilized and was occurred at values about 210 V. The breakdown in the conducting channel metal–electrolyte in the synthesis of oxide ceramic at a distance of 0,25 m exists no longer than 20 min. In this case, the coating is formed at a voltage of 180 V. The PEO process stabilizes during the first 9 min at a distance of 0.1 m between electrodes. However, the coatings are formed, in this case, for a voltage of 175 V.

In case, the OCC formed approximately at 260 V at the most distance between the electrodes (4.5 m) (electrolyte S2). It should also be noted that the breakdown of the natural oxide films on the anode occurs something faster – after 6 min. In an electrolyte S3, coatings are formed at a distance of 4.5 m at a voltage not much smaller than 200V. Reducing the distance between electrodes to 2.25 m leads to the ability to form a voltage coverage of an average of 155 V. At a distance between electrodes from 0.5 m or less, the coating is formed at about the same voltage, which is equal to 125 V. In such distances the process goes uniformly compared to the others: the voltage after breakdown practically does not change its value in the process of synthesis.

The composition change of the electrolyte also influences the value of the voltage generated. So the increasing of the concentration in the electrolyte KOH from 1 g/l to

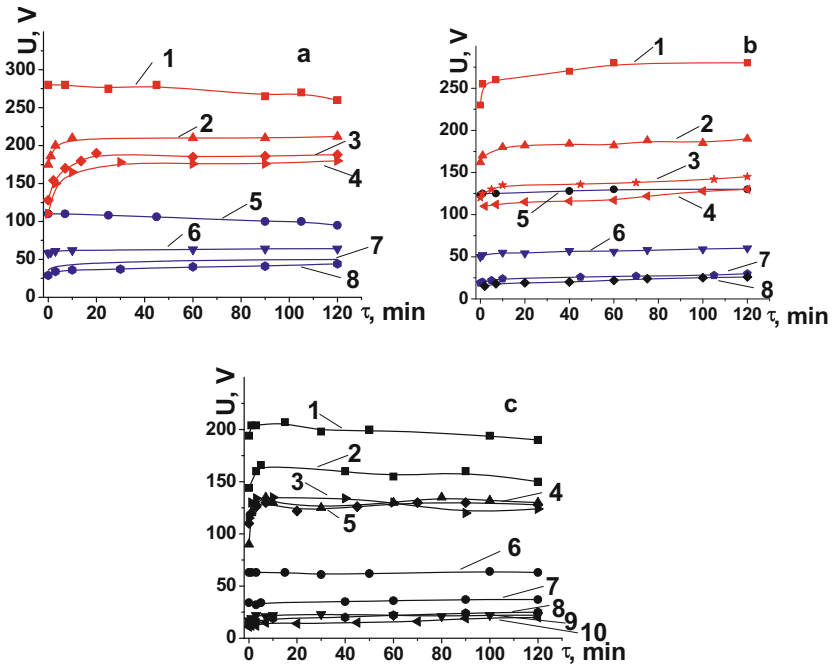


Fig. 3. a - Kinetics of anodic (1–4) and cathodic (5–8) tension in the 1g/l KOH electrolyte for the following distances between electrodes: 1 m (curves 1, 5); 0,5 m (2, 6); 0,25 m (3,7); 0,1 m (4, 8); b - kinetics of an anodic (1–4) and cathodic (5–8) tension in 3 g/l KOH + 2 g/l liquid glass electrolyte for the following distances between electrodes 4,5 m (curves 1, 5); 2,25 m (2, 6); 0,5 m (3,7); 0,05 m (4, 8); c - kinetics of anodic (1–5) and cathodic (6–10) tension in 5 g/l KOH + 6 g/l liquid glass electrolyte for the following distances between electrodes 4,5 m (curves 1, 6); 2,25 m (2, 7); 0,5 m (3, 8); 0,25 m (4, 9); 0,1 m (5, 10).

3 g/l and the adding 2 g/l of liquid glass makes it possible to reduce the synthesis voltage at the anode by approximately 85 V (curve 2 in Fig. 3a, and curve 3 in Fig. 3b). Further increase of electrolyte concentration up to 5 g/l KOH + 6 g/l of liquid glass allows synthesizing a coating for a voltage lower than 5 V compared to the previous electrolyte.

The stability of the process in time makes it possible to measure the total voltage over the cell length for different distances between the electrodes (Fig. 4).

The investigation of thickness and microhardness of OCC, which are synthesized in different electrolytes and at different distances between electrodes, are presented in Fig. 5a and b. It has been experimentally established that coatings synthesized in an electrolyte S2 at a distance more significant than the critical one (from 0.5 m to 4.5 m) are thicker than more complexly-doped electrolyte S3.

The microhardness of oxide ceramic coatings varies from 600 kg/mm² to 1100 kg/mm² (Fig. 5b). It has been established that the highest microhardness of 1100 kg/mm² has coatings that are synthesized in an electrolyte S2 at an inter-electrode distance of 0,25 m. The reduction of an electrolyte concentration makes it possible to form a coating with a microhardness of 950 kg/mm².

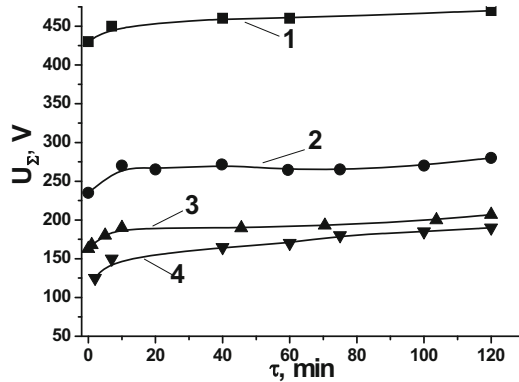


Fig. 4. Kinetics of the total tension in an electrolyte for the following distances between electrodes: 4,5 m (1); 2,25 m (2); 0,5 m (3); 0,05 m (4).

The studies showed that the coatings, which are synthesized in the electrolyte S2, have the best optimal thickness and microhardness. Consequently, we have researched the oxide ceramic durability formed in this electrolyte at distances from the electrodes of 0.05 m, 0.25 m, and 0.10 m.

Traditionally, the most common contact in technique is linear. Therefore, using this kind of contact in work [17, 18], the developed testing method of lubricants was illuminated, making it possible to diagnose the lubricity of materials correctly. It can be obtained first of all with the help of the step-by-step test. We have modernized this technique (methodic), and it has been adapted to dry friction conditions. It was revealed that the opposite element's friction surface is worked out secondary structures at the first stage (the initial stage of an embedding). At the second and third stages, the stability of the developed secondary structures is estimated on the criterion of the linear wear value. At the fourth stage, the generated secondary structures in time with a big friction path and wear resistance of estimated coatings are evaluated. As a result of the tests, we have gotten wear traces with the help of test samples, which are described in Fig. 2. Secondary structures on the surface of the opposite element are formed due to complex physical and chemical processes (temperature increase, chemical reactions).

We have found that the distance between the electrodes affects the wear intensity (E_f) of the oxide ceramic coating (Table 1).

During the experiment, the deterioration intensity of the oxide ceramic coating at each stage was determined (Table 2). Thus, at the first start-up stage (Fig. 6, stage I), E_f is the largest for the oxide ceramic, synthesized at a distance of 0.05 m. So, here the secondary structures on the opposite element can soon be developed. This part is straightforward for three researched samples (Fig. 7).

The stability of the generated secondary structures, estimated in the 2-nd and 3-rd sections of the curves, is ambiguous. So, for OCC, which is synthesized at a distance of the electrode 0.1 m, such structures are not stable and are changed over time (curve 2, Fig. 6). However, we can say it about two other curves, whose inclination angle practically does not change during the next 1000 m. At the IV stage, it is possible to

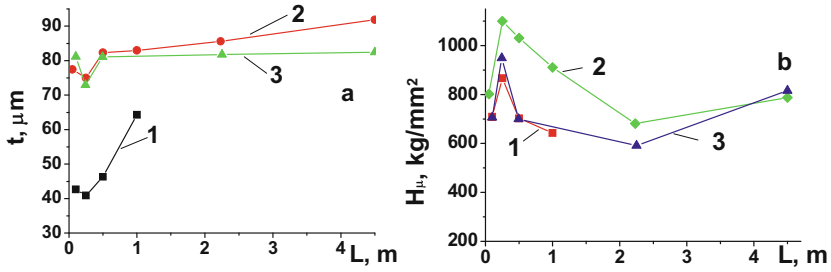


Fig. 5. Change of thickness (a) and microhardness (b) of the coatings obtained in 1 g/l KOH (1), 3 g/l KOH + 2 g/l l. g. (2), and 5 g/l KOH + 6 g/l l. g. (3) electrolytes at different distances between electrodes.

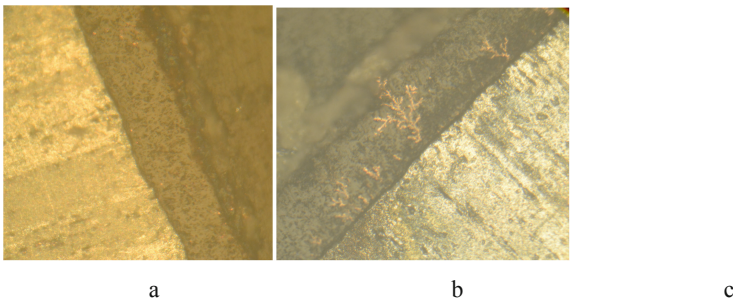


Fig. 6. OCC synthesized on alloy ENAW-2024 at a distance between the electrodes of 0,05 m (a) and 0,25 m (b) after microhardness researches (c) ($\times 200$) in the electrolyte S2.

Table 1. The friction intensity of OCC depending on the traversed path.

The friction intensity I , m		The traversed path L , m	
The distance from the electrode a , cm			
0.05	0.1	0.25	
11.4	12.9	12.5	500
23.4	25	26.2	1000
33.7	34.4	37.5	1500
47.2	40	51	2500

evaluate the wear resistance of researched coatings. Here all the curves change the angle of inclination (Sect. 4, Fig. 6).

We have seen from surface studies, E_f is the same for coatings on an aluminum alloy which are synthesized at a distance of 0.04 m and 0.25 m and is $0.135 \mu\text{m}/\text{m}$, whereas this distance for the covering is less than 2 times and equal to $0.0056 \mu\text{m}/\text{m}$ which is formed at a distance of 0.1 m.

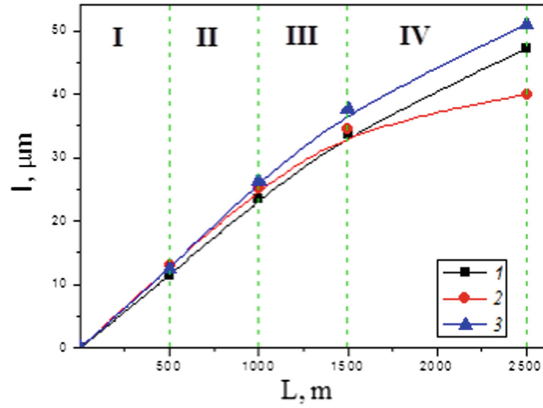


Fig. 7. The dependence of friction intensity I from traversed path L of OCC, which is synthesized through different distances from the electrode: 1 – 0.05 m, 2 – 0.10 m, 3 – 0.25 m.

Table 2. The deterioration rate of OCP, which are synthesized at different distances from the electrode at different stages.

№ of the sample	The deterioration rate of OCC E_f , $\mu\text{m}/\text{m}$			
	Friction stage			
	I	II	III	IV
1	0.0228	0.024	0.0206	0.0135
2	0.0258	0.0242	0.0188	0.0056
3	0.025	0.0274	0.0226	0.0135

5 Conclusions

It was established that the voltage between electrodes varies almost linearly regardless of the electrolyte composition and the distance between these electrodes at the constant current density, and the breakdown of the oxide lamina occurs in the first 10–20 min. It is experimentally set that the value of the synthesis voltage is influenced by the composition, electrolyte concentration, and the distance between the electrodes: an increase in the distance between the electrodes leads to an increase in the synthesis voltage.

It was found that at a critical distance of 25 cm, the minimum thickness of the coating is $75 \mu\text{m}$, which is caused by the depletion of the electrolyte between the electrodes. We propose, for partially reducing the negative influence of this effect, to increase the area of the auxiliary electrode.

It has been experimentally established that the microhardness of the OCC, which is formed on the critical distance, is the highest and is $1100 \text{ kg}/\text{mm}^2$. It is explained by increase the power of separate spark discharges and (or) increase the coverage of $\alpha\text{-Al}_2\text{O}_3$. It was investigated that the coatings of higher thickness and microhardness are obtained through the composition of an electrolyte 3 g/l KOH + 2 g/l l. g. In our

experiments on the durability of synthesized coatings, we have been determined that the highest friction resistance $0.056 \mu\text{m/m}$, is done by OCC, which is oxidized in plasma of spark discharges at a distance of 0.1 m.

For scientific substantiation of the reasons of the received results further, it is necessary to carry out the spectral analysis of the received coverings.

References

1. Cheng, Y., Cao, J., Peng, Z., et al.: Wear-resistant coatings formed on Zircaloy-2 by plasma electrolytic oxidation in sodium aluminate electrolytes. *Electrochim. Acta* **116**, 453–466 (2014)
2. Zhong, Y., Shi, L., Li, M., He, F., He, X.: Characterization and thermal shock behavior of composite ceramic coating doped with ZrO₂ particles on TC4 by micro-arc oxidation. *Appl. Surf. Sci.* **311**, 158–163 (2014)
3. Klappkov, M.D., Imbirovich, N., Posuvaylo, V.M., Ostapyuk, S.I.: Plasma-electrolyte oxidation of light alloys and spray layers. *Sci. Notes* **31**, 151–155 (2011)
4. Fazel, M., Salimijazi, H.R., Golozar, M.A., Garsivaz Jazi, M.R.: A comparison of corrosion, tribocorrosion and electrochemical impedance properties of pure Ti and Ti6Al4V alloy treated by micro-arc oxidation process. *Appl. Surf. Sci.* **324**, 751–756 (2015)
5. Kulesh, E.A., Piliptsov, D.G., Rogachev, A.V., Hong, J.X., Fedosenko, N.N., Kolesnyk, V.: Boron-carbon coatings: structure, morphology and mechanical properties. *J. Eng. Sci.* **7**(1), C1–C9 (2020). [https://doi.org/10.21272/jes.2020.7\(2\).c1](https://doi.org/10.21272/jes.2020.7(2).c1)
6. Aktuğ, S.L., Durdu, S., Kutbay, I., Usta, M.: Effect of Na₂SiO₃·5H₂O concentration on microstructure and mechanical properties of plasma electrolytic oxide coatings on AZ31 Mg alloy produced by twin roll casting. *Ceram. Int.* **42**, 1246–1253 (2016)
7. Snizhko, L.O.: The nature of anodic gas at plasma electrolytic oxidation. *Prot. Met. Phys. Chem. Surf.* **50**(6), 705–708 (2014). <https://doi.org/10.1134/S2070205114060215>
8. Banakh, O., Journot, T., Gay, P.-A., Matthey, J.: Synthesis by anodic-spark deposition of Ca- and P-containing films on pure titanium and their biological response. *Appl. Surf. Sci.* **378**, 207–215 (2016)
9. Snizhko, L.A., Kalinichenko, O.A., Misnyankin, D.A.: Synthesis of calcium phosphates on titanium. *Surf. Eng. Appl. Electrochem.* **52**(3), 257–262 (2016). <https://doi.org/10.3103/S106837551603011X>
10. Banakh, O., Snizhko, L., Journot, T.: The influence of the electrolyte nature and PEO process parameters on properties of anodized Ti-15Mo alloy intended for biomedical applications. *Metals* **8**(5), 370 (2018)
11. Abdulla, T., Yerokhin, A., Goodall, R.: Enhancement in specific strength of open cell aluminium foams through plasma electrolytic oxidation treatment. *Scripta Mater.* **75**, 38–41 (2014)
12. Gnedenkov, S.V., et al.: Composite hydroxyapatite-PTFE coatings on Mg-Mn-Ce Alloy for resorbable implant applications via a plasma electrolytic oxidation-based route. *J. Taiwan Inst. Chem. Eng.* **45**, 3104–3109 (2014)
13. Tian, X.B., Chu, P.K.: Experimental investigation of the electrical characteristics and initiation dynamics of pulsed high-voltage glow discharge. *J. Phys. D Appl. Phys.* **34**(3), 354–360 (2001)
14. Yerokhin, A., Parfenov, E.V., Liang, C.J., Mukaeva, V.R., Matthews, A.: System linearity quantification for in-situ impedance spectroscopy of plasma electrolytic oxidation. *Electrochem. Comm.* **27**, 137–140 (2013)
15. Yeung, W.K., Reilly, G.C., Matthews, A., Yerokhin, A.: In vitro biological response of plasma electrolytically oxidised and plasma sprayed hydroxyapatite coatings on Ti-6Al-4V alloy. *J. Biomed. Mat. Res.: B Appl. Biomater.* **101B**(6), 939–949 (2013)

16. Imbirovich, N., Klavkov, M.D., Posuvayilo, V.M., Povstyanoy, A.: Properties of oxide ceramic coatings on magnesium and titanium alloys which are synthesized in electrolyte plasma. *Powder Metall.* **1**(2), 54–60 (2015)
17. Stelmakh, A.U., Sidorenko, O., Kostyunik, R.E.: Methods of the identifying fuels and lubricants by antiwear and antifriction properties, taking into account the actual conditions of their work. *Technol. Syst.* **3**, 96–101 (2002)
18. Aksenov, O.F., Stelmakh, O.U., Shimchuk, S.P., Koba, V.P., Manso-Ur, J.I.: Methodology for determining the anti-trapping properties of lubricants by criteria of tribo characteristics of secondary structures which are formed in them. *Visnyk of NAU*, pp. 62–64 (2006)



Optimal Design of Composite Shelled Sandwich Structures with a Honeycomb Filler

Andrii Kondratiev¹  , Olexander Potapov² , Anton Tsaritsynskyi³ ,
and Tetyana Nabokina³ 

¹ O.M. Beketov National University of Urban Economy in Kharkiv, 17, Marshal Bazhanov St.,
Kharkiv 61002, Ukraine

andrii.kondratiev@kname.edu.ua

² Yuzhnoye Design Office, 3, Krivorozhskaya St., Dnipro 49008, Ukraine

³ National Aerospace University “Kharkiv Aviation Institute”, 17,
Chkalova St., Kharkiv 61070, Ukraine

Abstract. The multi-parameter problem of the optimal design of composite sandwich structures with the honeycomb filler has been solved. For this purpose, the optimization process was divided into several stages according to the reasonable levels of significance of the objective function’s parameters, i.e., minimal weight. At the first stage, preliminary analysis of thermal protection coatings of sandwich structures with the honeycomb filler is carried out, the most rational types thereof are found, the values of physical and mechanical characteristics, as well as the optimal ranges of variation and the initial value of the thickness of thermal protection coatings for different sections of the structure, are determined. At the second stage, the task of choosing the optimal relationship of the thickness of the thermal protection coating, height of the honeycomb filler, size of its cell, and thicknesses of bearing skins is solved, with simultaneous securing of the acceptable temperature ranges for the outer and inner surfaces of sandwich shells and bearing capacity of the rational variant in all critical areas. To further reduce the weight, the honeycomb filler structure is optimized at the third stage by varying the angle of opening of the cell of irregular hexagonal shape and coefficient of its shape in each section of the structure. Implementation of the suggested approach in weight optimization of a real object’s structural parameters showed its efficiency, expressed in a significant reduction of the optimal structure’s weight compared to its initial variant.

Keywords: Optimization · Minimum weight · Bearing skins · Composite materials · Thermal protection coating

1 Introduction

An increase in the efficiency of various applications’ modern structures is inseparably associated with the searching for and implementing new design and technology solutions [1, 2]. One of the essential directions in these search efforts concerning shell-type structures is creating and broadening sandwich structures. Elements of such structures

comprise two thin bearing skins and a lightweight honeycomb filler (HF) between them. Its nature predetermines this loading pattern's high efficiency; it is reliably proved theoretically and showed by experiments [3]. The development of sandwich structures is accompanied by the active introduction of polymeric composite materials (PCM) [4]. It significantly increases the weight efficiency of structures due to high specific characteristics of strength and stiffness of composite materials and the possibility of directed formation of the desired mechanical properties [5].

Peculiarities of designing sandwich structures with HF of minimum weight require the choice of design patterns consistent with the structure geometry and the range of external actions thereon. It limits the applicability of the analytical design patterns widely used in actual practice. The nature of variation in thicknesses of the bearing skins in PCM use is associated with the need to consider the change in their physical and mechanical characteristics (PhMC) due to varying reinforcement patterns. Wide opportunities of HF PhMC variation by changing its cell's geometrical parameters also complicate the formulation and implementation of the optimal designing of shell-type sandwich structures in the rigorous mathematical setting because of the growing number of variables. Considering a non-exhaustive list of peculiar features of shell-type sandwich structure designing mentioned above, the authors attempt to use the unconventional approach to synthesize the optimal structural parameters of a product and substantiated successive approximation them.

2 Literature Review

Despite a number of developed methods for optimizing parameters of the considered class of structures, which are widely used now, they are rather complex and time-consuming ones. The common feature of most of the works dealing with this problem is that the approaches suggested in them implement the analytical mathematical models quite similar in their content [6].

The basis of the approach showed in [7, 8] is the analytical mathematical model that allows establishing the general loss of stability of the conical and cylindrical honeycomb shell under the compressive force and uniform external pressure.

The papers [9, 10] show the analytical dependences obtained to determine the stress-strain behavior of honeycomb structures based on Lagrange's variational principle. However, these models demand the idealization of representation of the structure and types of external actions.

Authors of [11, 12], using the examples of natural structures, show the methodology for determining the areas of rational use of various structural arrangements of cylindrical composite shells. Nevertheless, descriptions of employed solution methods given in [11, 12] indicate significant idealization of objects' representation under consideration and external actions.

The paper [13] deals with optimizing cylindrical composite shells, which are homogeneous/inhomogeneous in thickness. As the bearing skins, the authors studied the PCM pack composed of layers of different types at fixed reinforcement angles. However, the above results were obtained under the action of isolated axial compression only.

The papers [14, 15] present the methods for determining the ultimate loads of shell-type composite structures. A common disadvantage of the papers is that the authors paid

considerable attention to the theory of ultimate load calculation based on the use of the composite materials' generalized characteristics. These characteristics of PCM can be obtained for individual samples of the structure only.

Optimization of the structure of bearing skins, taking into account the design and technological constraints on the thickness of the PCM pack, is the topic of [16]. However, the application of results to shell-type sandwich systems with HF under combined loading requires an appropriate generalization of the proposed algorithms. The paper [17] deals with the issues of optimization of HF parameters. The authors proposed a method for analytical forecasting of the maximum possible reduction of weight of the composite structures for space applications, taking into account their production's technological capabilities. However, a simplified design pattern is used in this paper, which is the reason for obtaining the knowingly approximate results. These simplifications are also used in other authors' works, for example [18, 19].

Consideration of HF structural parameters in the optimization, considering its production process, was implemented in [20]. However, the proposed method can be used to optimize the honeycomb shell parameters with a specific correction only, when they are divided into cylindrical panels being joined together. The paper [21] further develops the approach to weight optimization of structures such as the launcher's nose fairings. The minimum benefit (5%) in weight is shown due to the optimal reinforcement pattern compared to the quasi-homogeneous shell. Nevertheless, the adopted design patterns are highly simplified, which does not allow generalizing the results obtained.

A common disadvantage of the papers published in this domain is that a small number of variables are considered in optimization calculations. Given that the real composite sandwich structures have a relatively large number of design variables, the generalization of approaches suggested in the considered papers looks problematic.

At present, optimal designing of composite structures with the honeycomb filler is based on computer technologies. In the last decade, these technologies are intensively developed and implemented [22]. However, this optimization approach allows solving a specific problem only. As a rule, it does not provide an opportunity to generalize the results, considering technological constraints and other limitations [23]. An attempt to reduce the weight of honeycomb composite structures for space applications by optimizing their parameters based on the synthesis of computer technologies of finite-element analysis and analytical models was made [24]. The authors developed and implemented a method for optimization of parameters of the launcher's composite nose fairing. This paper's significant drawback is that the thermal effect is considered only by deterioration of the structural materials' physical and mechanical characteristics.

3 Research Methodology

As an object of research, the nose fairing (NF) within the space launcher vehicle's head unit is considered [21, 24, 25].

NF is a cylindrical-biconical module of 8590 mm long and 4000 mm in diameter, having a spherical tip with a radius of 720 mm. NF housing consists of two sandwich half-shells. All NF sections are connected with the use of metal stiffening rings. The spherical tip is made of glass fiber plastic; bearing skins are made of carbon PCM;

honeycombs of aluminum alloy with hexagonal cells act as fillers. The following design cases of loading were considered: loading of structural elements by surface pressure at the critical Mach number; maximum aerodynamic coefficients; maximum drag force; area of maximum velocity head. Calculated components of the bending moments M , shear forces Q , axial forces T in the NF design sections, and excessive non-uniform pressure P were taken as the loads on the NF. For determining the stress-strain behavior and optimization of design parameters of the NF under study, one of the software systems of the finite-element analysis was used.

The problem was being solved using linear equations from the theory of elasticity and buckling analysis. The general statement of the elastic theory problem for the orthotropic body contains equilibrium equations, generalized Hook's law, Cauchy relations, and boundary conditions. Theoretical solutions are obtained using the finite-element method. The Kirchhoff–Love hypothesis is applied for composite bearing skins. A linear distribution of cross-section height is considered for the HF, and deformations in transversal direction are not considered.

For the calculation and further optimization in the finite-element analysis software, NF is presented as a system of shells supported by stiffening rings.

Sandwich shells represent conical and cylindrical parts of NF. The multilayered second-order shell-type finite element with the relevant properties was taken during their discretization on the finite element mesh. Bearing skins were modeled in the form of packs of four layers of the considered PCM filler with the total thickness of $\delta_i = 1$ mm and reinforcement pattern $[0_{0.25s}; \pm 45_{0.5s}; 90_{0.25s}]$. HF is represented as a conventional layer of the multilayered finite element of $h = 25$ mm homogeneous in volume, with PhMC depending on the cell's geometrical configuration, the thickness of foil, and its PhMC. In discretization of the spherical tip, a single-layer shell-type finite element was used. Stiffening rings and elements of the NF's longitudinal joint were modeled by the corresponding cross-section beam elements. For the proper consideration of the condition of NF joining with the adjacent carrier sections (interstage section and payload adapter), it was modeled together with them.

Load on the head unit elements was applied as a pressure normal to the surface, distributed according to the given law within the limits of the relevant surface and the equivalent longitudinal and transverse force reduced to the nodes in each section. Bending moments in design sections were applied as the distributed pairs of forces were reduced to the corresponding section's nodes. The head unit was fixed along with the nodes of the lower stiffening ring of the interstage section on all movements, which corresponded to the condition of its joining with the second stage of the launcher.

Rationalization of the problem of optimal designing of carrier sections of the launcher's head unit (particularly NF), which are subject to the intensive thermal effects, provides the need for simultaneous optimization of their parameters structural arrangement and thermal protection coating (TPC). Therefore, preliminary analysis of employed TPC is carried out in the first block of the proposed optimization method (Fig. 1).

At the same time, possible recommendations are developed for the subsequent optimization of the thermal protection parameters, and the most rational types of it are determined concerning the NF under consideration; PhMC values are found, as well as the optimal ranges of variation and the initial value of TPC thickness for different NF

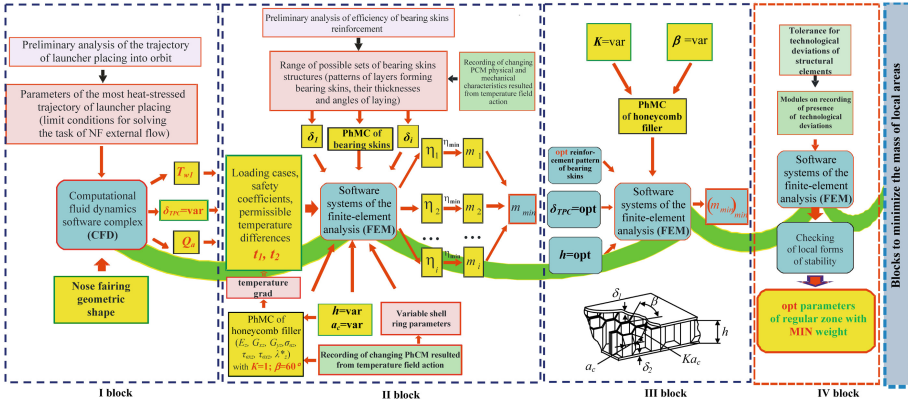


Fig. 1. Method of minimization of the weight of sandwich nose fairing with honeycomb filler at simultaneous thermal and strain loads.

sections. Boundary conditions for calculations of NF TPC are the aerodynamic heat flow Q_a and the maximum value of the NF structure’s temperature.

The second block of the proposed multistage mass optimization method solves the task of choosing the optimal ratio of thermal protection thickness δ_{TPC} , HF height h , HF cell size a_c , thicknesses of bearing skins δ and also securing the acceptable ranges of temperatures of the outer and inner surfaces of sandwich shells and bearing capacity of the rational variant in all critical areas, taking into account the deteriorations in the PhMC of the employed materials from the thermal effect. Optimization of these HF parameters at this stage is caused by the fact that, as the experience shows [19], heat-insulating properties of honeycombs mainly depend on the height and density, which is primarily determined by the cell size, and to a lesser extent, is conditioned by other parameters: angle of its opening β and coefficient of the shape K . As the optimization constraints relating to the bearing capacity of structural elements of the NF structure under study, layer-by-layer analysis according to Von-Mises–Hill criterion was carried out for layers forming the bearing skins. When determining HF’s required safety margins, the specified orthotropic filler’s adjusted characteristics were used [19, 21]. For isotropic materials, Von-Mises criterion was chosen. Besides, the modeled object’s stability margins as a whole k_{st} and possible forms of local losses of structural elements’ stability were the block’s active constraints. As an objective function is minimized, the structure’s weight equal to the weights of the NF’s structural components: thermal protection, bearing skins, and HF, is taken. While minimizing the objective function, the optimization module performs complete enumeration of the design variables specified. Therefore, while meeting the constraints for the acceptable ranges of temperatures and providing the bearing capacity for all normalized loading cases, consider the reduction of PhMC of the employed PCM. All design variables on a staged basis enter the optimization block where the task is solved concerning choosing the rational relationship of the required thickness of thermal protection δ_{TPC} . Parameters of structural arrangement and additional basic structure with the simultaneous securing of the permissible ranges of temperatures of the outer and inner surfaces of the unit under study, bearing capacity of

its rational variant in all critical areas, taking into account the deteriorations of PhMC of the employed materials from the thermal effect and observance of additional functional and technological constraints. To further reduce the NF weight at the final stage, HF structure is optimized by varying the angle of opening of the cell of irregular hexagonal shape β and coefficient of shape K in each NF section.

For getting the basic design before the optimization procedure, which is then can also be compared to the final result of the calculation, the initial construction of the NF was analyzed (Table 1).

Table 1. Results of initial NF construction analysis.

Indicator	Design loading cases				
	1	2	3	4	5
The maximum value of the Von Mises-Hill criterion for the layers forming the bearing skins of thicknesses: $\delta_i = 1.0$ mm	0.44	0.81	0.88	0.91	0.95
Maximum shear stress in HF					
HF cell side width, by sections: $a_{ci} = 5.0$ mm					
Cell shape coefficient, by sections $K_i = 1$					
The angle of cell opening, by sections: $\beta_i = 60^\circ$					
HF height, by sections: $h_i = 25$ mm					
$\tau_{xz \max}$, kPa	134	171	172	173	175
$\tau_{yz \max}$, kPa	23	27	52	72	72
NF stability margin k_{st}	2.81	1.78	1.69	1.68	1.67
Mass of bearing skins, kg	275.37				
Mass of HF, kg	57.03				
The total mass of bearing skins and HF, kg	332.4				

4 Results

As a result of the proposed multistage optimization technique, there was found a way to select optimal relations between TPC thickness δ_{TPC} , HF height h , cell size a_c , bearing skin thickness δ providing permissible temperature range between the outer and inner surface of sandwich shells as well as bearing capacity of final design within all critical areas of its structure.

Rational TPC thickness as a function of the permissible temperature of outer bearing skin is shown in Fig. 2.

Table 2 shows the results of optimization of the NF sandwich structure parameters.

The result of this stage of optimization of parameters of the NF sandwich structure is the decrease in its mass compared to the basic variant:

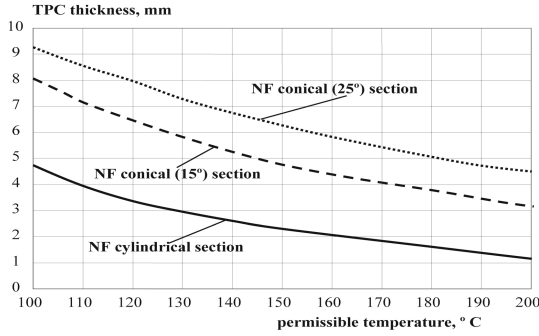


Fig. 2. Variation in TPC’s rational thickness depends on the permissible temperature of the outer bearing skin of the NF.

Table 2. Results of optimization of parameters of the NF sandwich structure.

Indicator	Design loading cases				
	1	2	3	4	5
The maximum value of the Von Mises-Hill criterion for the layers forming the bearing skins of thicknesses: $\delta_1 = 0.9 \text{ mm}; \delta_2 = 0.4 \text{ mm}; \delta_3 = 0.9 \text{ mm}; \delta_4 = 0.8 \text{ mm}$	0.62	0.9	0.95	0.97	0.98
Maximum shear stress in HF					
HF cell side width, by sections: $a_{c1} = 6.6 \text{ mm}; a_{c2} = 7.2 \text{ mm}; a_{c3} = 4.8 \text{ mm}; a_{c4} = 7.2 \text{ mm}$					
Cell shape coefficient, by sections $K_i = 1$					
The angle of cell opening, by sections: $\beta_i = 60^\circ$					
HF height, by sections: $h_1 = 15 \text{ mm}; h_2 = 25 \text{ mm}; h_3 = 18 \text{ mm}; h_4 = 19 \text{ mm}$					
$\tau_{xz \text{ max, kPa}}$	78	99	101	120	150
$\tau_{yz \text{ max, kPa}}$	9	11	33	37	37
NF stability margin k_{st}	1.55	1.2	1.15	1.13	1.1
Mass of bearing skins, kg	244.88				
Mass of HF, kg	34.22				
The total mass of bearing skins and HF, kg	279.10				

- bearing skins by $\frac{275.37-244.88}{275.37} 100\% = 11.07\%$ (30.49 kg);
- HF by $\frac{57.03-34.22}{57.03} 100\% = 40\%$ (22.81 kg);
- NF sandwich shells, as a whole, by $\frac{332.4-279.1}{332.4} 100\% = 16\%$ (53.3 kg).

Search for rational parameters of HF made it possible to decrease the mass of NF further. The obtained result was predicted in [7, 21], and the minimal mass is achieved with HF parameters: $\beta_i = 60^\circ$ and $K_i = 3$. With these values, the NF stability margin k_{st}

is not changed noticeably. The final optimization stage result is the additional reduction of NF weight compared to the variant where HF featured the regular hexagonal shape cell by $\frac{279.1-263.4}{279.1}100\% = 5.63\%$ (15.7 kg), and compared to the basic variant – by $\frac{332.4-263.4}{332.4}100\% = 21\%$ (69 kg).

After determining HF's rational structure, the data entered the optimization verification blocks, which confirmed our findings.

The distinctive feature of the suggested optimization method is the obtaining of maximum target efficiency from NF structures. The most of papers cited [6] above deal with the typical approach to the optimal designing of structures of the class under consideration, subjected to simultaneous strength and thermal loads, providing, as a rule, division of the general task into a number of subtasks to obtain the rational parameters for each type of action [9, 11]. As a result, even the individual optimal solutions of the tasks taken separately do not provide the final structure's integral optimality [7, 21]. In contrast to the above papers, the proposed method allows the optimization for all design cases of loading simultaneously, taking into account possible mechanisms of failure and loss of stability of structural elements. Consequently, the structure's resulting rational parameters are not optimal in each loading case, but they are rational concerning their totality. Furthermore, the permissible ranges of temperatures of the unit's outer and inner surfaces under study and the bearing capacity of its rational variant in all critical areas are provided, taking into account the deteriorations of employed materials' physical and mechanical characteristics from the thermal effect. The method allows determining the rational relationship of the thickness of thermal protection, bearing skins, and height of the HF in each section, which ultimately decreases the weight of the necessary thermal protection.

5 Conclusions

The research carried out allowed solving the multi-parameter problem of the optimal design of composite sandwich structures with the honeycomb filler without noticeable accuracy. For achieving this result, the optimization process was divided into several stages under the reasonable levels of significance of the parameters included in the objective function, i.e., minimal weight.

Implementation of the proposed approach for a real object's parameter optimization revealed its effectiveness in significant mass reduction compared to the basic design. The obtained results allow further development and improvement of the approach by including some auxiliary structural elements of composite sandwich structures with honeycomb filler.

References

1. Fomin, O., Logvinenko, O., Burlutsky, O., Rybin, A.: Scientific substantiation of thermal leveling for deformations in the car structure. *Int. J. Eng. Technol.* 7(4.3), 125–129 (2018). <https://doi.org/10.14419/ijet.v7i4.3.19721>
2. Bychkov, A.S., Kondratiev, A.V.: Criterion-based assessment of performance improvement for aircraft structural parts with thermal spray coatings. *J. Superhard Mater.* 41(1), 53–59 (2019). <https://doi.org/10.3103/S1063457619010088>

3. Nunes, J.P., Silva, J.F.: Sandwiched composites in aerospace engineering. In: *Advanced Composite Materials for Aerospace Engineering*, pp. 129–174 (2016). <https://doi.org/10.1016/b978-0-08-100037-3.00005-5>
4. Mustafa, L.M., Ismailov, M.B., Sanin, A.F.: Study on the effect of plasticizers and thermoplastics on the strength and toughness of epoxy resins. *Naukovyi Visnyk Natsionalnoho Hirnychoho Universytetu* **4**, 63–68 (2020). <https://doi.org/10.33271/nvngu/2020-4/063>
5. Rodichev, Y.M., Smetankina, N.V., Shupikov, O.M., Ugriimov, S.V.: Stress-strain assessment for laminated aircraft cockpit windows at static and dynamic loads. *Strength Mater.* **50**(6), 868–873 (2019). <https://doi.org/10.1007/s11223-019-00033-4>
6. Ganguli, R.: Optimal design of composite structures: a historical review. *J. Indian Inst. Sci.* **93**(4), 557–570 (2013)
7. Slyvyns'kyy, V., Gajdachuk, V., Gajdachuk, A., Slyvyns'ka, N.: Weight optimization of honeycomb structures for space applications. In: *Proceedings of The International Astronautical Congress, IAC 56. Our World Needs Space 6*, pp. 3611–3620 (2005). <https://doi.org/10.2514/6.iac-05-c2.3.07>
8. Slivinsky, M., Slivinsky, V., Gajdachuk, V., Gajdachuk, A., Kirichenko, V.: New possibilities of creating efficient honeycomb structures for rockets and spacecrafts. In: *55th International Astronautical Congress*, pp. 1–7 (2004). <https://doi.org/10.2514/6.iac-04-i.3.a.10>
9. D'Ottavio, M., Dozio, L., Vescovini, R., Polit, O.: Bending analysis of composite laminated and sandwich structures using sublaminated variable-kinematic Ritz models. *Compos. Struct.* **155**, 45–62 (2016). <https://doi.org/10.1016/j.compstruct.2016.07.036>
10. An, H., Chen, S., Huang, H.: Optimal design of composite sandwich structures by considering multiple structure cases. *Compos. Struct.* **152**, 676–686 (2016). <https://doi.org/10.1016/j.compstruct.2016.05.066>
11. Smerdov, A.A.: A computational study in optimum formulations of optimization problems on laminated cylindrical shells for buckling. I. Shells under axial compression. *Compos. Sci. Technol.* **60**, 2057–2066 (2000). [https://doi.org/10.1016/S0266-3538\(00\)00102-0](https://doi.org/10.1016/S0266-3538(00)00102-0)
12. Smerdov, A.A.: A computational study in optimum formulations of optimization problems on laminated cylindrical shells for buckling. II. Shells under external pressure. *Compos. Sci. Technol.* **60**, 2067–2076 (2000). [https://doi.org/10.1016/S0266-3538\(00\)00103-2](https://doi.org/10.1016/S0266-3538(00)00103-2)
13. Zheng, Q., Jiang, D., Huang, C., Shang, X., Ju, S.: Analysis of failure loads and optimal design of composite lattice cylinder under axial compression. *Compos. Struct.* **131**, 885–894 (2015). <https://doi.org/10.1016/j.compstruct.2015.06.047>
14. Totaro, G., Gürdal, Z.: Optimal design of composite lattice shell structures for aerospace applications. *Aerosp. Sci. Technol.* **13**, 157–164 (2009). <https://doi.org/10.1016/j.ast.2008.09.001>
15. Totaro, G.: Local buckling modelling of isogrid and anisogrid lattice cylindrical shells with hexagonal cells. *Compos. Struct.* **95**, 403–410 (2013). <https://doi.org/10.1016/j.compstruct.2012.07.011>
16. Karpov, Ya.S., Gagauz, P.M.: Structural optimization of composite panels under strength and stability restrictions. *Strength Mater.* **42**(6), 631–636 (2010). <https://doi.org/10.1007/s11223-010-9251-z>
17. Slyvyns'kyy, V., Slyvyns'kyy, M., Polyakov, N., Gajdachuk, A., Gajdachuk, V., Kirichenko, V.: Scientific fundamentals of efficient adhesive joint in honeycomb structures for aerospace applications. In: *Proceedings of the International Astronautical Congress, IAC 59. Our World Needs Space 8*, pp. 5307–5314 (2008)
18. Vijayakumar, S.: Parametric based design of CFRP honeycomb sandwich cylinder for a spacecraft. *Compos. Struct.* **65**, 7–12 (2004). [https://doi.org/10.1016/S0263-8223\(03\)00176-4](https://doi.org/10.1016/S0263-8223(03)00176-4)

19. Kondratiev, A., Gaidachuk, V., Nabokina, T., Tsaritsynskiy, A.: New possibilities of creating the efficient dimensionally stable composite honeycomb structures for space applications. In: Nechyporuk, M., Pavlikov, V., Kritskiy, D. (eds.) *Integrated Computer Technologies in Mechanical Engineering*. AISC, vol. 1113, pp. 45–59. Springer, Cham (2020). https://doi.org/10.1007/978-3-030-37618-5_5
20. Gaydachuk, V., Koloskova, G.: Mathematical modeling of strength of honeycomb panel for packing and packaging with regard to deviations in the filler parameters. *Eastern-Eur. J. Enterp. Technol.* **6**(1(84)), 37–43 (2016). <https://doi.org/10.15587/1729-4061.2016.85853>
21. Slyvyns'kyi, V., Gajdachuk, V., Kirichenko, V.: Basic parameters' optimization concept for composite nose fairings of launchers. In: *Proceedings of the 62nd International Astronautical Congress, IAC 2011*, vol. 9, pp. 5701–5710. Curran, Red Hook (2012)
22. Li, S., Li, X., Wang, Z., Wu, G., Lu, G., Zhao, L.: Finite element analysis of sandwich panels with stepwise graded aluminum honeycomb cores under blast loading. *Compos. A Appl. Sci. Manuf.* **80**, 1–12 (2016). <https://doi.org/10.1016/j.compositesa.2015.09.025>
23. Farrokhhabadi, A., Ahmad Taghizadeh, S., Madadi, H., Norouzi, H., Ataei, A.: Experimental and numerical analysis of novel multi-layer sandwich panels under three point bending load. *Compos. Struct.* **250**, 112631 (2020). <https://doi.org/10.1016/j.compstruct.2020.112631>
24. Slyvyns'kyi, V., Slyvyns'kyi, M., Polyakov, N., Gajdachuk, A., Gajdachuk, V., Kirichenko, V.: New concept for weight optimization of launcher nose firings made of honeycomb structures. In: *Proceedings of the International Astronautical Congress, IAC 57. Our World Needs Space 8*, pp. 5669–5683 (2006)
25. Milinevsky, G., Yatskiv, Y., Degtyaryov, O., Syniavskiy, I., Mishchenko, M., Rosenbush, V.: New satellite project Aerosol-UA: remote sensing of aerosols in the terrestrial atmosphere. *Acta Astronaut.* **123**, 292–300 (2016). <https://doi.org/10.1016/j.actaastro.2016.02.027>



Preparation and Characterization of a Biocomposite Based on Casein and Cellulose

Mykola Melnychuk¹(✉) , Victoria Malets¹ , Marcin Sosnowski² ,
Ivanna Mykhaylyuk¹, and Inna Boyarska¹ 

¹ Lutsk National Technical University, 75, Lvivska Street, Lutsk 43018, Ukraine
m.melnichuk@lntu.edu.ua

² Jan Dlugosz University in Czestochowa, 4/8, Waszyngtona, 42-200 Czestochowa, Poland

Abstract. The problems caused by synthetic waste have led to the need to develop new materials that can be environmentally safe for living organisms and biocompatible with the environment, replacing widely used synthetic polymers. IR spectroscopy was used to study the chemical composition of the composite and to detect harmful substances. The nature of the relationships of structural components in the compositions was studied using scanning electron microscopy. The impact strength was determined by the Charpy method. The nature of the interaction of system components at the microstructural level is investigated. In particular, the anisotropy of properties, which is ensured by the uniform distribution of cavities in the volume of the composite and good adhesion of microcellulose with casein binder, was investigated. It is established that the composite does not contain harmful, toxic substances and can be positioned as a biocomposite. This material has been shown to have sufficient impact characteristics, in particular, impact strength $a = 47 \text{ kJ/m}^2$ and can be used in the manufacture of food packaging, such as an alternative to polystyrene.

Keywords: Cellulose · Plant fibers · Biodegradable material · Casein · Food packaging · Chemical composition · Impact strength

1 Introduction

World oil reserves are rapidly declining. There are deepening global environmental problems such as accumulation of waste, pollution of ecosystems, and others. Such challenges have contributed to the development of an alternative to existing polymer materials [1]. Casein is widely used in the food, medical, woodworking industries, in particular, the long-known casein glue for wooden surfaces and casein primers, casein is added to paints, where it acts as a thickener and stabilizer, or it is added to textile products because in the presence of casein fibers do not give shrinkage during washing. One of the most relevant areas of its use in the manufacture of bioplastics capable of biodegradation [2].

In recent years, scientists are increasingly using natural fibers as reinforcements for composites. Natural fibers have many advantages, such as low specific gravity, low cost,

biological degradability, and higher mechanical properties such as stiffness and strength compared with synthetic fibers [3]. The most common plant fibers used as reinforcing materials are lignocellulosic materials (containing cellulose, hemicellulose, and lignin) and cellulose fibers. These materials can be obtained from many sources, such as sawdust, cotton, technical hemp, recycled corrugated cardboard, sugar cane [4], etc.

2 Literature Review

In recent years, research on materials derived from natural renewable sources has increased significantly. Examples of such materials are composites based on gelatin [5], dextrin [6], chitosan [7], polylactide [8] pectin [9, 10] and casein [11, 12]. As a result, knowledge about the functional characteristics of new materials and the scope of such natural polymers is constantly improving. Natural polymers, such as casein and pectin, are proteins and hydrogel-forming polysaccharides, so they are given special attention because they are biodegradable polymers. An additional advantage of casein is that they have no toxic effects.

Modification of the casein structure is the basis for developing new and improved technologies for biodegradable materials. One of the promising areas of this research is the creation of medical films and food packaging. However, solving this problem is not easy, because pure casein materials have low technological characteristics, such as very low strength and elasticity; they are easily soluble in water. Improving the properties can be achieved by obtaining composite materials based on casein reinforced with natural fibers. There are studies devoted to developing such materials, particularly the possibility of forming a copolymer of casein and methylcellulose and obtaining films [13].

To achieve the research goal, the following tasks were set: to obtain microcellulose from fibers and technical hemp trusts, determine the composite's chemical composition, and investigate the structure and chemical composition of the composite.

3 Research Methodology

Examination of the surface condition was performed using an optical digital microscope LEICA DMS300 (Leica Microsystems, Germany). The microstructure was examined using a Hitachi TM3000 (Hitachi High-Technologies Corporation, Japan) scanning electron microscope with the EDS SwiftED3000 microanalyzer system for quantitative and qualitative analysis (percentage of elements contained in the samples). FTIR spectrometer (Shimadzu, Japan) operating in the range of $4000\text{--}400\text{ cm}^{-1}$; at a resolution of 0.5, 1, 2, 4, 8, 16 cm^{-1} , was used to study the chemical composition. The signal-to-noise ratio $S/N = 30000:1$ for 1 min of spectrum collection to calculate peak-peak at a resolution of 4 cm^{-1} . The spectrometer is equipped with a Gladi ATR Vision Base Optics adapter from Pike Technologies, which allows measurements to be performed in the mode of attenuated total infrared reflection.

Impact tests were performed under current international standards ISO 179 by the Charpy method. For the study used a pendulum dill CEAST 9050 (Instron, USA).

Impact tests were performed using pendulum copra with a maximum energy of 25 J - CEAST 9050 (INSTRON). The hammer is intended for tests by the Charpy method at a temperature of +20 °C without an incision.

Technical hemp fibers were used to obtain microcrystalline cellulose, hereinafter “cellulose-1”; long flax (long flax fiber from long wetting trusts), then “cellulose-2”; and hemp fiber from dew-soak trusts of the spring harvest period, hereinafter “cellulose-3”. The method “Development of technology for obtaining cellulose from hemp fibers” was used as a basis for pulp production [14].

The cellulose fibers (Fig. 1) of flax and hemp were ground to a size of 7 ± 1 mm. The fibers were treated with a 1% solution of Trilon B ($C_{10}H_{18}N_2Na_2O_{10}$) for 30 min in a ratio of 10:1 at a temperature of 100 °C, to facilitate the removal of minerals from the resulting cellulose.



Fig. 1. Shredded fibers of technical hemp.

The process (Fig. 2) is carried out in a heat-resistant flask mounted on a flask heater connected to a reflux condenser.

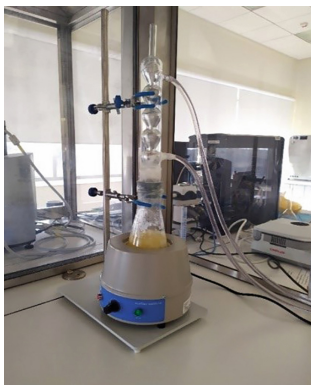


Fig. 2. The process of obtaining cellulose.

After obtaining cellulose for the manufacture of composites, the cellulose was further ground using a laboratory homogenizer, “CAT Unidrive X 1000”, at a speed of 20,800 rpm (Fig. 3). The crushed cellulose was filtered through filter paper and then dried at room temperature overnight.



Fig. 3. Cellulose-3, crushed using a homogenizer (photo from an optical microscope, magnification, $\times 1.25$).

4 Results

Samples with different percentages of cellulose in the range $\Theta = 25 \dots 50\%$ of the mass fractions were prepared for research. Casein glue of the Extra (B-107) brand of animal origin was chosen as a binder.

The adhesive is characterized by high reliability for gluing wooden surfaces and has no harmful emissions, so it is suitable for producing environmentally friendly composites. The powder was gradually poured into the water at room temperature with constant stirring to prepare the adhesive solution.

The glue was mixed to a uniform consistency using a porcelain mortar. Then cellulose was added, and the whole mass was thoroughly mixed.

The resulting mass is laid to the prepared aluminum molds, dimensions $10 \times 10 \times 100$.

The finished mass was dried in the mold in the air for 48 h, after which the finished samples were removed from the mold for research, and the samples were dried at temperatures of $60\text{--}80\text{ }^{\circ}\text{C}$, which accelerates the drying rate, but slightly increased the porosity of the structure. Structure studies were performed using a Leica DMS300 digital microscope. Figure 4 shows photographs of the macrostructure of samples filled with different cellulose fibers and different content of mass parts. The structure of the samples is cellulose fibers glued together with a matrix material. It should be noted that the filler is not evenly distributed in the matrix.

The homogeneity of the samples depends on the amount of filler and the size of the cellulose fibers. Also present in all samples structure defects (pores) of different diameters. The fibers are arranged in the matrix chaotically at different angles, which provides the system's inhomogeneity and anisotropy of properties.

Using an EDS adapter (SwiftED3000 (EDS X-Ray microanalyzer)), the chemical composition of the three types of cellulose obtained was studied. Table 1 shows the percentage of elements obtained during the study of cellulose.

The molecular formula of cellulose is $(\text{C}_6\text{H}_{10}\text{O}_5)_n$. According to research, cellulose contains the most carbon (53–55%) and oxygen (43–46%). Cellulose also contains hydrogen, but due to the atomic mass, less than 3 of this element, so it is impossible to detect during the study of the EDS prefix's chemical composition. Chemical test results

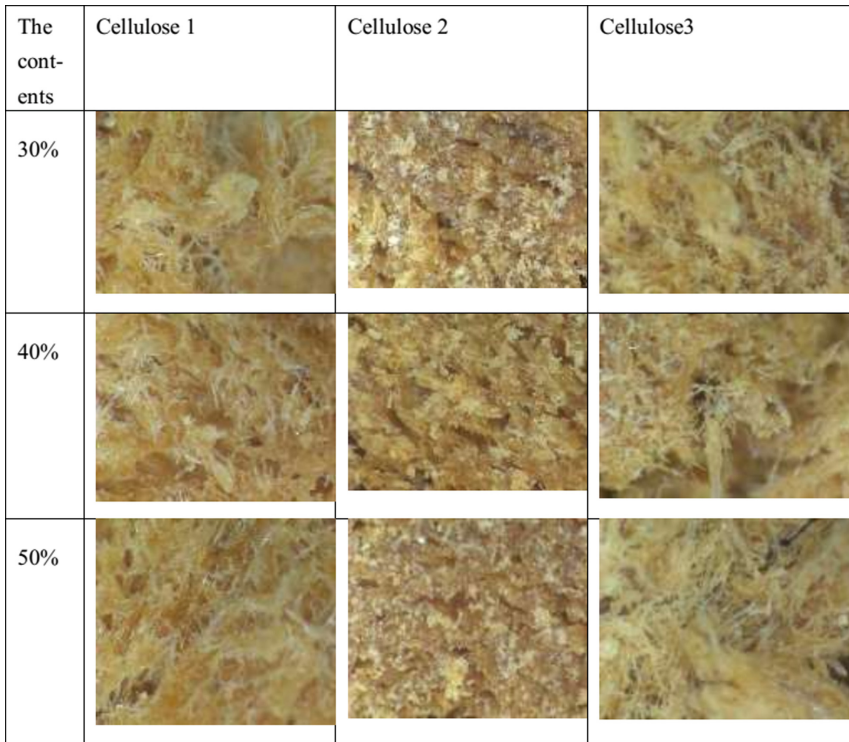


Fig. 4. Macrostructure of composites, $\times 6$.

Table 1. Percentage of elements in cellulose.

Sample	Percentage of elements [%]					
	C	O	Al	Br	Ca	Si
Cellulose -1	53.186	45.88	0.674	0.248	–	–
Cellulose -2	55.877	43.2424	0.7602	0.08	0.0392	0.0312
Cellulose -3	54.9292	44.8196	–	–	–	0.2512

show a small number of aluminum, bromine, calcium, and silicon elements. Their presence can be explained by contamination resulting from obtaining and contacting the holder on which the test samples were placed (Fig. 5).

The study results show that all three types of cellulose obtained do not contain harmful elements and heavy metals.

Figure 6 shows SEM samples' images with different types of filler with a degree of filling of 40% at magnification, $\times 310$ at a voltage of 5.0 kV. The photo clearly shows that the sample has structural defects (pores and cracks) ranging in size from 72.49 to 169.77 μm .

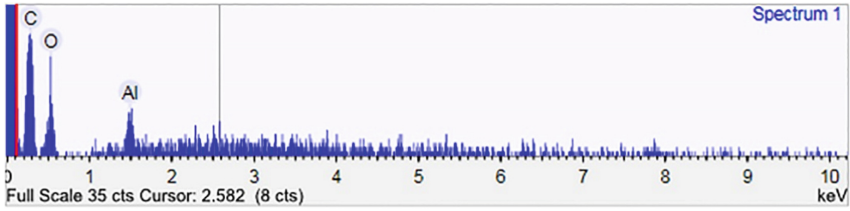


Fig. 5. Spectrum of EDS cellulose-1.

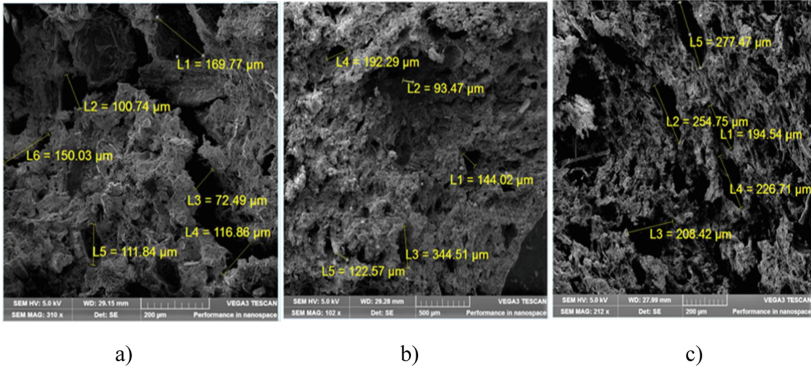


Fig. 6. Microstructure of the SEM image: a) I-type; II-type; III-type.

FTIR infrared spectroscopy, which includes registration and analysis of spectra (Fig. 7) of the tested samples' oscillations, was used to study the chemical composition of the finished samples. The study was conducted to analyze organic compounds and determine their structural features.

During the tests, all samples contain primary aliphatic amides in the range of $1600\text{--}1690\text{ cm}^{-1}$; $3310\text{--}3410\text{ cm}^{-1}$; $3160\text{--}3220\text{ cm}^{-1}$; and primary aliphatic alcohols in the range of $1000\text{--}1090\text{ cm}^{-1}$; $3200\text{--}3600\text{ cm}^{-1}$. Samples with cellulose-1 and cellulose-2 have aliphatic hydrocarbons in the range of $2840\text{--}2980\text{ cm}^{-1}$. Sample cellulose-2 and -3 have secondary aliphatic alcohols in the range of $950\text{--}980\text{ cm}^{-1}$; $1100\text{--}1150\text{ cm}^{-1}$; $3200\text{--}3600\text{ cm}^{-1}$. And only in one sample was found inorganic carbonate (Inorganic Carbonate Compounds) in the range of $1300\text{--}1510\text{ cm}^{-1}$.

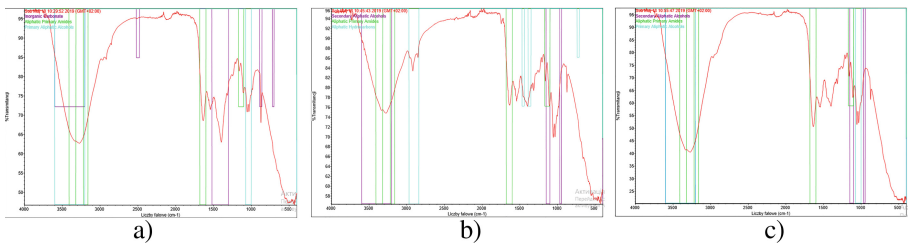


Fig. 7. Infrared absorption bands.

It should be noted that all tested samples showed a brittle fracture. The results are presented in Table 2.

Table 2. The results of measuring the toughness.

Cellulose content, %	Abs. en. (%)	$a_{b.n.}$ [KJ/m ²]	Energy [J]
0	10.31	6.93	0.34
30	30.85	25.31	1.24
40	32.06	32.65	1.61
50	47.07	46.94	2.35
60	49.12	37.96	1.86

No dependence of the samples’ impact strength on the type of cellulose was observed, but only on the content. According to the study results, the impact strength and absorbed impact energy increase almost linearly with an increase in the degree of filling to 50%, and at higher degrees of filling begins to decrease. Due to insufficient wetting of the binder.

To obtain a more detailed picture (the ability to resist shock load), these samples’ fracture surface (Fig. 8) was investigated using SEM.

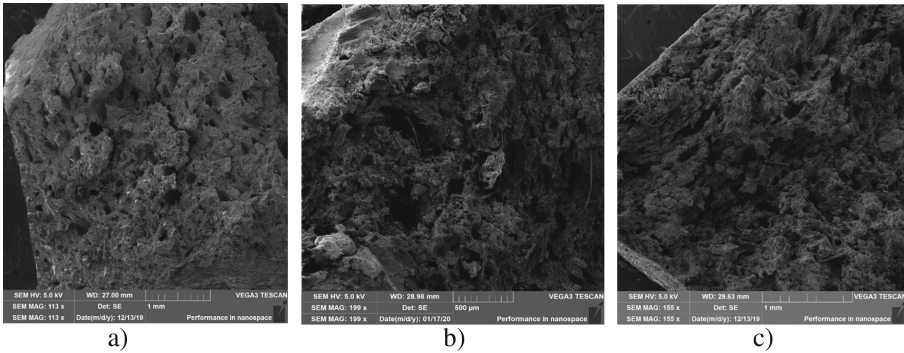


Fig. 8. Fracture of composite material, SEM × 150.

The photo shows that the cellulose fibers lie well in the matrix, there is no pulling of the fibers, and after the impact, there is a brittle fracture without signs of plastic deformation in the material. Regardless of the porosity, the material exhibits quite good mechanical properties.

Structural defects, pores of different diameters, the sizes of which range from 72 to 344 μm, which are a consequence of the composite’s high viscosity during molding, were also registered. However, these defects are characterized by a homogeneous (uniform) distribution in the structure, which does not adversely affect the material’s

mechanical properties; on the contrary, it increases the possibility of its use as a porous material. The fracture surface is characterized by the absence of a large number of pronounced microscopic chipping lines, which have significant branches, which indicates the structure of the system with a low-stress state.

5 Conclusions

The research is devoted to creating biomaterial that could be used as packaging material in food technology, medicine. Three types of crystalline cellulose were obtained from the fibers of technical hemp, flax, and hemp trusts. It was found that the quantitative yield of cellulose from different raw materials is the same, which in turn provides prospects for the production of cellulose from trusts. Because trust is essentially a waste in fiber production technology. Studies have confirmed that all three types of cellulose do not contain harmful substances and heavy metals, which gives grounds for using such types of fillers in materials for the food industry.

The chemical composition of casein-based composites was also investigated, and the results show that the material does not contain toxic or harmful substances in general.

The impact strength of the casein matrix increases to 47 kJ/m² for a composition filled with 50% by weight, the increase is due to the reinforcement of cellulose fibers, which corresponds to the impact strength of polystyrene, which is widely used for food packaging.

Therefore, the obtained results confirm the prospects for further research of this material. Accordingly, studies of tensile and flexural strength, thermal conductivity, and biodegradability of the composite will be performed.

References

- Suchada, C.: Current trends in biodegradable polyhydroxyalkanoates. *J. Biosci. Bioeng.* **110**, 621–632 (2010). <https://doi.org/10.1016/j.jbiosc.2010.07.014>
- Nagarajan, V., Mohanty, A.K., Misra, M.: Sustainable green composites: value addition to agricultural residues and perennial grasses. *ACS Sustain. Chem. Eng.* **1**(3), 325–333 (2013). <https://doi.org/10.1021/sc300084z>
- Melnychuk, M., Andrushko, O.: Influence of the scale factor of fibers and the temperature of structuring on the physical and mechanical characteristics of hemp fiber biocomposites. In: Ivanov, V., et al. (eds.) *DSMIE 2018. LNME*, pp. 108–116. Springer, Cham (2019). https://doi.org/10.1007/978-3-319-93587-4_12
- Faruk, O., Błędzki, A.K., Fink, H.-P., Sain, M.: Progress report on natural fiber reinforced composites. *Macromol. Mater. Eng.* **299**, 9–26 (2014). <https://doi.org/10.1002/mame.201300008>
- Stenekes, R.J.H., Franssen, O., Van Bommel, E.M.G., Cromelin, D.J.A., Hennink, W.E.: The use of aqueous PEG/Dextran phase separation for the preparation of dextran microspheres. *Int. J. Pharm.* **183**, 29–32 (1999). [https://doi.org/10.1016/s0378-5173\(99\)00038-1](https://doi.org/10.1016/s0378-5173(99)00038-1)
- Rosler, B., Kreuter, J., Scherer, D.: Collagen microparticles: preparation and properties. *J. Microencapsul.* **12**, 49–57 (1995). <https://doi.org/10.3109/02652049509051126>
- Wu, H., Wang, S., Fang, H., Zan, X., Zhang, J., Wan, Y.: Chitosan-polycaprolactone copolymer microspheres for transforming growth factor-β1 delivery. *Colloids Surf. B Biointerfaces* **82**, 602–608 (2011). <https://doi.org/10.1016/j.colsurfb.2010.10.024>

8. Liu, R., Ma, G.-H., Wan, Y.-H., Su, Z.-G.: Influence of process parameters on the size distribution of PLA microcapsules prepared by combining membrane emulsification technique and double emulsion–solvent evaporation method. *Colloids Surf. B Biointerfaces* **45**, 144–153 (2005). <https://doi.org/10.1016/j.colsurfb.2005.08.004>
9. Baracat, M.M., Nakagawa, A., Freitas, L.A.P., Freitas, O.: Microcapsule processing in a spouted bed. *Can. J. Chem. Eng.* **82**, 134–141 (2004). <https://doi.org/10.1002/cjce.5450820117>
10. Redigueri, C.F., Freitas, O., Lettinga, M.P., Tuinier, R.: Thermodynamic incompatibility and complex formation in pectin/caseinate mixtures. *Biomacromol* **8**, 3345–3354 (2007). <https://doi.org/10.1021/bm7004438>
11. Saravanan, M., Rao, K.P.: Pectin–gelatin and alginate–gelatin complex coacervation for controlled drug delivery: influence of anionic polysaccharides and drugs being encapsulated on physicochemical properties of microcapsules. *Carbohydr. Polym.* **80**, 808–816 (2010). <https://doi.org/10.1016/j.carbpol.2009.12.036>
12. Heidebach, T., Först, P., Kulozik, U.: Influence of casein-based microencapsulation on freeze-drying and storage of probiotic cells. *J. Food Eng.* **98**, 309–316 (2010). <https://doi.org/10.1016/j.jfoodeng.2010.01.003>
13. Grynchenko, N., Tyutyukova, D., Pyvovarov, P.: Modification of the structure and functional-technological properties of casein: scientific and applied aspects. *Food Sci. Technol.* **11**(1), 57–70 (2017). <https://doi.org/10.15673/fst.v11i1.305>. [in Ukrainian]
14. Barbash, V.A., Trembus, I.V., Sirotuk, S.V.: A method for producing microcrystalline cellulose from hemp fibers. *KPI Sci. News* **1**(117), 81–87 (2018). <https://doi.org/10.20535/1810-0546.2018.1.118670>. [in Ukrainian]



Advanced Technologies of Manufacturing Readily Removable Cores for Obtaining High-Quality Castings

Olga Ponomarenko¹ , Igor Grimzin² , Nataliia Yevtushenko¹  ,
Tatiana Lysenko³ , and Dmytro Marynenko¹ 

¹ National Technical University “Kharkiv Polytechnic Institute”, 2, Kyrpychova St., Kharkiv 61002, Ukraine

natalya0899@ukr.net

² Research and Production Center, European Engineering Technologies”, 101, Velyka Panasivska Street, Kharkiv 61017, Ukraine

³ Odessa National Polytechnic University, 1, Shevchenko Ave., Odessa 65044, Ukraine

Abstract. The work investigates the physical, mechanical, and technological properties of mixtures to manufacture cores in a foundry. The filler is technical salt, the binder is an aqueous solution of sodium silicate, and the hardener is a solution based on propylene carbonate on a silicate basis. These rods are used to make internal surfaces in thin-walled castings. The work proposes a new method of manufacturing cores based on cold-hardening mixtures (CHM), which harden at room temperature. The planned experiment was chosen as the basis for modeling the properties of the mixture. The following parameters were chosen as optimization parameters: compressive strength, friability, and durability. According to the developed mathematical models, the mixture composition was optimized. The optimum binder content is 4.0 to 6.0%, and the hardener content is 0.3 to 0.4%. A technological process of preparing CHM for readily removable salt cores has been developed. As a result, the surface quality of the internal surfaces of castings improved. The cycle of core production was reduced, and the casting cleaning costs were reduced due to the elimination of the decoring process; environmental safety of the technological process was provided to the use of non-toxic materials.

Keywords: Cold-hardening mixture · Binder · Hardener · Salt · Core · Mathematical model · Casting · Quality

1 Introduction

Modern mechanical engineering focuses on the widespread use of resource- and energy-saving technologies that provide high performance of parts and their minimal labor intensity. These include, first of all, casting technique. Casting ensures that the workpiece is as close as possible in size and configuration to the finished part.

At present, small-scale production uses a technique of nonferrous sand and plaster mold casting. There is a great variety in the scope of casting in these molds.

Turbine wheels with complex blades, thin-walled body parts [1, 2], and unique castings for artistic casting [3, 4] are obtained by casting in sand-plaster molds.

The advantages of this type of casting are as follows: obtaining castings with a clean surface and high precision comparable to the castings obtained by lost-wax casting and die casting; simplicity of the technological process of obtaining the casting on the model made of various materials (wood, plastic, plasticine, and metal); the low thermal conductivity of molds and their sufficient durability, which provides easy filling with a metal of difficult and thin-walled castings [5]. Besides, this technology makes it possible to obtain castings from several grams to tens of kilograms of various sizes [6, 7].

However, as of today, choosing a method of manufacturing the internal cavities remains one of the difficult tasks when obtaining thin-cavity parts. The method of obtaining thin cavities by machining is associated with the complexity of the technological process and high costs.

2 Literature Review

There is a way to obtain the internal cavities in castings by using cores. When pouring the mold, the cores are surrounded on every side by liquid metal, so they are to have a number of properties: high gas permeability, as well as strength, ductility, decorating ability, which is ensured by choosing the composition of the appropriate core mixture and core design [8, 9].

More than ten main technological processes are currently used for producing cores in industry, each of which has varieties, subtypes, and modifications.

In the context of foundry production, it is appropriate to use readily removable salt cores for sand and plaster mold casting, die casting, and lost-wax casting. One of the advantages of salt cores is that they do not need to be decorated, i.e., they can be easily removed from the finished part by dissolving in a non-toxic medium, such as water. Salt rods are removed from the castings due to their dissolution in water, while in the technological process, the operation of knocking out the rods from the castings disappears. However, such rods must have good physical and mechanical properties, qualitatively form the surface of the casting, have low shrinkage, and do not emit toxic substances when filling the mold with metal [10, 11].

As a rule, these cores are made of substances that do not enter into reactions with the release of gases, do not adversely affect the environment, either in the manufacture of cores or in the casting process [9]. Thus, when filling the mold with metal, no gases are formed, the quality of castings is improved, gas and shrinkage holes do not develop. When removing the cores, no residues occur that require particular disposal. Depending on the composition, the cores can be reused. Extracting salts from the liquid phase is possible, for example, by spray drying or evaporation.

As of today, there is a whole range of materials that are used for the manufacture of readily removable salt-based cores [11–13]. Salt cores can be obtained in various ways, such as casting, pressing, casting, and pressing [14, 15].

One of the emerging technologies for obtaining cores is cold-hardening mixtures (CHM) for their preparation. Fabricating cores from cold-hardening mixtures dates back to more than a few decades and now dominates in foundries, allowing obtaining as follows:

- High dimensional and mass accuracy of cores and castings;
- Short production cycle;
- Better sealing of cores in the mold pattern owing to the high flow properties of the core mixtures;
- Low energy consumption of the process;
- Using cheaper core patterns made of wood, plastics, and other materials;

The transition to the manufacture of cores from CHM dramatically improves the accuracy of castings, production practices, minimizes losses due to rejects, and reduces labor intensity.

However, the technology of obtaining salt cores based on cold-hardening mixtures has not been used and has been poorly known to date. Therefore, the development of readily removable cores based on cold-hardening mixtures in non-corrosive media receives priority in foundry production.

3 Research Methodology

The main objective of the study is to develop advanced technologies for the manufacture of cores in the foundry, in which the filler is technical salt, the binder is an aqueous solution of sodium silicate (*Recril Slow Set C*), and the hardener is a solution based on propylene carbonate on a silicate basis (*Dursil C1*).

Mixtures for CHM contain a filler, a binder, and a hardener. The filler is the basis of the mixture. This component gives the mixture the required compressive strength, fire resistance, and certain thermophysical characteristics. As a filler of the core mixture food-grade, salt NaCl is used. The shape, size, and homogeneity of its grain composition have a decisive impact on the properties of the mixture.

The binder envelops the grains of sand and separates them from each other by a thin layer. The binding components impart strength and ductility to the mixtures. Reducing the content of binding materials in the mixtures helps to reduce the amount of gases formed during the casting process, facilitate the conditions of the decoring process, and reduce the drying process of the cores.

Mixing the components is one of the main operations when preparing qualitative mixes. The properties of molding and core mixtures depend on the uniform distribution of binders in the volume of the mixture. The uniformity of distribution of components and creation of envelopes of binders around the grains of sand is reached in preparation of the mixture. The design of the working bodies of the mixer, the speed and time of mixing affect the formation of a high-quality dense film on the filler grains.

The proper sequence of introducing the mixture's components, the mixing time, the optimum mode of preparation of the mixture provide its homogeneity and the maximum durability.

Salt is the most common and widely mined mineral, without which it is impossible to imagine human life. Salt (NaCl) has over 14 thousand fields of application and is used in the food, chemical, oil and gas, fertilizer, and leather industries, and mechanical engineering, metalworking, ferrous and nonferrous metallurgy, medicine, public utilities, and agriculture. There is a technical one, fodder, tableted, and table salt. Technical salt

(also called halite or deposited salt) is a natural mineral product, the main chemical element of which is sodium chloride (NaCl).

The physical and chemical characteristics of halite are given in Table 1.

Table 1. Physical and chemical characteristics and types of halite.

Characteristics (mass fraction of the substance)	Premium	First	Second
Sodium chloride, %, no less than	98.1	96.5	93
Calcium ion, %, no more than	0.35	0.35	1.8
Magnesium ion, %, no more than	0.05	0.05	0.8
Sulfate ion, %, no more than	1	1.2	0.9
Potassium ion, %, no more than	0.1	0.1	2.2
Iron oxide, %, no more than	0.005	0.005	0.1
Insoluble residue, %, no more than	0.25	0.75	2.5
Moisture content, %, no more than	0.25	0.35	3.5

According to the particle size distribution, technical salt is divided into the types as follows:

- Type A: inclusions up to 1.2 mm not less than 85%, over 2.5 mm up to 3%;
- Type B: inclusions up to 2.5 mm 90%, over 4.5 mm up to 5%;
- Type C: inclusions up to 4.5 mm 85%, over 4.5 mm up to 15%;
- Type D: inclusions up to 20 mm 85%, over 20 mm up to 15%;
- Type E: blocks measuring (200 × 200 × 200) mm and (200 × 200 × 400) mm. influence.

The mixture components were chosen for the experiments: technical salt Type A, liquid hardener, and binder.

The core mixture was prepared as follows: the salt was sieved on a sieve with a mesh size of 0.315 mm, and then the hardener was added to the salt and mixed for three minutes, then the binder was introduced and mixed for another two minutes.

For studying the compressive strength of the proposed mixtures, standard specimens were prepared. A nine-seater press die was used for this purpose. In the press die, the specimens were kept for some time and then removed and tested after some time. It is usually 0, 30, 60, 90, 180 min, and 24 h.

The curing time of the specimens mainly depends on the amount of binder and hardener and the mixing time of the mixture.

The task of control and stabilization of the properties of mixtures is to select the optimum average values of the controlled characteristics of the mixtures and the allowable intervals of their change.

To stabilize and control the properties of core mixtures in the foundry, empirical and computational-analytical approaches are used. The formulation and technology for

preparing mixtures are developed and adjusted directly in production conditions with an empirical approach. With the computational and analytical approach, the parameters of the mixture preparation technology are determined using mathematical models.

The empirical approach to solving the problem is marked by high complexity, a significant risk of obtaining low-quality products in the process of developing technical conditions, and its results are suitable only for the specific conditions studied for the production of castings. Recommendations for selecting components and the formulation of mixtures are empirical, considering a limited number of variables. These recommendations are not reliable enough and cannot be used in other production conditions.

The calculation and analytical methods are the most progressive. The method is based on the use of a planned experiment. This approach opens up new opportunities for controlling the properties of molding mixtures due to process control efficiency when changing the properties of raw materials and the range of castings to be manufactured. Only based on this approach automated control systems of processes of preparation of molding mixes can be developed.

A planned experiment was performed to optimize the core mixture. Type 2^{3-1} planning (half-replicates of a complete factorial experiment for two variables) were used for the investigation.

The leading physical and mechanical indicators of the properties of the molding mixture were selected as optimization parameters (y): compressive strength, friability, durability (y_1, y_2, y_3). Mixtures with different percentages of binder and hardener were studied.

Durability is determined by the curing rate and depends mainly on the type of binder composition, the quality of the starting materials and their temperature, the ambient temperature, intensity, and duration of mixing.

The varied factors were as follows: the amount of binder (x_1) introduced into the mixture, the amount of hardener used (x_2); was chosen as a hardener.

The quantitative indicators of the components, the main levels, and intervals of variation of the factors are given in Table 2.

Table 2. Experimental conditions for CHM based on the *Recril Slow Set C* binder and *Dursil C1* hardener.

Independent variables	Amount of binder in %	Amount of hardener in %
Code	X1	X2
Main level	4	0.4
Variation interval	1	0.2
Upper level	5	0.6
Lower level	3	0.2

The physical and mechanical properties of the mixture were controlled as follows: compressive strength, friability, durability.

The mechanical properties of molding and core mixtures are among the main factors determining the possibility of obtaining high-quality castings.

The physical and mechanical properties were determined as an average of three specimens tested in parallel. The experiments specified by the planning matrix were carried out randomly, that is, in a random sequence. A table of random numbers sets their order. This makes it possible to exclude the influence of external factors on the experiment.

The planning matrix and indicators of the initial parameters of the molding mixture are shown in Table 3.

Table 3. Planning matrix.

Item No	X0	X1	X2	X1·X2	σcompression (compressive strength), MPa	Friability in %	Durability, min
					y1	y2	y3
1	+	+	+	+	2,05	0,37	16
2	+	–	+	–	1,07	0,54	10
3	+	+	–	–	1,9	0,7	24
4	+	–	–	+	1,15	1	15

The experiment planning matrix half-replicate 2^{3-1} . The mathematical model took into account the influence of individual factors and their paired interactions.

During the experiment, the reproducibility variance was determined. That is, the experimental error was considered. Parallel experiments assessed reproducibility. To do this, we carry out each experiment in the planning matrix three times. The coefficients of mathematical models were calculated, and their statistical significance was determined. The Student’s test determined the significance of the coefficients in mathematical models. We check the hypothesis about the adequacy of mathematical models using the Fisher criterion.

As a result of the planned experiment, the following regression equation was obtained (example (1), (2), (3)):

$$\sigma_{\text{compression}} = 1.54 + 0.43X_1 + 0.04X_2 + 0.06X_1X_2 \text{ [MPa]} \tag{1}$$

$$\text{Friability} = 1.11 - 0.08 X_1 - 0.23 X_2 - 0.43 X_1X_2, \text{ [%]} \tag{2}$$

$$\text{Durability} = 16.25 + 3.75X_1 - 3.25X_2, \text{ [min]} \tag{3}$$

In these equations, we use the values of the factors in the coded scale, which are calculated from the corresponding values in the natural scale by the following formulas:

$$X_1 = \frac{X_1 - 1,5}{0,5} \tag{4}$$

$$X_2 = \frac{X_2 - 3}{1} \quad (5)$$

4 Results

Figures 1, 2 and 3 show the effect of binder and hardener on the core mixture's strength, friability, and durability.

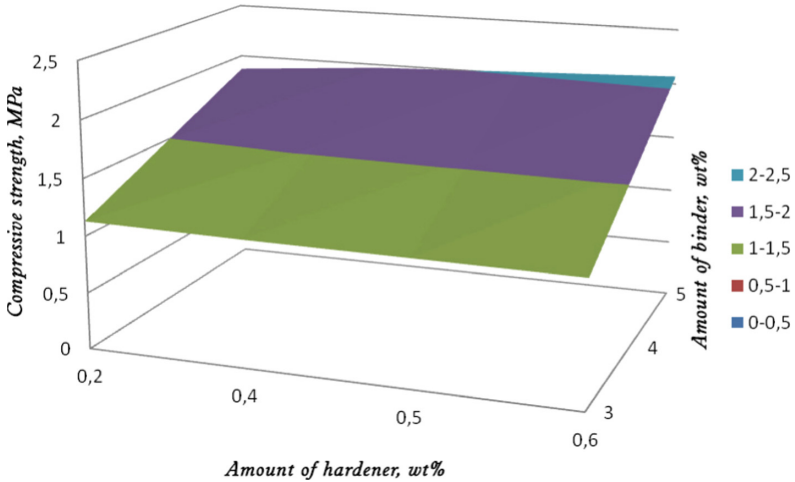


Fig. 1. Effect of the binder and the hardener on compressive strength.

The analysis of mathematical models showed the degree of influence of the quantitative indicators of the binder and hardener on durability, compressive strength, and friability. This coincides with the existing ideas about the properties of the mixture, which can be obtained during its preparation. With an increase in the amount of binder and hardener, the strength of the mixture increases. Consequently, an increase in the amount of binder, a more uniform enveloping of the grain surface occurs. The simultaneous increase in the hardener increases the binding properties of the film, and the bonds between the grains become stronger. Besides, the paired interactions of the components have a positive effect on the studied indicator of the strength of the mixture. The durability increases with an increase in the amount of binder and a decrease in the hardener. The more binder in the mixture, the slower the processes of reducing the quality indicators of the mixture. The friability decreases with an increase in the amount of binder and hardener. The indicators of the crumbling of the mixture remain at a reasonably low level in the entire range of variation of the components. This allows us to state that there will be no defects in castings due to blockages and sandy shells.

Based on the developed mathematical models, the optimal content of the binder was established, which is from 4.0 to 6.0% and the hardener from 0.3 to 0.4%.

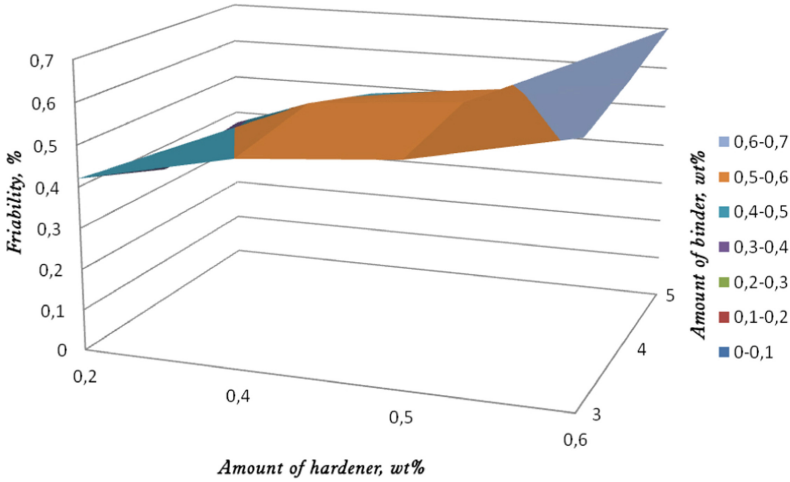


Fig. 2. Effect of the binder and the hardener on friability.

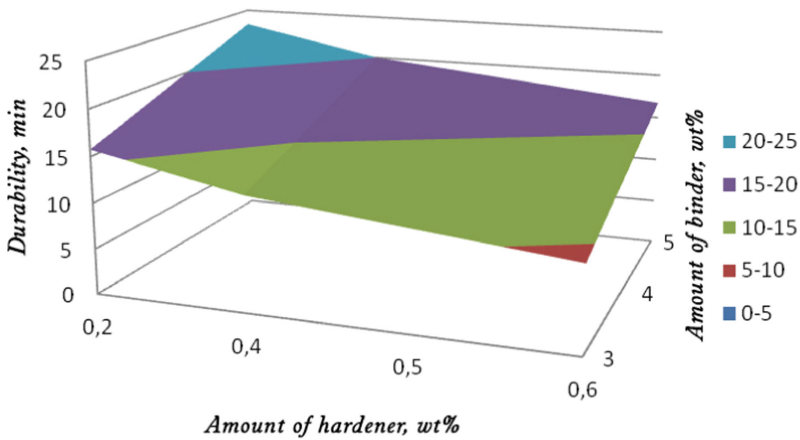


Fig. 3. Effect of the binder and the hardener on the durability of the mixture.

A technological process was developed for obtaining CHM for easily removable cores based on the research carried out. As a result, the quality of the surface of the inner surfaces of the castings was improved, the cycle for the manufacture of cores was shortened, the costs of cleaning the castings were reduced, and the environmental safety of the technological process was ensured.

5 Conclusions

In the current context of the development of foundry production, readily removable salt cores are used for obtaining internal cavities, holes, and channels of the most diverse and complex shapes in thin-walled castings. One of the advantages of salt cores is that

they do not need to be decorated. The obtained castings are placed in water, and the cores are dissolved in it. Therefore, salt cores in the manufacture of castings are a promising area in the foundry industry. The advantages of salt cores are that they are composed of substances that do not react with each other, with the release of gases that adversely affect the quality of castings or the environment, either in the manufacture of cores or in the process of filling molds with metal. This makes the process environmentally safe. For the first time in the work for the production of cores, the technology was used to prepare cold-hardening mixtures based on salt composition using the binder and hardener.

For simulating the properties of the core mixture, a planned experiment was performed. The main indicators of the properties of the molding mixture were selected as optimization parameters: compressive strength, friability, and durability. The amount of binder and the amount of hardener to be introduced into the mixture were chosen as variable factors.

The analysis of mathematical models showed the degree of influence of the quantitative indicators of the binder and hardener on durability, compressive strength, and friability. This coincides with the existing ideas about the properties of the mixture, which can be obtained during its preparation. With an increase in the amount of binder and hardener, the strength of the mixture increases. Consequently, with an increase in the amount of binder, a more uniform enveloping of the grain surface occurs. The simultaneous increase in the hardener increases the binding properties of the film, and the bonds between the grains become stronger. Besides, the paired interactions of the components have a positive effect on the studied indicator of the strength of the mixture. The durability increases with an increase in the amount of binder and a decrease in the hardener. The more binder in the mixture, the slower the processes of reducing the quality indicators of the mixture. The friability decreases with an increase in the amount of binder and hardener. The indicators of the crumbling of the mixture remain at a reasonably low level in the entire range of variation of the components. This allows us to state that there will be no defects in castings due to blockages and sandy shells. Based on the developed mathematical models, the optimal content of the binder was established, which is from 4.0 to 6.0% and the hardener from 0.3 to 0.4%.

A technological process of preparing a core CHM based on salt composition has been developed. The technological process of core preparation was tested in the conditions of Scientific production center “European Technologies of Mechanical Engineering” (Kharkiv, Ukraine), where it showed high efficiency: the surface quality of the internal surfaces of castings improved, the cycle of core production was reduced and the casting cleaning costs were reduced owing to the elimination of the decorating process; environmental safety of the technological process was provided owing to the use of non-toxic materials.

References

1. Holtzer, M., Kmita, A.: *Synthetic Resins. Mold and Core Sands in Metalcasting: Chemistry and Ecology*. Springer, Cham (2020)
2. Shah, S.R.: Design of a sand casting method using patterns made of sublime materials for casting intricate shapes. *J. Eng. Res. Appl.* **8**(12) (Part -I), 64–70 (2018)

3. Karpenko, V.M., Karpenko, V.M., Marukovich, E.I.: *Artistic casting: materials, technologies, equipment*. Belarus Science, Minsk (2019)
4. Livshits, V.B.: *Casting technology of art products*. URSS Publishing Group, Moscow (2017)
5. Zhang, Y., Zhang, J., Miao, Y., Duan, S.: Study on the thermal expansion performance of gypsum in the application of precision casting. In: *IOP Conference Series: Earth and Environmental Science*, vol. 330 (2019)
6. Livshits, V.B.: *Material processing technology*. Textbook. Benefit. Yurayt Publishing House, Moscow (2018)
7. Cantas, C., Baksan, B.: Effects of composition on the physical properties of water-soluble salt cores. *Int. Metalcast.* (2020)
8. Major-Gabrys, K.: Environmentally friendly foundry molding and core sands. *J. Mater. Eng. Perform.* **28**(7), 3905–3991 (2019)
9. Lyuty, R.V., Houri, I.M.: *Molding materials*. KPI named after I. Sikorsky, Kyiv (2020)
10. Lysenko, T.V. Yasyukov, V.V., Prokopovich, I.V.: *Casting shaping control concept*. Ecology, Odessa (2019)
11. Baganayi, F.C., Nyembwe, D.K., Polzin, H.: Optimisation of an environmentally friendly foundry inorganic binder core making process for the replacement of an organic binder. *MRS Adv.* **5**(25), 1323–1330 (2020). <https://doi.org/10.1557/adv.2020.225>
12. Schneider, M., Hofmann, T., Andrä, H., Lechner, P., Etmeyer, F., Volk, W., Steeb, H.: Modelling the microstructure and computing effective elastic properties of sand core materials. *Int. J. Solids Struct.* **143**, 1–17 (2018)
13. Liu, F., Tu, S., Gong, X., Li, G., Jiang, W., Liu, X., Fan, Z.: Comparative study on performance and microstructure of composite water-soluble salt core material for manufacturing hollow zinc alloy castings. *Mater. Chem. Phys.* **252**, 123257 (2020)
14. Huang, P.-H., Chien, S.-Y., Wu, P., Chou, C.-S.: Optimal design of high-strength water-soluble sand core for investment casting system. Thermodynamic analysis and experimental verification. *Mater. Des.* **189**, 108507 (2020)
15. Francis, V., Jaina, P.: Experimental investigations on fused deposition modelling of polymer-layered silicate nanocomposite. *J. Virtual Phys. Prototyping* **11**, 109–121 (2016)



The Use of Ion Bombardment Modeling as a Component of the Structural Engineering of Nanoperiodic Composite Structures

Oleg Sobol , Nataliia Pinchuk^(✉) , Andriy Meilekhov , and Mariia Zhadko 

National Technical University “Kharkiv Polytechnic Institute”,
2, Kyrpychova Street, Kharkiv 61002, Ukraine

Abstract. The influence of bias potential on the phase-structural state and hardness of nanolayer multi-period vacuum-arc coatings has been studied using modeling radiation damage during ion bombardment, phase-structural studies, and measurement of microhardness. A significant expansion of the defect formation area was revealed when using layers of multi-element (high-entropy) alloys. For the composition (TiZrAlVNbCr), the depth of defect formation reaches 30% of the total layer thickness (around 14 nm). It was found that for monometallic layers of the TiN/MoN system, the use of a constant potential of -230 V leads to the formation of the phase composition of TiN and γ -Mo₂N. The hardness of such a coating is 44 GPa. The use of a high-voltage potential (-1000 V) in a pulsed form allows the formation of TiN and an equilibrium MoN phase, reduces the micro deformation of crystallites, and increases the hardness to 47 GPa. The introduction of layers of high-entropy (TiZrAlVNbCr) alloy nitride into the nanocomposite instead of TiN layers, and thus obtaining a composite (TiZrAlVNbCr)N/MoN, even in a high-voltage pulse mode, leads to stabilization of the nonequilibrium (γ -Mo₂N) phase in molybdenum nitride layers. However, the feature of high-entropy alloys associated with low diffusion mobility and high distortion of the crystal lattice makes it possible to achieve the highest hardness of 54 GPa in such a nanocomposite.

Keywords: Computer simulation · Radiation damage · Nanoscale layers · High-entropy alloy · Crystallite size · Microdeformation · Hardness

1 Introduction

Multilayer coatings are characterized by uniquely high mechanical properties associated with a relatively high content of interfaces between layers, which is most pronounced for nanoperiodic structures [1–3]. Such boundaries prevent crack propagation in the coatings, changing the mechanism of destruction, thereby increasing the service life of the coatings [4, 5]. The multilayer coating construction allows combining high wear resistance, corrosion resistance, etc. Further development of this direction is the modification of the layer structure based on engineering approaches. One of the most promising approaches to structural engineering is the use of multi-element compositions in such

nanolayers, the formation of special structural states in them (for example, the creation of MAX phases (Ti_2AlC , Cr_2AlC) [6]). The use of the multi-element approach has led in recent years to create a new type of material – high-entropy alloys.

2 Literature Review

The concept of high-entropy alloys was first reported in 2004 by Yeh [7]. High-entropy alloy (HEA) consists of at least five basic elements with an atomic content of 5 at.% to 35 at.%, which form disordered solid solutions with a simple fcc/bcc crystal lattice structure instead of usually complex intermetallic compounds. Face-centered cubic (fcc) or body-centered cubic (bcc) lattices [8] are more easily formed in high-entropy alloys (HEA) due to the effect of high entropy of mixing compared to complex intermetallic compounds. Consequently, HEA has demonstrated excellent properties such as high resistance to high-temperature oxidation [9], high wear resistance [10], radiation [11], and corrosion resistance [12]. However, in the formation of nitride coatings, the classical concepts of optimizing elemental compositions and their effect on properties were not applicable. This applies to the greatest extent to vacuum-arc coatings for which high-energy deposition of all precipitating elements is provided [13].

In this regard, the question of the influence of each element in a multi-element nitride coating during the formation of a nitride layer during its deposition from strongly ionized flows remains relevant. This refers to how, when bombarded the surface, they affect the defectiveness of the structure because ions have different masses, as a result of which they can penetrate to different depths, creating a different distribution of defects. This determines the importance of introducing the stage of modeling ion bombardment by ions of different masses in structural engineering to achieve the required properties.

This research aimed to study the effect of the bias potential on the model distribution of defects in layers of mono- and multi-element nitrides of vacuum-arc nanoperiodic coatings, their phase-structural state, and hardness.

3 Research Methodology

Multilayer composites were obtained by the vacuum-arc method on a modernized Bulat-6 installation. The pressure of the working (nitrogen) atmosphere during the deposition of nitride layers was $p_N = 0.6$ Pa. Deposition was carried out from two sources of Mo, Ti, and (TiZrAlVNbCr) with the continuous rotation of samples fixed on the substrates at a speed of 8 rpm, the total deposition time of the coating was about 1 h. In contrast, the total thickness of the coating was 9 μm , and the thickness of the layers in the period was ~14–15 nm. A constant negative potential of the value $U_s = -200\dots230$ V was applied to the substrates in the deposition process, and a pulse potential $U_i = -1000$ V (pulse frequency $\tau = 7$ μs).

The modeling of processes during bombardment with accelerated ions was carried out using the STRIM software package [14].

The phase-structural analysis was carried out by X-ray diffractometry according to the θ - 2θ scheme (in reflection [15]) in Cu-k_α radiation on a DRON-4 setup. The division of the profiles into their components was carried out using the “NewProfile” software

package. Substructural characteristics were determined by the approximation method, and the macrostressed-strain state was studied using the X-ray tensiometry method (“ $a - \sin^2\psi$ ” method) [16–18].

Nanoindentation was carried out using a Mikron-Gamma micro indenter [19] with a Berkovich pyramid under loading within 20 G with automatic loading and unloading for 30 s.

4 Results

4.1 Modeling of Processes and Structural-Phase State of Nanocomposites of the TiN/MoN System

The TiN/MoN composite system was used as a model object when analyzing the effect of ion bombardment. The following systems, “Ti-MoN” and “Mo-TiN”, were used. The results are presented in Tables 1 and 2.

Table 1. Depth of ion penetration into the nitride coating and the number of vacancies that are formed during the deposition with the number of iterations 100.

U, V	Depth of ion penetration		Number of vacancies per 1 ion	
	h_{\max} , Å	h_{avg} , Å	c_{\max}	c_{avg}
Ti-MoN				
230	17	8.5	0.54	0.27
1000	32	16	1.1	0.55
Mo-TiN				
230	18	9	0.53	0.265
1000	31	15.5	1.1	0.55

A typical form of the distribution of ions for the number of iterations of 100 and 10,000 is shown in Fig. 1.

Analysis of the data presented in Tables 1 and 2 showed that the penetration depth of Ti and Mo ions in the studied systems has a close average value of 8.5–9 Å at $U = 230$ V and 15.5–16 Å at $U = 1000$ V with a small number of iterations 100. This number of iterations was used in work as an analog-comparison with a pulse action with a duration of 7 μs . With a large number of iterations (10,000), which can be compared with continuous exposure, the average depth increased to 12 Å (at $U = 230$ V) and 21 Å (at $U = 1000$ V). The number of vacancies has also increased proportionally. In this case, the ion/vacancy ratio remained close to 0.6.

The next stage of the study was to investigate the structural and phase states of multilayer TiN/MoN coatings. The results of X-ray diffraction studies are shown in Fig. 2. It can be seen that the formation of a polycrystalline state with separate layers of TiN (PDF card JCPDS 38-1420) and MoN (PDF card 25-1367) with a reduced period due to the lower nitrogen content occurs.

Table 2. Depth of ion penetration into the nitride coating and the number of vacancies that are formed during the deposition process with the number of iterations 10,000.

U, V	Depth of ion penetration		Number of vacancies per 1 ion	
	$h_{max}, \text{Å}$	$h_{avg}, \text{Å}$	c_{max}	c_{avg}
Ti-MoN				
230	24	12	0.55	0.275
1000	43	21.5	1.16	0.58
Mo-TiN				
230	22	11	0.7	0.35
1000	42	21	1.25	0.625

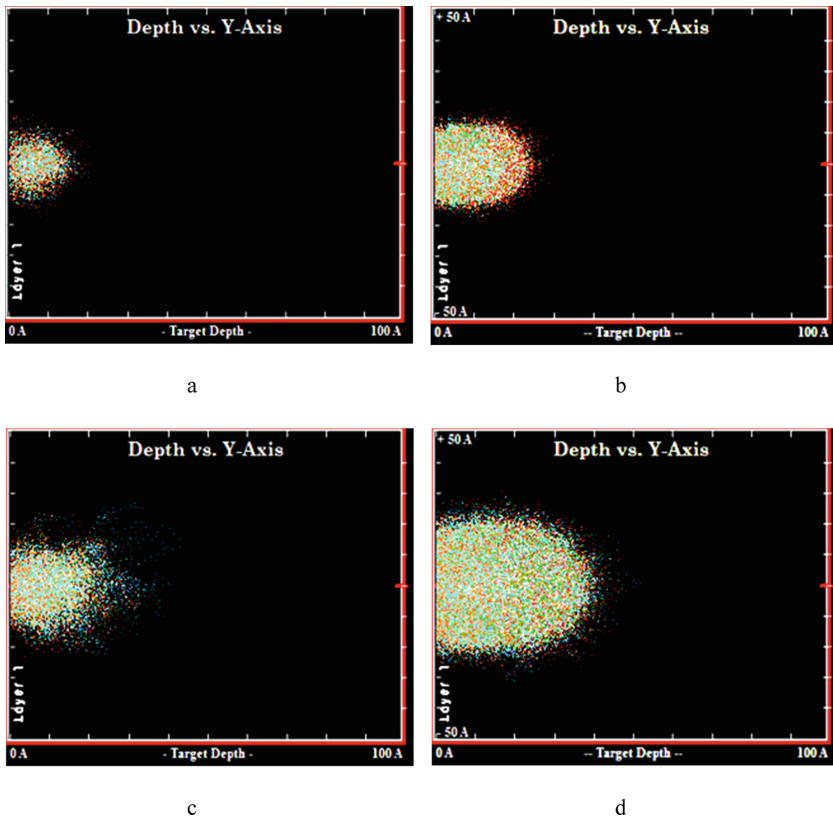
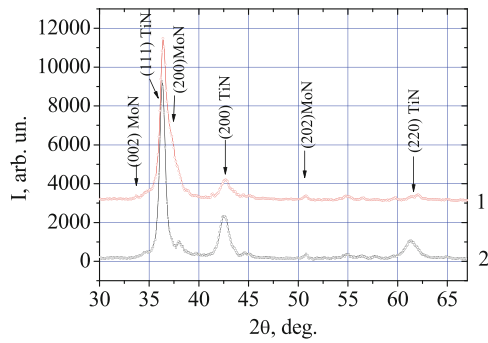
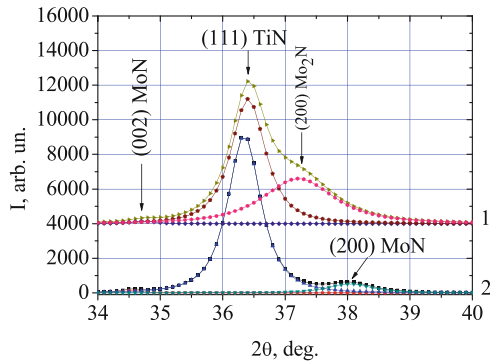


Fig. 1. Distribution of ions during the bombardment of the MoN coating with Ti ions: a – number of iterations 100, U = 230 V, b – number of iterations 10,000, U = 230 V, c – number of iterations 100, U = 1000 V, d – number of iterations 10,000, U = 1000 V.



a



b

Fig. 2. Sections of the diffraction spectra of coatings of the TiN/MoN system obtained at $p_N = 0.6$ Pa, $U_s = -230$ V: 1 – $U_i = 0$ V; 2 – $U_i = -1000$ V: a – the initial form of the diffraction spectra, b – the selected area with the decomposition of the diffraction profile into components $2\theta = 34\text{--}40^\circ$.

Thus, the impulse action allows the formation of a more equilibrium MoN phase.

After determining the substructural characteristics, it was established that in the coatings obtained without additional pulse exposure, the crystallite size (L) is 14 nm in the TiN layers and 7 nm in the MoN layers, the application of the pulse potential leads to an insignificant increase in L to 15 nm and 11 nm in the TiN layers and MoN, respectively. Microdeformation ($\langle \varepsilon \rangle$) was 0.8% in coatings obtained without impulse exposure and 0.47% with high-voltage exposure. Such a decrease in $\langle \varepsilon \rangle$ can be associated with relaxation processes occurring under high-voltage, high-energy impact at which displacement cascades are formed.

Indentation was used as a basic method for studying mechanical properties. The obtained microhardness values showed that using a pulsed high-voltage potential makes it possible to increase the hardness from 44 GPa to 47 GPa slightly. Such coatings are super hard. The transition to the superhard state is also facilitated by a high level

of compressive macro deformation, which reaches values of -2.7% and -2.35% , respectively.

4.2 Modeling of Implantation Processes, Structure, and Properties of MoN/(TiZrAlVNbCr)N Composites

To understand the processes occurring during the deposition of multi-element coatings, modeling was carried out using the SRIM program. The features of the impact of each element were tested on the following systems: “Ti-TiZrAlVNbCr”, “Zr-TiZrAlVNbCr”, “Al-TiZrAlVNbCr”, “V-TiZrAlVNbCr”, “Nb-TiZrAlVNbCr”, “Cr-TiZrAlVNbCr”, “Ti- MoN”, “Zr – MoN”, “Al – MoN”, “V – MoN”, “Nb-MoN”, “Cr – MoN”. The results of the modeling are presented in Tables 3 and 4.

Table 3. Depth of ion penetration into the multi-element coating and nitride coating MoN, as well as the number of vacancies that are initiated during the deposition process, $U = 200$ V at 100 and 10,000 iterations.

Layer	Depth of ion penetration		Number of vacancies per 1 ion	
	$h_{avg}^{100}, \text{Å}$	$h_{avg}^{10\,000}, \text{Å}$	c_{avg}^{100}	$c_{avg}^{10\,000}$
Ti ions				
MoN	8	10.5	0.275	0.28
TiZrAlVNbCr	9.75	13.5	0.225	0.2
Zr ions				
MoN	8.5	11	0.29	0.28
TiZrAlVNbCr	10.25	12.5	0.26	0.25
Al ions				
MoN	8	11.5	0.17	0.175
TiZrAlVNbCr	10	14.5	0.16	0.175
V ions				
MoN	7.5	10.5	0.25	0.255
TiZrAlVNbCr	8.5	12	0.21	0.2
Nb ions				
MoN	9	11	0.29	0.29
TiZrAlVNbCr	9.75	13	0.25	0.225
Cr ions				
MoN	8	10.5	0.3	0.225
TiZrAlVNbCr	10.25	12.5	0.265	0.19

From the data given in Tables 3 and 4, it can be seen that for a multi-element system, the tendency persists: the heavier the ion, the deeper it penetrates the coating and creates more defects. At the same time, as can be seen from the results obtained, even with the largest number of iterations (10,000), which can be compared with a continuous mode of exposure, the average penetration depth of ions does not exceed 1.5 nm (at $U = 200$ V) and 4.3 nm ($U = 1000$ V). Thus, the thickness of the radiation effect layer is about

5 nm on each side of the interlayer boundary. This exceeds the analogous effect for the TiN/MoN model system (for which $h_{\text{avg}} \sim 2.1$ nm) and can change the phase-structural state in the formed layers.

Table 4. Depth of ion penetration into the multi-element coating and nitride coating MoN and the number of vacancies that are initiated during the deposition process, $U = 1000$ V at 100 and 10,000 iterations.

Layer	Depth of ion penetration		Number of vacancies per 1 ion	
	$h_{\text{avg}}^{100}, \text{Å}$	$h_{\text{avg}}^{10\,000}, \text{Å}$	$c_{\text{avg}100}$	$c_{\text{avg}10\,000}$
Ti ions				
MoN	15	24.5	0.55	0.6
TiZrAlVNbCr	22.5	36	0.45	0.425
Zr ions				
MoN	13	20.5	0.7	0.7
TiZrAlVNbCr	18.5	29	0.55	0.55
Al ions				
MoN	18	30	0.375	0.4
TiZrAlVNbCr	26	42.5	0.35	0.36
V ions				
MoN	14	25	0.65	0.6
TiZrAlVNbCr	20.5	30	0.55	0.425
Nb ions				
MoN	14.5	22	0.7	0.7
TiZrAlVNbCr	17.5	33.5	0.56	52.5
Cr ions				
MoN	14	24	0.575	0.61
TiZrAlVNbCr	19.5	31	0.45	0.425

X-ray diffraction spectra for an MoN/(TiZrAlVNbCr)N multi-element coating are shown in Fig. 3. It can be seen that in this case, a three-phase state is formed from 2 phases with fcc and first phase bcc crystal lattice. In this case, the γ -Mo₂N phase forms in the molybdenum nitride layer, in contrast to the MoN phase (Fig. 1), formed in the TiN/MoN system at a shallower depth of influence of implanted ions.

Another feature of formation, in this case, is the appearance of a phase with a bcc lattice. This phase manifests itself at small angles, and its appearance, apparently, is associated with the formation on the coating surface of a characteristic “drop” phase of metal atoms. The base for this is the Al and Cr atoms, which are included in the multi-element composition and stimulate the formation of the droplet phase in the vacuum-arc method.

At large diffraction angles (Fig. 3b), reflections from the bcc phase are absent, since the informative depth (for Cu K α radiation, the depth is about 5 μm , which is about 1/2 of the coating thickness) of the formation effect of the bcc phase on the coating surface increases.

Measurement of the hardness of such coatings showed that its value reaches 54 GPa, which is higher than for similar conditions in the TiN/MoN system.

Thus, the use of multi-element alloys in the formation of nanocomposite layers increases the width of the radiation damage region. This is based on the different depths of defect formation in multi-element alloys. In this regard, the formation of isostructural phases with an fcc crystal lattice is stimulated in thin layers. However, even the formation of isostructural phases makes it possible to achieve high hardness in multi-element (high-entropy) layers. This is largely determined by the low diffusion capacity characteristic of such alloys due to the distortion of the crystal lattice.

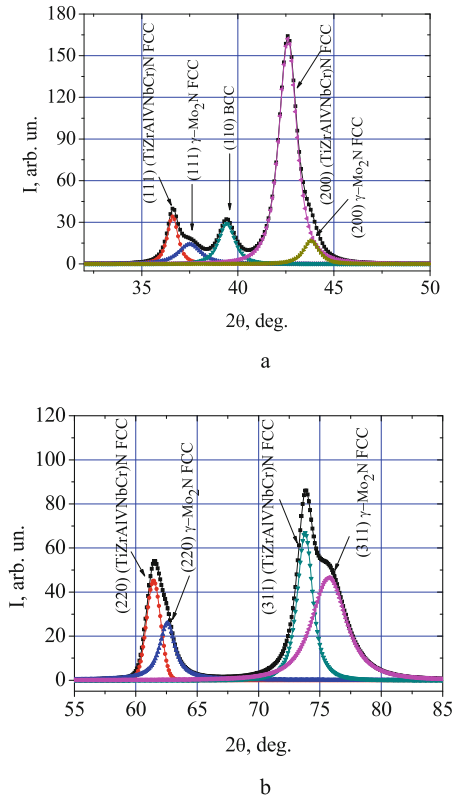


Fig. 3. Sections of diffraction spectra of coatings of the MoN/(TiZrAlVNbCr)N system after separation in the New Profile program, obtained at $p_N = 0.6$ Pa, $U_s = -200$ V, $U_i = -900$ V, $\tau = 7$ μ s, angular range 2θ : a – $(32-50)^\circ$, b – $(55-85)^\circ$.

5 Conclusions

Modeling of the ion bombardment process for two characteristic modes of displacement potentials -230 V (in constant mode) and high-voltage -1000 V (in pulsed form) was

carried out. It was found that for monometallic nitride layers of TiN and MoN, the average implantation depth is 1.1–1.2 nm, and the number of vacancies per ion is 0.28–0.35. A high-voltage bias in a pulsed form makes it possible to increase the average depth to 1.6 nm and the number of vacancies per ion to 0.55.

The use of comparative modeling of ion bombardment of (TiZrAlVNbCr) alloy elements made it possible to reveal a significant expansion of the depth of defect formation in such layers. For nanoperiodic vacuum-arc coatings with a layer thickness of 14–15 nm, the defect formation depth reaches 30% of the layer thickness. At the phase-structural level, this leads to the formation of isostructural phases in different layers of the periodic structure. These are the (TiZrAlVNbCr)N and α -Mo₂N phases with an fcc crystal lattice for the systems under study.

For nanoperiodic composites with a monometallic state of nitride layers, the use of a high-energy impact in a pulsed form allows the formation of more equilibrium structures with a different type of crystal lattice, such as MoN with a rhombic lattice.

At the substructural level, the high-voltage impact of bombarding ions (in a pulsed form) can significantly reduce the micro deformation of crystallites and increase their average size.

It was revealed that in nitrides based on multi-element (high entropy) alloys (which have low diffusion mobility and high lattice distortion due to the difference in atomic radii), it is possible to achieve an increase in hardness up to 54 GPa.

Since the trend of modern materials science is associated with a decrease in the thickness of layers to several nm (to increase the functional properties), the limitations of this study do not take into account the influence of the interface between nanolayers. Further research is planned in this direction.

Acknowledgment. This work was financially supported by the National Research Foundation of Ukraine (grant № 205 / 02.2020).

References

1. Chen, S.-F., et al.: The effect of Cr/Zr chemical composition ratios on the mechanical properties of CrN/ZrN multilayered coatings deposited by cathodic arc deposition system. *Surf. Coat. Technol.* **231**, 247–252 (2013)
2. Sobol', O.V., Meilekhov, A.A.: Conditions of attaining a superhard state at a critical thickness of nanolayers in multiperiodic vacuum-arc plasma deposited nitride coatings. *Tech. Phys. Lett.* **44**(1), 63–66 (2018)
3. Tokarev, O.A., Demchyshyn, A.V., Avtonomov, G.A.: The structure and mechanical properties of multilayer nanocrystalline TiN/ZrN coatings obtained by vacuum-arc deposition. *Process. Appl. Ceram.* **1**, 43–47 (2007)
4. Vereschaka, A., et al.: Investigation of the influence of the thickness of nanolayers in wear-resistant layers of Ti-TiN-(Ti, Cr, Al)N coating on destruction in the cutting and wear of carbide cutting tools. *Surf. Coat. Technol.* **385**(15), 125402 (2020)
5. Bayón, R., et al.: Corrosion-wear behaviour of PVD Cr/CrN multilayer coatings for gear applications. *Tribol. Int.* **42**(4), 591–599 (2009)
6. Maier, B.R., Garcia-Diaz, B.L., Hauch, B., Olson, L.C., Sindelar, R.L., Sridharan, K.: Cold spray deposition of Ti₂AlC coatings for improved nuclear fuel cladding. *J. Nucl. Mater.* **466**, 1–6 (2015)

7. Yeh, J.W., et al.: Nanostructured high-entropy alloys with multiple principal elements: novel alloy design concepts and outcomes. *Adv. Eng. Mater.* **6**(5), 299–303 (2004)
8. Zhang, Y., et al.: Microstructures and properties of high-entropy alloys. *Prog. Mater. Sci.* **61**, 1–93 (2014)
9. Tsai, K.Y., Tsai, M.H., Yeh, J.W.: Sluggish diffusion in Co-Cr-Fe-Mn-Ni high-entropy alloys. *Acta Mater.* **61**, 4887–4897 (2013)
10. Chuang, M.H., Tsai, M.H., Wang, W.R., Lin, S.J., Yeh, J.W.: Microstructure and wear behavior of Al_xCo_{1.5}CrFeNi_{1.5}Ti_y high-entropy alloys. *Acta Mater.* **59**, 6308–6317 (2011)
11. Lu, C.Y., et al.: Enhancing radiation tolerance by controlling defect mobility and migration pathways in multicomponent single-phase alloys. *Nat. Commun.* **7**, 13564–13572 (2016)
12. Liu, Y.X., Cheng, C.Q., Shang, J.L., Wang, R., Li, P., Zhao, J.: Oxidation behavior of high-entropy alloys Al_xCoCrFeNi (x = 0.15, 0.4) in supercritical water and comparison with HR3C steel. *Trans. Nonferrous Metals Soc. China* **25**, 1341–1351 (2015)
13. Jager, N., et al.: Evolution of structure and residual stress of a fcc/hex-AlCrN multi-layered system upon thermal loading revealed by cross-sectional X-ray nanodiffraction. *Acta Mater.* **162**, 55–66 (2019)
14. Ziegler, J.F., Ziegler, M.D., Biersack, J.P.: SRIM – the stopping and range of ions in matter. *Nucl. Instr. Meth. Phys. Res. B* **268**, 1818–1823 (2010)
15. Sobol', O.V., Shovkoplyas, O.A.: On advantages of X-ray schemes with orthogonal diffraction vectors for studying the structural state of ion-plasma coatings. *Tech. Phys. Lett.* **39**(6), 536–539 (2013)
16. Noyan, I.C., Cohen, J.B.: *Residual Stress Measurement by Diffraction and Interpretation*. Springer, New York (1987)
17. Genzel, C., Reinners, W.: A study of X-ray residual-stress gradient analysis in thin-layers with strong filer texture. *Phys. Stat. Solidi: A-Appl. Res.* **166**(2), 751–762 (1998)
18. Gargaud, P., Labat, S., Thomas, O.: Limits of validity of the crystallite group method in stress determination of thin film structures. *Thin Solid Films* **319**, 9–15 (1998)
19. Aznakayev, E.: Micron-gamma for estimation the physico-mechanical properties of micro-materials. In: *Proceedings of the International Conference “Small Talk – 2003”*, San Diego, California, USA, pp. 8–10 (2003)



Powder Technology and Software Tools for Microstructure Control of AlCu₂ Samples

Oleg Zabolotnyi¹ , Viktoriya Pasternak¹ , Nataliia Ilchuk¹ ,
Nataliia Huliieva¹ , and Dagmar Cagaňová² 

¹ Lutsk National Technical University, 75, Lvivska Street, Lutsk 43018, Ukraine

² Faculty of Materials Science and Technology, Slovak University of Technology, Bratislava,
25, Bottova Street, 917 24 Trnava, Slovak Republic

Abstract. The powder technology of structurally inhomogeneous materials of AlCu₂ sample formation is developed. The algorithm for image recognition of separate particles' microstructure of structurally inhomogeneous materials is formed and implemented in the Smart-eye software, which provides tools for analysis of surface and internal properties of structurally inhomogeneous materials. The developed powder technology is applied in obtaining the samples of AlCu₂, which are further analysed by the Smart-eye software. The structural characteristics of the starting material (AlCu₂), in particular porosity, were predicted. The analysis of the average results of the study of the microstructure of AlCu₂ particles is held, which shows that the developed models allow accurate control of the microstructure and properties of structurally inhomogeneous materials obtained based on powder technologies. Improvement of granulometric composition of structurally inhomogeneous materials is proved. Based on the obtained materials developed powder technology, it is possible to predict the structural characteristics of AlCu₂ raw materials at a qualitative level. Thus, it is possible to exercise to carry out practical realization of the received results on manufacture.

Keywords: Technology · Inhomogeneous materials · Metallographic analysis · Particles' · Smart-eye

1 Introduction

Modern mechanical engineering technologies are closely related to the development of modern production. The result is creating products from powder materials, which possess desired properties, e.g., strength, weight, porosity, and filtration coefficient. One of the ways to obtain such materials with qualitative indicators is the use of standard research methods. For this purpose, it is necessary to control all parameters of the manufacturing of a powder product. However, standard methods do not always allow to obtain the desired results of sample production AlCu₂. For improving the standard methods of research of powder metallurgy and study the perfect structure of materials that meet all the technical requirements of production, it is necessary to use a modern method of metallographic analysis. This method studies the destruction of the structure of the samples and predicts

the internal properties of the source materials. Therefore, the study of the features of the internal connections of the structure of AlCu_2 materials at the stage of their manufacture is a major problem of materials science.

2 Literature Review

40% of educators study the prediction of material properties worldwide. A relatively large number of researchers are engaged in studying the essential aspects of structurally heterogeneous materials at one time; one may refer to [1]. Scientific work is phenomenological [2] and whose quality indicators do not coincide with the manufactured finished materials [3]. As described in paper [4], the composition of the powders was obtained by chemical equations. Maintaining additional elements led to different porosity. Laboratory research [5] modeling plays an important role, which allows for research without carrying out expensive and time-consuming experiments.

It should be noted that much work has been done by research teams [6]. The result is the final product with the help of laboratory equipment (magnifying glass, microscope, and millimeter ruler). That does not allow one to investigate completely inhomogeneous materials. According to [7], the authors have investigated general analysis of structurally inhomogeneous materials. Different material parameters and boundary conditions were considered. The obtained interpolation dependences were obtained using the methods of boundary elements. In the study [8], all necessary conditions for the production of an aluminum matrix are considered. The great advantage of scientific work is that the microstructure of the source powders is considered using a laser.

Today's conditions state that research in mechanical engineering technology should be conducted at a higher level [9]. For improving the quality of powder technologies [10, 11], it should consider all the necessary technical requirements of modern production [12]. In turn, it is necessary to consider in detail AlCu_2 [13] and its basic properties [14]. Starting with the filling of powders [15] and ending with implementing the results at the enterprise [16]. The above materials indicate an imperfect level of research in this area, which leads to detailed methods of studying structurally inhomogeneous materials using technology.

3 Researches Methodology

The objective of the paper is to investigate study the internal connection of AlCu_2 with each other. Calculation of individual AlCu_2 segments considering all the features of the Smart-eye program.

It should be noted that the scheme for obtaining products from powders consists of the following main processes: obtaining powders and preparing the powder charge, under pressure forming and sintering of moulded products, and a method for controlling the properties of structurally inhomogeneous materials in order to improve the accuracy of obtaining the final product. For most structurally inhomogeneous materials, the main object of industrial control and analysis of structural transformations is their geometric structure (microstructure of samples), which can be represented as a set of two and three-dimensional elements in three-dimensional space. It is worth mentioning that an essential

practical task of metallographic analysis of structurally inhomogeneous materials is the obtainment of an estimate, which fixes the structural state of the material obtained as a result of a set of technological operations with known parameters (temperature, time, charge composition, particle size and shape, porosity, density, and others). The mass of powders forms a completely homogeneous bronze AlCu₂, consisting of 83% of copper and 17% of aluminium. In this case, a cylindrical sample: Ø = 30 mm, h = 60 mm was used. The percentage of the components' mass of the mixture that must be taken to prepare a cylindrical sample is presented in Table 1.

Table 1. The percentage of the components' mass of the covered mixture that must be taken to prepare a cylindrical sample Ø = 30 mm, h = 60 mm.

Sample	Al, %	Cu, %	Carbamide, %	Calcium carbonate, %	Σ, %
Sample A	30	30	30	10	100
Sample B	40	35	25	–	100
Sample C	30	30	20	20	100

The pressing procedure was carried out using a hydraulic press PSU-125. The pressing pressure had been changed from 50 to 80 MPa. Sintering of the formed powder products (blanks) was carried out in an electric furnace VMK – 1600. Sintering temperature varied in the range between 1550–1600 °C. The heating rate was 200°/hour, and isothermal exposure landed at – 1.5 h. The procedure of microscopic analysis was carried out according to the standard technique [9, 10]. The sample' lines were examined using the MMR-4 microscope model at ×600 and ×800 magnification. The digestion process was carried out with a 4% hydrochloric acid solution. Planar porosity was determined by the micrographs of the grinds using the Smart-eye application. The porosity was equal from 20% to 30%. The Smart-eye software allows for the determination of the necessary characteristics needed for qualitative and quantitative assessment of the structure of any material, including porous ones. The algorithm is as follows: let $b_{i,j}$ is the original image, the value of $b_{i,j}$ is equal to the brightness at the point $i, j \in D$, where: $i = 1, 2, \dots, n; j = 1, 2, 3, \dots, m$. The image $b_{i,j}$ of the real conditions, as well as the set of images of individual objects, will be equal to:

$$b_{i,j} = H_1(i, j) + H_2(i, j) + \dots + H_s(i, j) \tag{1}$$

where S is a number of real objects; $H_k(i, j)$ are images of the k -th object, $k = 1, 2, 3, \dots, s$.

The problem of image recognition, in this case, consists of finding all objects $H_k(i, j)$, which are determined from the criteria of homogeneity of the region by the formula:

$$\frac{\max_{P \in R} |f(P) - m|}{P} \times T, \tag{2}$$

where T is an initial value; P is the value in the field R ; m is an average value of pixels in the area P ; $f(P)$ is a function of the brightness distribution.

4 Results

4.1 Formation of Structurally Inhomogeneous Materials

The process of forming structurally inhomogeneous powder materials is as follows. In the first stage, the particles of raw materials move in the direction of the seal pressure. Large holes «pores» are filled. The deformation process does not occur. However, a high density of backfill is formed. In the second stage, the extrusion process takes place. That is, the free movement of materials stops, and as a result, deformation occurs. The sequence of the deformation process is as follows: soft deformation-elastic deformation-plastic deformation. The phenomenon of relationships between $AlCu_2$ contacts is observed. Thus, the granulometric composition of the powder is changing – the number of grains increases by crushing, and smaller particles arise by breaking down the grains under high pressure in the areas of contact. Compressed samples are represented in (Fig. 1).

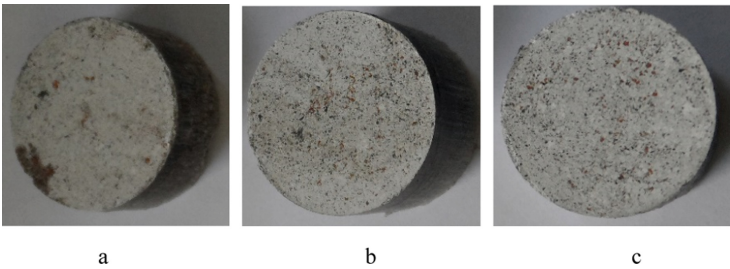


Fig. 1. Compressed samples $AlCu_2$: a – sample A; b – sample B; c – sample C.

Sintering of carved cylindrical products was carried out using an electric furnace. It should be noted that this oven has its special characteristics. This fully satisfies the technical requirements. A general overview of the sintered samples is shown in (Fig. 2).

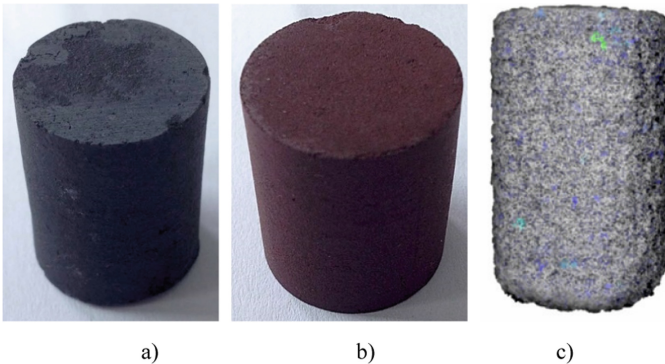


Fig. 2. General overview of the sintered samples $AlCu_2$: a – sample A; b – sample B; c – sample C.

The essential features of powder materials are the hardness and strength of the material [17, 18], which directly depends on the density of their crystal lattices in the volume of the controlled object (sample). The main foundation for this is the samples' chemical composition, oxidation state, particle size, concentration, and duration of exposure. The peculiarity of these studies is that the authors analyzed each particle of powders. The obtained results allowed us to confirm the high accuracy of calculations and to make the maximum description of the made samples. In this case, the «grains» were presented in photomicrographs as cut sections separated from each other by thick lines «boundaries». Also, «grains» can function with many areas of materials. The measurement was performed based on the total number of grains, which was carried out in millimeters. This method of monitoring the study of structurally inhomogeneous materials displays significant advantages: high sensitivity to the most dangerous defects, such as cracks and inclusions, the ability to control the density of powders, high productivity, and the ability to conduct control directly at the workplace without disrupting the process, as well as low-cost control and automation.

The Main Properties of Powders Based on the Analysis by the Smart-Eye Software Often, the practical implementation of the metallographic analysis of microimages (light, lumen, raster microscopy) considers the operations mentioned in the following paragraph. After loading the image of the object for study, pre-processed brightness and contrast adjustments were made. Then, it is necessary to carry out digital filtering. The next step is to transport the image of the micro-sections in their binary form and conduct segmentation. For interactive correction, computer visualization of the image was performed. Besides, at the final stage, the authors performed a statistical probability analysis of the distribution of particles and pores of powder materials. For detecting the image of homogeneous brightness areas in their characteristics, segmentation was performed, where different segments were likely to correspond to different structural elements. Preliminary analysis of the microstructure was performed on microsections of molding materials, which are presented in Fig. 3. The simplest and most common approach to solve the problem of image recognition is the so-called «limit discrimination method». In this case, the brightness matrix G turns into a binary matrix B , in which the non-zero elements correspond to the values of the original matrix and is biggest than the fixed threshold value $g_{\text{threshold}}$. Let us present the method of limiting discrimination as follows:

$$G = \begin{pmatrix} g_{11} & \dots & g_{1N} \\ \vdots & \ddots & \vdots \\ g_{M1} & \dots & g_{MN} \end{pmatrix} \rightarrow B = \begin{pmatrix} b_{11} & \dots & b_{1N} \\ \vdots & \ddots & \vdots \\ b_{1M} & \dots & b_{MN} \end{pmatrix} \quad (3)$$

where:

$$b_{ij} = \begin{cases} 1, & b_{ij} > g_{\text{threshold}} \\ 0, & b_{ij} \leq g_{\text{threshold}} \end{cases} \quad (4)$$

M and N – the dimensions of the micrometre matrix (computer units of length) image recognition, $g_{\text{threshold}}$ – is the threshold constant.

Figure 3, the authors presented a screenshot of the microstructure of the samples using the image recognition method.

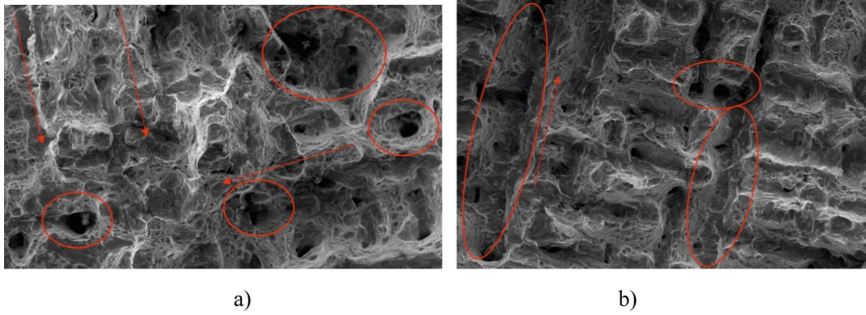


Fig. 3. Screenshot of the microstructure with magnification $\times 600$ where: a) before etching, b) after etching

From the study results, it was found that the upper layer of microsections was obtained with heterogeneous indicators. Furthermore, the interaction of functional bonds depends on the etching of $AlCu_2$ materials (Fig. 3, b). The etching process, the surface of the materials, and their relief increased due to the grinding and polishing of cylindrical products. At the same time, there was observed an increase in pores. The above studies made it possible to record the porosity of structurally inhomogeneous materials.

It should be noted that all digestive processes were carried out under the same conditions in order to provide certain deviations that may have occurred during the study. It is also important to note that the experiments help determining the basic physical and mechanical properties of the original composition of the materials and obtained materials. Figure 4 shows the fluctuations of the curves of the $AlCu_2$ experiments. The morphological analysis of the samples shows the variation of the components that function with each other.

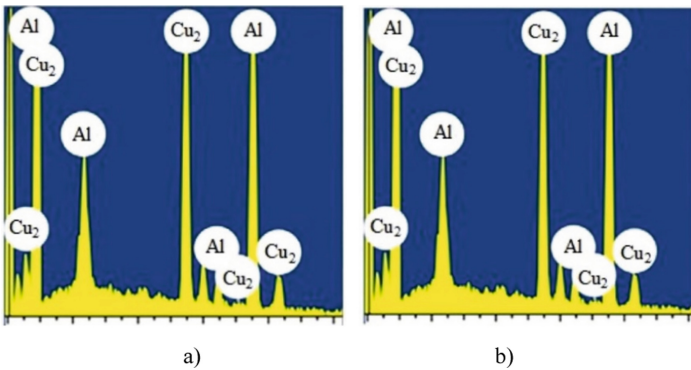


Fig. 4. The surface relief SNM with increasing $\times 600$ where: a) before etching, b) after etching.

The experiments show that the microstructure of the digestion samples in some areas differed. A larger digestive area (dark color) and a smaller digestive area (light color) were recorded. As a result, a microrelief was formed on the surface of the samples.

Table 2 presents the results of experiments performed in the Smart-eye software (Fig. 3 and 4). In turn, the total area of the particles is 41 178.48 mkm^2 , calibration coefficient 0.83 $\text{mm} \times \text{pixel}$, porosity 21.48%.

Table 2. Average experimental results of formation research AlCu₂.

Particle	X	Y	Width	Height	R _{min}	Convexity	Perimeter	Area	Quantity
1	0.9	0.74	0.83	34.17	4.450	0.50	60.00	9.7	0.67
2	1.67	0.75	30.83	47.50	9.32	0.80	55.04	10.13	0.83
3	5.83	0.76	11.67	18.33	1.86	0.61	55.82	10.51	0.61
4	8.33	0.78	9.17	7.50	0.83	0.39	27.74	19.44	0.46
5	30	0.79	7.50	7.50	2.36	0.75	27.71	31.60	0.74
6	6.67	0.80	8.33	11.67	1.18	0.63	37.69	62.15	0.79
7	4.17	0.80	61.67	34.17	0.83	0.38	50.83	68.40	0.40
8	9.17	0.83	5.00	15.00	0.83	0.56	37.34	43.75	0.57
9	4.17	0.83	15.00	12.50	0.90	0.61	50.33	39.79	0.86
10	7.50	0.83	10.83	7.50	0.83	0.62	33.76	48.26	0.77
11	8.83	0.83	15.00	11.67	3.44	0.74	49.87	22.92	0.89
12	10.6	0.83	11.67	11.67	2.36	0.73	42.93	46.04	0.75
13	8.33	0.83	5.83	3.33	1.80	0.73	37.24	11.81	0.72
14	9.17	0.72	22.50	24.17	4.17	0.65	92.55	11.11	0.87
15	9.84	2.50	18.33	25.83	1.18	0.63	78.50	78.47	0.82
16	9.17	0.83	5.83	6.67	0.83	0.63	20.15	17.01	0.76
17	5.0	2.50	7.50	19.17	0.83	0.40	49.70	72.22	0.53
18	6.67	4.17	3.33	7.50	0.90	0.45	18.90	10.07	0.51
19	5.83	5.00	14.17	10.00	0.90	0.53	43.92	85.07	0.80
20	9.17	7.50	5.83	7.50	1.18	0.63	23.12	20.49	0.69
21	9.67	8.33	5.00	5.83	0.20	0.59	16.71	7.29	0.47
22	5.0	10.8	1.67	8.33	0.19	0.65	18.65	5.21	0.27
23	7.50	10.5	7.50	7.50	0.90	0.61	26.40	34.38	0.89
24	9.17	13.3	5.00	11.67	0.83	0.52	28.75	19.10	0.42
25	3.3	13.8	9.17	13.33	2.36	0.70	39.36	66.67	0.78

Therefore, studies show that the behavior of particles of powder materials plays an important role, which from any point of view depends on the peculiarities of the formation of its microstructure. Based on the functional and internal relationships between the components of the studied materials and their physical and mechanical properties, it can be got a simple quality control method of the final product.

5 Conclusions

The paper develops a solid approach to design, obtainment, and control of structurally inhomogeneous materials based on powder technology. In particular, the developed models for image recognition and investigation of microstructures, both structural and inhomogeneous powder materials, allow to investigate and predict physical and mechanical properties of materials:

- linear dimensions, cross-sectional area, and perimeter of the intersection of structural components and phases;
- radius and volume of powder particles;
- distribution of particles structurally inhomogeneous materials in different forms and size, as well as the evaluation of angles of orientation;
- perimeters and cross-sectional area of ready products and the analysis of defects in the manufacture of structurally inhomogeneous materials.

References

1. Long, Z., Heng-wei, Z.: Sintering driving force of Al_2O_3 powders at the initial stage of pulse electric current sintering under thermoelastic diffusion. *Int. J. Mech. Mater. Eng.* **13**(1), 2–8 (2018)
2. Apurba Kanti, D., Chatterjee, P.: Study of deformation microstructure of nickel samples at very short milling times: effects of addition of $\alpha\text{-Al}_2\text{O}_3$ particles. *J. Theor. Appl. Phys.* **13**, 63–73 (2019)
3. Guo, F., Weihui, J., Jianmin, L.: A novel green nonaqueous sol-gel process for preparation of partially stabilized zirconia nanopowder. *Process. Appl. Ceram.* **11**(3), 220–224 (2017)
4. Li, W., Xu, F., Li, Y., Hu, X., Bo, D., Yu, X.: Discussion on microwave-matter interaction mechanisms by in situ observation of “core-shell” microstructure during microwave sintering. *Materials* **9**(3), 2–12 (2016)
5. Zabolotnyi, O., Pasternak, V., Andrushchak, I., Ilchuk, N., Svirzhevskiy, K.: Numerical simulation of the microstructure of structural-inhomogeneous materials. In: Ivanov, V., Trojanowska, J., Pavlenko, I., Zajac, J., Peraković, D. (eds.) *DSMIE 2020. LNME*, pp. 562–571. Springer, Cham (2020). https://doi.org/10.1007/978-3-030-50794-7_55
6. Yu, X., Xu, F., Dong, B., Li, W., Hu, X.: Discussion on the local magnetic force between reversely magnetized micro metal particles in the microwave sintering process. *Metals-Open Access Metall. J.* **7**(2), 2–11 (2017)
7. Sulym, H., Pasternak, I., Pasternak, V.: Boundary element modeling of pyroelectric solids with shell inclusions. *Mech. Mech. Eng.* **22**(3), 727–737 (2018)
8. Marchese, G., Aversa, A., Lorusso, M., Manfredi, D., Calignano, F.: Development and characterisation of aluminium matrix nanocomposites $\text{AlSi10Mg/MgAl}_2\text{O}_4$ by laser powder bed fusion. *Metals* **8**(3), 1–12 (2018)
9. Carneiro, Í., Viana, F., Vieira, M., Fernandes, J., Simões, S.: EBSD analysis of metal matrix nanocomposite microstructure produced by powder metallurgy. *Nanomaterials* **9**(6), 1–12 (2019)
10. Magnani, G., Galvagno, S., Sico, G., Portofino, S., Freda, C., Burresti, E.: Sintering and mechanical properties of $\beta\text{-SiC}$ powder obtained from waste tires. *J. Adv. Ceram.* **5**, 40–46 (2016)

11. Lytvynenko, A., et al.: Ensuring the reliability of pneumatic classification process for granular material in a rhomb-shaped apparatus. *Appl. Sci. (Switzerland)* **9**(8), 1604 (2019). <https://doi.org/10.3390/app9081604>
12. Zhang, Q., Xu, L.S., Guo, X.: Improvement of mechanical properties, microscopic structures, and antibacterial activity by Ag/ZnO nanocomposite powder for glaze-decorated ceramic. *J. Adva. Ceram.* **6**(3), 269–278 (2017). <https://doi.org/10.1007/s40145-017-0239-z>
13. Fathy, N., Ramadan, M., Hafez, K., Alghamdi, A., Halim, A.: Microstructure and induced defects of 6061 Al alloy after short times cyclic semi-solid heat treatment. *MATEC Web Conf.* **67**(5), 1–6 (2016)
14. Samar Reda, A., Hamid, A., Menam, A., Salah Elden, I., Haytham Abdelrafea, E., Hassan Abdel, S.: Laser powder cladding of Ti-6Al-4V α/β alloy. *Materials* **10**(11), 2–16 (2017)
15. Lin, Z., Tian-Shu, L., Tao-Tao, D., Tao-Tao, L., Feng, Q., Hong-Yu, Y.: Design of a new Al-Cu alloy manipulated by in-situ nanocrystals with superior high temperature tensile properties and its constitutive equation. *Mater. Des.* **181**(2), 1–12 (2019)
16. Vijay Ponraj, N., Azhagurajan, A., Vettivel, S.: Microstructure, consolidation and mechanical behaviour of Mg/n-TiC composite. *Alex. Eng. J.* **55**(2), 2077–2086 (2016)
17. Hu, W.J.: Effects of metal particles on cold spray deposition onto Ti-6Al-4V alloy via Abaqus/Explicit. *J. Eng. Sci.* **7**(2), E19–E25 (2020). [https://doi.org/10.21272/jes.2020.7\(2\).e4](https://doi.org/10.21272/jes.2020.7(2).e4)
18. Kubit, A., Faes, K., Jurczak, W., Bucior, M., Kluz, R.: Analysis of the properties of RFSSW lap joints of Alclad 7075–T6 aluminum alloy sheets under static and dynamic loads. *Technologia i Automatyżacja Montażu* **4**, 4–13 (2020)



Rational Choice of a Material for Orthopedic Insoles Based on the Mechanical Characteristics and Practical Application Purposes

Ruslan Zaloha¹ (✉) , Kostiantyn Dyadyura¹ , Viliam Zaloga¹ ,
and Michal Hatala² 

¹ Sumy State University, 2, Rymskogo-Korsakova Street, Sumy 40007, Ukraine
r.zaloha@tmvi.sumdu.edu.ua

² Technical University of Košice, 9 Letná, 042 00 Košice, Slovak Republic

Abstract. The general principles for the usage of polymer materials for the manufacturing of orthopedic products are discussed. The current choice of polymeric materials for orthopedic insoles and footwear is based on empirical evidence. In many cases, this choice is made subjectively because there is no information regarding each material's mechanical properties and their *in vitro* interaction. The insole functionality will depend on the mechanical properties of the used materials, the target functions of which are: amortization, energy absorption, stiffness, adaptation to the sole of the foot, filling of the cavities inside the shoe, and relieving pressure when walking. Accommodative insoles are suitable for patients with diabetes, early Charcot's disease, or any form of neuropathy, while functional insoles are best used for treating pronation, plantar fasciitis, and heel spur syndrome. This study aimed to provide objective criteria for selecting materials for orthopedic insoles based on their mechanical characteristics. The mechanical properties of the materials were quantified using standardized methods.

Keywords: Standardization · Foot insoles · Performance polymers · Polymer composite · Friction and wear · Additive manufacturing technology

1 Introduction

Customized orthopedic products are attracting increasing interest from the research community [1]. In order to reduce complaints about the musculoskeletal system, it is important to choose the right footwear. Orthopedic insoles have a corrective effect on the wearer [2]. They are designed to reduce and adequately distribute plantar pressure between the points of support and minimize the stress to which these points may be subjected. Orthopedic insoles can change the overall perception of comfort [3]. During walking, a new microclimate is created in shoes, temperature, and humidity, which are relatively higher than in the external environment [4].

Physical and mechanical properties such as elasticity, compressive stiffness, and friction coefficient are generally considered key requirements for evaluating and selecting suitable materials for orthopedic insoles [5]. Knowledge of materials' properties allows

for designing and manufacturing orthopedic insoles for every person's individual needs [6, 7]. It is also necessary to take into account previous experience: the presence of pain or injuries, neurophysiological and psychological problems, and the design, contour, and firmness of the insole [8, 9].

Considering the wide range of orthopedic materials and the limited selection of suitable characterization technologies, and the fact that the effectiveness of orthopedic insoles continues to be highly dependent on the repeated trial and error experience of individual orthopedists and practitioners, this study aimed to develop objective quantitative evaluation criteria for the orthopedic insoles material selection based on their mechanical characteristics and the purposes of their practical usage.

2 Literature Review

By 2021, the market for orthopedic foot insoles is projected to exceed \$ 3.6 billion. Such individual products have traditionally been made by hand or by subtractive methods, that is, by milling a sheet of material. The method for creating the insoles depends on its intended use. Recent advances in additive manufacturing (AM) technologies and the popularization of 3D printing through fused deposition modeling (FDM) have opened up new possibilities for the production of orthopedic insoles. These technologies allow for the addition of extra functions, such as the use of materials with antimicrobial properties or, at a structural level, zone control in 3D designs for increased shock absorption capacity. The most common materials for 3D printing are polymers. Most researches rely on the lowering of plantar pressure [6].

With the growing adoption of environmentally friendly manufacturing technologies, researchers focus on maximizing the effectiveness of materials used. The new standards have brought about major changes to manufacturing processes' energy efficiency, waste reduction, reuse, and recycling. Smart Manufacturing or Industry 4.0, which is well known in Europe, has been the latest technology trend globally.

Attention regarding environmental issues and sustainability has opened up another exciting research area, namely the blends of bio-based polymers and biodegradable polymers. However, the data about the purpose of the shoes and the insoles made from these materials is limited. Further qualitative research in this area is required.

To be suitable for orthopedic applications, polymeric materials that typically exhibit mechanical strength, lightness, ease of processing, versatility, and low cost, together with acceptable thermal and environmental resistance, must also have good abrasion and wear resistance. Achieving this objective is not easy since polymeric materials' viscoelasticity analyzes tribological properties and processes associated with such phenomena rather difficult. In general, orthopedic insoles fall into two broad categories: functional or accommodative [10].

Functional orthoses seek to control the talocalcaneal joint and foot biomechanics, while accommodative orthoses minimize foot function changes while providing relief and/or protection to specific areas of the foot [11]. The functionality of the insole depends on the mechanical properties of the composite materials used. Some of the target functions are cushioning, energy absorption, stiffness, adaptation to the sole of the foot, filling of the cavities inside the shoe, and relieving pressure on the selected area.

According to the research [12], accommodative insoles are suitable for patients with diabetes, early Charcot’s disease, or any form of neuropathy. Besides, they are often the best choice for patients with stiff foot structures or limited range of motion, such as those with a hollow foot, clubfoot, or post-polio syndrome [13]. Functional insoles are used to control the biomechanics of the subtalar joint and foot. They are usually made from thinner and stronger materials and include deep calcaneal cups and good longitudinal medial arches. These devices are best used for treating pronation, plantar fasciitis, and heel spur syndrome [14].

With the help of CAD, orthopedic products can be designed to achieve both functionality and accommodation simultaneously, as weight and size can be minimized. CAD allows for customizing the internal structure and changing the properties to meet specific needs [15].

3 Research Methodology

Polystyrene (PS), polyethylene (PE), polyurethane (PU), polypropylene (PP), and ethylene-vinyl acetate (EVA) were selected for comparative analysis. They are all foams. The last three of them are used the most commonly. Material samples were made using AM methods. This study examines the abrasion resistance of various materials.

In polymers, two very different wear mechanisms can occur, namely cohesive and interfacial wear processes, as schematically shown in Fig. 1.

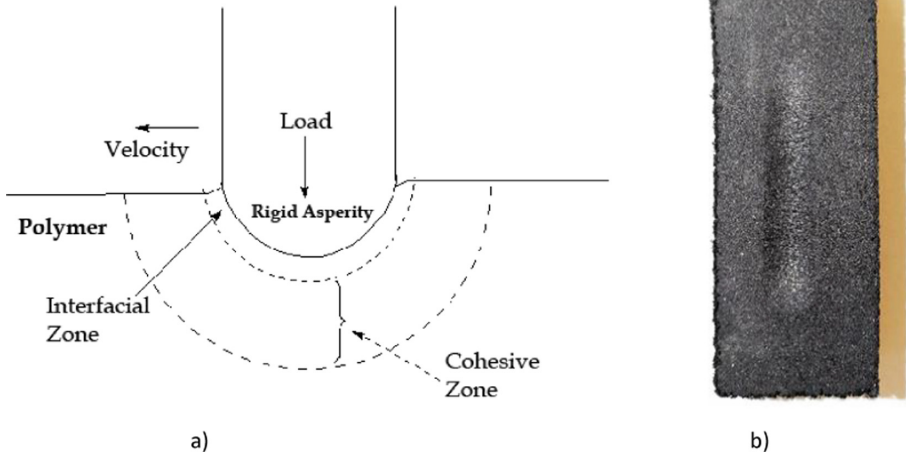


Fig. 1. Schematic image of the processes of cohesive and interfacial wear: a) Diagram of the strain; b) The sample after testing

The diagram illustrates the force acting on the sample in a tensile manner. In this case, internal stresses arise. These stresses are calculated as follows:

$$\sigma = \frac{F}{A}, \tag{1}$$

where F is the force acting over the cross-sectional area A .

The deformation is calculated as follows:

$$\varepsilon = \frac{\delta}{L_0}, \quad (2)$$

where δ is the change in the sample length, and L_0 is the initial sample length.

Depending on the material and the magnitude of the load on the sample, it will exhibit elastic or inelastic/plastic properties. Based on the results of testing materials with different stresses, it is possible to determine the proportionality of stress/strain (elastic modulus):

$$E = \frac{\sigma}{\varepsilon}. \quad (3)$$

Shear stress occurs when translational forces are created parallel to the surface area of the material.

The wear characteristics of polymeric materials depend on several factors, such as the wear mechanisms involved, the test method used, and the test pieces' volume and surface properties. A sample comparison for the mentioned materials was performed using an ASTM G133 friction tester. All samples were weighed before and after testing using a four-digit decimal scale. The difference in weight before and after the test and the coefficient of friction were evaluated. The difference in weight was analyzed to see how much material was removed from the sample. The percentage of wear loss was calculated for each specific sample in both one hour and two hours of testing.

The determination of rebound elasticity was carried out according to the method described in ISO 8307:2018 standard (Flexible cellular polymeric materials - Determination of resilience by ball rebound).

4 Results

The research results showed that several factors must be taken into account when choosing the material for the insole (Fig. 2). The material should be technologically easy to manufacture, have good durability and availability, favorable mechanical properties, subjective comfort, and be affordable. Research results (Table 1) show that the insole cavities will generate cushioning if the selected materials are not too stiff. Increasing material density and thickness will further enhance stability. Another important aspect when choosing a material is the ability to withstand permanent deformation. There are two types of structures: open cells and closed cells. The open cell structure absorbs energy due to the struts' deflection when the air is pushed out, compared to a closed-cell, where the walls flex when the air is compressed. Both procedures will deform under a certain load but return to their original shape when no load is applied unless the load becomes too high and causes ductility.

Due to the fact that its properties are on average superior to those of other materials, polypropylene was chosen as the most suitable material for the production of insoles. A more detailed list of its properties is presented in the following Table 2. Polypropylene material has high elongation at break, high tensile strength, and high abrasion resistance.

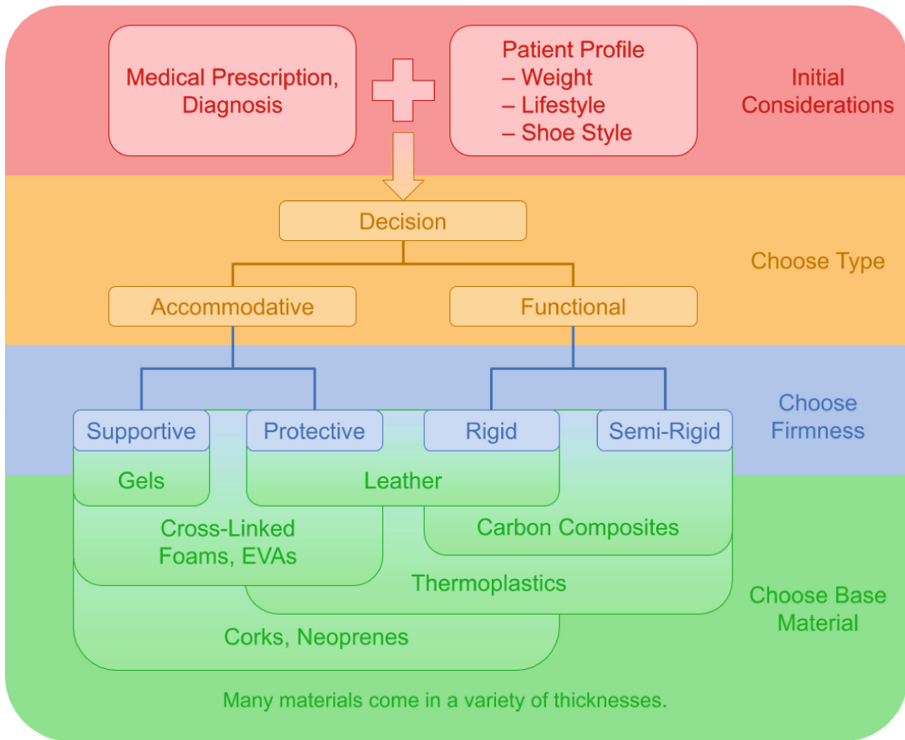


Fig. 2. Scheme of objective quantitative evaluation criteria for selecting materials for orthopedic insoles based on their mechanical characteristics and the purposes of their practical usage.

In addition, the innovative foam remains very flexible and soft over a wide temperature range. It also has good chemical resistance.

Based on this numerical work, an *in vivo* study was carried out regarding cushioning stiffness on the insole’s ability to reduce flat pressure and quantify the importance of systematic material selection. Moreover, the possibility of optimizing stiffness for a particular patient will also be investigated by examining the relationship between optimal stiffness and anthropometric parameters, which are usually measured in the clinic.

To ensure that the insoles work as expected, a survey was conducted on a sample of 60 people, of whom only six of the participants did not continue to wear insoles for various personal reasons. The study did not include participants who did not wear insoles. Preliminary sociodemographic data were assessed: (1) age, (2) gender, (3) height, (4) weight, (5) body mass index (BMI), and (6) foot size, chronic diseases with dysfunction of the motor apparatus, and the desired sensations during motor activity.

Gait analysis and balance/equilibrium control: Walking with soft safety shoes or midfoot safety shoes resulted in a significant decrease in mean trunk inclination ($p < 0.005$). Also, the mean hip flexion angle decreased for cushioned and midfoot shoes ($p < 0.002$). For soft shoes, the range of motion of the knee joint is increased. As expected,

Table 1. Comparative analysis of the chosen materials.

Properties	PS	PE	PU foam	PP	EVA
Density (g/cm^3)	0.01–0.03	0.03–0.06	0.02–0.4	0.02–0.06	0.2–0.7
Rebound	Poor	Fair	Fair	Good	Fair
Low-temperature resistance	Good	Fair	Fair	Good	Good
Toughness	Poor	Excellent	Good	Excellent	Fair
Mechanical properties	Poor	Good	Poor	Excellent	Fair
Weatherability	Poor	Fair	Fair	Excellent	Fair
Abrasion resistance	Poor	Good	Fair	Good	Poor
Environmental friendly	Poor	Excellent	Poor	Excellent	Fair

Table 2. Polypropylene properties and their values.

Mechanical properties	
Elongation at break	150–600%
Flexibility (flexural modulus)	1.2–1.6 GPa
Hardness rockwell M	1–30
Hardness shore D	70–83
Stiffness (flexural modulus)	1.2–1.6 GPa
Strength at break (tensile)	20–40 MPa
Strength at yield (tensile)	35–40 MPa
Toughness (notched izod impact at room temperature)	20–60 J/m
Toughness at low temperature (notched izod impact at low temperature)	27–107 J/m
Young modulus	1.1–1.6 GPa

the distribution of plantar pressure varies significantly between a shoe with a cushion or midfoot and a shoe without ergonomic components.

The maximum pressure values took place predominantly in the big toe with $4.90 \pm 1.19 \text{ N/cm}^2$, followed by the second and third metatarsal areas with $4.57 \pm 0.73 \text{ N/cm}^2$, followed by the first metatarsal area with $4.30 \pm 0.96 \text{ N/cm}^2$ followed by the fourth. And the fifth metatarsal region from $3.22 \pm 0.89 \text{ N/cm}^2$ when using the insole of the control foot and an aluminum insole of the foot, which reduces the maximum pressure to 1.55 ± 0.34 , 1.56 ± 0.75 , 1.09 ± 0.43 , and $1.07 \pm 0.59 \text{ N/cm}^2$, respectively ($p < 0.001$) with effect sizes of 3.828, 4.067, 4.315 and 2.847, respectively.

Compliance depends on the types of polymer pairs used, their relative amounts, the degree of miscibility, the nature and amount of the compatibilizer used, and the mixing method. The key issue is the polymer blending process, during which blends

undergo a complex combination of shear and elongation, and the evolution of the blend's microstructure becomes crucial and requires close attention.

5 Conclusions

The study's main findings are that fill density is the dominant factor in material and energy consumption, while layer height has the greatest impact on production time. Also, it simplifies the process of choosing the most suitable orthopedic products. As a result of the research, a block diagram has been developed to help in the design process of orthopedic insoles. The entire success of orthopedics depends on the patient's weight, shoe style, and lifestyle. Patient weight is critical information that the laboratory must have to make the right choice of material. The style of shoes a person wears will influence the type of orthopedics that suits them best. Knowing the type of orthopedic product, now we can choose the base material for the manufacturing. Multiple materials were compared, and polypropylene was found to have the most suitable properties. Mechanical tests have confirmed that optimal stiffness increases with increasing compressive load. For the first time, this study provides quantitative evidence for the importance of optimizing the stiffness of cushioning materials and lays the foundation for techniques that allow the optimization of material selection in the clinics. It also clarifies and complements the previous studies done by other researchers.

This study can be viewed as a pilot study which methodology can be used in further research. Further research is needed.

References

1. Kong, L., et al.: The effects of shoes and insoles for low back pain: a systematic review and meta-analysis of randomized controlled trials. *Res. Sports. Med.* **21**, 1–16 (2020)
2. Yurt, Y., Şener, G., Yakut, Y.: The effect of different foot orthoses on pain and health related quality of life in painful flexible flat foot: a randomized controlled trial. *Eur. J. Phys. Rehabil. Med.* **55**(1), 95–102 (2018)
3. Ghomian, B., et al.: Gait stability of diabetic patients is altered with the rigid rocker shoes. *Clin. Biomech.* **69**, 197–204 (2019)
4. Wang, J.-C., Dommati, H., Cheng, J.: A turnkey manufacturing solution for customized insoles using material extrusion process. In: Kumar, L.J., Pandey, P.M., Wimpenny, D.I. (eds.) *3D Printing and Additive Manufacturing Technologies*, pp. 203–216. Springer, Singapore (2019). https://doi.org/10.1007/978-981-13-0305-0_18
5. Molnár, I., Morovič, L.: 3D digitization and additive manufacturing technologies in medicine. *Res. Pap.* **26**(42), 165–170 (2018)
6. Davia-Aracil, M., Hinojo-Pérez, J., Jimeno-Morenilla, A., Mora-Mora, H.: 3D printing of functional anatomical insoles. *Comput. Ind.* **95**, 38–53 (2018)
7. Ma, Z., et al.: Design and 3D printing of adjustable modulus porous structures for customized diabetic foot insoles. *Int. J. Lightweight Mater. Manuf.* **2**(1), 57–63 (2019)
8. Tse, C.T.F., Ryan, M.B., Hunt, M.A.: Influence of foot posture on immediate biomechanical responses during walking to variable-stiffness supported lateral wedge insole designs. *Gait Posture* **81**, 21–26 (2020)

9. Casado-Hernández, I., et al.: Electromyographic evaluation of the impacts of different insoles in the activity patterns of the lower limb muscles during sport motorcycling: a cross-over trial. *Sensors* **9**(10), 2249 (2019)
10. Yuan, Z., Qin, W., Zhao, J.: Smart manufacturing for the oil refining and petrochemical industry. *Engineering* **3**(2), 179–182 (2017)
11. Shaw, K.E., et al.: The effects of shoe-worn insoles on gait biomechanics in people with knee osteoarthritis: a systematic review and meta-analysis. *Br. J. Sports Med.* **52**(4), 238–253 (2018)
12. Teffer, S., Woodburn, J., Collier, A., Gavanagh, P.: Virtually optimized insoles for offloading the diabetic foot: a randomized crossover study. *J. Biomech.* **60**, 157–161 (2017)
13. Schaper, N., Van Netten, J., Apelqvist, J., Lipsky, B., Bakker, K.: Prevention and management of foot problems in diabetes: a summary guidance for daily practice 2015, based on the IWGDF guidance documents. *Diabetes Metabol. Res. Rev.* **32**, 7–15 (2016)
14. Bai, D.Y., Yuan, Z.G., Shao, J.J., Zhu, T., Zhang, H.J.: Unstable shoes for the treatment of lower back pain: a meta-analysis of randomized controlled trials. *Clin. Rehabil.* **33**(11), 1713–1721 (2019)
15. Kurdi, A., Kan, W.H., Chang, L.: Tribological behaviour of high performance polymers and polymer composites at elevated temperature. *Tribol. Int.* **130**, 94–105 (2019)



Structure and Properties of Surface Bandage Shelves for the Gas Turbine Engine's Blades

Natalia Zaichuk¹ , Sergii Shymchuk¹ , Anatolii Tkachuk¹  ,
Yurii Feshchuk¹ , and Jacek Szczot²

¹ Lutsk National Technical University, 75, Lvivska Street, Lutsk 43018, Ukraine
a.tkachuk@lntu.edu.ua

² Airport Lublin SA, 6, Zesłańców Sybiru Street, 20008 Lublin, Poland

Abstract. Analysis of the properties of the materials from which the parts of a gas turbine engine are made showed that they must have a high melting point, high strength, high creep resistance, and be machined. Therefore, the best option for strengthening the blades of titanium alloy VT3–1 is the formation in the wear zone of a thermodynamically compatible, heat-resistant, and wear-resistant layer, which is different from the main material of the blade. Samples for research were cut from the bandage shelves of the compressor blade in the shank area: the first - with high-quality soldering relite, the second – the shelf is worn, and there is a defect in the form of a drop. It was found that the main titanium alloy has a homogeneous structure, and the surface of the defective coating has a lower roughness, microcracks. Its local areas differ in elemental composition. Clusters of pores explain the clear and wide grain boundaries of titanium alloy under defective soldering at the boundaries. Such clusters of defects are etched more strongly than the base metal, so the base alloy has a needle-like martensite hardened structure formed by rapid cooling in the air after soldering. It is proved that such defects are formed due to the violation of soldering technology. It is proposed to create a protective layer of composite material VTN-1 with tungsten particles, which contains solid parts of tungsten carbide and titanium-based solder VPr16, to strengthen the working blades in the wearing zone.

Keywords: Heat resistance · Soldering · Relit · Bandage shelf · Titanium alloy · Spectral analysis · Mechanical properties

1 Introduction

The basis of modern aircraft construction is a gas turbine engine (GTE). GTE blades are the most numerous parts. Their total number in the engine is about 3000 pieces. The reliability of gas turbine engines depends on the compressor and turbine blades' reliability, as they are the most loaded parts [1]. They are located in the gas stream and in the area of high temperatures, are designed to change the parameters of the engine and consist of a root or shank (Fig. 1, a), which serves to attach the blades in the housing, the working part - the blade washer and the top in the form of a spike on which the bandage tape connecting shovels is put on [2].

The gas turbine engine's blades work in the conditions of multiple heat changes, are exposed to high-temperature gas flows, and experience additional fuel components and products of its combustion [1, 3]. This effect causes high-temperature salt corrosion, which is a process of rapid oxidation and sulfidation of the blade's working surface under the influence of combustion products with high sulfur fuel and determines the service life of the aircraft. The study of the structure and surface properties of titanium alloy VT3–1 without soldering and with soldering of wear-resistant material will determine the best combination of mechanical, physical, and technological properties necessary to increase the wear resistance of the surface of the bandage shelves and increase the service life of the blade [4].

2 Literature Review

Turbine blades are widely used in modern gas turbine engines. The use of bandage shelves reduces alternating voltages from vibration loads and thus increases the gas turbine engine's overall service life and reliability [5]. However, in the operation of the working and nozzle blades resulting from significant contact stresses under conditions of friction and vibration at the contact points of the shelves, there is increased wear of the contact surfaces compared with the pin and the blade lock [6]. Ensuring parameter identification [7] for rising operating temperatures and aircraft engines' service life sharply intensifies the processes that lead to damage and destruction of the blades' contact surfaces, limiting their service life and reliability [8, 9].

In general, the following defects may occur during the operation of the blades:

- cracks in the main metal and surface cracking due to fatigue wear [10];
- damage to the surface layers of parts due to corrosion [11–13];
- increased operation of contact surfaces under the conditions of friction [14] and vibrations [15].

Despite all their advantages, Titanium alloys have low wear characteristics, which leads to the need to address the issues of increasing the service life of parts made of these materials and the problems of strengthening and repairing worn surfaces. This primarily applies to the contact surfaces of the bandage shelves of the blades of the compressor GTE. From the experience of aircraft repair units, it is known that one of the most profitable and effective ways to repair many engine parts is welding [4, 14]. However, the results of studies of the mechanism of wear of contact surfaces allow concluding that the best option to strengthen the blades is to create in the wear zone a layer of highly heat-resistant and wear-resistant material, different from the blade's material [2, 8, 16].

3 Research Methodology

Titanium alloys do not have entirely satisfactory tribotechnical properties, for most compressor blades of aircraft engines use the alloy VT3–1, which satisfies the performance characteristics, and its use is economically justified. Repair and restoration of these parts allow to extend service life and to reduce expenses at regular maintenance. Surfacing on

the blades of the wear-resistant and heat-resistant layer of VTN-1 alloy was performed by the vacuum-arc method.

The surface analysis of samples made of titanium alloy VT3–1 was performed. The sample's surface was studied using a REMMA electron microscope, a high-resolution scanning electron microscope, and an X-ray microanalyzer. The samples were cut from different parts of the compressor blade's bandage shelves (Fig. 1, a). The study's object was: samples cut from the bandage shelves on which the relite was qualitatively applied (Fig. 1, b) and one – from the shelf, which contained a defect in the form of a drop (Fig. 1, c). Samples from the scapula feather that are not subject to intensive wear were also examined.

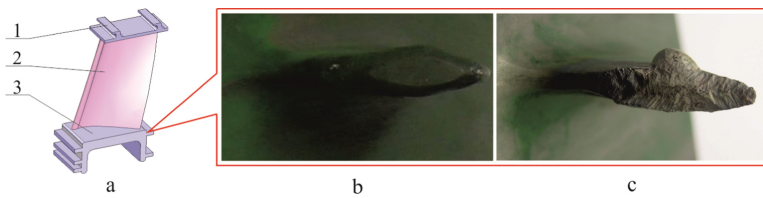


Fig. 1. The research object: a – the scheme of a shovel: 1 – shank; 2 - nib; 3 – top of the scapula with banding tape; b – high-quality soldering of wear-resistant material; c – soldering with a defect in the form of a drop.

Samples for research were cut from the bandage shelves after their operation and after soldering the relite. The samples' elemental composition was determined by X-ray microanalysis and electron microscopy [17, 18].

Investigations of mechanical properties were performed on the multifunctional “Micron-gamma” device by automatic registration during loading P on the indenter and the depth h of its immersion in the surface of the test material in the form of a load diagram $P = f(h)$.

4 Results

In particular, in this work, we studied the surface of samples made of titanium alloy VT3–1, cut from different parts of the compressor blade (Fig. 2).

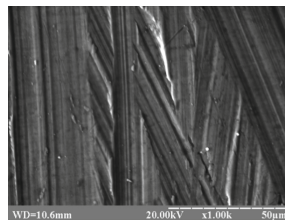


Fig. 2. Image of the section of titanium alloy VT3–1.

As a result of studies of the cut surface of the titanium alloy VT3–1, it was found that the alloy has a generally homogeneous structure (Fig. 3).

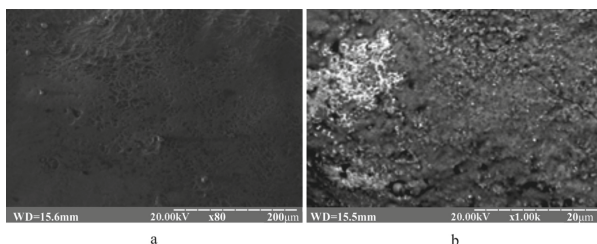


Fig. 3. The image of the samples’ surfaces with soldering: a - quality soldering, b - defective area.

There are also areas in the form of small inclusions. The surface structure indicates that the material is viscous and ductile, difficult to cut, and prone to sticking. The local analysis results indicate the homogeneity of the sample’s chemical composition and its compliance with the chemical composition of VT3–1. Spectral analysis performed on soldering (Fig. 4) shows a homogeneous distribution of chemical elements on the sample’s surface.

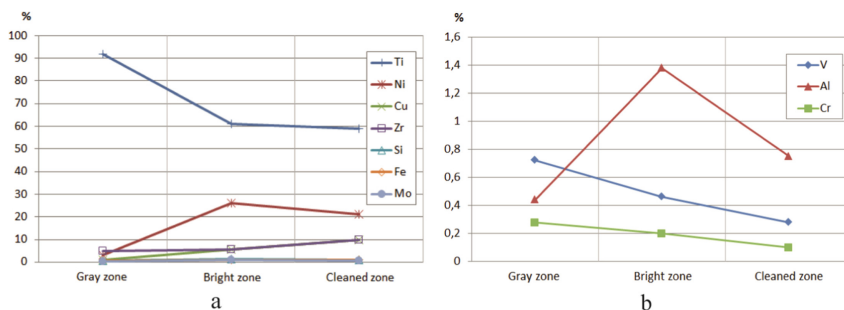


Fig. 4. Comparison of the chemical composition of different parts of the defective sample.

The defective coating surface is characterized by a slightly lower roughness than high-quality soldering, and there are sometimes small cracks (which do not pass the thickness of the coating). Local analysis of the plots shows that they differ in elemental composition. In (Fig. 4, a) shows a graph of changes in the content of chemical elements depending on the area where the study was conducted; Fig. 4, b shows Al, Cr, and V.

Heterogeneity of the chemical composition could arise due to a violation of the technological process of soldering. As a result, the shelf is unusable due to the presence in areas of very high Ti content with low thermal conductivity, prone to sticking and bulging.

Comparing the average values of the quantitative composition of qualitative soldering, defective area, and base material is shown in Table 1, graphical representation of the content of elements is presented in (Fig. 5). In (Fig. 5, b) the lower part (Fig. 5, a) – elements Mo, Fe, Si, V, the content of which does not exceed 2.4%.

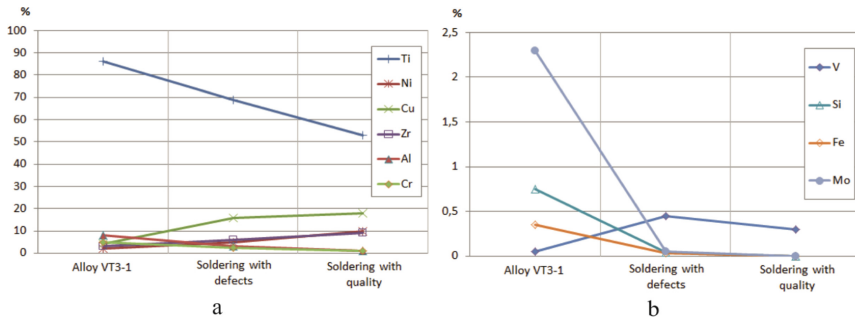


Fig. 5. Comparison of the chemical composition of different samples.

Table 1. Comparison of quantitative analysis of the elements of the base and soldering (accelerating voltage 20 kV).

Zone	The average content of elements, % ($\Sigma = 100$)									
	Al	Si	Ti	V	Cr	Fe	Mo	Ni	Cu	Zr
Quality soldering	0.52	–	51.7	0.29	11.72	–	–	10.85	16.47	8.97
Defective soldering	0.47	–	90.94	0.68	0.29	–	–	0.42	2.09	5.11
The base of the blade	8.09	0.77	86.71	–	0.75	0.34	2.34	–	–	–

It is possible to note that compared with a basis, the qualitative soldering contains the lowered quantity of Ti, Al, and the increased content of Cu, Ni, Zr. The defective area is characterized by an intermediate Ti content between the quality solder and the base. The content of Al, Cu, Zr, and V is close to its content in the quality solder.

All alloying elements increase the strength and reduce the ductility of titanium. Cu increases the stability during operation, increases the heat resistance of the alloy. Ni increases the strength and corrosion resistance of the coating. Zr increases the strength, heat resistance, and creep resistance of the coating at elevated temperatures.

Spectral analysis of the solders’ chemical composition revealed elements present in the solder VPr16 (Cr, Ni, Cu, Zr). Still, it did not reveal the presence on the surface of the reinforcing phase - relit (W and C). This can be explained by the fact that the relay particles have a density 2.5 times higher than the solder’s density, and in the process of soldering, they settle and, as a result, enrich the lower layers of the coating and deplete the upper ones. The studied samples’ structure is primarily homogeneous, although in

some areas, there is some inhomogeneity: local clusters of alloying elements or small pore size. They occur during the manufacture of the blade by injection molding when the cooling rate is significant, and the cross-section of the blade is small, gas or air bubbles do not have time to come to the surface. These structural defects are insignificant and do not affect the performance of the product. The structure of the initial alloy VT3-1 of the shoulder blades of the blade at the soldering point of the relit is significantly different from the structure of the pen and shank, which were not heated. On the etched section, the traces left after polishing are visible. This occurs since titanium alloy is a relatively soft material. They arise as a result of the hit of particles of a relit in a grinding zone. In such cases, it is recommended to use electrolytic polishing, which prevents defects of this type.

The microstructure of the solder also shows large grains with clear boundaries. Such grains are formed during microwave heating, and aging in soldering relit because the tendency of titanium to rapid grain growth at high temperatures is known. The presence of clear, wide grain boundaries of VT3-1 alloy under defective soldering is explained by the accumulation of pores and other defects at the boundaries such accumulations of defects are etched more strongly than the base metal. The alloy has a needle-like martensitic hardened structure formed due to rapid cooling in the air after soldering. Comparing the transition zones between quality soldering and base metal, and between defective soldering and base alloy, it should be noted that quality soldering has an equal gradual defect-free transition. While the boundary between defective soldering and the base metal is uneven, it is characterized by defects (pores, cracks). The microstructure of relite soldering is two-phase: light large WC crystals and etched dark areas of VPr16 solder. Light grains are very hard. The fine-grained equilibrium structure of the solder is less hard but more viscous, i.e., astringent.

In the soldering process, there are no phase reactions that radically change the reinforcing parts' composition and structure. Therefore, in the structure of the soldered layer, the relit particles, which provide high resistance to wear of the coating, should be evenly distributed and connected between themselves and the base material by solder. However, defective soldering has a heterogeneous structure: large, unevenly distributed relite grains, surrounded by an increased amount of solder. It has a fine-grained structure consisting of a β -phase. Relite grains, in contrast to solder, were not pickled because digestion was performed with a Kroll reagent designed to determine the structure of titanium alloys. Only traces of corrosion are observed on the relite grains.

In some areas of defective soldering, the coating is loose – you can see the area's presence with the structure of the main alloy of the blade VT3-1. Also, gas pores in this area have significant dimensions (up to 1 mm), smooth, smooth walls, and edges. High-quality soldering on the test sample is characterized by a uniform distribution of relit and a sufficient amount of solder. It covers the test sample's entire surface and forms a dense, high-quality defect-free coating that provides high hardness and strength during the blade's operation. An essential feature of the coating formation is the distribution of the reinforcing parts of the rafters in height. Tungsten carbide has a density 2.5 times higher than the solder's density, and in the process of soldering, it settles and, as a consequence, the enrichment of the lower layers of the coating and the depletion of the upper. The depleted upper layer is most clearly manifested by increasing the solder

content in the paste and increasing the thickness of the soldered layer. Relite particles can also settle under forces arising from the electromagnetic stirring of the liquid solder bath during induction heating by high-frequency currents. Practically on the thickness of the soldered layer 0.2–0.3 mm from the strengthened surface of the reinforcing parts has almost uniform character.

The contact action research and control of materials' physical and mechanical properties in the near-surface layers are. Contact deformation is associated with almost all modern methods of processing, strengthening, and joining materials (metal processing by pressure and cutting, grinding, polishing) and service properties of materials in the conditions of friction, fatigue, setting, wear. The study presents the results of reduced and non-reduced microhardness. The Martens method was used to determine the restored hardness, and the Meyer method was used to determine the non-reduced hardness. It should be noted that the Meyer microhardness is equal to the average pressure in the impression and quantitatively accurately expresses the physical essence of hardness. The standard microhardness (in this case, according to Martens) is less than the Meyer hardness as many times as the area of the impression surface calculated for the indenter of the accepted geometry is greater than the area of the projection of the impression. After conducting the research, the computer program using the "Micron-gamma" device displayed on the monitor the values of strength in tables for each of the samples.

Analyzing the data for these samples, we can say that the highest value of unrecovered microhardness has relite grains (21.02 GPa). They provided the overall increase in surface microhardness with quality soldering relite (average 5.51 GPa). Under the same loading conditions, the unrecovered hardness for other samples became slightly lower: for the sample with defective soldering 4.76 GPa, and the sample from the alloy VT3-1 approached 4 GPa (Table 2).

Table 2. Average values of microhardness of the studied surfaces.

The investigated surface	Restored microhardness H_{μ} , GPa	Unrestored microhardness H_{μ} , GPa
The surface of the sample from the alloy VT3-1	3.53	3.99
The surface of the sample with defective relite soldering	4.16	4.76
The surface of the sample with high-quality relite soldering	4.83	5.51
Relite grains	17.14	19.36

In (Fig. 6) shows histograms comparing the obtained average values of microhardness of the samples.

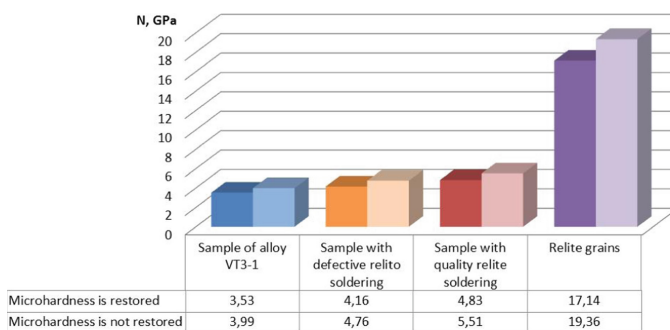


Fig. 6. Histogram comparing the average values of restored and unrestored microhardness of the studied samples.

A characteristic feature of titanium alloys is the low modulus of elasticity, which decreases with increasing temperature. Relite soldering allowed to increase this characteristic (Table 3), which will increase the part's rigidity and efficiency. Strength is one of the essential properties of the material. The tensile strength (σ_B), i.e., the maximum stress that can withstand the material when tested in titanium alloys, is quite high (Table 3), but in terms of wear, it is insufficient. Relite soldering provides an increase in the value of strength.

Table 3. Average values of mechanical properties of the studied samples.

The investigated surface	Young's modulus E, GPa	Plasticity index K	Tensile strength σ_B , GPa
The surface of the sample from the alloy VT3-1	133.46	0.78	0.879
The surface of the sample with defective relite soldering	132.80	0.76	1.022
The surface of the sample with high-quality relite soldering	136.22	0.75	1.151
Relite grains	178.67	–	1.532

In (Fig. 7, a) shows that the highest modulus of elasticity has a pattern with high-quality soldering, which is undoubtedly achieved by forming a high-quality coating and uniform grain distribution of the relay, which has a much higher Young's modulus. The lowest modulus of elasticity has a pattern with defective soldering, which could occur due to non-compliance with soldering technology. Analyzing the histograms comparing

the ductility (Fig. 7, b), we can say that one of the reasons for the low wear resistance of titanium alloys is high ductility. Relite soldering reduces ductility, providing increased hardness, strength, and durability.

Comparisons of the average values of the modulus of elasticity, ductility, and tensile strength are presented in (Fig. 5), (Fig. 6), (Fig. 7).

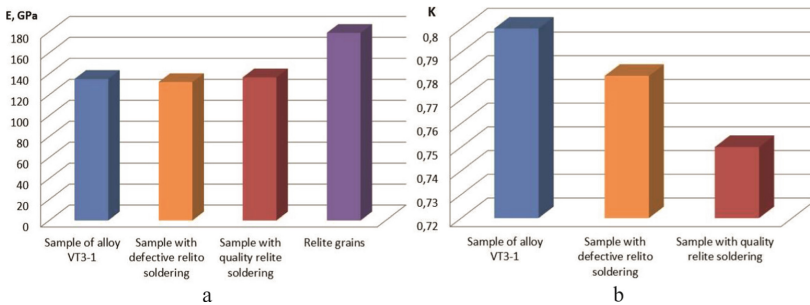


Fig. 7. Histogram comparing Young's modulus's average values (a) the average values plasticity of the studied samples (b).

Relite grains have high strength values (Fig. 7). They significantly increase the studied samples' tensile strength (by 30.9% compared to the sample of alloy VT3-1).

Examination of the samples revealed relit grains' presence, although a significant increase in mechanical properties is provided by relit powder, which is evenly distributed in the solder. Relite particles have a density 2.5 times higher than the solder's density. In the process of soldering, they settle and, as a consequence, the enrichment of the lower layers of the coating and the depletion of the upper ones. Reducing the content of relit in the upper layers of the coating has a positive value. It facilitates the machining of the soldered surface by decreasing the hardness of the upper layer.

5 Conclusions

The recommended option for strengthening the blades is to create a layer of heat-resistant and wear-resistant material VTN-1 in the wear zone, consisting of solid parts of tungsten carbide (relit) titanium-based solder VPr16 as a binder. Microstructural studies have shown that there have been no significant changes in the base alloy structure over the entire blade volume, although, in the alloy on the shelf shelves, grain growth and the formation of a martensitic needle structure occurred at the soldering point.

Physicomechanical parameters of samples from VT3-1 alloy and samples with defective and high-quality relite soldering showed a significant increase in mechanical properties of the sample with high-quality soldering in comparison with the sample from VT3-1 alloy: modulus of elasticity E by 2.1%, strength limit σ_B on 30.9%, unrecovered microhardness by 38.1%. The sample acquires such properties due to the high mechanical properties of the relite grains ($H\mu = 19.36$ GPa, $E = 178.67$ GPa, $\sigma_B = 1.532$ GPa) and the solder, which provides a strong connection of the relit grains with each other and with the main alloy.

The next stage of the study will be to determine the wear resistance and service life of the surfaces of the bandage shelves of the GTE blades, considering the above recommendations.

References

1. Alqallaf, J., Ali, N., Teixeira, J.A., Addali, A.: Solid Particle Erosion Behaviour and Protective Coatings for Gas Turbine Compressor Blades. A Review. *Processes* **8**(8), 984 (2020)
2. Hovorun, T.P., Pylypenko, O.V., Hovorun, M.V., Dyadyura, K.O.: Methods of obtaining and properties of wear-resistant coatings based on Ti and N and Ti. Al and N. *J. Nano-Electron. Phys.* **9**(2), 02026 (2017)
3. Blinkov, I.V., Volkhonsky, A.O., Anikin, V.N.: Phase composition and properties of wear-resistant Ti-Al-Cr-Zr-Nb-N coatings, obtained by physical vapor deposition. *Phys. Chem. Mater. Process.* **37**, 37–44 (2010)
4. Pogrebnjak, A.D., Bagdasaryan, A.A., Pshyk, A., Dyadyura, K.: Adaptive multicomponent nanocomposite coatings in surface engineering. *Phys. Usp.* **60**, 586–607 (2017)
5. Lei, X., et al.: Microstructure, Texture Evolution and Mechanical Properties of VT3-1 Titanium Alloy Processed by Multi-Pass Drawing and Subsequent Isothermal Annealing. *Metals* **7**(4), 131 (2017)
6. Kirchgaßner, M., Badisch, E., Franek, F.: Behaviour of iron-based hardfacing alloys under abrasion and impact. *Wear* **265**, 772–779 (2008)
7. Pavlenko, I., Trojanowska, J., Ivanov, V., Liaposhchenko, O.: Parameter identification of hydro-mechanical processes using artificial intelligence systems. *International Journal of Mechatronics and Applied Mechanics* **2019**(5), 19–26 (2019)
8. Tkachuk, A., Zablotskiy, V., Kononenko, A., Moroz, S., Prystupa, S.: Directed Formation of Quality, as a Way of Improving the Durability of Conjugated Parts of Friction Pairs. In: Ivanov, V., et al. (eds.) *DSMIE 2019. LNME*, pp. 370–377. Springer, Cham (2020). https://doi.org/10.1007/978-3-030-22365-6_37
9. Buchely, M.F., Gutierrez, J.C., León, L.M., Toro, A.: The effect of microstructure on abrasive wear of hardfacing alloys. *Wear* **259**, 52–61 (2005)
10. Coronado, J.J., Caicedo, H.F., Gómez, A.L.: The effects of welding processes on abrasive wear resistance for hardfacing deposits. *Tribol. Int.* **42**, 745–749 (2009)
11. Zhu, L., Jia, M.-P.: A new approach for the influence of residual stress on fatigue crack propagation. *Results Phys.* **7**, 2204–2212 (2017)
12. Lupyry, O., Hovorun, T., Vorobiov, S., Burlaka, A., Khvostenko, R.: Influence of heat treatment technologies on the structure and properties of the corrosion-resistant martensitic steel type AISI 420. *Journal of Engineering Sciences* **7**(2), C10–C16 (2020). [https://doi.org/10.21272/jes.2020.7\(2\).c2](https://doi.org/10.21272/jes.2020.7(2).c2)
13. Bagdasaryan, A.A., et al.: Structural and mechanical characterization of (TiZrNbHfTa)N/WN multilayered nitride coatings. *Mater. Lett.* **229**, 364–367 (2018)
14. Musil, J.: Hard nanocomposite coatings: thermal stability, oxidation resistance and toughness. *Surf. Coat. Technol.* **207**, 50–65 (2012)
15. Pavlenko, I., Ivanov, V., Kuric, I., Gusak, O., Liaposhchenko, O.: Ensuring Vibration Reliability of Turbopump Units Using Artificial Neural Networks. In: Trojanowska, J., Ciszak, O., Machado, J.M., Pavlenko, I. (eds.) *MANUFACTURING 2019. LNME*, pp. 165–175. Springer, Cham (2019). https://doi.org/10.1007/978-3-030-18715-6_14
16. Sanjay, K.T. Gopal Krishnan, R.: *Advances in Applied Surface Engineering*. Research Publishing Services, Singapore (2011).

17. Rudnev, V.S., Lukiyanchuk, I.V., Vasilyeva, M.S., Medkov, M.A., Adigamova, M.V., Sergienko, V.I.: Aluminum-and titanium-supported plasma electrolytic multicomponent coatings with magnetic, catalytic, biocide or biocompatible properties. *Surf. Coat. Technol.* **307**, 1219–1235 (2016)
18. Stephens, R., Fatemi, A., Stephens, R., Fuchs, O.H.: *Metal Fatigue in Engineering*, 2nd edn. Wiley, New Jersey (2001)

Author Index

A

Akimov, Oleg, [3](#)
Alexeyev, Alexander, [289](#)
Antosz, Katarzyna, [415](#)
Araújo, Adriana, [262](#)
Arhat, Roman, [12](#)

B

Balaniuk, Anna, [481](#)
Barz, Cristian, [472](#)
Basova, Yevheniia, [343](#)
Bekish, Iryna, [322](#)
Berladir, Kristina, [525](#)
Boyarska, Inna, [556](#)
Bucior, Magdalena, [315](#)
Bui, Vasyl, [322](#)
Burburska, Svitlana, [81](#)

C

Cagaňová, Dagmar, [585](#)
Chernenko, Serhii, [104](#)
Chernish, Andrii, [104](#)
Chumachenko, Tatiana, [453](#)
Cizsak, Olaf, [444](#)
Comes, Radu, [311](#)
Crisan, Liviu Adrian, [311](#)

D

Dašić, Predrag, [193](#)
Davydovitch, Andrei, [165](#)
Denysenko, Yuliia, [444](#)
Derevianchenko, Oleksandr, [21](#)
Diachun, Andrii, [385](#)
Dobrotvorskiy, Sergey, [343](#)

Dobrovolska, Ludmila, [343](#)
Dolmatov, Anatolii, [434](#)
Dubei, Olha, [153](#)
Dyadyura, Kostiantyn, [594](#)
Dzhemalyadinov, Ruslan, [353](#)
Dzhemelinskyi, Vitaliy, [62](#)
Dzhemilov, Eshreb, [353](#), [513](#)

E

Edl, Milan, [183](#), [343](#)
Emiroglu, Uğur, [513](#)

F

Fedorovich, Vladimir, [363](#)
Feshchuk, Yurii, [602](#)
Fomin, Oleksandr, [21](#)
Frolenkova, Olga, [453](#)

G

Garashchenko, Yaroslav, [31](#)
Gasanov, Magomedimin, [490](#)
Germashev, Anton, [373](#)
Glushko, Alyona, [31](#)
Grabis, Janis, [174](#)
Grimzin, Igor, [565](#)
Gusak, Oleksandr, [525](#)
Gutsalenko, Yuriy, [114](#)

H

Haidabrus, Bohdan, [165](#), [174](#)
Haikova, Tetiana, [12](#)
Haluzynskyi, Oleksandr, [81](#)
Harashchenko, Olena, [31](#)
Hatala, Michal, [594](#)

Hevko, Ivan, 385
 Honchar, Natalia, 395
 Horbunov, Andriy, 73
 Hovorun, Tetiana, 525
 Hrytsay, Ihor, 405, 501
 Huliieva, Nataliia, 585
 Hupka, Andriy, 385
 Husak, Ermin, 193
 Hutorov, Andrii, 463

I

Ilchuk, Nataliia, 585
 Imbirovych, Nataliia, 536
 Ivanov, Vitalii, 481
 Ivanova, Larysa, 490
 Ivanova, Maryna, 490
 Ivchenko, Oleksandr, 444

J

Jakym, Roman, 123

K

Kábele, Pavel, 183
 Karabegović, Edina, 193
 Karabegović, Isak, 193
 Karnaukh, Mykola, 213
 Khavkina, Olena, 395
 Klimov, Eduard, 104
 Kluz, Rafał, 415
 Klymenko, Nataliia, 453
 Klymenko, Stepan, 3
 Kobets, Olena, 31
 Kobets, Vitaliy, 301
 Kondratiev, Andrii, 546
 Kononenko, Serhii, 343
 Kornuta, Olena, 322
 Kornuta, Volodymyr, 322
 Korotun, Mykola, 444
 Kostyk, Kateryna, 3
 Koubovská, Michaela, 275
 Koval, Svitlana, 301
 Krol, Oleg, 41, 133
 Kryvenko, Maksym, 81
 Kuchuhurov, Mark, 373
 Kulieshov, Serhii, 332
 Kundrak, Janos, 363
 Kunitsyn, Maksym, 425
 Kurin, Maksym, 434
 Kусyі, Yaroslav, 52

L

Lamikiz, Aitzol, 62
 Larshin, Vasily, 203
 Lauwers, Bert, 373
 Lebedev, Vladimir, 453

Lesyk, Dmytro, 62
 Lishchenko, Natalia, 203
 Litovchenko, Petro, 73, 490
 Liubchenko, Vira, 301
 Logominov, Viktor, 373
 Lucamba, Aurélio, 262
 Luzan, Petro, 332
 Lyashuk, Oleg, 385
 Lysenko, Tatiana, 565
 Lysyi, Oleksandr, 203

M

Machado, José, 262
 Mahmić, Mehmed, 193
 Malandii, Tetiana, 289
 Malets, Victoria, 556
 Martinez, Silvia, 62
 Marynenko, Dmytro, 565
 Matzey, Ruslan, 481
 Medvid, Iulia, 472
 Meilekhov, Andriy, 575
 Melnychuk, Mykola, 556
 Mordyuk, Bohdan, 62
 Moshna, Alina, 289
 Muzylyov, Dmitriy, 213
 Mykhaylyuk, Ivanna, 556

N

Nabokina, Tetyana, 546
 Nechiporenko, Vladimir, 73
 Novikov, Dmytro, 463
 Novikov, Fedir, 463
 Novinkina, Julija, 165
 Nyshnyk, Serhii, 434

O

Oborskyi, Gennadiy, 481
 Onysko, Oleh, 472
 Orgiyan, Alexandr, 481

P

Panchuk, Vitalii, 472
 Pasichnyk, Vitalii, 81
 Pasternak, Viktoriya, 585
 Peksa, Janis, 223
 Penzev, Pavel, 3
 Pinchuk, Nataliia, 575
 Ponomarenko, Olga, 565
 Ponomarenko, Yevhen, 463
 Pop, Grigore Marian, 311
 Popovych, Ihor, 301
 Porkuian, Olga, 133
 Potapov, Olexander, 546
 Povstyanoy, Oleksandr, 536
 Priadko, Olga, 536

Protsenko, Serhiy, 174
Prydalnyi, Borys, 95
Pupan, Larisa, 114, 363
Puzyr, Ruslan, 12, 104
Puzyr, Viacheslav, 12
Pyzhov, Ivan, 363

R

Rakivnenko, Valeriya, 73
Rauch, Erwin, 233
Rodic, Vesna, 472
Ropyak, Liubomyr, 153
Rosenberger, Philipp, 243
Rudnev, Aleksandr, 114

S

Saló, Valentin, 73
Saltykov, Leonid, 3
Sevidova, Elena, 114
Shah, Vaibhav, 262
Shchetynin, Viktor, 12
Shelkovyi, Oleksandr, 143
Shkitsa, Lesya, 322
Shramenko, Natalya, 213
Shymchuk, Sergey, 536
Shymchuk, Sergii, 602
Sikirash, Yulia, 425
Šimon, Michal, 275
Sira, Yuliia, 104
Slipchuk, Andrii, 123
Sobol, Oleg, 575
Sokolov, Volodymyr, 41, 133
Sosnowski, Marcin, 556
Sosnytska, Natalia, 332
Stepanov, Dmytro, 395
Stepanov, Mykhaylo, 490
Stepanova, Oksana, 133
Strelchuk, Roman, 143
Stupnytskyy, Vadym, 405, 501
Suprun, Olena, 332
Szczot, Jacek, 602

T

Tick, Jozsef, 243
Titarenko, Oksana, 114
Titova, Olena, 332
Tkachuk, Anatolii, 602
Touggui, Youssef, 513
Trojanowska, Justyna, 253
Trojanowski, Piotr, 253
Tryshyn, Pavlo, 395
Trzepieciniski, Tomasz, 415
Tsaritsynskyy, Anton, 546
Tutko, Tetiana, 153

U

Uminsky, Sergey, 203
Usov, Anatoly, 425
Uysal, Alper, 513

V

Varela, Leonilde, 262
Vasiljeva, Tatjana, 165
Vinante, Eugenio, 233
Vnukov, Yuri, 373
Voloshkina, Irina, 363
Vovk, Yuriy, 385
Vytvytskyi, Vasyl, 153

X

Xianning, She, 501

Y

Yermolenko, Oleksii, 463
Yevtifeiev, Serhii, 453
Yevtushenko, Nataliia, 565

Z

Zabolotnyi, Oleg, 585
Zaichuk, Natalia, 602
Zaleta, Olha, 536
Zaloga, Viliam, 594
Zaloha, Ruslan, 594
Zhadko, Mariia, 575
Zoubek, Michal, 275